



UNIVERSITÉ
PARIS-SUD 11



Faculté des
sciences
d'Orsay

N° d'ordre: 2011PA112193

THÈSE

Présentée pour obtenir

LE GRADE DE DOCTEUR EN SCIENCES
DE L'UNIVERSITÉ PARIS-SUD XI

Spécialité: Physique théorique

par

Julien BAGLIO

Phenomenology of the Higgs at the hadron colliders: from the Standard Model to Supersymmetry.

Soutenue le Lundi 10 octobre 2011 devant le Jury composé de :

Pr.	Guido ALTARELLI	(Examineur)
Dr.	Abdelhak DJOUADI	(Directeur de thèse)
Pr.	Ulrich ELLWANGER	(Examineur)
Dr.	Louis FAYARD	(Rapporteur)
Dr.	Massimiliano GRAZZINI	(Rapporteur)
Pr.	Margarete MÜHLEITNER	(Examineur)
Dr.	Gavin SALAM	(Examineur)



Thèse préparée au
Département de Physique d'Orsay
Laboratoire de Physique Théorique (UMR 8627), Bât. 210
Université Paris-Sud 11
91 405 Orsay CEDEX

PHÉNOMÉNOLOGIE DU HIGGS AUPRÈS DES COLLISIONNEURS HADRONIQUES :
DU MODÈLE STANDARD À LA SUPERSYMMÉTRIE.

Résumé

Cette thèse, conduite dans le contexte de la recherche du boson de Higgs, dernière pièce manquante du mécanisme de brisure de la symétrie électrofaible et qui est une des plus importantes recherches auprès des collisionneurs hadroniques actuels, traite de la phénoménologie de ce boson à la fois dans le Modèle Standard (SM) et dans son extension supersymétrique minimale (MSSM). Après un résumé de ce qui constitue le Modèle Standard dans une première partie, nous présenterons nos prédictions pour la section efficace inclusive de production du boson de Higgs dans ses principaux canaux de production auprès des deux collisionneurs hadroniques actuels que sont le Tevatron au Fermilab et le grand collisionneur de hadrons (LHC) au CERN, en commençant par le cas du Modèle Standard. Le principal résultat présenté est l'étude la plus exhaustive possible des différentes sources d'incertitudes théoriques qui pèsent sur le calcul : les incertitudes d'échelles vues comme une mesure de notre ignorance des termes d'ordre supérieur dans un calcul perturbatif à un ordre donné, les incertitudes reliées aux fonctions de distribution de partons dans le proton/l'anti-proton (PDF) ainsi que les incertitudes reliées à la valeur de la constante de couplage fort, et enfin les incertitudes provenant de l'utilisation d'une théorie effective qui simplifie le calcul des ordres supérieurs dans la section efficace de production. Dans un second temps nous étudierons les rapports de branchement de la désintégration du boson de Higgs en donnant ici aussi les incertitudes théoriques qui pèsent sur le calcul. Nous poursuivrons par la combinaison des sections efficaces de production avec le calcul portant sur la désintégration du boson de Higgs, pour un canal spécifique, montrant quelles en sont les conséquences intéressantes sur l'incertitude théorique totale. Ceci nous amènera à un résultat significatif de la thèse qui est la comparaison avec l'expérience et notamment les résultats des recherches du boson de Higgs au Tevatron. Nous irons ensuite au-delà du Modèle Standard dans une troisième partie où nous donnerons quelques ingrédients sur la supersymétrie et sa mise en application dans le MSSM où nous avons cinq bosons de Higgs, puis nous aborderons leur production et désintégration en se focalisant sur les deux canaux de production principaux par fusion de gluon et fusion de quarks b . Nous présenterons les résultats significatifs quant à la comparaison avec aussi bien le Tevatron que les résultats très récents d'ATLAS et CMS au LHC qui nous permettront d'analyser l'impact de ces incertitudes sur l'espace des paramètres du MSSM, sans oublier de mentionner quelques bruits de fond du signal des bosons de Higgs. Tout ceci va nous permettre de mettre en avant le deuxième résultat très important de la thèse, ouvrant une nouvelle voie de recherche pour le boson de Higgs standard au LHC. La dernière partie sera consacrée aux perspectives de ce travail et notamment donnera quelques résultats préliminaires dans le cadre d'une étude exclusive, d'un intérêt primordial pour les expérimentateurs.

Mots-clefs : Modèle Standard, Higgs, Supersymétrie, Chromodynamique quantique, incertitudes théoriques.

Abstract

This thesis has been conducted in the context of one of the utmost important searches at current hadron colliders, that is the search for the Higgs boson, the remnant of the electroweak symmetry breaking. We wish to study the phenomenology of the Higgs boson in both the Standard Model (SM) framework and its minimal Supersymmetric extension (MSSM). After a review of the Standard Model in a first part and of the key reasons and ingredients for the supersymmetry in general and the MSSM in particular in a third part, we will present the calculation of the inclusive production cross sections of the Higgs boson in the main channels at the two current hadron colliders that are the Fermilab Tevatron collider and the CERN Large Hadron Collider (LHC), starting by the SM case in the second part and presenting the MSSM results, where we have five Higgs bosons and focusing on the two main production channels that are the gluon gluon fusion and the bottom quarks fusion, in the fourth part. The main output of this calculation is the extensive study of the various theoretical uncertainties that affect the predictions: the scale uncertainties which probe our ignorance of the higher-order terms in a fixed order perturbative calculation, the parton distribution functions (PDF) uncertainties and its related uncertainties from the value of the strong coupling constant, and the uncertainties coming from the use of an effective field theory to simplify the hard calculation. We then move on to the study of the Higgs decay branching ratios which are also affected by diverse uncertainties. We will present the combination of the production cross sections and decay branching fractions in some specific cases which will show interesting consequences on the total theoretical uncertainties. We move on to present the results confronted to experiments and show that the theoretical uncertainties have a significant impact on the inferred limits either in the SM search for the Higgs boson or on the MSSM parameter space, including some assessments about SM backgrounds to the Higgs production and how they are affected by theoretical uncertainties. One significant result will also come out of the MSSM analysis and open a novel strategy search for the Standard Higgs boson at the LHC. We finally present in the last part some preliminary results of this study in the case of exclusive production which is of utmost interest for the experimentalists.

Keywords : Standard Model, Higgs, Supersymmetry, QCD, theoretical uncertainties.

Remerciements

Trois années ont passé depuis que j'ai poussé pour la première fois les portes du Laboratoire de Physique Théorique d'Orsay, chaleureusement accueilli par son directeur Henk Hilhorst que je remercie beaucoup. Trois années d'une activité intense, aussi bien dans mes recherches scientifiques au LPT et au CERN, dans le groupe de physique théorique, où j'ai passé quelques mois à partir de la seconde année, que dans mes activités hors recherche au sein de l'université Paris-Sud 11. J'ai appris beaucoup et rencontré un certain nombre de personnes dont je vais me rappeler pour longtemps, si je ne les énumère pas ici qu'elles veuillent bien me pardonner cela ne signifie pas que je les ai pour autant oubliées.

Tout ceci n'aurait pu se faire sans les encouragements, les conseils et les discussions passionnées avec Abdelhak Djouadi, mon directeur de thèse qui a guidé ainsi mes premiers pas de professionnel dans ma carrière de physicien théoricien des particules élémentaires. Je l'en remercie profondément et j'espère qu'il aura apprécié notre collaboration autant que moi, aussi bien lors de notre travail qu'en dehors.

Je voudrais aussi remercier Rohini Godbole avec qui j'ai collaboré sur la passionnante physique du Higgs au Tevatron. Je ne peux non plus oublier Ana Teixeira pour son soutien constant et les nombreuses discussions passionnantes aussi bien scientifiques que personnelles que nous avons eues ensemble. Ma première année en tant que doctorant lui doit beaucoup.

Je remercie aussi tous les membres de mon jury de thèse et en particulier mes deux rapporteurs qui m'ont certainement maudit d'avoir écrit autant, non seulement pour le temps qu'ils auront pris pour assister à ma soutenance et lire ma thèse, mais aussi pour toutes leurs judicieuses remarques et questions.

Aussi bien le LPT que le CERN se sont révélés des lieux très enrichissants pour le début de ma carrière scientifique. Je voudrais profiter tout d'abord de ces quelques mots pour remercier les équipes administratives des deux laboratoires pour leur aide au jour le jour, toujours avec le sourire, et pour toute leur aide dans mes divers voyages scientifiques. Je remercie aussi tous les chercheurs de ces deux laboratoires pour toutes les discussions que j'ai eues et qui m'ont beaucoup appris. Je pense tout particulièrement à Asmâa Abada et à Grégory Moreau d'un côté, à Géraldine Servant et Christophe Grojean qui m'a invité à venir au CERN, de l'autre. Je ne peux bien sûr pas oublier les doctorants et jeunes docteurs du groupe de physique théorique du CERN, Sandeepan Gupta, Pantelis Tziveloglou et tous les autres, ainsi que Léa Gauthier, doctorante au CEA, que j'ai rencontrée au CERN : les magnifiques randonnées autour de Genève que nous avons faites ont été salutaires. Enfin je remercie aussi tous mes camarades doctorants et jeunes docteurs du SINJE à Orsay pour

tous les merveilleux moments que nous avons passés et toutes les discussions passionnées et passionnantes, je ne vous cite pas tous mais le cœur y est. Je pense quand même tout particulièrement à mes camarades ayant partagé mon bureau et bien plus, Adrien Besse et Cédric Weiland, mais aussi à Guillaume Toucas, Blaise Goutéraux et Andreas Goudelis. Jérémie Quevillon qui va prendre ma succession auprès de mon directeur de thèse n'est pas non plus oublié. Mes amis de Toulouse eux aussi sont loin d'avoir été oubliés et ont fortement contribué non seulement à rendre exceptionnel mon stage de Master 2 mais aussi ma première année de thèse, de loin en loin : merci à Ludovic Arnaud, Gaspard Bousquet, Arnaud Ralko, Clément Touya, Fabien Trouselet, mais aussi mes deux tuteurs Nicolas Destainville et Manoel Manghi.

Je ne peux terminer sans exprimer ma profonde gratitude à ma famille et à mes amis de longue date, qui se reconnaîtront. Anne, Charles, Elise, Gaetan, Lionel, Mathieu, Matthieu, Patrick, Pierre, Rayna, Sophie, Yiting et tous ceux que je n'ai pas cités mais qui sont dans mes pensées, ces mots sont pour vous ! Le mot de la fin revient à ma fiancée, Camille : sans ton profond amour et ton soutien constant, ces trois dernières années auraient été bien différentes, et certainement pas aussi fécondes. Merci pour tout.

Acknowledgments

Three years have now passed since my first steps in the Laboratoire de Physique Théorique at Orsay, where I have been warmly welcomed by its director Henk Hilhorst that I thank a lot. They have been very intense, both in the laboratory and at the CERN Theory Group in Geneva, where I spent some months starting from the second year. I have learnt much, either within these labs or outside, encountered many people that I will remember for a long time. If some of you are not cited in these acknowledgments, please be kind with me: that does not mean I have forgotten you.

This would have never been possible without the constant encouragement, advices and fruitful discussions with Dr. Abdelhak Djouadi, my thesis advisor, who guided my first steps in theoretical particle physics research. I hope he got as much great time as I had working with him and more than that.

I also would like to thank Pr. Rohini Godbole whom I worked with from time to time on Higgs physics at the Tevatron. I cannot also forget Dr. Ana Teixeira for her constant support and all the great discussions on various topics we had together. My first year as a PhD candidate was scientifically exciting thanks to her.

I am very grateful to all the members in the jury for my defence, for the time they would took and the useful comments. In particular I would like to thank my two referees who certainly have cursed me for the length of the thesis.

The LPT environnement as well as the CERN Theory Group have been proven to be very fruitful environnements for the beginning of my career. I then would like to thank the administrative staff from both laboratories for their constant help in day-to-day life and support when I had to travel for various workshops, conferences or seminars. I would like to thank all the members of these two groups for the very passionate discussions we had and where I have learnt a lot. I dedicate special thanks to Asmâa Abada and Grégory Moreau on the one side, Géraldine Servant and also Christophe Grojean, who invited me to come by, on the other side. I cannot forget the PhD candidates and post-doctoral researchers from the CERN Theory Group, Sandeepan Gupta, Pantelis Tziveloglou and all the others, not to forget Léa Gauthier, who is a PhD candidate at the CEA and was at CERN at that time: the hiking we did in the Jura and Alps around Geneva were great. I also would like to thank all my SINJE fellows at the LPT, with whom I had so many great time and passionate discussions; you are not all cited but I do not forget you. I dedicate special thanks to my office (and more than office) friends Adrien Besse and Cédric Weiland, and also to Blaise Goutéraux, Andreas Goudelis and Guillaume Toucas. The next PhD candidate, Jérémie Quevillon, who will follow my path, is also thanked for the discussions we had. I finally

cannot forget my friends from Toulouse, where I did my Master 2 internship and whom I collaborated with during my first PhD thesis year from time to time: many thanks to Ludovic Arnaud, Gaspard Bousquet, Arnaud Ralko, Clément Touya, Fabien Trouselet, and also to my two internship advisors Nicolas Destainville and Manoel Manghi.

I now end this acknowledgments by expressing my deep gratitude and love to my family and long-time friends who will recognize themselves. Anne, Charles, Elise, Gaetan, Lionel, Mathieu, Matthieu, Patrick, Pierre, Rayna, Sophie, Yiting and all the others, these words are for you! The last word is for Camille, my fiancée: without your deep love and constant support these three years would have been without doubts completely different and not as fruitful.

Contents

Introduction	1
I A brief review of the Standard Model of particle physics	5
1 Symmetry principles and the zoology of the Standard Model	6
1.1 A brief history of the Standard Model	6
1.2 Gauge symmetries, quarks and leptons	12
2 The Brout–Englert–Higgs mechanism	17
2.1 Why do we need the electroweak symmetry breaking?	17
2.2 The spontaneous electroweak symmetry breaking	21
II SM Higgs production and decay at hadron colliders	29
3 Where can the SM Higgs boson be hiding?	31
3.1 Theoretical bounds on the Higgs mass	31
3.2 Experimental bounds on the Higgs mass	39
4 Higgs production at the Tevatron	46
4.1 The main production channels	50
4.2 Scale variation and higher order terms	62
4.3 The PDF puzzle	70
4.4 EFT and its uncertainties	81
4.5 Combination and total uncertainty	85
4.6 Summary and outlook	92
4.A Appendix: analytical expressions for μ_R -NNLO terms in $gg \rightarrow H$	94

5	Higgs production at the LHC	96
5.1	The main channel at the LHC	97
5.2	The scale uncertainty	100
5.3	The PDF+ α_S uncertainty	103
5.4	EFT	107
5.5	Total uncertainty at 7 TeV	110
5.6	LHC results at different center-of-mass energies	115
5.7	Summary and outlook	121
6	Higgs decay and the implications for Higgs searches	122
6.1	Important channels for experimental search	122
6.2	Uncertainties on the branching ratios	127
6.3	Combination at the Tevatron	133
6.4	Combination at the LHC	135
6.5	The Tevatron exclusion limit	136
6.6	Summary of the results	142
III	The Minimal Supersymmetric extension of the Standard Model	144
7	Why Supersymmetry is appealing	146
7.1	The hierarchy problem	146
7.2	Coupling constants convergence at high energies	148
7.3	SUSY and Dark Matter searches	150
8	Formal SUSY aspects	153
8.1	SUSY Algebra	153
8.2	Superspace, superfields and superpotential	157

8.3	Soft SUSY breaking	162
9	The Minimal Supersymmetric Standard Model	165
9.1	Fields content: Higgs and SUSY sectors of the MSSM	165
9.2	The Higgs sector and the number of Higgs doublets	170
9.3	The MSSM is not the end of the story	178
IV	MSSM Higgs(es) production and decay	181
10	The MSSM Higgs sector at hadron colliders	183
10.1	SUSY corrections to Higgs couplings to fermions	183
10.2	Model independence of the results	187
11	MSSM Higgs production at the Tevatron	190
11.1	Gluon–gluon fusion and bottom quarks fusion	191
11.2	The scale uncertainty	195
11.3	The PDF and α_S uncertainties	196
11.4	The b -quark mass uncertainty	198
11.5	Summary and combination of the different sources of uncertainties	201
12	MSSM Higgs production at the LHC	203
12.1	Gluon–gluon fusion and bottom quarks fusion channels	203
12.2	The scale uncertainty at the LHC	205
12.3	The PDF and α_S uncertainties at the LHC	207
12.4	The b -quark mass issue	208
12.5	Combination and total uncertainty	210
12.6	The case of the charged Higgs production in association with top quark at the LHC	212

13 Higgs $\rightarrow \tau\tau$ channel and limits on the MSSM parameter space	221
13.1 The main MSSM Higgs branching ratios	221
13.2 Combination of production cross section and Higgs $\rightarrow \tau\tau$ decay	224
13.3 Impact of the theoretical uncertainties on the limits on the MSSM parameter space	231
13.4 Consequences on the SM $H \rightarrow \tau\tau$ search at the LHC	237
13.5 Summary and outlook	239
V Perspectives	241
14 Exclusive study of the gluon–gluon fusion channel	242
14.1 Exclusive SM Higgs production	243
14.2 SM Backgrounds	246
Conclusion	248
A Appendix : Synopsis	252
A.1 Introduction	252
A.2 Production et désintégration du boson de Higgs du Modèle Standard	256
A.3 Le Modèle Standard Supersymétrique Minimal (MSSM)	264
A.4 Production et désintégration des bosons de Higgs supersymétriques	268
A.5 Perspectives	274
References	276

List of Figures

1	Feynman diagrams at the Born level for the process $e^+e^- \rightarrow W^+W^-$	18
2	Higgs potential in the case of a real scalar field, depending on the sign of the mass term	22
3	Higgs potential in the case of the SM	22
4	Tree-level SM Higgs boson couplings to gauge bosons and fermions	26
5	One-loop SM Higgs boson couplings to the photons and the gluons	27
6	Feynman diagrams up to one-loop correction for the Higgs self-coupling	36
7	Theoretical bounds on the Higgs mass in function of the scale of new physics beyond the SM	39
8	Electroweak precision data	41
9	Indirect constraints on the SM Higgs boson mass	42
10	95%CL exclusion limit on the SM Higgs boson mass at the LEP collider	44
11	95%CL exclusion limit on the SM Higgs boson mass at the Tevatron collider	45
12	Feynman diagrams of the four main SM Higgs production channel	52
13	Some Feynman diagrams for NLO SM $gg \rightarrow H$ production	53
14	Some Feynman diagrams for NNLO SM $gg \rightarrow H$ production	54
15	NLO QCD corrections to $p\bar{p} \rightarrow V^*$	58
16	NNLO QCD corrections to $p\bar{p} \rightarrow V^*$	59
17	Total cross sections for Higgs production at the Tevatron in the four main channels	61
18	Scale variation in the $gg \rightarrow H$ process at the Tevatron	65
19	Scale variation in the $p\bar{p} \rightarrow WH$ process at the Tevatron	71
20	Comparison between different PDFs sets in $gg \rightarrow H$ at the Tevatron using CTEQ/ABKM/MSTW PDF sets for 90%CL uncertainties and MSTW/ABKM/HERA/JR for central predictions comparison	73
21	Comparison between MSTW PDFs set and ABKM PDFs set predictions in $gg \rightarrow H$ channel at the Tevatron as for the uncertainties related to PDF+ $\Delta\alpha_s$	77

22	The total PDF, PDF+ $\Delta^{\text{exp}}\alpha_s$ and PDF+ $\Delta^{\text{exp+th}}\alpha_s$ uncertainties in $gg \rightarrow H$ at the Tevatron using the MSTW PDFs set.	79
23	Central predictions for NNLO $p\bar{p} \rightarrow WH$ at the Tevatron using the MSTW, CTEQ and ABKM PDFs sets, together with their 90% CL PDF uncertainty	80
24	Comparison between MSTW PDFs set and ABKM PDFs set predictions in $p\bar{p} \rightarrow WH$ channel at the Tevatron as for the uncertainties related to PDF+ $\Delta\alpha_s$	80
25	b -loop uncertainty in $gg \rightarrow H$ at the Tevatron	83
26	EW uncertainties in $gg \rightarrow H$ at the Tevatron	85
27	Production cross sections for $gg \rightarrow H$ at the Tevatron together with the total theoretical uncertainties	90
28	Production cross sections for $p\bar{p} \rightarrow WH$ and $p\bar{p} \rightarrow ZH$ at the Tevatron together with the total theoretical uncertainties	92
29	Total cross sections for SM Higgs production at the LHC	99
30	Scale uncertainty at the LHC in $gg \rightarrow H$ at NNLO	102
31	PDF and $\Delta^{\text{exp,th}}\alpha_s$ uncertainties in $gg \rightarrow H$ at the LHC	104
32	Comparison between the predictions given by the four NNLO PDF sets for $gg \rightarrow H$ at the LHC	105
33	Uncertainties due to EFT in the top quark and bottom quark loops of $gg \rightarrow H$ at NNLO at the LHC	108
34	Total uncertainty due to the EFT approach in $gg \rightarrow H$ at NNLO at the LHC	110
35	Central prediction with its total uncertainty for $gg \rightarrow H$ at NNLO at the LHC	112
36	Central predictions for $gg \rightarrow H$ at NNLO at the LHC with $\sqrt{s} = 8, 9, 10$ TeV	116
37	Scale and total EFT uncertainties in $gg \rightarrow H$ at the LHC with $\sqrt{s} = 14$ TeV	119
38	PDF+ $\Delta^{\text{exp,th}}\alpha_s$ uncertainties and the comparison between the 4 NNLO PDF sets in $gg \rightarrow H$ at the LHC with $\sqrt{s} = 14$ TeV	119
39	Central prediction and total uncertainty in $gg \rightarrow H$ at NNLO at the LHC with $\sqrt{s} = 14$ TeV	119
40	SM Higgs decay channels on the interesting Higgs mass range	123

41	The Higgs decays branching ratios together with the total uncertainty bands	131
42	The production cross section times branching ratio for SM $p\bar{p} \rightarrow WH \rightarrow Wb\bar{b}$ and $gg \rightarrow H \rightarrow W^+W^-$ at the Tevatron together with the total uncertainty	134
43	The production cross section times branching ratio for SM $gg \rightarrow H \rightarrow W^+W^-$ at the LHC together with the total uncertainty	136
44	The SM Higgs boson production cross section $gg \rightarrow H$ at the Tevatron together with the total uncertainty using 4 different ways of adding the theoretical uncertainties	137
45	The CDF/D0 95%CL limit on the SM Higgs boson mass confronted to our theoretical expectations in a naive approach.	139
46	The luminosity needed by the CDF experiment to recover their current claimed sensitivity when compared to our theoretical expectations for the uncertainty	142
47	One-loop corrections to the Higgs boson mass within the SM	147
48	One-loop corrections to gauge couplings	149
49	$SU(3)_c \times SU(2)_L \times U(1)_Y$ gauge couplings running from the weak scale up to the GUT scale	150
50	Possible proton decay in SUSY theories without R-parity conservation	151
51	The constrained NMSSM parameter space	180
52	The impact of main one-loop SUSY corrections to the $\Phi b\bar{b}$ coupling in the MSSM at hadron colliders	188
53	Feynman diagrams for the bottom quark fusion process in the MSSM	194
54	The NLO $gg \rightarrow A$ and NNLO $b\bar{b} \rightarrow A$ cross sections at the Tevatron with $\tan\beta = 30$	195
55	Scale uncertainty in the $gg \rightarrow \Phi$ and $b\bar{b} \rightarrow \Phi$ processes at the Tevatron	196
56	PDF+ $\Delta^{\text{exp,th}}\alpha_s$ uncertainty in the $gg \rightarrow \Phi$ and $bb \rightarrow \Phi$ processes at the Tevatron	197
57	The comparison between the MSTW, ABKM and JR prediction for the NNLO bottom quark fusion cross section at the Tevatron	198

58	Specific b -quark mass uncertainties in the $gg \rightarrow \Phi$ and $b\bar{b} \rightarrow \Phi$ processes at the Tevatron	200
59	The $gg \rightarrow A$ and $b\bar{b} \rightarrow A$ cross sections at the Tevatron together with their different sources of uncertainty and the total uncertainties	201
60	The $gg \rightarrow \Phi$ and $b\bar{b} \rightarrow \Phi$ at the LHC for different center-of-mass energies . .	205
61	Scale uncertainty in the $gg \rightarrow \Phi$ and $b\bar{b} \rightarrow \Phi$ processes at the LHC	206
62	PDF+ $\Delta\alpha_s$ uncertainty in the $gg \rightarrow \Phi$ and $bb \rightarrow \Phi$ processes at the LHC . . .	207
63	Comparison between the different PDFs sets in the $gg \rightarrow \Phi$ and $b\bar{b} \rightarrow \Phi$ processes at the LHC	208
64	Specific b -quark mass uncertainties in the $gg \rightarrow \Phi$ and $b\bar{b} \rightarrow \Phi$ processes at the LHC	209
65	The $gg \rightarrow \Phi$ and $b\bar{b} \rightarrow \Phi$ cross sections at the LHC together with their different sources of uncertainty and the total uncertainties	210
66	LO $\sigma(gb \rightarrow t_{L,R}H^-)$ cross section and polarization asymmetry at the LHC in the MSSM in two benchmark scenarios as a function of $\tan\beta$	216
67	Scale and PDF dependence on top-charged Higgs asymmetry at the LHC . .	217
68	The impact of the NLO SUSY corrections on the top-charged Higgs asymmetry at the LHC with $\sqrt{s} = 14$ TeV	219
69	CP -odd A boson production in the $p\bar{p} \rightarrow A \rightarrow \tau^+\tau^-$ channel at the Tevatron together with the total uncertainty	225
70	The total uncertainties on the MSSM Higgs production in the $gg \rightarrow \Phi$ and $b\bar{b} \rightarrow \Phi$ channels at the LHC including the impact of the $\Phi \rightarrow \tau^+\tau^-$ branching fraction	226
71	CP -odd A boson production in the $pp \rightarrow A \rightarrow \tau^+\tau^-$ channel at the LHC together with the total uncertainty	231
72	The 95%CL limits on the MSSM parameter space using our theoretical uncertainties confronted to the Tevatron results	233
73	The 95%CL limits on the MSSM parameter space using our theoretical uncertainties confronted to the LHC results	234
74	Expectations at higher luminosity at the LHC for the 95%CL limits on the MSSM parameter space using our theoretical calculation	235

75	The MSSM Higgs analysis applied to the SM $H \rightarrow \tau^+\tau^-$ search channel compared to the ATLAS $H \rightarrow \gamma\gamma$ limits	238
76	Potentiel de Higgs dans le cas d'un champ scalaire réel selon le signe du terme de masse	255
77	Incertitude d'échelle dans le processus $gg \rightarrow H$ au Tevatron	259
78	Comparaison entre les prédictions des différentes collaborations de PDFs pour le canal $gg \rightarrow H$ au NNLO en QCD	259
79	Incertitude PDF+ $\Delta\alpha_s$ dans les canaux de production $gg \rightarrow H$ et $p\bar{p} \rightarrow HW$ au Tevatron	260
80	Sections efficaces de production inclusives des canaux $gg \rightarrow H$ et $p\bar{p} \rightarrow HV$ au Tevatron ainsi que les incertitudes théoriques totales associées	261
81	Sections efficaces de production inclusives du canal $gg \rightarrow H$ au LHC à 7 et 14 TeV ainsi que les incertitudes théoriques totales associées	262
82	Luminosité nécessaire à l'expérience CDF afin qu'elle obtienne la sensibilité qu'elle prétend avoir actuellement, en tenant compte de nos incertitudes théoriques	264
83	Les sections efficaces de production inclusives du boson de Higgs A du MSSM au Tevatron dans les canaux $gg \rightarrow A$ et $b\bar{b} \rightarrow A$ accompagnées des incertitudes théoriques	271
84	Les sections efficaces de production inclusives du boson de Higgs Φ du MSSM au LHC dans les canaux $gg \rightarrow \Phi$ et $b\bar{b} \rightarrow \Phi$ accompagnées des incertitudes théoriques	271
85	Les limites à 95% de niveau de confiance sur l'espace des paramètres du MSSM en tenant compte de nos incertitudes théoriques confrontées aux données du Tevatron et du LHC	273
86	L'analyse MSSM des bosons de Higgs neutres appliquée au canal de recherche $H \rightarrow \tau^+\tau^-$ du Modèle Standard, comparée aux résultats obtenus par ATLAS dans le canal $H \rightarrow \gamma\gamma$	274

List of Tables

1	The fermionic content of the Standard Model	13
2	The NNLO total Higgs production cross sections in the $gg \rightarrow H$ process at the Tevatron together with the detailed theoretical uncertainties as well as the total uncertainty	88
3	The NNLO total cross section for Higgs–strahlung processes at the Tevatron together with the detailed theoretical uncertainties and the total uncertainty	91
4	The total Higgs production cross sections in the four main production channels at the LHC with $\sqrt{s} = 7$ TeV	101
5	The NNLO total Higgs production cross sections in the $gg \rightarrow H$ process at the LHC with $\sqrt{s} = 7$ TeV together with the associated theoretical uncertainties	114
6	The NNLO total production cross section in the $gg \rightarrow H$ channel at the LHC with $\sqrt{s} = 8, 9, 10$ TeV	117
7	The NNLO total Higgs production cross section in the $gg \rightarrow H$ process at the LHC with $\sqrt{s} = 14$ TeV together with the associated theoretical uncertainties	120
8	The SM Higgs decay branching ratios in the $b\bar{b}$ and WW modes for representatives Higgs masses together with the different sources of uncertainties as well as the total uncertainty.	130
9	The SM Higgs decay branching ratios together with the total uncertainty for the most important decay channels	132
10	The superparticles and Higgs content of the MSSM before EWSB	167
11	The neutralinos, charginos and Higgs content of the MSSM after EWSB	167
12	The main MSSM CP –odd like Higgs bosons decay branching fractions together with their uncertainties	223
13	The central predictions in the MSSM $gg \rightarrow \Phi$ channel at the Tevatron together with the detailed uncertainties and the impact of the $\Phi \rightarrow \tau^+\tau^-$ branching fraction	227
14	The central predictions in the MSSM $b\bar{b} \rightarrow \Phi$ channel at the Tevatron together with the detailed uncertainties and the impact of the $\Phi \rightarrow \tau^+\tau^-$ branching fraction	228

15	The central predictions in the MSSM $gg \rightarrow \Phi$ channel at the IHC together with the detailed uncertainties and the impact of the $\Phi \rightarrow \tau^+\tau^-$ branching fraction	229
16	The central predictions in the MSSM $b\bar{b} \rightarrow \Phi$ channel at the IHC together with the detailed uncertainties and the impact of the $\Phi \rightarrow \tau^+\tau^-$ branching fraction	230
17	CMS cuts used in the SM exclusive study $gg \rightarrow H \rightarrow WW \rightarrow \ell\nu\ell\nu$ at the IHC	243
18	Results for the $gg \rightarrow H$ +jet cross sections with $M_H = 160$ GeV at the IHC with HNNLO and MCFM programs	244
19	Uncertainties on the exclusive production $gg \rightarrow H \rightarrow WW \rightarrow \ell\nu\ell\nu$ with $M_H = 160$ GeV at the IHC with HNNLO program	246
20	Uncertainties on the exclusive production $gg \rightarrow H \rightarrow WW \rightarrow \ell\nu\ell\nu$ with $M_H = 160$ GeV at the IHC with MCFM program	246
21	Central values and uncertainties for the $H \rightarrow WW$ SM backgrounds exclusive cross sections at the IHC	247
22	Contenu fermionique du Modèle Standard	253
23	Les superparticules et champs de Higgs du MSSM avant brisure électrofaible	267

Liste des publications

Cette page donne la liste de tous mes articles concernant le travail réalisé depuis 3 ans.

This page lists all the papers that I have written for 3 years in the context of my PhD work.

Articles publiés (published papers) :

Predictions for Higgs production at the Tevatron and the associated uncertainties, J. B. et A. Djouadi, JHEP **10** (2010) 064;

Higgs production at the LHC, J. B. et A. Djouadi, JHEP **03** (2011) 055;

The Tevatron Higgs exclusion limits and theoretical uncertainties: A Critical appraisal, J. B., A. Djouadi, S. Ferrag et R. M. Godbole, Phys.Lett.**B699** (2011) 368-371; erratum Phys.Lett.**B702** (2011) 105-106;

Revisiting the constraints on the Supersymmetric Higgs sector at the Tevatron, J. B. et A. Djouadi, Phys.Lett.**B699** (2011) 372-376;

The left-right asymmetry of the top quarks in associated top-charged Higgs bosons at the LHC as a probe of the parameter $\tan\beta$, J.B et al., Phys.Lett.**B705** (2011) 212-216.

Articles non-publiés (unpublished papers) :

Implications of the ATLAS and CMS searches in the channel $pp \rightarrow Higgs \rightarrow \tau^+\tau^-$ for the MSSM and SM Higgs bosons, J. B. et A. Djouadi, arXiv:1103.6247 [hep-ph] (soumis à Phys.Lett.**B**);

Clarifications on the impact of theoretical uncertainties on the Tevatron Higgs exclusion limits, J. B., A. Djouadi et R. M. Godbole, arXiv:1107.0281 [hep-ph].

Rapport de collaboration (review collaboration report) :

Handbook of LHC Higgs Cross Sections: 1. Inclusive Observables, LHC Higgs Cross Section Working Group, S. Dittmaier *et al.*, arXiv:1101.0593 [hep-ph].

Comptes-rendus de conférences (proceedings) :

Higgs production at the Tevatron: Predictions and uncertainties, J. B., ICHEP 2010, Paris (France), PoS **ICHEP2010** (2010) 048;

The Supersymmetric Higgs bounds at the Tevatron and the LHC, J.B., XLVI^e Rencontres de Moriond, EW interactions & unified theory, La Thuile (Italie), arXiv:1105.1085 [hep-ph].

Cette thèse est dédiée à mon père et à mes deux grand-pères, disparus bien trop tôt.

Dear Higgs Boson,

We know you're out there. We can feel you now. We know that you're afraid. You're afraid of us; you're afraid of change. We don't know the future. We didn't write this to tell you how this is going to end. We wrote this to tell you how it's going to begin.

As you know, our Large Hadron Collider has had some setbacks due to a.... uh... "transformer malfunction" but we know it was you. You sabotaged our machine. We hope you've been enjoying your vacation because we're scheduled to restart in September 2009 and we're pissed.

....so run and hide, asshole. Run and hide. If you should get careless and allow yourself to get detected by the Tevatron, we are going to be supremely disappointed; because we want to find you first, and when we do, rest assured we are not going to publish right away. We're going to teach you some manners first.

Love,

CERN



(From <http://abstrusegoose.com/118>)

*Et maintenant, apprends les vérités qui me restent à te découvrir,
Tu vas entendre de plus claires révélations.
Je n'ignore pas l'obscurité de mon sujet ;*

Lucrèce, dans De rerum natura, v. 902-943 livre I

*Les amoureux fervents et les savants austères
Aiment également, dans leur mûre saison,
Les chats puissants et doux, orgueil de la maison,
Qui comme eux sont frileux et comme eux sédentaires.*

Charles Baudelaire, dans Les Fleurs du Mal

Introduction

In this thesis, we wish to present some predictions for the Higgs boson(s) study at the two largest hadron colliders currently in activity: the Fermilab Tevatron collider and the CERN Large Hadron Collider (LHC). Our focus will be on the inclusive production cross sections and the decay branching fractions, first in the Standard Model which in itself is the topic of part [I](#) and then in its minimal supersymmetric extension which is the topic of part [III](#).

The study of the fundamental mechanisms of Nature at the elementary level has a long story and has known many milestones in the past sixty years. Physicists have built a theory, nowadays known as the Standard Model, to describe the elementary particles and their interactions, that are those of the strong, weak and electromagnetic, the two last being unified in a single electroweak interaction. It relies on the elegant concept of gauge symmetry within a quantum field theory framework and has known many experimental successes: despite decades of effort to surpass this model it is still the one that describes accurately nearly all the known phenomena¹. One of its key concepts is the spontaneous breakdown of electroweak symmetry: indeed in order to give mass to the weak bosons that mediate the weak interaction, a scalar field is introduced in the theory whose vacuum breaks the electroweak symmetry and gives mass to the weak bosons. In fact it also gives masses to the fermions and one piece of this mechanism remains to be discovered: the Higgs boson, the “Holy Grail” of the Standard Model. Its discovery is one of the main goal of current high energy colliders.

It is then of utmost importance to give theoretical predictions for the production cross sections and decay branching fractions of the Higgs boson at current colliders to serve as a guideline for experiments. However, the hadronic colliders are known to be very difficult experimental environments because of the huge hadronic, that is Quantum Chromodynamics (QCD), activity. This is also true on a theoretical side, which means that an accurate description of all possible sources of theoretical uncertainties is needed: this is precisely the main output of this thesis. We shall mention that in the very final stage of this thesis new results have been presented in the HEP–EPS 2011 conference; our work is to be read in the light of the results that were available before these newest experimental output which will be briefly commented in the conclusion.

Part [I](#) is entirely devoted to a review of the Standard Model. In section [1](#) we will draw a short history of the Standard Model and list its main milestones of the past sixty years, followed by a description of its main concepts. We will go into more details about the Higgs mechanism, which spontaneously breaks electroweak symmetry, in section [2](#): we will

¹We leave aside the neutrino mass issue.

review some reasons to believe that either the Higgs mechanism itself or something which looks like the Higgs mechanism is needed, and then how the Higgs boson emerges from the electroweak symmetry breaking and what are its couplings to fermions and bosons of the Standard Model.

Part II is the core of the Standard Model study of this thesis. Indeed the Higgs boson remains to be discovered and is one of the major research programs at current high energy colliders. The old CERN Large Electron Positron (LEP) collider has put some bounds on the possible value of the Higgs boson mass, which is above 114.4 GeV in the Standard Model at 95%CL. We will review in section 3 the current experimental and theoretical bounds on the Higgs mass. We then give our predictions for the Standard Model Higgs boson inclusive production cross section at the Tevatron in the two main production channels that are the gluon–gluon fusion and the Higgs–strahlung processes, giving all the possible sources of theoretical uncertainties: the scale uncertainty viewed as an estimation of the unknown higher–order terms in the perturbative calculation; the parton distribution functions (PDFs) uncertainties related to the non–perturbative QCD processes within the proton, and its related strong coupling constant issue; the uncertainty coming from the use of an effective theory approach to simplify the hard calculation in the gluon–gluon fusion process. We will specifically address the issue of the combination of all the uncertainties in section 4.5. We will then move on to the same study at the LHC, concentrating on its current run at a 7 TeV center–of–mass energy that we will name as the LHC for littler Hadron Collider; we will still give some predictions for the designed LHC at 14 TeV. We will finish this part II by the Higgs boson decay branching fractions predictions in section 6, together with a detailed study of the uncertainties that affect these predictions. It will be followed by the combination of the production cross sections and decay branching fractions into a single prediction, first at the Tevatron in section 6.3 and then at the LHC in section 6.4. We will then study the impact of our uncertainties on the Tevatron Higgs searches in section 6.5 and in particular put into question the Tevatron exclusion limits that are debated within the community.

Even if the Standard Model is a nice theory with great experimental successes, it suffers from some problems, both on the theoretical and experimental sides. It is known for example that the Higgs boson mass is not predicted by the Standard Model, and even not protected: higher order corrections in the perturbative calculation of the Higgs boson mass have the tendency to drive the mass up to the highest acceptable scale of the theory which means that we need a highly fine–tuning of the parameters to cancel such driving. It is known as the naturalness problem of the Standard Model. There are several ways to solve such a problem, and one of them is particularly elegant and relies on a new symmetry between

bosons and fermions: supersymmetry. This theoretical concept, born in the 1970s, has many consequences when applied to the Standard Model of particle physics and is actively searched at current high energy colliders. This will be the topic of part III in which we will review some of the reasons that drive the theorists to go beyond the Standard Model and in particular what makes supersymmetry interesting in this view in section 7, then move on to the description of the mathematical aspects of supersymmetry in section 8. We will finish this part III by a very short review of the minimal supersymmetric extension of the Standard Model, called the MSSM, in section 9. We will in particular focus on the Higgs sector of the theory and show that the MSSM needs two Higgs doublets to break the electroweak symmetry breaking and has thus a rich Higgs sector as five Higgs boson instead of a single one are present in the spectrum: two neutral CP -even, one CP -odd and two charged Higgs bosons.

After this review of supersymmetry and the MSSM we will reproduce in part IV the same outlines that have been developed in part II in the Standard Model case. We will first review the neutral Higgs sector at hadron colliders in section 10 and show that we can have a quite model-independent description for our predictions in the sense that they will hardly depend on most of the (huge) parameters of the MSSM but two of them, the mass of the CP -odd Higgs boson A and the ratio $\tan\beta$ between the vacuum expectation values of the two Higgs doublets. We will then give in section 11 our theoretical predictions for the neutral Higgs bosons inclusive production cross section at the Tevatron in the two main production channels that are the gluon-gluon fusion and the bottom quark fusions, the bottom quark playing a very important role in the MSSM at hadron colliders. We will reproduce the same study at the LHC in section 12 before giving the implications of our study on the $[M_A, \tan\beta]$ parameter space in section 13. We will first give in this last section our predictions for the main MSSM decay branching fractions and in particular the di-tau branching fraction that is of utmost importance for experimental searches. We will then compare our predictions together with their uncertainties to the experimental results obtained at the Tevatron and at the LHC that has now been running for more than a year at 7 TeV and given impressive results. We will see that the theoretical uncertainties have a significant impact on the Tevatron results, less severe at the LHC. We will finish section 13 by a very important outcome of our work: the possibility of using the MSSM neutral Higgs bosons searches in the di-tau channel for the Standard Model Higgs boson in the gluon-gluon fusion production channel followed by the di-tau decay channel in the low Higgs boson mass range 115–140 GeV.

Finally, we will give an outlook and draw some conclusions in part V together with some perspectives for future work. These rest on the next step on the road of the experiments,

that is an exclusive study of the Higgs bosons production channels. We shall give some early results in section 14 on the Standard Model Higgs boson at the IHC in the $gg \rightarrow H \rightarrow WW \rightarrow \ell\nu\ell\nu$ search channel together with an exclusive study of the main Standard Model backgrounds. This is also the current roadmap of the Higgs bosons theoretical community and this work is done in the framework of a collaboration on this topic.

Part I

A brief review of the Standard Model of particle physics

Summary

1	Symmetry principles and the zoology of the Standard Model	6
1.1	A brief history of the Standard Model	6
1.2	Gauge symmetries, quarks and leptons	12
2	The Brout–Englert–Higgs mechanism	17
2.1	Why do we need the electroweak symmetry breaking?	17
2.1.1	The unitarity puzzle	17
2.1.2	Masses and gauge invariance	19
2.2	The spontaneous electroweak symmetry breaking	21
2.2.1	Weak bosons masses and electroweak breaking	21
2.2.2	SM Higgs boson couplings	26

1 Symmetry principles and the zoology of the Standard Model

The Standard Model (SM) of particle physics is the current description of the fundamental constituents of our universe together with the interactions that occur between them. The SM was born in its current form in the seventies, after nearly twenty years of many experiments and theoretical reflexions on how to build a somewhat simple and elegant model to describe accurately the experimental results on the one hand and to make powerful predictions in order to have a falsifiable theory on the other hand. Its frameworks are relativistic quantum field theory and group theory to classify the different interactions. It also needs the key concept of spontaneous (electroweak) symmetry breaking in order to account for the masses of the different fields in the theory, the (weak) bosons as well as the matter fermions. Other reasons also push for such a theoretical concept and will be presented in the next sections.

We will in this section present a short review of the major historical points in the birth of the SM, and present its theoretical foundations. The focus on the electroweak symmetry breaking, in particular its minimal realization through the Brout–Englert–Higgs mechanism, will be discussed in the next section.

1.1 A brief history of the Standard Model

This subsection will sketch the different historical steps that have lead to the current form of the theory that describes the elementary particles and their interactions among each other, called the Standard Model (SM). This model has a very rich history over more than fifty years of the XXth century, not to mention all the diverse and fruitful efforts made before to attain this level of description of the elementary world. We will only select some (of the) outstanding events, both from the theoretical and experimental sides, to present the twisted path leading to the current Standard Model of particle physics.

The birth of modern QED

The first attempt to describe electromagnetic phenomena in the framework of special relativity together with quantum mechanics can be traced back in the 1920s. In particular Dirac was the first to describe the quantization of the electromagnetic fields as an ensemble of harmonic oscillators, and introduced the famous creation–annihilation operators [1]. In 1932 came Fermi with a first description of quantum electrodynamics [2], but physicists were blocked by the infinite results that did arise in the calculations beyond the first order

in perturbation theory.

Years after, the difficulty was solved by Bethe in 1947 [3] with the concept of renormalization, that is the true physical quantities are not the bare parameters of the theory, and thus the infinite that arise are absorbed in the physical quantities, leaving finite results in the end. This leads to the modern Quantum Electrodynamics (QED) with the key concept of gauge symmetry and renormalization, that was formulated by Feynman, Schwinger and Tomonaga [4–6] in the years 1950s and awarded by a Nobel prize in 1965. This is the first quantum field theory available and has been the root of all the SM ideas for the key concepts of gauge symmetry and renormalizability.

P violation and $V - A$ weak theory

It was long considered in physics that the parity symmetry was conserved: if we repeated an experiment with the experimental apparatus mirror reversed, the results would be the same as for the initial set-up. This assessment is true for any experiment involving electromagnetism or strong interaction, but that is not the case for weak interaction.

It was first proposed by Yang and Lee in 1956 that the weak interaction might indeed not respect P -symmetry [7]. This was observed in 1957 by Chien-Shiung Wu (“Madam Wu”) in the beta desintegration of cobalt 60 atoms [8]. Yang and Lee were then awarded the 1957 Nobel prize for their theoretical developments on this concept.

Up until that period, the weak interaction, that shapes the decay of unstable nuclei, was described by the Fermi theory in which the fermions interact through a four-particles vertex. The discovery of the P -violation lead to the construction of an effective $V - A$ theory where the tensor structure of the theory is correct and does respect the charge and parity violations. This $V - A$ theory was later on replaced by the electroweak theory, see below.

The quark description

In the first half of the XXth century the pattern of elementary particles was simple: the electron (and its antiparticle the positron, postulated by Dirac in 1931 and discovered in 1932 by Anderson), the proton and the neutron were the only known elementary particles at that time. The neutrino, first postulated by Pauli in its famous letter in 1930 to save the energy-momentum conservation in beta decay reactions² was discovered only in 1956.

Experimental particle physicists discovered numerous new particles (the “hadrons”) in

²The original name was “neutron” for neutral particle. Chadwick discovered in 1932 what would be the neutron, thus Fermi proposed the name “neutrino” meaning “little neutral one” in italian.

the 1950s and 1960s after the discovery of the pion in 1947, predicted by Yukawa in 1935, thus casting some doubts on the elementary nature both of the “older” particles such as the neutron and the proton and on the new zoo discovered. Gell–Man and Zweig proposed in 1964 a model of constituent particles of these hadrons and mesons that could explain the pattern seen by experimentalists, using only a limited number of new constituent particles: the quarks [9, 10]. They introduce the $SU(3)$ flavor symmetry with the three up, down and strange quarks. One year later the charm quark was proposed to improve the description of weak interactions between quarks, and in 1969 deep inelastic scattering experiments at the Stanford Linear Accelerator Center (SLAC) discovered point–like objects within the proton [11], an experimental proof of the compositeness of the hadrons. It is interesting to note that the term used for these new point–like objects was “parton”, proposed by Feynman, as the community was not entirely convinced that they were indeed the Gell–Mann’s quarks. Nowadays “parton” is still a word used in particle physics to name the different constituents of the hadrons (the quarks, antiquarks and gluons, the later being the bosons of the strong interaction).

The (nearly) final word on the quark model was given in 1974 when the J/Ψ meson was discovered [12, 13] and thus proved the existence of the charm quark, which was proposed by Glashow, Iliopoulos and Maiani in the GIM mechanism [14] in 1970 to explain the universality of weak interaction in the quark sector, preventing flavor changing neutral currents. The heaviest quark, that is the top quark, was finally discovered in 1995 at the Fermilab Tevatron collider [15, 16].

CP violation and the concept of generation

To explain both the universality and the $u \longleftrightarrow d$ transitions in weak interactions, Cabibbo introduced in 1963 what is known as the Cabibbo angle [17] and was used to write in the mass eigenstates basis the weak eigenstate for the down quark d . A year later, Cronin and his collaborators discovered that not only C and P symmetries are broken by weak interactions, but also the combined CP symmetry [18], studying the $K^0\bar{K}^0$ oscillations: the probability of oscillating from K^0 state into \bar{K}^0 state is different from that of the $\bar{K}^0 \rightarrow K^0$, indicating that T time reversal symmetry is violated. As the combined CPT is assumed to be conserved, this means that CP is violated.

As mentioned a few lines above, the GIM mechanism introduced a fourth quark, the charm quark c . It then restores universality in the weak coupling for the quarks, as we have now two weak eigenstates

$$\begin{aligned} |d'\rangle &= \cos \theta_c |d\rangle + \sin \theta_c |s\rangle \\ |s'\rangle &= -\sin \theta_c |d\rangle + \cos \theta_c |s\rangle \end{aligned} \quad (1.1)$$

coupled to respectively the u quark and the c quark. We thus have two generations in the quark sector, the first one is the (u, d) doublet and the second one is the (c, s) doublet. However, as explained in 1973 by Kobayashi and Maskawa extending the work initiated by Cabibbo, this is not sufficient to explain the CP violation observed by the 1964 experiment. Only with three generations could be introduced some CP violating effects through a phase angle, and thus extending the Cabibbo angle to what is known as the Cabibbo–Kobayashi–Maskawa (CKM) matrix [19]. Kobayashi and Maskawa were awarded the 2008 Nobel prize for this result³.

Yang–Mills theory and spontaneous symmetry breaking

We have seen a few lines above that the Fermi theory describing the weak interactions had been refined by the $V - A$ picture to take into account the P violation. Still the $V - A$ theory was known to be an effective theory as the theory was not renormalizable and did not allow for calculations beyond the first order in perturbation theory. The only gauge theory that was available at that time was QED, an abelian gauge theory, which obviously is not the right description of weak processes as it describes only light–matter interactions.

The first step toward the solution was set–up in 1954, when Yang and Mills developed a formulation of non–abelian gauge theories [20] in order to provide (initially) an explanation for the strong interaction at the hadron level (that we call nuclear interaction). Unfortunately the theory was not a success at first, as the gauge bosons must remain massless to preserve the symmetry of the theory, thus meaning that the weak interaction should be long–range; experimentally that is not the case.

The key result to solve this contradiction and then still use the elegant description of gauge theory is given in 1964 by Brout, Englert, Higgs, Guralnik, Hagen and Kibble after some important work on the concept of symmetry breaking from Nambu and Goldstone: the spontaneously gauge symmetry breaking [21–24] described by the Brout–Englert–Higgs mechanism. This will be presented in the following in details, but we can already remind the reader that the most important result is that it allows for the use of a Yang–Mills theory together with a description of massive gauge bosons for any gauge theory.

³Unfortunately the Nobel committee failed to recognize the important pionnering work from Cabibbo.

Interlude: from nuclear force to strong interaction

Before arriving to the final electroweak description that constitutes the heart of the SM, we recall the road leading to the description of the strong interaction between the quarks.

As stated above, Yang–Mills theory in 1954 was the first attempt to describe the interaction between the hadrons, that we call nuclear interaction, in a gauge formulation. After the introduction of the quark model by Gell–Mann in 1964 (see above) and the discovery of the quarks in 1969 (see above), it has been proposed that the quarks must have a new quantum charge, called color, to accommodate for the Pauli exclusion principle within some baryons [25]. This was experimentally observed in the SLAC experiments in 1969 which discovered point–like objects within the nucleon, as discussed earlier.

With the help of the discovery of asymptotic freedom [26, 27] in 1973 by Wilczek, Gross and Politzer (who share the 2004 Nobel prize for this result), that states that at very high energy quarks are free, and with a $SU(3)$ gauge Yang–Mills theory, Quantum Chromodynamics (QCD) was firmly established in the 1970s as being the theory of the strong interactions, with the gluons as the gauge bosons. Evidence of gluons was discovered in three jet events at PETRA in 1979 [28], giving further credits to QCD.

The nuclear interaction between the hadrons is then a residual force originating from the strong interaction between quarks (and gluons). However, as the strong coupling is indeed very strong at large distance (that is the confinement), preventing from the use of perturbation theory, an analytical description of the strong interaction within the hadrons at low energies is still to be found. This problem is now studied within the framework of lattice gauge theories which give spectacular results.

The weak neutral currents and the path to electroweak theory

As stated above it was known that the $V - A$ theory for the weak interaction was an effective theory, with difficulties calculating beyond the first order in perturbation theory. With the advent of Yang–Mills theory and the Brout–Englert–Higgs mechanism, describing the weak interaction with a gauge theory and in the same time allowing for massive weak bosons as dictated by the experiments, the weak interaction being a short distance interaction, it would be possible to account for a renormalizable description of the weak interaction.

During the 1960s there were many attempts to carry on this roadmap, trying lots of different gauge groups to account for the QED on the one hand, the weak interaction on the other hand, as both interactions play a role for lepton particles such as the electron. The gauge theory that did emerge was the $SU(2) \times U(1)$ model where the weak and electro-

magnetic interactions are unified in a single gauge theory description⁴, with contributions notably from Glashow [29], Salam [30] and Weinberg [31]. This model together with the Brout–Englert–Higgs mechanism predicts in particular that there should be a neutral weak boson Z^0 to be discovered and thus neutral currents.

A very important theoretical discovery was made in 1971 by 't Hooft, who demonstrated that the electroweak theory is indeed renormalizable [32, 33]. A year after, together with Veltman, he also described for the first time the dimensional regularization scheme for renormalizability calculation [34]. That gave prominent credits to the electroweak model as renormalizability allows for finite calculation at any order in perturbation theory. Physicists started to actively look for neutral currents which would be a great success for the electroweak theory.

The thrilling experimental discovery of these neutral currents happened in 1973 at CERN in the Gargamelle detector [35]. This established the electroweak theory as the correct theory describing the weak and electromagnetic interactions in an unified gauge theory view, preserving renormalizability and allowing for massive weak bosons. Glashow, Weinberg and Salam were awarded the 1979 Nobel prize for the electroweak model, 't Hooft was awarded the 1999 Nobel prize for the proof of its renormalizability.

The electroweak theory together with QCD describing strong interactions is what is called the Standard Model (SM) of particle physics.

***W* and *Z* bosons: the experimental success**

The final paragraph of this short history of the SM is devoted to the direct discovery of the massive W and Z in 1983. Indeed after the great success of the year 1973 where the weak neutral currents, predicted by the electroweak theory, were discovered at CERN, the weak bosons remained to be discovered.

The UA1 and UA2 experiment at the SPS proton–antiproton collider at CERN, conducted by Van der Meer and Rubbia, did the great discovery in 1983 [36, 37]. They were awarded the 1984 Nobel prize, an unexpected fast acknowledgement from the Nobel committee.

We are arrived at the end of our path along the history of the SM. This subsection does not pretend to cover all its aspects, sketching only some landmarks. What remains

⁴It is actually not a complete unified theory as the algebra describing the electroweak interaction is a product of two Lie algebras. Nevertheless as the description of the weak and electromagnetic interactions are intimately connected through the pattern of the electroweak symmetry breaking, see below, this can be viewed as at least a partial unification.

to be done? As put in light above the Brout–Englert–Higgs mechanism plays a key role in the formulation of the SM. However the Higgs boson related to this mechanism has yet to be found, despite nearly thirty years of intense research both at the CERN and Fermilab colliders. This motivates not only this thesis, but also the very exciting research program of current high energy colliders! We are all waiting for decisive answers in the coming years...

1.2 Gauge symmetries, quarks and leptons

Now that we have seen the major pages of the history of the Standard Model (SM), we review its content. Most of this subsection is based on Ref. [38] and the lecture notes of a master course on particle physics and gauge theories [39, 40]. As briefly discussed in the historical part of this section, the key concept behind the SM is that of symmetries. We will thus give the symmetry algebra of the SM that shapes the interactions between the fundamental particles.

The particle content

Each interaction is described by a quantum field theory based on a Lie algebra which describes the gauge symmetry of the interaction. The Lie algebra of the SM is $(SU(2)_L \times U(1)_Y) \times SU(3)_c$:

- $SU(3)_c$ describes the strong interaction among the quarks which are the colored fermions of the theory. This is the QCD theory.
- $SU(2)_L \times U(1)_Y$ describes the electroweak interaction between the quarks and the leptons. Y is the hypercharge of the fermions that are charged under $U(1)_Y$. This is the electroweak theory.

Each fermion is classified in irreducible representations of each individual Lie algebra, that is according to its quantum numbers C, I, Y which are respectively the color, the weak isospin and the hypercharge. The electric charge is then given by the Gell–Mann–Nishijima relation $Q = I_3^W + \frac{Y}{2}$. The SM fermion part is organised in three generations, which are three times a replication of the same structure: one charged lepton and one neutrino on the one hand, two quarks on the other hand.

The weak interaction maximally violates the parity symmetry: $SU(2)_L$ Lie algebra acts only on left-handed fermions. Apart from the neutrinos which are only left-handed in the

SM and massless⁵, all other fermions are both left and right-handed. Table 1 below gives the fermionic content of the SM ⁶.

Type	Name	Mass [GeV]	Spin	Charge	$(I^W, I_3^W)_L$	$SU(3)_c$ rep.
LEPTONS	ν_e	$< 2 \times 10^{-6}$	1/2	0	(1/2, 1/2)	1
	e	5.11×10^{-4}	1/2	-1	(1/2, -1/2)	1
	ν_μ	$< 1.9 \times 10^{-4}$	1/2	0	(1/2, 1/2)	1
	μ	1.06×10^{-1}	1/2	-1	(1/2, -1/2)	1
	ν_τ	$< 1.82 \times 10^{-2}$	1/2	0	(1/2, 1/2)	1
	τ	1.777	1/2	-1	(1/2, -1/2)	1
QUARKS	u	$(1.5 \leq m \leq 3.0) \times 10^{-3}$ ($\overline{\text{MS}}$)	1/2	2/3	(1/2, 1/2)	3
	d	$(3.0 \leq m \leq 7.0) \times 10^{-3}$ ($\overline{\text{MS}}$)	1/2	-1/3	(1/2, -1/2)	3
	c	1.28 ($\overline{\text{MS}}$)	1/2	2/3	(1/2, 1/2)	3
	s	9.5×10^{-2} ($\overline{\text{MS}}$)	1/2	-1/3	(1/2, -1/2)	3
	t	173.1	1/2	2/3	(1/2, 1/2)	3
	b	4.16 ($\overline{\text{MS}}$)	1/2	-1/3	(1/2, -1/2)	3

Table 1: The fermionic content of the Standard Model. Apart from the neutrinos which are left-handed only, all other fields are left and right-handed, the latter being $SU(2)_L$ gauge singlets.

In addition to the fermionic content there are the gauge bosons mediating the interactions and one scalar boson, the Higgs boson that we have already seen in the brief history of the SM. Before the electroweak symmetry breaking, we have in the electroweak sector:

- The three W_μ^a weak bosons that are the generators of the $SU(2)_L$ gauge algebra.
- The neutral B_μ boson that is the generator of the $U(1)_Y$ gauge algebra.
- The scalar Higgs doublet $\Phi = (\phi^+, \phi^0)$.

We also have 8 gluons g as generators of the non-broken $SU(3)_c$ color symmetry algebra. After electroweak symmetry breaking the electroweak bosons states mix and give

⁵Experimentally it has been proved that the neutrinos are indeed massive. The existence of the right-handed neutrinos is then still an open question.

⁶The value of the b and c -quark masses will be discussed in more details in section 6.2.

two charged weak bosons W^\pm , a neutral weak boson Z^0 and the photon γ which remains massless. We also retain one scalar degree of freedom: the Higgs boson.

The SM lagrangian

As stated in the historical subsection, in order to retain the gauge symmetry of the SM all fields must remain massless. More precisely, explicit mass terms for fermions in the form $m\bar{\psi}\psi$ would not break the $SU(3)_c$ gauge symmetry but would violate $SU(2)_L$ symmetry, as such a term is indeed a product $m(\bar{\psi}_L\psi_R + \bar{\psi}_R\psi_L)$. One of the terms in the product does not change under $SU(2)_L$ transformation, which thus means that the product is not invariant. Moreover the same argument applies for weak bosons (sketched in a different way as we are dealing with bosons). How to account for the mass of the weak bosons and of the fermions, which manifestly exist according to experiments?

The solution within the SM is precisely the Brout–Englert–Higgs mechanism that will be described in the next section: we add to the theory a scalar doublet which will generate through spontaneous symmetry breaking the masses of the weak bosons, and also of the fermions through Yukawa interactions.

We will only write down the lagrangian of the unbroken electroweak symmetry for one generation, as the two others are an exact mathematical replica (apart from the Yukawa sector). The broken lagrangian will be described in the following section when dealing with weak gauge bosons masses. We use the notation $L = (\nu_e, e)_L$, $Q = (u, d)_L$ for the left doublets, and we have e_R , u_R and d_R for the right-handed electron, up and down quarks. The Higgs doublet is $\Phi = (\phi^+, \phi_0)$.

We use Y for the generator of the $U(1)_Y$ algebra and the three generators T^a of the $SU(2)_L$ algebra are taken as the half of the 2×2 Pauli matrices

$$T^a = \frac{1}{2}\tau^a; \quad \tau_1 = \begin{pmatrix} 0 & 1 \\ 1 & 0 \end{pmatrix}, \quad \tau_2 = \begin{pmatrix} 0 & -i \\ i & 0 \end{pmatrix}, \quad \tau_3 = \begin{pmatrix} 1 & 0 \\ 0 & -1 \end{pmatrix} \quad (1.2)$$

with the commutation relations between these generators given by

$$[T^a, T^b] = i\epsilon^{abc}T_c \quad \text{and} \quad [Y, Y] = 0 \quad (1.3)$$

where ϵ^{abc} is the usual antisymmetric tensor. For the strong sector we use the eight Gell–Mann 3×3 U^a matrices as the generators of $SU(3)_c$ symmetry associated with the eight gluons G_μ^a , with

$$[U^a, U^b] = if^{abc}U_c \quad \text{with} \quad \text{Tr}[U^a U^b] = \frac{1}{2}\delta_{ab} \quad (1.4)$$

where f^{abc} are the structure constants of the Lie algebra. We then have the field strengths for the gauge bosons given by

$$\begin{aligned} G_{\mu\nu}^a &= \partial_\mu G_\nu^a - \partial_\nu G_\mu^a + g_s f^{abc} G_\mu^b G_\nu^c \\ W_{\mu\nu}^a &= \partial_\mu W_\nu^a - \partial_\nu W_\mu^a + g \epsilon^{abc} W_\mu^b W_\nu^c \\ B_{\mu\nu} &= \partial_\mu B_\nu - \partial_\nu B_\mu \end{aligned} \quad (1.5)$$

g_s and g are, respectively, the coupling constants of $SU(3)_c$ and $SU(2)_L$ gauge algebras. The non-abelian structure of the strong and weak interaction leads to non-trivial interactions among respectively the gluons and the weak bosons, with triple and quartic couplings.

In order to have a locally gauge invariant lagrangian we have to write a covariant derivative for the fermions. The minimal coupling between the fermionic matter fields and the gauge bosons, with g_Y as the $U(1)_Y$ coupling constant, is defined as

$$D_\mu \psi = \left(\partial_\mu - ig_s U_a G_\mu^a - ig T_a W_\mu^a - ig_Y \frac{Y_q}{2} B_\mu \right) \psi \quad (1.6)$$

In the covariant derivative 1.6 it has to be understood that only the relevant part is to be taken: g_s and g couplings are irrelevant for the case of a right-handed electron for example.

The SM Lagrangian is then written in the following way:

$$\begin{aligned} \mathcal{L}_{\text{SM}} &= \mathcal{L}_{\text{gauge}} + \mathcal{L}_{\text{fermion}} + \mathcal{L}_{\text{scalar}} \\ \mathcal{L}_{\text{gauge}} &= -\frac{1}{4} G_{\mu\nu}^a G_a^{\mu\nu} - \frac{1}{4} W_{\mu\nu}^a W_a^{\mu\nu} - \frac{1}{4} B_{\mu\nu} B^{\mu\nu} \\ \mathcal{L}_{\text{fermion}} &= \bar{L} i D_\mu \gamma^\mu L + \bar{e}_R i D_\mu \gamma^\mu e_R + \bar{Q} i D_\mu \gamma^\mu Q + \\ &\quad \bar{u}_R i D_\mu \gamma^\mu u_R + \bar{d}_R i D_\mu \gamma^\mu d_R \\ &\quad (-\lambda_e \bar{L} \Phi e_R - \lambda_{ij} \bar{L}_i \Phi q_j + \text{h.c.}) \\ \mathcal{L}_{\text{scalar}} &= (D_\mu \Phi)^\dagger (D_\mu \Phi) - V(\Phi), \quad V(\Phi) = \mu^2 \Phi^\dagger \Phi + \lambda (\Phi^\dagger \Phi)^2 \end{aligned} \quad (1.7)$$

$V(\Phi)$ is a potential term for the scalar field, and will be studied in the following section. The Yukawa interactions in $\mathcal{L}_{\text{fermions}}$ give rise to the mass of the fermions coupled to the Higgs field through λ_e for the electron (more generally the charged leptons), and $(\lambda_{ij})_{1 \leq i, j \leq 3}$ for the 6 quarks. The diagonalization of the λ_{ij} matrix gives the CKM matrix which is then involved in the couplings between the weak bosons and the quarks. We also remind the reader that the $\lambda_{ij} \bar{L}_i \Phi q_j$ is a formal form actually involving both $\bar{L}_i \Phi q_j$ and $\bar{L}_i \tilde{\Phi} q_j$ terms where $\tilde{\Phi} = i\tau_2 \Phi^*$ in order to give a mass to up-type quarks.

2 The Brout–Englert–Higgs mechanism

After the presentation of the lagrangian of the SM in the previous section we now turn our attention to the electroweak symmetry breaking. The first question to be answered is: why do we need the electroweak symmetry breaking in the description of the SM? For example, as already stated, we now through the experiment that weak bosons should be massive, as the weak interaction is that of short–range; but explicit mass terms are prohibited if we want to preserve gauge symmetry principles.

This will be discussed in details in the following subsection. We will then present the spontaneous electroweak symmetry breaking using one scalar weak doublet, which is known as the Brout–Englert–Higgs mechanism [21–24]. We will deduce the weak bosons masses and the Higgs boson couplings to fermions and bosons.

2.1 Why do we need the electroweak symmetry breaking?

2.1.1 The unitarity puzzle

As presented in the historical part, the effective Fermi theory was the first attempt to describe the weak interaction in a quantum framework. The neutron and proton interactions were described in an effective four–point vertex, which in the end results in a cross section which grows with the center–of–mass energy \sqrt{s} . This means that the theory at some point has lost unitarity and cannot make reliable predictions: a reliable quantum theory should arrange for having the sum of the probabilities of every possible event to be equal to one, hence conserving the unitarity.

When taking into account the mass of the W boson we restore unitarity at the Fermi scale. Nevertheless we still face a potential disaster at higher energy: if we study for example the scattering of two W bosons we obtain a growth of the cross section with higher center–of–mass energy, still destroying unitarity beyond the Fermi scale. We thus have to cure the theory in order to restore unitarity in all processes, then preserving its prediction power and the ability to calculate reliable quantities.

The crucial point that has been developed in 1973 in Refs. [41,42] is that of the following: if we impose the SM (without the Higgs field as introduced in standard textbooks by requiring spontaneous symmetry breaking) to remain unitary at the Born level in perturbation theory we end up precisely with two requirements:

- The fermion–bosons interactions should be that of Yang–Mills theory.

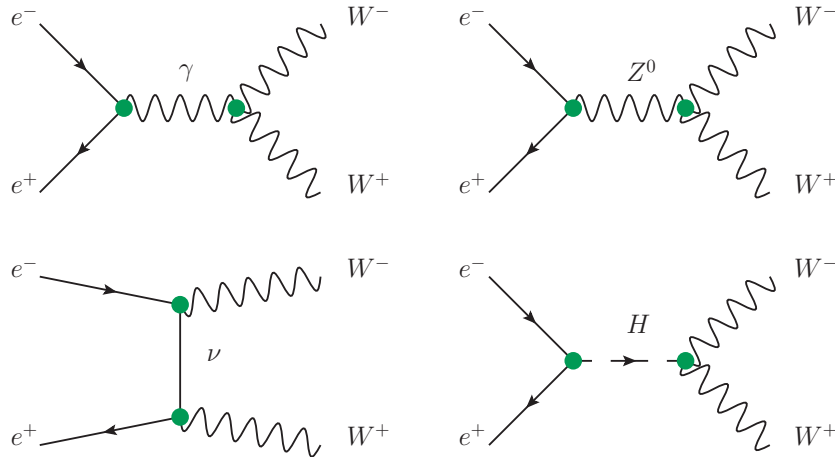


Figure 1: Feynman diagrams at the tree-level for WW production in e^+e^- annihilation.

- The theory needs at least a scalar doublet whose couplings to fermions and bosons are precisely that of the Higgs mechanism type. The self-couplings are also that of the Higgs type.

This very important result should be interpreted as proving the existence of something to restore unitarity in weak processes that is, either the Higgs doublet and subsequently the Higgs boson itself, or something which *looks exactly like the Higgs doublet and reproducing its properties*. This second proposition is what should remain in mind when dealing with electroweak symmetry breaking: the $SU(2)_L \times U(1)_Y$ symmetry has to be broken to restore unitarity, even if we do not think about the weak bosons masses puzzle. Indeed, if the gauge symmetry were preserved we would not have included new symmetry breaking scalar degree of freedom, hence not have had the precise type of fermion–scalar and boson–scalar interactions that are those of gauge breaking type.

To demonstrate this intimate connection between the scalar degrees of freedom and the unitarity requirement, we present the case of the WW production through electron–positron annihilation. The four Feynman diagrams are depicted in Fig. 1.

Let us suppose for a while that the fourth Feynman diagram involving the Higgs boson exchange does not exist. If we are interested in the production of longitudinal W bosons, as the electron are massive we need to cancel the cross section divergence arising because the electron can have an helicity distinct from that of its chirality. If this problem might seem to be not so critical, the electron mass being small, this is certainly not the case if we replace the electron by the top quark, a process that should be described by the theory. This divergence is then proportional to m_e and has to be cancelled by a new contribution also proportional to m_e . To avoid some tedious questions when using particles with spin higher than $3/2$, this new contribution should be of spin zero.

This two last conditions are precisely fulfilled with the Higgs boson contribution of the fourth Feynman diagram that we now take into account and that restores the unitarity of this process!

This very important result, leading to the conclusion that something should be discovered at hadron colliders at the electroweak scale, whether it is the SM Higgs boson or its beyond-the-SM colleagues, or anything else which looks like the Higgs boson (e.g. composite Higgs boson, extra-dimensions mimick, etc.), has also been extended in Ref. [43] for arbitrary scalar multiplets. We should then keep in mind the intimate link between unitarity requirement and the existence of (a) new scalar degree(s) of freedom in the electroweak theory.

2.1.2 Masses and gauge invariance

So far we have addressed the formal problem of requiring that the theory remains predictive and thus at least preserve unitarity in high energy processes. The last subsection has shown that this precise requirement of preserving unitarity leads to the existence of either the Higgs mechanism (and the Higgs boson), or the existence of something which looks like the Higgs boson.

We take here the other way around by looking at what the experiment tells us. We want to use gauge symmetry formalism in order to describe the fundamental interactions at the high energy scale as it has been proved to be a very powerful tool in the description of quantum electromagnetic processes. The problem that we have is that Nature gives us massive weak bosons, the interaction being of short length scale; it turns out that explicit mass terms are prohibited in the lagrangian as to preserve gauge invariance.

If we do not have any mass terms nor take into account the scalar part in the SM lagrangian 1.7, this gauge transformations preserve the lagrangian:

$$\begin{aligned}
L(x) \rightarrow L'(x) &= e^{i\alpha_a(x)T^a + i\beta(x)Y + i\gamma_a(x)U^a} L(x) \\
R(x) \rightarrow R'(x) &= e^{i\beta(x)Y + i\gamma_a(x)U^a} R(x) \\
W_\mu^a(x) \rightarrow W_\mu'^a(x) &= W_\mu^a(x) - \frac{1}{g} \partial_\mu \alpha^a(x) - \epsilon_{abc} \alpha^b(x) W_\mu^c(x) \\
G_\mu^a(x) \rightarrow G_\mu'^a(x) &= G_\mu^a(x) - \frac{1}{g_s} \partial_\mu \gamma^a(x) - \epsilon_{abc} \gamma^b(x) G_\mu^c(x) \\
B_\mu(x) \rightarrow B_\mu'(x) &= B_\mu(x) - \frac{1}{g_Y} \partial_\mu \beta(x)
\end{aligned} \tag{2.1}$$

It is of course understood that the $SU(3)_c$ gauge transformation acts only on the quark and gluons fields.

Let us suppose that we now add explicit mass terms in the lagrangian 1.7 (again we exclude at this stage the scalar part as we are interested in proving that we need it, without explicit mass terms), taking as an example the hypercharge boson B_μ (which is exactly like the case of a massive photon). We write down its gauge transformation as:

$$\frac{1}{2}M_B^2 B_\mu B^\mu \rightarrow \frac{1}{2}M_B^2 \left(B_\mu - \frac{1}{g_Y} \partial_\mu \beta \right) \left(B^\mu - \frac{1}{g_Y} \partial^\mu \beta \right) \neq \frac{1}{2}M_B^2 B_\mu B^\mu \quad (2.2)$$

which does not preserve $U(1)_Y$ gauge invariance. This means that we cannot account for the mass of the weak bosons while preserving gauge invariance with explicit mass terms in the lagrangian.

We also have a similar problem when dealing with fermions. Indeed we obviously observe a massive electron, not to mention the heavy quarks. We would then include a mass term $-m_f \bar{\psi}_f \psi_f$ in the lagrangian. This does not break $SU(3)_c$ nor $U(1)_Y$, but if we rewrite this mass term using chirality degrees of freedom we have:

$$-m_f \bar{\psi}_f \psi_f = -m_f \bar{\psi}_f \left(\frac{1}{2}(1 - \gamma_5) + \frac{1}{2}(1 + \gamma_5) \right) \psi_f = -m_f (\bar{\psi}_{fR} \psi_{fL} + \bar{\psi}_{fL} \psi_{fR}) \quad (2.3)$$

which manifestly violates $SU(2)_L$ gauge symmetry since Ψ_{fL} is a member of a doublet while Ψ_{fR} is a member of a singlet.

Thus, the incorporation by hand of mass terms for gauge bosons and fermions leads to a manifest breakdown of the local $SU(2)_L \times U(1)_Y$ gauge invariance. We then have at a first look either to give up the fact that we do observe masses for weak bosons and for fermions, which of course is unacceptable, or we have to give up the principle of (exact) gauge symmetry.

The spontaneous electroweak symmetry breaking is a solution which avoids both of the problematic answers given above: we still preserve the gauge symmetry of the theory, but the vacuum breaks the electroweak symmetry and gives rise to massive gauge bosons and fermions in the spectrum. In the following subsection we will sketch the Higgs mechanism which is the simplest procedure to do so.

2.2 The spontaneous electroweak symmetry breaking

We have seen that we are bound to add something to the gauge content of the SM in order to both preserve unitarity and give masses to the weak bosons, which are known to be massive. The most simple solution is known as the Brout–Englert–Higgs mechanism [21–24] and will be presented in this subsection. We will see how to obtain the weak bosons masses, and then we will review the Higgs boson coupling to fermions and bosons that will be used in the following sections when dealing with the SM Higgs boson production and decay at the hadron colliders.

2.2.1 Weak bosons masses and electroweak breaking

The Higgs mechanism

This subsection is built upon Refs. [44] and [45]. We start by taking the full SM lagrangian 1.7, that is not only the gauge and fermion parts but also the scalar part. We thus add a new $SU(2)_L$ scalar doublet to the usual content of the theory:

$$\Phi = \begin{pmatrix} \phi^+ \\ \phi^0 \end{pmatrix}$$

with $Y = +1$ hypercharge. Φ is also a color singlet. We remind the reader that the scalar part of the SM lagrangian 1.7 is

$$\mathcal{L}_{\text{scalar}} = (D_\mu \Phi)^\dagger (D_\mu \Phi) - V(\Phi), \quad V(\Phi) = \mu^2 \Phi^\dagger \Phi + \lambda (\Phi^\dagger \Phi)^2$$

The vacuum expectation value of the Higgs doublet is given by the minimum of $V(\Phi)$. We first note that $\lambda > 0$ is required to have a potential bounded from below, thus insuring a stable vacuum. We then have the two situations depicted in Fig. 2 for a one dimensional scalar field.

If $\mu^2 > 0$ we then have a positive potential everywhere, whose minimum is $\langle 0 | \Phi | 0 \rangle = 0$: we have not achieved anything new.

We will then suppose that $\mu^2 < 0$, which is the hypothesis building the Brout–Englert–Higgs mechanism [21–24] that we apply in the SM. In that case we obtain a minimum

$$\phi_0^2 \equiv \langle 0 | |\Phi|^2 | 0 \rangle = -\frac{\mu^2}{2\lambda} \equiv \frac{v^2}{2} \quad (2.4)$$

In the case of the $SU(2)_L$ doublet, the potential is depicted in Fig. 3 below.

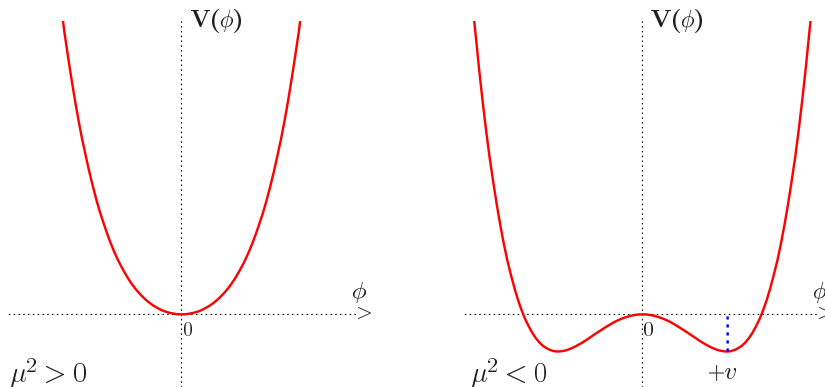


Figure 2: Higgs potential in the case of a real scalar field, depending on the sign of the mass term. This figure is taken from Ref. [45].

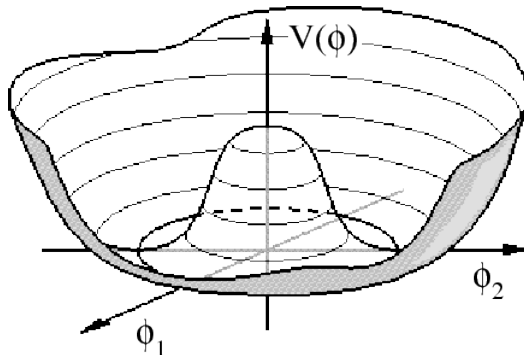


Figure 3: Higgs potential in the SM, also known as the “mexican hat”.

The vacuum expectation value (vev) still preserves a $U(1)$ symmetry, but has broken the $SU(2)$ symmetry: we thus have a spontaneously breaking of the original SM gauge algebra down to a residual $U(1)$ symmetry which, as seen later, is the electromagnetic $U(1)$ gauge algebra.

To make a physical interpretation of the lagrangian we will expand Φ around its minimum which will give us the physical degree of freedom. The neutral component of the doublet field Φ will develop a vacuum expectation value

$$\langle \Phi \rangle_0 \equiv \langle 0 | \Phi | 0 \rangle = \begin{pmatrix} 0 \\ \frac{v}{\sqrt{2}} \end{pmatrix} \quad \text{with} \quad v = \left(-\frac{\mu^2}{\lambda} \right)^{1/2} \quad (2.5)$$

We have chosen this direction so as to preserve $U(1)_{\text{EM}}$. We then write the field Φ in terms of four fields $\theta_{1,2,3}(x)$ and $H(x)$ around the minimum, and at first order we have:

$$\Phi(x) = \begin{pmatrix} \theta_2 + i\theta_1 \\ \frac{1}{\sqrt{2}}(v + H) - i\theta_3 \end{pmatrix} = e^{i\theta_a(x)\tau^a(x)/v} \begin{pmatrix} 0 \\ \frac{1}{\sqrt{2}}(v + H(x)) \end{pmatrix} \quad (2.6)$$

The second expression is crucial: as the theory remains gauge invariant we can always make a $SU(2)_L$ gauge transformation with the parameter $-\theta^a(x)/v$, which means that we chose a particular gauge, called the unitary gauge or U-gauge:

$$\Phi(x) \rightarrow e^{-i\theta_a(x)\tau^a(x)} \Phi(x) = \frac{1}{\sqrt{2}} \begin{pmatrix} 0 \\ v + H(x) \end{pmatrix} \quad (2.7)$$

We have to expand the scalar part of the lagrangian 1.7 in this gauge, we obtain:

$$\begin{aligned} V(\Phi) &= \frac{1}{2}\mu^2(v + H(x))^2 + \frac{1}{4}\lambda(v + H(x))^4 \\ &= -\mu^2 H(x)^2 + \lambda v H(x)^3 + \frac{1}{4}\lambda H(x)^4 + \text{constant} \end{aligned}$$

and

$$\begin{aligned} |D_\mu \Phi|^2 &= \left| \left(\partial_\mu - ig \frac{\tau_a}{2} W_\mu^a - ig_Y \frac{1}{2} B_\mu \right) \Phi \right|^2 \\ &= \frac{1}{2} \left| \begin{pmatrix} \partial_\mu - \frac{i}{2}(gW_\mu^3 + g_Y B_\mu) & -\frac{ig}{2}(W_\mu^1 - iW_\mu^2) \\ -\frac{ig}{2}(W_\mu^1 + iW_\mu^2) & \partial_\mu + \frac{i}{2}(gW_\mu^3 - g_Y B_\mu) \end{pmatrix} \begin{pmatrix} 0 \\ v + H \end{pmatrix} \right|^2 \\ &= \frac{1}{2}(\partial_\mu H)^2 + \frac{1}{8}g^2(v + H)^2 |W_\mu^1 - iW_\mu^2|^2 + \frac{1}{8}(v + H)^2 |gW_\mu^3 - g_Y B_\mu|^2 \end{aligned}$$

We define the physical fields W_μ^\pm , Z_μ and A_μ as:

$$W^\pm = \frac{1}{\sqrt{2}}(W_\mu^1 \mp iW_\mu^2), \quad Z_\mu = \frac{gW_\mu^3 - g_Y B_\mu}{\sqrt{g^2 + g_Y^2}}, \quad A_\mu = \frac{gW_\mu^3 + g_Y B_\mu}{\sqrt{g^2 + g_Y^2}} \quad (2.8)$$

With this new basis we finally obtain the physical interpretation of the scalar part of the lagrangian:

$$\begin{aligned}
\mathcal{L}_{\text{scalar}} = & \frac{1}{2} (\partial_\mu H)^2 - \frac{1}{2} (-2\mu^2) H^2 + \\
& \left(\frac{g^2 v^2}{4} \right) W_\mu^+ W^{-\mu} + \frac{1}{2} \left(\frac{(g^2 + g_Y^2) v^2}{4} \right) Z_\mu Z^\mu + \\
& \left(\frac{g^2 v}{2} \right) H W_\mu^+ W^{-\mu} + \left(\frac{(g^2 + g_Y^2) v}{4} \right) H Z_\mu Z^\mu + \\
& \left(\frac{g^2}{4} \right) H^2 W_\mu^+ W^{-\mu} + \left(\frac{(g^2 + g_Y^2)}{8} \right) H^2 Z_\mu Z^\mu + \\
& - (\lambda v) H^3 - \left(\frac{\lambda}{4} \right) H^4 + \text{constant} \tag{2.9}
\end{aligned}$$

The spontaneous breakdown of $SU(2)_L \times U(1)_Y$ has achieved our goal of obtaining masses for the weak bosons. They can be read in the second line of Eq. 2.9 as:

$$M_W = \frac{gv}{2}, \quad M_Z = \frac{v\sqrt{g^2 + g_Y^2}}{2}, \quad M_A = 0 \tag{2.10}$$

not to mention the Higgs mass itself $M_H^2 = -2\mu^2$.

The photon A_μ remains massless as the remaining $U(1)_{\text{EM}}$ is unbroken while the three weak bosons W^\pm and Z^0 are now massive. The three degree of freedom θ_μ^a of the original Higgs doublet, which are Goldstone bosons, have been absorbed by the W^\pm and Z^0 bosons to obtain their longitudinal components, which means that the number of degree of freedom is still conserved when looking at the lagrangian before and after the electroweak symmetry breaking. We are left with one scalar degree of freedom: the Higgs boson.

The remaining lines of Eq. 2.9 give the couplings of the Higgs boson H with the gauge bosons, and also its trilinear and quartic self-couplings.

If we recall the fermionic part of the SM lagrangian which also contains Higgs field couplings to fermion, we can also generate the fermion masses using Φ and $\tilde{\Phi} = i\tau_2 \Phi^*$. Starting from

$$\mathcal{L}_{\text{Yukawa}} = -\lambda_e \bar{L} \Phi e_R - \lambda_d \bar{Q} \Phi d_R - \lambda_u \bar{Q} \tilde{\Phi} u_R + h.c. \tag{2.11}$$

where we have left out the CKM issue and only dealt with the first generation, again we expand the expression around the vev:

$$\begin{aligned}
\mathcal{L}_{\text{Yukawa}} = & - \left(\frac{\lambda_e v}{\sqrt{2}} \right) \bar{e} e - \left(\frac{\lambda_u v}{\sqrt{2}} \right) \bar{u} u - \left(\frac{\lambda_d v}{\sqrt{2}} \right) \bar{d} d \\
& - \left(\frac{\lambda_e}{\sqrt{2}} \right) \bar{e} H e - \left(\frac{\lambda_u}{\sqrt{2}} \right) \bar{u} H u - \left(\frac{\lambda_d}{\sqrt{2}} \right) \bar{d} H d \tag{2.12}
\end{aligned}$$

We then have the fermion masses:

$$m_e = \frac{\lambda_e v}{\sqrt{2}} \quad , \quad m_u = \frac{\lambda_u v}{\sqrt{2}} \quad , \quad m_d = \frac{\lambda_d v}{\sqrt{2}} \quad (2.13)$$

and also the Higgs–fermion–fermion couplings $\lambda_f/\sqrt{2}$. We thus have generated the masses of both the weak vector bosons W^\pm, Z and the fermions, while preserving the $SU(2)_L \times U(1)_Y$ gauge symmetry, which is now spontaneously broken or hidden, together with a preservation of both the color $SU(3)_c$ and electromagnetic $U(1)_{\text{EM}}$ gauge symmetries. This constitutes the Higgs mechanism applied to the Standard Model. The SM refers actually to the gauge symmetries together with the Higgs mechanism.

The fundamental parameters

We list in this small paragraph the main fundamental parameters of the SM that will be used in the following sections.

- *Weak coupling and the Fermi constant:* The weak couplings in the lagrangian are g and g_Y for the $SU(2)_L \times U(1)_Y$ gauge algebra. This can be related to the Fermi constant $G_F = 1.6637 \times 10^{-5} \text{ GeV}^{-2}$, by taking the low energy limit of the electroweak theory:

$$\frac{g^2}{8M_W^2} = \frac{G_F}{\sqrt{2}} \quad (2.14)$$

using the W mass given in Eq. 2.10, we have the value of the vev

$$v = (G_F \sqrt{2})^{-1/2} \simeq 246 \text{ GeV} \quad (2.15)$$

- *The Weinberg angle:* we can relate the W and Z bosons masses through what is called the Weinberg angle θ_W :

$$\begin{aligned} \sin \theta_W &\equiv \frac{g_Y}{\sqrt{g^2 + g_Y^2}} = 0.23150 \\ g_Y &= g \tan \theta_W \quad , \quad M_Z = \frac{M_W}{\cos \theta_W} \end{aligned} \quad (2.16)$$

This leads to

$$\rho \equiv \frac{M_W^2}{M_Z^2 \cos^2 \theta_W} = 1 \quad (2.17)$$

and this value is hardly changed when taking into account radiative corrections, a statement which can be related to a global $SU(2)$ custodial symmetry in the SM. This imposes constraints on any theory that goes beyond the SM.

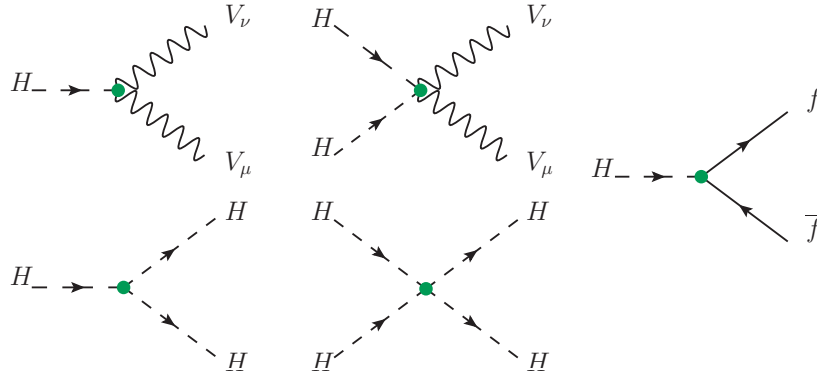


Figure 4: Tree-level SM Higgs boson couplings to gauge bosons and fermions.

- *Strong and electromagnetic constants:* the electromagnetic coupling constant is related to the $SU(2)_L \times U(1)_Y$ coupling constants through $e = g \sin \theta_W$. We have at the scale M_Z :

$$\begin{aligned} \alpha_s(M_Z^2) &\equiv \frac{g_s^2}{4\pi} = 0.1172 \text{ (LEP2)} \\ \alpha(M_Z^2) &\equiv \frac{e^2}{4\pi} = 1/(128.951) \end{aligned} \quad (2.18)$$

The value of the strong coupling constant will be particularly important when dealing with Higgs boson production and decay at hadron colliders; this will be discussed in more details in the following part [II](#).

- *W and Z masses:* the current measured values of the W and Z masses are

$$M_W = 80.420 \text{ GeV} , M_Z = 91.1876 \text{ GeV} \quad (2.19)$$

2.2.2 SM Higgs boson couplings

We finish this presentation of the SM by giving the Higgs couplings to gauge bosons and fermions in a compact form. These couplings will play a crucial role in the following parts as they dictate the dynamics of the SM Higgs boson in production and decays.

The couplings of the Higgs boson H with the gauge bosons as well as its trilinear and quartic self-couplings can be read in [Eq. 2.9](#), while the SM Higgs boson coupling to fermions can be read in [Eq. 2.12](#). These tree-level couplings are depicted in [Fig. 4](#) below.

When taking into account the number of identical particles in the vertex, this gives

$$\begin{aligned}
 g_{HVV} &= \frac{2M_V^2}{v} (\times i g_{\mu\nu}) & , & & g_{HHVV} &= \frac{2M_V^2}{v^2} (\times i g_{\mu\nu}) \\
 g_{HHH} &= -\frac{3M_H^2}{v} (\times i) & , & & g_{HHHH} &= -\frac{3M_H^2}{v^2} (\times i) \\
 g_{Hf\bar{f}} &= -\frac{m_f}{v} (\times i) & & & & & (2.20)
 \end{aligned}$$

There are two additional couplings which are of utmost importance for the study of the Higgs boson, either within or beyond the SM. Indeed, even if the Higgs is not charged nor colored, it may have a coupling to the photon and the gluons at the one-loop level, as shown in Fig. 5. These couplings come through a fermionic triangular loop which carries the absent quantum number of the Higgs boson.

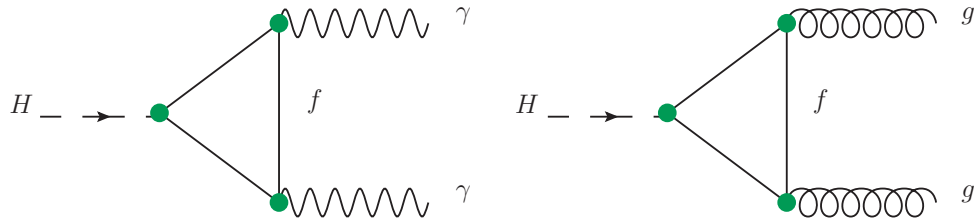


Figure 5: One-loop SM Higgs boson couplings to the photons and the gluons.

The gluon-gluon-Higgs coupling will play a major role in the production of the Higgs boson at hadron colliders. Now that we have ended describing the Standard Model and the Higgs mechanism, we are ready to study the SM Higgs production and decay at the two hadron colliders in activity.

Part II

SM Higgs production and decay at hadron colliders

Summary

3	Where can the SM Higgs boson be hiding?	31
3.1	Theoretical bounds on the Higgs mass	31
3.1.1	Unitarity constraint	31
3.1.2	Constraint from the perturbativity of the self-Higgs coupling . .	35
3.1.3	Triviality constraint	36
3.1.4	Stability requirement and lower bound on Higgs mass	37
3.1.5	Combination of the theoretical bounds	38
3.2	Experimental bounds on the Higgs mass	39
3.2.1	Indirect searches through precision data	40
3.2.2	Direct searches at the LEP collider	43
3.2.3	Direct searches at the Tevatron collider	44
4	Higgs production at the Tevatron	46
4.1	The main production channels	50
4.1.1	The gluon-gluon fusion	51
4.1.2	The Higgs-strahlung production channels	57
4.1.3	The VBF and associated heavy quarks channels	60
4.2	Scale variation and higher order terms	62
4.2.1	The case of $gg \rightarrow H$ production	64
4.2.2	The scale variation uncertainty in Higgs-strahlung processes . .	69
4.3	The PDF puzzle	70
4.3.1	PDF uncertainties in gluon-gluon fusion	73
4.3.2	The case of Higgs-strahlung processes	79
4.4	EFT and its uncertainties	81
4.4.1	The b -loop uncertainty	82

4.4.2	The electroweak uncertainty	84
4.5	Combination and total uncertainty	85
4.6	Summary and outlook	92
4.A	Appendix: analytical expressions for μ_R -NNLO terms in $gg \rightarrow H$	94
5	Higgs production at the LHC	96
5.1	The main channel at the LHC	97
5.2	The scale uncertainty	100
5.3	The PDF+ α_S uncertainty	103
5.4	EFT	107
5.5	Total uncertainty at 7 TeV	110
5.6	LHC results at different center-of-mass energies	115
5.6.1	The case of the LHC with $\sqrt{s} = 8, 9, 10$ TeV	115
5.6.2	The case of the designed LHC at $\sqrt{s} = 14$ TeV	116
5.7	Summary and outlook	121
6	Higgs decay and the implications for Higgs searches	122
6.1	Important channels for experimental search	122
6.1.1	$H \rightarrow b\bar{b}$ channel	123
6.1.2	$H \rightarrow V^*V^*$ channel	124
6.1.3	$H \rightarrow \gamma\gamma$ channel	125
6.1.4	A comment on the $H \rightarrow gg$ channel	126
6.1.5	$H \rightarrow \tau^+\tau^-$ channel	127
6.2	Uncertainties on the branching ratios	127
6.2.1	The parametric uncertainties	127
6.2.2	The final uncertainties on the branching ratios	129
6.3	Combination at the Tevatron	133
6.4	Combination at the LHC	135
6.5	The Tevatron exclusion limit	136
6.6	Summary of the results	142

3 Where can the SM Higgs boson be hiding?

The section 2 was devoted to the Higgs mechanism itself and its remnant particle, the Higgs boson. This key particle, predicted by the Standard Model and at the core of the electroweak symmetry breaking, has been yet to be discovered for nearly 40 years. Large particle physics experiments have promoted its search as prominent, such as in the LEP era [46] and at the Tevatron collider. It is also one of the key searches at the newest Large Hadron Collider (LHC) at CERN.

Before starting to study the Higgs boson production at the two current hadronic colliders and then its decay, we will review the current theoretical and experimental bounds on its mass which is not predicted by the Standard Model.

3.1 Theoretical bounds on the Higgs mass

The Higgs boson mass is not predicted by the Standard Model. Hence the only prediction that can be made is on the range of validity for M_H as to be sure that the Standard Model is still a valid and consistent theory. The theoretical bounds on the Higgs mass are precisely derived on these requirements: we probe the mass range in which the SM does not break down and where perturbation theory is still applicable, before new phenomena occur. These limits include constraints from the unitarity required in scattering amplitudes, the perturbativity of the Higgs self-coupling and considerations about the stability of the vacuum of the theory. We summarize and combine all the limits in the last subsection.

3.1.1 Unitarity constraint

The SM is embedded within the framework of quantum field theory. As for any consistent quantum theory, where the description is probabilistic in the sense that any physical observable has a probability to be measured by an observer, the total probability is conserved and equal to the unity. In the context of the scattering amplitudes within the SM, it means that we require that the S -matrix, which encodes all the necessary information between the initial and final states, is unitary. We thus want that the SM to be unitary in that sense, which will translate into an upper bound for the SM Higgs boson mass.

It was actually one of the main arguments to abandon the Fermi theory of the weak interaction, together with the requirement of accommodate within a gauge theory the fact that experimentally the weak bosons are to have a mass. To take an example the weak process $\nu_\mu e \rightarrow \nu_e \mu$ is proportional to the Mandelstam variable s , which then violates unitarity at

a certain point as we should instead have $\sigma(\nu_\mu e \rightarrow \nu_e \mu) = \mathcal{O}(s^{-1})$. If we go further the unitarity constraint applied to all SM processes does even lead to the requirement of the Higgs field itself, as presented in section 2.1.1⁷. In some sense, we can think about the SM as the theory which cures the unitarity problem at the Fermi scale $\Lambda \sim 300$ GeV.

However there is still some potential unitarity concern in the SM, at much higher energies than the Fermi scale, in particular if it is believed that the SM is valid up to the Planck scale⁸. We take as an example the ZZ scattering, looking in particular at the longitudinal component $Z_L Z_L$ scattering. This scattering is (one of) the focus point of the spontaneously electroweak symmetry breaking as the Z_L is one of the degrees of freedom of the unbroken Higgs field. The situation is that of the Fermi theory: the $Z_L Z_L$ interaction grows with the momenta of the ingoing particles, which then may lead to a violation of the unitarity requirement. Considering that at high center-of-mass energies we can work directly with the corresponding Goldstone bosons for the scattering of the longitudinal component, we obtain very easily

$$\mathcal{A}(Z_L^0 Z_L^0 \rightarrow Z_L^0 Z_L^0) = - \left[3 \frac{M_H^2}{v^2} + \left(\frac{M_H^2}{v} \right)^2 \frac{1}{s - M_H^2} + \left(\frac{M_H^2}{v} \right)^2 \frac{1}{t - M_H^2} \right] \quad (3.1)$$

where s, t are the Mandelstam variables (the center-of-mass energy s is the square of the sum of the momenta of the initial or final states, while t is the square of the difference between the momenta of one initial and one final state).

In order to study the unitarity of this amplitude we use the partial wave decomposition of the scalar amplitude on the Legendre polynomials basis:

$$\mathcal{A} = 16\pi \sum_{k=0}^{\infty} (2k+1) a_k P_k(\cos \theta) \quad (3.2)$$

with a_k being the partial waves along the angular momentum k and θ the scattering angle in the center-of-mass frame. We recall the reader that the Legendre polynomials is an orthogonal basis of the vector space $\mathbb{R}[X]$. In particular we have the orthonormal condition

$$\int_{-1}^1 d \cos \theta P_k(\cos \theta) P_l(\cos \theta) = \frac{2}{2k+1} \delta_{kl} \quad (3.3)$$

⁷To be more rigorous this leads to the requirement of a new scalar degree of freedom which exactly looks like the Higgs field of the SM. This does not mean that this new degree of freedom is elementary and it may well be a strongly coupled composite bound state, as proposed in many Higgsless theories [47, 48].

⁸That is not the current belief of the community, though. If SM were indeed valid up to the Planck scale we would stop working on particle physics! That would be a shame for young particle physicists and we hope that Nature does not trick us with that. . . .

where δ_{kl} is the Kronecker symbol. Since for a $2 \rightarrow 2$ process, the cross section is given by $d\sigma/d\Omega = |\mathcal{A}|^2/(64\pi^2s)$ with $d\Omega = 2\pi d\cos\theta$, the total cross section is

$$\begin{aligned}\sigma &= \frac{8\pi}{s} \sum_{k=0}^{\infty} \sum_{l=0}^{\infty} (2k+1)(2l+1) a_k a_l^* \int_{-1}^1 d\cos\theta P_k(\cos\theta) P_l(\cos\theta) \\ &= \frac{16\pi}{s} \sum_{k=0}^{\infty} (2k+1) |a_k|^2\end{aligned}\quad (3.4)$$

We now use the optical theorem which relates the imaginary part of the amplitude taken on the beam line $\mathcal{A}(\theta = 0)$ and the total cross section σ :

$$\sigma = \frac{1}{s} \text{Im} [\mathcal{A}(\theta = 0)] = \frac{16\pi}{s} \sum_{k=0}^{\infty} (2k+1) |a_k|^2 \quad (3.5)$$

This leads to the unitary conditions [49, 50]

$$\begin{aligned}|a_k|^2 = \text{Im}(a_k) &\iff [\text{Re}(a_k)]^2 + [\text{Im}(a_k)]^2 = \text{Im}(a_k) \\ &\iff [\text{Re}(a_k)]^2 + \left[\text{Im}(a_k) - \frac{1}{2}\right]^2 = \frac{1}{4}\end{aligned}\quad (3.6)$$

We thus obtain the equation of a circle of radius $\frac{1}{2}$ and center $(0, \frac{1}{2})$ in the plane $[\text{Re}(a_\ell), \text{Im}(a_\ell)]$. The real part lies between $-\frac{1}{2}$ and $\frac{1}{2}$, we obtain the unitarity condition which follows:

$$|\text{Re}(a_\ell)| < \frac{1}{2} \quad (3.7)$$

The kinematics of the process gives $t = \frac{-s}{2}(1 - \cos\theta)$. If we use the orthonormality relation of the Legendre polynomials and knowing that $P_0(x) = 1$ we easily obtain the $J = 0$ partial wave $a_0 = \frac{1}{32\pi} \int_{-1}^1 \mathcal{A}(\cos\theta) d\cos\theta$. Using the t variable this transforms in

$$a_0 = \frac{1}{16\pi s} \int_{-s}^0 dt \mathcal{A}(t) \quad (3.8)$$

We then obtain for the $\mathcal{A}(Z_L^0 Z_L^0 \rightarrow Z_L^0 Z_L^0)$:

$$a_0 = -\frac{M_H^2}{16\pi v^2} \left[3 + \frac{M_H^2}{s - M_H^2} - \frac{M_H^2}{s} \ln \left(1 + \frac{s}{M_H^2} \right) \right] \quad (3.9)$$

If we now assume that the Higgs boson mass to be much smaller than \sqrt{s} and then use the unitarity condition 3.7 we obtain

$$M_H \leq \frac{8\pi v^2}{3} \Rightarrow M_H \lesssim 710 \text{ GeV} \quad (3.10)$$

The same analysis has to be done for any channel of the theory: $W_L^+W_L^-$, HH , Z_LH , $W_L^\pm H$, $W_L^\pm Z_L$, etc. The condition obtained in Eq. 3.10 is formally valid only at tree-level, and since the Higgs boson self-coupling becomes strong for large Higgs masses, $\lambda = M_H^2/(2v^2)$, the argument could be destroyed if radiative corrections are taken into account. This is then only a perturbative tree-level unitarity limit. The complete perturbative unitarity argument should then be given within the context of a perturbative expansion analysis and assuring that the SM remains a perturbative theory where the radiative corrections are not too large. Taking this into account and with all the channel in the theory, the unitarity constraint is (incidentally!) still the one given by Eq. 3.10 [51–53].

We could adopt a different point of view and look the other way around where M_H is taken very large, and we would then obtain a bound on the possible compatible \sqrt{s} energies [54]. We take the example of the $W_L^+W_L^-$ channel. We take the limit $s \gg M_H^2$ in Eq. 3.9 where the number 3 is replaced by the number 2, and then apply the unitarity condition 3.7 to obtain

$$\sqrt{s} \leq v\sqrt{16\pi} \Rightarrow \sqrt{s} \lesssim 1.7 \text{ TeV} \quad (3.11)$$

Considering all the possible channels this reduces to

$$\sqrt{s} \lesssim 1.2 \text{ TeV} \quad (3.12)$$

Therefore we face two possibilities: either some new physics should manifest at the TeV scale range if the Higgs boson is very massive (or not existing at all), or the unitarity breakdown is canceled by large high-order terms which signal the failure of perturbation theory and the loss of the predictive power of the SM. The last possibility is of course a nightmare that we would avoid, and then we have two final reasonable conclusions:

- i) the SM Higgs boson exists and its mass should be bounded, $M_H \lesssim 710 \text{ GeV}$, in order to retain unitarity.
- ii) the SM Higgs boson is very massive or does not exist: then new physics effects are to emerge at the TeV scale.

3.1.2 Constraint from the perturbativity of the self-Higgs coupling

Even if we forget about the unitarity issue, the requirement of having a perturbative theory in particular with processes involving the Higgs self-coupling will induce an upper bound on the Higgs boson mass. Indeed it is known that for large values of the Higgs boson mass the perturbation theory is lost. If we take the SM Higgs decay into massive gauge bosons, we obtain (see Ref. [45]):

$$\Gamma(H \rightarrow ZZ) = \frac{M_H^3}{32\pi v^2} \left[1 + 3\hat{\lambda} + 62\hat{\lambda}^2 + \mathcal{O}(\hat{\lambda}^3) \right] \quad (3.13)$$

with $\hat{\lambda} = \lambda/(16\pi^2)$. We recall that we have $M_H^2 = 2\lambda v^2$. Thus if we require that the perturbativity of the calculation remains, that is each term in the expansion is smaller than its predecessor, we can derive an upper bound on the Higgs boson mass. Indeed if we have $M_H \simeq 2.5$ TeV the 1-loop term is of order 1, $3\hat{\lambda} = 1$, breaking the perturbativity. We can reduce this bound even more with the limit $3\hat{\lambda} = 62\hat{\lambda}^2$ where the 1-loop term is of order the 2-loop term, we then have $M_H \simeq 960$ GeV in this limit. Thus we have to impose $M_H \ll 1$ TeV to retain the perturbativity of the expansion.

The jeopardy of perturbation theory at large Higgs masses can also be seen in the scattering of longitudinal gauge bosons from which were derived above the upper bound on M_H using perturbative unitarity argument. In the case of the $W_L^+ W_L^- \rightarrow W_L^+ W_L^-$ scattering, the radiative corrections have been calculated at one and two loops in Refs. [55–58]. The logarithmic scale dependence found in these corrections can be absorbed in a running λ coupling through Renormalization Group analysis and we find (see Ref. [45]):

$$\sigma(W_L^+ W_L^- \rightarrow W_L^+ W_L^-) \sim \frac{1}{s} \hat{\lambda}(s) \left(1 - 48.64\hat{\lambda} + 333.21\hat{\lambda}^2 \right) \quad (3.14)$$

Here, the coefficients of the corrections are much larger than in Higgs decays and in fact, the one-loop correction become of order unity already for $\lambda(s)$ values close to 3, that transforms into $M_H \simeq 700$ GeV.

The perturbativity of the self-Higgs coupling in the end implies that $M_H \lesssim 700$ GeV in order to keep a calculable perturbative theory. We then obtain a bound that is very close to that obtained using the unitarity argument.

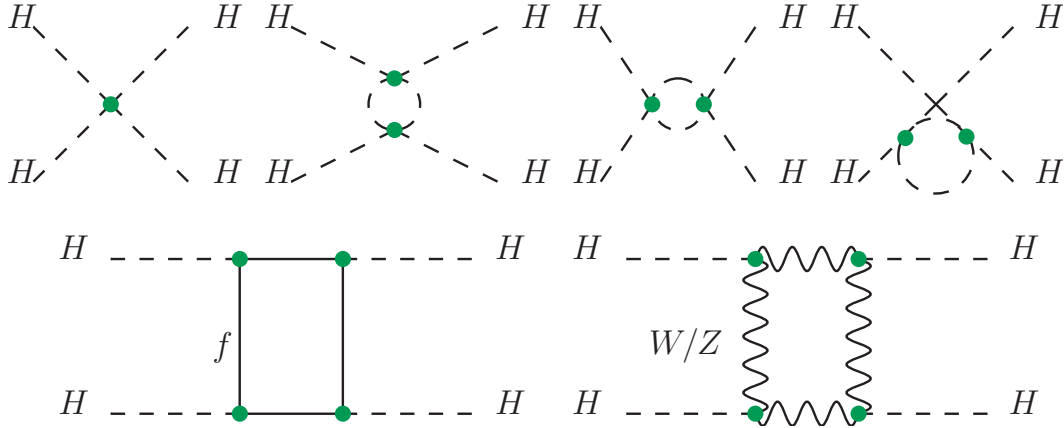


Figure 6: Feynman diagrams up to one-loop correction for the quartic Higgs self-coupling.

3.1.3 Triviality constraint

The triviality constraint is closely related to the vacuum stability that is the next constraint that will be discussed. An interacting theory is said to be trivial when the coupling is indeed null, which means that it is actually a non-interacting theory. The scalar sector of the SM is a ϕ^4 -theory, and for these theories to remain perturbative at all scales it is required that the theory is trivial: $\lambda = 0$, and thus the Higgs boson is massless [49, 50, 59–65].

We will take another point of view, and look at the Renormalization Group Equation (RGE) for the quartic Higgs coupling λ and require that it remains finite and the theory perturbative. It will define a range for the scale where the SM is valid and thus we will obtain an upper bound for the Higgs mass. Fig. 6 shows the tree-level Higgs self-coupling together with its one-loop corrections. These contribute to the β -function for the λ -coupling; as we are interested in the high λ regime the leading terms will only deal with the Higgs-Higgs couplings. In this limit the RGE equation is written at the one-loop order as [66–72]:

$$\frac{d\lambda(Q^2)}{d \ln Q^2} = \frac{3}{4\pi^2} \lambda^2(Q^2) \quad (3.15)$$

When choosing the electroweak symmetry breaking scale $Q_0 = v$ as the reference scale we then obtain

$$\lambda(Q^2) = \frac{\lambda(v^2)}{1 - \frac{3}{4\pi^2} \lambda(v^2) \ln \frac{Q^2}{v^2}} \quad (3.16)$$

The triviality is recovered at small energy scale $Q \ll v$ where $\lambda \rightarrow 0$. The other limit will give us the bound that we are looking for. Indeed at a certain point we see that λ

becomes infinite if we increase the energy scale Q . We thus reach a Landau pole, at the scale

$$\Lambda_P = v \exp\left(\frac{2\pi^2}{3\lambda(v^2)}\right) = v \exp\left(\frac{4\pi^2 v^2}{3M_H^2}\right) \quad (3.17)$$

If we would like that the scale Λ_P be large, the Higgs mass should be small. If we assume the SM to be valid up to the Planck scale and then take $\Lambda_P \simeq 10^{19}$ GeV this requires a light Higgs boson mass $M_H \lesssim 145$ GeV. If we take a small cut-off $\Lambda_P \simeq 10^3$ GeV, the Higgs boson can be heavier, $M_H \lesssim 750$ GeV. In particular, if the cut-off is set at the Higgs boson mass itself, $\Lambda_P = M_H$, this implies that $M_H \lesssim 700$ GeV. Nevertheless we should bear in mind that all the calculations presented so far use the perturbation theory and if λ becomes too large the calculation becomes non-consistent. According to Ref. [45], simulations of gauge theories on the lattice save the argument as the rigorous bound that is obtained is $M_H \lesssim 640$ GeV [73, 74], in a good agreement with the perturbative results obtained in this paragraph.

3.1.4 Stability requirement and lower bound on Higgs mass

To obtain a lower bound on the Higgs mass we retain in the RGE equation 3.15 all the terms at the one-loop order, in particular the fermionic corrections depicted in Fig. 6 as the Higgs boson couplings is proportionnal to the fermion masses. The one-loop RGE equation for the Higgs self-coupling 3.15 becomes, including all weak and fermion masses:

$$\frac{d\lambda}{d \ln Q^2} = \frac{1}{16\pi^2} \left[12\lambda^2 + 12\frac{m_t^2}{v^2}\lambda - 12\frac{m_t^4}{v^4} - \frac{3}{2}\lambda(3g_2^2 + g_1^2) + \frac{3}{16}(2g_2^4 + (g_2^2 + g_1^2)^2) \right] \quad (3.18)$$

where g_1, g_2 are respectively the hypercharge and weak coupling constants. The triviality bounds are marginally affected, but in an important way as the scale of physics beyond the SM will now depend on the precise value of the top quark mass, which explains why the top sector is of such great importance in the quest for new physics. The large impact of the additional fermionic and bosonic contributions to the Higgs self-coupling β -function is for very small values of λ . For $\lambda \ll \frac{m_t}{v}, g_1, g_2$, the RGE can be approximated by

$$\frac{d\lambda}{d \ln Q^2} \simeq \frac{1}{16\pi^2} \left[12\lambda^2 - 12\frac{m_t^4}{v^4} + \frac{3}{16}(2g_2^4 + (g_2^2 + g_1^2)^2) \right] \quad (3.19)$$

This translates into the solution

$$\lambda(Q^2) = \lambda(v^2) + \frac{1}{16\pi^2} \left[-12\frac{m_t^4}{v^4} + \frac{3}{16}(2g_2^4 + (g_2^2 + g_1^2)^2) \right] \ln \frac{Q^2}{v^2} \quad (3.20)$$

The top quark contribution becomes dominant for $\lambda \rightarrow 0$ and indeed drives the self-coupling to negative values, which then imply that the vacuum is not stable anymore. If we want to have a bounded scalar potential and thus a vacuum we should keep $\lambda(Q^2) > 0$ [75–79] and then the Higgs boson mass should have the lower bound

$$M_H^2 > \frac{v^2}{8\pi^2} \left[-12 \frac{m_t^4}{v^4} + \frac{3}{16} (2g_2^4 + (g_2^2 + g_1^2)^2) \right] \ln \frac{Q^2}{v^2} \quad (3.21)$$

Thus we have a lower bound limit dependent on the cut-off Λ_P that is the appearance of the new physics. We thus obtain

$$\begin{aligned} \Lambda_P \sim 10^3 \text{ GeV} &\Rightarrow M_H \gtrsim 70 \text{ GeV} \\ \Lambda_P \sim 10^{16} \text{ GeV} &\Rightarrow M_H \gtrsim 130 \text{ GeV} \end{aligned} \quad (3.22)$$

3.1.5 Combination of the theoretical bounds

As stated in Ref. [45] (nearly) all the bounds presented up until now were derived in a perturbative approach at the one-loop level at most. The use of the most advanced results helps to improve the limits [79–82].

In particular the β functions of all SM couplings have been calculated up to two loops and can then be included in the analysis of the Higgs boson mass. From Ref. [45] we extract for the λ Higgs self-coupling

$$\frac{d\lambda}{d \ln Q^2} \equiv \beta_\lambda = 24 \frac{\lambda^2}{(16\pi^2)} - 312 \frac{\lambda^3}{(16\pi^2)^2} \quad (3.23)$$

At the two-loop level the λ coupling can reach an ultraviolet fixed point where $\beta_\lambda = 0$. This means that the value of the cut-off scale can be lower than obtained above. The stability bound is again obtained by the requirement that $\lambda(Q^2) > 0$ and we use a two-loop β function retaining all the Higgs, weak boson and fermion corrections, including matching conditions, that is the precise relation between the physical masses of the gauge bosons and the top quark and their corresponding couplings.

We obtain [82] the Roman plot shown in Fig. 7 for the stability and triviality bounds on the Higgs boson mass. The graph displays the allowed values for the Higgs boson mass in function of the scale Λ for new physics effects. The upper band is the triviality limit and the lower band is the stability limit. These are bands instead of lines in order to take into account some theory and experimental uncertainties in the determination (e.g. scale dependence, input top quark mass, etc.).

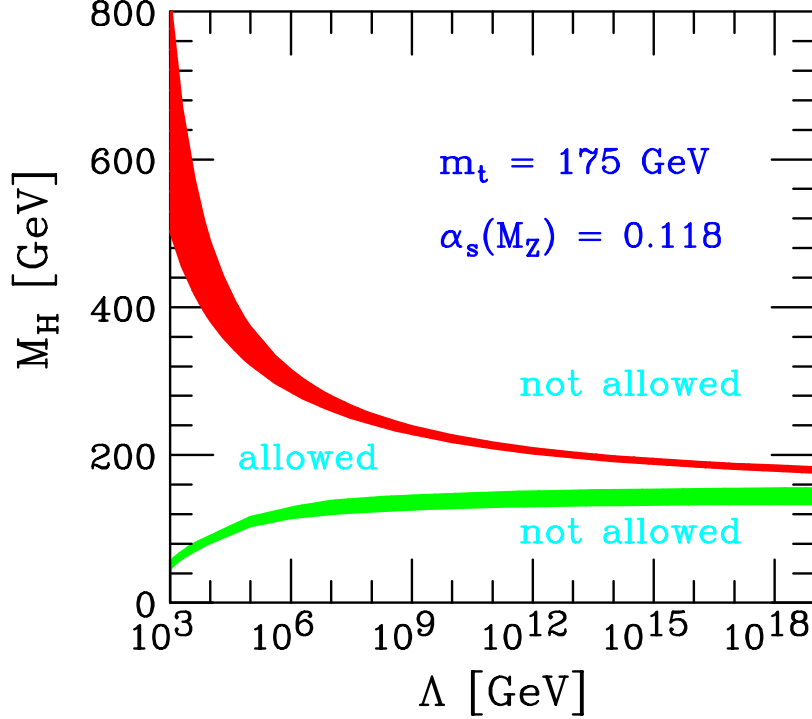


Figure 7: The triviality (upper) bound and the vacuum stability (lower) bound on the Higgs boson mass as a function of the New Physics or cut-off scale Λ for a top quark mass $m_t = 175 \pm 6$ GeV and $\alpha_s(M_Z) = 0.118 \pm 0.002$; the allowed region lies between the bands and the colored/shaded bands illustrate the impact of various uncertainties. Taken from Ref. [82] according to Ref. [45].

In the end the Higgs boson mass is allowed to be in the range

$$50 \text{ GeV} \lesssim M_H \lesssim 750 \text{ GeV} \quad (3.24)$$

when new physics is to arise at the TeV scale, taking also into account the unitarity constraint. If we require that the SM be valid up to the Grand Unification scale, $\Lambda_{\text{GUT}} \simeq 10^{16}$ GeV, the Higgs boson mass should lie in the range

$$130 \text{ GeV} \lesssim M_H \lesssim 180 \text{ GeV} \quad (3.25)$$

3.2 Experimental bounds on the Higgs mass

The experimental quest for the evidence of the SM Higgs boson has started more than twenty years ago, at the CERN Large Electron Positron (LEP) collider. As the Higgs boson has sizeable contributions to radiative corrections to many processes in the SM, its existence can be probed through its effects on electroweak observables. Hence we can obtain indirect constraints on its mass. We will also present of course the constraints obtained with its direct search both at the LEP collider and the Fermilab Tevatron collider. We

note that the last constraint, obtained at the Tevatron, will be challenged in the following chapters of this thesis.

3.2.1 Indirect searches through precision data

The SM has been tested in many experiments for decades and the results have reached a very high precision. It then imposes stringent conditions on new physics phenomena as well as on the Higgs boson itself, the only yet unknown SM particle to be discovered.

We will summarize the electroweak precision data used to constraint indirectly the SM Higgs boson mass, classified by the different experiments:

- *LEP1 searches:* LEP1 was the first era of running for the LEP collider, when the designed center-of-mass energy was 110 GeV (the actual energy used was 45.6 GeV per beam near the Z peak). This has given us much information on the Z lineshape: the Z mass, the total Z width Γ_Z , the peak hadronic cross section $\sigma^{\text{had}} \equiv \sigma(e^+e^- \rightarrow \text{hadrons})$, the ratio $R_{\ell,c,b}$ between the Z partial decay width into leptons, charm and bottom quarks, and the total hadronic Z decay width, the forward-backward asymmetries A_{FB}^f for leptons and heavy c, b quarks, the τ polarization asymmetry A_{pol}^τ , etc.
- *LEP2 searches:* LEP2 was the second step for the LEP collider when the designed energy did reach 209 GeV center-of-mass energy in 2000, the year of the end of the collider operations. It has given valuable information on the W boson: its mass M_W , the total decay width Γ_W , again the different asymmetries that are used to measure $\sin^2 \theta_W$ through the lepton channel, the hadronic contribution $\Delta_{\text{had}}^{(5)} \alpha$ to the value of α , etc. As discussed in the next subsection the Higgs boson was also hunted directly at LEP2.
- *SLC searches:* The Stanford Linear Collider (SLC) experiments in the beginning of the nineties have given unique results at the high precision level in electroweak physics thanks to its very polarized beams. The longitudinal polarization asymmetry A_{LR}^f which has been measured at the SLC thus gives the best individual measurement of $\sin^2 \theta_W$. It has also measured the left-right forward-backward asymmetries for the heavy b, c quarks, $A_{LR,FB}^{b,c}$.
- *Tevatron searches:* The Fermilab Tevatron collider has started to operate in 1987 and will end running in the end of 2011. It has given precise measurements of the W mass, the total decay width Γ_W and in particular of the top quark mass m_t , which were discovered at the Tevatron in 1995. Being a proton-antiproton collider it is also a good place to measure asymmetries. Its most important experimental program is the search for the Higgs boson, and as discussed later it has given direct constraints on its mass.

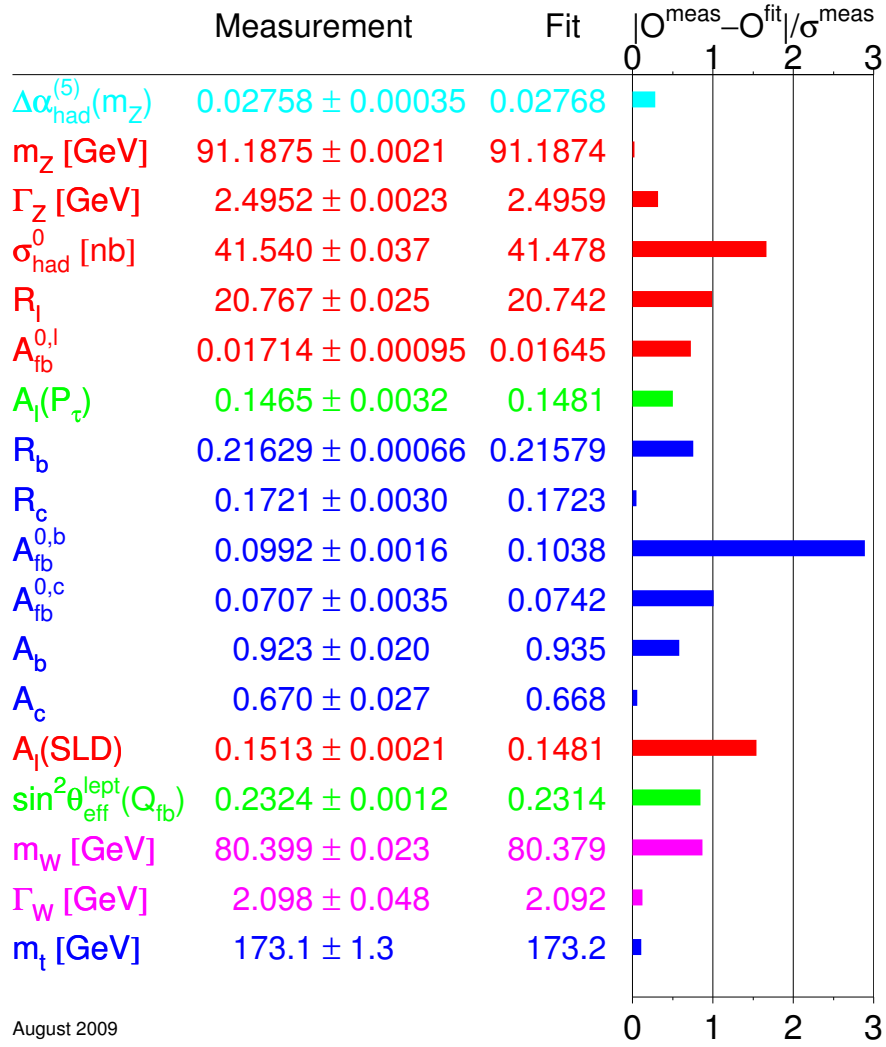


Figure 8: The SM fits results compared to the data for electroweak precision observables, together with the standard deviations. Figure taken from the LEP EW Working Group webpage, dated on August 2009.

- In addition there are high-precision measurements at low energies, for example the ν_μ - and $\bar{\nu}_\mu$ -nucleon deep-inelastic scattering cross sections, from which we can extract a determination of $\sin^2\theta_W$ through the measure of the Z couplings to fermions, both the right-handed and the left-handed.

The comparison with the SM calculation of all these precision data is displayed in Fig. 8 which has been taken from LEP ElectroWeak Working Group webpage. The theoretical predictions are in a very good agreement with the data, apart from a tension in the measure of the forward-backward asymmetry for the b -quark which is nearly 3σ away from the SM value.

When combining all these precision data measurements, stringent constraints on SM

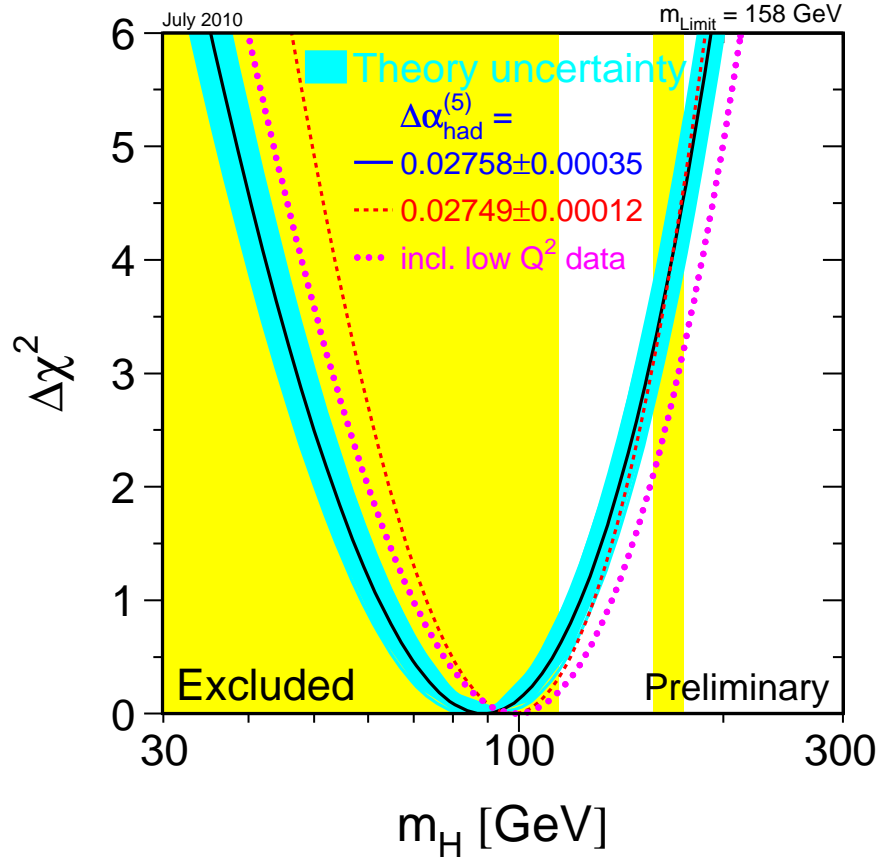


Figure 9: The $\Delta\chi^2$ of the fit of the electroweak precision data to the predictions of the SM as a function of the SM Higgs mass value. The solid line include all data but the low energies data, and the effect of varying the $\Delta_{\text{had}}^{(5)}\alpha$ is also shown.

the Higgs boson mass can be obtained. When one performs a fit on all the data, the $\Delta\chi^2 = \chi^2 - \chi_{\text{min}}^2$ of the fit displayed in Fig. 9 is obtained, depending on the Higgs boson mass.

On the left of the plot the area depicted in yellow (shaded), close to the minimum value of the fit, is the excluded limit by the LEP2 experiments as discussed just below. The small yellow (shaded) band on the right of the plot displays the limits set by the Tevatron run II experiments, again discussed later on. The fitted SM Higgs boson mass is then

$$M_H = 89_{-26}^{+35} \text{ GeV} \quad (3.26)$$

and the 95%CL upper bound is

$$M_H \leq 158 \text{ GeV at 95\%CL} \quad (3.27)$$

This last limit can be a bit relaxed if the direct search limits at the LEP and the Tevatron colliders are taken into account in the fit, leading to $M_H \leq 185$ GeV at 95%CL. The data thus strongly disfavour a very heavy SM Higgs boson $M_H \lesssim 700$ GeV which anyway is (nearly) outside the theoretical bounds presented above.

It should be worth mentioning that the SM fit is not as good because of the nearly 3σ deviation of the forward–backward asymmetry of the b -quark $A_{\text{fb}}^{0,b}$. Nevertheless if this quantity were removed from the fit, the obtained central value for the Higgs boson mass together with the uncertainties would fall below the direct search limit, increasing the tension between the central value from the EW fit and the bounds obtained by the direct searches.

3.2.2 Direct searches at the LEP collider

Direct searches of the SM Higgs boson started at the LEP collider in the LEP1 era, but the interesting results have been obtained during the LEP2 era when $\sqrt{s} = 209$ GeV. The dominant production channel is the Higgs–strahlung $e^+e^- \rightarrow ZH$, see Refs. [83–89]. The search has been conducted in several final states topologies:

- *Final state $b\bar{b}\nu\bar{\nu}$* : this final state is obtained with $H \rightarrow b\bar{b}$ together with $Z \rightarrow \nu\bar{\nu}$.
- *Final state $b\bar{b}\ell^+\ell^-$* : with $\ell = e, \mu$ this is obtained with the same SM Higgs decay as above but with a leptonic Z decay $Z \rightarrow \ell^+\ell^-$.
- *Final state $b\bar{b}\tau^+\tau^-$* : this topology is obtained through two different channels, $e^+e^- \rightarrow (H \rightarrow b\bar{b}) (Z \rightarrow \tau^+\tau^-)$ and $e^+e^- \rightarrow (H \rightarrow \tau^+\tau^-) (Z \rightarrow b\bar{b})$ as the two Higgs decay channel are sizeable, see section 6.

Even if there were tantalizing results in the end of year 2000 of the observation of a SM Higgs boson around 115 GeV, the excess of 1.7σ (after a re–evaluation as the first claimed observation was of 2.9σ evidence) was not significant enough to claim a discovery [46]. The combination of the results from the OPAL, L3, DELPHI and ALEPH experiments at LEP has set an exclusion limit

$$M_H > 114.4 \text{ GeV at } 95\% \text{CL} \quad (3.28)$$

This is displayed in Fig. 10, which shows the statistical CL_s for the signal plus background hypothesis as a function of the Higgs boson mass. If the CL_s is below 0.05 the Higgs boson mass is excluded. The expected exclusion is found to be $M_H > 115.3$ GeV, the discrepancy with the observed exclusion being due to the excess discussed above.

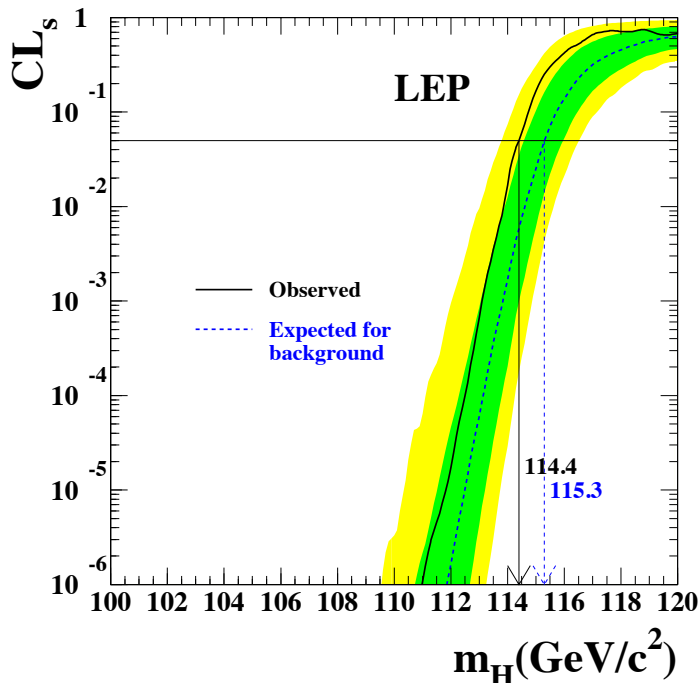


Figure 10: Confidence level CL_s for the signal plus background hypothesis in the Higgs production at LEP2. The black (solid) line is for the observed value, the blue (dashed) line is for the expected value. The intersection between the horizontal line $CL_s = 0.05$ with the data lines define the lower 95%CL limit on the SM Higgs boson mass. Figure taken from Ref. [46].

It is worth mentioning that this direct search limit is rather robust as it has been obtained in pure electroweak processes (at LO). In particular the theoretical uncertainties on the predicted cross section times branching ratios used for the comparison with the data are very small; this has to be compared with the direct search limit discussed in the following at the Tevatron collider which is a hadron collider.

3.2.3 Direct searches at the Tevatron collider

The direct search for the SM Higgs boson at the Fermilab Tevatron collider is its major experimental program and started more than a decade ago. The production channel will be discussed in details in the next section, but we can already mention briefly that there are two dominant channels, the Higgs-strahlung processes $p\bar{p} \rightarrow HV$ with $V = W, Z$ for low Higgs mass searches $M_H \lesssim 135$ GeV, and the gluon-gluon fusion channel $gg \rightarrow H$ for high Higgs mass searches $M_H \gtrsim 135$ GeV. The most important decay channels used at the Tevatron are the hadronic $H \rightarrow b\bar{b}$ decay for low Higgs mass searches and the bosonic $H \rightarrow W^{(*)}W^{(*)}$ for high Higgs mass searches. Again, this will be discussed in details in the following, see section 6.1.

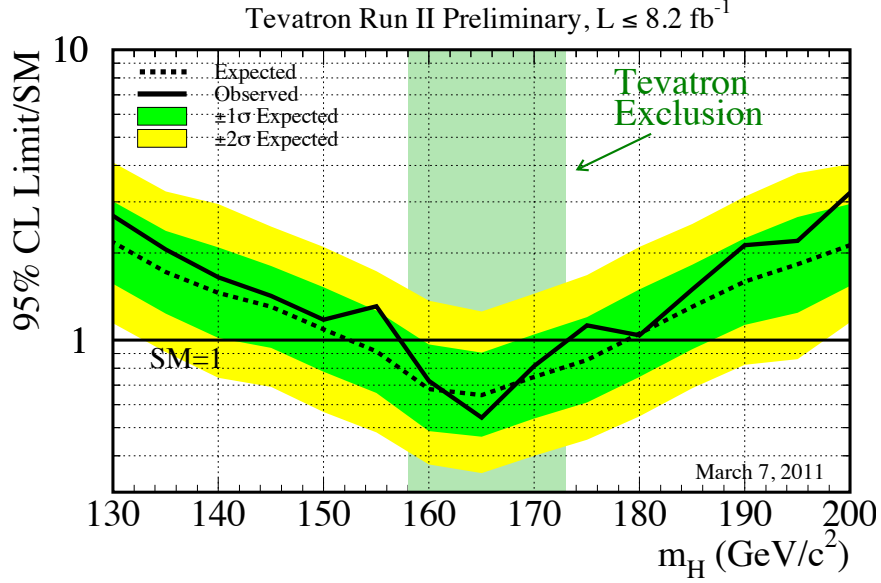


Figure 11: Ratio R between the 95%CL exclusion cross section and the predicted SM cross section as a function of the SM Higgs boson mass at the Tevatron run II. The solid black line shows the observed value and the dashed black lines shows the expected value. When the lines fall below the $R = 1$ the Higgs boson mass is excluded at 95%CL. This exclusion band is displayed by the light green (shaded) band. Figure taken from Ref. [93].

The Tevatron has collected enough luminosity to be sensitive to Higgs signal for $M_H \simeq 165$ GeV, but has not yet seen the elusive particle. For the first time since the LEP experiments it was able to produce a new exclusion limit in the year 2008 [90] which then was extended in the next years [91, 92] to reach the current exclusion limit [93] at 95%CL:

$$M_H \leq 158 \text{ GeV or } M_H \geq 173 \text{ GeV at 95\%CL} \quad (3.29)$$

This is displayed in Fig. 11 where the ratio between the 95%CL exclusion limit on the Higgs cross section and the SM prediction is shown as a function of the SM Higgs boson mass. When the ratio falls below the unity the SM Higgs boson mass is excluded.

We remind the reader that this impressive result has been obtained at a hadron collider. Contrary to the result 3.28 obtained at the LEP collider, which is rather robust and theoretically well behaved, the exclusion limit at the Tevatron is based upon a comparison between data and SM prediction at a hadron collider, which are well known to be plagued with various theoretical uncertainties as discussed in this thesis. We will see that these limits are put into question, see Refs. [94, 95], and that will be discussed in particular in section 6.5.

4 Higgs production at the Tevatron

The Fermilab Tevatron collider has started its operation back in 1987 and has been the home of major particle physics discoveries, e.g. the discovery of the top quark in 1995 which leads to a Nobel prize. The Higgs search program is currently one of the most important research plan for the collider. In this context, the CDF and D0 experiments at the Tevatron have collected enough data to be sensitive to the Standard Model Higgs boson. The two collaborations recently performed a combined analysis on the search for this particle and excluded at the 95% confidence level the possibility of a Higgs boson in the mass range between 158 and 173 GeV [90–93] (see section 3.2). We are thus entering a new era in the quest of the Higgs particle as this is the first time that the mass range excluded by the Large Electron–Positron (LEP) collaborations in the late 1990s, $M_H \geq 114.4$ GeV [46], is extended.

Although current hadronic colliders have a center-of-mass energy that is greater than the LEP energy, which is good to produce new physics events, QCD interactions are dominant and plague the theoretical prediction with various sources of uncertainties in contrast with the predictions obtained at LEP where the production cross sections were mainly sensitive to (small) electroweak effects which are well under control. Among these are the contributions of yet uncalculated higher order corrections which can be important as the strong coupling constant α_s is rather large; the errors due to the folding of the partonic cross sections with the parton distribution functions (PDFs) to obtain the production rates at the hadronic level; and the errors on some important input parameters such as α_s . An accurate calculation of the estimation of these uncertainties is then mandatory in order to have a complete theoretical prediction for the production rates and eventually the production cross section times branching ratio prediction. It would allow for a consistent comparison with the experimental data available at the Tevatron which are described in term of exclusion bounds⁹.

At the Tevatron, only two production channels are important for the Standard Model Higgs boson¹⁰. In the moderate to high mass range, $140 \text{ GeV} \lesssim M_H \lesssim 200 \text{ GeV}$, the Higgs boson decays dominantly into W boson pairs (with one W state being possibly off

⁹An example of such a situation is the $p\bar{p} \rightarrow b\bar{b}$ production cross section that has been measured at the Tevatron (and elsewhere) and which was a factor of two to three larger than the theoretical prediction, before higher order effects and various uncertainties were included [96].

¹⁰The CDF/D0 exclusion limits [90, 92] have been obtained by considering a large variety of Higgs production and decay channels (36 and 54 exclusive final states for, respectively, the CDF and D0 collaborations) and combining them using artificial neural network techniques. However, as will be seen later, only a few channels play a significant role in practice.

mass-shell) [97, 98] and the main production channel is the gluon–gluon fusion mechanism $gg \rightarrow H$ [99] which proceeds through heavy (mainly top and, to a lesser extent, bottom) quark triangular loops. The Higgs particle is then detected through the leptonic decays of the W bosons, $H \rightarrow WW^{(*)} \rightarrow \ell^+ \nu \ell^- \bar{\nu}$ with $\ell = e, \mu$, which exhibits different properties than the $p\bar{p} \rightarrow W^+W^- \rightarrow \ell\ell$ plus missing energy continuum background [100].

It is well known that the $gg \rightarrow H$ production process is subject to extremely large QCD radiative corrections [101–112]. In contrast, the electroweak radiative corrections are much smaller, being at the level of a few percent [113–118] as in the case of Higgs production at the LEP collider. For the corrections due to the strong interactions, the K -factor defined as the ratio of the higher order (HO) to the lowest order (LO) cross sections, consistently evaluated with the α_s value and the PDF sets at the chosen order,

$$K_{\text{HO}} = \sigma^{\text{HO}}|_{(\alpha_s^{\text{HO}}, \text{PDF}^{\text{HO}})} / \sigma^{\text{LO}}|_{(\alpha_s^{\text{LO}}, \text{PDF}^{\text{LO}})}, \quad (4.1)$$

is about a factor of two at next-to-leading order (NLO) [101–105] and about a factor of three at the next-to-next-to-leading order (NNLO) [107–109]. In fact, this exceptionally large K -factor is what allows a sensitivity on the Higgs boson at the Tevatron with the presently collected data. Nevertheless, the K -factor is so large that one may question the reliability of the perturbative series, despite of the fact that there seems to be kind of a convergence of the series as the NNLO correction is smaller than the NLO correction¹¹.

In the low mass range, $M_H \lesssim 140$ GeV, the main Higgs decay channel is $H \rightarrow b\bar{b}$ [97] and the gg fusion mechanism cannot be used anymore as the $gg \rightarrow H \rightarrow b\bar{b}$ signal is swamped by the huge QCD jet background. The Higgs particle has then to be detected through its associated production with a W boson $q\bar{q} \rightarrow WH$ [119] which leads to cleaner $\ell\nu b\bar{b}$ final states [120]. Additional topologies that can also be considered in this context are $q\bar{q} \rightarrow WH$ with $H \rightarrow WW^* \rightarrow \ell\nu\nu$ or the twin production process $q\bar{q} \rightarrow ZH$ with the subsequent decays $H \rightarrow b\bar{b}$ and $Z \rightarrow \nu\bar{\nu}$ or $\ell^+\ell^-$. Other production/decay channels are expected to lead to very low rates and/or to be affected with too large QCD backgrounds.

At the Tevatron, the Higgs–strahlung processes $q\bar{q} \rightarrow VH$ with $V = W, Z$ receive only moderate higher order corrections: the QCD corrections increase the cross sections by about 40% at NLO [121–125] and 10% at NNLO [126], while the impact of the one–loop electroweak corrections is small, leading to a $\approx 5\%$ decrease of the cross sections [127]. Thus, in contrast to the gluon–gluon fusion process, the production cross sections in the Higgs–strahlung processes should be well under control. The purpose of this section is to study the Higgs boson production at the Tevatron in these two main search channels, including all

¹¹At LHC energies, the problem of the convergence of the perturbative series is less severe as the QCD K -factor is only ~ 1.7 at NLO and ~ 2 at NNLO in the relevant Higgs mass range.

relevant higher order QCD and electroweak corrections, using the latest MSTW 2008 set of PDFs [128]¹² and comparing with other PDFs set available on the market. The calculation has been performed in various recent analyses [111, 118] for the gluon–gluon fusion process and CDF/D0 collaborations for example used their normalized cross sections to produce the Higgs mass 95% CL limits [90, 92] in their combined analysis. The results were published in [94] and were the first update for the Higgs–strahlung production channels $q\bar{q} \rightarrow VH$ with the newest PDFs available on the market. The Tevatron analyses before July 2010 used the normalised cross sections available in Refs. [130, 131] which make use of the old MRST2002 set of PDFs [132], a parametrisation that was approximate as it did not include the full set of evolved PDFs at NNLO. For completeness, an update of the cross sections for the two other single Higgs production channels at hadron colliders will also be presented briefly: the weak boson fusion $p\bar{p} \rightarrow qqH$ [85, 133–137] and the associated production with top quark pairs $p\bar{p} \rightarrow t\bar{t}H$ [138–144]. These channels play only a minor role at the Tevatron but have also been included in the CDF/D0 analysis [90, 92].

The study of the Higgs boson production will also include a comprehensive investigation of all possible sources of uncertainties mentioned earlier that have a significant impact on the central prediction for the two main search channels. We will first discuss the choice of the central renormalization scale μ_R and factorization scale μ_F in the gluon–gluon fusion mechanism and explain why some choices have been made about the order of calculation. We will then begin the study of the uncertainties with the analysis of the unknown higher order effects, which are usually estimated by exploring the cross sections dependence on the renormalization scale μ_R and the factorization scale μ_F . In most recent analyses, the two scales are varied within a factor of two from a median scale which is considered as the most natural one. We show that this choice slightly underestimates the higher order effects and we use a criterion that allows a more reasonable estimate of the latter: the range of variation of the two scales μ_R and μ_F should be the one which allows the uncertainty band of the LO/NLO cross section to match the central value of the cross section at the highest calculated order. In the case of $gg \rightarrow H$, for the uncertainty band of the LO cross section to reach the central result of the NNLO cross section, a variation of μ_R and μ_F within a factor of ~ 3 from the central value $\mu_R = \mu_F = \frac{1}{2}M_H$ is required; this choice of central scale will also be discussed. When the scales are varied within the latter range, one obtains an uncertainty on the NNLO cross section of $\approx 18\%$, which is slightly larger than what is usually assumed in inclusive calculation. We will see that we obtain result that is comparable with what is used in current Tevatron combined analysis and which comes from 0,1,2 jets bin analysis [112].

¹²The PDFs are available in Ref. [129].

We then discuss the errors resulting from the folding of the partonic cross sections with the parton densities, considering not only the recent MSTW set of PDFs as in Refs. [111, 112, 118], but also two other PDF sets that are available in the literature: CTEQ [145]¹³ and ABKM [147]¹⁴. We will also make a comprehensive comparison of all the NNLO available PDFs set on the market: apart from MSTW and ABKM we will also consider HERAPDF [149] and JR09 [150]. In the case of the cross section for the $gg \rightarrow H$ process at the Tevatron, we find that while the PDF uncertainties evaluated within the same scheme are moderate, as also shown in Refs. [111, 112, 118], the central values of the cross sections obtained using the three schemes can be widely different. We show that it is only when the experimental as well as the theoretical errors on the strong coupling constant α_s are accounted for that one obtains results that are consistent when using the MSTW/CTEQ and ABKM schemes. As a result, the sum of the PDF+ $\Delta^{\text{exp}}\alpha_s$ and $\Delta^{\text{th}}\alpha_s$ uncertainties, that we evaluate using a set-up recently proposed by the MSTW collaboration to determine simultaneously the errors due to the PDFs and to α_s , is estimated to be at least a factor of two larger than what was generally assumed in earlier analyses before the publication of Ref. [94]. We will also show that the error we obtain is actually comparable to what should be taken when using the PDF4LHC recommendation [151].

Finally, a third source of potential errors is considered in the gg fusion mechanism: the one resulting from the use of an effective field theory approach, in which the loop particle masses are assumed to be much larger than the Higgs boson mass, to evaluate the NNLO contributions. While this error is very small in the case of the top-quark contribution at the Tevatron, it is at the percent level in the case of the b -quark loop contribution at NNLO QCD where the limit $M_H \ll m_b$ cannot be applied and where the b -loop is indeed totally absent as there are no b -loop NNLO calculation available up until now. This is also the case of the three-loop mixed QCD-electroweak radiative corrections that have obtained in the effective limit $M_H \ll M_W$, which lead to a few percent uncertainty. In addition, an uncertainty of about 1% originates from the freedom in the choice of the input b -quark mass in the Hgg amplitude. The total uncertainty in this context is thus not negligible and amounts to a few percent.

We then address the important issue of how to combine the theoretical errors originating from these different sources. Since using the usually adopted procedures of adding these errors either in quadrature, as is done by the experimental collaborations for instance, or linearly as is generally the case for theoretical errors, lead to either an underestimate or to an overestimate of the total error, we propose a procedure that seems to be more adequate. One first determines the maximal and minimal values of the cross sections obtained from

¹³The PDFs are available in Ref. [146].

¹⁴The PDFs are available in Ref. [148].

the variation of the renormalization and factorization scales, and then estimate directly on these extrema cross sections the combined uncertainties due to the PDFs and to the experimental and theoretical errors on α_s . The other smaller theoretical uncertainties, such as those coming from the use of the effective approach in $gg \rightarrow H$, can be then added linearly to this scale, PDF and α_s combined error.

We will in the end show that the total theoretical error that we obtain is nearly twice the one often quoted in the literature and used for the Tevatron analyses. In particular, in the case of the most sensitive Higgs production channel at the Tevatron, $gg \rightarrow H \rightarrow \ell\nu\nu$, the overall uncertainty on the NNLO total cross section is found to be of the order of $\pm 40\%$. This is significantly larger than the uncertainty of $\approx \pm 20\%$ assumed by the CDF/D0 combined Higgs search analysis. As a result, we believe that the exclusion range given by the Tevatron experiments for the Higgs mass in the Standard Model, $158 \text{ GeV} \leq M_H \leq 173 \text{ GeV}$, should be discussed in the light of these results and that will be discussed in section 6.5.

4.1 The main production channels

We present the procedure used to obtain the central or “best” values of the total cross sections for SM Higgs production at the Tevatron. We recall the reader that we mainly concentrate on the two main search channels, that is the gluon–gluon fusion and Higgs–strahlung processes, but we also mention very briefly the two other productions channels for single Higgs production: the vector boson fusion and the associated Higgs production with top quark pairs.

The Higgs production at hadron colliders, as for any hadronic process, requires that the partonic elements which actually collide have to be extracted from the initial (anti)protons. This is summarized by the factorization procedure which is behind the concept of parton distribution functions (PDFs): a PDF for a parton Y evaluated at the scale Q and for a momentum fraction x is the probability to extract from the (anti)proton the parton Y at the scale Q with a linear momentum $x \times \vec{P}$ where \vec{P} is the initial linear momentum of the (anti)proton. We then have to factorize the PDF with the partonic production cross section.

If we call S for the center–of–mass energy and \hat{s} for the partonic center–of–mass energy, x_1 for the momentum fraction of the first parton and x_2 for the momentum fraction of the second parton, we have $\hat{s} = x_1 x_2 S$ in the massless limit for the two incoming partons, which is always the case at current hadronic colliders (we just have to compare the mass of the (anti)proton which is nearly 1 GeV to the Tevatron 1.96 TeV center–of–mass energy). We then have

$$\sigma(p\bar{p} \rightarrow AB) = \sum_{i,j} \int_0^1 f_i(x_1) dx_1 \int_0^1 f_j(x_2) dx_2 \hat{\sigma}_{ij}(\hat{s} = x_1 x_2 S) \Theta(\hat{s} \geq (M_A + M_B)^2) \quad (4.2)$$

where $\hat{\sigma}_{i,j}$ is the partonic cross section $ij \rightarrow AB$ and Θ is the usual step function. The dependence of the PDFs over the scale Q called the factorization scale μ_F has been made implicit in the equation above for simplification. We sum over all possible initial partonic states and we could also include additional jets in the production denoted collectively by X . If we make the following variable replacement $x_2 = \frac{\hat{s}}{x_1 S}$ we obtain

$$\sigma(p\bar{p} \rightarrow AB) = \sum_{i,j} \int_0^1 dx_1 f_i(x_1) \int_{(M_A+M_B)^2}^{x_1 S} \frac{d\hat{s}}{S} f_j\left(\frac{\hat{s}}{x_1 S}\right) \hat{\sigma}_{ij}(\hat{s}) \quad (4.3)$$

then followed by the reordering of the interval of variation of \hat{s} and x_1 which then gives

$$\sigma(p\bar{p} \rightarrow AB) = \sum_{i,j} \int_{(M_A+M_B)^2}^S d\hat{s} \frac{\hat{\sigma}_{ij}(\hat{s})}{S} \int_{\hat{s}/S}^1 f_i(x_1) f_j\left(\frac{\hat{s}}{x_1 S}\right) \frac{dx_1}{x_1} \quad (4.4)$$

We finally use the following variables: $\tau_{AB} = \frac{(M_A + M_B)^2}{S}$, $\tau = \frac{\hat{s}}{S}$ and obtain

$$\sigma(p\bar{p} \rightarrow AB) = \sum_{i,j} \int_{\tau_{AB}}^1 d\tau \hat{\sigma}_{ij}(\hat{s} = \tau S) \int_{\tau}^1 f_i(x) f_j\left(\frac{\tau}{x}\right) \frac{dx}{x} \quad (4.5)$$

The quantity $\frac{d\mathcal{L}^{ij}}{d\tau}(\tau) = \int_{\tau}^1 f_i(x) f_j\left(\frac{\tau}{x}\right) \frac{dx}{x}$ is called the ij luminosity. This quantity encodes all the necessary information that is stored in the PDFs.

We are now ready to describe the calculation of the production cross sections of the two main channels at the Tevatron.

4.1.1 The gluon–gluon fusion

The production rate for the $gg \rightarrow H + X$ process, where X denotes the additional jets that appear at higher orders in QCD, is evaluated following the Eq. 4.5. We then define the

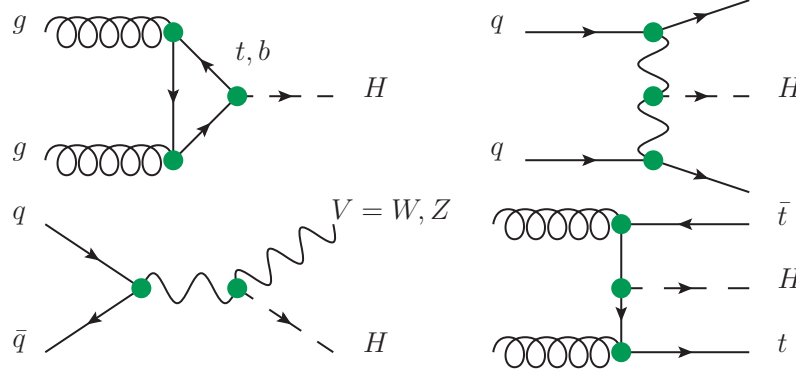


Figure 12: The Feynman diagrams for the four main channels for SM Higgs production at hadron colliders as discussed in the text: the gluon–gluon fusion $gg \rightarrow H$ (upper left), the vector boson fusion $q_1q_2 \rightarrow q_1q_2H$ (upper right), the Higgs–strahlung channels $q\bar{q} \rightarrow VH$ with $V = W, Z$ (lower left) and the associated top quark production $p\bar{p} \rightarrow t\bar{t}H$ (lower right).

variable $\tau_H = \frac{M_H^2}{S}$ which is our τ_{AB} , and we also define a new variable $z = \frac{\tau_H}{\tau}$ which quantify the departure from the soft–gluon limit $z \rightarrow 1$ where $\hat{s} \rightarrow S$ with no jets production.

This cross section is already a loop calculation at leading order (LO) in QCD, as it involves in the SM triangular quark loops, mainly the top quark and in a lesser extent the bottom quark, see Fig. 12. We write the total cross section in α_s expansion as

$$\sigma(p\bar{p} \rightarrow H) = \sum_{(ij)} \int_{\tau_H}^1 d\tau \frac{d\mathcal{L}^{ij}}{d\tau}(\tau) \alpha_s^2 \sigma^0 \left(\delta_{ij}^{(0)}(z) + \frac{\alpha_s}{\pi} \delta_{ij}^{(1)}(z) + \left(\frac{\alpha_s}{\pi} \right)^2 \delta_{ij}^{(2)}(z) + \dots \right) \quad (4.6)$$

(ij) means either gg which occurs already at LO, or qg and $q\bar{q}/qq/qq'$ pairs which occur from the NLO, see Fig. 13 for typical NLO diagrams. σ^0 is the LO kernel and $\delta_{ij}^{(K)}$ is the K th order correction to the total cross section induced by a (ij) partonic initial state. We have

$$\sigma^0 = \frac{G_F}{288\pi\sqrt{2}} \left| \frac{3}{4} \sum_q A(\tau_q) \right|^2 \quad (4.7)$$

with $G_F = 1.16637 \times 10^{-5} \text{ GeV}^{-2}$ as the Fermi constant. In Eq. 4.7 we have $\tau_q = \frac{M_H^2}{4m_q^2}$

and

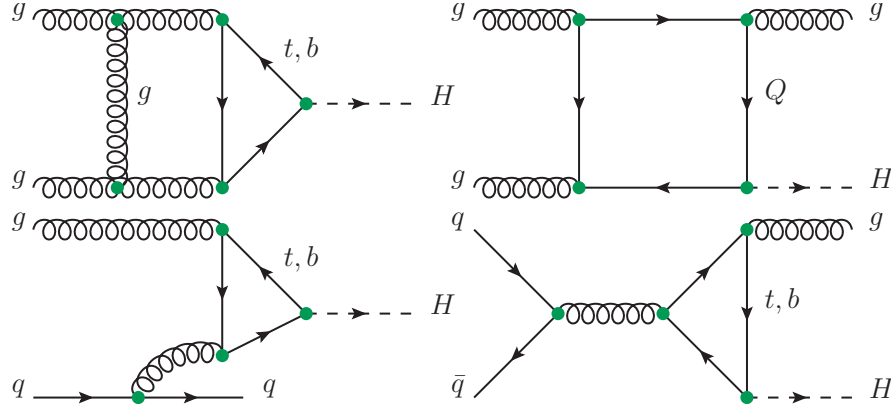


Figure 13: Some Feynman diagrams for the NLO corrections to $gg \rightarrow H$ SM Higgs production channel.

$$A(\tau) = 2 \left(\frac{1}{\tau} + \frac{\tau - 1}{\tau^2} f(\tau) \right)$$

$$f(\tau) = \begin{cases} \arcsin^2 \sqrt{\tau} & \tau \leq 1 \\ -\frac{1}{4} \left[\ln \frac{1 + \sqrt{1 - \tau^{-1}}}{1 - \sqrt{1 - \tau^{-1}}} - i\pi \right]^2 & \tau \geq 1 \end{cases} \quad (4.8)$$

The cross section for SM Higgs production in gluon–gluon fusion is then evaluated in the following way. Up to NLO in QCD we use the Fortran code `HIGLU` [152]¹⁵ which includes the complete set of radiative corrections at this order, taking into account the full dependence on the top and bottom quark masses [105]. We also want to take into account the NNLO corrections that are known in an effective approach where only the dominant top quark contribution is included in the limit where the top mass is taken as infinite [107–109], see Fig. 14 for some NNLO diagrams. These contributions are implemented into the code taking the analytical expression given in Ref. [108]. We rescale the NNLO correction by the full m_t dependent Born cross section, an approximation which at NLO is accurate at the level of a few percent for Higgs masses below the $t\bar{t}$ kinematical threshold, $M_H \lesssim 300$ GeV [105, 106].

The dependence on the renormalization scale μ_R and the factorization scale μ_F of the partonic NNLO cross sections has been reconstructed from the scale independent expressions of Ref. [108] using the fact that the full hadronic cross sections do not depend on them and the α_s running between the μ_F and μ_R scales¹⁶. Indeed, the complete cross section taking into account all orders in perturbation theory should not depend on the (unphysical) renormalization and factorization scales; we first take $\mu_F = \mu_R = \mu$ and we then have

¹⁵The public code is available in Ref. [153].

¹⁶The analytical expressions for the scale dependence have only been given in Ref. [109] in the limit $\mu_F = \mu_R$ from which one can straightforwardly obtain the case $\mu_F \neq \mu_R$ as stated in the text (see also Ref. [154]).

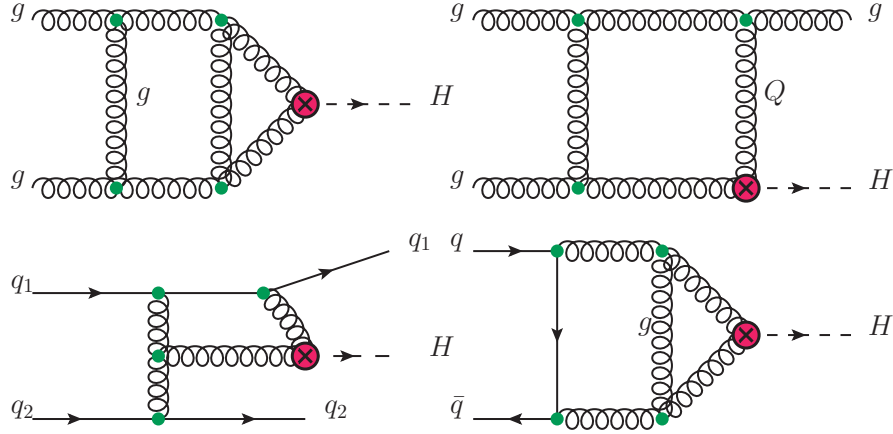


Figure 14: Some Feynman diagrams for the NNLO corrections to $gg \rightarrow H$ SM Higgs production channel in the infinite top mass limit. The red circle with a cross represents the effective Hgg vertex where the top quark has been integrated out.

$\frac{d\sigma}{d\ln\mu^2} = 0$. This equation is then expressed in term of the evolution of the partonic cross section convoluted with DGLAP evolution for the PDFs, which expressed order by order in α_s gives the dependence on the scale μ of $\hat{\sigma}_{ij}$ (see also Ref. [108]).

In the end we can obtain the final μ_R -dependent terms using the evolution of the strong coupling constant α_s between $\alpha_s(\mu = \mu_F)$ and $\alpha_s(\mu_R)$. For NNLO terms the LO evolution is nearly enough:

$$\alpha_s(\mu_F) = \alpha_s(\mu_R) \left(1 + \alpha_s(\mu_R) b_0 \ln \left(\frac{\mu_R^2}{\mu_F^2} \right) \right) \quad (4.9)$$

with $b_0 = \frac{33 - 2n_f}{12\pi}$ as the first term in the β -function of QCD strong coupling constant α_s , where n_f stands for the number of active flavors in the running (here $n_f = 5$). The NLO running of α_s with $b_1 = \frac{153 - 19n_f}{24\pi^2}$ is needed only for the NNLO gg virtual correction coming from the LO gg diagram. The complete μ_R -dependent terms at NNLO are available in the appendix 4.A of this section.

What will be the choice for the central scale $\mu_0 = \mu_R = \mu_F$? The usual choice would be to use $\mu_0 = M_H$ as it seems to be the most natural scale fixed by the dynamics of the process. Some results using this scale choice can be found in the first pages of Ref. [94] and have been derived before some criticisms, made by the members of the Tevatron New Physics and Higgs working group (TEVNPHWG) of the CDF and D0 collaborations [155] concerning the theoretical modeling of the $gg \rightarrow H$ production cross section proposed in the beginning of Ref. [94] appeared on the web in May 2010. A new analysis was then derived with a new central scale $\mu_0 = \frac{1}{2}M_H$ after ICHEP 2010 (in July 2010) as we got

aware of the criticisms only during ICHEP¹⁷ where the new combined analysis of CDF and D0 for the Higgs search at the Tevatron was released [91, 157]. This new analysis addressed the criticisms and reinforced the conclusion of the first pages of Ref. [94]¹⁸. We will then use in the rest of the thesis the scale choice $\mu_0 = \frac{1}{2} M_H$ as explained below.

Although soft-gluon resummation contributions for the total cross section have been calculated up to next-to-next-to-leading logarithm (NNLL) [110] we do not include them in our calculation. There are also other additional estimated small contributions at N³LO [159] as well as beyond the soft NNLL approximation [160–163] that we do not include. There are some reason to do so, that we explain in three points:

- these corrections are known only for the inclusive total cross section and not for the cross sections when experimental cuts are incorporated; this is also the case for the differential cross sections [164–167] and many distributions that are used experimentally, which have been evaluated only at NNLO at most. Even if we concentrate on the total cross section in this work, we should have in mind that these results are then used in experimental analyses which also take differential cross sections. In order to be fully consistent in the whole analysis, our total cross section should be calculated at NNLO. This interpretation is strengthened by the CDF/D0 analysis itself [91–93], as the $gg \rightarrow H$ cross section in this analysis has been broken into three pieces which yield different final state signal topologies for the main decay $H \rightarrow WW^{(*)} \rightarrow \ell\nu\nu$, namely $\ell\nu\nu+0\text{jet}$, $\ell\nu\nu+1\text{jet}$ and $\ell\nu\nu+2\text{jets}$ or more:

$$\sigma_{gg \rightarrow H}^{\text{NNLO}} = \sigma_{gg \rightarrow H}^{0\text{jet}} + \sigma_{gg \rightarrow H}^{1\text{jet}} + \sigma_{gg \rightarrow H}^{\geq 2\text{jets}} \quad (4.10)$$

These channels have been analyzed separately and these individual components, with $\sigma_{gg \rightarrow H}^{0\text{jet}}$ evaluated at NNLO, $\sigma_{gg \rightarrow H}^{1\text{jet}}$ evaluated at NLO and $\sigma_{gg \rightarrow H}^{\geq 2\text{jets}}$ evaluated at LO, represent respectively $\approx 60\%$, $\approx 30\%$ and $\approx 10\%$ of the total $gg \rightarrow H$ cross section at NNLO. Since these three pieces add up to $\sigma_{gg \rightarrow H}^{\text{NNLO}}$, why using different normalisation for these jet cross sections and the total sum, and include soft-gluon resummation in the latter and not in the former?

- it is theoretically not very consistent to fold a resummed cross section with PDF sets which do not involve any resummation, as is the case for the presently available PDF sets which at at most at NNLO. Even if the effects of the resummation on the PDFs might be rather small in practice, this has also been discussed in details in Ref. [168].
- it is well known that the NNLL contributions increase the NNLO result by a factor of $\sim 10\text{--}15\%$ at the Tevatron [110]. This increase can be very closely approached by

¹⁷The results with $\mu_0 = m_H$ were also presented in ICHEP, see Ref. [156].

¹⁸This was presented in the Higgs Hunting workshop in Orsay which followed ICHEP [158].

evaluating the NNLO cross section at $\mu_0 = \frac{1}{2}M_H$ [118, 169] which is one of the reasons to use this central scale choice, which is then fully consistent with the point b) while taking into account this $\sim 10\text{--}15\%$ increase in the total cross section¹⁹.

We see here that a central scale $\mu_0 = \frac{1}{2}M_H$ seems more appropriate while sticking at NNLO order. In fact there is also another reason why this scale choice is particularly appropriate for gluon–gluon fusion. As pointed out by Anastasiou and collaborators some time ago [118, 169] (see also Ref. [45]), lowering the central value of the renormalization and factorization scales from $\mu_0 = M_H$ to $\mu_0 = \frac{1}{2}M_H$ improves the convergence of the perturbative series and is more appropriate to describe the kinematics of the process. Recalling that if the scale value $\mu_0 = \frac{1}{2}M_H$ is chosen, the central value of $\sigma_{gg \rightarrow H}^{\text{NNLO}}$ increases by more than 10%, we then end with a NNLO calculation with no difference between $\sigma_{gg \rightarrow H}^{\text{NNLO}}(\mu_0 = \frac{1}{2}M_H)$ and $\sigma_{gg \rightarrow H}^{\text{NNLL}}(\mu_0 = M_H)$ as calculated for instance in [111], which is fully consistent with the PDF order, and which improves the convergence of the perturbative series. All of these reasons explain this central scale choice used in the rest of our analysis.

For the electroweak part, we include the complete one–loop corrections to the $gg \rightarrow H$ amplitude which have been calculated in Ref. [117] taking into account the full dependence on the top/bottom quark and the W/Z boson masses. These corrections are implemented in the so–called partial factorization scheme in which the electroweak correction δ_{EW} is simply added to the QCD corrected cross section at NNLO, $\sigma^{\text{tot}} = \sigma^{\text{NNLO}} + \sigma^{\text{LO}}(1 + \delta_{EW})$. In the alternative complete factorization scheme discussed in Ref. [117], the electroweak correction $1 + \delta_{EW}$ is multiplied by the fully QCD corrected cross section, $\sigma^{\text{tot}} = \sigma^{\text{NNLO}}(1 + \delta_{EW})$ and, thus, formally involves terms of $\mathcal{O}(\alpha_s^3\alpha)$ and $\mathcal{O}(\alpha_s^4\alpha)$ which have not been fully calculated. Since the QCD K –factor is large, $K_{\text{NNLO}} \approx 3$, the electroweak corrections might be overestimated by the same factor. We have also included the mixed QCD–electroweak corrections at NNLO due to light-quark loops [118]. These are only part of the three–loop $\mathcal{O}(\alpha\alpha_s)$ corrections and have been calculated in an effective approach that is valid only when $M_H \lesssim M_W$ and which cannot be so easily extrapolated to M_H values above this threshold; this will be discussed in more details in the next section. In Ref. [118], it has been pointed out that this procedure, i.e. adding the NLO full result and the mixed QCD–electroweak correction in the partial factorization scheme, is equivalent to simply including only the NLO electroweak correction in the complete factorization scheme.

¹⁹This choice of ignoring the contributions beyond NNLO has also been adopted in Ref. [112] in which the theoretical predictions have been confronted to the CDF/D0 results, the focus being the comparison between the distributions obtained from the matrix elements calculation with those given by the event generators and Monte-Carlo programs used by the experiments. They find excellent agreement with NNLL calculation at a central scale $\mu_0 = M_H$

We finally fold the partonic cross section with the MSTW PDF set [128], setting as mentioned above the renormalization and factorization scales at $\mu_R = \mu_F = \frac{1}{2}M_H$. We obtain for the Tevatron energy $\sqrt{s} = 1.96$ TeV the central values displayed in Fig. 17 for the gluon–gluon fusion production cross sections as a function of the Higgs mass on the entire interesting range for the Tevatron experiment. Our results for the total cross sections are in an excellent agreement with those given in Refs. [90–93, 111]. For instance, for $M_H = 160$ GeV, we obtain with our procedure a total $p\bar{p} \rightarrow H + X$ cross section of $\sigma^{\text{tot}} = 427$ fb, compared to the value $\sigma^{\text{tot}} = 434$ fb quoted in Refs. [90–93, 111]. The small difference comes from the different treatment of the electroweak radiative corrections (partial factorization plus mixed QCD–electroweak contributions in our case versus complete factorization in Ref. [111]) and another one percent discrepancy can be attributed to the numerical uncertainties in the various integrations of the partonic sections²⁰.

We should also note that for the Higgs mass value $M_H = 160$ GeV, we obtain $K \simeq 2.15$ for the QCD K –factor at NLO and $K \simeq 2.8$ at NNLO. These numbers are slightly different from those presented in Ref. [112], $K \simeq 2.4$ and $K \simeq 3.3$, respectively. The reason is that the b –quark loop contribution, for which the K –factor at NLO is significantly smaller than the one for the top quark contribution [105] has been ignored for simplicity in the latter paper; this difference will be discussed in section 4.4.

4.1.2 The Higgs–strahlung production channels

The Higgs–strahlung processes $q\bar{q} \rightarrow WH$ and $q\bar{q} \rightarrow ZH$ are also evaluated using Eq. 4.5. The variable τ_{AB} is $\tau_{HV} = \frac{(M_H + M_V)^2}{S}$. It has been shown (see Ref. [45]) that this process can be interpreted as the Drell–Yan production $p\bar{p} \rightarrow V^*$ of a virtual vector boson which then splits into a real vector boson V and a Higgs boson H [172]. We could then write $\hat{\sigma}_{ij} = \hat{\sigma}(ij \rightarrow V^*) \times \frac{d\Gamma}{dk^2}$ where k^2 is the mass of the virtual vector boson V^* , which is subject to vary between τ_{HV} and S . If we rewrite the equality we can obtain $\frac{d\Gamma}{dk^2} = \frac{\hat{\sigma}_{ij}^{\text{LO}}}{\hat{\sigma}^{\text{LO}}(ij \rightarrow V^*)}$.

²⁰We have explicitly verified, using the program HRESUM [170, 171] which led to the results of Ref. [111], that our NNLO cross section is in excellent agreement with those available in the literature. In particular, for $M_H = 160$ GeV and scales $\mu_R = \mu_F = M_H$, one obtains $\sigma^{\text{NNLO}} = 380$ fb with HRESUM compared to $\sigma^{\text{NNLO}} = 374$ fb in our case; the 1.5% discrepancy being due to the different treatment of the electroweak corrections and the integration errors. Furthermore, setting the renormalization and factorization scales to $\mu_R = \mu_F = \frac{1}{2}M_H$, we find $\sigma^{\text{NNLO}} = 427$ fb which is in excellent agreement with the value $\sigma^{\text{NNLO}} = 434$ fb obtained in Ref. [118] and with HRESUM, as well as the value in the NNLL approximation when the scales are set at their central values $\mu_R = \mu_F = M_H$. This gives us confidence that our implementation of the NNLO contributions in the NLO code HIGLU, including the scale dependence, is correct.

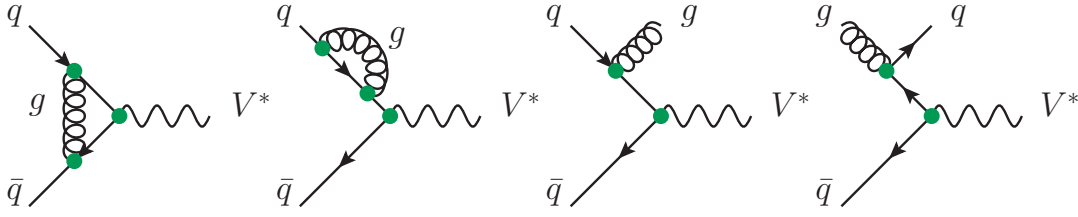


Figure 15: NLO QCD corrections to virtual vector boson production $p\bar{p} \rightarrow V^*$.

In the end, using Eq. 4.5 and the fact that we have to integrate the variable $Z = \frac{k^2}{S\tau}$ between $\frac{\tau_{HV}}{\tau}$ and 1:

$$\sigma(p\bar{p} \rightarrow HV) = \int_{\tau_{HV}}^1 \sum_{(ij)} \frac{d\mathcal{L}^{ij}}{d\tau}(\tau) \int_{\tau_{HV}/\tau}^1 dZ \hat{\sigma}_{ij}^{\text{LO}}(\tau Z S) \Delta_{ij}(ij \rightarrow V^*) \quad (4.11)$$

In Eq. 4.11 the quantity Δ_{ij} describes the corrections to the partonic Drell–Yan process $ij \rightarrow V^*$. At LO we thus have $\Delta_{ij} = \delta_{iq}\delta_{j\bar{q}}$ (with δ as the Kronecker symbol) as only the $q\bar{q}$ partonic initial state contributes with no QCD correction, Higgs–strahlung processes being pure electroweak processes at LO. We can calculate $\hat{\sigma}_{ij}$ directly and use the factorization with the Drell–Yan process for HO corrections. We obtain

$$\hat{\sigma}_{ij} = \delta_{iq}\delta_{j\bar{q}} \frac{G_F^2 M_V^4}{288\pi\hat{s}} (\hat{v}_q^2 + \hat{a}_q^2) \sqrt{\beta} \frac{\beta + 12M_V^2/\hat{s}}{(1 - M_V^2/\hat{s})} \quad (4.12)$$

where $\beta = \left(1 - \frac{M_V^2}{\hat{s}} - \frac{M_H^2}{\hat{s}}\right)^2 - 4\frac{M_V^2 M_H^2}{\hat{s}^2}$ is the phase–space two bodies function. \hat{v}_q and \hat{a}_q stand for the reduced axial and vector fermion–gauge boson couplings: $\hat{v}_q = \hat{a}_q = \sqrt{2}$ for $V = W$, $\hat{v}_q = 2I_3(q) - 4Q_q \sin\theta_W$ and $\hat{a}_q = 2I_3(q)$ for $V = Z$ where I_3 is the weak isospin z –projection, $\sin\theta_W$ stands for the Weinberg angle and Q_q is the electric charge of the quark q .

We then add the NLO corrections in the Drell–Yan process, see Fig. 15 for the Feynman diagrams. The exact expressions for the NLO QCD corrections can be found in Refs. [45, 121–125]. The NNLO corrections for $p\bar{p} \rightarrow HV$ have been presented in Ref. [126] and use the NNLO Drell–Yan corrections [107, 173, 174], see Fig. 16 for some Feynman diagrams. It is worth mentioning that there are other specific corrections for Higgs–strahlung processes which occur at NNLO and that have nothing to do with the Drell–Yan process $p\bar{p} \rightarrow V^*$, such as the $gg \rightarrow ZH$ channel. They have been reviewed in Ref. [45] and what comes out is that we can neglect them at the Tevatron both for W and Z bosons (the $gg \rightarrow ZH$ channel

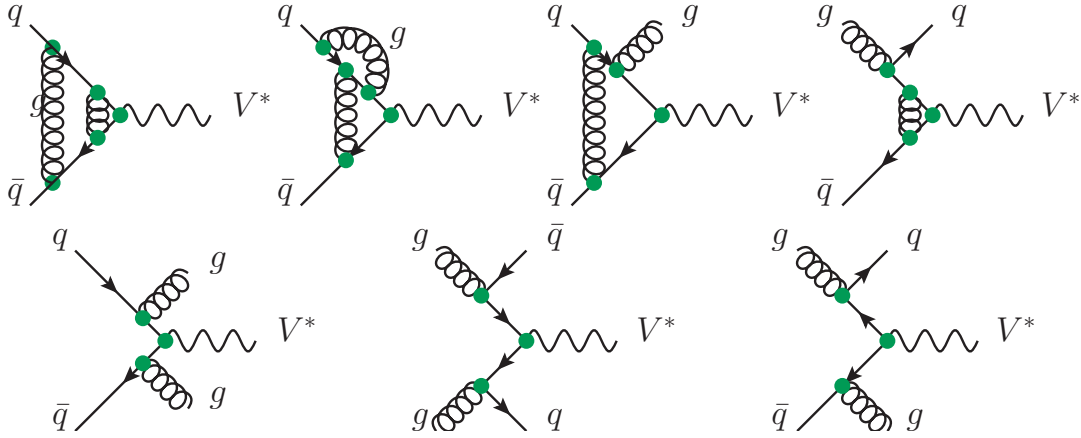


Figure 16: Some Feynman diagrams for NNLO QCD corrections to virtual vector boson production $p\bar{p} \rightarrow V^*$.

does not exist for W channel for example and is at the permille level at the Tevatron for the Z channel).

The total Higgs–strahlung cross sections are then calculated in the following way. We use the Fortran code `V2HV` [153] which evaluates the full cross sections at NLO in QCD. The NNLO QCD contributions to the cross sections [126], as well as the one–loop electroweak corrections evaluated in Ref. [127], are incorporated in the program `V2HV` by us. The central scale adopted in this case is the invariant mass of the HV system, $\mu_R = \mu_F = M_{HV} = (p_H + p_V)^2$.

Folding the partonic cross sections with the MSTW parton distribution functions [128] and setting the renormalization and factorization scales at the most natural values $\mu_R = \mu_F = M_{HV}$, we obtain for the Tevatron energy $\sqrt{s} = 1.96$ TeV, the central values displayed in Fig. 17 for the $p\bar{p} \rightarrow VH$ Higgs production cross sections as a function of the Higgs mass. Note that including the combined HERA data and the Tevatron $W \rightarrow \ell\nu$ charge asymmetry data in the MSTW2008 PDF set [175] might lead to an increase of the $p\bar{p} \rightarrow (H+)Z/W$ cross sections by $\approx 3\%$; a small change in $\sigma(gg \rightarrow H)$ is also expected.

The central values of the cross sections of Higgs–strahlung from W and Z bosons that we obtain are comparable to those given in Refs. [90, 130, 131], with at most a $\sim 2\%$ decrease in the low Higgs mass range, $M_H \lesssim 140$ GeV. The reason is that the quark and antiquark densities, which are the most relevant in these processes and are more under control than the gluon densities, are approximately the same in the new MSTW2008 and old MRST2002 sets of PDFs (although the updated set includes a new fit to run II Tevatron and HERA inclusive jet data). We should note that for $M_H = 115$ GeV for which the production cross sections are the largest, $\sigma^{\text{WH}} = 175$ fb and $\sigma^{\text{ZH}} = 104$ fb, the QCD K –factors are ~ 1.2 (1.3) at NLO (NNLO), while the electroweak corrections decrease the LO cross

sections by $\approx -5\%$. The correcting factors do not change significantly for increasing M_H values for the Higgs mass range relevant at the Tevatron.

We make here a small comment which will simplify the analysis of the theoretical uncertainties affecting the central predictions. Since in this case, the NNLO QCD corrections and the one-loop electroweak corrections have been obtained exactly and no effective approach was used, only the scale variation and the PDF+ α_s uncertainties have to be discussed. In addition, since the NNLO gluon-gluon fusion contribution to the cross section in the $p\bar{p} \rightarrow ZH$ case, which is absent in $p\bar{p} \rightarrow WH$, is very small at the Tevatron and because the scales and phase space are only slightly different for the $p\bar{p} \rightarrow WH$ and ZH processes, as the difference $(M_Z^2 - M_W^2)/\hat{s}$ is tiny, the kinematics and the K -factors for these two processes are very similar. We will thus restrict our analysis to the WH channel but the same results will hold for the ZH channel.

4.1.3 The VBF and associated heavy quarks channels

We have also evaluated the cross sections of the two sub-leading processes $qq \rightarrow V^*V^*qq \rightarrow Hqq$ and $q\bar{q}/gq \rightarrow t\bar{t}H$ that we also include in Fig. 17 for completeness, we have not entered into very sophisticated considerations. We have simply followed the procedure outlined in Ref. [45] and used the public Fortran codes again given in Ref. [153]. The vector boson total cross section is evaluated at NLO in QCD [136, 137] at a scale $\mu_R = \mu_F = Q_V$ (where Q_V is the momentum transfer at the gauge boson leg), while the presumably small electroweak corrections, known for the LHC [176], are omitted. We have not included the recent partial NNLO QCD corrections presented in Refs. [177, 178], as they do not modify greatly the central cross section that interest us in this small update. We have not estimated the uncertainties affecting these calculations.

In the case of associated $t\bar{t}H$ production, the LO cross section is evaluated at scales $\mu_R = \mu_F = \frac{1}{2}(M_H + 2m_t)$ but is multiplied by a factor $K \sim 0.8$ over the entire Higgs mass range to account for the bulk of the NLO QCD corrections [141–144]. In the latter case, we use the updated value $m_t = 173.1$ GeV for the top quark mass [179]. The only other update compared to the cross section values given in Ref. [45] is thus the use of the recent MSTW set of PDFs.

The cross sections for the vector boson fusion channel in which the recent MSTW set of PDFs is used agree well with those given in Refs. [90, 91, 93, 180]²¹. In the case of the $t\bar{t}H$ associated production process, a small difference is observed compared to Ref. [45] in which the 2005 $m_t = 178$ GeV value is used: we have a few percent increase of the

²¹The values from Ref. [180] can be found in [181].

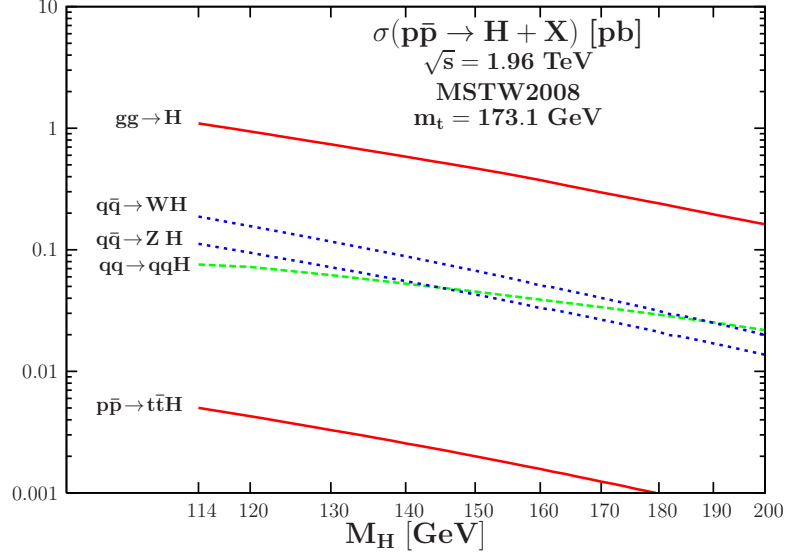


Figure 17: The total cross sections for Higgs production at the Tevatron as a function of the Higgs mass. The MSTW set of PDFs has been used and the higher order corrections are included as discussed in the text.

rate due the presently smaller m_t value which provides more phase space for the process, overcompensating the decrease due to the smaller top-quark Yukawa coupling. This is shown in Fig. 17 as a function of the Higgs mass.

Before closing this subsection, let us make a few remarks on the Higgs decay branching ratios and on the rates for the various individual channels that are used to detect the Higgs signal at the Tevatron, bearing in mind that this will be discussed in more details in section 6. In the interesting range $160 \text{ GeV} \leq M_H \leq 175$ for which the Tevatron experiments are most sensitive, the branching ratio for the $H \rightarrow WW$ is largely dominant, being above 90%. In addition, in this mass range, the $gg \rightarrow H$ cross section is one order of magnitude larger than the cross sections for the $q\bar{q} \rightarrow WH, ZH$ and $qq \rightarrow qqH$ processes as for $M_H \sim 160 \text{ GeV}$ for instance, one has $\sigma(gg \rightarrow H) = 425 \text{ fb}$ compared to $\sigma(WH) \simeq 49 \text{ fb}$, $\sigma(ZH) \simeq 31 \text{ fb}$ and $\sigma(qqH) \simeq 40 \text{ fb}$. Thus, the channel $gg \rightarrow H \rightarrow W^*W^*$ represents, even before selection cuts are applied, the bulk of the events leading to $\ell\nu\nu + X$ final states, where here X stands for additional jets or leptons coming from W, Z decays as well as for jets due to the higher order corrections to the $gg \rightarrow H$ process. In the lower Higgs mass range, $M_H \lesssim 150 \text{ GeV}$, all the production channels above, with the exception of the vector boson $qq \rightarrow qqH$ channel which can be selected using specific kinematical cuts, should be taken into account but with the process $q\bar{q} \rightarrow WH \rightarrow \ell\nu b\bar{b}$ being dominant for $M_H \lesssim 130 \text{ GeV}$. This justifies the fact that we concentrate mainly on the gluon-gluon fusion and Higgs-strahlung production channels for the study of the theoretical predictions both for the central cross sections and the theoretical uncertainties; the inclusion of the other

channels would marginally affect our results, especially in the Higgs mass region around $M_H = 160$ GeV where the Tevatron is the most sensitive: the effect would be below the percent level due to the huge impact of the $H \rightarrow WW$ branching fraction.

4.2 Scale variation and higher order terms

The effect of unknown (yet to be calculated) higher order contributions to production cross sections and differential distributions at hadron colliders is usually estimated by studying the variation of these observables, evaluated at the highest known perturbative order, with the renormalization scale defining the strong coupling constant α_s scale and the factorization scale μ_F at which the matching between the perturbative calculation of the matrix elements, that is the partonic cross section, and the non-perturbative part which is described in the parton distribution functions, is performed. These two scales are unphysical and should be viewed as a technical artefact; indeed the dependence of the final result on these two scales should be null, as when all orders of the perturbative series are summed, the observables should be scale independent. This scale dependence appears only because the perturbative series are truncated, as only its few first orders are evaluated in practice. This is the reason this scale dependence is taken as a guess of the impact of the higher order contributions.

Starting from a median scale μ_0 which, with a smart guess, is considered as the most “natural” scale of the process and absorbs potentially large logarithmic corrections, the current convention is to vary these two scales within the range

$$\mu_0/\kappa \leq \mu_R, \mu_F \leq \kappa\mu_0. \quad (4.13)$$

with the constant factor κ to be determined. One then uses the following equations to calculate the deviation of, for instance, a cross section $\sigma(\mu_R, \mu_F)$ from the central value evaluated at scales $\mu_R = \mu_F = \mu_0$,

$$\begin{aligned} \Delta\sigma_\mu^+ &= \max_{(\mu_R, \mu_F)} \sigma(\mu_R, \mu_F) - \sigma(\mu_R = \mu_F = \mu_0), \\ \Delta\sigma_\mu^- &= \sigma(\mu_R = \mu_F = \mu_0) - \min_{(\mu_R, \mu_F)} \sigma(\mu_R, \mu_F). \end{aligned} \quad (4.14)$$

This procedure is by no means a true measure of the higher order effects and should be viewed only as providing a guess of the lower limit on the scale uncertainty. The variation of the scales in the range of Eq. 4.13 can be individual with μ_R and μ_F varying independently in this domain, with possibly some constraints such as $1/\kappa \leq \mu_R/\mu_F \leq \kappa$ in order not to generate “artificially large logarithms”, or collective when, for example, keeping one of

the two scales fixed, say to μ_0 , and vary the other scale in the chosen domain. Another possibility which is often adopted, is to equate the two scales, $\mu_0/\kappa \leq \mu_R = \mu_F \leq \kappa\mu_0$, a procedure that is possibly more consistent as most PDF sets are determined and evolved according to $\mu_R = \mu_F$, but which has no theoretical ground as the two scales enter different parts of the calculation (renormalization versus factorization).

The choice of the variation domain for a given process, hence the constant factor κ in Eq. 4.13, is somewhat arbitrary and a matter of taste: depending on whether one is optimistic or pessimistic, that is whether one believes or not that the higher order corrections to the process are under control, it can range from $\kappa=2$ to much higher values.

In most recent analyses of production cross sections at hadron colliders, a kind of consensus has emerged and the domain,

$$\frac{1}{2}\mu_0 \leq \mu_R, \mu_F \leq 2\mu_0, \quad \frac{1}{2} \leq \mu_R/\mu_F \leq 2, \quad (4.15)$$

has been generally adopted for the scale variation. A first remark is that the condition $\frac{1}{2} \leq \mu_R/\mu_F \leq 2$ to avoid the appearance of large logarithms might seem too restrictive: after all, these possible large logarithms can be viewed as nothing else than the logarithms involving the scales and if they are large, it is simply a reflection of a large scale dependence. A second remark is that in the case of processes in which the calculated higher order contributions are small to moderate and the perturbative series appears to be well behaved²², the choice of such a narrow domain for the scale variation with $\kappa = 2$, appears reasonable, as will be seen when we will study the scale dependence of the Higgs–strahlung processes. However, this might be a complete different story when dealing with processes in which the calculated radiative corrections turn out to be extremely large. As the higher order contributions might also be significant in this case, the variation domain of the renormalization and factorization scales might have to be extended and a range with a factor κ substantially larger than two may seem more appropriate²³.

²²This is indeed the case for some important production processes at the Tevatron, such as the Drell–Yan process $p\bar{p} \rightarrow V$ [173, 174, 182, 183], weak boson pair production [184–188] and even top quark pair production [189–191] once the central scale is taken to be $\mu_0 = m_t$, which have moderate QCD corrections.

²³This would have been the case, for instance, in top–quark pair production at the Tevatron if the central scale were fixed to the more “natural” value $\mu_0 = 2m_t$ (instead of the value $\mu_0 = m_t$ usually taken [189–191]) and a scale variation within $\frac{1}{4}M_H \leq \mu_R, \mu_F \leq 4M_H$ were adopted. Another well known example is Higgs production in association with b –quark pairs in which the cross section can be determined by evaluating the mechanism $gg/q\bar{q} \rightarrow b\bar{b}H$ [192] or $b\bar{b}$ annihilation, $b\bar{b} \rightarrow H$ [193–195]. The two calculations performed at NLO for the former process and NNLO for the later one, are consistent only if the central scale is taken to be $\mu_0 \approx \frac{1}{4}M_H$ instead of the more “natural” value $\mu_0 \approx M_H$, see Ref. [131] (page 5). Again, without prior knowledge of the higher order corrections, it would have been wiser, if the central scale $\mu_0 = M_H$ had been adopted, to assume a wide domain, e.g. $\frac{1}{4}M_H \leq \mu_R, \mu_F \leq 4M_H$, for the scale variation. Note that

4.2.1 The case of $gg \rightarrow H$ production

In the case of the $gg \rightarrow H$ production process, the most natural value for the median scale would be the Higgs mass itself, $\mu_0 = M_H$, and if the effects of the higher order contributions to the cross section is again usually estimated by varying μ_R and μ_F as in Eq. 4.15, i.e. with the choice $\frac{1}{\kappa} \leq \mu_R/\mu_F \leq \kappa$ and $\kappa = 2$, we obtain at the Tevatron a variation of approximately $\pm 15\%$ of the NNLO cross section with this specific choice [107, 108] and the uncertainty drops to the level of $\approx \pm 10\%$ in the NNLL approximation.

As we have stated in the former section that it is wiser to choose $\mu_0 = \frac{1}{2}M_H$ as the central scale, e.g. as in. Ref. [118], the variation domain $\frac{1}{4}M_H \leq \mu_R = \mu_F \leq M_H$ is then adopted, leading also to a $\approx 15\%$ uncertainty.

Nevertheless, as the K -factor is extraordinarily large in the $gg \rightarrow H$ process, $K_{\text{NNLO}} \approx 3$, the domain of Eq. 4.15 for the scale variation seems too narrow. If this scale domain was chosen for the LO cross section for instance, the maximal value of $\sigma(gg \rightarrow H)$ at LO would have never caught, and by far, the value of $\sigma(gg \rightarrow H)$ at NNLO, as it should be the case if the uncertainty band with $\kappa = 2$ were indeed the correct “measure” of the higher order effects. Only for a much larger value of κ that this would have been the case.

Here, we will use a criterion which allows an empirical evaluation of the effects of the still unknown high orders of the perturbative series and, hence, the choice of the variation domain of the factorization and renormalization scales in a production cross section (or distribution). This is done in two steps:

1. The domain of scale variation, $\mu_0/\kappa \leq \mu_R, \mu_F \leq \kappa\mu_0$, is derived by calculating the factor κ which allows the uncertainty band of the lower order cross section resulting from the variation of μ_R and μ_F , to reach the central value (i.e. with μ_R and μ_F set to μ_0), of the cross section that has been obtained at the higher perturbative order.
2. The scale uncertainty on the cross section at the higher perturbative order is then taken to be the band obtained for a variation of the scales μ_R and μ_F within the same range and, hence, using the same κ value.

In the case of the $gg \rightarrow H$ process at the Tevatron, if the lower order cross section is taken to be σ^{LO} and the higher order one σ^{NNLO} , this is shown in the left-hand side of

 even for the scale choice $\mu_0 \approx \frac{1}{4}M_H$, the K -factor for the $gg \rightarrow b\bar{b}H$ process remains very large, $K_{\text{NNLO}} \approx 2$ at the Tevatron. In addition, here, it is the factorization scale μ_F which generates the large contributions $\propto \ln(\mu_F^2/m_b^2)$ in a 5 flavour scheme and not the renormalization scale which can be thus kept at the initial value $\mu_R \approx M_H$. We will study this process in the section 11.1 and 12.1 in part IV when dealing with MSSM Higgs production.

Fig. 18. The figure shows the uncertainty band of σ^{LO} resulting from a scale variation in the domain

$$\frac{1}{2}M_H/\kappa \leq \mu_R, \mu_F \leq \kappa \frac{1}{2}M_H$$

with $\kappa = 2, 3, 4$, which is then compared to σ^{NNLO} evaluated at the central scale $\mu_R = \mu_F = \frac{1}{2}M_H$. We first observe that, as expected, the uncertainty bands are larger with increasing values of κ .

The important observation that one can draw from this figure is that it is only for $\kappa=4$, i.e. a variation of the scales in a range that is much wider than the one given in Eq. 4.15 that the uncertainty band of the LO cross section becomes very close to (and still does not yet reach for low Higgs mass values) the curve giving the NNLO result. Thus, as the scale uncertainty band of $\sigma^{\text{LO}}(gg \rightarrow H)$ is supposed to provide an estimate of the resulting cross section at NNLO and beyond, the range within which the two scales μ_R and μ_F should be varied must be significantly larger than $\frac{1}{2}\mu_0 \leq \mu_R, \mu_F \leq 2\mu_0$.

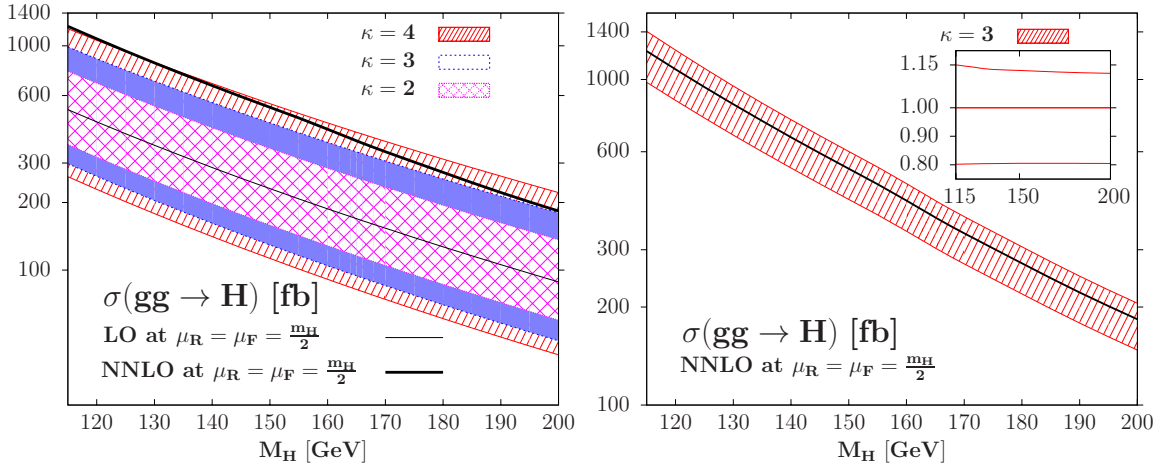


Figure 18: Left: the scale variation of $\sigma_{gg \rightarrow H}^{\text{LO}}$ as a function of M_H in the domain $\mu_0/\kappa \leq \mu_R = \mu_F \leq \kappa\mu_0$ for $\mu_0 = \frac{1}{2}M_H$ with $\kappa = 2, 3$ and 4 compared to $\sigma_{gg \rightarrow H}^{\text{NNLO}}(\mu_R = \mu_F = \frac{1}{2}M_H)$. Right: the uncertainty band of $\sigma_{gg \rightarrow H}^{\text{NNLO}}$ as a function of M_H for a scale variation $\mu_0/\kappa \leq \mu_R = \mu_F \leq \kappa\mu_0$ with $\mu_0 = \frac{1}{2}M_H$ and $\kappa = 3$. In the inserts shown are the relative deviations.

Nevertheless, one might be rightfully reluctant to use σ^{LO} as a starting point for estimating the higher order effects, as it is well known that it is only after including at least the next-order QCD corrections that a cross section is somewhat stabilized and, in the particular case of the $gg \rightarrow H$ process, the LO cross section does not describe correctly the kinematics as, for instance, the Higgs transverse momentum is zero at this order. We thus explore also the scale variation of the NLO cross section σ^{NLO} instead of that of σ^{LO} and compare the resulting uncertainty band to the central value of the cross section again

at NNLO (we refrain here from adding the $\sim 15\%$ contribution at NNLL as well as those arising from higher order corrections, such as the estimated N³LO correction [159]). On the other hand, the choice of $\mu_0 = \frac{1}{2}M_H$ incorporate much of the higher order correction already at LO as it lowers the K -factors drastically.

If we had chosen to compare NLO band with NNLO central predictions with the central scale choice $\mu_0 = \frac{1}{2}M_H$, we would have been within the band $\kappa = 2$ and touching the lower limit of the $\kappa = 3$ band²⁴. In addition, this is only for low Higgs masses that we cannot reach the $\kappa = 3$ LO band with NNLO central prediction. Thus, to attain the (N)LO values of the $gg \rightarrow H$ cross section at the Tevatron with the scale variation of the NLO cross section, when both cross sections are taken at the central scale choice, we believe that the right choice is the value $\kappa = 3$, and hence a domain of scale variation that is wider than that given in Eq. 4.15. This choice of the domains of scale variation might seem somewhat conservative at first sight. However, we emphasise again that in view of the huge QCD corrections which affect the cross section of this particular process, and which almost spoil completely the convergence of the perturbative series, this choice appears to be justified, even if the choice of the central scale adopted here helps to reduce these giant K -factors. In fact, this scale choice is not so unusual and in Refs. [108–110, 196–198] for instance, scale variation domains comparable to those discussed here, and sometimes even wider, have been used for illustration.

In addition, we have mentioned that the scales μ_R and μ_F are varied independently and with no restriction such as $\frac{1}{3} \leq \mu_R/\mu_F \leq 3$ for instance. In fact, this is only a general statement and this requirement has absolutely no impact on the NNLO analysis as the minimal and maximal values of $\sigma_{gg \rightarrow H}^{\text{NNLO}}$ due to scale variation are obtained for equal μ_R and μ_F values: for a central scale $\mu_0 = M_H$, we have $\sigma_{\min}^{\text{NNLO}}$ for $\mu_R = \mu_F = 3\mu_0$ and $\sigma_{\max}^{\text{NNLO}}$ for $\mu_R = \mu_F = \frac{1}{3}\mu_0$. We then choose for simplicity to take μ_R and μ_F as equal so that there is no more discussion about the possibility of generating artificially large logarithms if we take two widely different μ_R/μ_F scales.

Thus, in our analysis, rather than taking the usual choice for the scale domain of variation with $\kappa = 2$ given in Eq. 4.15, we will adopt the slightly more conservative possibility given by the wider variation domain²⁵

²⁴see here the Ref. [94] where this point is mentioned in a footnote. C. Anastasiou is thanked for a discussion on this point.

²⁵One might argue that since in the case of $\sigma(gg \rightarrow H)$, the NLO and NNLO contributions are both positive and increase the LO rate, one should expect a positive contribution from higher orders (as is the case for the re-summed NNLL contribution) and, thus, varying the scales using $\kappa = 2$ is more conservative, as the obtained maximal value of the cross section would be smaller than the value that one would obtain for e.g. $\kappa = 3$. However, one should not assume that the higher order contributions always increase the

$$\frac{1}{3}\mu_0 \leq \mu_R = \mu_F \leq 3\mu_0, \quad \mu_0 = \frac{1}{2}M_H \quad (4.16)$$

Having made this choice for the factor κ , we now estimate the higher order effects of $\sigma(gg \rightarrow H)$ evaluated at the highest perturbative order that we take to be NNLO, ignoring again the known small contributions beyond this fixed order.

The uncertainty bands resulting from scale variation of $\sigma^{\text{NNLO}}(gg \rightarrow H)$ at NNLO in the domain given by Eq. 4.16 is shown in the right-hand side of Fig. 18 as a function of M_H . As expected, the scale uncertainty is slightly larger for $\kappa = 3$ than for $\kappa = 2$. Averaged over the entire Higgs mass range, the final scale uncertainty is about $\simeq +15\%, -20\%$. If we had chosen the usual domain $\frac{1}{2}\mu_0 \leq \mu_R = \mu_F \leq 2\mu_0$, the scale variation would have been of about $\approx +10\%, -12\%$ for $M_H \approx 160$ GeV. The minimal cross section is obtained for the largest values of the two scales as stated above, $\mu_F = \mu_R = \kappa\frac{1}{2}M_H$, while the maximal value is obtained for the lowest value of the renormalization scale, $\mu_R = \frac{1}{\kappa}\frac{1}{2}M_H$, almost independently of the factorization scale μ_F , but with a slight preference for the lowest μ_F values, $\mu_F = \frac{1}{\kappa}\frac{1}{2}M_H$.

We should note that the $\approx 10\%$ scale uncertainty obtained in Ref. [111] and adopted in earlier publications by the CDF/D0 collaborations [90] is even smaller than the ones discussed above. The reason is that it is the resummed NNLL cross section, again with $\kappa = 2$ and $\frac{1}{2} \leq \mu_R/\mu_F \leq 2$, that was considered, and the scale variation of σ^{NNLL} is reduced compared to that of σ^{NNLO} in this case. As one might wonder if this milder dependence also occurs for our adopted κ value, we have explored the scale variation of σ^{NNLL} in the case of $\kappa = 3$, without the restriction $\frac{1}{3} \leq \mu_R/\mu_F \leq 3$. Using again the program HRESUM [171], we find that the difference between the maximal value of the NNLL cross section, obtained for $\mu_R \approx M_H$ and $\mu_F \approx 3M_H$, and its minimal value, obtained for $\mu_F \approx \frac{1}{3}M_H$ and $\mu_R \approx 3M_H$, is as large as in the NNLO case (this is also true for larger κ values). The maximal decrease and maximal increase of σ^{NNLL} from the central value are still of about $\pm 20\%$ in this case. Hence, the relative stability of the NNLL cross section against scale variation, compared to the NNLO case, occurs only for $\kappa = 2$ and may appear as accidentally due to a restrictive

lower order cross sections. Indeed, had we taken the central scales at $\mu_R = \mu_F = \frac{1}{5}M_H$, the NNLO (and even NNLL) corrections would have reduced the total cross section evaluated at NLO, see a remark made in Ref. [94]. Hence, the higher order contributions to $\sigma(gg \rightarrow H)$ could well be negative beyond NNLO and could bring the value of the production cross section close to the lower range of the scale uncertainty band of σ^{NNLO} . Another good counter-example of a cross section that is reduced by the higher order contributions is the process of associated Higgs production with top quark pairs at the Tevatron where the NLO QCD corrections decrease the LO cross section by $\sim 20\%$ [141–144] once the central scale is chosen to be $\mu_0 = \frac{1}{2}(2m_t + M_H)$.

choice of the variation domain. However, if the additional constraint $1/\kappa \leq \mu_F/\mu_R \leq \kappa$ is implemented, the situation would improve in the NNLL case, as the possibility $\mu_F \approx \frac{1}{\kappa}M_H$ and $\mu_R \approx \kappa M_H$ which minimizes σ^{NNLL} would be absent and the scale variation reduced. Nevertheless, even in this case, the variation of σ^{NNLL} for $\kappa = 3$ is of the order of $\approx \pm 15\%$ and, hence, the scale uncertainty is larger than what is obtained in the domain of Eq. 4.15.

It is important to notice that if the NNLO $gg \rightarrow H$ cross section, evaluated at $\mu_0 = M_H$, is broken into the three pieces with 0,1 and 2 jets, and one applies a scale variation for the individual pieces in the range $\frac{1}{2}\mu_0 \leq \mu_R, \mu_F \leq 2\mu_0$, one obtains with selection cuts similar to those adopted by the CDF/D0 collaborations [112]:

$$\Delta\sigma/\sigma|_{\text{scale}} = 60\% \cdot \begin{pmatrix} +5\% \\ -9\% \end{pmatrix} + 29\% \cdot \begin{pmatrix} +24\% \\ -23\% \end{pmatrix} + 11\% \cdot \begin{pmatrix} +91\% \\ -44\% \end{pmatrix} = \begin{pmatrix} +20.0\% \\ -16.9\% \end{pmatrix} \quad (4.17)$$

Averaged over the various final states with their corresponding weights, an error on the “inclusive” cross section which is about $+20\%$, -17% is derived²⁶. This is very close to the result obtained in the CDF/D0 analysis [91–93] which quotes a scale uncertainty of $\approx \pm 17.5\%$ on the total cross section, when the weighted uncertainties for the various jet cross sections are added. Thus, our alleged conservative choice $\frac{1}{3}\mu_0 \leq \mu_R = \mu_F \leq 3\mu_0$ for the scale variation of the total inclusive cross section $\sigma_{\text{gg} \rightarrow \text{H}}^{\text{NNLO}}$, leads to a scale uncertainty that is very close to that obtained when one adds the scale uncertainties of the various jet cross sections for a variation around the more consensual range $\frac{1}{2}\mu_0 \leq \mu_R, \mu_F \leq 2\mu_0$.

We also note that when breaking $\sigma_{\text{gg} \rightarrow \text{H}}^{\text{NNLO}}$ into jet cross sections, an additional error due to the acceptance of jets is introduced; the CDF and D0 collaborations, after weighting, have estimated it to be $\pm 7.5\%$. We do not know if this weighted acceptance error should be considered as a theoretical or an experimental uncertainty. But this error, combined with the weighted uncertainty for scale variation, will certainly increase the total scale error in the CDF/D0 analysis, possibly (and depending on how the errors should be added) to the level where it almost reaches or even exceeds our own supposedly “conservative” estimate.

We could finally give another reason for a more conservative choice of the scale variation domain for σ^{NNLO} , beyond the minimal $\frac{1}{2}M_H \leq \mu_R, \mu_F \leq 2M_H$ range. It is that it is well known that the QCD corrections are significantly larger for the total inclusive cross section than for that on which basic selection cuts are applied; see e.g. Refs. [164–167]. This can be seen from the recent analysis of Ref. [112], in which the higher order corrections to the inclusive cross section for the main Tevatron Higgs signal, $gg \rightarrow H \rightarrow \ell\nu\nu$, have been compared to those affecting the cross section when selection cuts, that are very similar to those adopted by the CDF and D0 collaborations in their analysis (namely lepton selection and isolation, a minimum requirement for the missing transverse energy due to the neutrino-

²⁶The error might be reduced when including higher-order corrections in the 1 jet and 2 jet cross sections.

nos, and a veto on hard jets to suppress the $t\bar{t}$ background), are applied. The output of this study is that the K -factor for the cross section after cuts is $\sim 20\text{--}30\%$ smaller than the K -factor for the inclusive total cross section (albeit with a reduced scale dependence). For instance, one has $K_{\text{cuts}}^{\text{NNLO}} = 2.6$ and $K_{\text{total}}^{\text{NNLO}} = 3.3$ for $M_H = 160$ GeV and scales set to $\mu_F = \mu_R = M_H$.

Naively, one would expect that this $\sim 20\text{--}30\%$ reduction of the higher order QCD corrections when selection cuts are applied, if not implemented from the very beginning in the normalisation of the cross section after cuts that is actually used by the experiments (which would then reduce the acceptance of the signal events, defined as $\sigma_{\text{cuts}}^{\text{NNLO}}/\sigma_{\text{total}}^{\text{NNLO}}$), to be at least reflected in the scale variation of the inclusive cross section and, thus, accounted for in the theoretical uncertainty. This would be partly the case for scale variation within a factor $\kappa = 3$ from the central scale, which leads to a maximal reduction of the $gg \rightarrow H \rightarrow \ell\nu\nu$ cross section by about 20%, but not with the choice $\kappa = 2$ made in Refs. [90–93] which would have led to a possible reduction of the cross section by $\approx 10\%$ only²⁷.

4.2.2 The scale variation uncertainty in Higgs–strahlung processes

We finish this subsection by the discussion of the theoretical uncertainties in the Higgs strahlung mechanism $q\bar{q} \rightarrow VH$, following the same line of arguments as in the previous subsection.

To evaluate the uncertainties due to the variation of the renormalisation and factorisation scales in the Higgs–strahlung processes, the choice of the variation domain is in a sense simpler than for the $gg \rightarrow H$ mechanism. Indeed, as the process at leading order is mediated only by massive gauge boson exchange and is then a pure electroweak process at the partonic level, only the factorisation scale μ_F appears when the partonic cross section is folded with the q and \bar{q} luminosities and there is no dependence on the renormalisation scale μ_R at this order. It is only at NLO, when gluons are exchanged between or radiated from the q, \bar{q} initial states, that both scales μ_R and μ_F appear explicitly.

Using the proposed criterion for the estimate of the perturbative higher order effects, we thus choose again to consider the variation domain of the scales from their central values, $\mu_0/\kappa \leq \mu_R, \mu_F \leq \kappa\mu_0$ with $\mu_0 = M_{HW}$, of the NLO cross section to determine the value of the factor κ to be used at NNLO²⁸. We display in the left-hand side of Fig. 19

²⁷The discussion is, however, more involved as one has to consider the efficiencies obtained with the NNLO calculation compared to that obtained with the Monte–Carlo used by the experiments; see Ref. [112].

²⁸It is clear that in this case the comparison with the LO prediction would be no use as the scale uncertainty is a pure QCD uncertainty; the LO partonic cross section being a pure electroweak process, we

the variation of the NLO cross section $\sigma^{\text{NLO}}(p\bar{p} \rightarrow WH)$ at the Tevatron as a function of M_H for three values of the constant κ which defines the range spanned by the scales, $M_{HW}/\kappa \leq \mu_R, \mu_F \leq \kappa M_{HW}$. One sees that, in this case, a value $\kappa = 2$ is sufficient (if the scales μ_R and μ_F are varied independently in the chosen domain) in order that the uncertainty band at NLO reaches the central value of the cross section at NNLO. In fact, the NLO uncertainty band would have been only marginally affected if one had chosen the values $\kappa = 3, 4$ or even 5. This demonstrates that the cross sections for the Higgs–strahlung processes, in contrast to $gg \rightarrow H$, are very stable against scale variation, a result that is presumably due to the smaller $q\bar{q}$ color charges compared to gluons, $\approx C_F/C_A$, that lead to more moderate QCD corrections.

In the right–hand side of Fig. 19, the NNLO $p\bar{p} \rightarrow WH$ total cross section is displayed as a function of M_H for a scale variation $\frac{1}{2}M_{HW} \leq \mu_R, \mu_F \leq 2M_{HW}$. Contrary to the $gg \rightarrow H$ mechanism, the scale variation within the chosen range is rather mild and only a $\sim 0.7\%$ (at low M_H) to 1.2% (at high M_H) uncertainty is observed for the relevant Higgs mass range at the Tevatron. This had to be expected as the K –factors in the Higgs–strahlung processes, $K_{\text{NLO}} \approx 1.4$ and $K_{\text{NNLO}} \approx 1.5$, are substantially smaller than those affecting the gg fusion mechanism and one expects perturbation theory to have a better behavior in the former case. This provides more confidence that the Higgs–strahlung cross section is stable against scale variation and, thus, that higher order effects should be small.

4.3 The parton distribution functions puzzle

The second (and sometimes the most important) source of theoretical uncertainties on production cross sections and distributions at hadron colliders is due to the still imperfect parametrisation of the parton distribution functions (PDFs). Within a given parametrisation, for example the one in the MSTW scheme, these uncertainties are estimated as follows [132, 199, 200]. The scheme is based on a Hessian matrix method which enables a characterization of a parton parametrization in the neighborhood of the global χ^2 minimum fit and gives an access to the uncertainty estimation through a set of PDFs that describes this neighborhood. The corresponding PDFs are constructed by: *i*) performing a global fit of the data using N_{PDF} free parameters ($N_{\text{PDF}} = 15$ or 20, depending on the scheme); this provides the nominal PDF or reference set denoted by S_0 ; *ii*) the global χ^2 of the fit is increased to a given value $\Delta\chi^2$ to obtain the error matrix, this value is subject to vary between different collaborations; *iii*) the error matrix is diagonalized to obtain N_{PDF} eigen-

would not be consistent to compare a full NNLO calculation with a scale variation at LO induced only by the PDF through the factorization scale μ_F .

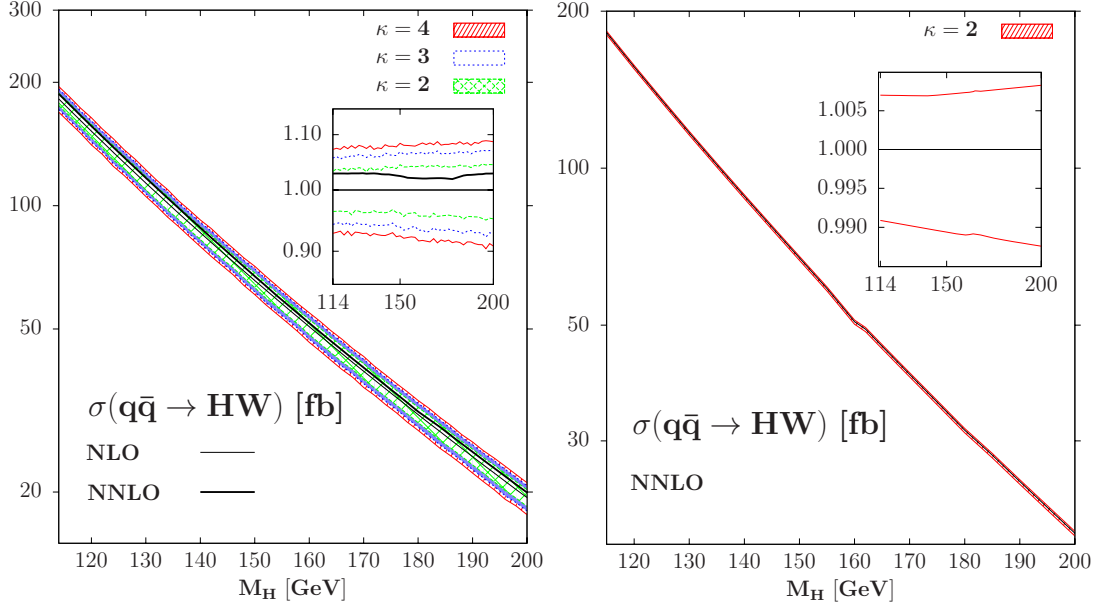


Figure 19: Left: the scale dependence of $\sigma(p\bar{p} \rightarrow WH)$ at NLO for variations $M_{HV}/\kappa \leq \mu_R, \mu_F \leq \kappa M_{HV}$ with $\kappa = 2, 3$ and 4, compared to the NNLO value; in the insert, shown are the variations in percentage and where the NNLO cross section is normalized to the NLO one. Right: the scale dependence of $\sigma(p\bar{p} \rightarrow WH)$ at NNLO for a variation in the domains $M_{HV}/2 \leq \mu_R = \mu_F \leq 2M_{HV}$; the relative deviations from the central value are shown in the insert.

vectors corresponding to N_{PDF} independent directions in the parameter space; (*iv*) for each eigenvector, up and down excursions are performed in the tolerance gap, $T = \sqrt{\Delta\chi_{\text{global}}^2}$, leading to $2N_{\text{PDF}}$ sets of new parameters, denoted by S_i , with $i = 1, 2N_{\text{PDF}}$. It is worth mentioning that the NNPDF collaboration [201] does not use this method and rely on Monte-Carlo replication sample to generate its uncertainty PDF sets.

These sets of PDFs can be used to calculate the uncertainty on a cross section σ in the general following way: one first evaluates the cross section with the nominal PDF S_0 to obtain the central value σ_0 , and then calculates the cross section with the S_i PDFs, giving $2N_{\text{PDF}}$ values σ_i , and defines, for each σ_i value, the deviations

$$\sigma_i^\pm = |\sigma_i - \sigma_0| \quad \text{when } \sigma_i \gtrless \sigma_0 \quad (4.18)$$

The uncertainties are summed quadratically to calculate the cross section, including the error from the PDFs that are given at the 68% or 90% confidence level (CL),

$$\sigma_0 \Big|_{-\Delta\sigma_{\text{PDF}}^-}^{+\Delta\sigma_{\text{PDF}}^+} \quad \text{with } \Delta\sigma_{\text{PDF}}^\pm = \left(\sum_i \sigma_i^{\pm 2} \right)^{1/2} \quad (4.19)$$

The procedure outlined above has been applied to estimate the PDF uncertainties in the Higgs production cross sections in the gluon-gluon fusion mechanism at the Tevatron

in Refs. [111, 118]. This has led to a 90% CL uncertainty of $\approx 6\%$ for the low mass range $M_H \approx 120$ GeV to $\approx 10\%$ in the high mass range, $M_H \approx 200$ GeV. These uncertainties were adopted in the early CDF/D0 combined Higgs search and represented the second largest source of errors after the scale variation. This has been shown since that at least in the case of the gluon–gluon fusion mechanism it underestimated the PDF uncertainties for at least the first reason that will be mentioned below, if not for that of the second that concerns the strong coupling constant α_s itself, see in the next pages.

First of all, the MSTW collaboration [128] is not the only one which uses the above scheme for PDF error estimates, as the CTEQ [145] and ABKM [147] collaborations, for instance, also provide similar schemes, as well as NNLO JR set [150] appeared in 2010 or HERAPDF [149] (NNPDF set [201] also allows for error estimates even if their method is a bit different). It is thus more appropriate to compare the results given by the different sets and take into account the possibly different errors that are obtained. In addition, as the parameterisations of the PDFs are different in the various PDF schemes, we might obtain different central values for the cross sections and the impact of this difference should also be addressed²⁹.

These two aspects will be taken into account in the following. We will begin the analysis by looking at the PDF uncertainties given separately by MSTW, ABKM and CTEQ. Even if in the case of CTEQ collaboration there is no NNLO PDFs set yet available, we can still use the available NLO sets, evaluate the PDF errors on the NLO cross sections and take these errors as approximately available at NNLO once we rescale the cross sections by including the NNLO corrections. This constitutes a good approximation for error estimates that is our goal in this first analysis.

We then will analyze the results obtained with the current four NNLO PDFs sets available on the market, that are the MSTW collaboration, the ABKM PDFs set, the HERA PDF 1.0 and the JR 09 PDF set, comparing only the central values. This will be full of information and we will see that there are too many differences between the predictions to discard the problem. Note that this PDF “puzzle” has been the subject of a recommendation by the PDF4LHC group, see [151]. This will also be discussed.

²⁹This difference should not come as a surprise as, even within the same scheme, there are large differences when the PDF sets are updated. For instance, as also pointed out in Refs. [111, 118], $\sigma^{\text{NNLO}}(gg \rightarrow H)$ evaluated with the MRST2004 set is different by more than 10% compared to the current value obtained with the MSTW2008 set, as a result of a corrected treatment of the b, c densities among other improvements.

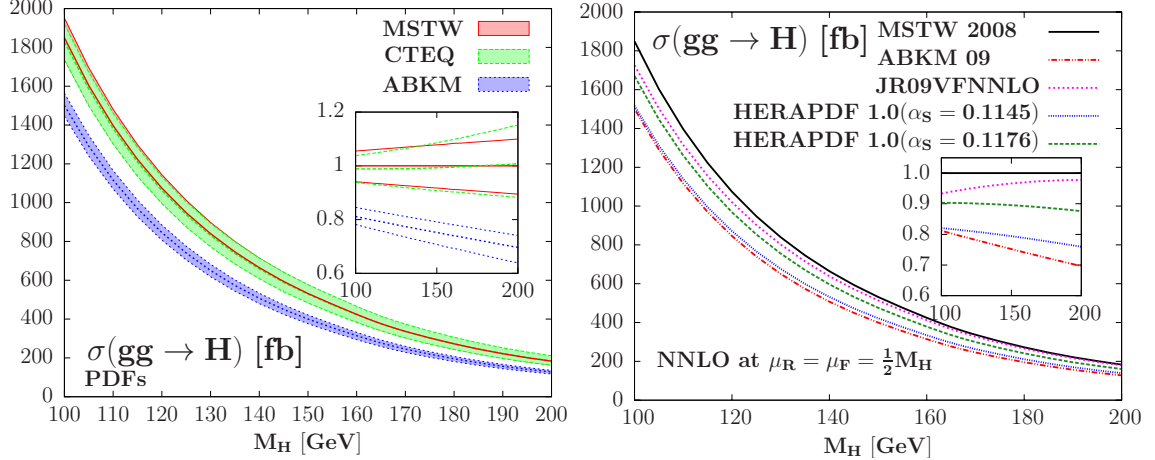


Figure 20: Left: the central values and the 90%CL PDF uncertainty bands in the NNLO cross section $\sigma(gg \rightarrow H + X)$ at the Tevatron when evaluated within the MSTW, CTEQ and ABKM schemes. In the insert, shown in percentage are the deviations within a given scheme and the CTEQ and ABKM central values when the cross sections are normalized to the MSTW central value. Right: the $gg \rightarrow H$ cross section as a function of M_H when the four NNLO PDF sets, MSTW, ABKM, JR and HERAPDF, are used. In the inserts, shown are the deviations with respect to the central MSTW value

4.3.1 PDF uncertainties in gluon–gluon fusion

In the case of the $gg \rightarrow H$ cross section at the Tevatron, the 90% CL PDF errors using the first three schemes discussed above (namely MSTW, CTEQ, ABKM) are shown in the left–hand side of Fig. 20 as a function of M_H . The spread of the cross section due to the PDF errors is approximately the same in the MSTW and CTEQ schemes, leading to an uncertainty band of less than 10% in both cases. For instance, in the MSTW scheme and in agreement with Refs. [111, 118], we obtain a $\sim \pm 6\%$ error for $M_H = 120$ GeV and $\sim \pm 9\%$ for $M_H = 180$ GeV; the errors are only slightly asymmetric and for $M_H = 160$ GeV, one has $\Delta\sigma_{\text{PDF}}^+/\sigma = +8.1\%$ and $\Delta\sigma_{\text{PDF}}^-/\sigma = -8.6\%$. The errors are relatively smaller in the ABKM case in the entire Higgs mass range and, for instance, we obtain a $\Delta\sigma_{\text{PDF}}^\pm/\sigma \approx \pm 5\%$ (7%) error for $M_H = 120$ (180) GeV.

The left–hand side of Fig. 20 opens a very important issue: the (very!) large discrepancy between the central values of the cross sections calculated with the different PDFs sets, with MSTW/CTEQ on the one hand and ABKM on the other hand, even when taking into account their individual uncertainties. This problem has been discussed in [147, 199, 202] and is a long–standing issue still pending in the community. Indeed, the use of the ABKM parametrisation results in a cross section that is $\sim 25\%$ smaller than the cross section evaluated with the MSTW or CTEQ PDFs. Thus, even if the PDF uncertainties evaluated within a given scheme turn out to be relatively small and apparently well under control,

the spread of the cross sections due to the different parameterisations can be much more important.

If one uses the old way of estimating the PDF uncertainties (i.e. before the advent of the PDF error estimates within a given scheme) by comparing the results given by different PDF parameterisations, one arrives at an uncertainty defined as

$$\begin{aligned}\Delta\sigma_{\text{PDF}}^+ &= \max(\sigma_{\text{MSTW}}^0, \sigma_{\text{CTEQ}}^0, \sigma_{\text{ABKM}}^0) - \sigma_{\text{MSTW}}^0 \\ \Delta\sigma_{\text{PDF}}^- &= \sigma_{\text{MSTW}}^0 - \min(\sigma_{\text{MSTW}}^0, \sigma_{\text{CTEQ}}^0, \sigma_{\text{ABKM}}^0)\end{aligned}\quad (4.20)$$

where the central value of the $gg \rightarrow H$ cross section is taken to be that given by the MSTW nominal set S_0 ³⁰. Hence, for $M_H = 160$ GeV for instance, one would have $\Delta\sigma_{\text{PDF}}^+ \approx 1\%$ given by the small difference between the CTEQ and MSTW central values of the cross section and $\Delta\sigma_{\text{PDF}}^- \approx -25\%$ given by the large difference between the ABKM and MSTW central values.

To make the discussion solid and consistent, we have compared the central predictions obtained when calculating the NNLO hadronic $gg \rightarrow H$ cross section using the various available NNLO sets on the market: besides the already mentioned ABKM [147] and MSTW [128] sets, we have also included the HERA PDF set [149] and the JR 09 set [150]. The result is displayed in the right-hand side of Fig. 20. As can be seen, there is a very large spread in the four predictions, in particular at large M_H values where the poorly constrained gluon densities at high- x are involved. The largest rate is obtained with MSTW, but the cross section using the ABKM set is $\approx 30\%$ lower for $M_H \approx 160$ GeV. That would mean that using the naive way to estimate this spread would end-up with an approximate -30% uncertainty only due to PDF uncertainty! Nearly similar results would have been obtained using HERAPDF set³¹ with the smaller $\alpha_s(M_Z)$ value, with an approximate 22% decrease of the cross section for $M_H \approx 160$ GeV.

Nevertheless we would like to keep considering the MSTW scheme for at least two reasons: first because it is the widest used PDF scheme and then allows for comparison with other calculation and especially with the numbers used in [90–93], and then because the MSTW scheme include the di-jet Tevatron run II data which are of utmost importance

³⁰We do not include in this comparison the uncertainties obtain within a given PDF set, which would add 5% to 7% to the uncertainty quoted.

³¹It is often argued against the HERAPDF scheme, which uses consistently only HERA data to determine the flavour decomposition, that it does not use any jet (Tevatron or DIS) data which is in principle important in the determination of the gluon densities. However, HERAPDF describes well not only the Tevatron jet data but also the W, Z data. Since this is a prediction beyond leading order, it has also the contributions of the gluon included. This gives an indirect test that the gluon densities are predicted in a satisfactory way. See also Ref. [203].

in this context. We will of course not discard the discrepancy outlined above, and try to solve it within the MSTW scheme.

Indeed, the spread of the predictions does not only result from the different gluon densities used (and it is well known that these densities are less severely constrained by experimental data than light quark densities, especially at high Bjorken- x values), but also from the difference in the value of the strong coupling constant α_s which is fitted altogether with the PDF sets. The $gg \rightarrow H$ process is very special in light of this issue, as this process is already a one-loop calculation at LO which is proportional to the square of α_s and the large NLO and NNLO QCD contributions are, respectively, of $\mathcal{O}(\alpha_s^3)$ and $\mathcal{O}(\alpha_s^4)$. The α_s value used in the ABKM set, $\alpha_s(M_Z^2) = 0.1129 \pm 0.0014$ at NLO in the BMSM scheme [204], is $\approx 3\sigma$ smaller than the one in the MSTW set $\alpha_s(M_Z^2) = 0.12018 \pm 0.014$ at NLO. Similar difference arise with the HERA PDF set ($\alpha_s(M_Z^2) = 0.1135$ or 0.1176 at NNLO depending on the PDF set) or with JR 09 set ($\alpha_s(M_Z^2) = 0.1124 \pm 0.0020$ at NNLO) when compared to MSTW value displayed in Eq. 4.21³². Since the K -factors for the gluon-gluon fusion process are very large at the Tevatron, $K_{\text{NLO}} \sim 2$ and $K_{\text{NNLO}} \sim 3$, a one percent uncertainty in the input value of α_s will generate a $\approx 3\%$ uncertainty in $\sigma^{\text{NNLO}}(gg \rightarrow H)$.

$$\alpha_s(M_Z^2) = 0.11707^{+0.0014}_{-0.0014} \text{ (68\%CL)} \quad ^{+0.0032}_{-0.0032} \text{ (90\%CL)} \quad \text{at NNLO} \quad (4.21)$$

Experimental collaborations are now aware of this issue and have started in 2010 to take into account related “ α_s ” uncertainties in the quoted number they use for their analysis, see [92, 93]. This uncertainty was certainly lacking in earlier Tevatron analysis [90, 91] and that was after the output of Ref. [94] that the incorporation of such an uncertainty was widely accepted.

In general, α_s is fitted together with the PDFs: the PDF sets are only defined for the special value of α_s obtained with the best fit and, to be consistent, this best value of α_s that we denote α_s^0 , should also be used for the partonic part of the cross section. Indeed there is an interplay between the PDFs and the value of α_s and, for instance, a larger value of α_s would lead to a smaller gluon density at low x [199]. The MSTW collaboration released last year a new set-up which allows for a simultaneous evaluation of the errors due to the PDFs and those due to the experimental uncertainties on α_s of Eq. 4.21, taking into account the possible correlations [199]. The procedure to obtain the different PDFs and their associated errors is similar to what was presented in the introduction of this subsection, but provided

³²The significant difference between the world average α_s value [205] and the one from deep-inelastic scattering (DIS) data used in the PDFs is connected to that issue.

is a collection of five PDF+error sets for different α_s values: the best fit value α_s^0 and its 68% CL and 90% CL maximal and minimal values.

Using the following equations to calculate the PDF error for a fixed value of α_s ,

$$\begin{aligned} (\Delta\sigma_{\text{PDF}}^{\alpha_s})_+ &= \sqrt{\sum_i \left\{ \max \left[\sigma(\alpha_s, S_i^+) - \sigma(\alpha_s^0, S_0), \sigma(\alpha_s, S_i^-) - \sigma(\alpha_s^0, S_0), 0 \right] \right\}^2}, \\ (\Delta\sigma_{\text{PDF}}^{\alpha_s})_- &= \sqrt{\sum_i \left\{ \max \left[\sigma(\alpha_s^0, S_0) - \sigma(\alpha_s, S_i^+), \sigma(\alpha_s^0, S_0) - \sigma(\alpha_s, S_i^-), 0 \right] \right\}^2}, \end{aligned} \quad (4.22)$$

we then compare these five different values and finally arrives, with α_s^0 as the best-fit value of α_s given by the central values of Eq. 4.21 and S_0 the nominal PDF set with this α_s value, at the 90% CL PDF+ $\Delta^{\text{exp}}\alpha_s$ errors given by [199]

$$\begin{aligned} \Delta\sigma_{\text{PDF}+\alpha_s^{\text{exp}}}^+ &= \max_{\alpha_s} \left(\left\{ \sigma(\alpha_s^0, S_0) + (\Delta\sigma_{\text{PDF}}^{\alpha_s})_+ \right\} - \sigma(\alpha_s^0, S_0) \right), \\ \Delta\sigma_{\text{PDF}+\alpha_s^{\text{exp}}}^- &= \sigma(\alpha_s^0, S_0) - \min_{\alpha_s} \left(\left\{ \sigma(\alpha_s^0, S_0) - (\Delta\sigma_{\text{PDF}}^{\alpha_s})_- \right\} \right). \end{aligned} \quad (4.23)$$

Using this procedure, we have evaluated the PDF+ $\Delta^{\text{exp}}\alpha_s$ uncertainty on the NNLO $gg \rightarrow H$ total cross section at the Tevatron and the result is displayed in the left-hand side of Fig. 21 as a function of M_H . The PDF+ $\Delta^{\text{exp}}\alpha_s$ error ranges from $\approx \pm 11\%$ for $M_H = 120$ GeV to $\approx \pm 14\%$ for $M_H = 180$ GeV with, again, a slight asymmetry between the upper and lower values; for a Higgs mass $M_H = 160$ GeV, one has $\Delta\sigma_{\text{PDF}+\alpha_s}^{\pm}/\sigma = {}_{-12.0\%}^{+12.8\%}$. That is, the experimental uncertainty on α_s adds a $\approx 5\%$ error to the PDF error alone over the entire M_H range relevant at the Tevatron.

Nevertheless, this larger PDF+ $\Delta^{\text{exp}}\alpha_s$ uncertainty compared to the PDF uncertainty alone does not yet reconcile the evaluation of MSTW and ABKM (in this last scheme the $\Delta^{\text{exp}}\alpha_s$ uncertainty has not been included since no PDF set with an error on α_s is provided) of the $gg \rightarrow H$ cross section at the Tevatron, the difference between the lowest MSTW value and the highest ABKM value being still at the level of $\approx 10\%$.

In order to (at least partially) reconcile the MSTW and ABKM/HERA predictions which differ drastically, we introduce the impact of the theoretical uncertainty on the value of α_s . So far, only the impact of the experimental errors on α_s has been discussed, while it is well known that the strong coupling constant is also plagued by theoretical uncertainties due to scale variation or ambiguities in heavy quark flavor scheme definition. This theoretical uncertainty has been estimated in Ref. [128] to be at least $\Delta^{\text{th}}\alpha_s = \pm 0.003$ at NLO which turns out to be ± 0.002 at NNLO. The estimate of Refs. [206, 207] leads to a slightly larger uncertainty, $\Delta^{\text{th}}\alpha_s = \pm 0.0033$. We will begin by using the MSTW uncertainty, that is

$$\Delta_{\text{NNLO}}^{\text{th}}\alpha_s = 0.002 \quad (4.24)$$

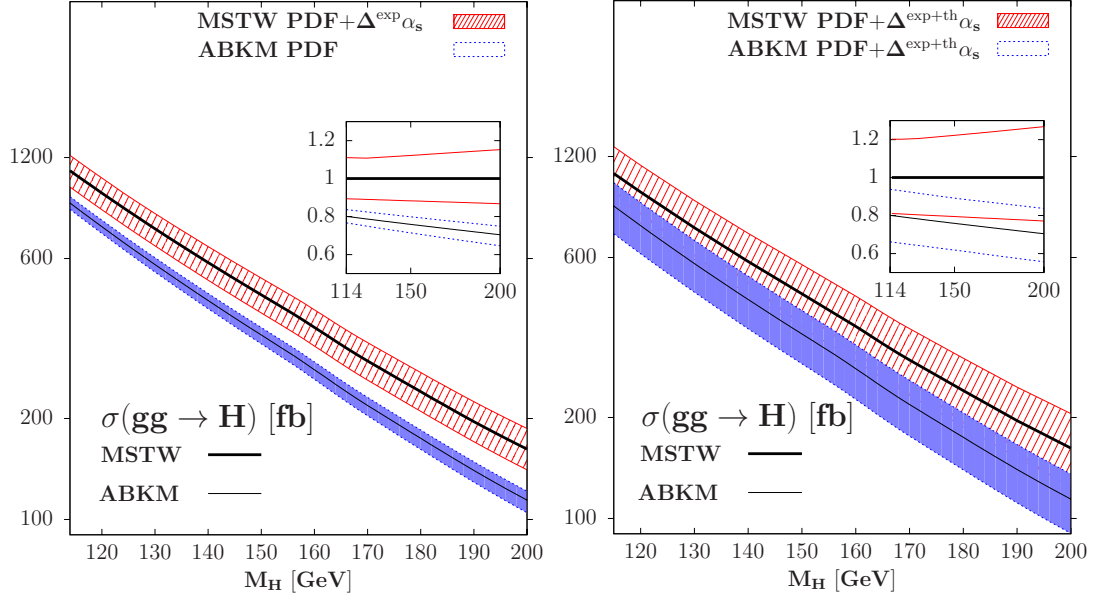


Figure 21: Left: the PDF+ $\Delta^{\text{exp}}\alpha_s$ uncertainties in the MSTW scheme and the PDF uncertainties in the ABKM schemes on the $gg \rightarrow H$ cross section at the Tevatron as a function of M_H . Right: the PDF+ $\Delta^{\text{exp}}\alpha_s + \Delta^{\text{th}}\alpha_s$ uncertainties in the MSTW scheme using the new set-up and the PDF+ $\Delta^{\text{exp}}\alpha_s + \Delta^{\text{th}}\alpha_s$ error in the ABKM scheme using a naive procedure. In the inserts, shown are the same but with the cross sections normalized to the MSTW central cross section.

To calculate in a consistent way the uncertainty due to this α_s variation, we use the fixed- α_s NNLO PDF grid also provided by the MSTW collaboration, which is a set of central PDFs but at fixed values of α_s different from the best-fit value. Values of α_s in a range comprised between 0.107 and 0.127 in steps of 0.001 are selected, which then include the values $\alpha_s^0 \pm 0.002$ that we will use for our estimation. We also point out that this also allows for a broader range of $\Delta^{\text{th}}\alpha_s$ value, that we will use in the following. Using this PDF grid with the theoretical error on α_s of Eq. 4.24 implemented, the upper and lower values of the cross sections will be given by

$$\begin{aligned} \Delta\sigma_{\text{PDF}+\alpha_s^{\text{th}}}^+ &= \sigma(\alpha_s^0 + \Delta^{\text{th}}\alpha_s, S_0(\alpha_s^0 + \Delta^{\text{th}}\alpha_s)) - \sigma(\alpha_s^0, S_0(\alpha_s^0)) \\ \Delta\sigma_{\text{PDF}+\alpha_s^{\text{th}}}^- &= \sigma(\alpha_s^0, S_0(\alpha_s^0)) - \sigma(\alpha_s^0 - \Delta^{\text{th}}\alpha_s, S_0(\alpha_s^0 - \Delta^{\text{th}}\alpha_s)) \end{aligned} \quad (4.25)$$

with again $S_0(\alpha_s)$ being the MSTW best-fit PDF set at the fixed α_s value which is either α_s^0 or $\alpha_s^0 \pm \Delta^{\text{th}}\alpha_s$. For the calculation with ABKM set, we use a naive estimate, that is use the central PDF set at the central $\alpha_s(M_Z^2)$ but with different $\alpha_s(M_Z^2)$ values, as this PDFs set does not provide different PDFs set according to a variation in the value of the strong coupling constant.

Nevertheless with this procedure and the value adopted in Eq. 4.24 the uncertainty is still far from solving the issue. Indeed, as pointed in Ref. [94], taking this additional

uncertainty with the value of $\Delta^{\text{th}}\alpha_s$ in Eq. 4.24 would have reconciled the MSTW/CTEQ and ABKM/HERA prediction only in the case where $\mu_0 = M_H$. When switching to $\mu_0 = \frac{1}{2}M_H$, it seems that this increases the spread between the different PDFs sets predictions. We will then take as $\Delta^{\text{th}}\alpha_s$ the difference between the strong coupling constant value in the MSTW set and in the ABKM set. This gives in the end

$$\Delta_{(2)}^{\text{th}}\alpha_s(M_Z^2) = 0.004 \quad (4.26)$$

Note that despite of the fact that the uncertainty on α_s is that of a theoretical and is not at the 90% CL, we will take the PDF+ $\Delta^{\text{th}}\alpha_s$ error that one obtains using Eq. 4.25 to be at the 90% CL. In this way we will be able to add the uncertainty to the rest: to obtain the total PDF+ α_s uncertainty, we then add in quadrature the PDF+ $\Delta^{\text{exp}}\alpha_s$ and PDF+ $\Delta^{\text{th}}\alpha_s$ uncertainties,

$$\Delta\sigma_{\text{PDF}+\alpha_s^{\text{exp}}+\alpha_s^{\text{th}}}^{\pm} = \left((\Delta\sigma_{\text{PDF}+\alpha_s^{\text{exp}}}^{\pm})^2 + (\Delta\sigma_{\text{PDF}+\alpha_s^{\text{th}}}^{\pm})^2 \right)^{1/2}. \quad (4.27)$$

The result for the total PDF+ α_s 90% CL uncertainty on $\sigma^{\text{NNLO}}(gg \rightarrow H)$ in the MSTW scheme using the procedure outlined above is shown in the right-hand side of Fig. 21 as a function of M_H and compared to the result when the PDF error in the ABKM scheme is combined with the $\Delta^{\text{exp}}\alpha_s$ and $\Delta^{\text{th}}\alpha_s$ uncertainties using the naive procedure briefly mentioned previously as, in this case, no PDF with an α_s value different from that obtained with the best-fit is provided. Stretching the range of $\Delta^{\text{th}}\alpha_s$ to $\Delta^{\text{th}}\alpha_s = 0.004$ thus helps to reconcile MSTW and ABKM predictions as can be seen on the graph, the two uncertainty bands overlapping.

We then compare MSTW PDF, PDF+ $\Delta^{\text{exp}}\alpha_s$ and the total PDF+ $\Delta^{\text{exp+th}}\alpha_s$ uncertainties in Fig. 22. The total uncertainty due to the PDF and theoretical and experimental errors on the strong coupling constant α_s is now significant, and amounts to $\pm 15\%$ to 20% on the central cross section depending on the M_H value. This is still a bit larger than the 12.5% error which has been assumed in the most recent CDF/D0 combined analyses [92,93], and of course even larger than the $\approx \pm 8\%$ assumed in the earliest Tevatron analysis [90]) where the strong coupling constant uncertainties were lacking.

In any case we face the situation where we have large differences in the predictions obtained using the various PDFs set on the market. This is what we call the ‘‘pdf puzzle’’; this is also discussed in Ref. [208] which analyzes the question of the discrepancy between global fits and DIS fits predictions, assessing that this can be related to NMC data handling in the PDFs.

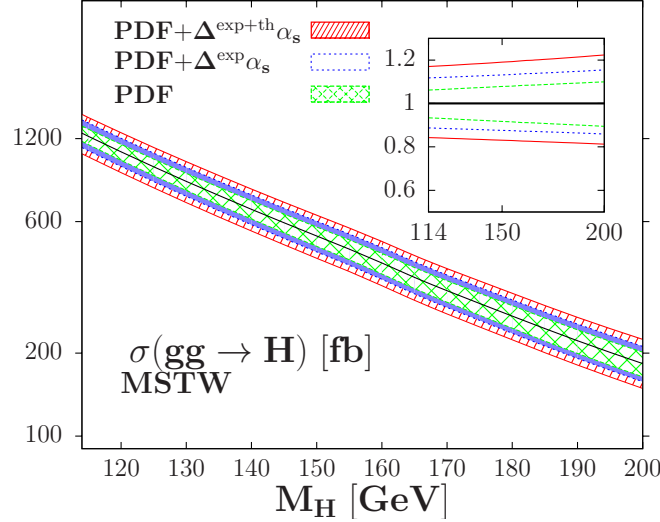


Figure 22: The 90% CL PDF, PDF, PDF+ $\Delta^{\text{exp}}\alpha_s$ and PDF+ $\Delta^{\text{exp+th}}\alpha_s$ uncertainties on $\sigma_{gg\rightarrow H}^{\text{NNLO}}$ in the MSTW parametrisation. In the inserts, shown in % are the deviations with respect to the central MSTW value.

4.3.2 The case of Higgs–strahlung processes

In the case of the associated Higgs boson production with a W boson, $p\bar{p} \rightarrow WH$, we follow the same line of arguments developed above in the case of the gluon–gluon fusion. We recall that the case of the associated production with a Z boson is absolutely similar to that of the W boson.

We thus calculate the PDF, PDF+ $\Delta^{\text{exp}}\alpha_s$ and PDF+ $\Delta^{\text{exp+th}}\alpha_s$ 90% CL uncertainties in the MSTW scheme and compare it to what could be obtained using the ABKM PDFs set. In this case we use the $\Delta^{\text{th}}\alpha_s$ value of Eq. 4.26 as it is sufficient to reconcile the different predictions as seen in the results below.

The results are displayed in Fig. 23 and Fig. 24 for the Tevatron center–of–mass energy 1.96 TeV and for Higgs mass relevant in the Tevatron SM Higgs searches. The spread of the MSTW/CTEQ/ABKM schemes is displayed in Fig. 23. The uncertainty bands are of order $\pm 4\%$ in CTEQ/MSTW schemes and slightly larger in ABKM PDFs set. The discrepancy between central predictions is of order 10% which is nearly three times less than compared to the gluon–gluon fusion case. This does not constitute a surprise as at LO the Higgs–strahlung processes use quark densities which are better known than gluon density. However, contrary to the gluon–gluon fusion case, the MSTW/CTEQ and ABKM bands almost touch each other.

In the left–hand side of Fig. 24, we show the bands resulting from the PDF+ $\Delta^{\text{exp}}\alpha_s$

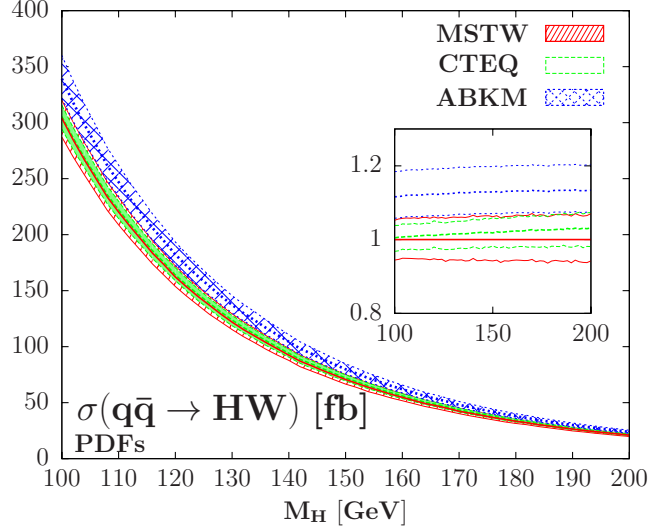


Figure 23: The central values and the PDF uncertainties in the cross section $\sigma(p\bar{p} \rightarrow WH)$ at the Tevatron when evaluated within the MSTW, CTEQ and ABKM schemes. In the insert, the relative deviations from the central MSTW value are shown.

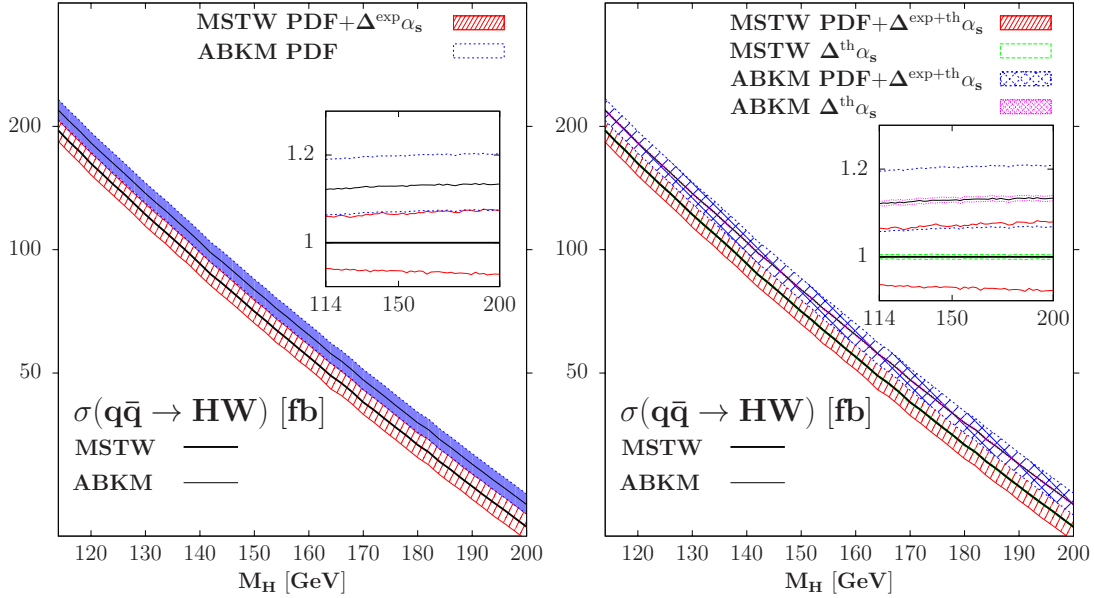


Figure 24: Left: the PDF uncertainties in the MSTW and ABKM schemes when the additional experimental errors on α_s is included in MSTW as discussed in the text; in the insert, the relative deviations from the central MSTW value are shown. Right: the same as in a) but when the theoretical error on α_s is added in both the MSTW and ABKM cases.

uncertainty in the MSTW mixed scheme, while the right-hand side of the figure shows the uncertainty bands when the additional theoretical error $\Delta^{\text{th}}\alpha_s$ is included in both the MSTW scheme using Eq. 4.27 and ABKM scheme using the naive estimate and Eq. 4.25. As expected, the errors due to the imprecise value of α_s are much smaller than in the

$gg \rightarrow H$ mechanism, as in Higgs–strahlung, the process does not involve α_s in the Born approximation and the K –factors are reasonably small, $K_{\text{NNLO}} \lesssim 1.5$. Hence, $\Delta^{\text{exp}}\alpha_s$ generates an additional error that is about $\approx 2\%$ when included in the PDF fits, while the error due to $\Delta^{\text{th}}\alpha_s$ is about one to two percent.

In any case, the total PDF+ $\Delta^{\text{exp}}\alpha_s$ + $\Delta^{\text{th}}\alpha_s$ uncertainty is at the level of ≈ 7 – 8% in the MSTW scheme, that is slightly larger than the errors due to the PDFs alone, and we again have a significant overlap between the MSTW and ABKM uncertainty band but with the use of MSTW theoretical error estimate of $\Delta^{\text{th}}\alpha_s = 0.002$.

To conclude this subsection we would like to insist on the fact that the procedure that we have used is only one particular way of handling the PDF puzzle which is still currently pending and on active investigation by theorists, especially in the view of the LHC predictions. In particular we could also have used the difference between the central predictions given by the different NNLO PDFs set on the market, that is the MSTW, ABKM, HERA and JR sets. The PDF uncertainty, when compared to the central MSTW prediction, would have ended being of order -30% , $+0\%$ in the critical range $155 \leq M_H \leq 180$ GeV, as seen in the right–hand side of Fig. 20 .

We also note that there is another recipe that has been suggested by the PDF4LHC working group for evaluating PDF uncertainties for NNLO cross sections (besides taking the envelope of the predicted values obtained using several PDF sets) [209]: take the 68% CL MSTW PDF+ $\Delta^{\text{exp}}\alpha_s$ error and multiply it by a factor of two [210]. In our case, this would lead to an uncertainty of $\approx \pm 25\%$ which, for the minimal value, is close to the recipe discussed just above, and is larger than what we obtain when considering the PDF+ $\Delta^{\text{exp+th}}\alpha_s$ uncertainty given by MSTW. This gives some credits to our way of handling the PDF issue.

4.4 Effective field theory and its uncertainties

This subsection is intended to cover a specific issue in the gluon–gluon fusion production channel and will not concern the Higgs–strahlung mechanism. Indeed, while both the QCD and electroweak radiative corrections to the process $gg \rightarrow H$ have been calculated exactly at NLO taking into account both the top quark and the bottom quarks loop with the exact finite mass of both quark flavours, these corrections are derived at NNLO only in an effective field theory (EFT) approach in which the loop particles are assumed to be very massive, $m \gg M_H$, and integrated out. Thus these corrections have only been calculated for the top loop and currently there are no NNLO corrections for the b –quark loop available.

4.4.1 The b -loop uncertainty

At the Born level, taking into account only the dominant contribution of the top quark loop and working in the limit $m_t \rightarrow \infty$ provides an approximation [105, 106] that is only good at the 10% level for Higgs masses below the $t\bar{t}$ kinematical threshold, $M_H \lesssim 350$ GeV. The difference from the exact result is mainly due to the absence of the contribution of the b -quark loop: although the b -quark mass is small, the $gg \rightarrow H$ amplitude exhibits a dependence $\propto m_b^2/M_H^2 \times \ln^2(m_b^2/M_H^2)$ which, for relatively low values of the Higgs mass, generates a non-negligible contribution that interferes destructively with the dominant top-quark loop contribution. In turn, when considering only the top quark loop in the Hgg amplitude, the approximation $m_t \rightarrow \infty$ is extremely good for Higgs masses below $2m_t$, compared to the amplitude with the exact top quark mass dependence as shown in Refs. [107–109].

In the NLO approximation for the QCD radiative corrections, it has been shown [105] that the exact K -factor when the full dependence on the top and bottom quark masses is taken into account, $K_{\text{NLO}}^{\text{exact}}$, is smaller than the K factor obtained in the approximation in which only the top quark contribution is included and the asymptotic limit $m_t \rightarrow \infty$ is taken, $K_{\text{NLO}}^{m_t \rightarrow \infty}$. The reason is that when only the b -quark loop contribution is considered in the Hgg amplitude (as in the case of supersymmetric theories in which the b -quark Yukawa coupling is strongly enhanced compared to its Standard Model value [211], see section 11), the K -factor for the $gg \rightarrow H$ cross section at the Tevatron is about $K \sim 1.2$ to 1.5, instead of $K \sim 2.4$ when only the top quark is included in the loop. The approximation of infinite loop particle mass significantly improves when the full t, b mass dependence is included in the LO order cross section and $\sigma_{\text{NLO}}^{m_t \rightarrow \infty} = K_{\text{NLO}}^{m_t \rightarrow \infty} \times \sigma_{\text{LO}}(m_t, m_b)$ gets closer to the cross section $\sigma_{\text{NLO}}^{\text{exact}}$ in which the exact m_t, m_b dependence is taken into account.

The difference between $\sigma_{\text{NLO}}^{\text{exact}}$ and $\sigma_{\text{NLO}}^{m_t \rightarrow \infty}$ at Tevatron energies is shown in Fig. 25 as a function of the Higgs mass we show that there is a few percent discrepancy between the two cross sections. As mentioned previously, in the Higgs mass range $115 \text{ GeV} \lesssim M_H \lesssim 200$ GeV relevant at Tevatron energies, this difference is only due to the absence of the b -quark loop contribution and its interference with the top quark loop in the Hgg amplitude and not to the fact that the limit $m_t \gg M_H$ is taken.

At NNLO, because of the complexity of the calculation, only the result in the effective approach in which the loop particle masses are assumed to be infinite is available. In the case of the NNLO QCD corrections [107–109], the b -quark loop contribution and its interference with the contribution of t -quark loop is therefore missing. Since the NNLO correction increases the cross section by $\sim 30\%$, the question whether this missing piece might

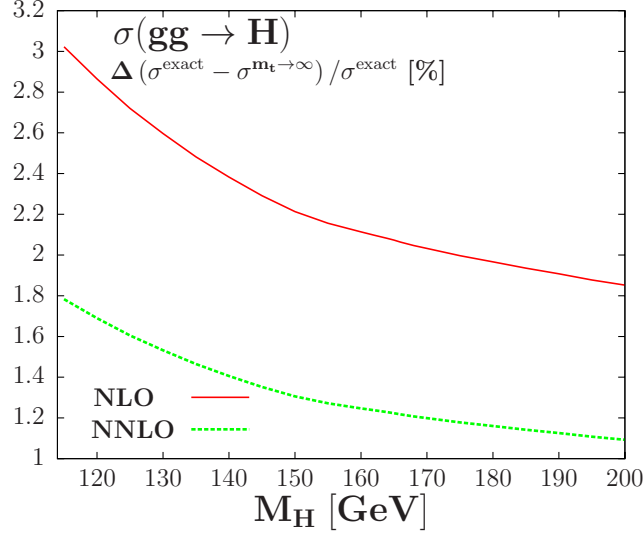


Figure 25: Relative difference (in %) at Tevatron energies and as a function of M_H between the exact NLO and NNLO $gg \rightarrow H$ cross sections $\sigma_{\text{NLO/NNLO}}^{\text{exact}}$ and the cross section in the effective approach with an infinite top quark mass $\sigma_{\text{NLO/NNLO}}^{m_t \rightarrow \infty}$.

lead to an overestimate of the total K -factor should be asked. We will assume that it might be indeed the case and assign an error on the NNLO QCD result which is approximately the difference between the exact result $\sigma_{\text{NLO}}^{\text{exact}}$ and the approximate result $\sigma_{\text{NLO}}^{m_t \rightarrow \infty}$ obtained at NLO while taking the exact LO result and shown in Fig. 25, but rescaled with the relative magnitude of the K -factors that is obtained at NLO and NNLO, i.e. $K_{\text{NLO}}^{m_t \rightarrow \infty} / K_{\text{NNLO}}^{m_t \rightarrow \infty}$. This leads to an uncertainty on the NNLO cross section which ranges from $\sim \pm 2\%$ for low Higgs values $M_H \sim 120$ GeV at which the b -quark loop contribution is significant at LO, to the level of $\sim \pm 1\%$ for Higgs masses above $M_H \sim 180$ GeV for which the b -quark loop contribution is much smaller. This uncertainty is not really taken into account in the scale uncertainty, as we are not only missing the b -loop contribution but also, and mainly if we compare to what happens at NLO, the (likely negative) top-bottom interference at NNLO which can be significant. This interference term cannot be really well estimated through NNLO scale variation as the latter will mainly estimate missing N^3LO terms.

In addition we should also assign to the b -quark contribution an error originating from the freedom in choosing the input value of the b -quark mass in the loop amplitude and the scheme in which it is defined³³. Indeed, apart from the difference obtained when using the b -quark pole mass, $M_b^{\text{pole}} \approx 4.7$ GeV, as we have done here, or the running $\overline{\text{MS}}$ mass evaluated at the scale of the b -quark mass, $\bar{m}_b^{\text{MS}}(M_b) \sim 4.2$ GeV, there is an additional $\frac{4}{3} \frac{\alpha_s}{\pi}$ factor which enters the cross section when switching from the on-shell to the $\overline{\text{MS}}$ scheme. This leads to an error of approximately 1% on the total cross section, over the M_H range

³³We thank M. Spira for reminding us of this point.

that is relevant at the Tevatron. In contrast, according to very recent calculations [212–215], the $m_t \rightarrow \infty$ limit is a very good approximation for the top–quark loop contribution to $\sigma(gg \rightarrow H)$ at NNLO as the higher order terms, when expanding the amplitude in power series of $M_H^2/(4m_t^2)$, lead to a difference that is smaller than one percent for $M_H \lesssim 300$ GeV.

4.4.2 The electroweak uncertainty

The other part of the calculation that is concerned by an effective theory approach deals with the electroweak corrections in $gg \rightarrow H$ production channel. As mentioned previously, while the $\mathcal{O}(\alpha)$ NLO corrections have been calculated with the exact dependence on the loop particle masses [117], the mixed QCD–electroweak corrections due to light quark loops at $\mathcal{O}(\alpha\alpha_s)$ have been evaluated [118] in the effective theory approach where the W, Z bosons have been integrated out and which is only valid for $M_H \ll M_W$. These contributions are approximately equal to the difference between the exact NLO electroweak corrections when evaluated in the complete factorization and partial factorization schemes [118].

However, as the results for the mixed corrections are only valid at most for $M_H < M_W$ and given the fact that the δ_{EW} electroweak correction at $\mathcal{O}(\alpha)$ exhibits a completely different behavior below and above the $2M_W$ threshold³⁴, one should be cautious and assign an uncertainty to this mixed QCD–electroweak correction, even if this may overestimate the uncertainty due to EFT effects. Conservatively, we then have chosen in Ref. [94] to assign an error that is of the same size as the $\mathcal{O}(\alpha\alpha_s)$ contribution itself. This is equivalent to assigning an error to the full $\mathcal{O}(\alpha)$ contribution that amounts to the difference between the correction obtained in the complete factorization and partial factorization schemes as done in Ref. [117]. As pointed out in the latter reference, this reduces to adopting the usual and well–established procedure that has been used at LEP for attributing uncertainties due to unknown higher order effects. We then obtain an uncertainty ranging from 1.5% to 3.5% for Higgs masses below $M_H \lesssim 2M_W$ and below 1.5% for larger Higgs masses as is shown in Fig. 26.

Finally, we should note that we do not address here the issue of the threshold effects from virtual W and Z bosons which lead to spurious spikes in the $\mathcal{O}(\alpha)$ electroweak correction in the mass range $M_H = 160$ – 190 GeV which includes the Higgs mass domain that is most

³⁴Indeed, the NLO electroweak correction δ_{EW} of Ref. [117] is positive below the WW threshold $M_H \lesssim 2M_W$ for which the effective approach is valid in this case and turns to negative for $M_H \gtrsim 2M_Z$ for which the effective approach cannot be applied and the amplitude develops imaginary parts. This behavior can also be seen in Fig. 26 which, up to the overall normalisation, is to a very good approximation the δ_{EW} correction factor given in Fig. 1 of Ref. [117] for $M_H \lesssim 2M_Z$.

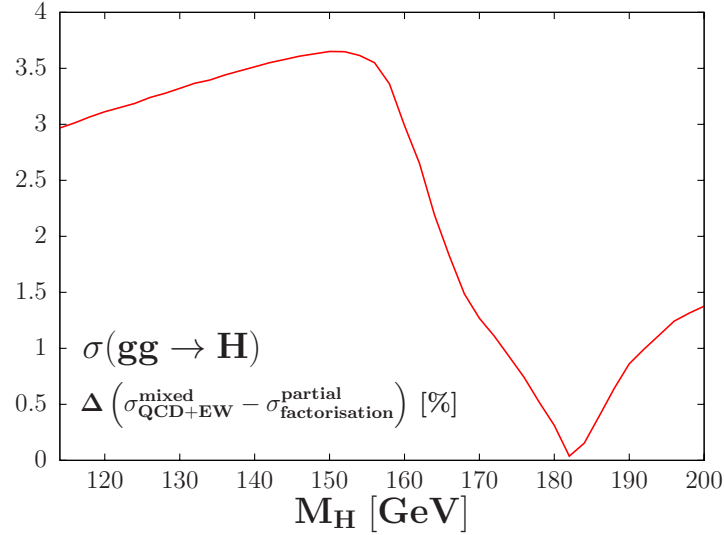


Figure 26: Relative difference (in %) between the complete factorization and partial factorization approaches for the electroweak radiative corrections to the NLO $gg \rightarrow H$ cross section at the Tevatron as a function of M_H .

relevant at the Tevatron (the same problem occurs in the case of the $p\bar{p} \rightarrow HV$ cross sections once the electroweak corrections are included). These singularities are smoothed by including the finite widths of the W/Z bosons, a procedure which might introduce potential additional theoretical ambiguities that has been ignored in the analysis of Ref. [94] upon which is constructed a large part of this thesis.

4.5 Combination and total uncertainty

We present in this subsection the tables which summarize the individual sources of theoretical uncertainties, and we discuss how to combine them to obtain the overall theoretical uncertainty. We start with the gluon–gluon fusion process and then turn our attention to the Higgs–strahlung channels.

The central cross section in the $gg \rightarrow H$ process at the Tevatron, as well as the various associated theoretical uncertainties, are summarized in Table 2. For a set of Higgs mass values that is relevant at the Tevatron (we choose a step of 5 GeV as done by the CDF and D0 experiments [90–93] except in the critical range 160–170 GeV where a 2 GeV step has been adopted), the second column of the table gives the central values of the total cross section at NNLO (in fb) for the renormalization and factorization scale choice $\mu_R = \mu_F = \frac{1}{2}M_H$, when the partonic cross sections are folded with the MSTW parton densities. The following columns give the errors on the central value of the cross section originating from the various sources discussed in subsection 4.2/4.3/4.4, namely, the uncertainties due to the

scale variation in the adopted range $\frac{1}{3}\mu_0 \leq \mu_R, \mu_F \leq 3\mu_0$ with $\mu_0 = \frac{1}{2}M_H$, the 90% CL errors due to the MSTW PDF, PDF+ $\Delta^{\text{exp}}\alpha_s$ and PDF+ $\Delta^{\text{exp}}\alpha_s + \Delta^{\text{th}}\alpha_s$ uncertainties as well as the estimated uncertainties from the use of the effective approach in the calculation of the NNLO QCD (the b -quark loop contribution and its interference with the top-quark loop) and electroweak (difference between the complete and partial factorization approaches) radiative corrections.

The largest of these errors, $\sim +15, -20\%$, is due to the scale variation, followed by the PDF+ $\Delta^{\text{exp}}\alpha_s + \Delta^{\text{th}}\alpha_s$ uncertainties which are at the level of $\approx 15\%$; the errors due to the effective theory approach (including that due to the definition of the b -quark mass) are much smaller, being of the order of a few percent for both the QCD and electroweak parts.

The very important issue which remains to be solved is how to combine these various uncertainties. We present here the procedure that was developed in Ref. [94] and then used for the following analyses at the LHC and in the MSSM (see the following sections). In accord with Refs. [112, 210], there is currently a vivid debate whether to add these errors in quadrature as done, for instance, by the CDF and D0 collaborations³⁵ [216–218] or not, and we believe that quadratic addition should be the accurate procedure when dealing with theoretical uncertainties.

To begin with, the uncertainties associated to the PDF parameterisations should be viewed as theoretical errors and they have been considered as such since a long time. Indeed, although the PDF sets use various experimental data which have intrinsic errors which then induce “might-be” statistical grounds, the main uncertainty is due to the theoretical assumptions which go into the different parameterizations. This uncertainty cannot be easily quantified within one given parametrization but it is reflected in the spread of the central values given by the various PDF parameterizations that are available. If the PDF uncertainty is defined as to be the difference in the cross sections when using the different available PDF sets, as recommended for example by the PDF4LHC recommendation [151], this uncertainty has no statistical ground.

For the scale uncertainty, the situation is of course clear: it has no statistical ground at all and any value of the cross section in the uncertainty band is as respectable as another³⁶.

³⁵In earlier analyses, the CDF collaboration [216, 217] adds in quadrature the 10.9% scale uncertainty obtained at NNLL with a scale variation in the range $\frac{1}{2}M_H \leq \mu_R, \mu_F \leq 2M_H$ with a 5.1% uncertainty due to the errors on the MSTW PDFs (not including the errors from α_s), resulting in a 12% total uncertainty. The D0 collaboration [217, 218] assigns an even smaller total error, 10%, to the production cross section. This has changed a lot in the most recent analyses where they quote an approximate 20% total uncertainty using PDF+ α_s uncertainties and jet-analysis for scale uncertainties which amounts to $\simeq 18\%$.

³⁶In statistical language, both the scale and PDF uncertainties have a flat prior. See Refs. [95, 210] for a more elaborated discussion on this subject. It is worth mentioning that Ref. [210] recommends a linear

The same is also true for the uncertainties due to the use of an effective approach: they should be viewed as purely theoretical uncertainties and thus be added linearly with each others.

As a result, the scale and PDF uncertainties, cannot be combined in quadrature as done, for instance, by the CDF and D0 collaborations. This is especially true as in the $gg \rightarrow H$ process, a strong correlation between the renormalization and factorization scales that are involved (and that we have equated here for simplicity, $\mu_R = \mu_F$), the value of α_s and the gg densities is present. For instance, decreasing (increasing) the scales will increase (decrease) the $gg \rightarrow H$ cross section not only because of the lower (higher) $\alpha_s(\mu_R^2)$ value that is obtained and which decreases (increases) the magnitude of the matrix element squared (that is proportional to α_s^2 at leading order and the cross section is minimal/maximal for the highest/lowest $\mu_R = \mu_F$ values), but also because at the same time, the gg densities become smaller (larger) for higher (smaller) $\mu_F = \sqrt{Q^2}$ values. Some of these issues have been discussed in details in Ref. [209]. On the other hand, if we add everything linearly it might appear too conservative and also because of the aforementioned reasons.

We then have proposed a rather simple procedure to combine at least the two largest uncertainties, those due to the scale variation and to the PDF+ α_s uncertainties that may avoid the drawbacks of the two other possibilities mentioned above and have been presented for the first time in Ref. [94]. We review this procedure below.

One first derives the maximal and minimal values of the production cross sections when the renormalization and factorization scales are varied in the adopted domain, that is, $\sigma_0 \pm \Delta\sigma_\mu^\pm$ with σ_0 being the cross section evaluated for the central scales $\mu_R = \mu_F = \mu_0$ and the deviations $\Delta\sigma_\mu^\pm$ given in Eq. 4.14. We then evaluate, on these maximal and minimal cross sections from scale variation, the PDF+ $\Delta^{\text{exp}}\alpha_s$ as well as the PDF+ $\Delta^{\text{th}}\alpha_s$ uncertainties (combined in quadrature) using the new MSTW set-up, i.e as in Eq. (4.27) but with σ_0 replaced by $\sigma_0 \pm \Delta\sigma_\mu^\pm$.

We then obtain the maximal and minimal values of the cross section when scale, PDF and α_s (both experimental and theoretical) uncertainties are included,

$$\begin{aligned}\sigma_{\text{max}}^{\mu+\text{PDF}+\alpha_s} &= (\sigma_0 + \Delta\sigma_\mu^+) + \Delta(\sigma_0 + \Delta\sigma_\mu^+)_{\text{PDF}+\alpha_s^{\text{exp}}+\alpha_s^{\text{th}}}, \\ \sigma_{\text{min}}^{\mu+\text{PDF}+\alpha_s} &= (\sigma_0 - \Delta\sigma_\mu^-) - \Delta(\sigma_0 - \Delta\sigma_\mu^-)_{\text{PDF}+\alpha_s^{\text{exp}}+\alpha_s^{\text{th}}}.\end{aligned}\quad (4.28)$$

To these new maximal and minimal cross sections, we finally add in the case of gluon-gluon fusion the smaller EFT uncertainty, that is the one resulting from the missing b -loop at NNLO and the small EW uncertainties. This last addition is linear as these errors have

combination.

M_H	$\sigma_{gg \rightarrow H}^{\text{NNLO}}$ [fb]	scale	PDF	PDF+ α_s^{exp}	α_s^{th}	EW	b-loop	total	% total
100	1849	+318 -371	+102 -109	+210 -201	+219 -199	+45 -45	+42 -42	+817 -648	+44.2% -35.0%
105	1603	+262 -320	+91 -98	+184 -176	+192 -174	+41 -41	+39 -39	+700 -565	+43.7% -35.3%
110	1397	+219 -277	+83 -89	+163 -156	+170 -152	+37 -37	+35 -35	+602 -496	+43.1% -35.5%
115	1222	+183 -242	+75 -81	+144 -138	+151 -134	+33 -33	+32 -32	+521 -437	+42.6% -35.7%
120	1074	+156 -211	+69 -73	+129 -123	+135 -119	+30 -30	+29 -29	+454 -386	+42.2% -36.0%
125	948	+134 -186	+63 -67	+115 -110	+121 -106	+28 -28	+24 -24	+397 -342	+41.9% -36.1%
130	839	+115 -164	+57 -61	+104 -99	+108 -94	+25 -25	+21 -21	+349 -304	+41.5% -36.2%
135	746	+100 -145	+53 -56	+94 -89	+98 -84	+23 -23	+18 -18	+309 -272	+41.4% -36.5%
140	665	+88 -129	+48 -51	+85 -80	+88 -76	+21 -21	+16 -16	+275 -243	+41.4% -36.6%
145	594	+78 -115	+45 -47	+77 -73	+80 -68	+19 -19	+14 -14	+246 -218	+41.4% -36.8%
150	532	+69 -103	+41 -44	+70 -66	+73 -61	+17 -17	+13 -13	+221 -197	+41.6% -37.0%
155	477	+61 -92	+38 -40	+64 -60	+67 -55	+15 -15	+10 -10	+198 -176	+41.5% -37.0%
160	425	+54 -82	+35 -37	+58 -54	+60 -50	+11 -11	+9 -9	+175 -155	+41.3% -36.6%
162	405	+51 -78	+33 -35	+56 -52	+58 -48	+9 -9	+8 -8	+166 -146	+40.9% -36.2%
164	386	+48 -75	+32 -34	+53 -50	+55 -45	+8 -8	+8 -8	+158 -139	+40.9% -36.0%
165	377	+47 -73	+31 -33	+52 -48	+54 -44	+7 -7	+8 -8	+154 -135	+40.8% -35.9%
166	368	+46 -71	+31 -33	+51 -47	+53 -44	+6 -6	+8 -8	+150 -132	+40.9% -35.8%
168	352	+44 -68	+30 -31	+49 -46	+51 -42	+5 -5	+8 -8	+144 -126	+40.9% -35.7%
170	337	+42 -65	+29 -30	+47 -44	+49 -40	+4 -4	+7 -7	+137 -119	+40.6% -35.4%
175	303	+37 -59	+26 -28	+43 -40	+45 -36	+2 -2	+6 -6	+122 -106	+40.4% -35.1%
180	273	+33 -53	+24 -26	+39 -36	+41 -33	+1 -1	+6 -6	+111 -95	+40.6% -34.9%
185	245	+30 -47	+22 -24	+36 -33	+38 -30	+1 -1	+6 -6	+101 -87	+41.1% -35.3%
190	222	+27 -43	+21 -22	+33 -30	+35 -27	+2 -2	+5 -5	+92 -79	+41.4% -35.7%
195	201	+24 -39	+19 -20	+31 -28	+32 -25	+2 -2	+3 -3	+83 -72	+41.4% -35.8%
200	183	+22 -35	+18 -19	+28 -26	+30 -23	+2 -2	+3 -3	+77 -67	+42.0% -36.3%

Table 2: The NNLO total Higgs production cross sections in the $gg \rightarrow H$ process at the Tevatron (in fb) for given Higgs mass values (in GeV) at a central scale $\mu_F = \mu_R = \frac{1}{2}M_H$. Shown also are the corresponding shifts due to the theoretical uncertainties from the various sources discussed, as well as the total uncertainty when all errors are added using the procedure described in the text.

no correlations with the scale and PDF uncertainties³⁷.

³⁷In the case of the b -loop contribution, the K -factor when varying the scale from the central value

The two last columns of Table 2 display the maximal and minimal deviations of the $gg \rightarrow H$ cross section at the Tevatron when all uncertainties are added, as well as the percentage deviations of the cross section from the central value. We should note that the actual PDF+ α_s uncertainty and the uncertainty from the use of the effective theory approach are different from those of Table 2, which are given for the best value of the cross section, obtained for the central scale choice $\mu_F = \mu_R = \frac{1}{2}M_H$; nevertheless, the relative or percentage errors are approximately the same for σ_0 and $\sigma_0 \pm \Delta\sigma_\mu^\pm$.

Doing so for the $gg \rightarrow H$ NNLO cross section with a central scale $\mu_0 = \frac{1}{2}M_H$, we obtain the total error shown in Fig. 27, that we compare to the $\approx \pm 22\%$ error assumed in the CDF/D0 analysis. For $M_H = 160$ GeV for example, we obtain $\Delta\sigma/\sigma \approx +41\%, -37\%$, that is a spread from the central value $\sigma_0 = 425$ fb which is up to $\sigma^{\max} = 600$ fb and down to $\sigma^{\min} = 270$ fb. This is also shown in Table 2 in the last columns where all theoretical uncertainties are combined. This large variation of approximately $\pm 40\%$ is seen on the entire Higgs mass range. We should also note that the central cross section displayed in Fig. 27 is in excellent agreement with Ref. [111]; the striking new result is then the large uncertainties that we have found.

Hence, our procedure for the combination does not reduce to a linear sum of all uncertainties. If we had added linearly all errors, we would have had, for the negative part at $M_H = 160$ GeV, a total uncertainty of $\Delta\sigma/\sigma \approx -42\%$, compared to the value -37% with our procedure. On the other hand, one has an error of $\approx -30\%$, i.e. close to the total error assumed by CDF/D0 if the scale and PDF+ α_s uncertainties were added in quadrature and the EFT approach error linearly (the latter being ignored by the CDF/D0 collaborations). We also want to point out that the Ref. [210] in its last section recommends a procedure of combination which is linear, as the prior on the different theoretical uncertainties are not gaussian. Thus our combination is far from being too conservative or exaggerated.

The consequences on the exclusion limits quoted by CDF and D0 collaborations on the Higgs mass range between 158 and 173 GeV [91–93] will be discussed in the section 6.5. We can already tell that they should be taken with caution in the light of our uncertainties.

We now discuss the results in the Higgs-strahlung processes and similarly to the $gg \rightarrow H$ case we display in Table 3 the central values of the cross sections for $p\bar{p} \rightarrow WH$ and $p\bar{p} \rightarrow ZH$ at the Tevatron, evaluated at scales $\mu_R = \mu_F = M_{HV}$ with the MSTW set of PDFs (second and third columns). In the remaining columns, we display only the WH

$\frac{1}{2}M_H$ to the values $\approx \frac{1}{6}M_H$ or $\approx \frac{3}{2}M_H$, which maximise and minimise the cross section, might be slightly different and thus, the error will not be exactly that given in Table 2. However, since the entire effect is very small, we will ignore this tiny complication here.

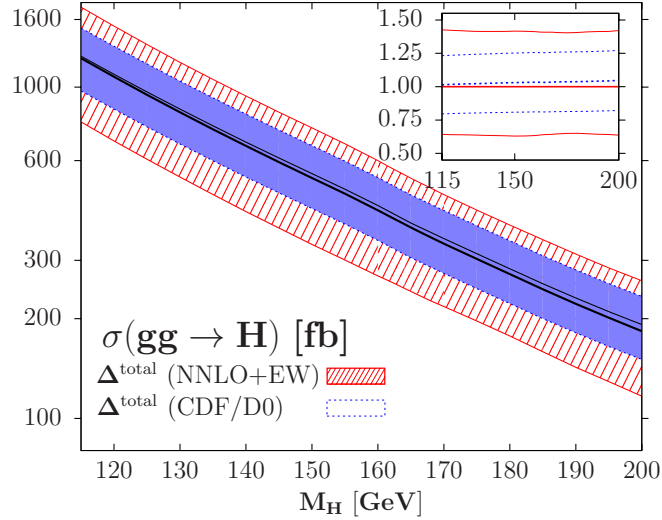


Figure 27: The production cross section $\sigma(gg \rightarrow H)$ at NNLO for the QCD and NLO for the electroweak corrections at the Tevatron at a central scale $\mu_F = \mu_R = \frac{1}{2}M_H$ with the uncertainty band when all theoretical uncertainties are added using our procedure. It is compared to $\sigma(gg \rightarrow H)$ at NNLL [111] with the errors quoted by the CDF/D0 collaboration [91–93]. In the insert, the relative deviations compared to the central value are shown.

channel results about the uncertainties coming from the scale variation (with $\kappa = 2$), the PDF, mixed PDF+ $\Delta^{\text{exp}}\alpha_s$ and PDF+ $\Delta^{\text{exp}}\alpha_s + \Delta^{\text{th}}\alpha_s$ uncertainties in the MSTW scheme. In the last columns, we give the total error and its percentage; this percentage error is, to a very good approximation, the same in the $p\bar{p} \rightarrow ZH$ channel which explains why we have chosen to study the W boson channel only, recalling that the result for the Z boson channel are in a very good approximation obtained by rescaling the absolute error by the correct central value.

In contrast to the $gg \rightarrow H$ mechanism, since the errors due to scale variation are rather moderate in this case, there is no large difference between the central cross section σ_0 and the cross sections $\sigma_0 \pm \Delta\sigma_\mu^\pm$ and, hence, the PDF, PDF+ $\Delta^{\text{exp}}\alpha_s$ and PDF+ $\Delta^{\text{exp}}\alpha_s + \Delta^{\text{th}}\alpha_s$ errors on σ^0 are, to a good approximation, the same as the errors on $\sigma_0 \pm \Delta\sigma_\mu^\pm$ displayed in Table 3.

The total uncertainty is once more summarized in Fig. 28, where the cross sections for WH and ZH associated production at the Tevatron, together with the total uncertainty bands (in absolute values in the main frame and in percentage in the insert), are displayed as a function of the Higgs mass. The total error on the cross sections in the Higgs–strahlung processes is about $\pm 9\%$ in the entire Higgs mass range, possibly 1% to 2% smaller for low M_H values and $\sim 1\%$ larger for high M_H values, as displayed in the figure. Thus, the theoretical errors are much smaller than in the case of the $gg \rightarrow H$ process and the cross sections for the Higgs–strahlung processes are well under control. Nevertheless, it is worth

M_H	σ_{HW}	σ_{HZ}	scale	PDF	PDF+ α_s^{exp}	α_s^{th}	total	% total
115	174.5	103.9	+1.3 -1.6	+10.5 -9.1	+10.7 -10.7	+1.3 -0.9	+12.1 -12.3	+7% -7%
120	150.1	90.2	+1.1 -1.4	+9.2 -8.1	+9.6 -9.4	+1.2 -0.9	+10.7 -10.9	+7% -7%
125	129.5	78.5	+0.9 -1.3	+7.5 -6.8	+8.6 -8.7	+1.1 -0.8	+9.6 -10.0	+7% -8%
130	112.0	68.5	+0.8 -1.1	+6.8 -6.4	+7.2 -7.5	+1.1 -0.8	+8.0 -8.6	+7% -8%
135	97.2	60.0	+0.7 -1.0	+5.6 -5.5	+6.7 -6.6	+1.0 -0.7	+7.4 -7.6	+8% -8%
140	84.6	52.7	+0.6 -0.9	+5.6 -4.5	+5.8 -5.7	+0.9 -0.7	+6.5 -6.6	+8% -8%
145	73.7	46.3	+0.5 -0.8	+4.4 -4.1	+5.4 -5.2	+0.9 -0.7	+5.9 -6.0	+8% -8%
150	64.4	40.8	+0.5 -0.7	+4.2 -3.9	+4.4 -4.3	+0.8 -0.6	+5.0 -5.0	+8% -8%
155	56.2	35.9	+0.4 -0.6	+3.4 -3.1	+4.2 -4.1	+0.7 -0.6	+4.6 -4.7	+8% -8%
160	48.5	31.4	+0.4 -0.6	+3.3 -3.0	+3.6 -3.3	+0.7 -0.5	+4.1 -4.0	+8% -8%
162	47.0	30.6	+0.4 -0.5	+3.4 -2.8	+3.5 -3.3	+0.7 -0.5	+3.9 -3.8	+8% -8%
164	44.7	29.1	+0.3 -0.5	+3.1 -2.7	+3.4 -3.4	+0.6 -0.5	+3.7 -3.9	+8% -9%
165	43.6	28.4	+0.3 -0.5	+2.8 -2.4	+3.4 -3.3	+0.6 -0.5	+3.8 -3.8	+8% -8%
166	42.5	27.8	+0.3 -0.5	+3.0 -2.6	+3.1 -3.0	+0.6 -0.5	+3.4 -3.5	+8% -8%
168	40.4	26.5	+0.3 -0.5	+2.8 -2.4	+3.1 -2.9	+0.6 -0.5	+3.4 -3.4	+9% -8%
170	38.5	25.3	+0.3 -0.4	+2.9 -2.2	+3.0 -2.7	+0.6 -0.5	+3.3 -3.1	+9% -8%
175	34.0	22.5	+0.3 -0.4	+2.2 -1.9	+2.7 -2.6	+0.5 -0.4	+3.0 -3.0	+9% -9%
180	30.1	20.0	+0.2 -0.4	+2.1 -1.8	+2.2 -2.2	+0.5 -0.4	+2.5 -2.6	+8% -9%
185	26.9	17.9	+0.2 -0.3	+1.8 -1.5	+2.1 -2.1	+0.5 -0.4	+2.3 -2.4	+9% -9%
190	24.0	16.1	+0.2 -0.3	+1.6 -1.6	+1.8 -1.8	+0.4 -0.3	+2.1 -2.1	+9% -9%
195	21.4	14.4	+0.2 -0.3	+1.3 -1.2	+1.8 -1.7	+0.4 -0.3	+2.1 -2.0	+10% -10%
200	19.1	13.0	+0.2 -0.2	+1.4 -1.2	+1.5 -1.4	+0.4 -0.3	+1.8 -1.7	+9% -9%

Table 3: The central values of the cross sections for the $p\bar{p} \rightarrow WH$ and ZH processes at the Tevatron (in fb) for given Higgs mass values (in GeV) with, in the case of the WH channel, the uncertainties from scale variation, PDF, PDF+ $\Delta^{\text{exp}}\alpha_s$ and $\Delta^{\text{th}}\alpha_s$, as well as the total uncertainty when all errors are added using the procedure described in the text.

mentionning that the total uncertainty that is obtained in our analysis is almost twice as large as the total 5% uncertainty assumed by the CDF and D0 collaborations in their combined analysis of this channel [90–93].

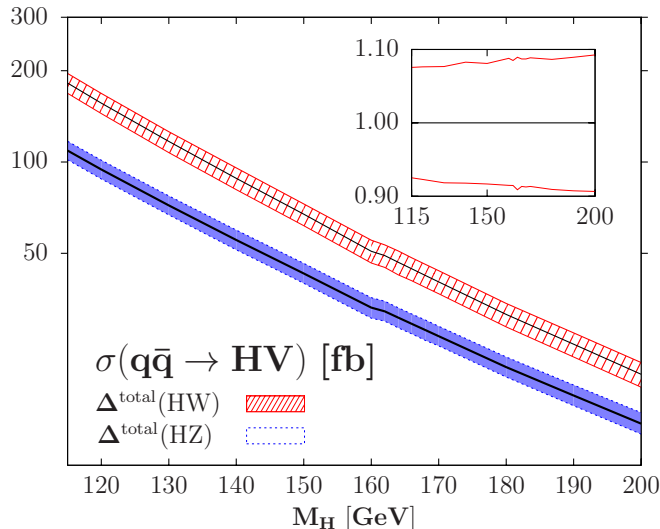


Figure 28: The production cross section $\sigma(p\bar{p} \rightarrow WH)$ and $\sigma(p\bar{p} \rightarrow ZH)$ at NNLO in QCD and electroweak NLO at the Tevatron evaluated with the MSTW set of PDFs, together with the uncertainty bands when all the theoretical errors are added. In the insert, the relative deviations from the central MSTW value are shown in the case of $\sigma(p\bar{p} \rightarrow WH)$.

Before closing this section, we point out that the uncertainties in the Higgs–strahlung processes can be significantly reduced by using the Drell–Yan processes of massive gauge boson production as standard candles, as first suggested in Ref. [219]. Indeed, normalizing the cross sections of associated WH and ZH production to the cross sections of single W and Z production, respectively, allows for a cancellation of several experimental errors such as the error on the luminosity measurement, as well as the partial cancellation (since the scales that are involved in the $p\bar{p} \rightarrow V$ and HV processes are different) theoretical errors such as those due to the PDFs, α_s and the higher order radiative corrections.

4.6 Summary and outlook

In this section were presented the theoretical predictions for the Standard Model Higgs boson production total cross section at the Tevatron in the two main channels, the gluon–gluon fusion $gg \rightarrow H$ and the Higgs–strahlung processes $p\bar{p} \rightarrow VH$, where V stands for either the W or the Z boson. We have assumed a central scale $\mu_F = \mu_R = \mu_0$ to be $\mu_0 = \frac{1}{2}M_H$ for the gluon–gluon fusion process and $\mu_0 = M_{HV}$ (the invariant mass of the pair HV) for the Higgs–strahlung processes, and calculated the cross section up to NNLO in QCD and EW corrections.

We have then estimated the theoretical uncertainties associated to the prediction: the scale uncertainty, the uncertainties from the PDF parametrisation and the associated error on α_s , as well as uncertainties due to the use of the EFT approach for the mixed QCD–

electroweak radiative corrections and the b -quark loop contribution in the gluon–gluon fusion case. The major result is that we obtain in the critical region for Higgs searches at the Tevatron, that is the region $M_H = 158\text{--}173$ GeV, an overall theoretical uncertainty of order $\pm 40\%$ when using our procedure of combination of the uncertainties. That is twice the uncertainty used in the experimental analyses of the CDF/D0 collaborations [91–93]. This is a mere consequence of the different ways to combine the individual scale and PDF+ α_s uncertainties and, to a lesser extent, the impact on the theoretical uncertainty on α_s and the EFT uncertainties which have not been considered by the CDF/D0 collaborations. The uncertainty obtained in the Higgs–strahlung mechanism is of order $\pm 8\%$, which implies that this process is much more under control than the gluon–gluon fusion mechanism. The uncertainty is also twice the one assumed in low Higgs mass searches at the Tevatron [91–93].

The consequence of this doubling of the errors will be analyzed in section 6.5. Before that we now turn our attention on the Higgs production at the other hadron colliders which has started to run in 2010 in the TeV energy range: the CERN Large Hadron Collider (LHC). Indeed, it is of crucial importance to analyze the theoretical uncertainties affecting the Higgs production at the LHC as it is the designed machine to discover the Higgs boson: theoretical uncertainties have an impact not only on the discovery of the elusive boson but also on its couplings to fermions and gauge bosons [220–222].

4.A Appendix: analytical terms for NNLO μ_R -dependent corrections to $gg \rightarrow H$ total cross section

We present in this appendix the exact analytical expressions for the NNLO corrections which include μ_R terms. Even if this expressions can be recovered in a straightforward way, they are not presented in the current literature and it may be of use to present them in their all extent.

We write $\hat{\sigma}_{ij} = \sigma_0 \alpha_s^2(\mu_R) \left(\eta_{ij}^{(0)} + \frac{\alpha_s(\mu_R)}{\pi} \eta_{ij}^{(1)} + \left(\frac{\alpha_s(\mu_R)}{\pi} \right)^2 \eta_{ij}^{(2)} \right)$ with

$$\sigma_0 = \frac{G_F}{288\pi\sqrt{2}} \left| \frac{3}{4} \sum_q A(\tau_q) \right|^2$$

and z is the variable defined as $z = \frac{\tau_H}{\tau}$. We separate the expression of $\hat{\sigma}_{gg}$ in two pieces as done in the literature: the soft+virtual part containing the virtual corrections as well as the soft-gluon terms with \mathcal{D}_i plus-distributions, and the hard part containing the polylogarithms. We then have:

- For $\hat{\sigma}_{ij}$ with $ij = qq, \bar{q}\bar{q}, qq', q\bar{q}', \bar{q}q', \bar{q}\bar{q}'$ there are no $\frac{\mu_R}{\mu_F}$ -terms in $\eta_{ij}^{(2)}$.
- For $\hat{\sigma}_{q\bar{q}}$ we have $\delta\eta_{q\bar{q}}^{(1)} = 0$ and :

$$\delta\eta_{q\bar{q}}^{(2)} = (33 - 2n_f) \ln \left(\frac{\mu_R^2}{\mu_F^2} \right) \frac{8}{27} (1 - z)^3 \quad (4.29)$$

- For $\hat{\sigma}_{gq}$ we have $\delta\eta_{gq}^{(1)} = 0$ and :

$$\begin{aligned} \delta\eta_{gq}^{(2)} = & \frac{33 - 2n_f}{4} \ln \left(\frac{\mu_R^2}{\mu_F^2} \right) \left[\frac{2}{3} \ln \left(\frac{m_H^2}{\mu_F^2} \right) - 1 + 2z - \frac{1}{3}z^2 \right. \\ & \left. - \frac{2}{3} (1 + (1 - z)^2) \ln \left(\frac{z}{(1 - z)^2} \right) \right] \end{aligned} \quad (4.30)$$

- For $\hat{\sigma}_{gg}^{\text{soft+virtual}}$ we have $\delta\eta_{gg}^{(1),s+v} = \frac{33 - 2n_f}{6} \ln\left(\frac{\mu_R^2}{\mu_F^2}\right)$ and :

$$\begin{aligned}
\delta\eta_{gg}^{(2),s+v} &= \frac{(33 - 2n_f)^2}{48} \ln^2\left(\frac{\mu_R^2}{\mu_F^2}\right) \delta(1 - z) + 3(33 - 2n_f) \mathcal{D}_1(z) \ln\left(\frac{\mu_R^2}{\mu_F^2}\right) \\
&+ \frac{3}{2} (33 - 2n_f) \ln\left(\frac{m_H^2}{\mu_F^2}\right) \ln\left(\frac{\mu_R^2}{\mu_F^2}\right) \mathcal{D}_0(z) \\
&+ \ln\left(\frac{\mu_R^2}{\mu_F^2}\right) \left(3\zeta(2) \frac{33 - 2n_f}{2} + \frac{1395 - 104n_f}{24}\right) \delta(1 - z)
\end{aligned} \tag{4.31}$$

- For $\hat{\sigma}_{gg}^{\text{hard}}$ we have $\delta\eta_{gg}^{(1),h} = 0$ and :

$$\begin{aligned}
\delta\eta_{gg}^{(2),h} &= \frac{3}{2} (33 - 2n_f) \ln\left(\frac{\mu_R^2}{\mu_F^2}\right) \ln\left(\frac{\mu_F^2}{m_H^2}\right) z (2 - z(1 - z)) \\
&- \frac{3}{2} (33 - 2n_f) \frac{\ln z}{1 - z} \ln\left(\frac{\mu_R^2}{\mu_F^2}\right) (1 - z(1 - z))^2 \\
&- 3(33 - 2n_f) \ln\left(\frac{\mu_R^2}{\mu_F^2}\right) z \ln(1 - z) (2 - z(1 - z)) \\
&- \frac{33}{8} (33 - 2n_f) \ln\left(\frac{\mu_R^2}{\mu_F^2}\right) (1 - z)^3
\end{aligned} \tag{4.32}$$

5 Higgs production at the LHC

The CERN proton–proton collider successfully started its operations in 2009 at a center–of–mass energy of 900 GeV and then really in 2010 but at a reduced center of mass energy of 7 TeV [223]. It has been running in physics mode for more than one year up until now and has collected enough data to produce already interesting results. Indeed the quest for the SM Higgs boson has began and some results have been presented in Refs. [224, 225].

In order to distinguish between the current early run at 7 TeV and the designed run at an energy close to 14 TeV, we will call the early 7 TeV experiment as the LHC for littler Hadron Collider. The LHC will also be sensitive to the SM Higgs particle and in particular be competitive with the Tevatron experiment once the accumulated luminosity will be at least of order 1 fb^{-1} [210, 223, 226, 227]. However, with the present expectations, the Tevatron and presumably also the LHC will only be able to exclude the existence of the SM Higgs particle in some given mass range. We will present in this section some results for the LHC energy and also for SM Higgs boson production at the designed $\sqrt{s} = 14 \text{ TeV}$ LHC.

The situation at the LHC is much in the same way as what has to be carefully done at the Tevatron: both are hadron colliders which then imply that the predictions are plagued with various theoretical uncertainties. The exclusion of Higgs mass regions relies crucially on the theoretical predictions for the production cross sections for the Higgs signal as well as for the relevant SM backgrounds, and this was discussed in detail in the last section. We remind the reader that the main production channel at the Tevatron which were presented are the top and bottom quark loops mediated gluon–gluon fusion mechanism $gg \rightarrow H$ [99] with the Higgs decaying into WW pairs which lead to $\ell\nu\ell\bar{\nu}$ (with $\ell = e, \mu$) final states [100] and the Higgs–strahlung processes $q\bar{q} \rightarrow VH$ (with $V = W, Z$) [119] with the subsequent $H \rightarrow b\bar{b}$ and $V \rightarrow \ell + X$ decays of the Higgs and the associated gauge bosons.

At the LHC, the Higgs–strahlung processes, as well as as other production channels such as weak vector–boson fusion and associated Higgs production with top quark pairs, have too small cross sections and/or are plagued with too large QCD backgrounds. This implies that the gluon–gluon fusion process with the Higgs boson decaying into $H \rightarrow WW \rightarrow \ell\ell\nu\bar{\nu}$, $H \rightarrow ZZ \rightarrow 2\ell + X$, where X stands for charged leptons, neutrinos and eventually also jets including b –quark jets, and to a lesser extent $H \rightarrow \gamma\gamma$ final states, will be mostly relevant. At a center of mass energy $\sqrt{s} = 7 \text{ TeV}$ and with 1 fb^{-1} of data, recent studies by the ATLAS and CMS collaborations have shown that the mass range $M_H \approx 150\text{--}190 \text{ GeV}$ can be excluded at 95%CL if no Higgs signal is observed [226, 227]. This is the reason why we will only concentrate in this section in the theoretical predictions in the gluon–gluon fusion

production channel.

We will reproduce the same line of arguments developed in section 4 and presented in Ref. [94]. We present an analysis of the gluon–gluon fusion production channel for SM Higgs production $gg \rightarrow H$ at the LHC, beginning with the theoretical prediction for the Higgs production cross sections, including all the relevant higher order QCD and electroweak corrections. We then analyze the various uncertainties that affect them. We show that the scale and PDF uncertainties, as well as the non–negligible uncertainty due to the use of an effective approach in the calculation of QCD and electroweak higher order corrections beyond next–to–leading order, add up to $\approx 25\text{--}30\%$ depending on the considered Higgs mass range. If we compare with what has been obtained in section 4.5 for the Tevatron case, the total uncertainty at the LHC is significantly smaller than that obtained at the Tevatron, as a result of smaller QCD radiative corrections and a better knowledge of the gluon distribution function at the energies relevant at the LHC.

We will also give some predictions for different center–of–mass energies. Indeed the LHC commissioning group did think about running the LHC at intermediate center–of–mass energies of 8, 9, 10 TeV before the long shut–down of the accelerator in order to complete design operations needed for the full–fledged 14 TeV LHC [223]. This has been finally abandoned and the CERN accelerator will run at 7 TeV until the one year shut–down for the design of the 14 TeV run [228]. Nevertheless we will give the central cross sections predictions for these intermediate energies, as well as a detailed analysis of the gluon–gluon fusion production channel for the full–fledged LHC with $\sqrt{s} = 14$ TeV. The main result that we obtain is that while the production cross sections for the SM Higgs particle are higher at energies $\sqrt{s} = 8\text{--}14$ TeV compared to $\sqrt{s} = 7$ TeV, the overall theoretical uncertainties affecting the predictions do not change much.

5.1 The main channel at the LHC (or LHC at 7 TeV)

The hierarchy in the production channels for the SM Higgs boson at the LHC does not substantially change when compared to the situation at the Tevatron collider presented in section 4. The main production channel remains the gluon–gluon fusion channel $gg \rightarrow H$ proceeding through triangular top and bottom quark loops [99] and as stated in the introduction of this section we will discard the analysis of the other sub–dominant production channels, due to the fact that the LHC analysis is mostly relevant only in the gluon–gluon fusion channel. As stated in the Tevatron analysis this process is known to be subject to extremely large QCD radiative corrections [101–105, 107–111, 118, 159, 160, 163] that can be described by an associated K –factor defined as the ratio of the higher order (HO) to the

LO cross sections, consistently evaluated with the value of the strong coupling α_s and the PDF taken at the considered order, see Eq. 4.1.

The NLO corrections in QCD are known both for infinite [101–104] and finite [105] loop quark masses and, at $\sqrt{s} = 7$ TeV, lead to a K -factor $K_{\text{NLO}} \sim 1.8$ in the low Higgs mass range, if the central scale of the cross section is chosen to be the Higgs mass. We remind the reader that it has been shown in Ref. [105] that working in an effective field theory (EFT) approach in which the top quark mass is assumed to be infinite is a very good approximation for Higgs mass values below the $t\bar{t}$ threshold $M_H \lesssim 2m_t$, provided that the leading order cross section contains the full m_t and m_b dependence. The calculation of the NNLO contribution has then been done [107–109] only in the EFT approach where $M_H \ll 2m_t$ and, at $\sqrt{s} = 7$ TeV, it leads to a $\approx 25\%$ increase of the cross section with $K_{\text{NNLO}} \sim 2.5$. The comparison with the Tevatron K -factors shows that the QCD corrections to $gg \rightarrow H$ at $\sqrt{s} = 7$ TeV are thus smaller than the corresponding ones at the Tevatron as the K -factors in this case are $K_{\text{NLO}} \approx 2$ and $K_{\text{NNLO}} \approx 3$ (with a central scale equal to M_H). At the LHC with $\sqrt{s} = 14$ TeV, the K -factors are even smaller, $K_{\text{NLO}} \approx 1.7$ and $K_{\text{NNLO}} \approx 2$.

The NNLL resummation of soft gluons increases the cross section by slightly less than 10% [110, 111] and as in the Tevatron case and for the same reasons, we do not include this effect and mimick the 10% increase by using as the central scale

$$\mu_R = \mu_F = \mu_0 = \frac{1}{2}M_H \quad (5.1)$$

We recall the reader that this central scale choice improves the convergence of the perturbative series and is more appropriate to describe the kinematics of the process [169]. We again also include the electroweak corrections known exactly up to NLO [113–117] and which contribute at the level of a few percent; there are also small mixed NNLO QCD–electroweak effects which have been calculated [118] in an effective approach valid for $M_H \ll M_W$ that are also included in our calculation.

We use the same procedure described in 4.1 for the calculation of the production cross sections³⁸: we use the Fortran code HIGLU [153] with our modification in order to include the complete NLO corrections for the top and bottom quark loops and the NNLO corrections for the top loop in the infinite mass limit; grids for the electroweak corrections are provided within the code and we also implement the NNLO mixed QCD–EW corrections in our calculation. The production cross sections are shown at the LHC with $\sqrt{s} = 7$ TeV in Fig. 29 for an updated value of the top quark mass $M_t = 172.5$ GeV³⁹ and when the

³⁸Other updates of the $gg \rightarrow H$ cross section at the LHC can be found in Refs. [111, 118, 203, 229–231].

³⁹in accord with most predictions at the LHC, see Ref. [210].

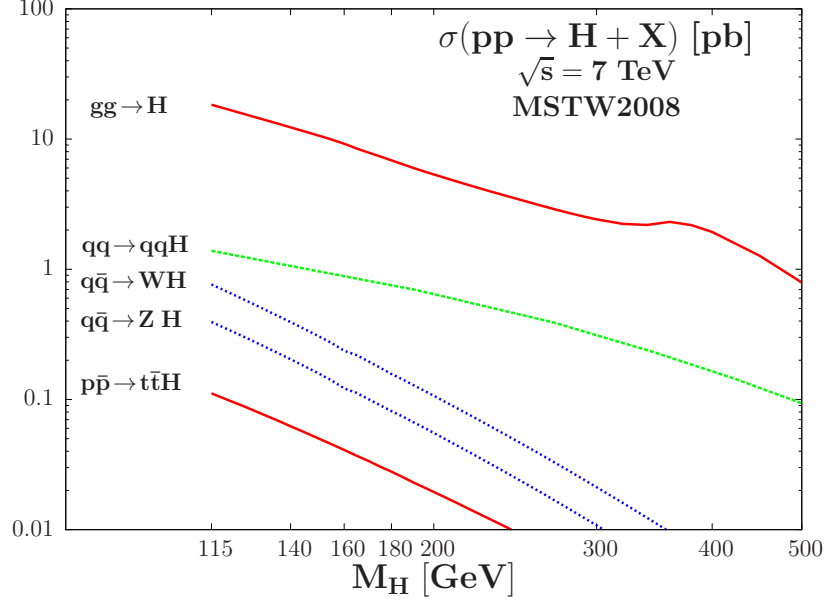


Figure 29: The total cross sections for Higgs production at the LHC with $\sqrt{s} = 7$ TeV as a function of the Higgs mass. The MSTW set of PDFs has been used and the higher order corrections are included as discussed in the text.

partonic cross section is folded with the NNLO MSTW2008 public set of PDFs [128]. The renormalization and factorization scales are fixed to the central values of Eq. 5.1. Our results published in Ref. [232] agree with those given in Refs. [111, 118] and updated in Ref. [210] within a few percent.

As in the Tevatron calculation we also display in Fig. 29 for completeness the cross sections for the three other Higgs production channels at hadron colliders that we evaluate using the programs of Ref. [153]:

- i)* the Higgs-strahlung processes $q\bar{q} \rightarrow HV$ with $V = W, Z$ that are known exactly up to NNLO in QCD [106, 121–126, 173, 174] and up to NLO for the electroweak corrections [127]; they are evaluated at $\mu_0 = M_{HV}$ (the invariant mass of the HV system) for the central scale⁴⁰;
- ii)* the weak vector boson fusion channel $qq \rightarrow Hqq$ evaluated at the scale $\mu_0 = Q_V$ (the momentum transfer at the gauge boson leg) in which only the NLO QCD corrections [106, 136, 137] have been included; the NNLO corrections have been found to be very small [177, 178] and we omit the electroweak corrections [176], as was done in the Tevatron calculation earlier;

⁴⁰Here, the QCD K -factors are moderate, $K_{\text{NNLO}} \sim 1.5$ and the electroweak corrections reduce the cross section by an amount of $\approx 3 - 8\%$. For the evaluation of the cross section, we have used the NLO code V2HV [153] in which we implemented these higher order contributions. Our results agree with those of Ref. [210].

iii) associated Higgs production with top quark pairs in which only the leading order contribution is implemented but at a central scale $\mu_0 = \frac{1}{2}(M_H + 2m_t)$, which is a good approximation at these energies as the NLO K -factor is very close to unity [141–144], see also Ref. [210].

The hierarchy shows a small difference compared to that of the Tevatron, as the vector boson fusion production channel becomes the second most important production channel at the LHC whereas it was next to the Higgs-strahlung processes at the Tevatron. It is also demonstrated in Fig. 29 that the $gg \rightarrow H$ process is by far dominating in the entire Higgs mass range, with a cross section that is one to two orders of magnitudes larger than in the other production channels. Table 4 displays the values of the cross sections for the five Higgs production processes for a selection of Higgs masses relevant at the LHC.

5.2 The scale uncertainty

In the calculation of production cross sections and kinematical distributions at hadron colliders, as the perturbative series are truncated and the results are available only at a given perturbative order, there is a residual dependence of the observables on the renormalization scale μ_R which defines the strong coupling constant α_s and on the factorization scale μ_F at which the matching between the perturbative matrix elements calculation and the non-perturbative parton distribution functions is performed. The uncertainty due to the variation of these two scales is then viewed as an estimate of the unknown (not yet calculated) higher-order terms and is rather often the dominant source of theoretical uncertainties.

This picture has been sketched in section 4.2 and we will use the same techniques for the estimation of this scale uncertainty induced by the missing higher order terms. We start at the median scale $\mu_R = \mu_F = \mu_0 = \frac{1}{2}M_H$ for which the central or “best” value of the cross section is obtained, and we vary the two scales μ_R and μ_F within the intervall defined in 4.2:

$$\mu_0/\kappa \leq \mu_R, \mu_F \leq \kappa \times \mu_0$$

with the value of the constant $\kappa = 2, 3, 4, \dots$, to be chosen. The constant κ is again chosen as to catch the NNLO central calculation with the (N)LO scale uncertainty bandd⁴¹.

⁴¹In the case of the $gg \rightarrow H$ process, the maximal (minimal) cross sections at a given fixed order in perturbation theory (in particular at NNLO) is obtained for the scale choices $\mu_R = \mu_F = \mu_0/\kappa$ ($\kappa\mu_0$); there

M_H	$\sigma_{gg \rightarrow H}^{\text{NNLO}}$	$\sigma_{qq \rightarrow Hqq}^{\text{NLO}}$	$\sigma_{q\bar{q} \rightarrow HW}^{\text{NNLO}}$	$\sigma_{q\bar{q} \rightarrow HZ}^{\text{NNLO}}$	$\sigma_{pp \rightarrow t\bar{t}H}^{\text{LO}}$
115	18347.4	1386.1	764.1	394.0	111.5
120	16844.6	1313.2	664.8	343.2	98.7
125	15509.2	1259.5	580.0	300.3	87.9
130	14322.6	1192.1	507.5	263.2	78.1
135	13260.6	1148.6	446.0	231.4	69.8
140	12305.6	1087.0	392.9	203.6	62.3
145	11446.4	1051.5	347.3	180.0	56.0
150	10665.9	1006.2	307.1	159.1	50.2
155	9936.4	964.6	272.0	140.4	45.3
160	9205.9	908.4	236.8	121.7	40.9
165	8470.8	875.3	218.9	112.3	37.0
170	7872.3	842.5	196.0	100.6	33.7
175	7345.3	796.6	175.6	90.2	30.5
180	6861.2	768.0	156.8	81.2	27.9
185	6416.3	732.8	142.7	74.0	25.4
190	6010.0	705.0	129.3	67.1	23.1
195	5654.8	683.8	117.5	60.9	21.2
200	5344.1	651.5	106.8	55.3	19.5
220	4357.0	556.7	74.4	38.4	14.0
240	3646.4	479.6	52.9	27.2	10.4
260	3110.7	411.6	38.4	19.7	7.8
280	2706.4	360.7	28.3	14.5	6.1
300	2415.4	312.6	21.2	10.8	4.8

Table 4: The total Higgs production cross sections (in fb) in the processes $gg \rightarrow H$, vector–boson fusion $qq \rightarrow Hqq$, Higgs–strahlung $q\bar{q} \rightarrow HW.HZ$ and associated production $pp \rightarrow t\bar{t}H$ at the LHC with $\sqrt{s} = 7$ TeV for given Higgs mass values (in GeV) with the corresponding central scales described in the main text. The MSTW sets of PDFs have been used at the relevant order.

is thus no relevant restriction to put on the intervall of variation in practice and we will usually use the simplification $\mu_R = \mu_F$.

At the LHC with $\sqrt{s} = 7$ TeV, at $\mu_0 = \frac{1}{2}M_H$, the value $\kappa = 2$ is enough as to catch the NNLO central prediction with the NLO uncertainty band of $\sigma^{\text{NLO}}(gg \rightarrow H)$. This result still nearly holds if we use the LO bands to catch the NNLO central prediction, as the LO bands nearly touch the NNLO central prediction.

Adopting the range

$$\frac{1}{2}\mu_0 \leq \mu_R, \mu_F \leq 2\mu_0 \quad (5.2)$$

with $\mu_0 = \frac{1}{2}M_H$ for the cross section $\sigma^{\text{NNLO}}(gg \rightarrow H)$, the scale variation displayed in Fig. 30 as a function of M_H is obtained; it is compared to a variation with a factor $\kappa = 3$. In the insert, we present the maximal and minimal variations of $\sigma^{\text{NNLO}}(gg \rightarrow H)$ compared to the central value. We can see that for $\kappa = 2$, a scale uncertainty of $\approx \pm 10\%$ is obtained in the low mass range, $M_H \approx 120$ GeV, which decreases to the level of $\approx -8\%, +4\%$ at high masses, $M_H \approx 500$ GeV. If the domain for scale variation were extended to $\kappa = 3$, the uncertainty band would have increased to $\approx \pm 17\%$ in the low Higgs mass range as shown in Fig. 30. Using at the LHC the value $\kappa = 2$ instead of $\kappa = 3$ can be related to the fact that the higher order QCD corrections in the gluon–gluon fusion process at the LHC are smaller than that of the Tevatron case where we have then used $\kappa = 3$ and hence a larger domain for the scale variation.

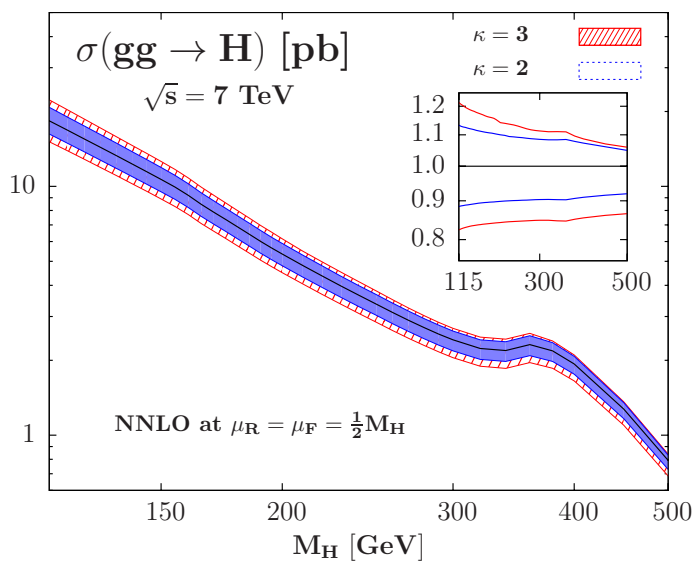


Figure 30: The scale uncertainty band of $\sigma^{\text{NNLO}}(gg \rightarrow H)$ at the LHC as a function of M_H for a scale variation in the domain $M_H/(2\kappa) \leq \mu_R, \mu_F \leq \kappa \times \frac{1}{2}M_H$ for $\kappa = 2$ and 3; in the insert, shown are the relative deviations from the central value with a scale $\mu_R = \mu_F = \frac{1}{2}M_H$.

5.3 The PDF+ α_S uncertainty

The second major source of uncertainty in the Higgs production in the gluon–gluon fusion at the LHC is again related to the imprecise determination of the parton distribution functions (PDFs), much in the same way at the Tevatron. This uncertainty, as shown later, is even more important at the LHC as for high Higgs mass values it becomes the largest uncertainty.

As discussed in the Tevatron case, see 4.3, there exist many different PDFs parametrizations on the market. We thus have different way to estimate the PDF uncertainty on the total production cross section and again we will summarize our lines of argument as in the Tevatron case.

The first method is the so-called Hessian method where, besides the best fit PDF with which the central values of the cross sections are evaluated, a set of $2N_{\text{PDF}}$ PDF parameterizations is provided that reflect the $\pm 1\sigma$ variation of all (N_F) parameters that enter into the global fit. These uncertainties are thus mostly due to the experimental errors in the various data that are used in the fits. Taking the NNLO public set provided by the MSTW collaboration [128, 199] for instance, the PDF uncertainty at the 90% CL that is obtained at the LHC for the NNLO $gg \rightarrow H$ cross section is shown (by the red lines and red band) in Fig. 31 as a function of M_H . For low Higgs masses, the uncertainty is at the level of 5% but it increases to reach the level of $\approx 8\%$ at high Higgs masses, $M_H \approx 500$ GeV. If only the (more optimistic) 68%CL errors are to be considered, the previous numbers have to be divided by ≈ 1.6 .

The thorough analysis conducted for the gluon–gluon Higgs production at the Tevatron has demonstrated that these (Hessian) uncertainties are not sufficient as they do not account for the theoretical assumptions entering into the parametrizations of the PDFs and which explain why there are so many different PDFs sets on the market. It is therefore very difficult to estimate within a given set the uncertainties behind these different assumptions. Nevertheless, an accurate determination of the PDFs uncertainty requires that we take into account this spread observed in the theoretical predictions using the different NNLO PDFs sets that are available.

As stated in section 4.3, one possible way to estimate this more accurate uncertainty is to compare the results for the central values of the cross section (and hence, using the best fit PDFs only) when using the different NNLO sets of PDFs which involve, in principle, different assumptions. We display in Fig. 32 the values of $\sigma^{\text{NNLO}}(gg \rightarrow H)$ calculated with our procedure when folding the partonic cross section with the gluon densities that are

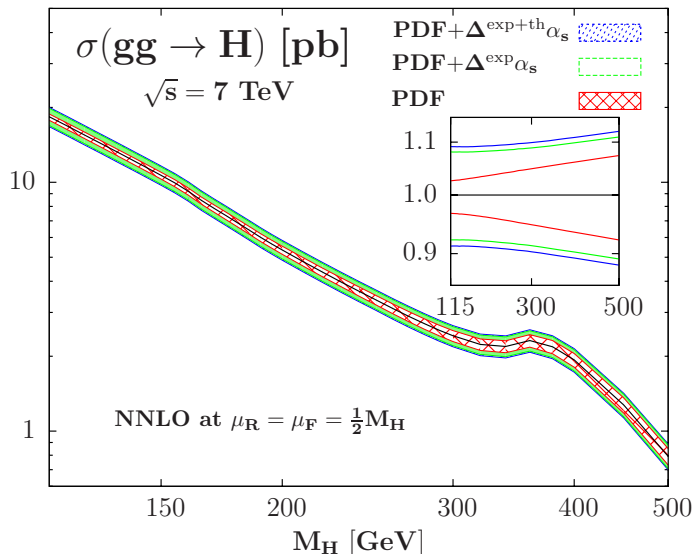


Figure 31: The central values and the 90% CL PDF, PDF+ $\Delta^{\text{exp}}\alpha_s$ and PDF+ $\Delta^{\text{exp}}\alpha_s+\Delta^{\text{th}}\alpha_s$ uncertainty bands in $\sigma^{\text{NNLO}}(gg \rightarrow H + X)$ at the IHC when evaluated within the MSTW scheme. In the inserts, shown are the same but with the cross sections normalized to the central cross section.

predicted by the four PDF sets⁴² that have parameterizations at NNLO: MSTW [128], JR 09 [150], ABKM [147] and HERAPDF [149]. In the latter case, two sets are provided: one with the value $\alpha_s(M_Z^2) = 0.1176$ that is close to the world average value [205] and the MSTW best-fit $\alpha_s(M_Z^2) = 0.1171$ [128], and one with the value $\alpha_s(M_Z^2) = 0.1145$ used also in the ABKM set [147], that is close to the preferred values that one obtains using deep-inelastic scattering data alone.

The Fig. 32 shows that there are significant differences between the various NNLO PDFs sets predictions. Indeed, while the differences in the cross sections are moderate in the low Higgs mass range, being of the order of 10% or less, there is a significant difference at higher Higgs masses, $\mathcal{O}(25\%)$ for $M_H \approx 500$ GeV. Even with the same α_s input or best-fit values, HERAPDF with $\alpha_s(M_Z^2) = 0.1176$ and MSTW results are strikingly different. For the large M_H values, this discrepancy is mainly due to the gluon densities at moderate to high Bjorken- x values which are less constrained by the data (in particular if the Tevatron high E_T jet data are not included as is the case of the ABKM and HERAPDF sets).

⁴²We discard in this analysis the two other major PDF collaborations on the market, the CTEQ collaboration [145] and the NNPDF collaboration [201] as their PDF sets were only provided at the NLO order in QCD when this analysis has been done. We also point out that the analysis conducted in section 4.3 has shown that the MSTW and CTEQ parametrizations are very similar, hence we could easily believe that this should be in much the same way at the IHC. It is worth mentioning that the NNPDF collaboration has released an update during the final stage of the writing of the thesis, which includes a NNLO PDFs set [233]. Their PDF fit is close to that of the MSTW collaboration.

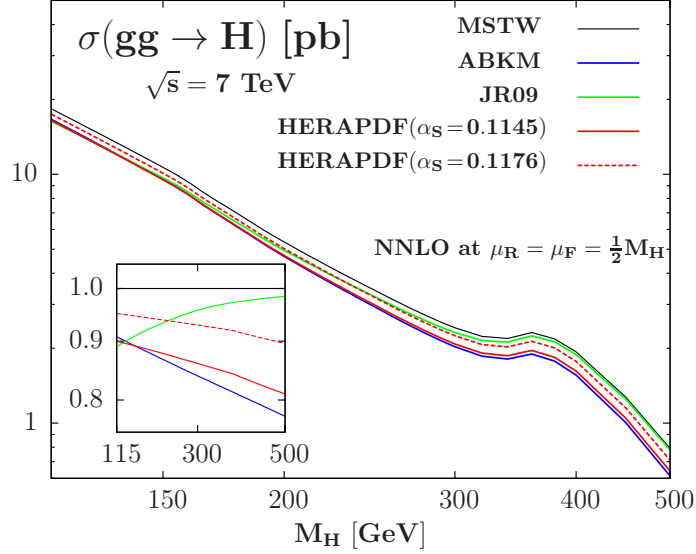


Figure 32: The central values of the NNLO cross section $\sigma(gg \rightarrow H + X)$ at the IHC as a function of M_H when evaluated in the four schemes which provide NNLO PDFs. In the inserts, shown are the same but with the cross sections normalized to the MSTW central cross section.

We again encounter the same situation developed at the Tevatron and discussed earlier. The comparison between the estimate using only one PDF set with the usual Hessian method displayed in Fig. 31 and the estimate comparing the central predictions with various NNLO PDF sets, displayed in Fig. 32, leads to very different uncertainty estimations. That is why the inclusion of the uncertainty due to the value of α_S is crucial as pointed out in Refs. [94, 232] and explained in details in section 4.3. If the reader reads carefully the legend of Fig. 32 he will see that even within one PDF set, say the HERAPDF set, the value of α_S could change drastically depending on the PDF fit that is done. Indeed this value is fitted altogether with the PDF, but the difference in the value of $\alpha_S(M_Z^2)$ alone is not enough to explain the striking differences in the various predictions and we should think about the differences in the shape of the gluon densities. We will then also use this additional source of uncertainty in the case of the Higgs production in gluon–gluon fusion at the IHC.

We recall that we use the MSTW scheme [199] with

$$\alpha_s(M_Z^2) = 0.1171^{+0.0014}_{-0.0014} \text{ (68\% CL) or } ^{+0.0032}_{-0.0032} \text{ (90\% CL) at NNLO} \quad (5.3)$$

We have evaluated the 90% CL correlated PDF+ $\Delta^{\text{exp}}\alpha_S$ uncertainties and the result is shown in Fig. 31 (green band and green lines) as a function of M_H . The uncertainties that we have obtained, as displayed in Fig. 31, are much larger than the uncertainties solely due to the PDF Hessian errors. At low Higgs masses we even double the uncertainty. Nevertheless, in much the same way as in the case of the Tevatron predictions, we cannot yet reconcile MSTW and ABKM/HERAPDF predictions, particularly at high Higgs masses.

We then miss something that would be able to explain the spread of the different PDF sets predictions using only one PDF scheme.

We will thus consider, in addition to the correlated PDF+ $\Delta^{\text{exp}}\alpha_s$ uncertainty, the one that comes from the theoretical uncertainty on the value of the strong coupling constant, stemming from the truncation of the perturbation series, the different heavy flavour scheme in the various PDF collaborations, and so on. If we compare the world average value for $\alpha_s(M_Z^2)$ and the value obtained using only deep-inelastic scattering data, the difference is significant. Considering this additional source of uncertainty then helps to reconcile the different Higgs production cross section predictions.

The MSTW collaboration estimates the theoretical uncertainty to be $\Delta^{\text{th}}\alpha_s = 0.003$ at NLO [199], which gives $\Delta^{\text{th}}\alpha_s = 0.002$ at most at NNLO. Using a fixed α_s NNLO grid with central PDFs given by the MSTW collaboration, with α_s values different from the best-fit value (in the range 0.107–0.127 with steps of 0.001 and which thus include the values $\alpha_s(M_Z^2) = 0.1171 \pm 0.002$ at NNLO), we have evaluated this uncertainty. Adding it in quadrature to the PDF+ $\Delta^{\text{exp}}\alpha_s$ uncertainty, we obtain at the LHC a total PDF+ $\Delta^{\text{exp}}\alpha_s + \Delta^{\text{th}}\alpha_s$ uncertainty of $\approx 11\% - 15\%$ depending on the Higgs mass. At least for not too heavy Higgs bosons, this larger uncertainty reconciles the MSTW and ABKM/HERAPDF predictions⁴³.

If we compare the situation at the LHC with the results we obtained in the Tevatron study in section 4.3 we see that for $M_H \lesssim 200$ GeV we obtain smaller uncertainties, approximately $\pm 11\%$ compared to the $\approx \pm 15\text{--}20\%$ uncertainty of $\sigma^{\text{NNLO}}(gg \rightarrow H)$ at the Tevatron. This is due to the better control on the behavior of the gluon density at moderate- x values which are relevant for the LHC compared to high- x values relevant for the Tevatron. In addition to this remark we point out the fact that we required to extend $\Delta^{\text{th}}\alpha_s$ to the value of 0.004 in the Tevatron study in order to reconcile MSTW prediction with that of ABKM. This is nearly done at the LHC with the much smaller value of $\Delta^{\text{th}}\alpha_s = 0.002$ as estimated by the MSTW collaboration.

We again stress that this procedure is by no mean universal and unique. If we compare

⁴³In order to be as much thorough as possible, we could also take into account the effects due to the bottom and charm quark masses on the PDFs. Indeed, a change in the fitted masses for these quarks may affect the gluon splitting which in turn alters the shape of the gluon-gluon luminosity in $gg \rightarrow H$. We have estimated quantitatively this effect by using the m_b and m_c dependent MSTW PDFs [234] with $m_c = 1.40 \pm 0.15$ GeV and $m_b = 4.75 \pm 0.05$ GeV. In the case of the charm quark, we obtain an approximate 0.2% change at $M_H = 115$ GeV and at most $\approx 1.5\%$ change at $M_H = 500$ GeV. In the case of the b -quark, the change is below the percent level. As we add in quadrature these uncertainties to obtain the total PDF+ $\Delta^{\text{exp+th}}\alpha_s$ uncertainty, these additional sources are totally negligible and will not be included in the end.

to the results obtained with the use of the PDF4LHC recommendation [151], that is to take the 68%CL MSTW PDF+ $\Delta^{\text{exp}}\alpha_s$ band and multiply it by a factor of two⁴⁴ we obtain a slightly larger uncertainty while we obtained a comparable uncertainty in the Tevatron analysis. This is not much a surprise as Fig. 32 displays a very large discrepancy between the various NNLO predictions that cannot be handled in a satisfactory way by the PDF4LHC recommendation. Nevertheless we obtain similar uncertainties, a situation which gives us some confidence in our way of trying to handle the still pending PDF puzzle.

5.4 Effective field theory approximation

The last source of theoretical uncertainties that we consider is the one specific to the gluon–gluon fusion production channel, and that was already discussed in section 4.4 in the case of the Tevatron collider.

Indeed, although NLO QCD and EW corrections for the $gg \rightarrow H$ cross section are known precisely with no approximation, the calculation at the NNLO order is done in an effective theory (EFT) approach where the particles running in the loop are assumed to have an infinite mass, or more precisely to have a much heavier mass than that of the produced Higgs boson. We will thus take into account an uncertainty related to that approximation, both for QCD and EW corrections.

At NLO in QCD, the approximation $m_t \gg M_H$ for the contribution of the top quark in the loop is rather good for Higgs masses below the $t\bar{t}$ threshold, $M_H \lesssim 340$ GeV, in particular when the full quark mass dependence of the leading order cross section $\sigma_{\text{exact}}^{\text{LO}}$ is taken into account [105]. At NNLO, this approximation for the top quark contribution seems also to be accurate as studies of the effect of a finite m_t value in expansions of $M_H/(2m_t)$ have shown a difference below the percent level with respect to the EFT calculation for $M_H \lesssim 300$ GeV [212–215]. At the Tevatron this result was enough to keep us looking at the uncertainty related to the finiteness of the top quark mass as the results were derived in the interesting Higgs mass range of $115 \leq M_H \leq 200$ GeV for the Tevatron experiments.

The situation at the LHC is quite different: the ATLAS/CMS experiments have been designed to look for the Higgs boson in its entire mass range $115 \leq M_H \leq 1000$ GeV⁴⁵ which reduces at $\sqrt{s} = 7$ TeV to the mass range $115 \leq M_H \leq 600$ GeV. The EFT approach

⁴⁴More precisely the procedure advocated by the PDF4LHC group is to use the envelop of MSTW,CTEQ and NNPDF prediction at the NLO level, rescaled to the central NNLO MSTW prediction. As argued in [210] this is equivalent to the procedure outlined in the main text.

⁴⁵the upper bound should be in fact approximately 800 GeV, related to the theoretical bounds on the SM Higgs mass, see section 3.1.

should then definitely not be valid for Higgs masses beyond the $t\bar{t}$ threshold, that is beyond $M_H \geq 350$ GeV, where the $gg \rightarrow H$ amplitude develops imaginary parts. This can be seen at NLO where both the exact and the approximate results are known. We will thus include an uncertainty related to the use of the EFT approach for $M_H \gtrsim 2m_t$ which is taken as the difference between $\sigma_{\text{exact}}^{\text{NLO}}$ and $\sigma_{m_t \rightarrow \infty}^{\text{NLO}}$ when the exact top quark mass dependence is included in the LO cross section and when this difference is rescaled with the relative magnitudes of the NLO and NNLO K -factors, i.e. $K_{m_t \rightarrow \infty}^{\text{NLO}}/K_{m_t \rightarrow \infty}^{\text{NNLO}}$.

In the left-hand side of Fig. 33 we display the difference between the exact calculation and the EFT calculation, both at NLO and NNLO QCD order, for $\sqrt{s} = 7$ TeV. As expected the difference is very small for $M_H \leq 350$ GeV where the EFT approach is very well motivated, and then oscillate around the 2% level up to 400 GeV from which the error increases very fast. For $M_H \gtrsim 500$ GeV we obtain an uncertainty larger than 5% and thus we cannot treat this uncertainty as being negligible in contrast with the Tevatron analysis [94].

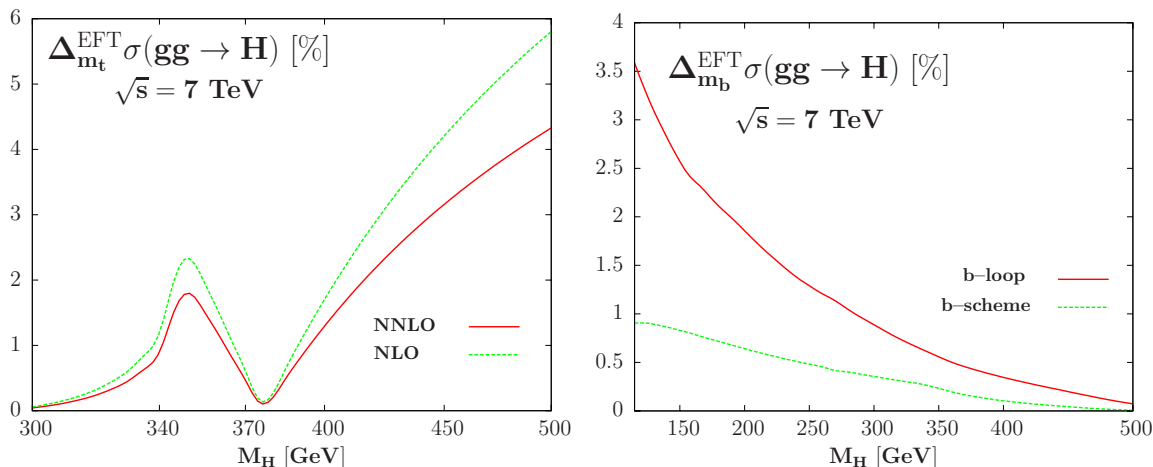


Figure 33: The estimated uncertainties (in %) due to the use of the EFT approach in the evaluation of $\sigma(gg \rightarrow H)$ at NNLO for the top quark loop contribution for Higgs masses beyond $2m_t$ (left) and for the bottom-quark loop contributions (right).

The two other sources of uncertainty that enter in the EFT approach have already been encountered in the Tevatron analysis. Indeed it is well known that of course the EFT approximation is not valid at all for the bottom quark loop in the gluon-gluon fusion as the bottom quark mass is small. The omission of this contribution at LO leads to a $\approx 10\%$ difference compared to the exact case. The inclusion of the bottom quark loop actually decreases the cross section because of the significant negative interference between the top and the bottom quark loops, the contribution of the bottom quark loop itself being rather small. Neglecting this contribution then actually overestimates the NLO (and also the NNLO) cross section and this approximation cannot be taken into account in the scale

variation performed at NNLO because of the absence of the top–bottom interference at NNLO.

In order to estimate the uncertainty due the missing b -loop contribution at NNLO, we simply follow the previous procedure for the top quark: we assign an error on the NNLO QCD result which is approximately the difference between the exact result $\sigma_{\text{exact}}^{\text{NLO}}$ and the approximate result $\sigma_{m_t \rightarrow \infty}^{\text{NLO}}$ obtained at NLO but rescaled with the relative magnitude of the K -factors that one obtains at NLO and NNLO for the top-loop, i.e. $K_{m_t \rightarrow \infty}^{\text{NLO}}/K_{m_t \rightarrow \infty}^{\text{NNLO}}$. This procedure is the one that has been used in section 4.4 in the study of the EFT approach at the Tevatron collider. This leads to the uncertainty on the $\sigma^{\text{NNLO}}(gg \rightarrow H)$ at $\sqrt{s} = 7$ TeV that is shown in the right-hand side of Fig. 33. Below $M_H \sim 120$ GeV where the b -loop plays an important role the uncertainty is not negligible, reaching the order of $\pm 3\%$. For Higgs mass above $M_H \sim 300$ GeV the uncertainty is below the percent level and thus completely negligible especially in the view of the EFT uncertainty due to the top-loop foreseen in the previous lines.

In addition to this missing loop uncertainty, there is some freedom in the choice of the renormalization scheme for the b -quark mass in the $gg \rightarrow H$ amplitude: either the on-shell scheme in which the pole mass is $m_b \approx 4.7$ GeV or the $\overline{\text{MS}}$ scheme in which the mass $\overline{m}_b(\overline{m}_b) \approx 4.2$ GeV is adopted. This leads to a difference of $\approx 1\%$ in the b -quark loop contribution at NLO that we will take as an additional uncertainty due to the scheme dependence. This scheme dependence will also be discussed in part IV when dealing with MSSM $gg \rightarrow$ Higgs production at the Tevatron and the LHC. Note that this cannot be taken into account with the scheme dependence as these are two widely different scales: the scheme dependence is probed around $\mu_0 = \frac{1}{2}M_H$ while the scheme dependence can be actually probed around $\mu = \overline{m}_b(\overline{m}_b)$.

The last source of EFT uncertainties is the mixed QCD–EW corrections that have been calculated at NNLO [118] in an EFT approach with $M_{W/Z} \gg M_H$. Obviously this limit is not valid in practice as Higgs mass above 115 GeV are probed at hadron colliders. Some caution should be taken when including this correction and we have made the choice to assign an uncertainty that is of the same size as the contribution of this correction itself, as in Refs. [94,232] and in section 4.4⁴⁶. This uncertainty is comparable in size to the difference between the electroweak correction calculated exactly at NLO [116,117] evaluated in the partial factorization scheme, where the correction $\sigma^{\text{LO}}\Delta_{\text{EW}}$ is added to the QCD corrected

⁴⁶According to a discussion with C. Anastasiou we tend to somewhat underestimate the quality of the approximation which may be valid, up to a certain point, above the $M_{W/Z}$ threshold. Nevertheless, in the view of the smallness of this (still non-negligible) uncertainty, we decide to stick to our procedure for the entire Higgs mass range.

cross section, and the EW corrections calculated in the complete factorization scheme where the NNLO cross section is multiplied by $1 + \Delta_{\text{EW}}$. This generates an additional uncertainty of $\approx 3\%$ at most, nearly exactly the same as discussed in section 4.4 for the Tevatron.

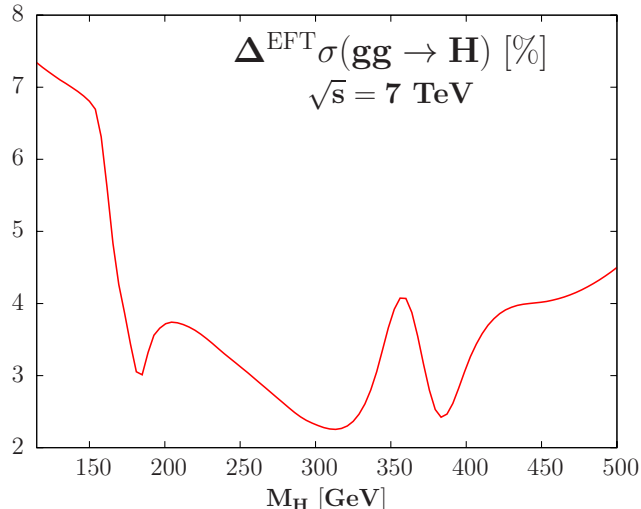


Figure 34: The estimated total uncertainty (in %) at LHC energies and as a function of M_H from the use of the EFT approach for the calculation of the $gg \rightarrow H$ amplitude at NNLO and from the scheme dependence of the b -quark mass.

Adding the uncertainties from these three sources linearly, the resulting overall uncertainty is displayed in Fig. 34 as a function of M_H . It amounts to $\approx 7\%$ in the low Higgs mass range, drops to the level of $\approx 4\%$ in the mass range $M_H \approx 200\text{--}400$ GeV, and then increases to reach the level of $\approx 6\%$ at 600 GeV, as a result of the bad $M_H \ll 2m_t$ approximation for the top loop contribution. Since this is a pure theoretical uncertainty with no statistical grounds, it should be added linearly to the uncertainty from scale variation, as will be done in the next subsection.

5.5 Total uncertainty at 7 TeV

We have described in the previous subsection the different sources of theoretical uncertainties affecting our prediction. The last task which remains to be done is the final combination in order to obtain the overall theoretical uncertainty on the $gg \rightarrow H$ production cross section at the LHC.

As discussed in section 4.5 and also in [95], the uncertainty associated to the PDFs(+ α_s) should be considered as a pure theoretical uncertainty despite the fact that the fit is done on experimental data using χ^2 techniques. Indeed this is the only reasonable way to handle the PDF puzzle, that is the very large discrepancy between the various predictions with the different NNLO PDFs sets on the market. In this way we consider the different theoretical

assumptions in the determination of the parton densities, and consider the PDF(+ α_s) uncertainty to have no statistical ground⁴⁷ and not added in quadrature with the scale uncertainty and the EFT uncertainty which are purely theoretical beyond any doubts.

We will thus summarize the three possible ways to combine the various uncertainties, that have been presented in Ref. [232].

- A) The first procedure has been presented for the first time in [94] and has been used in the section 4.5 in order to obtain the total uncertainty at the Tevatron in the gluon–gluon fusion channel, taking into account the possible correlation between the scale and the PDFs (that are evaluated at a given factorization scale). We calculate the extremal cross sections regarding to the scale variation and then apply on this minimal/maximal cross section our evaluation of the PDF+ $\Delta^{\text{exp+th}}\alpha_s$ uncertainty, with the factorization and renormalization scales fixed at the values corresponding to the minimal and maximal cross sections with respect to scale variation⁴⁸. We then add linearly the smaller EFT uncertainty to obtain the overall theoretical uncertainty on the central prediction. This procedure labeled as procedure “A” is our preferred way of handling with the total uncertainty.
- B) The second procedure, labeled as procedure “B”, is simply the linear addition of the scale, EFT/scheme and PDF+ α_s uncertainties, as all of them are considered as pure theoretical uncertainties. This procedure is the one advocated by Ref. [210]. The final uncertainty that is obtained is in general slightly larger than what can be obtained with the procedure A described above.
- C) The third and last procedure labeled as procedure “C” is to consider the PDF uncertainty as being the spread of the four NNLO central predictions with the four NNLO PDFs sets, using the MSTW parametrization as the central set. Since the maximal cross section for $gg \rightarrow H$ is obtained with the MSTW parametrization and the minimal one with the ABKM set, as displayed in Fig. 32, the total uncertainty on the production cross section will be on the one hand the linear addition of the scale and EFT uncertainties evaluated with the MSTW PDF set for the upper uncertainty, on the other hand the linear addition of the scale and EFT uncertainties evaluated with the ABKM PDF set for the lower uncertainty, adding the difference between the MSTW and the ABKM predictions.

⁴⁷In statistical language, the PDF uncertainties should be considered as having a flat prior, exactly like the scale uncertainty. A more elaborated discussion can be found in [210] where the recommended combination is that of the linear type.

⁴⁸This procedure has been in fact already proposed, together with other possibilities which give similar results, in Ref. [189] where top quark pair production at hadron colliders was discussed.

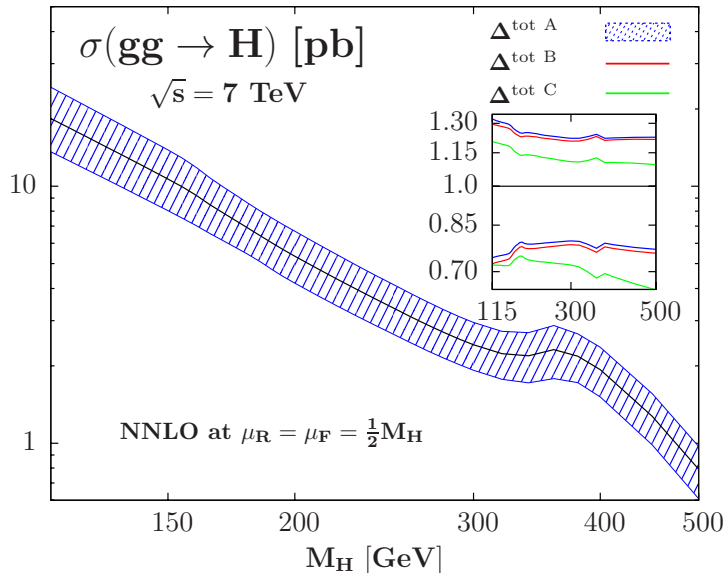


Figure 35: The production cross section $\sigma(gg \rightarrow H)$ at NNLO at the LHC with $\sqrt{s} = 7$ TeV, including the total theoretical uncertainty band when all the individual uncertainties are combined using the three procedures A, B and C described in the text. In the inserts, the relative deviations from the central cross section value are shown.

The overall theoretical uncertainties on $gg \rightarrow H$ cross section at the 7 TeV LHC that we obtain when using the three ways A, B, C of handling with the final combination are displayed in Fig.35 as a function of the Higgs mass. With the procedure A, the uncertainty amounts to $\approx -23\%$, $+25\%$ for $M_H \lesssim 160$ GeV, reduces to $\approx -21\%$, $+22\%$ for $M_H \gtrsim 200$ GeV to reach the value $\approx \pm 22\%$ at $M_H \approx 500$ GeV⁴⁹. With the procedure B, that is when the various sources of uncertainties are added linearly, the total uncertainty that is obtained is nearly the same as in the case of the procedure A, but slightly smaller (2 to 3%) for the upper uncertainty and slightly higher for the lower uncertainty. We remind the reader that this procedure is advocated by Ref. [210]; the results obtained with the procedure A are then reasonable. In the case of procedure C, as we use for the central prediction of $\sigma^{\text{NNLO}}(gg \rightarrow H)$ the MSTW PDF set, the upper uncertainty is simply the sum of the scale and scheme uncertainties which add to less than 20% in the entire Higgs mass and are thus much smaller (in particular in the low Higgs mass range) than in procedures A and B. This is a different story for the lower uncertainty as in addition to the scale and EFT uncertainties we have to take into account the difference between the MSTW and ABKM

⁴⁹Note that the overall uncertainty on $\sigma^{\text{NNLO}}(gg \rightarrow H)$ at the LHC is significantly smaller than what has been obtained at the Tevatron in section 4.5 and published in [94], where the procedure A for the combination has been used ($\approx -35\%$, $+40\%$). This is a result of the reduction of both the scale and the PDF uncertainties at $\sqrt{s} = 7$ TeV compared to $\sqrt{s} = 1.96$ TeV, because of the reduction of the QCD K -factors at the LHC compared to the Tevatron and also because of the gluon density itself which has a less uncertain behavior for not too heavy Higgs bosons.

predictions. In this case, the overall uncertainty is comparable to what is obtained using the procedures A and B in the low Higgs mass range where the difference between MSTW and ABKM is of the order of 10% and, hence, the Hessian MSTW PDF+ α_s uncertainty alone. It becomes much larger at higher M_H values where the difference between the MSTW and ABKM predictions becomes significant. A significant example can be taken at $M_H = 500$ GeV where an uncertainty of $\approx -35\%$ is obtained in procedure C, compared to $\approx -23\%$ using procedures A and B.

M_H	σ	Scale [%]	PDF+ $\Delta_{\alpha_s}^{\text{exp+th}}$ [%]	EFT [%]	A [%]	B [%]	C [%]
115	18.35	+9.1 -10.2	+9.1 -8.8	± 7.3	+27.8 -24.6	+25.6 -26.3	+16.4 -26.8
120	16.84	+8.9 -10.2	+9.1 -8.8	± 7.3	+27.5 -24.5	+25.3 -26.2	+16.2 -26.8
125	15.51	+8.8 -9.9	+9.1 -8.8	± 7.2	+27.1 -24.1	+25.1 -25.8	+16.0 -26.7
130	14.32	+8.5 -9.8	+9.1 -8.8	± 7.1	+26.7 -24.0	+24.7 -25.6	+15.6 -26.7
135	13.26	+8.4 -9.6	+9.1 -8.8	± 7.0	+26.4 -23.7	+24.5 -25.4	+15.4 -26.6
140	12.31	+8.3 -9.5	+9.1 -8.8	± 7.0	+26.2 -23.6	+24.3 -25.2	+15.3 -26.7
145	11.45	+8.2 -9.5	+9.1 -8.8	± 6.9	+26.0 -23.6	+24.2 -25.2	+15.1 -26.8
150	10.67	+8.1 -9.5	+9.1 -8.8	± 6.8	+25.8 -23.5	+24.0 -25.1	+14.9 -26.9
155	9.94	+7.9 -9.4	+9.1 -8.8	± 6.6	+25.4 -23.2	+23.6 -24.8	+14.5 -26.8
160	9.21	+7.8 -9.4	+9.1 -8.8	± 5.9	+24.4 -22.7	+22.8 -24.2	+13.7 -26.4
165	8.47	+7.7 -9.4	+9.1 -8.8	± 4.9	+23.4 -21.7	+21.7 -23.1	+12.6 -25.5
170	7.87	+7.7 -9.4	+9.1 -8.8	± 4.2	+22.7 -21.0	+21.1 -22.5	+11.9 -25.0
175	7.35	+7.6 -9.4	+9.1 -8.9	± 3.7	+22.0 -20.5	+20.4 -21.9	+11.3 -24.6
180	6.86	+7.5 -9.3	+9.2 -8.9	± 3.1	+21.4 -19.9	+19.8 -21.3	+10.6 -24.2
185	6.42	+7.4 -9.3	+9.2 -8.9	± 3.0	+21.1 -19.8	+19.6 -21.2	+10.4 -24.2
190	6.01	+7.4 -9.3	+9.2 -8.9	± 3.4	+21.5 -20.3	+20.0 -21.7	+10.8 -24.9
195	5.65	+7.4 -9.3	+9.2 -8.9	± 3.6	+21.8 -20.5	+20.3 -21.9	+11.0 -25.2
200	5.34	+7.3 -9.3	+9.3 -9.0	± 3.7	+21.8 -20.6	+20.3 -21.9	+11.0 -25.4
210	4.81	+7.2 -9.3	+9.3 -9.0	± 3.7	+21.7 -20.6	+20.2 -22.0	+10.9 -25.8
220	4.36	+7.2 -9.2	+9.3 -9.1	± 3.6	+21.6 -20.6	+20.2 -21.9	+10.9 -26.0
230	3.97	+7.0 -9.2	+9.4 -9.2	± 3.5	+21.4 -20.5	+19.9 -21.8	+10.5 -26.2
240	3.65	+7.0 -9.2	+9.5 -9.2	± 3.3	+21.1 -20.5	+19.8 -21.8	+10.3 -26.5
250	3.37	+6.9 -9.2	+9.5 -9.3	± 3.1	+20.9 -20.4	+19.5 -21.6	+10.0 -26.6
260	3.11	+6.8 -9.2	+9.6 -9.4	± 3.0	+20.6 -20.3	+19.3 -21.6	+9.7 -26.8
270	2.89	+6.7 -9.2	+9.7 -9.5	± 2.8	+20.5 -20.2	+19.1 -21.4	+9.4 -27.0
280	2.71	+6.8 -9.2	+9.8 -9.5	± 2.6	+20.5 -20.1	+19.2 -21.4	+9.4 -27.2
290	2.55	+6.8 -9.1	+9.8 -9.6	± 2.4	+20.3 -20.0	+19.1 -21.1	+9.2 -27.2
300	2.42	+6.7 -9.1	+9.9 -9.7	± 2.3	+20.2 -19.9	+18.9 -21.1	+9.0 -27.4
320	2.23	+6.7 -9.2	+10.1 -9.9	± 2.3	+20.2 -20.1	+19.0 -21.4	+9.0 -28.2
340	2.19	+6.9 -9.2	+10.3 -10.1	± 3.0	+21.4 -21.1	+20.2 -22.3	+10.0 -29.6
360	2.31	+7.0 -9.2	+10.5 -10.3	± 4.1	+22.5 -22.3	+21.6 -23.6	+11.0 -31.3
380	2.18	+6.3 -9.1	+10.7 -10.5	± 2.5	+20.4 -20.9	+19.6 -22.2	+8.8 -30.3
400	1.93	+5.9 -8.8	+11.0 -10.7	± 3.1	+20.7 -21.5	+20.0 -22.7	+9.0 -31.3
450	1.27	+5.0 -8.4	+11.6 -11.3	± 4.0	+21.4 -22.6	+20.5 -23.8	+9.0 -33.4
500	0.79	+4.4 -8.1	+12.2 -11.9	± 4.5	+22.1 -23.3	+21.1 -24.5	+8.9 -35.2
600	0.31	+3.7 -7.7	+13.3 -13.0	± 6.6	+24.5 -26.1	+23.7 -27.3	+10.4 -40.0

Table 5: The NNLO total Higgs production cross sections in the $gg \rightarrow H$ process at the LHC with $\sqrt{s} = 7$ TeV (in pb) for given Higgs mass values (in GeV) at a central scale $\mu_F = \mu_R = \frac{1}{2}M_H$. Shown also are the corresponding shifts due to the theoretical uncertainties from the various sources discussed (first from scale, then from PDF+ $\Delta_{\alpha_s}^{\text{exp+th}}$ at 90%CL and from EFT), as well as the total uncertainty when all errors are added using the procedures A, B and C described in the text.

The results obtained in this section are summarized in Table 5⁵⁰. The $gg \rightarrow H$ production cross section for values of the Higgs mass relevant at the LHC with $\sqrt{s} = 7$ TeV are given together with the uncertainties from scale variations, the PDF+ $\Delta^{\text{exp+th}}\alpha_s$ uncertainty in the MSTW scheme and the uncertainty due the use of the EFT approach beyond the NLO order. The combined uncertainties obtained using the three procedures A, B and C proposed above are also given.

5.6 LHC results at different center-of-mass energies

As stated in the introduction of this section, the LHC commissioning group had thought about the idea of raising gradually the center-of-mass energy at the LHC, by going from 7 TeV to 14 TeV through intermediate 8, 9, 10 TeV center-of-mass energies [223] in order to increase significantly the luminosity beyond the 1 fb^{-1} level without having to change much the accelerator design. Even if this idea was abandoned in the beginning of year 2011 [228] we will present some results concerning these intermediate energies and then give a detailed analysis of the case of the full-fledged LHC at $\sqrt{s} = 14$ TeV.

5.6.1 The case of the LHC with $\sqrt{s} = 8, 9, 10$ TeV

We use the same recipe for the calculation of the central predictions, namely a calculation at NNLO order in QCD and EW corrections, with a central scale $\mu_0 = \mu_R = \mu_F = \frac{1}{2}M_H$, using the MSTW 2008 NNLO PDFs set. The results for $\sigma^{\text{NNLO}}(gg \rightarrow H)$ are displayed for $\sqrt{s} = 8, 9$ and 10 TeV in Fig. 36 as a function of M_H . They are also available numerically in Table 6 for the relevant Higgs mass values .

As shown in Fig. 36, in the low Higgs mass range $M_H \approx 120$ GeV the cross section $\sigma(gg \rightarrow H)$ is approximately 20%, 40% and 100% higher at, respectively, $\sqrt{s} = 8, 9$ and 10 TeV, compared to $\sqrt{s} = 7$ TeV. At higher Higgs masses, $M_H \gtrsim 300$ GeV, the increase of the cross section is slightly larger as the phase space available for the Higgs production is reduced at lower energies.

It has been verified that the expectations for the theoretical uncertainties does not change significantly between the LHC at 7 TeV and the intermediate 8, 9, 10 TeV center-of-mass energies. At most we obtain a 2% decrease due to the better behaviour of the gluon density

⁵⁰An extended table for Higgs masses up to 1 TeV can be found in the gg -fusion section of Ref. [210]. The full table has not been displayed in this thesis as we want to insist on the fact that predictions for Higgs mass above 600 GeV are irrelevant at the LHC, as the center-of-mass energy and the luminosity are too small to obtain a viable signal.

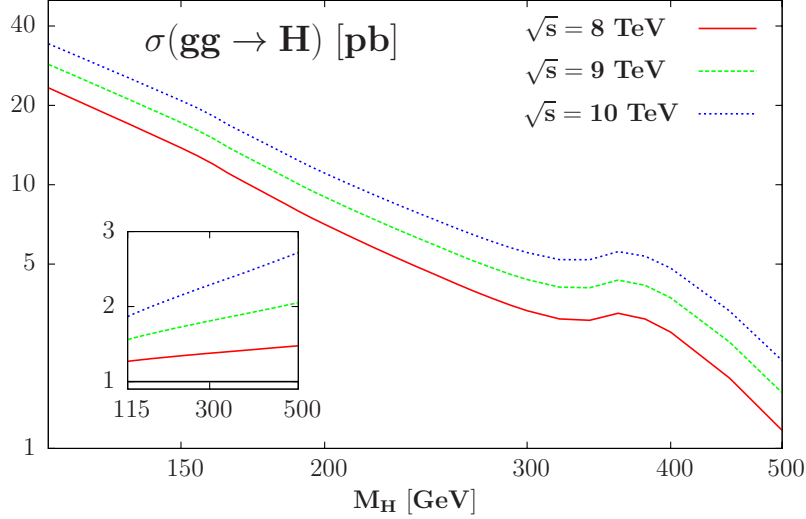


Figure 36: The production cross section $\sigma(gg \rightarrow H)$ at NNLO as a function of M_H at the LHC with center of mass energies of $\sqrt{s} = 8, 9$ and 10 TeV. In the inserts, the relative increase compared to the cross section at $\sqrt{s} = 7$ TeV are shown.

at high Higgs masses. To a very good approximation, we can therefore view the results of the scale, EFT and PDF+ $\Delta^{\text{exp+th}}\alpha_s$ uncertainties as well as the final combination (in either procedure A, B or C) all given in Table 5 for the $\sqrt{s} = 7$ TeV case as being the same at the LHC for the intermediate $\sqrt{s} = 8, 9, 10$ TeV.

5.6.2 The case of the designed LHC at $\sqrt{s} = 14$ TeV

We end this subsection with the case of the designed LHC, with $\sqrt{s} = 14$ TeV. It is expected to collect at least $\sim 30 \text{ fb}^{-1}$ of data, a luminosity that should allow either to discover the SM Higgs boson or to exclude its existence at 95%CL in its entire mass range $115 \leq M_H \lesssim 800$ GeV.

We use exactly the same outlines that were developed throughout this section for the case of the LHC at $\sqrt{s} = 7$ TeV. The results for the gluon–gluon fusion Higgs production cross section at the LHC with $\sqrt{s} = 14$ TeV are displayed in Figs. 37 (for the scale uncertainty), 38 for the PDF+ $\Delta^{\text{exp+th}}\alpha_s$ uncertainty and 39 for the overall combination. The numerical results can also be found in Table 7.

The main differences are highlighted in the next points:

- The scale uncertainty is estimated by varying μ_R and μ_F in the domain $\frac{1}{4}M_H \leq \mu_R = \mu_F \leq M_H$, as was the case for the LHC at 7 TeV. The result does not significantly change when comparing to the LHC case: we obtain a variation of approximately

M_H	$\sigma_{gg \rightarrow H}^{8 \text{ TeV}}$	$\sigma_{gg \rightarrow H}^{9 \text{ TeV}}$	$\sigma_{gg \rightarrow H}^{10 \text{ TeV}}$	M_H	$\sigma_{gg \rightarrow H}^{8 \text{ TeV}}$	$\sigma_{gg \rightarrow H}^{9 \text{ TeV}}$	$\sigma_{gg \rightarrow H}^{10 \text{ TeV}}$
115	23.31	28.63	34.26	210	6.39	8.15	10.07
120	21.46	26.42	31.68	220	5.82	7.44	9.22
125	19.81	24.44	29.37	230	5.33	6.84	8.50
130	18.34	22.68	27.30	240	4.91	6.32	7.88
135	17.03	21.10	25.44	250	4.55	5.88	7.34
140	15.84	19.67	23.76	260	4.22	5.47	6.85
145	14.77	18.38	22.24	270	3.94	5.13	6.44
150	13.80	17.21	20.86	280	3.70	4.83	6.08
155	12.89	16.10	19.55	290	3.50	4.58	5.78
160	11.97	14.98	18.22	300	3.33	4.37	5.53
165	11.04	13.85	16.87	320	3.10	4.09	5.20
170	10.28	12.92	15.77	340	3.06	4.07	5.19
175	9.62	12.11	14.80	360	3.26	4.35	5.58
180	9.00	11.36	13.90	380	3.09	4.15	5.36
185	8.44	10.66	13.08	400	2.76	3.73	4.83
190	7.92	10.03	12.32	450	1.85	2.53	3.32
195	7.47	9.47	11.65	500	1.17	1.62	2.15
200	7.07	8.99	11.07	600	0.47	0.68	0.92

Table 6: The cross sections in the $\sigma^{\text{NNLO}}(gg \rightarrow H)$ at the LHC with $\sqrt{s} = 8, 9, 10$ TeV (in pb) for given Higgs mass values (in GeV) at a central scale $\mu_F = \mu_R = \frac{1}{2}M_H$ using the MSTW PDF set.

$\pm 10\%$ at low Higgs masses and nearly $\pm 5\%$ at high Higgs masses, as displayed in the left part of Fig. 37.

- The EFT/scheme uncertainty is almost exactly the same than at $\sqrt{s} = 7$ TeV, as its most important component enters as a multiplicative factor in the $gg \rightarrow H$ amplitude but is larger starting from $M_H \gtrsim 500$ GeV. This is exemplified in the right part of Fig. 37.
- The left part of Fig. 38 demonstrates that there is still a very large spread in the different predictions when folding the partonic $gg \rightarrow H$ cross section with the gluon luminosities given by the four NNLO PDFs sets available. The results obtained within the MSTW scheme for the 90%CL PDF, PDF+ $\Delta^{\text{exp}}\alpha_s$ and the combined PDF+ $\Delta^{\text{exp+th}}\alpha_s$ uncertainties are displayed in the right part of Fig. 38. A slightly smaller PDF+ α_s uncertainty than at the LHC is obtained, of order 1 to 2%, since lower Bjorken x values are probed.

- The overall uncertainty on $\sigma^{\text{NNLO}}(gg \rightarrow H)$ displayed in Fig. 39 is more or less the same at 14 TeV than at 7 TeV in the low Higgs mass range, but is slightly smaller for heavier Higgs bosons. As an example, we obtain for $M_H = 500$ GeV a total $\approx \pm 21\%$ uncertainty at 14 TeV compared to $\approx \pm 23\%$ at 7 TeV. We note that we have restricted to procedure A as we believe it is the most reasonable procedure as discussed in section 5.5.

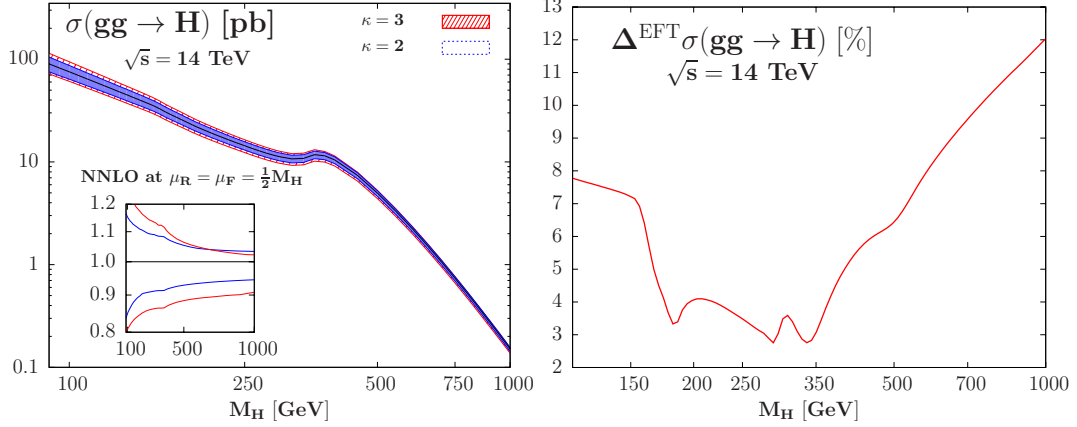


Figure 37: The uncertainty bands of $\sigma_{gg \rightarrow H}^{\text{NNLO}}$ from scale variation with $\kappa = 2$ (left) and the total EFT uncertainty (right) at $\sqrt{s} = 14$ TeV as a function of M_H .

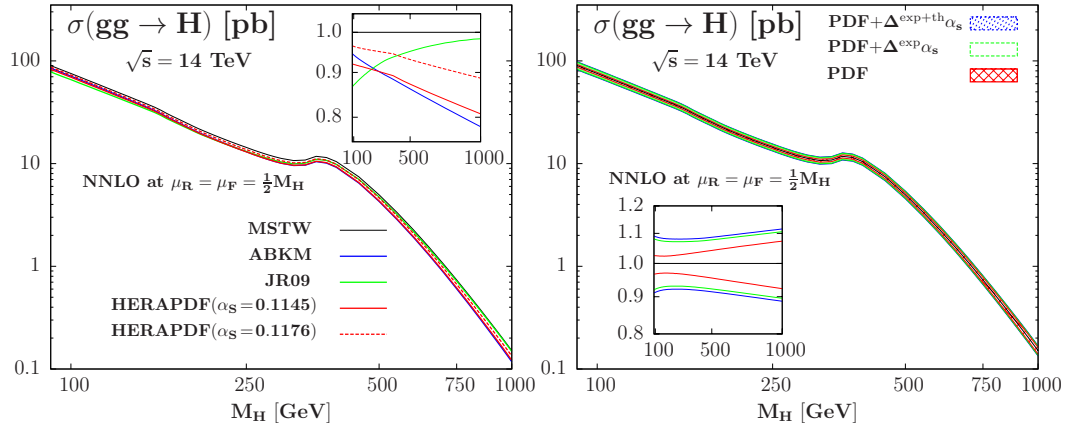


Figure 38: The PDF uncertainties in $\sigma^{\text{NNLO}}(gg \rightarrow H)$ at the LHC with $\sqrt{s} = 14$ TeV as a function of M_H . Left: the central values when using the four NNLO PDFs and right: the 90% CL PDF, PDF+ $\Delta^{\text{exp}}\alpha_s$ and PDF+ $\Delta^{\text{exp}}\alpha_s + \Delta^{\text{th}}\alpha_s$ uncertainties in the MSTW scheme.

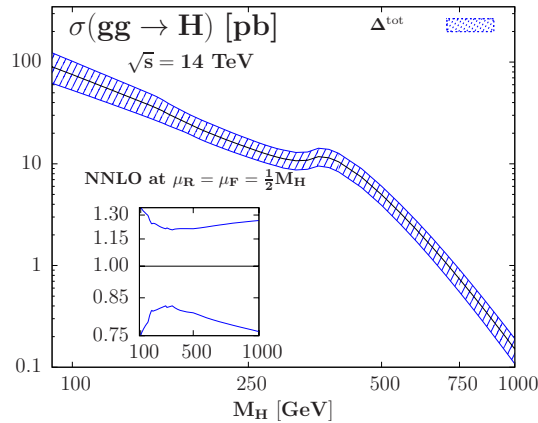


Figure 39: The cross section $\sigma^{\text{NNLO}}(gg \rightarrow H)$ at the LHC with the uncertainty band when all theoretical uncertainties are added using our procedure A described in the text.

M_H	$\sigma_{gg \rightarrow H}^{\pm\Delta_\mu \pm\Delta_{\text{PDF}} \pm\Delta_{\text{EFT}}}$	A	B	M_H	$\sigma_{gg \rightarrow H}^{\pm\Delta_\mu \pm\Delta_{\text{PDF}} \pm\Delta_{\text{EFT}}}$	A	B
115	59.37 ^{+9.4%+8.7%+7.8%} _{-12.2%-8.5%-7.8%}	+28.1%	+25.8%	240	15.30 ^{+7.0%+8.0%+3.7%} _{-8.2%-7.8%-3.7%}	+20.0%	+18.7%
120	55.20 ^{+9.2%+8.6%+7.7%} _{-11.9%-8.4%-7.7%}	+27.8%	+25.5%	250	14.38 ^{+6.9%+8.0%+3.5%} _{-8.2%-7.8%-3.5%}	+19.7%	+18.4%
125	51.45 ^{+9.0%+8.5%+7.6%} _{-11.6%-8.4%-7.6%}	+27.4%	+25.1%	260	13.52 ^{+6.8%+8.0%+3.3%} _{-8.1%-7.8%-3.3%}	+19.4%	+18.1%
130	48.09 ^{+8.9%+8.5%+7.5%} _{-11.4%-8.3%-7.5%}	+27.2%	+25.0%	270	12.79 ^{+6.7%+8.0%+3.1%} _{-8.1%-7.8%-3.1%}	+19.1%	+17.9%
135	45.06 ^{+8.7%+8.4%+7.5%} _{-11.1%-8.2%-7.5%}	+26.8%	+24.6%	280	12.17 ^{+6.7%+8.0%+2.9%} _{-8.1%-7.8%-2.9%}	+18.9%	+17.7%
140	42.30 ^{+8.5%+8.4%+7.4%} _{-10.8%-8.2%-7.4%}	+26.4%	+24.3%	290	11.65 ^{+6.6%+8.0%+2.8%} _{-8.0%-7.8%-2.8%}	+18.6%	+17.4%
145	39.80 ^{+8.4%+8.3%+7.3%} _{-10.6%-8.1%-7.3%}	+26.0%	+24.0%	300	11.22 ^{+6.5%+8.0%+3.4%} _{-8.0%-7.8%-3.4%}	+19.2%	+18.0%
150	37.50 ^{+8.3%+8.3%+7.2%} _{-10.4%-8.1%-7.2%}	+25.8%	+23.8%	320	10.70 ^{+6.5%+8.1%+3.1%} _{-8.0%-7.9%-3.1%}	+18.8%	+17.8%
155	35.32 ^{+8.1%+8.3%+7.0%} _{-10.2%-8.1%-7.0%}	+25.3%	+23.4%	340	10.83 ^{+6.5%+8.1%+2.8%} _{-8.0%-7.9%-2.8%}	+18.4%	+17.4%
160	33.08 ^{+8.0%+8.2%+6.3%} _{-10.0%-8.0%-6.3%}	+24.4%	+22.6%	360	11.77 ^{+6.4%+8.1%+3.5%} _{-8.0%-8.0%-3.5%}	+19.0%	+18.1%
165	30.77 ^{+7.9%+8.2%+5.3%} _{-9.8%-8.0%-5.3%}	+23.1%	+21.4%	380	11.46 ^{+6.0%+8.2%+4.4%} _{-7.7%-8.1%-4.4%}	+19.5%	+18.6%
170	28.89 ^{+7.8%+8.2%+4.5%} _{-9.7%-8.0%-4.5%}	+22.3%	+20.6%	400	10.46 ^{+5.6%+8.2%+5.0%} _{-7.4%-8.1%-5.0%}	+19.7%	+18.9%
175	27.24 ^{+7.8%+8.2%+4.0%} _{-9.5%-7.9%-4.0%}	+21.6%	+20.0%	450	7.42 ^{+5.0%+8.4%+6.0%} _{-7.0%-8.3%-6.0%}	+20.0%	+19.3%
180	25.71 ^{+7.7%+8.2%+3.5%} _{-9.4%-7.9%-3.5%}	+20.9%	+19.3%	500	4.97 ^{+4.6%+8.6%+6.4%} _{-6.7%-8.6%-6.4%}	+20.4%	+19.7%
185	24.28 ^{+7.6%+8.1%+3.3%} _{-9.1%-7.9%-3.3%}	+20.6%	+19.0%	550	3.32 ^{+4.3%+8.9%+7.4%} _{-6.5%-8.8%-7.4%}	+21.3%	+20.7%
190	22.97 ^{+7.6%+8.1%+3.8%} _{-9.1%-7.9%-3.8%}	+21.0%	+19.5%	600	2.24 ^{+4.1%+9.2%+8.3%} _{-6.3%-9.1%-8.3%}	+22.1%	+21.6%
195	21.83 ^{+7.5%+8.1%+4.0%} _{-9.0%-7.9%-4.0%}	+21.1%	+19.6%	650	1.53 ^{+3.9%+9.5%+9.0%} _{-6.2%-9.4%-9.0%}	+22.7%	+22.4%
200	20.83 ^{+7.4%+8.1%+4.1%} _{-8.8%-7.9%-4.1%}	+21.0%	+19.5%	700	1.05 ^{+3.8%+9.8%+9.6%} _{-6.1%-9.6%-9.6%}	+23.4%	+23.2%
210	19.10 ^{+7.3%+8.1%+4.1%} _{-8.6%-7.8%-4.1%}	+20.9%	+19.5%	800	0.52 ^{+3.5%+10.4%+10.5%} _{-6.0%-10.2%-10.5%}	+24.6%	+24.4%
220	17.64 ^{+7.2%+8.1%+4.0%} _{-8.4%-7.8%-4.0%}	+20.6%	+19.3%	900	0.27 ^{+3.4%+11.0%+11.3%} _{-5.9%-10.7%-11.3%}	+25.6%	+25.7%
230	16.38 ^{+7.1%+8.0%+3.8%} _{-8.3%-7.8%-3.8%}	+20.4%	+19.0%	1000	0.15 ^{+3.3%+11.5%+12.0%} _{-5.8%-11.3%-12.0%}	+26.4%	+26.9%

Table 7: The NNLO total Higgs production cross sections in the $gg \rightarrow H$ process at the LHC with $\sqrt{s} = 14$ TeV (in pb) for given Higgs mass values (in GeV) at a central scale $\mu_F = \mu_R = \frac{1}{2}M_H$. We also display the corresponding shifts due to the theoretical uncertainties from the various sources discussed (first from scale, then from PDF+ $\Delta^{\text{exp+th}}\alpha_s$ at 90%CL and from EFT), as well as the total uncertainty when all errors are added using the procedures A and B described in the text.

Table 7 which displays the cross sections together with the individual and overall theoretical uncertainties for the Higgs masses relevant at the LHC summarizes the results obtained at the full-fledged LHC with $\sqrt{s} = 14$ TeV.

5.7 Summary and outlook

In this section were presented the theoretical predictions for the Standard Model Higgs boson production total cross section at the early LHC, that is the LHC at 7 TeV, in the gluon–gluon fusion $gg \rightarrow H$ that is the main channel. We have assumed a central scale $\mu_F = \mu_R = \mu_0$ to be $\mu_0 = \frac{1}{2}M_H$ and calculated the cross section up to NNLO in QCD and EW corrections.

We have then estimated the theoretical uncertainties associated to the prediction: the scale uncertainty, the uncertainties from the PDF parametrisation and the associated error on α_s , as well as uncertainties due to the use of the EFT approach for the mixed QCD–electroweak radiative corrections and the b -quark loop contribution in the gluon–gluon fusion case. We have followed the recipe proposed for the first time in the case of the Tevatron collider and presented in section 4.5 for the combination of the different sources of uncertainties. The results that we obtain in the case of the LHC are smaller than at the Tevatron, mainly because the QCD corrections are smaller at the LHC, the K -factor being smaller. There is also a better behaviour of the gluon density at the high Bjorken x values probed at the LHC.

We have also given some predictions for the intermediate center–of–mass energies $\sqrt{s} = 8, 9, 10$ TeV as well as for the full–fledged $\sqrt{s} = 14$ TeV LHC. The total uncertainty is in all cases nearly the same as for the LHC with $\sqrt{s} = 7$ TeV.

We have finished the analysis of the production cross section. Before the investigation of the consequences on the experimental results we have to analyze the crucial Higgs decay branching ratios in the next section.

6 Higgs decay branching ratios and the implication on Higgs searches at hadron colliders

The last two sections have been devoted to the Higgs production itself, following the main production channels at the Tevatron and LHC colliders. The focus has been on the total cross section regardless of the Higgs decay channel. This section is then devoted to the crucial study of the Higgs decay branching ratios, as the experiments are looking for the traces of the Higgs boson in their detectors, which then require that the Higgs decay chain has to be well understood.

We will first review the most important channels for experimental searches at the Tevatron and the LHC. The main reference for this subsection is Ref. [45]. We then discuss the theoretical uncertainties affecting the Higgs decay branching ratios, that have not been considered in the experimental analyses [93, 226, 227] up until now and is under active investigation in Ref. [210, 232]. Indeed, while the Higgs decays into lepton and gauge boson pairs are well under control (as mainly small electroweak effects are involved), the partial decays widths into quark pairs and gluons are plagued with uncertainties that are mainly due to the imperfect knowledge of the bottom and charm quark masses and the value of the strong coupling constant α_s . This was first studied in Ref. [235] and the analysis presented in Ref. [232] was an update of this previous result, and will be the subject of this section. We show that at least in the intermediate mass range, $M_H \approx 120\text{--}150$ GeV, where the SM Higgs decay rates into $b\bar{b}$ and W^+W^- final states have the same order of magnitude, the parametric uncertainties on these two main Higgs decay branching ratios are non-negligible, being of the order of 3 to 10% at the 1σ level.

6.1 Important channels for experimental search

We present in this subsection the main channels used at the Tevatron and the LHC for the experimental searches of the SM Higgs boson. We display in Fig. 40 the decay pattern on the Higgs mass range that is relevant for the current search at the Tevatron and in particular at the LHC, which will illustrate the comments that follow for each important decay mode. We already point out that the reader can find most of the information relative to the LHC case in Refs. [236–238] which summarize all the efforts made by the two major ATLAS and CMS collaborations.

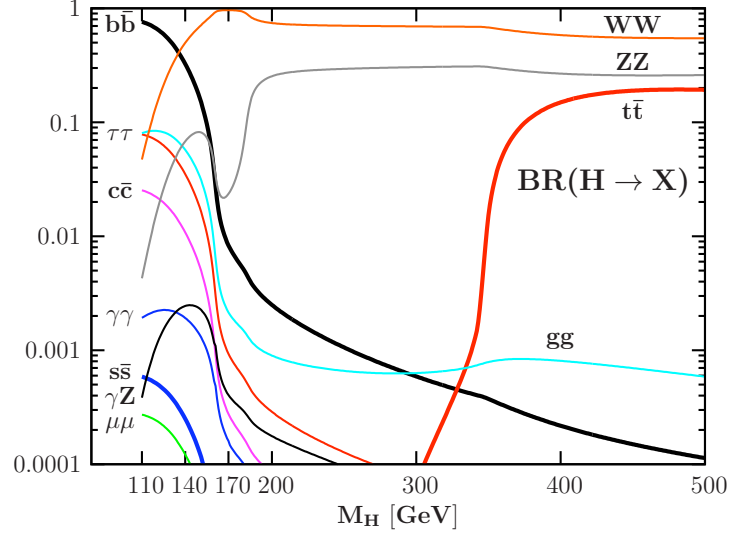


Figure 40: SM Higgs boson decay branching ratios on the Higgs mass range relevant at the Tevatron and the LHC, calculated with the programm HDECAY [97].

6.1.1 $H \rightarrow b\bar{b}$ channel

The partial width of the decay of the Higgs boson into quark pairs is given at LO in QCD by

$$\Gamma(H \rightarrow q\bar{q}) = \frac{3G_F}{4\pi\sqrt{2}} M_H m_q^2 \left(1 - 4\frac{m_q^2}{M_H^2}\right)^{3/2} \quad (6.1)$$

Eq. 6.1 then shows that the partial width is proportionnal to the square of the quark mass for not too light Higgs masses, which means that the dominant channel will be for the bottom quark. This partial width receives large NLO QCD corrections, and the quark mass has to be taken in the $\overline{\text{MS}}$ renormalization scheme in order to absorb large logarithms corrections. We refer the reader to Ref. [45], page 39. In Refs. [239, 240] the NNLO QCD corrections have been calculated as well as the three-loops $\mathcal{O}(\alpha_s^2 G_F m_t^2)$ in Refs. [241, 242].

The decay of the SM Higgs boson in quark pairs is one of the most important channels for experimental searches in particular for the bottom quark. This is the dominant mode for light Higgs masses $M_H \lesssim 135$ GeV at the Tevatron through the Higgs production in the Higgs-strahlung channel $p(p/\bar{p}) \rightarrow VH$ with V being either a W or a Z boson [243].

This mode is the golden mode at the Tevatron for the low Higgs mass searches, with $\ell\nu b\bar{b}$, $\ell\ell b\bar{b}$ and $\nu\bar{\nu} b\bar{b}$ final states where the requirements of isolated leptons and missing energy help to reduce the background. The use of b -tagging techniques crucially improves the signal-over-background ratio and is used along with neural network techniques for the signal reconstruction and the rejection of $p\bar{p} \rightarrow VV$, $p\bar{p} \rightarrow t\bar{t}$ and $p\bar{p} \rightarrow t + X$ backgrounds,

see Ref. [244] and Ref. [244] (page 69).

The situation at the LHC is not as good as the QCD background is far too large. Only with a luminosity of order 30 fb^{-1} at the full-fledged LHC we may obtain a 3σ evidence at $M_H = 120 \text{ GeV}$ [245, 246]. This decay mode also exists in association with a SM Higgs production through associated top quark production $pp \rightarrow t\bar{t}H$ and can improve the LHC search, but this requires a very challenging b -tagging with four bottom quarks in the final state. A clear evidence is beyond the reach of the LHC at 7 TeV and requires a luminosity greater than 100 fb^{-1} at the LHC to claim a discovery with only this channel [247–250].

6.1.2 $H \rightarrow V^*V^*$ channel

As displayed in Fig. 40 the Higgs decay channels involving a pair of weak bosons are the dominant channels for Higgs mass above $M_H = 135 \text{ GeV}$. These channels are thus of utmost importance both at the Tevatron and the LHC colliders.

We should distinguish between two regimes: either above the WW and ZZ thresholds where both weak bosons are real and then follow their own decay chains, or below the thresholds where we have off-shell weak bosons and thus three and four-body decays. The partial width for the $H \rightarrow VV$ with both V bosons being on-shell is given at LO by

$$\Gamma(H \rightarrow VV) = \frac{G_F M_H^3}{16\sqrt{2}\pi} A_V \sqrt{1-4z} (12z^2 - 4z + 1), \quad x = \frac{M_V^2}{M_H^2} \quad (6.2)$$

The symmetry factor A_V is either $A_W = 2$ or $A_Z = 1$. We see that for very heavy Higgs bosons we have $\Gamma(H \rightarrow VV) \propto M_H^3$ which means, this channel being largely dominant, that $\Gamma_H^{\text{tot}} \propto M_H^3$ for very heavy Higgs bosons. It implies that considering the Higgs boson still as a particle is far from obvious given that its width is comparable to its mass.

In order to obtain the decay width where the two weak bosons are off-shell we have to take into account the total decay width of the weak bosons through a Breit–Wigner modelisation and use Eq. 6.2 with general p_1^V and p_2^V momentum. It then has the expression given in Ref. [251]:

$$\Gamma(H \rightarrow V^*V^*) = \frac{1}{\pi^2} \int_0^{M_H^2} dp_1^2 \frac{M_V \Gamma_V}{(M_V - p_1^2)^2 + M_V^2 \Gamma_V^2} \int_0^{(M_H - p_1)^2} dp_2^2 \frac{M_V \Gamma_V}{(M_V - p_2^2)^2 + M_V^2 \Gamma_V^2} \Gamma(p_1^2, p_2^2, M_H^2) \quad (6.3)$$

with $\Gamma(p_1^2, p_2^2, M_H^2)$ being given by Eq. 6.2 but with $p_1^2 \neq M_V^2$ and $p_2^2 \neq M_V^2$. NLO

corrections have been calculated in Refs. [252–258] as well as higher order corrections up to NNLO [259] that are summarized in Ref. [45] page 58.

Higgs searches through these decay channels are very powerful, using either the gluon–gluon fusion production mode, the vector boson fusion mode or the Higgs–strahlung processes:

- $H \rightarrow W^{(*)}W^{(*)}$: the Higgs decaying into a pair of W bosons is very promising when the Higgs has been produced in the gluon–gluon fusion channel or the Higgs–strahlung process $p(p/\bar{p}) \rightarrow HW$. The channel $gg \rightarrow H \rightarrow WW \rightarrow \ell\nu\ell\nu$ is the most powerful channel at the Tevatron for high Higgs masses $M_H \gtrsim 135$ GeV searches and very promising at the LHC even at low Higgs masses around $M_H = 120$ GeV, see Refs. [238, 260]. We have to know very precisely the WW and ZZ backgrounds as well as top quark pair production in order to observe a clear excess of events in the distributions. Spin correlation and suitable cuts help to improve the significance. The process $p\bar{p} \rightarrow HW \rightarrow WWW, WWZ$ at the Tevatron is not very useful as the production cross section is too small. It is more promising at the LHC for Higgs masses between $M_H = 160$ GeV and $M_H = 180$ GeV, see Ref. [45] page 122. Finally the WW/ZZ fusion followed by the $H \rightarrow WW^{(*)}$ decay is very useful at the LHC with the jet veto techniques. A 3σ evidence in this channel can be obtained with a luminosity of order 30 fb^{-1} , see Ref. [261].
- $H \rightarrow Z^{(*)}Z^{(*)}$: in association with the Higgs boson production through gluon–gluon fusion, this is the golden channel for high Higgs mass searches $M_H \gtrsim 2M_Z$ both at the Tevatron and the LHC [262–264], where in the latter case a discovery can already be claimed for a Higgs mass $M_H \simeq 150$ GeV with a 5 fb^{-1} luminosity [238], and with a 8 fb^{-1} luminosity in the CMS detector on the entire high mass range (except for $M_H \simeq 170$ GeV where 100 fb^{-1} in this channel is needed), see Ref. [236]. The main background is the ZZ production which can be removed with a side–bands study and the interpolated in the signal region. This channel is not useful with other production channels because of the smallness of the production cross section and the very high backgrounds.

6.1.3 $H \rightarrow \gamma\gamma$ channel

The $H \rightarrow \gamma\gamma$ channel as well as the $H \rightarrow gg$ decay process that will be discussed below are loop–induced processes. These processes are known up to NNLO in EW corrections and NNLO in QCD corrections in the infinite quark mass limit in the loops, see page 58 of Ref. [45]. The expression for the LO partial decay widths are similar to what has been obtained for the $gg \rightarrow H$ production channel with the same functions A and f involved,

see Eq. 4.8:

$$\Gamma(H \rightarrow \gamma\gamma) = \frac{G_F \alpha_{\text{EM}}^2 M_H^3}{128 \pi^3 \sqrt{2}} \left| \sum_{\text{fermions}} N_c Q_f^2 A \left(\frac{M_H^2}{m_f^2} \right) + B \left(\frac{M_H^2}{M_W^2} \right) \right|^2 \quad (6.4)$$

with $N_c = 3$ for the quarks, $N_c = 1$ for the leptons, Q_f being the electric charge of the fermion f and B as the form factor

$$B(\tau) = - \left(2 + \frac{3}{\tau} + 3 \frac{(2\tau - 1)}{\tau^2} f(\tau) \right) .$$

This decay channel is the best mode for light Higgs mass searches $M_H \lesssim 150$ GeV at the LHC [265–269], and has been used in Tevatron experimental analyses for $M_H \leq 130$ GeV but as a sub-dominant channel and only to improve the efficiency of the experimental programm with multivariate techniques. Even if the branching fraction is small as can be seen in Fig. 40, its very clean final state compensate the trickiness of the analyses. Both $pp \rightarrow VH$ and $gg \rightarrow H$ production channels are used even if the former is not as useful as the latter. The backgrounds are similar in both cases. The QCD background from jets that fake photons is huge and require a very efficient triggering of the electromagnetic calorimeters of ATLAS and CMS detectors. These backgrounds can be determined by the measurements of the side-bands in the invariant di-photon mass distribution. Nevertheless this channel require a large amount of data as a small bump in the di-photon mass distribution is searched.

At low luminosities the combination of all production channels is required: $gg \rightarrow H \rightarrow \gamma\gamma$, $gg \rightarrow H \rightarrow \gamma\gamma + \text{jets}$, $pp \rightarrow HW \rightarrow \gamma\gamma\ell\nu$ and $pp \rightarrow t\bar{t}H \rightarrow b\ell\nu\bar{b}\bar{\ell}\bar{\nu}\gamma\gamma$ will enhance the statistics and we may then have a 5σ discovery though this decay mode with a luminosity of order 30 fb^{-1} and already a 3σ evidence for $\mathcal{L} = 10 \text{ fb}^{-1}$ [238].

6.1.4 A comment on the $H \rightarrow gg$ channel

The $H \rightarrow gg$ channel will be discussed in the following subsection, even if it adds little to the experimental searches. We just mention that the theoretical predictions follow a very similar recipe compared to that of the di-photon decay channel presented above. We have at LO:

$$\Gamma(H \rightarrow gg) = \frac{G_F \alpha_s^2 M_H^3}{36 \pi^3 \sqrt{2}} \left| \frac{3}{4} \sum_{b,t} A \left(\frac{M_H^2}{m_q^2} \right) \right|^2 \quad (6.5)$$

We will discuss in brief this channel when dealing with the uncertainties that affect its

branching fraction. The QCD corrections are known up to $\mathcal{O}(\alpha_s^2)$ order in the infinite top mass approximation, see Ref. [270].

6.1.5 $H \rightarrow \tau^+ \tau^-$ channel

The last important decay channel for experimental searches is the only leptonic channel that is not swamped by the other decay channels. The partial width at LO is given in Eq. 6.1 where we replace m_q by m_τ and divide the result by the factor of 3, as the tau lepton has no color factor. The NLO and NNLO corrections follow what has been presented in the $H \rightarrow b\bar{b}$ subsection above.

The production channel which allows for a search in this decay mode is at first look only the vector boson fusion $pp \rightarrow qqH$ process. It has been considered in particular in LHC analyses for the intermediate Higgs mass $M_H \in [120 \text{ GeV} ; 140 \text{ GeV}]$ range [271] (page 56), where for a luminosity of order 30 fb^{-1} a 6σ combined statistical significance can be obtained when considering all possible decay products of the τ 's. The major backgrounds are found to be QCD production $pp \rightarrow Zjj$ with the Z boson decaying into a di- τ pair. This can be measured in the side-bands of the invariant mass distribution of the lepton pair and then extrapolated in the signal region.

In the section 13.4 of this thesis we will present a possible new way for the use of this decay channel in association with gluon-gluon fusion Higgs production.

6.2 Uncertainties on the branching ratios

The sections 4 and 5 have introduced the detailed analysis of the theoretical uncertainties affecting the production channels for the SM Higgs boson. We need to perform the same investigation when dealing with the Higgs decay branching ratios in order to obtain in the end a combined cross section times branching ratios analysis with all sources of theoretical uncertainties taken into account.

6.2.1 The parametric uncertainties

An analysis of the uncertainties affecting the Higgs branching ratios has been performed long ago in Ref. [235]. This section, based on the results published in Ref. [232], update the earlier results by taking into account the parametric uncertainties on the value of the strong coupling constant $\alpha_s(M_Z)^2$ as well as the value of the bottom quark and charm quark masses. These uncertainties are taken as being experimental which means that we

will not take into account the theoretical uncertainty on the value of α_s in this analysis, mainly because the impact would be negligible in the view of the final combination of the uncertainties on the branching fractions. As we consider these uncertainties as experimental they have a statistical ground, and we will choose to stick at the 68%CL (i.e. 1σ level) for the choice of the error interval.

We will then use this following recipe:

- a) The strong coupling constant α_s plays a very important role either at LO for the $H \rightarrow gg$ channel or beyond LO when dealing with the QCD corrections; the uncertainty will be thus significant on the branching ratios. We adopt for consistency reasons the same value that we have used for the determination of the central predictions for the production cross section in the former sections: $\alpha_s(M_Z^2) = 0.1171 \pm 0.0014$ at NNLO at the 68%CL.
- b) In Ref. [232] we used $\overline{\text{MS}}$ masses evaluated at the mass itself as starting points for the b and c quarks, with the central values and the uncertainties taken directly from Ref. [205]⁵¹. Their uncertainties were larger than those considered in Ref. [272] with quite the same central values. In a recent discussion within the LHC Higgs Cross Section Working Group a new agreement has been reached and the results presented in the following will use $\overline{m}_b(\overline{m}_b) = 4.16 \pm 0.06$ GeV and $\overline{m}_c(\overline{m}_c) = 1.28 \pm 0.03$ GeV, which then transform into pole masses $M_b = 4.49 \pm 0.06$ GeV and $M_c = 1.41 \pm 0.03$ GeV with a 1-loop calculation⁵², as the parameters in Ref. [205] were seen to be too conservative on the one side, the parameters in Ref. [272] being seen a little too optimistic on the other side. When we will quote separately the impact of these uncertainties on the Higgs branching ratio, we will assume the central value $\alpha_s(M_Z^2) = 0.1171$ at NNLO for the strong coupling constant⁵³.
- c) For the $H \rightarrow gg$ channel we will consider only the parametric uncertainties quoted above. At NNLO, the pure theoretical scale uncertainty is of the order 10% but since the branching ratio is small it migrates into an error of less than 1%. In addition, the N³LO contribution would reduce this scale variation to the level of a few percent at most and this uncertainty can be safely neglected. The same analysis can be done for the

⁵¹with these starting inputs and the value of $\alpha_s(M_Z^2)$ given in point a), the central values of the b, c pole masses are $M_b = 4.71$ GeV and $M_c = 1.54$ GeV using a 2-loops calculation with variation ranges of, respectively, 4.64–4.90 GeV and 1.42–1.63 GeV. For the pole bottom-quark mass, the central value is rather close to the one adopted in the MSTW scheme for parameterizing the parton densities [128], $M_b = 4.75$ GeV, and it was expected that the difference would have no practical impact

⁵²We greatly thank A. Singer for having clarified the discussion about the final values to be taken.

⁵³We thank M. Spira for having clarified the link between the order at which the transformation from $\overline{\text{MS}}$ masses to pole masses is done and the correlation between α_s and the uncertainties on the quark masses.

other channel that we will consider in the following, meaning that the scale variation uncertainties will be neglected in the rest of the section.

All these three points mentioned above and in particular the last point c) are dependant on the interval of variation for the Higgs mass. Indeed for $M_H \gtrsim 350$ GeV the $H \rightarrow t\bar{t}$ opens up, as displayed in Fig. 40. We should then perform a detailed analysis of this channel for these high mass regime and in particular take into account the scale variation. Nevertheless this channel might play a role only for Higgs masses greater than $M_H \simeq 400 - 450$ GeV, where we reach the possibility of the LHC at 7 TeV, not to mention the Tevatron experiments. This is why its analysis has been totally discarded in this thesis.

6.2.2 The final uncertainties on the branching ratios

In order to calculate the central values for the branching ratios together with the associated uncertainties we use the latest version 3.80 of the program HDECAY [97] available, which calculates the partial and total Higgs decay widths including the relevant QCD and electroweak higher order corrections. It is worth mentioning that the version used in Ref. [232] was older: the results presented in this section are then an update of the previous results published in this latter reference. We will use the parameters discussed above and add in quadrature the final errors that we obtain in order to present the total uncertainties on the different branching ratios considered. We stress that the result we obtain are very similar to those presented in Ref. [232] in the crucial decay channels that are the $H \rightarrow b\bar{b}$ and $H \rightarrow W^{(*)}W^{(*)}$ modes. Thus the conclusion of Ref. [232] remains globally unchanged.

We obtain the branching ratios (BR) shown in Fig. 41 as a function of the Higgs mass, including the total uncertainty bands. We present in Table 8 the branching ratios for the main decay modes $H \rightarrow b\bar{b}$ and $H \rightarrow W^{(*)}W^{(*)}$, for selected values of the Higgs mass, $M_H = 120, 135$ and 150 GeV, together with the individual and total uncertainties. The uncertainties (in percentage) on the branching ratios for the $H \rightarrow \tau^+\tau^-$ and $H \rightarrow ZZ, \gamma\gamma$ channels are the same as those affecting the $H \rightarrow WW$ mode. In Table 9, we display the branching ratios for the various decays as well as their corresponding total uncertainties for a selection of Higgs masses that are relevant for the LHC and the Tevatron colliders. Fig. 41 displays the branching ratios for Higgs mass up to $M_H = 200$ GeV. The numbers above this mass are not useful as the uncertainties for the only relevant channels, that are the ZZ and WW modes, drop to the level of 0%. We will thus not include the values for Higgs mass above 200 GeV and up to $M_H = 500$ GeV in Table 9 but they are of course available on demand.

The largest total errors are by far the ones that affect $\text{BR}(H \rightarrow c\bar{c})$ which are of the

order of 8%. In contrast the errors on $\text{BR}(H \rightarrow gg)$ are at the level of a few to 5% at most and the errors in the WW channel do not exceed 3%. In the case of the $H \rightarrow c\bar{c}$ channel, it is mainly due to the uncertainty on the input charm-quark mass \bar{m}_c and, to a lesser extent, to the uncertainty on α_s ; their combination leads to a very strong variation of the charm-quark mass at the high scale μ , $\bar{m}_c(\mu) \propto [\alpha_s(\mu)]^{12/13}$. For the $H \rightarrow gg$ channel the uncertainty is mainly due to the uncertainty on α_s , and in both cases, the error on the input b -quark mass leads to a 3% uncertainty at most. Nevertheless, since the branching ratios for these two decays are small, at most a few percent in the Higgs mass range of interest, the associated uncertainties will affect the Higgs total width, and hence the branching ratios for the other decay channels, in a less significant way.

channel	M_H	BR(%)	Δm_c	Δm_b	$\Delta \alpha_s$	ΔBR
$H \rightarrow b\bar{b}$	120	65.40	+0.2% -0.2%	+1.1% -1.1%	+0.6% -0.6%	+1.3% -1.3%
	135	41.01	+0.1% -0.1%	+1.9% -1.9%	+1.1% -1.1%	+2.2% -2.2%
	150	16.07	+0.1% -0.1%	+2.7% -2.7%	+1.5% -1.5%	+3.1% -3.1%
$H \rightarrow WW$	120	14.06	+0.2% -0.1%	+2.1% -2.0%	+1.1% -1.0%	+2.4% -2.2%
	135	39.86	+0.1% -0.1%	+1.3% -1.3%	+0.6% -0.6%	+1.5% -1.4%
	150	69.45	+0.0% -0.1%	+0.5% -0.5%	+0.2% -0.2%	+0.6% -0.5%

Table 8: The Higgs decay branching ratio $\text{BR}(H \rightarrow b\bar{b})$ and $\text{BR}(H \rightarrow WW)$ (in %) for given Higgs mass values (in GeV) with the corresponding uncertainties from the various sources discussed in the text; the total uncertainties (adding the individual ones in quadrature) are also shown.

The uncertainty on the $H \rightarrow b\bar{b}$ decay channel that is the most important channel at the Tevatron for low Higgs mass searches, depends strongly on the considered Higgs mass range. For $M_H \lesssim 120$ GeV where the branching ratio is $\text{BR}(H \rightarrow b\bar{b}) \gtrsim 65\%$ and thus largely the dominant channel, the uncertainty is less than a percent, reaching the percent level at $M_H = 110$ GeV. This is mainly due to the fact that as the channel is dominant, the $b\bar{b}$ partial width is the major component of the total width and the errors partly cancel in the branching ratio. There is, however, a residual error coming from the input bottom mass and to a lesser extent α_s and the charm mass errors. This is also exemplified by the comparison between the results presented in this section and the former results of Ref. [232] where the errors on the input bottom mass were larger: we see that the errors on the branching fractions were also correspondingly larger.

In the mass range $M_H \approx 120$ –150 GeV, the partial widths for $H \rightarrow b\bar{b}$ and WW decays have the same magnitude (we reach the crossing region of the two decay modes) and the two branching ratios have larger uncertainties. The uncertainty on $\text{BR}(H \rightarrow b\bar{b})$ increases

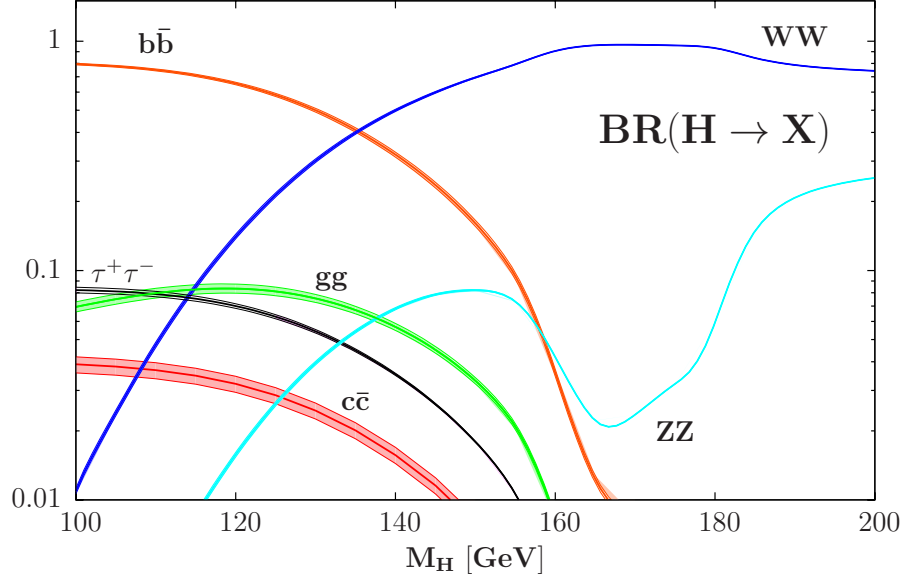


Figure 41: The Higgs decay branching ratios as a function of M_H including the total uncertainty bands from the 1σ errors on the input quark masses and the coupling α_s (the individual errors have been added in quadrature).

from 1% at $M_H \approx 120$ GeV to approximately 3%, that is the triple, at $M_H \approx 150$ GeV. At the same time, the uncertainty on $\text{BR}(H \rightarrow WW)$, which is the same as the one on $\text{BR}(H \rightarrow ZZ^*)$ and $\text{BR}(H \rightarrow \gamma\gamma)$, drops from $\pm 2.5\%$ at $M_H \approx 120$ GeV to $\pm 0.5\%$ at $M_H \approx 150$ GeV. In this case \bar{m}_c has nearly no impact as $\text{BR}(H \rightarrow c\bar{c})$ is small. For higher Higgs masses, $M_H \gtrsim 160$ GeV, the Higgs width is mainly controlled by the $H \rightarrow WW$ decay and then jointly with $H \rightarrow ZZ$ for $M_H \gtrsim 2M_Z$. The uncertainty on the branching ratio $\text{BR}(H \rightarrow WW)$ drops to nearly 0%. The uncertainty on $\text{BR}(H \rightarrow b\bar{b})$ remains at the 8% level but this has no impact as the branching ratio is far too small to be relevant.

For Higgs masses beyond $M_H \gtrsim 350$ GeV, the decay channel $H \rightarrow t\bar{t}$ opens up and has a branching ratio of $\approx 20\%$ at $M_H \approx 500$ GeV dropping to less than 10% for $M_H \lesssim 400$ GeV or $M_H \gtrsim 700$ GeV. It will be affected by the uncertainties on m_t, α_s as well as by some electroweak contributions from the Higgs self-couplings. This leads to a total uncertainty that is estimated to be below the 5% level [210], which translates to an uncertainty of less than 1% in the branching ratios for the important decays $H \rightarrow WW, ZZ$.

Thus, the uncertainties on the important Higgs branching ratios $\text{BR}(H \rightarrow WW, ZZ, \gamma\gamma)$ as well as $\text{BR}(H \rightarrow b\bar{b})$ can be significant in the intermediate mass range $M_H \approx 120\text{--}150$ GeV where the $b\bar{b}$ and WW decays are competing with each other. Even if the uncertainty remains reasonable in this new analysis, at most 8%, this should be taken into account in experimental analyses. We also see that the conclusions remain the same as in Ref. [232] even if the uncertainties have been reduced by a factor of 2.

M_H	$b\bar{b}$	Δ^{tot}	$c\bar{c}$	Δ^{tot}	gg	Δ^{tot}	WW	ZZ	$\tau\tau$	$\gamma\gamma$	Δ^{tot}
100	79.48	+0.8% -0.8%	3.90	+7.8% -8.3%	6.94	+5.2% -5.0%	1.09	0.11	8.22	0.16	+2.9% -2.8%
105	77.69	+0.8% -0.9%	3.81	+7.8% -8.3%	7.50	+5.1% -4.9%	2.39	0.21	8.11	0.18	+2.8% -2.7%
110	74.96	+1.0% -1.0%	3.68	+7.8% -8.3%	7.97	+5.0% -4.8%	4.75	0.43	7.89	0.19	+2.7% -2.6%
115	70.95	+1.1% -1.1%	3.48	+7.8% -8.2%	8.27	+4.8% -4.7%	8.54	0.86	7.53	0.21	+2.6% -2.5%
120	65.40	+1.3% -1.3%	3.21	+7.9% -8.2%	8.34	+4.6% -4.5%	14.06	1.57	7.00	0.22	+2.4% -2.2%
125	58.32	+1.6% -1.6%	2.86	+7.9% -8.1%	8.11	+4.4% -4.2%	21.35	2.62	6.29	0.23	+2.1% -2.0%
130	50.00	+1.9% -1.9%	2.45	+7.9% -8.1%	7.56	+4.1% -4.0%	30.13	3.95	5.43	0.22	+1.8% -1.8%
135	41.01	+2.2% -2.2%	2.01	+8.0% -8.1%	6.72	+3.8% -3.7%	39.86	5.42	4.49	0.21	+1.5% -1.4%
140	32.02	+2.5% -2.5%	1.57	+8.1% -8.1%	5.68	+3.6% -3.5%	49.92	6.82	3.53	0.19	+1.1% -1.1%
145	23.60	+2.8% -2.8%	1.16	+8.2% -8.1%	4.51	+3.4% -3.3%	59.82	7.86	2.62	0.17	+0.8% -0.8%
150	16.07	+3.1% -3.1%	0.79	+8.3% -8.2%	3.31	+3.2% -3.1%	69.45	8.21	1.79	0.14	+0.5% -0.6%
155	9.47	+3.3% -3.3%	0.46	+8.3% -8.2%	2.09	+3.0% -3.0%	79.28	7.33	1.06	0.10	+0.3% -0.3%
160	3.58	+3.6% -3.5%	0.18	+8.3% -8.3%	0.84	+2.9% -2.8%	90.63	4.19	0.40	0.05	+0.1% -0.1%
165	1.23	+3.6% -3.6%	0.06	+8.4% -8.3%	0.30	+2.8% -2.8%	95.97	2.22	0.14	0.02	+0.0% -0.0%
170	0.82	+3.7% -3.6%	0.04	+8.5% -8.3%	0.21	+2.8% -2.7%	96.43	2.35	0.09	0.02	+0.0% -0.0%
175	0.63	+3.7% -3.6%	0.03	+8.5% -8.3%	0.17	+2.8% -2.8%	95.84	3.21	0.07	0.01	+0.0% -0.0%
180	0.51	+3.7% -3.6%	0.02	+8.4% -8.4%	0.15	+2.8% -2.7%	93.28	5.94	0.06	0.01	+0.0% -0.0%
185	0.40	+3.7% -3.6%	0.02	+8.5% -8.4%	0.12	+2.8% -2.7%	84.52	14.86	0.05	0.01	+0.0% -0.0%
190	0.32	+3.7% -3.6%	0.02	+8.5% -8.4%	0.10	+2.8% -2.7%	78.72	20.77	0.04	0.01	+0.0% -0.0%
195	0.28	+3.7% -3.7%	0.01	+8.4% -8.4%	0.10	+2.7% -2.7%	75.89	23.66	0.03	0.01	+0.0% -0.0%
200	0.25	+3.7% -3.6%	0.01	+8.4% -8.4%	0.09	+2.7% -2.7%	74.26	25.34	0.03	0.01	+0.0% -0.0%

Table 9: The Higgs decay branching ratios (in %) for given Higgs mass values (in GeV) with the corresponding total uncertainties from the various sources discussed in the text.

6.3 Combination at the Tevatron

The section 6.2 above has introduced the branching ratios together with their uncertainties that are of parametric nature and have thus be combined with a quadratic addition. We need in the end to combine both the production cross section and the branching fractions in order to obtain a complete prediction for each specific search channel.

This combination is in general complicated to perform when several production and decay channels are involved. Unfortunately that is the case at the Tevatron where both $p\bar{p} \rightarrow HV$ and $gg \rightarrow H$ production channels on the one hand, both $H \rightarrow b\bar{b}$ and $H \rightarrow W^{(*)}W^{(*)}$ on the other hand have to be considered especially in the intermediate mass range $M_H \simeq 135$ GeV. In addition to this difficulty we should also take into account two important issues:

- i)* The total Higgs decay width becomes large at high Higgs masses and thus should be taken into account in the processes $p(p/\bar{p}) \rightarrow H + X \rightarrow X' + X$ where the narrow width approximation for the Higgs boson propagator fails.
- ii)* We should take into account interferences between the signal and background, as for example in $gg \rightarrow H \rightarrow VV$ and $gg \rightarrow VV$.

These two issues will not be addressed in this thesis, and we refer the reader to a work in progress [273]. We also note that there are anti-correlations between the different decay rates as the sum of all branching ratios is equal to unity.

Combining the uncertainty in the production rate and the uncertainty in the Higgs decay branching ratios is then not obvious at all. We should also think about the difference between the pure theoretical uncertainties considered in the case of the production cross sections and the uncertainties on the branching ratios which (mainly) come from experimental errors on the input parameters α_s and the quark masses. In statistical language this means that we should make a combination of a flat prior uncertainty and a gaussian prior uncertainty. In addition, there is one parameter which is common in the calculation of the branching ratios and the production cross sections: the coupling α_s . The uncertainty on α_s will affect at the same time $\sigma(gg \rightarrow H)$ and $\text{BR}(H \rightarrow X)$; it occurs that in both the Higgs production and in Higgs decays the minimal (maximal) values are obtained with the minimal (maximal) value of α_s when the error $\Delta^{\text{exp}}\alpha_s$ is included.

We will then adopt a simple method that is a linear addition of the errors on the Higgs branching ratios to the theoretical uncertainties on the production cross section, keeping in mind that if there are anti-correlations between the production and the decay chain

the related uncertainty should nearly vanish. For consistency reason we should increase the uncertainty due to the experimental errors on the strong coupling constant α_s in the branching ratios as in the production cross sections we have taken the 90%CL PDF + $\Delta^{\text{exp}}\alpha_s$ uncertainty. We will present results for the two main search channels $p\bar{p} \rightarrow HV$ followed by $H \rightarrow b\bar{b}$ decay and $p\bar{p} \rightarrow H$ through gluon–gluon fusion followed by $H \rightarrow W^+W^-$ decay. In the intermediate Higgs mass range the two decay compete each other. The combination of the two channels should then take into account the correlations between the two decay channels on the one hand, and should also take into account the relative importance of the two production channels on the other hand. We thus have a mean with anti-correlated uncertainties on the b -quark mass between the two decay chains. The final result will be used in section 6.5 in order to compare with the experimental results [91–93].

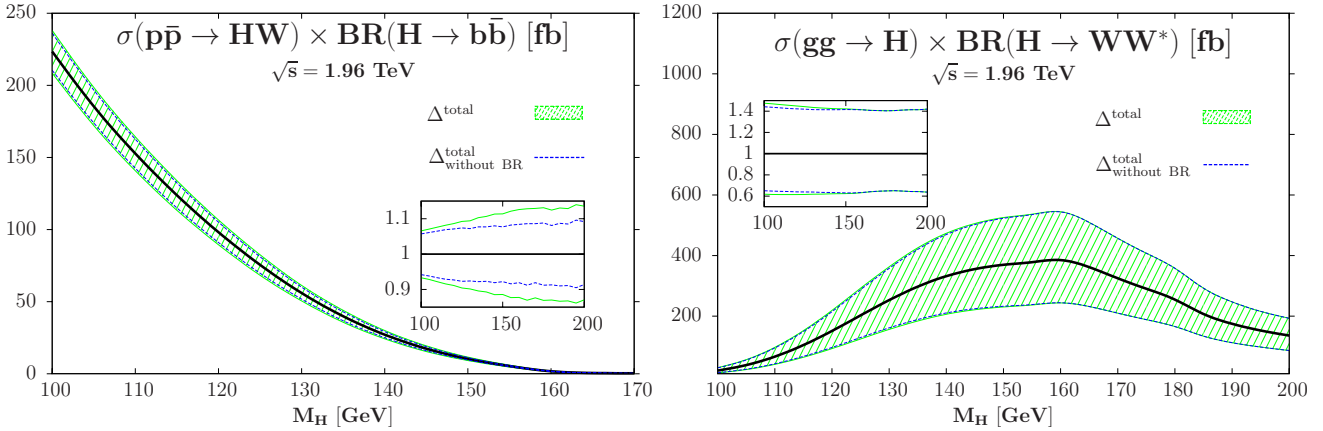


Figure 42: The production cross section times branching ratio for the process $p\bar{p} \rightarrow H \rightarrow b\bar{b}$ (left) and $gg \rightarrow H \rightarrow WW$ (right) at the Tevatron with $\sqrt{s} = 1.96$ TeV, including the total theoretical uncertainty band when the errors in the decay branching ratios are taken into account. In the inserts the relative deviations are shown.

The results for $\sigma(p\bar{p} \rightarrow HW) \times \text{BR}(H \rightarrow b\bar{b})$ and $\sigma(gg \rightarrow H) \times \text{BR}(H \rightarrow W^{(*)}W^{(*)})$ are displayed in Fig. 42 as a function of the relevant Higgs masses at the Tevatron, together with the total uncertainty when taking into account that on the branching ratio. The left of Fig. 42 shows the result for the dominant search channel for low Higgs masses in the $H \rightarrow b\bar{b}$ decay channel. It is then demonstrated that the uncertainties on the branching ratio are really sizeable and have to be taken into account. They add $\sim 5\%$ total uncertainty to be compared to the $\pm 7\%$ uncertainty on the production cross section alone. We note that the total $\sigma(p\bar{p} \rightarrow HW \rightarrow b\bar{b})$ plays no role at all above $M_H \gtrsim 160$ GeV as the total cross section times branching ratio tends to the null value.

The right of Fig. 42 shows the main channel for high Higgs masses searches in the $H \rightarrow W^{(*)}W^{(*)}$ channel, including the total uncertainty with or without those of the branching ratio included. The effect of the total uncertainty on the branching ratio is only visible in

the region $M_H \approx 100\text{--}150$ GeV where the errors on $\text{BR}(H \rightarrow WW)$, dominated in practice by the errors in the decay channel $H \rightarrow b\bar{b}$, is significant. Above the $M_H \gtrsim 2M_W$ threshold, the branching ratio uncertainty is nearly null which means that it has no effect in the Higgs mass range $M_H \approx 150\text{--}180$ GeV to which both the Tevatron and the LHC are most sensitive.

The net result is that even if the uncertainties on the branching ratios play no role in the range where the Tevatron experiment is the most sensitive, that is the range $M_H \in [150 ; 180]$ GeV, they have to be taken into account for $M_H \lesssim 150$ GeV in both the $H \rightarrow b\bar{b}$ and WW channels.

6.4 Combination at the LHC

The situation at the LHC and even at the LHC with $\sqrt{s} = 14$ TeV the situation is much simpler compared to that of the Tevatron. Indeed only the $gg \rightarrow H$ production channel is to be considered in practice, only the decays $H \rightarrow WW, ZZ$ and to a lesser extent $H \rightarrow \gamma\gamma$ are relevant. Since we have considered only the dominant QCD uncertainties, these decays are affected by the same uncertainties as discussed in previous section 6.2 and displayed in the last column of Table 9.

In this case, we obtain the combined uncertainty of $\sigma^{\text{NNLO}}(gg \rightarrow H) \times \text{BR}(H \rightarrow VV^*)$ at the LHC that is displayed in Fig. 43 in the case of the $H \rightarrow WW$ decay as a function of M_H . Besides the uncertainty on the cross section which is shown by the dashed lines, we display the effect of adding the error on the $H \rightarrow WW$ branching ratio as shown by the full lines which slightly increase the overall uncertainty. As expected this is only visible in the region where the uncertainties are sizeable for $M_H \leq 150$ GeV where the uncertainty on the branching fraction is in practice dominated by the uncertainty on the partial decay width $H \rightarrow b\bar{b}$. Above the WW thresold the uncertainty drops to the null value, meaning that in particular there is no need to consider this uncertainty in the high Higgs mass regime, as seen above in the case of the Tevatron colliders. However as already stated the total Higgs width as well as the interference between the signal and the background become significant at high masses and should be taken into account in both the production cross section and the decay widths [210].

In the case of the $H \rightarrow ZZ, \gamma\gamma$ (and $\tau\tau$) decays, since the errors on the branching ratios are the same as those affecting $\text{BR}(H \rightarrow WW)$, the overall uncertainties in $\sigma \times \text{BR}$ can also be seen from Fig. 43: only the normalization of the branching ratio is different and can be obtained for a specific decay mode from Table 9.

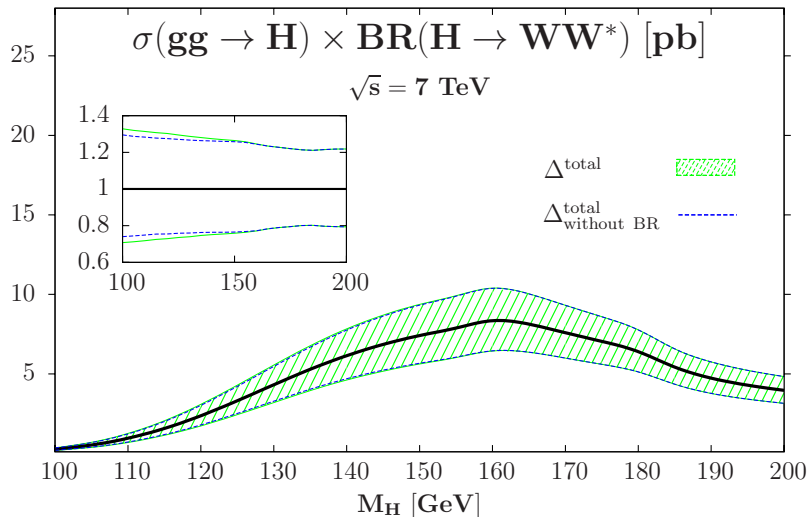


Figure 43: The production cross section times branching ratio for the process $gg \rightarrow H \rightarrow WW$ at the LHC with $\sqrt{s} = 7$ TeV, including the total theoretical uncertainty band when the errors in the decay branching ratios are taken into account. In the inserts the relative deviations are shown.

6.5 The Tevatron exclusion limit

After having calculated the production cross sections together with their theoretical uncertainties in section 4 at the Tevatron, the branching ratios that are relevant in section 6.2 and made the combination in section 6.3, we are now ready to compare with the experimental results given by the CDF and D0 collaborations [90–93].

The comparison with low mass Higgs searches results shows that while the Tevatron collaborations use an approximate 5% uncertainty on the main search channel $p\bar{p} \rightarrow WH \rightarrow Wb\bar{b}$, we have found a total uncertainty of nearly 15% taking into account all possible sources of uncertainties. In particular the uncertainties on the branching fractions are sizeable and add up to nearly 5%, when this has been overlooked by experimental collaborations. Nevertheless, it does not change significantly the main result on the 95%CL exclusion for the SM Higgs boson mass in the [115 : 150] GeV mass range.

The situation in the high Higgs mass range is completely different. This is the key range at the Tevatron as the experiments are the most sensitive for Higgs mass $M_H \sim 165$ GeV: indeed, the CDF and D0 experiments claim that they exclude a SM Higgs boson at 95%CL for $158 \leq M_H \leq 173$ GeV. In section 4.5 we have found a total uncertainty of order $\pm 40\%$, to be compared with the nearly $\pm 20\%$ used by the experimental collaborations. This has to be analyzed in detail to see whether it has an impact on the exclusions bounds [91–93]. In addition we should add the uncertainties on the branching ratios, but as can be seen on Fig. 42 they have no impact for $M_H \gtrsim 150$ GeV. In the intermediate Higgs mass range

$130 \lesssim M_H \lesssim 150$ GeV where both search channels $p\bar{p} \rightarrow WH \rightarrow Wb\bar{b}$ and $gg \rightarrow H \rightarrow W^{(*)}W^{(*)}$ compete each other, the uncertainties on the two branching ratios have to be taken into account.

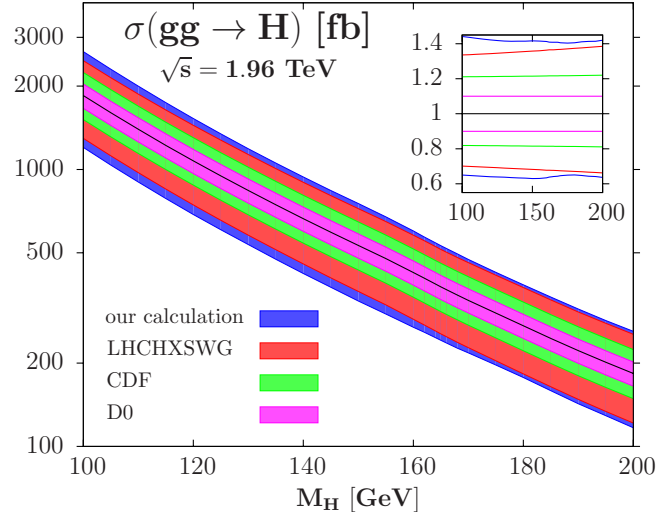


Figure 44: The SM Higgs boson production cross section $gg \rightarrow H$ at the Tevatron including the total theoretical uncertainty band when the uncertainties are combined using our procedure, those of CDF/D0 experiment or the recommendation of the LHC Higgs Cross Section Working Group [210].

We display in Fig. 44 the comparison between our calculation on the production cross section and the CDF/D0 expectations on the one hand, the prediction using the way of handling the theoretical uncertainties described in Ref. [210] on the other hand. The CDF and D0 experiments simply add in quadrature the uncertainties from the scale variation and the PDF+ α_s uncertainties obtained through the Hessian method and ignore the smaller EFT uncertainty. They obtain an overall uncertainty of order 20% on the inclusive cross section. As stated in the former section, see section 4.5, we believe that this is not reasonable and has little justification. Indeed, the uncertainties associated to the PDFs in a given scheme should be viewed as purely theoretical uncertainties (due to the theoretical assumptions in the parameterization) despite of the fact that they are presented as the 1σ or more departure from the central values of the data included in the PDF fits. They should be equivalent to the spread of the different predictions when use the four NNLO PDFs sets available on the market and thus having no statistical interpretation⁵⁴ and thus combined linearly with the uncertainties from the scale variation and the EFT approach which are pure theoretical uncertainties. This is the procedure recommended, for instance, by the LHC Higgs Cross Section Working Group [210] that is also displayed in Fig. 44. Our

⁵⁴If we want to use a stastical analysis we then should use a flat prior and not a gaussian prior to handle the PDF puzzle.

procedure has been proposed first in Ref. [94] where we apply the combined PDF- α_s uncertainties directly on the maximal/minimal cross sections with respect to scale variation⁵⁵, and then adds linearly the small uncertainty from the EFT approach. This last procedure, that we have used here, provides an overall uncertainty that is similar (but slightly smaller) to that obtained with the linear sum of all uncertainties.

In the mass range $M_H \approx 160$ GeV with almost the best sensitivity, our procedure gives an approximate +41%, -37% total uncertainty, to be compared to the $\approx 10\%$ and $\approx 20\%$ uncertainties assumed, respectively, by the CDF and D0 collaborations. The comparison with the LHC Higgs cross section working group recommendation use the uncertainties from scale (+20%, -17% on the sum of the jet cross sections⁵⁶ and PDFs (+16%, -15% when the MSTW 68% CL PDF + $\Delta^{\text{exp}}\alpha_s$ error is multiplied by a factor of two following the PDF4LHC recommendation) [151], leading to a total of $\approx +36\%$, -32% for $M_H \approx 160$ GeV. Thus, the uncertainty that we assume is comparable to the one obtained using the LHC procedure [210], the difference being simply due to the additional $\mathcal{O}(5\%)$ uncertainty from the use of the EFT approach that we also include. In the end this demonstrates that our total uncertainty is certainly not too conservative and then has to be taken seriously.

We display in Fig. 45 the comparison between the experimental results presented in Refs. [91–93] and our theoretical expectations. This presentation is of course naive, as the true combination of the different channel is very difficult, given the fact that many channels are involved. Nevertheless we know in practice that two channels only matter at the Tevatron, that are the $H \rightarrow b\bar{b}$ after Higgs-strahlung production for low Higgs mass searches and the $H \rightarrow W^{(*)}W^{(*)}$ channel after gluon-gluon fusion Higgs production for high Higgs mass searches. We pay a particular attention in the intermediate Higgs mass range where both channel are to be considered, and we take into account the correlation between the two decay channel.

If we want to claim a 95%CL exclusion we should require that the observed line be below the lower band of the SM prediction. That is not the case when we compare with our prediction, thus we believe that the Tevatron experiment have not excluded the SM Higgs boson in the Higgs mass range $158 \leq M_H \leq 175$ GeV.

The comparison displayed above is indeed not precise. We should plug directly our prediction in the experimental analysis as some uncertainties have been already taken into

⁵⁵We remind the reader that a similar procedure has also been advocated in Ref. [189] for top quark pair production.

⁵⁶An additional uncertainty of $\approx 7.5\%$ from jet acceptance is introduced when considering the Higgs+jet cross sections. We will consider it to be experimental and, when added in quadrature to others, it will have little impact.

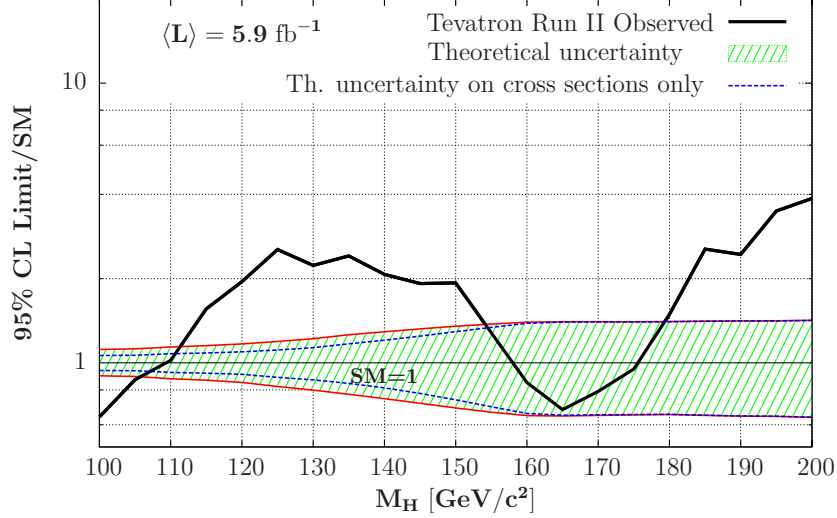


Figure 45: The SM Higgs boson production cross section $gg \rightarrow H$ at the Tevatron including the total theoretical uncertainty band when the uncertainties are combined using our procedure, those of CDF/D0 experiment or the recommendation of the LHC Higgs Cross Section Working Group [210].

account by the experiments in the calculation of the SM line of Fig. 45. Nevertheless we advocate to separate experimental and theoretical results on such a graph in order to make the comparison more relevant. We will in the next consider different scenarios and give the results published in Ref. [95] where the procedure described below has been used. The reader should note that this work is based on the former results of the Tevatron experiments when the luminosity was of order 5.9 fb^{-1} . The new result of the CDF experiment use a luminosity of 7.1 fb^{-1} ; nevertheless our conclusions will remain, especially that the new Tevatron results have induced a slightly reduction of the exclusion range from 158–175 GeV down to 158–173 GeV.

Before describing the more precise way of handling the comparison between our results and those of the CDF/D0 collaborations, we stress again that the comparison between our values and those assumed by the experimental collaborations becomes even worse when the cross section is evaluated with another set of PDFs. For instance, with the ABKM PDF parametrization, there is a reduction of $\approx 25 - 30\%$ of the normalisation compared to the central value adopted in the CDF/D0 combined analysis. We should also take into account the uncertainties on the backgrounds in order to make complete predictions. The by far largest background is $p\bar{p} \rightarrow W^+W^-$ for which CDF/D0 assume the inclusive cross section to be $\sigma = 11.34_{-4.3\%}^{+4.9\%}(\text{scale})_{-2.5\%}^{+3.1\%}(\text{PDF})$ pb. We have reevaluated the rate using MCFM [274] and find $\sigma = 11.55_{-6\%}^{+5\%}(\text{scale})_{-8\%}^{+5\%}(90\% \text{CL PDF})$ pb using the MSTW scheme (the errors due to α_s are negligible here) which gives $\sigma = 11.55_{-14\%}^{+11\%}$ pb if the errors are added according to our procedure developed for the signal cross section. If we adopt the ABKM or HERAPDF

sets, we would obtain a rate of, respectively, 12.35 pb and 11.81 pb. i.e. nearly 9% higher in the maximal case. We will thus consider that $\sigma(p\bar{p} \rightarrow W^+W^-)$ can be $\approx 10\%$ larger/lower than assumed by CDF/D0.

Thus if the $\approx 20\%$ total uncertainty assumed by the CDF collaboration is adopted, one can consider three scenarios:

1. The first scenario is a reduction of $\sigma_{gg \rightarrow H}^{\text{NNLO}}$ by $\approx 20\%$ to account for the difference between the quadratic and (almost) linear ways of combining the individual uncertainties.
2. The second scenario is simply to adopt the normalisation obtained using the ABKM PDFs which gives an $\approx 30\%$ reduction of $\sigma_{gg \rightarrow H}^{\text{NNLO}}$ in the critical region. In both scenarios 1 and 2, the remaining $\approx 20\%$ uncertainty due to scale variation and the EFT will correspond to the overall theoretical uncertainty that has been assumed in the Tevatron analysis.
3. The additional third scenario will be to consider the same assumptions in the first scenario for the signal and change the normalization of the $p\bar{p} \rightarrow WW$ background by $\pm 10\%$.

In Ref. [95], the exploration of the Tevatron exclusion limit is based on the CDF study published in Ref. [275] which provides with all the necessary details. In the analysis of the $gg \rightarrow H \rightarrow WW \rightarrow \ell\nu\nu$ signal, the production cross section has been broken into the three pieces which yield different final state signal topologies, namely $\ell\nu\nu+0$ jet, $\ell\nu\nu+1$ jet and $\ell\nu\nu+2$ jets or more. These channels which represent, respectively, $\approx 60\%$, $\approx 30\%$ and $\approx 10\%$ of the total $\sigma_{gg \rightarrow H}^{\text{NNLO}}$ [112], have been studied separately. In the $\ell\nu\nu+0$ jet and $+1$ jet samples, two configurations have been analyzed, one with a high and one with a low signal over background ratio (depending on the quality of the lepton identification). In addition, a sample with a low invariant mass for the two leptons, $M_{\ell\ell} \leq 16$ GeV, has been included. Five additional channels resulting from the contributions of the Higgs–strahlung processes are also included: $p\bar{p} \rightarrow VH \rightarrow VWW$ leading to same sign dilepton and to trilepton final states. These channels give rather small signal rates, though.

One then estimates the necessary relative variation of the integrated luminosity needed to reproduce the currently quoted sensitivity of the CDF collaboration, if the normalization of the Higgs signal cross section (as well as the corresponding backgrounds) is different from the one assumed to obtain the results. In Ref. [95] it has first been tried to reproduce as closely as possible the CDF results for a Higgs mass $M_H = 160$ GeV for which the

sensitivity is almost the best. They have used the information given in Ref. [275], that is the background, signal and data numbers for all the search channels of Tables I–VIII, and also their neural network outputs for the 10 search channels (each one for the signals, backgrounds and data) presented in Figs. 2,4,⋯,16 to build the background only and the background plus signal hypotheses, implemented them in the program `MCLimit` [276] and used a ratio of log-likelihood “à la LEP” as a test-statistic for which we combined the above channels; this provided the 95 %CL/ σ_{SM} sensitivity limit on the Higgs boson at the considered mass of $M_H = 160$ GeV. A median expected 95 %CL/ σ_{SM} limit of $S_0 = 1.35$ has been obtained, to be compared to $S_0 = 1.05$ in the CDF analysis; for the observed 95 %CL/ σ_{SM} limit, the agreement is better as we obtain 1.35 compared to 1.32. As the CDF and D0 collaboration agree in their methods only within 10% accuracy for the same input Monte Carlo and data [277], it is believed that the procedure is satisfactory enough to be used in the three scenarios described above.

The first two scenarios discussed previously which, in practice, when compared to the CDF/D0 results, reduce the normalisation of the $gg \rightarrow H \rightarrow WW \rightarrow \ell\nu\nu$ signal cross section by approximatively 20% when all the uncertainties are added using our procedure, approximatively 30% when the ABKM set is used to derive the central value of the cross section, will be considered. The third scenario adds the effect of the background uncertainties. The authors of Ref. [95] then estimate the relative variation of the sensitivity and increase the integrated luminosity until we recover our initial sensitivity. Finally, it is assumed that the obtained relative variations of the sensitivity, as well as the required luminosity to reproduce the initial sensitivity, would be the same for the CDF experiment.

For each scenario, the expected signals and the corresponding backgrounds at the Tevatron have been multiplied by a luminosity factor that has been varied. For each value of the luminosity factor, the corresponding median expected 95%CL/ σ_{SM} has been estimated and normalized to the initial sensitivity $S_0 = 1.35$ obtained above. We display in Fig. 46 the final result, where the Tevatron luminosity is shown as a function of the obtained normalized sensitivity. The luminosity needed to recover the current S_0 CDF sensitivity is given by the intersection of the vertical blue line with the luminosity curves. The third scenario where the normalization of the background cross sections is changed by approximatively $\pm 10\%$ ⁵⁷ has also been considered. The final result is that if $\sigma_{gg \rightarrow H}^{\text{NNLO}}$ is lowered by 20%, a luminosity of $\approx 8 \text{ fb}^{-1}$, compared to 5.9 fb^{-1} used in [275] would be required for the same analysis to obtain the current sensitivity. If the rate is lower by 30%, the required luminosity should increase to $\approx 10 \text{ fb}^{-1}$, i.e. nearly a factor of two, to obtain the CDF

⁵⁷The correlation between signal and background is implicitly taken into account as we use the results of Ref. [275]; we assume though that it is almost the same when another PDF set is adopted for both signal and background.

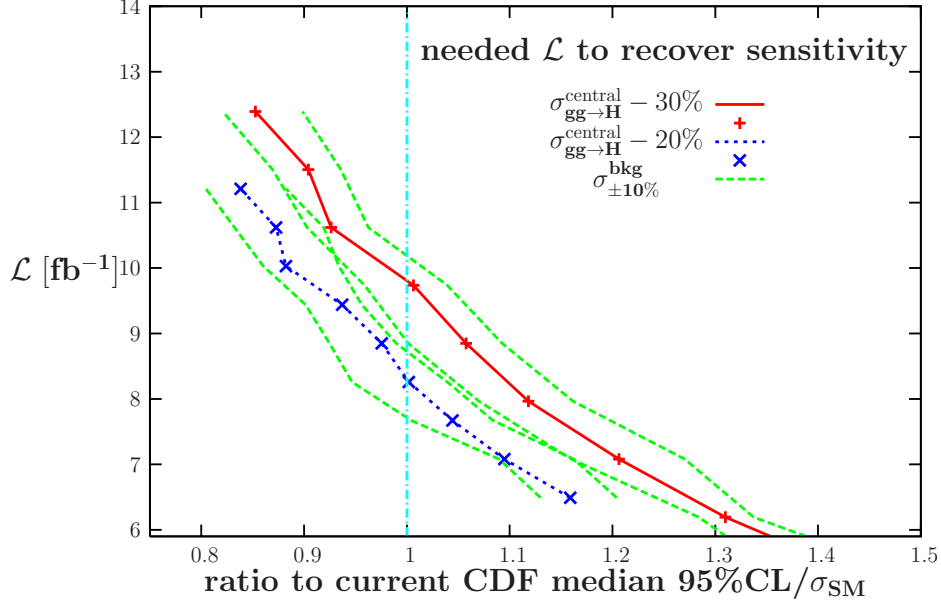


Figure 46: The luminosity needed by the CDF experiment to recover the current sensitivity (with 5.9 fb^{-1} data) when the $gg \rightarrow H \rightarrow \ell\ell\nu\nu$ signal rate is lowered by 20 and 30% and with a $\pm 10\%$ change in the $p\bar{p} \rightarrow WW$ dominant background. Figure taken from Ref. [95].

sensitivity with 5.9 fb^{-1} ; as the newest CDF analysis with 7.1 fb^{-1} leads to a slightly worse exclusion limit $158 \leq M_H \leq 173 \text{ GeV}$, we believe that recovering this last exclusion limit should require $\approx 13 \text{ fb}^{-1}$, that is still a factor of two than the current used luminosity. In the third scenario, we see that increasing/decreasing the background will degrade/improve the sensitivity and an $\approx 10\%$ higher/lower luminosity would be required to recover the sensitivity.

6.6 Summary of the results

After the results of sections 4 and 5 on the production cross sections we have given in this section our theoretical prediction of the Higgs decay branching fractions, together with a detailed analysis of the parametric uncertainties that affect the predictions.

We have found that in the two main decay search channels $H \rightarrow b\bar{b}$ and $H \rightarrow W^{(*)}W^{(*)}$ the uncertainties are sizeable and have some impact in the intermediate mass range $130 \lesssim M_H \lesssim 150 \text{ GeV}$. We then have combined the production cross section and decay branching ratio in section 6.3 for the Tevatron and section 6.4 for the LHC and found that in particular for the $p\bar{p} \rightarrow WH \rightarrow Wb\bar{b}$ channel at the Tevatron the uncertainties are more important than for the production cross section alone.

We then have compared our results with those of the CDF and D0 experiments. We

have presented a naive approach that has cast some doubts on the 95%CL exclusion limit. This is then confirmed by a more rigorous approach that we have presented in the end of section 6.5, where we conclude that the reduction of the signal by 30% as would be the case if the ABKM set were used for its normalization, would reopen the entire mass range $M_H = 158\text{--}173$ GeV excluded by the CDF/D0 analysis with 12.6 fb^{-1} combined data: this means that even if our uncertainties are viewed as being too conservative (which we believe is certainly not the case, as demonstrated above) the exclusion limit critically depends on the considered PDF. That is a non-satisfactory situation which needs to be cured and in particular the PDF case is still open, see for example Refs. [278–280] on the comparison between DIS-only and global fits that is still strongly disputed between the experts. We also note that the exclusion limit is also disputed in Ref. [281] with arguments different from that presented in this thesis. Henceforth the Tevatron results on the SM Higgs boson mass is strongly debated within the community.

This results put an end to the first two parts of this thesis that have been devoted to the study of the Higgs boson within the Standard Model. However this is not the end of the story, as there are strong indications that new physics beyond the SM is needed to describe the sub-atomic world, just to mention the experimental proof of the neutrinos masses which are not included in the SM⁵⁸. We will then turn our attention to one of the most popular beyond-the-SM scenario: supersymmetric theories. Part III will introduce the theoretical concepts of supersymmetry (SUSY) and its application to the minimal extension of the SM, called the MSSM. Part IV will give our results on the SUSY Higgs boson(s) production and decay at the Tevatron and LHC colliders.

⁵⁸This can be accommodated in some ways without introducing new physics, e.g. with a right-handed neutrino yet-to-be-seen put by hand in the theory; this is not a satisfactory way as we do not have any (good) explanation why this right-handed neutrino has not yet been observed.

Part III

The Minimal Supersymmetric extension of the Standard Model

Summary

7	Why Supersymmetry is appealing	146
7.1	The hierarchy problem	146
7.2	Coupling constants convergence at high energies	148
7.3	SUSY and Dark Matter searches	150
8	Formal SUSY aspects	153
8.1	SUSY Algebra	153
8.1.1	The Coleman–Mandula and HLS theorems	153
8.1.2	The Wess–Zumino free–field model	156
8.2	Superspace, superfields and superpotential	157
8.2.1	The chiral superfield	158
8.2.2	The vector superfield	159
8.2.3	The superpotential	160
8.3	Soft SUSY breaking	162
8.3.1	General soft SUSY beaking	162
8.3.2	What is the origin of soft SUSY breaking?	163
9	The Minimal Supersymmetric Standard Model	165
9.1	Fields content: Higgs and SUSY sectors of the MSSM	165
9.1.1	Superfields and (super)particles content	165
9.1.2	The MSSM lagrangian	167
9.1.3	Some experimental constraints on the sparticles masses	170
9.2	The Higgs sector and the number of Higgs doublets	170
9.2.1	The number of Higgs doublet in the MSSM	171
9.2.2	The electroweak symmetry breaking in the MSSM	171

9.2.3	The masses and couplings of the MSSM Higgs bosons	173
9.3	The MSSM is not the end of the story	178

7 Why Supersymmetry is appealing

The first two parts of this thesis were devoted to the extensive study of the Higgs boson phenomenology at hadron colliders within the SM theory. However we have already stated that this theory is bound to be considered as an effective model of a more elaborated theory yet-to-be-discovered: indeed, there are many models on the market that go beyond the SM, none of them being well established by experiments.

We will study in the following sections one of the most appealing scenarios beyond the SM: the minimal extension of the SM in the context of supersymmetry (SUSY). This theory will be presented in the following sections but to begin with we remind the reader that SUSY is a symmetry between bosons and fermions: it relates these two degrees of freedom through new fermionic operators, and any supersymmetric lagrangian has to be invariant by the exchange of the bosonic and fermionic degrees of freedom grouped in one same multiplet. We will first give some reasons why SUSY is a very appealing theory and then in the two next sections introduce its formal aspects and application to the minimal extension of the SM.

7.1 The hierarchy problem

When the Standard Model was described in section 1.1, one of the key arguments in going from the old $V - A$ theory for the weak interaction to the current electroweak theory was that it enables calculations beyond the Fermi scale and in particular the weak electron-neutrino scattering be well behaved at high center-of-mass energies, that is the unitarity requirement. However, we have seen that the SM itself is not free from potential unitarity problem and we have assessed bounds on the SM Higgs boson following from the unitarity requirement. This exercise, along other ways of obtaining theoretical bounds on the SM Higgs boson, has shown that the scalar sector of the SM is in some sense ill-defined: it concentrates most of the difficulties of the SM, as it is an unstable sector not protected by any symmetry, and this will be presented in this subsection.

The major problem of the Higgs boson mass is that quantum corrections of this fundamental parameter of the theory is of quadratically divergent type. If we take the one-loop corrections, they are described by the Feynman diagrams depicted in Fig. 47 below.

If we take for example the first fermionic diagram, the typical contribution is

$$\Pi_{HH}^f(0) = -4iN_f \left(\frac{\lambda_f}{\sqrt{2}} \right)^2 \frac{1}{8\pi^2} \int_0^{+\infty} dk k^3 \frac{k^2 + m_f^2}{(k^2 - m_f^2)^2} \quad (7.1)$$

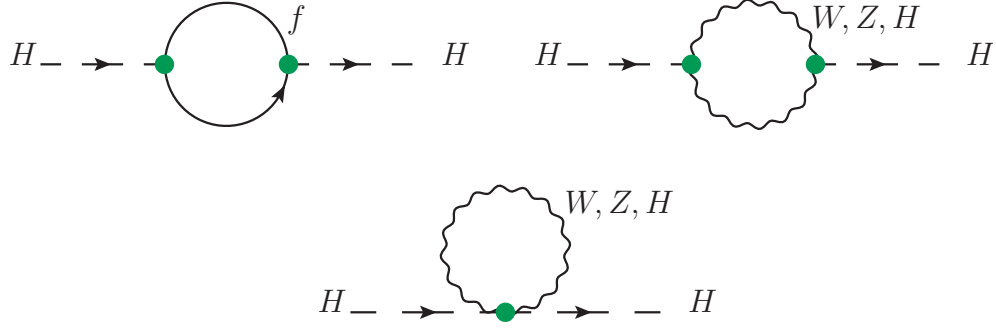


Figure 47: Feynman diagrams for one-loop corrections to the Higgs boson mass within the SM: fermionic loops (upper left), 3-points bosonic vertex (upper right) and 4-points bosonic vertex (lower).

were N_f is 3 for a quark, 1 for a lepton. If we rewrite the integrand it reads

$$\begin{aligned} \frac{k^3(k^2 + m_f^2)}{(k^2 - m_f^2)^2} &= \frac{k^3}{k^2 - m_f^2} + \frac{2m_f^2 k^3}{(k^2 - m_f^2)^2} \\ &= k + 3m_f^2 \frac{k}{k^2 - m_f^2} + 2m_f^4 \frac{k}{(k^2 - m_f^2)^2} \end{aligned}$$

which contains a quadratic divergence as the first term, after the integration with a cut-off Λ at high k momentum, gives a term proportionnal to Λ^2 . The actual dominant contribution, taking into account self-Higgs interactions and weak bosons contributions along that of the fermionic, reads [45, 211]:

$$\Delta M_H^2 = \frac{3\Lambda^2}{8\pi^2 v^2} (M_H^2 + 2M_W^2 + M_Z^2 - 4m_t^2) \quad (7.2)$$

This is a very severe divergence which is retained even after renormalization. Indeed, if the SM were to be valid up to the Planck scale $\Lambda_P \simeq 10^{18}$ GeV the Higgs boson mass would be attracted to that scale and would have a mass of order Λ_P : we would need a counterterm that is hugely fine-tuned in order to keep the Higgs boson mass below the theoretical bounds of order 1 TeV as presented in section 3.1. If we forget about the bosonic contributions to the Higgs boson mass, we see that the correction in Eq. 7.2 does not depend on M_H : this means that even if we were to set $M_H = 0$ we still would have the same problem. No symmetry then protects the SM Higgs boson to be driven to high masses, hence making this parameter unnatural. This is exactly the naturalness problem of the SM, see Ref. [282, 283]. The related question, which is the gauge hierarchy problem, is why the new physics scale that drives the SM Higgs boson mass, is much heavier than say M_Z which is typical of the electroweak scale, see also Ref. [284].

How to solve this technical (but theoretically unsatisfactory) problem? One solution would be to introduce new degrees of freedom which would arrange themselves to cancel out

exactly the contributions of the standard bosons and fermions. We start from Eq. 7.1 where the leading quadratic divergence reads $\Delta M_H^2 = -\lambda_f^2 \Lambda^2 / 8\pi^2$ (we discard in this analysis the additional N_f factor that is irrelevant for the point discussed). We follow Refs. [284, 285]; we introduce N new complex scalar fields \tilde{f} with

$$\mathcal{L}_{\tilde{f}\tilde{f}H} = -\frac{1}{2}\lambda_{\tilde{f}}H^2|\tilde{f}|^2 - \lambda_{\tilde{f}}vH|\tilde{f}|^2 \quad (7.3)$$

This induces two types of corrections to the Higgs boson mass following the two bosonic diagrams in Fig. 47, and again when writing only the quadratic divergence it reads:

$$\Pi_{HH}^{\tilde{f}}(0) = Nv\frac{\lambda_{\tilde{f}}}{16\pi^2}\Lambda^2 \quad (7.4)$$

If we combine Eqs. 7.1 and 7.4 we see that the cancellation of quadratic divergences, in other words having $\Pi_{HH}^f + \Pi_{HH}^{\tilde{f}} = \mathcal{O}(\ln \Lambda)$, can be obtained provided that

$$N = 2, \quad \lambda_{\tilde{f}} = \lambda_f^2 \quad (7.5)$$

This result is of utmost importance: it means that if we introduce a symmetry between bosonic and fermionic degrees of freedom that arranges to follow Eq. 7.5 we can solve the naturalness of the SM. Following Ref. [211, 284] we can even go further and cancel the logarithmic divergence without renormalization analysis if we impose $m_f = m_{\tilde{f}}$. We are even tempted to assign for each fermion f , which has a left and right chirality, two new complex scalar partners \tilde{f}_R and \tilde{f}_L where the index refers to the original fermionic degree of freedom and not any chirality for the scalar fields. Note that the total number of degree of freedom is conserved by this assignment.

This is exactly the virtue of SUSY which is a symmetry between bosons and fermions: each SM boson and each SM fermion has its own (super)partner, respectively a fermion and a boson. The relationship between the standard particles and these new degrees of freedom ensures that we get rid of quadratic divergencies, thus solving the weak hierarchy problem. This is one particularly elegant reason why SUSY is a very appealing theory beyond the SM.

7.2 Coupling constants convergence at high energies

We now turn our attention to a less severe problem as it deals with speculative questions. For centuries atomic and then sub-atomic physics have tried to unify the description of fundamental processes, starting from the unification of electricity and magnetism into a

single electromagnetic interaction, currently described by QED. It is then strongly believed that the current electroweak⁵⁹ and strong interactions unify at a very high energy scale, $\Lambda_{\text{GUT}} \simeq 10^{16}$ GeV. Several attempts have been made for forty years and the most well-known solution is the long-celebrated $SU(5)$ theory [286] (see also Ref. [287]). This model is nowadays excluded because of the too short proton life-time and the disagreement between the measured Weinberg angle $\sin^2 \theta_W$ and the predicted value of the $SU(5)$ model; nevertheless it provides a very useful example of a grand unified theory.

Gauge couplings are renormalized and thus running couplings. The running proceeds through quantum loop corrections, see Fig. 48 for typical diagrams at the 1-loop order, and is described through renormalization group equations [288, 289]

$$\begin{aligned} \frac{d\alpha_i}{d \ln Q^2} &= -b_i \alpha_i^2, \quad \alpha_i \equiv \frac{g_i^2}{4\pi} \quad (g_L \equiv g) \\ b_s &= \frac{23}{12\pi}, \quad b_L = \frac{19}{64\pi}, \quad b_Y = -\frac{41}{40\pi} \end{aligned} \quad (7.6)$$

with the SM coefficients taken at the 1-loop order. The hypercharge coupling constant α_Y has been rescaled by a factor of 5/3 in order to match unified gauge description in the covariant derivation.

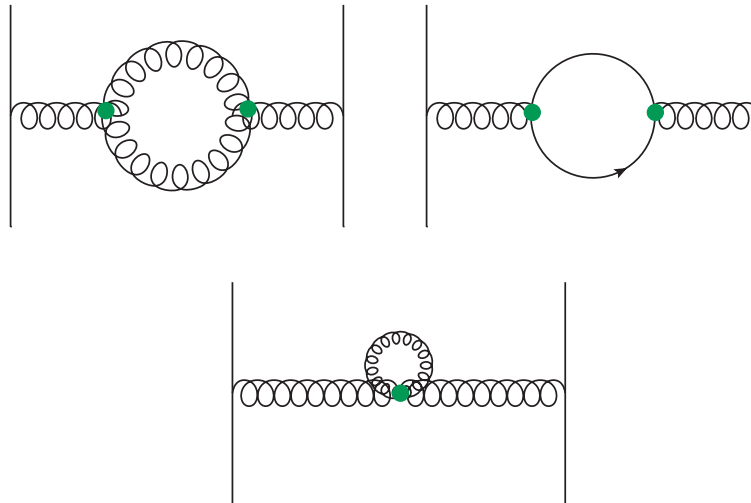


Figure 48: Feynman diagrams for typical one-loop corrections to a generic gauge coupling. The gauge-gauge vertex diagrams are only relevant for non-abelian gauge symmetries.

Fig. 49 shows on the left the resulting running within the SM, assuming no new particles content between the weak scale and the GUT scale. The three gauge couplings seem to

⁵⁹We want to point out in passing that the weak and electromagnetic interactions are partially unified in the electroweak framework: the gauge algebra $SU(2)_L \times U(1)_Y$ has two couplings constants, whereas we should only have a single Lie group X with a single coupling constant g_X to really have unification. This is the goal of any Grand Unified Theory, with the additional strong interaction unification to the electroweak interaction.

meet at high energy but not exactly: unification is not exactly achieved if we do not assume new particles content between the weak scale and the GUT scale, assuming that the new degree of freedom required by grand unification have a mass of order Λ_{GUT} ⁶⁰ and thus not contributing to the RGE [286].

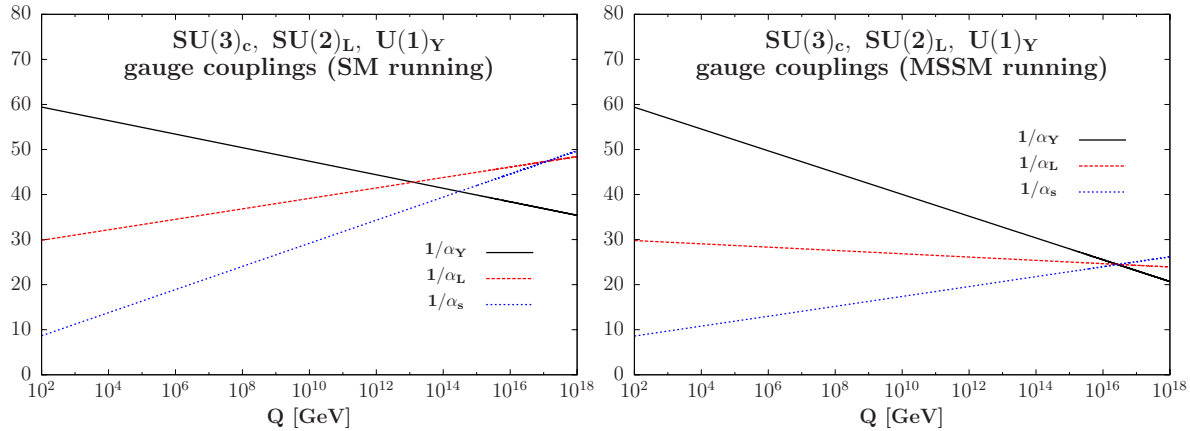


Figure 49: $SU(3)_c \times SU(2)_L \times U(1)_Y$ gauge couplings running from the weak scale up to the GUT scale, within the SM (left) and within the MSSM (right).

The right part of Fig. 49 reproduces the same exercise but replacing the RGE parameters by those obtained assuming new particles content due to the additional particles within the minimal supersymmetric extension of the SM, called the MSSM. Indeed the running of the three gauge couplings is expected to change as higher-order corrections involve new fermions and bosons (the so-called superpartners of the standard particles). We thus have

$$b_Y \rightarrow -\frac{33}{20\pi}, \quad b_L \rightarrow -\frac{1}{4\pi}, \quad b_s \rightarrow \frac{3}{4\pi} \quad (7.7)$$

which now allow the three gauge couplings to perfectly match at $Q \simeq 10^{16}$ GeV [289]. This is a spectacular reason why the addition of SUSY to the SM is very elegant: it helps to push toward an actual unification of the three sub-atomic interactions.

7.3 SUSY and Dark Matter searches

The two subsections above have presented two technical reasons that explain why SUSY is an interesting solution to both internal problems of the SM and external difficulties in the wish to obtain a Grand Unified Theory (GUT) where all the interactions are unified in a single Lie algebra, with all the coupling constants merged into a single one at very high

⁶⁰There is no reason why this should not be the case: if that were the case we would have to introduce a mechanism explaining why these new particles had a reduced mass.

energy. We will in this subsection present an experimental reason of introducing SUSY, connected to cosmology puzzles.

Indeed, all the cosmological observations⁶¹ point out to the existence of an unknown matter component of the Universe which amounts to nearly 23% of the total energy density of our current Universe [292–294]. If we take the exact numbers from Ref. [294] we have

$$\Omega_{\text{DM}} = 0.229, \text{ to be compared to } \Omega_{\text{baryon}} = 0.046 \quad (7.8)$$

This matter density is more than four times the density of standard matter that we know, which means that there is a very large amount of the Universe that is yet to be understood, not to mention the nearly 73% of dark energy density that is even more mysterious and drives the current acceleration of the expansion of the Universe. Particle physics is then confronted to a critical problem: how to account for this missing 23% piece of the Universe, which is absent from the SM? Any theory that goes beyond the SM ought to provide for realistic dark matter candidates.

If we come back to SUSY, we remind that we have introduced new fermions and bosons in the theory, as a consequence of the symmetry between bosonic and fermionic degrees of freedom. We then have new vertexes and in particular we should care about the proton decay. Indeed, the proton lifetime is estimated to be larger than 10^{32} years, thus any theory beyond the SM (where the proton is stable) must respect this lower bound, which means in practice to assure that the proton remains stable. Strictly speaking, this is not possible with the most general SUSY extension of the SM: for example we could have the decay $p \rightarrow e^+ \pi^0$ as depicted in Fig. 50 below.

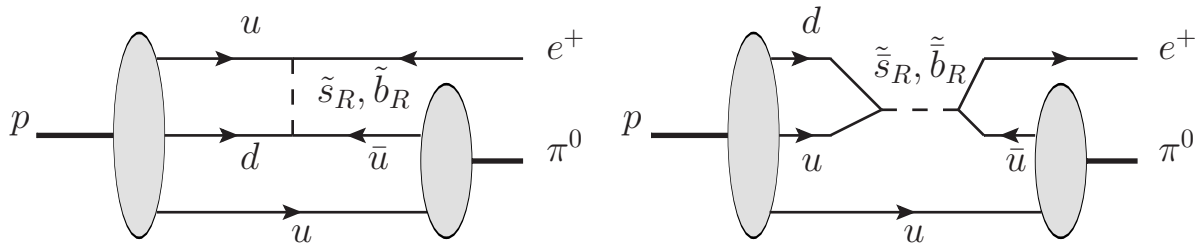


Figure 50: Some Feynman diagrams for the proton decay into a pion and a positron $p \rightarrow e^+ \pi^0$ through SUSY vertexes when R -parity is violated.

⁶¹We here take the (standard) point of view that general relativity still holds at such large scales. However this is nothing more than a mere assumption, general relativity not being tested as such large scales. There are alternative cosmological attempts to explain the cosmological observations such as the galaxies profiles without the standard Λ -CDM model based on general relativity on the cosmological scales, which does not require a dark matter component, see Ref. [290, 291] for example. However we will not come into such unnecessary discussions for the rest of the thesis.

This can be cast away if we impose, as is the case in the minimal supersymmetric extension of the SM, a new global discrete symmetry called R -parity [295]: we assign a multiplicative number $R = (-1)^{3B+L+2S}$, where B , L and S stand respectively for the baryon number, the lepton number and the spin. It reduces in the end to $R = +1$ for standard matter, and $R = -1$ for superpartners. R -parity is connected to the $B - L$ conservation, indeed we have $(-1)^{3B+L+2S} = (-1)^{3(B-L)+2S}$. Any reaction is now supposed to conserve this R number. This discrete symmetry can be seen as a relic of a global $U(1)_R$ symmetry broken down to a Z_2 subgroup, see Ref. [284] page 359.

We can now evade the problem of the proton decay: as the quarks (u,d) are standard particles their R -number is equal to one, thus it forbids any vertex with only one superpartner involved such as the violating vertexes in Fig. 50.

How is this statement connected to our cosmological problem? If we introduce R -parity to block the proton decay, it has also a very interesting consequence: superparticles ought to be produced in pairs, and if the proton is to be stable on the one hand, we can easily make the same statement for the lightest supersymmetric particle. Hence we predict that any supersymmetric spectrum following R -parity conservation must have a stable particle!

The lightest supersymmetric particle (LSP) in the context of the minimal supersymmetric extension of the SM is a neutral mixture of the superpartners of the weak bosons and Higgs bosons⁶² called the neutralino χ_1^0 . This is a stable, neutral, massive particle, hence an ideal candidate for the dark matter component of the Universe (see Ref. [296] for a review on this topic). This is worth mentioning that this LSP is nothing more than just one candidate among many others. Nevertheless the LSP explication for dark matter is one of the most popular scenerios that could explain the origin of dark matter.

⁶²The plural form is not accidental: we will see later on that there must be at least two Higgs doublets in the MSSM.

8 Formal SUSY aspects

Now that we have introduced some reasons to explain our interest in supersymmetric theories, we are ready to sketch some formal aspects of supersymmetry. Basically, as stated in the section 7 above, supersymmetry (SUSY) is a symmetry between bosons and fermions: each scalar boson has a spin $\frac{1}{2}$ partner, each spin $\frac{1}{2}$ fermion has a spin 0 partner, each vector boson has a spin $\frac{1}{2}$ partner⁶³. A theory is said to be supersymmetric when the exchange of any pair of partners leaves the action invariant. We will see that it is a very elegant extension of the usual Poincaré algebra and in some sense “natural”.

The first subsection will introduce the super-algebra, following the outlines of a very famous theoretical physics theorem that shapes any extension of the Poincaré algebra. We will then give some hints of the superspace formalism that allow for a compact description of the supermultiplets. We will end by the introduction to SUSY breaking, one of the most important issue in the study of SUSY theories that is still to be solved.

8.1 Graded Lie Algebra and the Coleman–Mandula theorem

The mathematical formalism of SUSY theories is based on the concept of graded Lie algebras which generalizes the usual Lie algebras to encompass anticommutators as well as Lie brackets. The actual shape of SUSY algebra is dictated by very powerful formal theorems: the Coleman–Mandula theorem [297] and the Haag–Lopuszanski–Sohnius (HLS) theorem [298] which generalizes the Coleman–Mandula theorem and leads to SUSY graded Lie algebra. We will not prove these theorems in this section, but discuss their consequences.

8.1.1 The Coleman–Mandula and HLS theorems

We will follow Refs. [284, 299] in this paragraph. The statement of the Coleman–Mandula theorem is:

With the following assumptions:

- a) *The S-matrix is based on a local, relativistic quantum field theory in four-dimensional spacetime;*
- b) *For a given mass, there is only a finite number of different particles associated to one-particle states;*

⁶³Here we leave aside the case of the graviton and its gravitino superpartner of spin $\frac{3}{2}$.

c) *There is an energy gap between the vacuum and the one-particle states; the most general Lie algebra of symmetries of the S -matrix contains the Poincaré algebra and a finite number of Lorentz scalar operators B_l which must belong to a compact Lie algebra.*

This theorem then puts some restrictions on the form of the symmetries than can be imposed on the S -matrix: any Lie algebra not of the type of the Poincaré algebra shall be in direct sum with the Poincaré algebra, that is, if we define the generator as T^a and the structure constants f_{abc} we have:

$$[T^a, T^b] = f_{abc}T^c, \quad [T^a, P_\mu] = [T^a, M_{\mu\nu}] = 0 \quad (8.1)$$

where $M_{\mu\nu}$ is the Lorentz generator, P_μ the translation generator. We see that this imposes severe restrictions to any *bosonic* symmetry (represented by a gauge Lie algebra), but what if we introduce a *fermionic* symmetry? This is precisely the spirit of SUSY, in which graded Lie algebras escape the Coleman–Mandula theorem by using anticommutators in addition to the usual Lie commutators. The HLS theorem then states that the only graded Lie algebra which is compatible with the Coleman–Mandula theorem assumptions is precisely that of the supersymmetry algebra which will be described below.

The HLS theorem precisely states the following (see also Ref. [284], page 31):

The Lie algebra which follows the assumptions of the Coleman–Mandula theorem is a Z_2 graded Lie algebra which odd generators belong to the representations $(\mathbf{0}, \frac{1}{2})$ and $(\frac{1}{2}, \mathbf{0})$ of the Lorentz algebra and even generators are a direct sum of the Poincaré generators and other symmetry generators.

This puts a restriction over the form of the new fermionic symmetry that we want to introduce through the anticommutators: this must be represented by a set of two (Q, \bar{Q}) generators which are of spin $\frac{1}{2}$, but not higher. The minimal choice is to take a set of two Majorana spinors $(Q_a, \bar{Q}_{\dot{a}})$ (ie where the spinor is invariant under charge conjugation) and we will use Weyl two-components notation; in four-components notation with Dirac spinors we would have one Majorana spinor

$$Q = \begin{pmatrix} Q_a \\ \bar{Q}_{\dot{a}} \end{pmatrix}$$

We will give the final super–Poincaré algebra relations. If we follow the HLS theorem, we see that the anticommutator $\{Q_a, \bar{Q}_{\dot{a}}\}$ has no choice but to be proportionnal to P_μ (if

not it would violate the Coleman–Mandula theorem). This precisely dictates the final shape of the super–Poincaré algebra:

$$\begin{aligned}
\{Q_a, \bar{Q}_b\} &= 2\sigma_{ab}^\mu P_\mu \\
\{Q_a, Q_b\} &= \{\bar{Q}_a, \bar{Q}_b\} = 0 \\
[Q_a, P_\mu] &= [\bar{Q}_a, P_\mu] = 0 \\
[P_\mu, P_\nu] &= 0 \\
[Q_a, M_{\mu\nu}] &= (\sigma_{\mu\nu})_a^b Q_b
\end{aligned} \tag{8.2}$$

where we recall that $\sigma^{\mu\nu} \equiv \frac{i}{4}\sigma^{[\mu}\bar{\sigma}^{\nu]}$, σ^μ being the usual set of Pauli matrices, $\sigma^0 = \bar{\sigma}^0 = I$, $\sigma^{1,2,3} = -\bar{\sigma}^{1,2,3}$. In four–components notation with only one four–components Majorana generator Q the super–Poincaré algebra 8.2 reads (see Ref. [284] page 34)

$$\begin{aligned}
\{Q_a, Q_b\} &= -2(\gamma^\mu C)_{ab} P_\mu \\
[Q_a, P_\mu] &= 0 \\
[P_\mu, P_\nu] &= 0 \\
[Q_a, M_{\mu\nu}] &= (\Sigma^{\mu\nu})_a^b Q_b
\end{aligned} \tag{8.3}$$

where this time we have $\Sigma^{\mu\nu} \equiv \frac{i}{4}\gamma^{[\mu}\gamma^{\nu]}$ and the charge conjugate operator $C \equiv \nu\gamma^2\gamma^0$ in Dirac representation.

Using the SUSY algebra we can derive two important consequences:

- *In each supermultiplet spanning a representation of the SUSY algebra there is an equal number of bosons and fermions:* if we introduce the operator $(-1)^{2S}$ which takes +1 eigenvalue on bosonic states and -1 eigenvalue on fermionic states, and take a closed supermultiplet $\{|i\rangle\}$ with a definite (non–zero) p_μ momentum, we have

$$\begin{aligned}
\text{Tr} [(-1)^{2S} \{Q_a, Q_b\}] &= \text{Tr} [(-1)^{2S} Q_a Q_b] + \text{Tr} [(-1)^{2S} Q_b Q_a] \\
&= \text{Tr} [(-1)^{2S} Q_a Q_b] + \text{Tr} [Q_a (-1)^{2S} Q_b] \\
&= \text{Tr} [(-1)^{2S} Q_a Q_b] - \text{Tr} [(-1)^{2S} Q_a Q_b] = 0
\end{aligned}$$

using the cyclicity of the trace operator and the fact that $\{(-1)^{2S}, Q_a\} = 0$, as can be easily verified. If we replace the anticommutator by the first equality of Eq. 8.3 it reads

$$\text{Tr} [(-1)^{2S} P_\mu] = p_\mu \text{Tr} (-1)^{2S} = 0$$

discarding the constant γ^μ factor. Having chosen $p_\mu \neq 0$ this reduces to

$$\text{Tr} (-1)^{2S} = n_B - n_F = 0 \tag{8.4}$$

where n_F (n_B) stands for the total number of fermionic states (bosonic states) within the supermultiplet. This is thus exactly the result we were looking for.

- *Each superpartner must have the same mass within a SUSY multiplet:* indeed if SUSY is exact, $[Q_a, P_\mu] = 0$ implies that $[Q_a, P^2] = 0$.

We want to note that the super–Poincaré algebra has two important features: the first is that it is an extension of the usual space–time symmetry and thus can be considered also as a space–time symmetry, making SUSY a fundamental symmetry; the second feature is that as the anticommutator of two supersymmetry generators Q gives the translation generator P_μ , it means that if we gauge SUSY we also gauge the usual space–time symmetry. Thus there is an intimate connexion between SUSY and gravity which is described in the context of supergravity theories [299]. It is sometimes said that gravity is “the square–root of SUSY”.

8.1.2 The Wess–Zumino free field model as an example of a SUSY lagrangian

We close this subsection by giving the most simple example of a SUSY lagrangian, the free field model called the massless non–interacting Wess–Zumino model [300], following the outlines of Ref. [285]. To parametrize a SUSY transformation we introduce an infinitesimal ϵ Grassmann parameter, which implies using the super–Poincaré algebra of Eq. 8.2 that $[\epsilon Q, \bar{\epsilon} \bar{Q}] = 2\bar{\epsilon} \sigma^\mu \bar{\epsilon} P_\mu$.

In the Wess–Zumino model we have one complex scalar field and one left–handed Weyl spinor field. The former is the superpartner of the latter; if we count the number of degrees of freedom we see that we have on–shell 2 bosonic and 2 fermionic degrees of freedom; nevertheless we would like to describe the most general lagrangian in the view of the quantum corrections. This means that we have to introduce an auxiliary scalar field F in order to match the 4 fermionic degree of freedoms off-shell. This constitute the chiral supermultiplet. The lagrangian is written as:

$$\mathcal{L} = \bar{\psi} \bar{\sigma}^\mu \partial_\mu \psi - \partial^\mu \phi^* \partial_\mu \phi + F^* F \quad (8.5)$$

In Eq. 8.5 we see explicitly that F is an auxiliary field, as its equation of motion is $F^* = F = 0$. Its has a mass dimension of 2 which is unusual for a scalar field. A SUSY transformation is written as

$$\begin{aligned} \delta_\epsilon \psi &= (\epsilon Q + \bar{\epsilon} \bar{Q}) \psi \\ \delta_\epsilon \phi &= (\epsilon Q + \bar{\epsilon} \bar{Q}) \phi \\ \delta_\epsilon F &= (\epsilon Q + \bar{\epsilon} \bar{Q}) F \end{aligned} \quad (8.6)$$

which reads [285, 299]

$$\begin{aligned}
\delta_\epsilon \phi &= \sqrt{2}\epsilon\psi \\
\delta_\epsilon \psi &= \iota\sqrt{2}\sigma^\mu \bar{\epsilon} \partial_\mu \phi + \sqrt{2}\epsilon F \\
\delta_\epsilon F &= \iota\sqrt{2}\bar{\epsilon} \bar{\sigma}^\mu \partial_\mu \psi
\end{aligned} \tag{8.7}$$

In Eq. 8.7 the role of F is to close the SUSY algebra, that is $[\epsilon Q, \bar{\epsilon} \bar{Q}] = 2\bar{\epsilon} \sigma^\mu \bar{\epsilon} P_\mu$, even in the off-shell case. The lagrangian 8.5 is then invariant up to a total space-time derivative:

$$\delta \mathcal{L} = \partial_\mu (iF \bar{\psi} \bar{\sigma}^\mu \epsilon + \epsilon \sigma^\nu \bar{\sigma}^\mu \psi \partial_\nu \phi^* + \epsilon \psi \partial^\mu \phi^* + \bar{\epsilon} \bar{\psi} \partial^\mu \phi) \tag{8.8}$$

The action is then fully SUSY invariant. We will see in the next section how to introduce in a simple way interactions which follow SUSY invariance, through the concept of superpotential.

8.2 Superspace, superfields and superpotential

We introduce in this subsection the superspace and superfield formalism which is a very compact and elegant formulation of SUSY, enlightening its deep connection with space-time symmetries. We will follow Refs. [284, 299].

The first step is to introduce the superspace: this is simply the usual space-time with the coordinates $x \equiv x_\mu = (ct, X, Y, Z)$ enlarged to include two additional two-components Grassmann (anticommuting) coordinates $\theta, \bar{\theta}$. We then have $\theta\theta \equiv \theta^a \theta_a$ and $\bar{\theta}\bar{\theta} \equiv \bar{\theta}^{\dot{a}} \bar{\theta}_{\dot{a}}$, but $\theta_a \theta_b = -\theta_b \theta_a$, $\theta_a \bar{\theta}_b = -\bar{\theta}_b \theta_a$. This means that any product of $\theta, \bar{\theta}$ which contains more than three $\theta/\bar{\theta}$ terms vanishes.

We introduce fields on this superspace, which we call superfields. By the virtue of the Grassmann coordinates, any superfield \mathcal{F} can be expanded in a finite serie of $\theta, \bar{\theta}$ variables:

$$\begin{aligned}
\mathcal{F}(x, \theta, \bar{\theta}) &= \phi(x) + \sqrt{2}\theta\psi(x) + \sqrt{2}\bar{\theta}\bar{\chi}(x) + \theta\theta M(x) + \bar{\theta}\bar{\theta} N(x) + \\
&\quad \theta\sigma^\mu \bar{\theta} A_\mu(x) + \theta\theta \bar{\theta} \bar{\lambda}(x) + \bar{\theta}\bar{\theta} \theta \zeta(x) + \frac{1}{2} \theta\theta \bar{\theta}\bar{\theta} D(x)
\end{aligned} \tag{8.9}$$

As the operators ϵQ and $\bar{\epsilon} \bar{Q}$ follow an ordinary Lie algebra, it is tempting to use the following SUSY transformation representation $\exp(\iota(x^\mu P_\mu + \epsilon Q + \bar{\epsilon} \bar{Q}))$ [299]. A linear SUSY transformation then reads in the superspace as

$$(x^\mu, \theta, \bar{\theta}) + \delta(x^\mu, \theta, \bar{\theta}) = (x^\mu - \iota\theta\sigma^\mu \bar{\epsilon} + \iota\epsilon\sigma^\mu \bar{\theta}, \theta + \epsilon, \bar{\theta} + \bar{\epsilon}) \tag{8.10}$$

which then induces the following linear representation of the supersymmetric generators

$$\begin{aligned}
Q_a &= -\imath \left(\frac{\partial}{\partial \theta^a} + \imath \sigma^\mu_{ab} \bar{\theta} \frac{\partial}{\partial x^\mu} \right) \\
\bar{Q}_a &= -\imath \left(\frac{\partial}{\partial \bar{\theta}^a} + \imath \theta \sigma^\mu_{ba} \frac{\partial}{\partial x^\mu} \right) \\
\delta \mathcal{F} &= \imath (\epsilon Q + \bar{\epsilon} \bar{Q}) \mathcal{F}
\end{aligned} \tag{8.11}$$

We are now ready to present the chiral and vector superfields that are used to construct the SUSY extension of the SM.

8.2.1 The chiral superfield

The chiral superfield will associate the standard fermionic fields with their spin 0 superpartners. In order to have a SUSY invariant definition, we shall construct a SUSY covariant derivative. As $P_\mu = -\imath \partial_\mu$ commute with Q but not $\partial_\theta \equiv \frac{\partial}{\partial \theta^a}$ nor $\partial_{\bar{\theta}}$. Following Ref. [284] we define

$$\begin{aligned}
\mathcal{D}_a &\equiv \partial_{\theta^a} - \imath \sigma^\mu_{ab} \bar{\theta}^b \partial_\mu \\
\bar{\mathcal{D}}_{\dot{a}} &\equiv -\partial_{\bar{\theta}^{\dot{a}}} + \imath \theta^b \sigma^\mu_{b\dot{a}} \partial_\mu
\end{aligned} \tag{8.12}$$

with which we define the (left) chiral superfield to follow these two equivalent conditions:

$$\mathcal{D}_a \Phi^\dagger = 0 \quad \text{or} \quad \bar{\mathcal{D}}_{\dot{a}} \Phi = 0 \tag{8.13}$$

This gives this component decomposition

$$\begin{aligned}
\Phi(x, \theta, \bar{\theta}) &= \phi(x) - \imath \theta \sigma^\mu \bar{\theta} \partial_\mu \phi(x) - \frac{1}{4} \theta \theta \bar{\theta} \bar{\theta} \partial_\mu \partial^\mu \phi(x) + \\
&\quad \sqrt{2} \theta \psi(x) + \frac{\imath}{\sqrt{2}} \theta \theta \partial_\mu \psi \sigma^\mu \bar{\theta} + \theta \theta F(x)
\end{aligned} \tag{8.14}$$

The SM fermion field will be $\psi(x)$, its scalar superpartner will be $\phi(x)$ and called a sfermion. The field $F(x)$ will be the auxiliary field necessary to ensure SUSY invariance in the off-shell case. Any product of chiral superfields will still be a superfield [284, 299]; the F -component of a chiral superfield, that is the $\theta\theta$ component, transforming as a total spatial derivative under a SUSY transformation, the F -component of any product of chiral superfields is a candidate for any lagrangian describing a SUSY invariant action.

The product $\Phi^\dagger \Phi$ is not a chiral superfield; nevertheless its highest $\theta\theta\bar{\theta}\bar{\theta}$ component is SUSY invariant up to a total derivative like any $\theta\theta\bar{\theta}\bar{\theta}$ component, and reads

$$F^* F + \frac{1}{2} \partial_\mu \phi^* \partial^\mu \phi - \frac{1}{4} (\phi \partial_\mu \partial^\mu \phi^* + \text{h.c.}) + \frac{1}{2} \imath \psi \sigma^\mu \partial_\mu \bar{\psi} + \imath \frac{1}{2} \bar{\psi} \bar{\sigma}^\mu \partial_\mu \psi \tag{8.15}$$

This will constitute the kinetic part of the chiral superfield. We then can rewrite the Wess–Zumino massless free lagrangian of Eq. 8.5 simply as

$$\mathcal{L}_{\text{free}} = \frac{\partial\Phi^\dagger\Phi}{\partial\bar{\theta}\bar{\theta}\theta\theta} \equiv \Phi^\dagger\Phi|_{\theta\theta\bar{\theta}\bar{\theta}} \quad (8.16)$$

8.2.2 The vector superfield

The second type of superfield will yield the gauge vector bosons. We impose a reality condition which define a vector superfield

$$V^\dagger = V \quad (8.17)$$

We can then use the general superfield written in Eq. 8.9 to obtain the expression of a vector superfield, but we will simplify the task in the next lines.

Following strictly Ref. [284] it is interesting to note that if we use a chiral superfield Λ the superfield $V = \imath\Lambda - \imath\Lambda^\dagger$ is a vector superfield. This implies the following abelian super–gauge transformation $V' = V + \imath\Lambda(x, \theta, \bar{\theta}) - \imath\Lambda^\dagger(x, \theta, \bar{\theta})$. This is indeed a gauge transformation as Λ is a function of the super–space coordinates. We are free to chose a particular gauge, the Wess-Zumino gauge in which a vector superfield reduces to

$$V = \theta\sigma^\mu\bar{\theta}A_\mu(x) + \theta\theta\bar{\theta}\bar{\lambda}(x) + \bar{\theta}\bar{\theta}\theta\lambda(x) + \frac{1}{2}\theta\theta\bar{\theta}\bar{\theta}D(x) \quad (8.18)$$

The SM gauge boson field will be $A_\mu(x)$, its fermionic superpartner will be $\lambda(x)$ and called the gaugino. The $D(x)$ field is that of the auxiliary necessary to ensure SUSY invariance even in the off–shell case, as did the $F(x)$ field in the case of a chiral superfield. As stated in Ref. [284] the D –term has the very interesting virtue to remains invariant under a supergauge transformation, making this term a very good candidate for writing supergauge and SUSY invariant lagrangian. It is actually very easy to introduce a $U(1)$ supergauge theory by taking a chiral superfield Φ and a vector superfield V , with

$$\begin{aligned} \Phi &\rightarrow \Phi' = e^{-2\imath g Y_\Phi V} \Phi \\ \Phi^\dagger &\rightarrow \Phi'^\dagger = e^{2\imath g Y_\Phi V} \Phi^\dagger \\ V &\rightarrow V' = V + \imath(\Lambda - \Lambda^\dagger) \end{aligned} \quad (8.19)$$

where Y_Φ is the $U(1)$ charge of the superfield Φ . A vector field is of zero mass dimension and thus can be exponentiated, which means that we can define

$$\mathcal{L}_{\text{kinetic}} = \Phi^\dagger e^{2g Y_\Phi V} \Phi|_{\theta\theta\bar{\theta}\bar{\theta}} \quad (8.20)$$

to be the lagrangian part containing both the kinetic term for the chiral superfield (the first factor in the exponential expansion) and the gauge invariant interacting term (i.e. the usual covariant derivative). The extension to an non-abelian supergauge theory follows the same pattern, that is introducing a gauge multiplet of chiral superfields Φ_I and then write down (in the Wess–Zumino gauge):

$$\begin{aligned}\Phi_I &\rightarrow \Phi'_I = (e^{-2ig_2 T_a \Lambda^a})_{IJ} \Phi_J \\ V_a T^a &\rightarrow V'_a T^a = V_a T^a + \imath (\Lambda_a T^a - (\Lambda_a T^a)^\dagger) + \frac{\imath}{2} [V, \Lambda_a T^a + (\Lambda_a T^a)^\dagger]\end{aligned}\quad (8.21)$$

with T^a as the usual generators of the non-abelian gauge algebra. Note that the a notation is here a non-abelian gauge index and not a spinorial index.

We now end this paragraph by giving the superfield–strength W which is a chiral superfield (see Ref. [284] page 65):

$$W_A = -\frac{1}{4} \overline{\mathcal{D}}_{\dot{B}} \overline{\mathcal{D}}^{\dot{B}} \mathcal{D}_A V, \quad W_A^\dagger = -\frac{1}{4} \mathcal{D}_B \mathcal{D}^B \overline{\mathcal{D}}_{\dot{A}} V \quad (8.22)$$

with A as a spinorial index. This superfield contains the usual field–strength tensor $F_{\mu\nu}$. We then define

$$\mathcal{L}_{\text{gauge kinetic}} = \frac{1}{4} \left(W_A W^A + W_A^\dagger W^{\dagger A} \right) \Big|_{\theta\theta} \quad (8.23)$$

which is coherent as we have a sum of product of chiral superfields which itself is also a chiral superfield, thus its F -term is SUSY invariant.

8.2.3 The superpotential

The last remaining piece that is needed to write down the most complete SUSY (renormalizable) lagrangian is the interaction among the scalar fields and between the scalars and fermions fields. The most simple way to introduce these interactions is to use a superpotential, in much the same spirit as above for the definition of the covariant derivative.

As the product of chiral superfields is also a superfield, the definition of a renormalizable superpotential is a superfield \mathcal{W} restricted by the following conditions:

1. It is an holomorphic expression of Φ_i chiral superfield, thus not containing any Φ^\dagger superfield;
2. It does not contain any product higher than $\Phi_i \Phi_j \Phi_k$ to ensure renormalizability;

The same conditions hold for the \mathcal{W}^\dagger superfield where we replace Φ_i by Φ_i^\dagger everywhere. The induced term in the lagrangian will be simply the F -term of the superpotential. The final lagrangian for a $U(1)$ gauge interaction among chiral superfields Φ_i mediated by a vector superfield V then writes

$$\begin{aligned}
\mathcal{L} &= \mathcal{L}_{\text{kinetic}} + \mathcal{L}_{\text{interaction}} \\
\mathcal{L}_{\text{kinetic}} &= \frac{1}{4} \left(W_A W^A + W_A^\dagger W^{\dagger A} \right) \Big|_{\theta\theta} + \left(\sum_i \Phi_i^\dagger e^{2gY_{\Phi_i} V} \Phi_i + \eta V \right) \Big|_{\theta\theta\bar{\theta}\bar{\theta}} \\
\mathcal{L}_{\text{interaction}} &= \mathcal{W}(\Phi_i) \Big|_{\theta\theta} + \text{h.c.} \\
&= \left(\sum_i (h_i \Phi_i) + \frac{1}{2} m_{ij} \Phi_i \Phi_j + \frac{1}{6} \lambda_{ijk} \Phi_i \Phi_j \Phi_k \right) \Big|_{\theta\theta} + \text{h.c.} \quad (8.24)
\end{aligned}$$

in which h_i is a complex number, m_{ij} and λ_{ijk} are complex tensors symmetric in their indices, and we have also included a D -term ηV with η being real, as the D -term of any vector superfield is both SUSY and supergauge invariant. The generalization to non-abelian gauge interactions is straightforward.

The use of the Lagrangian equations for the auxiliary fields which can then be eliminated gives

$$F_i = -\bar{\mathcal{W}}_i \equiv - \frac{\partial \mathcal{W}^\dagger}{\partial \Phi_i^\dagger} \Big|_{\theta=\bar{\theta}=0}, \quad F_i^* = -\mathcal{W}_i \equiv - \frac{\partial \mathcal{W}}{\partial \Phi_i} \Big|_{\theta=\bar{\theta}=0} \quad (8.25)$$

In the lagrangian 8.24 the scalar potential then reads

$$V(\phi_i) = \sum_i |F_i|^2 + \frac{1}{2} |D|^2 = \sum_i |\mathcal{W}_i|^2 + \frac{1}{2} |\eta + g\phi_i^* \frac{Y_{\Phi_i}}{2} \phi|^2 \quad (8.26)$$

where the D -term comes from the vector superfield and is dictated by SUSY and gauge invariance. The Yukawa interactions among scalar fields and fermion fields reads

$$\mathcal{L}_{\text{Yukawa}} = -\frac{1}{2} \left(\psi_i \psi_j \frac{\partial \mathcal{W}}{\partial \Phi_i \Phi_j} \Big|_{\theta=\bar{\theta}=0} + \text{h.c.} \right) \quad (8.27)$$

The superpotential then controls the shape of the scalar potential which is of utmost importance when dealing with spontaneous gauge symmetry breaking. We have finished the description of SUSY lagrangian in the very compact and elegant superspace description which generalizes the usual space-time field formalism. If we look at the lagrangian 8.24 the writing of interacting term is as in the usual field formalism, but with ordinary fields replaced by superfields and taking the F or D terms in the end. This is why the superspace description is so powerful.

8.3 Soft SUSY breaking

Up until now we have dealt with exact SUSY lagrangians, that are known to be renormalizable, see Ref. [301]. However experiments tells us that SUSY is broken: indeed as seen in section 8.1 we should observe the exact superpartner of the electron, that is a scalar selectron with the same mass $m_{\tilde{e}} = 511 \text{ keV}$. That is obviously not the case, hence SUSY has to be broken.

8.3.1 General soft SUSY beaking

If we recall the virtues of SUSY introduced in section 7 we do want to break SUSY *but still keeping these virtues*, and in particular the resolution of the weak hierarchy problem explained in section 7.1. We recall that if we take a Dirac fermion f and its scalar superpartners \tilde{f}_L, \tilde{f}_R , exact SUSY which cancels completely the 1-loop corrections to the Higgs mass leads to $m_f = m_{\tilde{f}_L} = m_{\tilde{f}_R}$, no trilinear $A_f H \tilde{f}_L \tilde{f}_R^*$ coupling and the Yukawa equality $\lambda_{\tilde{f}} = \lambda_f^2$. We still want to cancel quadratic divergences and thus keep the equality $\lambda_{\tilde{f}} = \lambda_f^2$, but break the equality $m_f = m_{\tilde{f}_{L,R}}$ and allow for $A_f \neq 0$, which means that logarithmic divergences will arise to be renormalized by the standard procedures. An explicit SUSY breaking that ensures these conditions is called soft SUSY breaking: only terms of mass dimension not higher than three are authorized in the soft SUSY breaking part of the lagrangian [301–303]. We thus have

$$\begin{aligned} \mathcal{L} &= \mathcal{L}_{\text{SUSY}} + \mathcal{L}_{\text{soft}} \\ \mathcal{L}_{\text{soft}} &= -\phi_i^*(m^2)_{ij}\phi_j + \left(\frac{1}{6}f_{ijk}A_{ijk}\phi_i\phi_j\phi_k - \frac{1}{2}(B\mu)_{ij}\phi_i\phi_j + \sum_i h_i C_i \phi_i + \text{h.c.} \right) \\ &\quad - \frac{1}{2} \left(\sum_\alpha M_\alpha \lambda_\alpha^a \lambda_\alpha^a + \text{h.c.} \right) \end{aligned} \quad (8.28)$$

M_α is the mass term for the gauginos λ_α^a , a being a gauge index for a given algebra G_α ; $(m^2)_{ij}$ is an hermitian matrix describing the mass terms for the sfermions, $h_i C_i$, $(B\mu)_{ij}$ and $f_{ijk}A_{ijk}$ being the tadpole, bilinear and trilinear scalar couplings. $\mathcal{L}_{\text{soft}}$ obviously breaks SUSY as there are no fermions nor gauge bosons within it. We note for consistency that h_i , μ_{ij} and f_{ijk} are SUSY invariant factors that come from the superpotential, see Eq. 8.24 with m replaced by μ (thus reserving m for the SUSY breaking sfermions masses terms).

The tadpole arises only with gauge singlet; as it does not appear in the minimal supersymmetric extension of the SM, we will discard this term in the rest of the thesis.

8.3.2 What is the origin of soft SUSY breaking?

It is obvious that this way of SUSY breaking is not satisfactory: we would like to have the same receipt as for the electroweak symmetry breaking, namely a spontaneous breakdown of supersymmetry that is more elegant than just explicit breaking and could explain the origin of the various SUSY breaking terms. This is one of the most tedious questions in SUSY theoretical studies nowadays and we get several mechanisms on the market, none of them being convincing in every situation. We will not come into details but rather present how can spontaneous SUSY breaking arise and what will be the impact on phenomenological studies.

In exact SUSY theories the hamiltonian is always positive, as we get, see Refs [284, 285, 299],

$$H = P_0 = \frac{1}{4}(Q_1\bar{Q}_1 + Q_2\bar{Q}_2 + \bar{Q}_1Q_1 + \bar{Q}_2Q_2) \quad (8.29)$$

If the vacuum is SUSY invariant, we should have $\delta|\Omega\rangle = \iota(\epsilon Q + \bar{\epsilon}\bar{Q})|\Omega\rangle = 0$ for any pair of $\epsilon, \bar{\epsilon}$ parameters, that is $Q|\Omega\rangle = \bar{Q}|\Omega\rangle = 0$. It then turns that **if SUSY is exact the vacuum state $|\Omega\rangle$ must have a vanishing energy**. The minimum of the scalar potential must be zero in exact SUSY theories.

Taking the other point of view, it means that as long as the scalar potential is non zero at its global minimum, we have spontaneously broken SUSY: this can be done through auxiliary F or D terms which are the only non physical fields that can play this role, as the scalar potential contains these two fields. A SUSY breaking through F -terms is called the O’Raifeartaigh mechanism [304], if we use D -terms it is called the Fayet–Iliopoulos mechanism [305]. Only F -terms ensure a spontaneously SUSY breaking with non-abelian gauge theories, see Ref. [284] page 140.

In any phenomenological theory which incorporates spontaneous symmetry breaking, such as the constrained minimal extension of the SM, the spontaneous breakdown of SUSY is assumed to arise in a “hidden sector” of the theory at the GUT scale. This hidden sector has only very small couplings (if any) to the phenomenological sector (or visible sector) and we need messengers, that is superfields that share some interactions between the hidden sector and the visible sector. There are several ways of achieving such a goal (see Refs. [284, 285] for more details), one of the most popular using gravity interactions in the minimal supergravity theory (mSUGRA). In that case SUSY is broken in the hidden sector by some vev $\langle F \rangle$ and we get the soft term in the visible sector through gravitationnal

interactions, that is:

$$m_{\text{soft}} \simeq \frac{\langle F \rangle}{M_P} \quad (8.30)$$

In this model we have the graviton and its superpartner the gravitino. The goldstino fermion, relic of the spontaneous breakdown of SUSY (in much the same way as the Goldstone boson in spontaneously broken bosonic gauge symmetry), becomes part of the gravitino field which then has got a mass. We then use renormalization group equations (RGE) to evolve the couplings from the GUT scale down to the SUSY scale where the phenomenological SUSY terms, in particular the soft SUSY beaking terms, are defined. We will present in the next section the minimal set of parameters at the GUT scale for a mSUGRA model in the MSSM.

9 The Minimal Supersymmetric Standard Model

In this part III we have already given some reasons why it is interesting to study supersymmetry by itself and we have given the SUSY formalism to construct supersymmetric theories. The content of this section is to apply these theoretical foundations to the building of a minimal extension of the SM, called the Minimal Supersymmetric Standard Model or MSSM in short. This will be minimal in the sense that we incorporate as minimal number of fields as possible. We will see that it leads to a richer Higgs phenomenology that will be discussed in the next part IV.

The first subsection will introduce the MSSM, the second subsection will explain in more details the Higgs sector; the last subsection will be an opening to theories beyond the MSSM, explaining that this latter model is not at all the end of the story for SUSY phenomenology, by introducing the famous μ -problem in the MSSM.

9.1 Fields content: Higgs and SUSY sectors of the MSSM

The sections 8.2 and 8.3 have introduced all the elements that are necessary for the minimal supersymmetric extension of the Standard Model, called the MSSM. We will give in this subsection all the superfields of the MSSM together with the soft SUSY breaking part of the lagrangian.

9.1.1 Superfields and (super)particles content

The MSSM is still based on the Lie algebra $SU(2)_L \times U(1)_Y \times SU(3)_c$. We will then introduce twelve vector superfields: the three $SU(2)_L$ superfields V_W^a , the hypercharge superfield V_Y and the eight $SU(3)_c$ superfields V_c^a .

All the chiral superfield are left handed in the MSSM. We will then introduce

$$L_i = \begin{pmatrix} L_{\nu_i} \\ L_{e_i} \end{pmatrix}, \quad \bar{E}_i \quad (9.1)$$

where the right-handed singlet leptons are represented by the chiral superfields \bar{E}_i containing e_R^C and \tilde{e}_R^* ⁶⁴. In this way all the chiral superfields are left-handed, which will be

⁶⁴The bar notation does not mean any (hermitian) conjugation, it is rather a notation in order to remind the reader that we deal with the charge conjugate of the original spinor, as we deal with left chiral superfield only.

useful for the writing of the superpotential. We have the following chiral superfields for the quarks:

$$Q_i = \begin{pmatrix} Q_{u_i} \\ Q_{d_i} \end{pmatrix}, \bar{U}_i, \bar{D}_i \quad (9.2)$$

where the same rule presented for the leptonic superfields also apply for the quark superfields. The index i runs from 1 to 3, labeling the generations.

We finally introduce the Higgs superfield, but in the context of the MSSM we have two Higgs superfields H_1 and H_2 . We will review in the next subsection (some of) the reasons to introduce more than one Higgs superfield, but it can already be noted that for consistency reason due to the analyticity of the superpotential, we should have one Higgs superfield devoted to the coupling to up-type quarks and another Higgs superfield devoted to the coupling to down-type quarks, as we cannot take the charge conjugate of only one Higgs field as in the case of the SM; otherwise we would break the analyticity of the superpotential. We thus have two $\mathbf{2}$ $SU(2)_L$ superfields doublets, H_u with hypercharge +1 and H_d with hypercharge -1:

$$H_u = \begin{pmatrix} H_u^+ \\ H_u^0 \end{pmatrix}, H_d = \begin{pmatrix} H_d^0 \\ H_d^- \end{pmatrix} \quad (9.3)$$

We list in the Table 10 below the new superparticles and Higgs fields in the MSSM in addition to the usual SM fields. It should be noted that by construction the higgsinos and gauginos are four-component Majorana spinors, thus their own charge conjugate.

After electroweak symmetry (and SUSY) breaking the Higgs and the gauginos/higgsinos sectors are affected by mixing between the different gauge eigenstates. We finally obtain 2 CP -even neutral Higgs bosons h, H , one CP -odd neutral Higgs boson A and two charged Higgs bosons H^\pm ; four neutral gauginos χ_i^0 called the neutralinos and four charged gauginos $\chi_{1,2}^\pm$ called the charginos. This is summarized in Table 11 below:

The ratio between the two Higgs vacuum expectation values (vev) v_u and v_d :

$$\tan \beta = \frac{v_u}{v_d} \quad (9.4)$$

is a fundamental parameter in the MSSM controlling much of its phenomenology as will be seen later on for example when dealing with Higgs production in the MSSM. We will discuss in more details the Higgs sector in the next subsection.

Type	Name	Spin	$SU(3)_c$ rep.	$SU(2)_L$ rep.	$U(1)_Y$ charge
SLEPTONS	$\tilde{\nu}_e, \tilde{e}_L, \tilde{\nu}_\mu, \tilde{\mu}_L, \tilde{\nu}_\tau, \tilde{\tau}_L$	0	1	2	-1
	$\tilde{e}_R, \tilde{\mu}_R, \tilde{\tau}_R$	0	1	1	2
SQUARKS	$\tilde{u}_L, \tilde{d}_L, \tilde{s}_L, \tilde{c}_L, \tilde{t}_L, \tilde{b}_L$	0	3	2	1/3
	$\tilde{u}_R, \tilde{c}_R, \tilde{t}_R$	0	3	1	-4/3
	$\tilde{d}_R, \tilde{s}_R, \tilde{b}_R$	0	3	1	2/3
GAUGINOS	\tilde{B}	1/2	1	1	1
	$\tilde{W}_1, \tilde{W}_2, \tilde{W}_3$	1/2	1	3	0
	\tilde{g}	1/2	8	1	0
HIGGSINOS	$\tilde{h}_u^+, \tilde{h}_u^0$	1/2	1	2	1
	$\tilde{h}_d^0, \tilde{h}_d^-$	1/2	1	2	-1
HIGGS	h_u^+, h_u^0	0	1	2	1
	h_d^0, h_d^-	0	1	2	-1

Table 10: The superparticles and Higgs content of the MSSM before the electroweak symmetry breaking.

Name	Spin	gauge eigenstates	mass eigenstates
Higgs	0	$h_u^+, h_u^0, h_d^0, h_d^-$	h, H, A, H^\pm
Neutralinos	1/2	$\tilde{W}_3, \tilde{B}, \tilde{h}_u^0, \tilde{h}_d^0$	$\tilde{\chi}_1^0, \tilde{\chi}_2^0, \tilde{\chi}_3^0, \tilde{\chi}_4^0$
Charginos	1/2	$\tilde{W}_{1,2}, \tilde{h}_u^+, \tilde{h}_d^-$	$\tilde{\chi}_1^\pm, \tilde{\chi}_2^\pm$

Table 11: The neutralinos, charginos and Higgs bosons in the MSSM after electroweak symmetry breaking.

9.1.2 The MSSM lagrangian

We are now ready to write down the MSSM lagrangian using all the superfields listed above, following the formal techniques described in the previous section 8. We will separate the lagrangian in the SUSY invariant part and the soft SUSY breaking part:

$$\mathcal{L}_{\text{MSSM}} = \mathcal{L}_{\text{SUSY}}^{\text{MSSM}} + \mathcal{L}_{\text{soft}}^{\text{MSSM}} \quad (9.5)$$

with

$$\begin{aligned}
\mathcal{L}_{\text{SUSY}}^{\text{MSSM}} &= \mathcal{L}_{\text{gauge}} + \mathcal{L}_{\text{matter}} + \mathcal{L}_{\text{Higgs}} \\
\mathcal{L}_{\text{gauge}} &= (W_c^a W_c^a + W_W^a W_W^a + W_Y W_Y)|_{\theta\theta} + \text{h.c.} \\
\mathcal{L}_{\text{matter}} &= \sum_{i=1}^3 \left(L_i^\dagger e^{(2gT_a V_W^a + g_Y Y_{L_i} V_Y)} L_i + \bar{E}_i^\dagger e^{g_Y Y_{E_i} V_Y} \bar{E}_i + \right. \\
&\quad \left. Q_i^\dagger e^{(2g_s V_c^a R_a + 2gT_a V_W^a + g_Y Y_{Q_i} V_Y)} Q_i + \bar{U}_i^\dagger e^{(-2g_s V_c^a \bar{R}_a + g_Y Y_{\bar{U}_i} V_Y)} \bar{U}_i + \right. \\
&\quad \left. \bar{D}_i^\dagger e^{(-2g_s V_c^a \bar{R}_a + g_Y Y_{\bar{D}_i} V_Y)} \bar{D}_i \right) \Big|_{\theta\theta\bar{\theta}\bar{\theta}} \\
\mathcal{L}_{\text{Higgs}} &= \left(H_u^\dagger e^{(2gT_a V_W^a + g_Y Y_{H_u} V_Y)} H_u + \right. \\
&\quad \left. H_d^\dagger e^{(2gT_a V_W^a + g_Y Y_{H_d} V_Y)} H_d \right) \Big|_{\theta\theta\bar{\theta}\bar{\theta}} + \mathcal{W}_{\text{MSSM}} \Big|_{\theta\theta} + \text{h.c.} \tag{9.6}
\end{aligned}$$

where a is a gauge index, T_a are the three $SU(2)_L$ generators acting on the $\mathbf{2}$ representations, R_a are the eight $SU(3)_c$ generators acting on the $\mathbf{3}$ representations and \bar{R}_a their complex conjugates acting on the $\bar{\mathbf{3}}$ representations. $\mathcal{W}_{\text{MSSM}}$ is the MSSM superpotential which is governed by gauge invariance and R -parity. Indeed in the SM both L and B are conserved, thus the natural assumption of the minimal supersymmetric extension of the SM is to assume R -parity which is related to the $B-L$ invariance. The superpotential contains both the Yukawa interactions and the SUSY invariant scalar potential, and then reads [284]:

$$\mathcal{W}_{\text{MSSM}} = -\mu H_u \cdot H_d - \lambda_{ij}^e (H_d \cdot L_i) \bar{E}_j - \lambda_{ij}^d (H_d \cdot Q_i) \bar{D}_j - \lambda_{ij}^u (Q_i \cdot H_u) \bar{U}_j \tag{9.7}$$

where $Q \cdot R \equiv \epsilon_{AB} Q^A R^B$ for A, B as $SU(2)_L$ indices and $\epsilon_{01} = -\epsilon_{10} = -1$. From this superpotential we can extract the SUSY invariant scalar potential that will be introduced in the next subsection when dealing specifically with the Higgs sector of the MSSM.

The last piece that remains is the soft SUSY breaking part. We start from the general lagrangian in Eq. 8.28, retaining only the gauge and R -parity invariant terms, in particular we discard the tadpole terms as the MSSM does not contain any gauge singlet. It eventually

reads

$$\begin{aligned}
-\mathcal{L}_{\text{soft}}^{\text{MSSM}} = & (m_{\tilde{q}}^2)_{ij} \tilde{q}_{iL}^* \tilde{q}_{jL} + (m_{\tilde{l}}^2)_{ij} \tilde{l}_{iL}^* \tilde{l}_{jL} + (m_{\tilde{e}}^2)_{ij} \tilde{e}_{iR}^* \tilde{e}_{jR} + (m_{\tilde{u}}^2)_{ij} \tilde{u}_{iR}^* \tilde{u}_{jR} + \\
& (m_{\tilde{d}}^2)_{ij} \tilde{d}_{iR}^* \tilde{d}_{jR} + m_{H_u}^2 h_u^\dagger h_u + m_{H_d}^2 h_d^\dagger h_d - (B\mu h_u \cdot h_d + \text{h.c.}) + \\
& \left(\lambda_{ij}^e A_{ij}^e (h_d \cdot \tilde{l}_{iL}) \tilde{e}_{jR}^* + \lambda_{ij}^d A_{ij}^d (h_d \cdot \tilde{q}_{iL}) \tilde{d}_{jR}^* + \right. \\
& \left. \lambda_{ij}^u A_{ij}^u (\tilde{q}_{iL} \cdot h_u) \tilde{u}_{jR}^* + \text{h.c.} \right) + \frac{1}{2} \left(M_1 \tilde{B} P_L \tilde{B} + M_2 \tilde{B} P_R \right) + \\
& \frac{1}{2} \left(M_2 \tilde{W}_a P_L \tilde{W}_a + M_2^* \tilde{W}_a P_R \tilde{W}_a \right) + \\
& \frac{1}{2} \left(M_3 \tilde{g}_a P_L \tilde{g}_a + M_3^* \tilde{g}_a P_R \tilde{g}_a \right)
\end{aligned} \tag{9.8}$$

where the fields have been defined in Table. 10 and with $P_L \equiv (1 - \gamma_5)/2$, $P_R \equiv (1 + \gamma_5)/2$ being the left and right chiral projectors. The repeated gauge index a are summed implicitly. M_i are the complex Majorana gauginos SUSY breaking mass parameters, $m_{1,2}$ are the real Higgs SUSY breaking mass parameters. The sleptons and squarks mass parameters are 3×3 hermitian matrices. Finally the trilinear couplings $A_{ij}^{e,u,d}$ are 3×3 complex matrices of mass dimension; the B parameter is real and is also of mass dimension.

If one counts all the new parameters, the general (or unconstrained) MSSM has 134 new parameters. This huge parameter space needs to be reduced to allow for viable phenomenological studies: that is the case in the constrained versions of the MSSM (cMSSM) where some assumptions such as no CP -violating mass matrices, mass unification at GUT scale, universality of the two first generations of squarks and sleptons, etc. As the origin of many new parameters lies in the soft SUSY breaking part of the MSSM, many phenomenological studies assume a definite SUSY breaking scheme at higher scale, such as the mSUGRA scheme, that induces the soft SUSY breaking parameters through renormalisation group evolution (RGE) of the parameters down to the weak scale. In such constrained version of the MSSM, everything is typically controlled by four parameters:

$$m_0, M_{1/2}, A_0, \tan \beta, \text{sign}(\mu) \tag{9.9}$$

where m_0 is the common scalar mass, $M_{1/2}$ is the common gaugino mass, A_0 is the common trilinear coupling, $\tan \beta$ is the vev ratio and $\text{sign}(\mu)$ is the sign of the invariant SUSY parameter μ .

9.1.3 Some experimental constraints on the sparticles masses

We end this subsection by giving some experimental limits to the mass of the yet-to-be-observed sparticles. These limits have been obtained at the LEP, Tevatron⁶⁵ and very recently LHC colliders in the ATLAS [306,307] and CMS [308,309] experiments. The limits are usually given within the cMSSM, that is assuming R -parity, gauginos mass unification at the GUT scale, first and second generations universality in the squark sector along with the condition $m_{\tilde{q}_L} = m_{\tilde{q}_R}$. We have at 95%CL:

$$\begin{aligned} m_{\tilde{\chi}_1^0} &> 46 \text{ GeV}, & m_{\tilde{\chi}_2^0} &> 62.4 \text{ GeV}, \\ m_{\tilde{\chi}_3^0} &> 99.9 \text{ GeV}, & m_{\tilde{\chi}_4^0} &> 116 \text{ GeV}, & m_{\tilde{\chi}_1^\pm} &> 94 \text{ GeV} \end{aligned} \quad (9.10)$$

Apart from the lightest neutralino, these limits assume $1 \leq \tan \beta \leq 40$. We also have for the gluinos

$$\begin{aligned} m_{\tilde{g}} &> 308 \text{ GeV}; & m_{\tilde{g}} &\gtrsim 500 - 700 \text{ GeV} \text{ if assuming } m_{\tilde{q}} = m_{\tilde{g}} \\ & & &\text{and depending on the mSUGRA parameters} \end{aligned} \quad (9.11)$$

The squarks limits strongly depends on the parameter space point. Nevertheless the gross limit either at LEP/Tevatron or at the LHC points out to

$$m_{\tilde{q}} \gtrsim 400 - 500 \text{ GeV} \quad (9.12)$$

which can be loosen for the stop and sbottom masses:

$$m_{\tilde{b}} > 89 \text{ GeV}, \quad m_{\tilde{t}} > 95 \text{ GeV} \quad (9.13)$$

The limits on the sleptons use the same assumptions as for the charginos and neutralinos and read:

$$m_{\tilde{e}_R} > 107 \text{ GeV}, \quad m_{\tilde{\mu}_R} > 94 \text{ GeV}, \quad m_{\tilde{\tau}_R} > 81.9 \text{ GeV} \quad (9.14)$$

9.2 The Higgs sector and the number of Higgs doublets

After having presented the full MSSM we move on to a more detailed analysis of its Higgs sector that will be discussed at hadron colliders in the next part IV. We first remind the reason to introduce two Higgs doublet instead of the minimal choice in the SM; we then present the Higgs scalar potential in the MSSM and the electroweak symmetry breaking, intimately connected to that of SUSY; we end by presenting the masses and couplings of the MSSM Higgs bosons.

⁶⁵For the LEP and Tevatron searches, see the review in Ref. [211]. We have taken the PDG limits [205] for these experiments.

9.2.1 The number of Higgs doublet in the MSSM

We have already presented one reason to introduce two Higgs doublets within the MSSM. Indeed the mathematical formulation of the MSSM requires that the superpotential, encoding all the SUSY invariant interactions between the chiral superfields that represent the fermions and their sfermions superpartners, to be a holomorphic expression of these superfields. In particular this means that there will be no Φ^\dagger term that was used in the case of the SM to give rise to up-type quark using the $\tilde{\phi} = i\tau_2\phi^*$ field. In other words, $\mathbf{2}$ and $\bar{\mathbf{2}}$ $SU(2)_L$ representations are not equivalent in SUSY theories contrary to the case of the SM.

Even if we were not to look for a way to give a mass to fermions we would require two Higgs doublets. Indeed, we know that the SM is free from gauge anomalies and in particular the Adler–Bardeen–Jackiw anomalies originating from triangular fermionic loops with axial–vector current couplings [310]. Gauge anomalies would be disastrous, spoiling the renormalizability and the gauge identities, but the fact that the sum of the hypercharges of all the fifteen chiral fermions (or charges, related to hypercharges through the Gell–Mann–Nishijima relation, see section 1.2) is zero in the SM explains the vanishing of these chiral anomalies, $\text{Tr}(Y_f) = \text{Tr}(Q_f) = 0$. In the MSSM, SUSY introduces new fermions in the theory as superpartners of the standard bosons, in particular in the higgsino sector. If we were to have only one Higgs doublet with a definite hypercharge, we would be left with the charged higgsino not cancelled by anything in the trace sum rule and thus the anomaly cancellation would be spoiled. With two doublets of Higgs fields with opposite hypercharge, the cancellation of chiral anomalies still takes place [311].

We now have two solid reasons to introduce two Higgs doublet within the MSSM, making the minimal supersymmetric extension of the SM a particular case of 2 Higgs doublet models (2HDM), more precisely a 2HDM of type II, see Ref. [44] for a review. We will now sketch the electroweak symmetry breaking within the MSSM.

9.2.2 The electroweak symmetry breaking in the MSSM

We recall that we use the following Higgs doublets:

$$h_u = \begin{pmatrix} h_u^+ \\ h_u^0 \end{pmatrix}, \quad h_d = \begin{pmatrix} h_d^0 \\ h_d^- \end{pmatrix} \quad (9.15)$$

We first need to write down the Higgs scalar potential in the MSSM. We break the

potential into a SUSY invariant part and a soft part

$$V = V_{\text{SUSY}} + V_{\text{soft}} \quad (9.16)$$

where V_{SUSY} comes from the superpotential 9.7 and the gauge D -terms while V_{soft} comes from the soft SUSY breaking lagrangian in Eq. 9.8. We then have [211, 285]:

$$\begin{aligned} V_{\text{SUSY}} &= |\mu|^2 (|h_u^0|^2 + |h_d^0|^2 + |h_u^+|^2 + |h_d^-|^2) + \\ &\quad \frac{(g^2 + g_Y^2)}{8} (|h_d^0|^2 + |h_d^-|^2 - |h_u^0|^2 - |h_u^+|^2)^2 + \\ &\quad \frac{g^2}{2} |h_d^{0*} h_u^+ + h_d^{-*} h_u^0|^2 \\ V_{\text{soft}} &= m_{H_u}^2 (|h_u^0|^2 + |h_u^+|^2) + m_{H_d}^2 (|h_d^0|^2 + |h_d^-|^2) + \\ &\quad B\mu (h_u^+ h_d^- - h_u^0 h_d^0 + \text{c.c.}) \end{aligned} \quad (9.17)$$

We want that the minimum of the scalar potential V breaks $SU(2)_L \times U(1)_Y$ down to $U(1)_{\text{EM}}$. Without any loss of generality we can assume that $\langle h_u^+ \rangle = 0$ at the minimum using the freedom of a gauge $SU(2)_L$ rotation. Together with the minimization equation $\partial V / \partial h_u^+ = 0$ we obtain $\langle h_d^- \rangle = 0$, a result that could have been predicted as the vacuum should not break $U(1)_{\text{EM}}$ thus not being charged. We are left with:

$$\langle h_u \rangle = \frac{1}{\sqrt{2}} \begin{pmatrix} 0 \\ v_u \end{pmatrix}, \quad \langle h_d \rangle = \frac{1}{\sqrt{2}} \begin{pmatrix} v_d \\ 0 \end{pmatrix} \quad (9.18)$$

with v_u and v_d real positive numbers. A $U(1)$ rotation of the fields h_u^0 and h_d^0 can make $B\mu$ as a real positive number too, thus the potential does conserve CP at tree-level.

The pattern of the vacuum expectation value is more complicated than compared to the SM case as we now have two vacuum expectation values (vev) v_u and v_d . The coupling of the Higgs doublets to the gauge bosons remain as in the SM case, thus we can define the weak bosons masses to be the same as in the SM case, that is:

$$\begin{aligned} v_u^2 + v_d^2 &= v_{\text{SM}}^2 \simeq 246 \text{ GeV}, \\ M_W &= \frac{1}{2} g v_{\text{SM}}, \quad M_Z = \frac{1}{2} \sqrt{g^2 + g_Y^2} v_{\text{SM}} \end{aligned} \quad (9.19)$$

SUSY being broken the scalar potential is not always positive. V must be bounded from below to develop a vev; along the so-called D -flat direction $|h_u^0| = |h_d^0|$ the quartic term vanishes and the stability requirement thus imposes the following condition [211, 284, 285]:

$$m_{H_u}^2 + m_{H_d}^2 + 2|\mu|^2 > 2B\mu \quad (9.20)$$

This relation must hold at any perturbative order, that is even in the case where the coefficients become running quantities. In addition we need to be sure that a linear combination of the two neutral Higgs fields has a negative mass squared term in order to have spontaneous electroweak symmetry breaking. The mass matrix is $\partial V/\partial h_u^0 \partial h_d^0$ and the quadratic part of V reads

$$\begin{pmatrix} h_u^{0*} & h_d^0 \end{pmatrix} \begin{pmatrix} m_{H_u}^2 + |\mu|^2 & -B\mu \\ -B\mu & m_{H_d}^2 + |\mu|^2 \end{pmatrix} \begin{pmatrix} h_u^0 \\ h_d^{0*} \end{pmatrix} \quad (9.21)$$

and its trace being positive because of Eq. 9.20 its determinant must be negative:

$$(B\mu)^2 > (m_{H_u}^2 + |\mu|^2)(m_{H_d}^2 + |\mu|^2) \quad (9.22)$$

If not the stable minimum is along the D -flat direction $\langle h_u^0 \rangle = \langle h_d^0 \rangle = 0$. The very interesting remark is that the two conditions 9.20 and 9.22 are not fulfilled if $m_{H_u}^2 = m_{H_d}^2$ and in particular if these two soft SUSY breaking terms vanish. This means that the electroweak symmetry breaking in the MSSM requires that SUSY be broken: there is a deep connection between SUSY and electroweak symmetry breakings. Furthermore the electroweak symmetry breaking can be driven radiatively: starting from a very high energy input scale where $m_{H_u}^2 = m_{H_d}^2$ (even equal to zero before SUSY breaking in the hidden sector), RGE evolution with the top/stop and bottom/sbottom contributions does lift the degeneracy, ending with $m_{H_u}^2 < 0$ or $m_{H_u}^2 \ll m_{H_d}^2$. This is known as the radiative electroweak symmetry breaking [312–314] which is a very elegant way to obtain a gauge symmetry breaking, not having imposed at first the negative value of the squared mass in the scalar potential.

9.2.3 The masses and couplings of the MSSM Higgs bosons

Charged Higgs, CP -even and CP -odd neutral Higgs masses

We have seen in the previous subsection the Higgs scalar potential of the MSSM which controls the electroweak symmetry breaking. We will now diagonalize the equation 9.17 to obtain the physical Higgs bosons states.

We will expand the Higgs fields around the minimum (v_u, v_d) :

$$h_u = \frac{1}{\sqrt{2}} \begin{pmatrix} \sqrt{2}h_u^+ \\ (h_u^0 + iG_u^0 + v_u) \end{pmatrix}, \quad h_d = \frac{1}{\sqrt{2}} \begin{pmatrix} (h_d^0 + iG_d^0 + v_d) \\ \sqrt{2}h_d^- \end{pmatrix} \quad (9.23)$$

where this time all the fields but those of the charged are reals (we use the same notation for the full fields and the expanded fields, but there should be no confusion from now on).

The first step is to expand the scalar potential at the minimum only, which gives

$$V_{\min} = \frac{1}{2}m_1^2 v_d^2 + \frac{1}{2}m_2^2 v_u^2 - B\mu v_u v_d + \frac{g^2 + g_Y^2}{32} (v_d^2 - v_u^2)^2 \quad (9.24)$$

where we have $m_1^2 \equiv m_{H_d}^2 + |\mu|^2$ and $m_2^2 \equiv m_{H_u}^2 + |\mu|^2$. Using $\partial V_{\min}/\partial v_u = \partial V_{\min}/\partial v_d = 0$ this gives the two consistency conditions below:

$$\begin{aligned} m_1^2 &= B\mu \tan \beta - \frac{1}{2}M_Z^2 \cos(2\beta) \\ m_2^2 &= B\mu \cotan \beta + \frac{1}{2}M_Z^2 \cos(2\beta) \end{aligned} \quad (9.25)$$

when we have used $v_u = v \cos \beta$ and $v_d = v \sin \beta$ together with the expression of M_Z in term of SM vacuum expectation value v . The consistency conditions of Eq. 9.25 implies a reduction of the number of free parameters in the Higgs sector.

We rewrite the scalar potential of Eq. 9.17 in terms of the real fields:

$$\begin{aligned} V &= \frac{1}{2}m_1^2 \left((v_d + h_d^0)^2 + G_d^{02} + 2|h_d^-|^2 \right) + \frac{1}{2}m_2^2 \left((v_u + h_u^0)^2 + G_u^{02} + 2|h_u^+|^2 \right) - \\ &\frac{1}{2}B\mu \left((v_u + h_u^0 + iG_u^0)(v_d + h_d^0 + iG_d^0) + \text{c.c.} - 2h_u^+ h_d^- + \text{c.c.} \right) + \\ &\frac{1}{4}g^2 |(v_d + h_d^0 + iG_d^0)h_u^+ + (v_u + h_u^0 + iG_u^0)h_d^-|^2 + \frac{1}{32} \times \\ &(g^2 + g_Y^2) \left((v_d + h_d^0)^2 + G_d^{02} + 2|h_d^+|^2 - (v_u + h_u^0)^2 - G_u^{02} - 2|h_u^-|^2 \right)^2 \end{aligned} \quad (9.26)$$

We will now read each quadratic part of the potential depending on our interest in the CP -even neutral Higgs bosons (h_u^0, h_d^0), the CP -odd neutral Higgs bosons (G_u^0, G_d^0) or the charged Higgs bosons (h_u^+, h_d^-).

- CP -odd Higgs boson A :

We read the quadratic part in Eq. 9.26:

$$\begin{aligned} V_{\text{quadratic}}^A &= \frac{1}{2}m_1^2 G_d^{02} + \frac{1}{2}m_2^2 G_u^{02} + \frac{1}{2}B\mu(G_d^0 G_u^0 + G_u^0 G_d^0) + \\ &\frac{1}{32} (g^2 + g_Y^2) \left(2v_u^2 G_u^{02} + 2v_d^2 G_d^{02} - 2v_u^2 G_d^{02} - 2v_d^2 G_u^{02} \right) \\ &= \frac{1}{2} (G_u^0, G_d^0) \begin{pmatrix} m_2^2 + \frac{1}{8}(g^2 + g_Y^2)(v_u^2 - v_d^2) & B\mu \\ B\mu & m_1^2 - \frac{1}{8}(g^2 + g_Y^2)(v_u^2 - v_d^2) \end{pmatrix} \begin{pmatrix} G_u^0 \\ G_d^0 \end{pmatrix} \\ &= \frac{1}{2} (G_u^0, G_d^0) \begin{pmatrix} B\mu \cotan \beta & B\mu \\ B\mu & B\mu \tan \beta \end{pmatrix} \begin{pmatrix} G_u^0 \\ G_d^0 \end{pmatrix} \end{aligned} \quad (9.27)$$

where we have used in the last line the two consistency conditions in Eq. 9.25. The vanishing determinant together with the non-vanishing trace implies a neutral Goldstone boson (which combines with the Z boson to give its mass) and a massive CP -odd Higgs boson A . We then have

$$\begin{pmatrix} G^0 \\ A \end{pmatrix} = \begin{pmatrix} \cos \beta & -\sin \beta \\ \sin \beta & \cos \beta \end{pmatrix} \begin{pmatrix} G_d^0 \\ G_u^0 \end{pmatrix}, \quad M_A^2 = \frac{2B\mu}{\sin(2\beta)}, \quad M_{G^0}^2 = 0 \quad (9.28)$$

In the unitarity gauge the Goldstone boson disappears as in the SM case.

- CP -even Higgs bosons (h, H):

We do the same exercise from Eq. 9.26 with the real components of the neutral Higgs fields:

$$\begin{aligned} V_{\text{quadratic}}^{HH} &= \frac{1}{2}m_1^2 h_d^0{}^2 + \frac{1}{2}m_2^2 h_u^0{}^2 - \frac{1}{2}B\mu(h_u^0 h_d^0 + h_d^0 h_u^0) + \\ &\quad \frac{1}{32}(g^2 + g_Y^2) \left(6v_u^2 h_u^0{}^2 + 6v_d^2 h_d^0{}^2 - 2v_u^2 h_d^0{}^2 - 2v_d^2 h_u^0{}^2 - 8v_u v_d h_u^0 h_d^0 \right) \\ &= \frac{1}{2} \begin{pmatrix} h_u^0 & h_d^0 \end{pmatrix} \mathcal{M}_H \begin{pmatrix} h_u^0 \\ h_d^0 \end{pmatrix} \end{aligned} \quad (9.29)$$

with \mathcal{M}_H being the following mass matrix

$$\begin{aligned} \mathcal{M}_H &= \begin{pmatrix} m_2^2 + \frac{1}{8}(g^2 + g_Y^2)(3v_u^2 - v_d^2) & -\frac{1}{4}(g^2 + g_Y^2)v_u v_d - B\mu \\ -\frac{1}{4}(g^2 + g_Y^2)v_u v_d - B\mu & m_1^2 + \frac{1}{8}(g^2 + g_Y^2)(3v_d^2 - v_u^2) \end{pmatrix} \\ &= \begin{pmatrix} M_A^2 \cos^2 \beta + M_Z^2 \sin^2 \beta & -(M_A^2 + M_Z^2) \sin \beta \cos \beta \\ -(M_A^2 + M_Z^2) \sin \beta \cos \beta & M_A^2 \sin^2 \beta + M_Z^2 \cos^2 \beta \end{pmatrix} \end{aligned} \quad (9.30)$$

where in the last line we have used both the consistency conditions of Eq. 9.25 and the result of Eq. 9.28 on the CP -odd Higgs mass M_A^2 . The determinant of the mass matrix does not vanish, meaning that the spectrum contains two physical CP -even Higgs bosons conventionally named h for the lightest and H for the heaviest. The rotation matrix is more complicated than in the CP -odd case. Together with the physical masses we have

$$\begin{aligned} \begin{pmatrix} h \\ H \end{pmatrix} &= \begin{pmatrix} \cos \alpha & -\sin \alpha \\ \sin \alpha & \cos \alpha \end{pmatrix} \begin{pmatrix} h_u^0 \\ h_d^0 \end{pmatrix} \\ M_{h,H}^2 &= \frac{1}{2} \left(M_A^2 + M_Z^2 \mp \sqrt{(M_A^2 + M_Z^2)^2 - 4M_A^2 M_Z^2 \cos(2\beta)^2} \right) \end{aligned} \quad (9.31)$$

with the mixing angle α given by

$$\begin{aligned} \cos(2\alpha) &= -\cos(2\beta) \frac{M_A^2 - M_Z^2}{M_H^2 - M_h^2} \\ \sin(2\alpha) &= -\sin(2\beta) \frac{M_H^2 + M_h^2}{M_H^2 - M_h^2} \end{aligned} \quad (9.32)$$

- *Charged Higgs boson H^\pm :*

We end with the charged Higgs boson mass matrix. From Eq. 9.26 we read:

$$\begin{aligned}
V_{\text{quadratic}}^{H^\pm} &= m_1^2 |h_d^-|^2 + m_2^2 |h_u^+|^2 + B\mu (h_u^+ h_d^- + h_u^- h_d^+) + \\
&\quad \frac{1}{4} g^2 (v_d^2 |h_u^+|^2 + v_u^2 |h_d^-|^2 + v_u v_d (h_u^+ h_d^- + h_u^- h_d^+)) + \\
&\quad \frac{1}{16} (2v_u^2 |h_u^+|^2 + 2v_d^2 |h_d^-|^2 - 2v_d^2 |h_u^+|^2 - 2v_u^2 |h_d^-|^2) \\
&= \begin{pmatrix} h_u^+ & h_d^+ \end{pmatrix} \mathcal{M}_{H^\pm} \begin{pmatrix} h_u^- \\ h_d^- \end{pmatrix} \tag{9.33}
\end{aligned}$$

with \mathcal{M}_{H^\pm} being the following charged Higgs matrix

$$\begin{aligned}
\mathcal{M}_{H^\pm} &= \begin{pmatrix} m_2^2 + \frac{1}{4} g^2 v_d^2 + \frac{1}{8} (g^2 + g_Y^2) (v_u^2 - v_d^2) & B\mu + \frac{1}{4} g^2 v_u v_d \\ B\mu + \frac{1}{4} g^2 v_u v_d & m_1^2 + \frac{1}{4} g^2 v_u^2 - \frac{1}{8} (g^2 + g_Y^2) (v_u^2 - v_d^2) \end{pmatrix} \\
&= \begin{pmatrix} (M_A^2 + M_W^2) \cos^2 \beta & (M_A^2 + M_W^2) \sin \beta \cos \beta \\ (M_A^2 + M_W^2) \sin \beta \cos \beta & (M_A^2 + M_W^2) \sin^2 \beta \end{pmatrix} \tag{9.34}
\end{aligned}$$

Again the vanishing determinant and the non-vanishing trace signal a pair of Goldstone bosons G^\pm (which give the mass to the charged W^\pm bosons) and two physical charged Higgs bosons H^\pm . The rotation matrix is the same as in the case of the CP -odd Higgs boson and we have

$$\begin{pmatrix} G^\pm \\ H^\pm \end{pmatrix} = \begin{pmatrix} \cos \beta & -\sin \beta \\ \sin \beta & \cos \beta \end{pmatrix} \begin{pmatrix} h_d^\pm \\ h_u^\pm \end{pmatrix}, \quad M_{H^\pm}^2 = M_A^2 + M_W^2, \quad M_{G^\pm}^2 = 0 \tag{9.35}$$

At tree-level we then have two parameters only which control the Higgs sector: the vevs ratio $\tan \beta$ and the CP -odd Higgs boson mass M_A . All the other masses and mixing angles (and also couplings, see below) follow from these two inputs. We also have a strong hierarchy in the spectrum and in particular $M_h \leq M_Z$. However it is well known that the radiative corrections (hopefully!) enhance the MSSM Higgs bosons masses (see Ref. [211] for a review): indeed we have stop/top contribution which increases the lightest Higgs boson and according to Ref. [285] we have at the one-loop order

$$\Delta(M_h^2) = \frac{3}{4\pi^2} \cos^2 \alpha \lambda_t^2 m_t^2 \ln \left(\frac{m_{\tilde{t}_1} m_{\tilde{t}_2}}{m_t^2} \right) \tag{9.36}$$

which helps having the lightest Higgs boson h above the LEP bound $M_{H_{\text{SM}}} > 114.4$ GeV as often the Higgs boson h is SM-like, thus bounded by the experimental SM limits. Including all known corrections up to three-loops order (see Refs. 185 to 194 in Ref. [285] for some of them) we have

$$M_h^2 \lesssim 135 \text{ GeV} \tag{9.37}$$

with $m_t = 173.1$ GeV (see Ref. [211] page 68). Direct searches at LEP have also put the followings lower bounds [315]:

$$M_{h,H} \gtrsim 92.6 \text{ GeV}, \quad M_A \gtrsim 93.4 \text{ GeV}, \quad M_{H^\pm} \gtrsim 78.6 \text{ GeV} \quad (9.38)$$

Higgs bosons couplings to fermions

Due to the huge number of new states in the MSSM, we will not give the full list⁶⁶. As we are interested in the Higgs production at hadron colliders in the main channels, we will simply give the couplings that are of interest to our goal: the couplings of the Higgs bosons to fermions.

We recall that the Yukawa interactions come directly from the superpotential \mathcal{W} through (in four-components notation):

$$\mathcal{L}_{\text{Yukawa}} = -\frac{1}{2} \sum_{ij} \left(\bar{\psi}_{iL} \frac{\partial \mathcal{W}}{\partial \Phi_i \partial \Phi_j} \Big|_{\theta=\bar{\theta}=0} \psi_{jL} + \text{h.c.} \right) \quad (9.39)$$

Using the MSSM superpotential written in Eq. 9.7 and introducing the chiral projector operators $P_{L,R}$ we have for the first generation [211], the scheme being repeated for the other two:

$$\mathcal{L}_{\text{Yukawa}} = -\lambda_u (\bar{u} P_L u h_u^0 - \bar{u} P_L d h_u^+) - \lambda_d (\bar{d} P_L d h_d^0 - \bar{d} P_L u h_d^-) + \text{h.c.} \quad (9.40)$$

In the lagrangian 9.40 above we have used the full Higgs fields without any expansion around the minimum. The fermion masses are generated when the neutral components of the Higgs fields acquire their vacuum expectation values; they read in terms of the Yukawa couplings, using the expansion of Eq. 9.23 with $v_u = v \sin \beta$ and $v_d = v \tan \beta$, v being the SM vacuum expectation value:

$$m_u = \lambda_u \sin \beta \frac{v}{\sqrt{2}}, \quad m_d = \lambda_d \cos \beta \frac{v}{\sqrt{2}} \quad (9.41)$$

We now expand the Higgs fields around their vevs using the physical fields expressed with Eqs. 9.28, 9.31, 9.35:

$$\begin{aligned} \mathcal{L}_{\text{Yukawa}} = & -\frac{m_u}{v \sin \beta} \left(\bar{u} u (H \sin \alpha + h \cos \alpha) - i \bar{u} \gamma_5 u A \cos \beta \right) \\ & -\frac{m_d}{v \cos \beta} \left(\bar{d} d (H \cos \alpha - h \sin \alpha) - i \bar{d} \gamma_5 d A \sin \beta \right) \\ & + \frac{1}{v \sqrt{2}} V_{ud} \left[H^+ \bar{u} \left(m_d \tan \beta (1 + \gamma_5) + m_u \cotan \beta (1 - \gamma_5) \right) d \right] \\ & + \frac{1}{v \sqrt{2}} V_{ud}^* \left[H^- \bar{d} \left(m_d \tan \beta (1 - \gamma_5) + m_u \cotan \beta (1 + \gamma_5) \right) u \right] \end{aligned} \quad (9.42)$$

⁶⁶The full list is available in standard textbooks and reviews, see e.g. Refs. [211, 284].

with V_{ud} the CKM matrix element which is present in the case of the quarks. The lagrangian of Eq. 9.42 is repeated for the two other generations and has the same structure. The MSSM Higgs boson couplings to fermions are thus given by

$$\begin{aligned}
G_{h uu} &= i \frac{m_u \cos \alpha}{v \sin \beta}, & G_{H uu} &= i \frac{m_u \sin \alpha}{v \sin \beta}, & G_{A uu} &= \frac{m_u}{v} \cot \beta \gamma_5 \\
G_{h dd} &= -i \frac{m_d \sin \alpha}{v \cos \beta}, & G_{H dd} &= i \frac{m_d \cos \alpha}{v \cos \beta}, & G_{A dd} &= \frac{m_d}{v} \tan \beta \gamma_5 \\
G_{H^+ \bar{u} d} &= -\frac{i}{\sqrt{2}v} V_{ud} \left(m_d \tan \beta (1 + \gamma_5) + m_u \cot \beta (1 - \gamma_5) \right) \\
G_{H^- u \bar{d}} &= -\frac{i}{\sqrt{2}v} V_{ud}^* \left(m_d \tan \beta (1 - \gamma_5) + m_u \cot \beta (1 + \gamma_5) \right)
\end{aligned} \tag{9.43}$$

What can be noted from these couplings? First we have to say that directly for the charged Higgs bosons H^\pm and the pseudoscalar A boson their couplings to up-type fermions (u, c, t quarks) are suppressed as $\tan \beta$ grows whereas their couplings to down-type fermions (d, s, b quarks and charged leptons) are greatly enhanced. This has a great impact on MSSM Higgs production at colliders as will be seen in the next part IV, as in the heavy quarks sector we have a very strong coupling between the A boson and the bottom quark whereas the At coupling is strongly suppressed. This side remark is also true for the CP -even Higgs bosons h, H , as if we rescale their couplings to those of the SM we have:

$$\begin{aligned}
g_{h dd} &= -\frac{\sin \alpha}{\cos \beta} = \sin(\beta - \alpha) - \tan \beta \cos(\beta - \alpha) \\
g_{h uu} &= \frac{\cos \alpha}{\sin \beta} = \sin(\beta - \alpha) + \cot \beta \cos(\beta - \alpha) \\
g_{H dd} &= \frac{\cos \alpha}{\cos \beta} = \cos(\beta - \alpha) + \tan \beta \sin(\beta - \alpha) \\
g_{H uu} &= \frac{\sin \alpha}{\sin \beta} = \cos(\beta - \alpha) - \cot \beta \sin(\beta - \alpha)
\end{aligned} \tag{9.44}$$

which means that (though depending of the magnitude of $\cos(\beta - \alpha)$ or $\sin(\beta - \alpha)$) the $dd(uu)$ coupling of either the h or H boson are enhanced (suppressed) by a factor $\tan \beta$.

9.3 The MSSM is not the end of the story

This last subsection will close the presentation of the MSSM and is intended as a door opened to theories beyond the minimal supersymmetric extension of the SM. Indeed it is well known that the MSSM suffers from difficulties even if it solves many problems within the SM, some having been highlighted in section 7. It then should be fair to present the limitations of this thesis and to put in perspectives the beauty of the MSSM.

One of the celebrated issues is the so-called “ μ problem” which can be traced as a naturalness issue. Indeed, let us start with the two equalities in Eq. 9.25 which have to be fulfilled to obtain a consistent electroweak vacuum. These can be rewritten as

$$\begin{aligned} B\mu &= \frac{(m_{H_u}^2 - m_{H_d}^2) \tan(2\beta) - M_Z^2 \sin(2\beta)}{2} \\ |\mu|^2 &= \frac{\sin^2 \beta m_{H_u}^2 - \cos^2 \beta m_{H_d}^2}{\cos(2\beta)} - \frac{1}{2} M_Z^2 \end{aligned} \quad (9.45)$$

The two equalities in Eq. 9.45 above highlight the μ -problem: $m_{H_{u,d}}^2$ being soft SUSY breaking terms they are at most two orders of magnitude of M_Z^2 , which means that on the overall μ has to be of the order of the soft SUSY breaking terms and cannot be null in order to have a correct electroweak symmetry breaking. This is unnatural as μ is a SUSY invariant term which then is naturally of the order of the highest scale of the theory, that are either the GUT scale where SUSY is broken or even the Planck scale. What is the mechanism which forces a SUSY invariant parameter to be of the same order of the soft terms⁶⁷?

One (elegant) solution is to introduce a new singlet superfield S in the theory, which then extends to the NMSSM for Next-to-MSSM [316, 317] which was actually born even before the MSSM. Two new couplings λ and κ are introduced in the lagrangian and the superpotential reads

$$\begin{aligned} \mathcal{W}_{\text{NMSSM}} &= -\lambda S H_u \cdot H_d - \frac{1}{3} \kappa S^3 - \lambda_{ij}^e (H_d \cdot L_i) \bar{E}_j \\ &\quad - \lambda_{ij}^d (H_d \cdot Q_i) \bar{D}_j - \lambda_{ij}^u (Q_i \cdot H_u) \bar{U}_j \end{aligned} \quad (9.46)$$

the trilinear S^3 term is necessary to prevent the NMSSM lagrangian to possess a \mathbf{Z}_3 symmetry which would lead to domain walls in cosmology. An effective μ term is generated when S acquires a vev:

$$\mu_{\text{eff}} = \lambda \langle S \rangle \quad (9.47)$$

which is then naturally of the order of the soft SUSY breaking terms, thus solving the μ -problem. The soft SUSY breaking terms read

$$-\mathcal{L}_{\text{soft}} = -\mathcal{L}_{\text{MSSM soft}} + m_S^2 s^2 - \frac{1}{3} \kappa A_\kappa s^3 - \lambda A_\lambda s h_1 \cdot h_2 \quad (9.48)$$

The phenomenology is richer than in the MSSM. Indeed the new singlet superfield adds two Higgs fields and two Higgsino fields, which mix with other fields to end up with [318, 319]:

⁶⁷One might argue that this is a rather subjective argument to go beyond the MSSM, Nature being perhaps “unnatural”. However one of the arguments to introduce supersymmetry is precisely the naturalness argument applied on the Higgs boson mass. It would be rather strange to reject the naturalness argument on the one hand and to accept it on the other hand.

- 3 CP -even Higgs bosons $h_{1,2,3}$;
- 2 CP -odd Higgs bosons a_1, a_2 ;
- 5 neutralinos $\tilde{\chi}_{1..5}^0$.

The lightest neutralino can be singlino-like, affecting the dark matter searches. The next-to-lightest supersymmetric particle (NLSP) can be charged, ending up with long-lived $\tilde{\tau}$ tracks thus being a golden signal for the NMSSM⁶⁸. All these features are reviewed in Ref. [320]; it is worth mentioning that adding this new singlet in the theory reduces the MSSM fine-tuning, that is the requirement of having large corrections to the lightest MSSM Higgs boson in order to cross the M_Z value. Indeed the NMSSM lightest Higgs boson can be very light in the case of large singlet composition thus evading the LEP bounds, and the SM-like boson can be heavier than in the case of the MSSM.

We end this perspectives subsection by mentioning that the constrained version of the NMSSM (cNMSSM) can be very predictive: if all the experimental constraints are taken into account and in particular the WMAP constraints on the dark matter density, the cNMSSM can be described in practice by a single parameter as shown in Ref. [321] and depicted in Fig. 51 below.

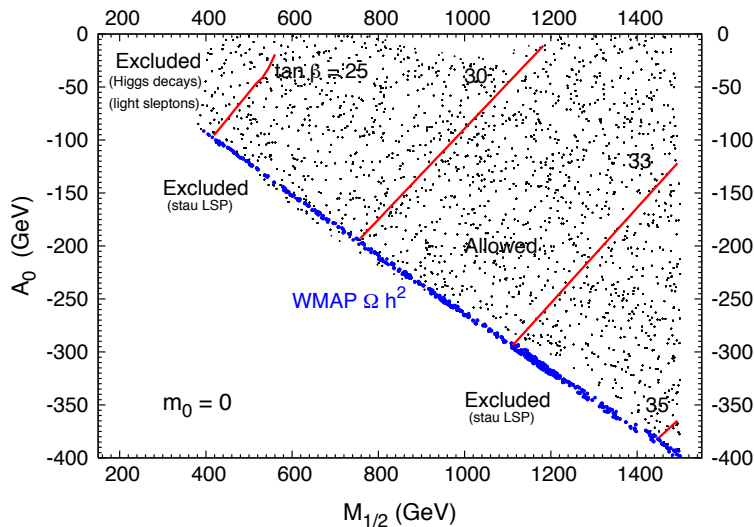


Figure 51: The viable cNMSSM parameter space in the $[M_{1/2}, A_0]$ plane. Figure taken from Ref. [321].

We have now ended the sketch of the MSSM and its essential features in the view of our goal, that is the study of the MSSM Higgs bosons production and decay at hadron colliders. We will now enter in the core of this study by moving on part IV.

⁶⁸This can also happen in the MSSM with gauge-mediated SUSY breaking though.

Part IV

MSSM Higgs(es) production and decay

Summary

10	The MSSM Higgs sector at hadron colliders	183
10.1	SUSY corrections to Higgs couplings to fermions	183
10.2	Model independence of the results	187
11	MSSM Higgs production at the Tevatron	190
11.1	Gluon–gluon fusion and bottom quarks fusion	191
11.1.1	The gluon–gluon fusion in the MSSM	192
11.1.2	The bottom quarks fusion in the MSSM	193
11.2	The scale uncertainty	195
11.3	The PDF and α_S uncertainties	196
11.4	The b -quark mass uncertainty	198
11.5	Summary and combination of the different sources of uncertainties . . .	201
12	MSSM Higgs production at the LHC	203
12.1	Gluon–gluon fusion and bottom quarks fusion channels	203
12.2	The scale uncertainty at the LHC	205
12.3	The PDF and α_S uncertainties at the LHC	207
12.4	The b -quark mass issue	208
12.5	Combination and total uncertainty	210
12.6	The case of the charged Higgs production in association with top quark at the LHC	212
13	Higgs $\rightarrow \tau\tau$ channel and limits on the MSSM parameter space	221
13.1	The main MSSM Higgs branching ratios	221
13.2	Combination of production cross section and Higgs $\rightarrow \tau\tau$ decay	224
13.2.1	The combination at the Tevatron	224

13.2.2	The combination at the LHC	226
13.3	Impact of the theoretical uncertainties on the limits on the MSSM parameter space	231
13.3.1	The Tevatron results	232
13.3.2	The LHC results	233
13.3.3	The expectations at the LHC	234
13.4	Consequences on the SM $H \rightarrow \tau\tau$ search at the LHC	237
13.5	Summary and outlook	239

10 The MSSM Higgs sector at hadron colliders

Part III was devoted to a brief summary of the reasons to go beyond the SM and in particular why SUSY is appealing. It has introduced the MSSM, the minimal extension of the SM, in which the Higgs phenomenology is particularly rich with five Higgs bosons in the spectrum. The purpose of this last part of the thesis is to study the MSSM Higgs bosons production and decay at the two major hadron colliders in activity, which will grossly reproduce the same outlines as done in part II.

We have seen in sections 9.1 and 9.2 the Higgs content of the MSSM; we need to study in this section how the Higgs couplings to fermions are affected by specific SUSY corrections which are in addition to that of the standard QCD and electroweak. We will then deduce from this analysis that the modelisation that we chose for the Higgs bosons production and decay will be somewhat model independent in the sense that it will hardly depend from the GUT scale parameters, wether it would be that of minimal supergravity, anomaly mediation or gauge mediation.

10.1 SUSY corrections to Higgs couplings to fermions

We have presented in section 9.2 the tree-level analysis of the Higgs sector of the MSSM. The need for quite large radiative corrections to the Higgs bosons masses is illustrated by the tree-level upper bound for the lightest CP -even Higgs boson h , $M_h \lesssim M_Z$. As this scalar boson has not been observed at LEP2 this limit should be crossed with the MSSM radiative corrections that also affect the Higgs couplings to the other fields. A thorough review has been done in Ref. [211] (see also references herein) from page 45 and we will only reproduce its main features and in particular list the regimes that we are interested in.

We should first mention that we have already presented some radiative corrections in section 9.2 in particular in the case of the lightest Higgs boson h in order to illustrate the impact of radiative corrections on the tree-level upper bound. Depending on the value of $\tan\beta$ and the relative value of M_A as compared to M_Z we may have h approaching its maximal value $M_h^{\max} \simeq 135$ GeV. We are mainly interested in the Higgs-fermions couplings in the view of the Higgs production at hadron colliders in the main production channels that involve Higgs-fermions couplings. The one-loop vertex corrections modifying the tree-level Lagrangian can be implemented in an effective lagrangian written as [44];

$$\begin{aligned}
 -\mathcal{L}_{\text{Yukawa}} &= \epsilon_{ij} \left[(\lambda_b + \delta\lambda_b) \bar{b}_R h_d^i Q_L^j + (\lambda_t + \delta\lambda_t) \bar{t}_R Q_L^i h_u^j + (\lambda_\tau + \delta\lambda_\tau) \bar{\tau}_R h_d^i L^j \right] \\
 &+ \Delta\lambda_b \bar{b}_R Q_L^i h_u^{i*} + \Delta\lambda_\tau \bar{\tau}_R L^i h_u^{i*} + \Delta\lambda_t \bar{t}_R Q_L^i h_d^{i*} + \text{h.c.}
 \end{aligned}
 \tag{10.1}$$

Thus, at this order, in addition to the expected corrections $\delta\lambda_{t,b}$ which alter the tree-level Lagrangian, a small contribution $\Delta\lambda_t$ ($\Delta\lambda_b$) to the top (bottom) quark will be generated by the doublet h_u (h_d). The top and bottom quark Yukawa couplings, defining $\lambda_b\Delta_b = \delta\lambda_b + \Delta\lambda_b \tan\beta$ and $\lambda_t\Delta_t = \delta\lambda_t + \Delta\lambda_t \cotan\beta$, are then given by

$$\lambda_b = \frac{\sqrt{2}m_b}{v \cos\beta} \frac{1}{1 + \Delta_b}, \quad \lambda_t = \frac{\sqrt{2}m_t}{v \sin\beta} \frac{1}{1 + \Delta_t} \quad (10.2)$$

The (approximate) corrections $\Delta_{t,b}$ are the same affecting the b and t quarks in the MSSM and is a way, known as the “ Δ_b approximation”, to resum large corrections into an effective parameter that gives for example in the case of the b quark

$$\bar{m}_b^{\text{MSSM}}(M_Z^2) \simeq \frac{\bar{m}_b^{\text{SM}}(M_Z^2)}{1 - \Delta_b} \quad (10.3)$$

with

$$\begin{aligned} \Delta_b &\simeq \left(\frac{2\alpha_s}{3\pi} \mu m_{\tilde{g}} I(m_{\tilde{g}}^2, m_{\tilde{b}_1}^2, m_{\tilde{b}_2}^2) + \frac{\lambda_t^2}{16\pi^2} A_t \mu I(\mu^2, m_{\tilde{t}_1}^2, m_{\tilde{t}_2}^2) \right) \tan\beta \\ I(x, y, z) &= \frac{xy \ln(x/y) + yx \ln(y/z) + xz \ln(z/x)}{(x-y)(y-z)(z-x)} \end{aligned} \quad (10.4)$$

The b quark corrections are then enhanced by $\tan\beta$ factors while those affecting the top quark are only sizable for large A_t or μ values. These corrections will affect the Yukawa couplings and in the case of the neutral Higgs boson couplings to bottom quarks, we may write

$$\begin{aligned} g_{hbb} &\simeq -\frac{\sin\bar{\alpha}}{\cos\beta} \left[1 - \frac{\Delta_b}{1 + \Delta_b} (1 + \cotan\bar{\alpha} \cotan\beta) \right] \\ g_{Hbb} &\simeq +\frac{\cos\bar{\alpha}}{\cos\beta} \left[1 - \frac{\Delta_b}{1 + \Delta_b} (1 - \tan\bar{\alpha} \cotan\beta) \right] \\ g_{Abb} &\simeq \tan\beta \left[1 - \frac{\Delta_b}{1 + \Delta_b} \frac{1}{\sin^2\beta} \right] \end{aligned} \quad (10.5)$$

where $\bar{\alpha}$ is the one-loop corrected α mixing angle in the CP -even Higgs bosons sector; g_{ijk} describe the MSSM couplings normalized to those of the SM.

As shown in Ref. [211] there is a strong variation of the couplings depending on the value of M_A around the critical value M_h^{max} . For $M_A \lesssim M_h^{\text{max}}$ the lighter h boson couplings to up-type fermions are suppressed, while the couplings to down-type fermions are enhanced, with the suppression/enhancement being stronger at high $\tan\beta$ values. For $M_A \gtrsim M_h^{\text{max}}$, the normalized h couplings approach the unity value and reach the values of the SM Higgs couplings, $g_{hff} = 1$, for $M_A \gg M_h^{\text{max}}$. The situation of the H boson couplings to fermions is just opposite: they are close to unity for $M_A \lesssim M_h^{\text{max}}$, while for $M_A \gtrsim M_h^{\text{max}}$,

the H couplings to up-type (down-type) fermions are strongly suppressed (enhanced). For $M_H \gg M_h^{\max}$, the H boson couplings become approximately equal to those of the A boson which couples to down-type and up-type fermions proportionally to, respectively, $\tan \beta$ and $\cotan \beta$.

We thus have typical regime that are of interest in our study, they are listed below.

- 1) *The decoupling regime:* either for large values of $M_A \gtrsim 300$ GeV at low $\tan \beta$ or for $M_A \gtrsim M_h^{\max}$ at high $\tan \beta$, the lightest CP -even Higgs boson h becomes SM-like while the heavier H becomes CP -odd like and decouples [322]: we have in the spectrum h SM-like with $M_h \lesssim M_h^{\max} \simeq 135$ GeV, (H, A, H^\pm) with nearly the same mass and couplings to other particles. In particular the H couplings to weak bosons become suppressed as in the case of the A boson where they are forbidden by CP invariance.

This behaviour is already manifest at tree-level, and the only significant change due to radiative corrections is the thresold for the A boson mass, which rises from M_Z to M_h^{\max} [323]. We have for $M_A^2 \gg M_Z^2$ and $\tan \beta \gg 1$:

$$\begin{aligned} g_{HVV} &= \cos(\beta - \alpha) \longrightarrow -\frac{2M_Z^2}{M_A^2 \tan \beta} \sim 0 \\ g_{hVV} &= \sin(\beta - \alpha) \longrightarrow -\frac{2M_Z^4}{M_A^4 \tan^2 \beta} \sim 1 \end{aligned} \quad (10.6)$$

for the weak bosons couplings and we have

$$\begin{aligned} g_{hUU} &\longrightarrow 1 - \frac{2M_Z^2}{M_A^2 \tan^2 \beta} \sim 1 \\ g_{hDD} &\longrightarrow 1 + \frac{2M_Z^2}{M_A^2} \sim 1 \\ g_{HUU} &\longrightarrow -\cotan \beta \left(1 + \frac{2M_Z^2}{M_A^2} \right) \sim -\cotan \beta \\ g_{HDD} &\longrightarrow \tan \beta \left(1 - \frac{2M_Z^2}{M_A^2 \tan^2 \beta} \right) \sim \tan \beta \end{aligned} \quad (10.7)$$

for the fermions couplings.

It is then manifest that for $M_A \gg M_Z$, g_{HVV} vanishes while g_{hVV} reaches the SM value (that is unity in term of normalized couplings). We recover for the CP -even Higgs couplings to fermions the same behaviour: the couplings of the h boson approach those of the SM Higgs boson, $g_{hUU} = g_{hDD} = 1$, while the couplings of the H boson reduce, up to a sign, to those of the pseudoscalar Higgs boson, $g_{HUU} \simeq g_{Auu} = \cotan \beta$ and $g_{HDD} \simeq g_{Add} = \tan \beta$.

- 2) *The anti-decoupling regime:* this regime is exactly the opposite of the decoupling regime: for a light pseudoscalar Higgs boson $M_A \gg M_h^{\max}$ the lighter CP -even Higgs boson mass is given at tree-level by $M_h \simeq M_A |\cos 2\beta|$ while the heavier CP -even Higgs mass is given by $M_H \simeq M_Z (1 + M_A^2 \sin^2 2\beta / M_Z^2)$. At large values of $\tan \beta$, this is this time the h boson which is degenerate in mass with the pseudoscalar Higgs boson A while the H boson has a mass $M_H \simeq M_h^{\max}$ when taking into account the radiative corrections [324]. The role of the h and H bosons are thus reversed compared to the decoupling regime. Again the effect of radiative corrections is in practice to level up the M_A thresold from M_Z to M_h^{\max} . The h boson has then the couplings that behave as those of the pseudoscalar Higgs boson A , while the H boson couplings are SM-like:

$$\begin{aligned} g_{huv} &\longrightarrow \cotan \beta \quad , \quad g_{hdd} \longrightarrow -\tan \beta \\ g_{Huv} &\longrightarrow 1 \quad , \quad g_{Hdd} \longrightarrow 1 \end{aligned} \quad (10.8)$$

and the H couplings to gauge bosons are SM-like, while the lighter h boson is degenerate in mass with the pseudoscalar Higgs boson, $M_h \simeq M_A$ and has approximately the same couplings, that is, very suppressed couplings to gauge bosons.

- 3) *The intense coupling regime:* the last interesting regime for our study is the situation where the mass M_A of the pseudoscalar A boson is close to the maximal possible value for the lightest CP -even Higgs boson M_h^{\max} (which corresponds to a mass close to the mass of the Z boson M_Z at tree-level). The three neutral Higgs bosons have nearly the same mass (also nearly equal to that of the charged Higgs boson), $M_h \sim M_H \sim M_A \sim M_h^{\max}$. The mass degeneracy is more effective when $\tan \beta$ is large; this is the so-called intense-coupling regime discussed in details in the case of hadron colliders in Ref. [325] referenced by Ref. [211].

More precisely, this regime is defined as the one where the two CP -even Higgs bosons h and H are almost degenerate in mass which implies that this degeneracy enlarges to the pseudoscalar boson A as well. We have in this regime two possibilities:

$$\begin{aligned} M_A \gtrsim M_h^{\max} &\Rightarrow M_H \simeq M_A \quad \text{and} \quad M_h \simeq M_h^{\max} \\ M_A \lesssim M_h^{\max} &\Rightarrow M_h \simeq M_A \quad \text{and} \quad M_H \simeq M_h^{\max} \end{aligned} \quad (10.9)$$

Therefore the A boson is always degenerate in mass with one of the CP -even Higgs bosons, that we will call Φ_A , while the other CP -even Higgs particle, called Φ_H , is very close in mass with M_h^{\max} which in passing is equivalent as being the minimal value for the H boson. In addition, the CP -even Φ_A boson will have almost the same couplings as A , while the Φ_H particle will have almost the couplings of the SM Higgs boson. We actually recover in a different situation the two regime described in the first two points, depending on the value of M_A relative to that of M_h^{\max} .

Two other regimes, the intermediate-coupling and the vanishing-coupling regimes, are not listed above because they do not scope our study, see Ref. [211] for more details. In all cases above the interesting feature is that one of the two CP -even Higgs boson behaves exactly like the CP -odd A boson, the other being SM-like. This greatly simplifies the study as we can take the SM results of part II for the study of the SM-like CP -even Higgs boson and only study the case of the A boson for the two other neutral Higgs bosons.

10.2 Model independence of the results

We will now present our set-up for the calculation of the cross sections and decay branching fractions at hadron colliders. As presented above three regimes are of great interest: the decoupling, anti-decoupling and intense coupling regimes. In all of them we are in the following situation: one of the CP -even Higgs boson behaves as the CP -odd Higgs boson, the other is SM-like. We will then denote the A boson and the H/h CP -odd-like boson by Φ , and study the Φ production and decay at hadron colliders. As stated in Ref. [326], this study is somewhat model-independent in the following sense that will review the arguments presented in the mentioned reference.

In both production and decay processes, we will actually assume the $b\bar{b}\Phi$ coupling to be SM-like, $\lambda_{\Phi b\bar{b}} = m_b/v$; this means that to obtain true cross sections the results have to be rescaled by a factor of $\tan^2 \beta$. What justifies the use of SM-like reduced couplings (apart from the $\tan \beta$ factor)? This follow from three reasons:

- i)* our study is conducted in the case of the regimes mentioned in the previous subsection; in these cases as explained above one of the CP -even Higgs boson behaves like the CP -odd A boson and thus share its production and decay amplitudes. The only exception is for the intense coupling regimes where the three neutral Higgs bosons have similar enhanced couplings to down-type quarks. As the squares of the CP -even Higgs couplings add to the square of the CP -odd Higgs coupling, and since $M_H \approx M_h \approx M_A$, we still recover our approximation provided that the cross section times branching ratios for the three h, H, A particles are added;
- ii)* as the pseudoscalar A boson does not couple to squarks of the same flavor ($A\tilde{q}_i\tilde{q}_i$ couplings are forbidden by CP -invariance), there is no superparticle contribution in the $gg, b\bar{b} \rightarrow A$ processes (to be discussed later on) at leading order and higher order SUSY corrections are suppressed. In the CP -even Higgs case, there are additional superparticle contributions to $gg \rightarrow H(h)$ originating mainly from stop and sbottom squarks loops. However, these contributions are damped by the squark mass squared

and are not similarly enhanced by $m_b \tan \beta$ factors; they thus remain small so that they can be safely neglected in most cases;

iii) the most important reason is the last one: the relevant effect of supersymmetric contributions appears through the Δ_b term in the Δ_b approximation as stated in the previous subsection. This correction can be significant as it grows with $\tan \beta$ and is obviously SUSY model dependant. However in the case of our study, that is the production times branching fraction, this correction almost cancel out between production and decay, the remaining part having no practical impact in the view of the large QCD uncertainties whatever benchmark scenario to be considered. Indeed as shown in Ref. [326] the impact of the Δ_b approximation is

$$\begin{aligned} \sigma \times \text{BR} &\longrightarrow \frac{\sigma}{(1 + \Delta_b)^2} \times \frac{\Gamma(\Phi \rightarrow \tau\tau)}{(1 + \Delta_b)^{-2}\Gamma(\Phi \rightarrow b\bar{b}) + \Gamma(\Phi \rightarrow \tau\tau)} \\ &\approx \sigma \times \text{BR} \times \left(1 - \frac{1}{5}\Delta_b\right) \end{aligned} \quad (10.10)$$

assuming $\text{BR}(\Phi \rightarrow \tau^+\tau^-) \approx 10\%$. Thus, unless the Δ_b correction is extremely large, it will lead to only a few percent correction at most to the cross section times decay branching ratio.

The impact of the Δ_b approximation is shown below:

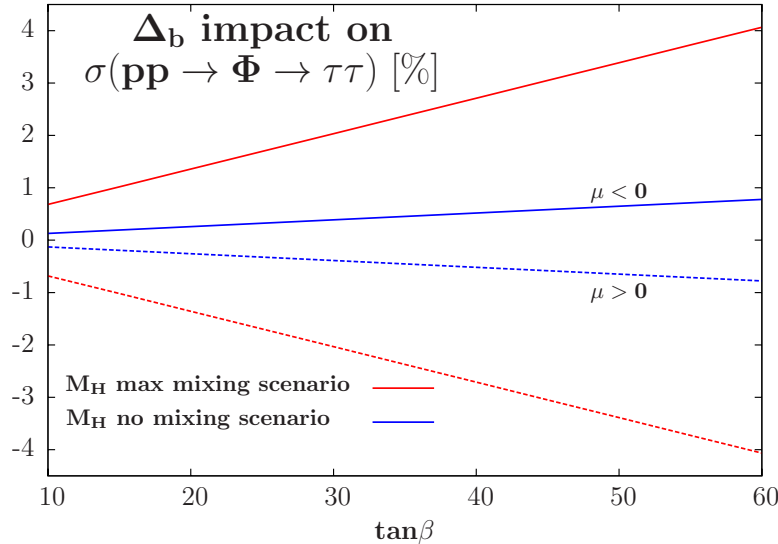


Figure 52: The impact (in %) of the Δ_b supersymmetric radiative correction on the cross section times branching ratio $\sigma[pp \rightarrow A + H(h)] \times \text{BR}[A/H(h) \rightarrow \tau^+\tau^-]$ as a function of $\tan \beta$ in two of the benchmark scenarios of Ref. [327] for both signs of μ .

We have used in Fig. 52 the program FeynHiggs [328] to evaluate the Δ_b correction, and we display for a fixed value of M_A and as a function of $\tan \beta$, the impact of the Δ_b

correction on $\sigma(gg + b\bar{b} \rightarrow \Phi) \times \text{BR}(\Phi \rightarrow \tau\tau)$. This is done in two benchmark scenarios for the CP -conserving MSSM proposed in Ref. [327]: the maximal M_h^{max} mixing and the M_h^{min} no-mixing Higgs scenarios⁶⁹, with the two possible signs of the higgsino parameter μ ; these two benchmark scenarios enter in the regimes described in the previous subsection.

We see that in both cases the quality of our approximation for the $pp \rightarrow \Phi \rightarrow \tau^+\tau^-$ cross section is always very good, the difference with the exact result including the Δ_b correction being less than 2% for $\tan\beta \lesssim 30$ (and $\lesssim 4\%$ for $\tan\beta \lesssim 60$), which is negligible in view of the large QCD uncertainties that affect the cross section as studied in the following sections. The quality of the Δ_b approximation itself has been discussed in Ref. [331] which states that this accurately reproduces the exact one-loop SQCD corrections. Nevertheless in the final stage of the writing of the thesis some preliminary results presented in Ref. [315] with new SUSY contributions show that this might not be the case in every scenarios (and in particular in the so-called α^{eff} scenario that has been ruled out though), thus softening a bit our model independence argument. Nevertheless it remains quite accurate in the main benchmark scenarios discussed in this thesis. We will then use the SM-like couplings to the A boson and multiply by a factor of $2 \tan^2\beta$ to account for the degeneracy between the A and one of the CP -even Higgs bosons, to obtain the true $pp \rightarrow \Phi \rightarrow \tau^+\tau^-$ cross section⁷⁰. In fact, our results also hold in a general two-Higgs doublet model in which two Higgs particles have the same mass and the same enhanced couplings to down-type fermions, as the relevant parameters are again $\tan\beta$ and M_A .

We summarize our set-up developed in this subsection: we will study the production and decay of the pseudoscalar A boson that is similar to one of the CP -even Higgs boson, these two states being collectively denoted by Φ . We will only present results with $\tan\beta = 1$ and with SM-like couplings, which is an excellent approximation; the actual results are recovered provided that the results are multiplied by a factor of $2 \tan^2\beta$. We are now ready to study the MSSM Higgs bosons production at the Tevatron and the LHC. We will then study the combination with the branching fractions and finish by the impact of our study on the MSSM parameter space.

⁶⁹The gluophobic scenario is now ruled out as it leads to light gluinos $m_{\tilde{g}} = 500$ GeV) and squarks ($m_{\tilde{q}} \approx 350$ GeV) which have been excluded by the recent ATLAS and CMS analyses [329, 330]. The small α_{eff} , which leads to $\tilde{m}_g = 500$ GeV and $\tilde{m}_q = 800$ GeV is probably also excluded, in particular if the various ATLAS and CMS analyses are combined. This latter scenario leads to a huge (and probably rather problematic) Δ_b value but the effect on the cross section times branching ratio is again less than 10% for $\tan\beta \lesssim 30$.

⁷⁰We note in passing that this approximation is very useful in practice as it prevents the need of large grids to tackle numerically every MSSM scenario as well as CPU time consuming scans of the supersymmetric parameter space.

11 MSSM Higgs production at the Tevatron

The section 4 has been devoted to the production of the SM Higgs boson at the Tevatron. The search of this remnant of the spontaneous breaking of the electroweak symmetry is one of the main goal of the present high energy colliders and in particular of the Tevatron program. We have seen in section 9.2 that the Higgs sector is extended in supersymmetric theories [284] and in particular in the minimal extension, the MSSM, two Higgs doublet are required and leads to the existence of five Higgs bosons: two CP -even h and H , a CP -odd A and two charged H^\pm particles [44, 211]. We will study the production and later on the decay of the neutral Higgs bosons at the Tevatron.

We have seen in section 9.2 that two parameters are needed to describe the Higgs sector of the MSSM at tree-level: the mass M_A of the pseudoscalar boson and the ratio of vacuum expectation values of the two Higgs fields, $\tan\beta$, that is expected to lie in the range $1 \lesssim \tan\beta \lesssim 50$ from theoretical analysis, see Ref. [211] for a review. The section 10.1 has presented the main regimes in which our analysis is conducted, thus we will denote collectively the A boson and the CP -even state which behaves like the A boson as $\Phi = A, H(h)$. They are almost degenerate in mass and have the same properties: no couplings to gauge bosons, while the couplings to isospin down-type (up-type) quarks and charged leptons are (inversely) proportional to $\tan\beta$.

This means that for $\tan\beta \gtrsim 10$, the Φ boson couplings to bottom quarks and τ -leptons are strongly enhanced while those to top quarks are suppressed. As a result, the phenomenology of these states becomes rather simple. To a very good approximation, the Φ bosons decay almost exclusively into $b\bar{b}$ and $\tau^+\tau^-$ pairs with branching ratios of, respectively, $\approx 90\%$ and $\approx 10\%$, while the other decay channels are suppressed to a negligible level [97]. The main production mechanisms for these particles are those processes which involve the couplings to bottom quarks. At hadron colliders, these are the gluon-gluon fusion mechanism, $gg \rightarrow \Phi$, which dominantly proceeds through b -quark triangular loops [99, 105] and bottom-quark fusion, $b\bar{b} \rightarrow \Phi$ [193–195, 332], in which the bottom quarks are directly taken from the protons in a five active flavor scheme [192, 333]. The latter process is similar to the channel $p\bar{p} \rightarrow b\bar{b}\Phi$ when no b -quarks are detected in the final state [192, 333]. We will study these two processes at the Tevatron and later on in this thesis at the LHC, leaving the study of the branching fractions and in particular their combination with production cross sections for the last section.

With its successful operation in the last years, the Fermilab Tevatron collider has now collected a substantial amount of data which allows the CDF and D0 experiments to be sensitive to the MSSM Higgs sector. Stringent constraints beyond the well established LEP

bounds $M_A, M_h \gtrsim M_Z$ and $\tan \beta \gtrsim 3$ [46], have been set on the MSSM parameter space $[M_A, \tan \beta]$ using the process $gg, b\bar{b} \rightarrow \Phi \rightarrow \tau^+\tau^-$. Moderate A masses, $M_A \approx 100\text{--}200$ GeV, together with high $\tan \beta$ values, $\tan \beta \gtrsim 30$, have been excluded at the 95% confidence level (CL) [334–336].

However the experimental analyses cited above have not taken into account the theoretical uncertainties that affect the production and decay rates, which can be important despite of the fact that some higher order perturbative corrections to these processes are known. These are mainly due to the unknown higher order corrections in perturbation theory as in the SM case, the still not satisfactory parametrization of the parton distribution functions (PDFs), as well as the parametric uncertainties stemming from the not very precisely measured values of the strong coupling constant α_s and the bottom quark mass m_b which plays a significant role in the MSSM contrary to the SM case. We will present in the following the results published in Ref. [337] concerning the thorough analysis of the theoretical uncertainties of production cross section of the Φ boson at the Tevatron, in the set-up summarized in the end of section 10.2. We will see that they can affect by nearly 50% the production rates, thus having a great impact of the combined analysis of the MSSM Higgs bosons by CDF and D0 experiments [336] that have put high constraints on the MSSM $[M_A, \tan \beta]$ parameter space.

11.1 Gluon–gluon fusion and bottom quarks fusion

Our study as said before will be in the context of the regimes where at least two of the neutral Higgs bosons are almost degenerate. Indeed it is the case in most benchmark scenarios [327] as in the maximal mixing scenario where $X_t = A_t - \mu/\tan \beta \sim \sqrt{6}M_S$, M_S being the common squark mass and leading to $M_h^{\max} = 135$ GeV [338–340], or the no-mixing scenario where $X_t \approx 0$ which leads to a lower M_h^{\max} value.

The Higgs Yukawa couplings to bottom quarks plays a major role in the analysis that will be presented in this section and this explains why we concentrate on the two main production channels that are the gluon–gluon fusion and the bottom quarks fusion. Indeed because of CP invariance which forbids A couplings to gaugebosons at tree-level, the pseudoscalar A boson cannot be produced in the Higgs-strahlung and vector boson fusion processes; only the $gg \rightarrow A$ fusion as well as associated production with heavy quark pairs, $q\bar{q}, gg \rightarrow Q\bar{Q}A$, will be in practice relevant (additional processes, such as associated production of CP -even and CP -odd Higgs particles, have too small cross sections). This will therefore be also the case of the CP -even H and h particles in, respectively, the decoupling and anti-decoupling scenario. As mentioned earlier, in almost the entire parameter space

for large enough $\tan\beta$ values, the couplings of one of the CP -even Higgs particles are SM-like which means that we can use again the results presented in part II, while the couplings of the other CP -even particle are the same as those of the pseudoscalar A boson, on which we will focus in the rest of our discussion. At the tree level, this coupling is given in terms of the b -quark mass, the SM vacuum expectation value v and $\tan\beta$, by

$$\lambda_{\Phi bb} = \frac{\sqrt{2}m_b}{v \cos\beta} \xrightarrow{\tan\beta \gg 1} \frac{\sqrt{2}m_b}{v} \tan\beta, \quad \Phi = A, H (h) \quad (11.1)$$

First of all, in the MSSM, one usually uses the modified dimensional reduction $\overline{\text{DR}}$ scheme which, contrary to the $\overline{\text{MS}}$ scheme, preserves Supersymmetry. In the case of the b -quark mass, the relation between the $\overline{\text{DR}}$ and $\overline{\text{MS}}$ running masses at a given scale μ reads [341]

$$\overline{m}_b^{\overline{\text{DR}}}(\mu) = \overline{m}_b^{\overline{\text{MS}}}(\mu) \left[1 - \frac{1}{3} \frac{\alpha_s(\mu^2)}{\pi} - \frac{\alpha_s^2(\mu^2)}{\pi^2} + \dots \right] \quad (11.2)$$

where the strong coupling constant α_s is also evaluated at the scale μ and additional but small electroweak contributions are present. Since the difference between the quark masses in the two schemes is not very large, $\Delta m_b/m_b \sim 1\%$, to be compared with an “experimental” error on $\overline{m}_b(\overline{m}_b)$ of the order of a few percent, we will neglect the difference as commonly done at least in unconstrained SUSY models with no RGE evolution of the parameters from a higher scale. We will thus adopt this approximation at least when we quote the central values of the cross sections; nevertheless we will discuss later on the impact of the b -mass renormalization scheme on the theoretical uncertainties. We will not include SUSY corrections to the Yukawa coupling as explained and justified in the previous section: the analysis will thus be somewhat model independent and we will focus on the standard QCD uncertainties. However if one is interested by the genuine SUSY corrections [342–351] they can be evaluated using the program HIGLU for instance in the case of the gluon–gluon fusion production channel.

11.1.1 The gluon–gluon fusion in the MSSM

The first production channel that we consider is the gluon–gluon fusion as in the SM case. As we are in moderate to high $\tan\beta$ regime in our set-up, the top-loop is suppressed and only the b -loop is included. As the b -quark mass is very small compared to the Higgs masses, chiral symmetry approximately holds and the cross sections are approximately the same for the CP -even $H (h)$ and CP -odd A bosons⁷¹. The QCD corrections are known only to NLO for which the exact calculation with finite loop quark masses is available [105].

⁷¹This is only true if the SUSY particle loop contributions are not included. In the case of the CP -even particles, their relative contribution are suppressed at high enough $\tan\beta$ and we will ignore them here as

Contrary to the SM case, they increase only moderately the production cross sections. The calculation of the higher order corrections that have been made available for the SM Higgs boson, the NNLO QCD corrections (performed in the infinite quark mass limit) and the NLO electroweak corrections (the dominant part of which arises because of the large Higgs- $t\bar{t}$ Yukawa coupling) do not apply here and will be thus ignored. In order to match the SM calculation which reproduces the results for the SM-like CP -even Higgs boson in order to approach properly the decoupling and anti-decoupling regime, we will adopt the central scale $\mu_0 = \frac{1}{2}M_\Phi$.

We will evaluate the cross section with such a central scale using the program HIGLU [152, 153] with only the dominant loop contribution of the bottom quark loop included. We work in the $\overline{\text{MS}}$ scheme for the renormalization of the b -quark mass, that is $\overline{m}_b(\overline{m}_b)$. The resulting partonic cross sections are then folded with the latest MSTW sets of PDFs [128, 199, 234] consistently at the NLO order in perturbation theory. We will use $\tan\beta = 1$: to obtain the true numbers a factor of $\tan^2\beta$ has to be included (and then doubled to obtain the full $gg \rightarrow A + h/H$ cross section).

11.1.2 The bottom quarks fusion in the MSSM

In the case of the $pp \rightarrow b\bar{b}\Phi$ processes, the NLO QCD corrections have been calculated in Ref. [192, 333] and turn out to be rather large, in contrast to $pp \rightarrow t\bar{t}$ +Higgs production. Because of the small m_b value, the cross sections develop large logarithms $\ln(Q^2/m_b^2)$ with the scale Q being typically of the order of the factorization scale, $\mu_F \sim M_\Phi \gg m_b$. These logarithms can be resummed via the Altarelli-Parisi equations by considering the b -quark as a massless parton and using heavy quark distribution functions at a scale $\mu_F \sim Q$ in a five active flavor scheme. In this scheme, the inclusive process where one does not require to observe the b quarks is simply the $2 \rightarrow 1$ process $b\bar{b} \rightarrow \Phi$ at leading order [332]. If the observation of a high- p_T final b -quark is required, one has to consider its NLO corrections [193, 195] and in particular the $2 \rightarrow 2$ process $gb \rightarrow \Phi b$, which indeed generates the p_T of the b -quark. Requiring the observation of two b quarks in the final state, we have to consider the $2 \rightarrow 3$ process $gg \rightarrow b\bar{b}\Phi$ discussed above, which is the leading mechanism at NNLO [194]. Thus, instead of $q\bar{q}, gg \rightarrow b\bar{b}\Phi$, we will consider the process $b\bar{b} \rightarrow \Phi$ for which the cross section is known up to NNLO in QCD [193–195], with corrections that are

stated in the previous section. In the case of the A boson, the SUSY contributions appear only at two-loops and they can be safely neglected. Indeed these additionnal SUSY contributions in $gg \rightarrow H/h$ do not appear in $gg \rightarrow A$ but they are very small for a large SUSY breaking scale, $M_\Phi \ll M_S$ as seen in Ref. [351]. In addition the Δ_b term is again negligible as stated in the previous section, and that can be seen from the almost identical tables XI–XIV and Figs. 4 of Ref. [336] that describe four benchmark scenarios [327].

of moderate size if: the bottom quark mass in the Yukawa coupling is defined at the scale M_Φ to absorb large logarithms $\ln(\mu_R^2/m_b^2)$; the factorization scale, that we will set here equal to the renormalization scale, is chosen to be small, $\mu_F = \mu_R = \mu_0 = \frac{1}{4}M_\Phi$. Fig. 53 below displays some typical Feynman diagrams for bottom quarks fusion in this set-up.

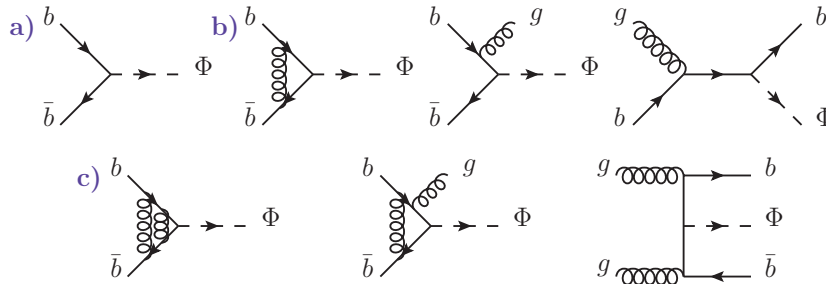


Figure 53: Typical Feynman diagrams up to next-to-next-to-leading order in QCD in the bottom quark fusion production channel in the MSSM. The five flavors scheme has been adopted.

The evaluation of the cross section up to NNLO is done using the program `bbh@nnlo`⁷² with a central scale $\mu_R = \mu_F = \mu_0 = \frac{1}{4}M_A$ as appropriate for this process according to Ref. [194]. We work in the $\overline{\text{MS}}$ scheme for the bottom quark mass evaluated at the scale of the process, $\overline{m}_b(\mu_R)$. The resulting partonic cross sections are then folded again with the MSTW2008 set of PDFs consistently at the NNLO order in in perturbation theory. We again assume $\tan\beta = 1$, the actual cross sections being obtained after a multiplication by a factor of $\tan^2\beta$.

The results for the cross sections $\sigma(gg \rightarrow \Phi)$ and $\sigma(b\bar{b} \rightarrow \Phi)$ are shown in Fig. 54 below for the Higgs mass range that is relevant at the Tevatron, $M_\Phi = 90\text{--}200$ GeV and with $\tan\beta = 30$ as an example. We have compared our values with those given by the program that has been used by the CDF and D0 collaborations for their cross section normalization, `FeynHiggs` [328]. This program, initially supposed to only provide precise values for the MSSM Higgs masses and couplings, gives also grids for production cross sections which should be used with care. For the $b\bar{b} \rightarrow \Phi$ channel, we obtain cross sections that are $\approx 30\%$ smaller. The reason is that `FeynHiggs` simply provides the values given in the original paper [194] which uses the outdated MRST2002 set of PDFs which are only partly at NNLO. In the case of $gg \rightarrow \Phi$, the agreement is better as we obtain a cross section that is only $\approx 10\%$ higher, due to the different central scale and renormalization scheme for m_b that have been used. The comparison between the two process shows that the dominant process from $M_\Phi \gtrsim 135$ GeV is the bottom quarks fusion. Both production cross sections are far greater than the similar processes in the SM: this adds up more odds to find the Higgs boson at the Tevatron.

⁷²We thank R. Harlander for providing us with the code.

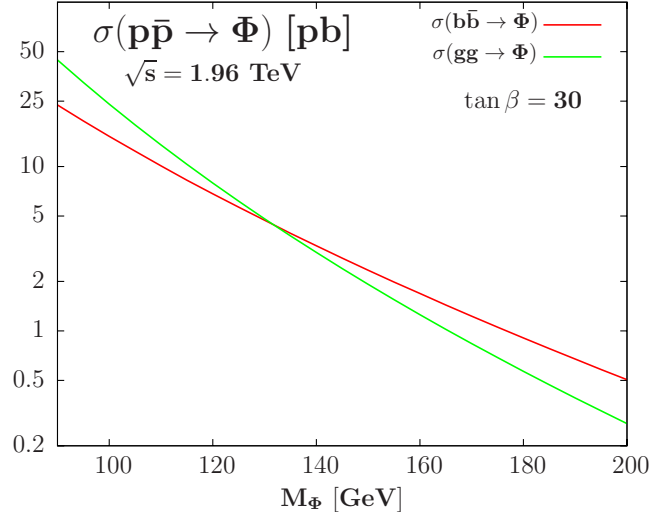


Figure 54: The normalization of the cross sections $\sigma_{gg \rightarrow \Phi}^{\text{NLO}}$ and $\sigma_{b\bar{b} \rightarrow \Phi}^{\text{NNLO}}$ at the Tevatron as a function of M_Φ when using the MSTW PDFs and $\tan \beta = 30$.

11.2 The scale uncertainty

We will follow the guideline that has been developed in part II in the case of the SM Higgs production. We start the evaluation of the theoretical uncertainties by looking at the scale uncertainty. In order to estimate the missing higher orders in perturbation theory we usually use a variation of the renormalization and factorization scales in the domains $\mu_0/\kappa \leq \mu_R, \mu_F \leq \kappa\mu_0$ around the central scales μ_0 , with sometimes the additional restriction $1/\kappa \leq \mu_R/\mu_F \leq \kappa$ imposed.

In the case of the $gg \rightarrow \Phi$ process, as for the SM Higgs boson at the LHC, the scale uncertainty is evaluated by allowing for a variation of the renormalization and factorization scales within a factor of two around the central scale, $\frac{1}{2}\mu_0 \leq \mu_R, \mu_F \leq 2\mu_0$ with $\mu_0 = \frac{1}{2}M_\Phi$; this is enough in the case of the bottom quark loop at NLO in view of our procedure developed in part II where we required that the LO band catch the NLO central result to define the constant factor κ .

However for the $b\bar{b} \rightarrow \Phi$ case we will extend the domain of scale variation to a factor of three around the central scale $\mu_0 = \frac{1}{4}M_\Phi$, $\frac{1}{3}\mu_0 \leq \mu_R, \mu_F \leq 3\mu_0$ and impose an additional restriction $1/3 \leq \mu_R/\mu_F \leq 3$. There are several reasons to do so, the first being that we would like to include the scheme dependence in the renormalization of the bottom quark as seen later on; this adds to the scale uncertainty and as the bottom quark mass in the bottom quark fusion is defined at the renormalization scale itself, one way to consider this additional source of uncertainty is to include it in the scale uncertainty by extending the domain of variation for the renormalization and factorization scales. A second reason is that it is well known that when the same final states are considered, the cross sections

in the $b\bar{b} \rightarrow \Phi$ process in the five-flavor scheme and in the $q\bar{q}, gg \rightarrow b\bar{b}\Phi$ channel in the four-flavor scheme differ significantly (see Ref. [131] page 5) and only by allowing a wider domain for scale variation and, hence, a larger scale uncertainty that the two results become consistent with each other. To illustrate the much larger scale uncertainty that is possible in the $b\bar{b} \rightarrow \Phi$ case, we display the results in Fig. 55 below in much the same way as in Ref. [210].

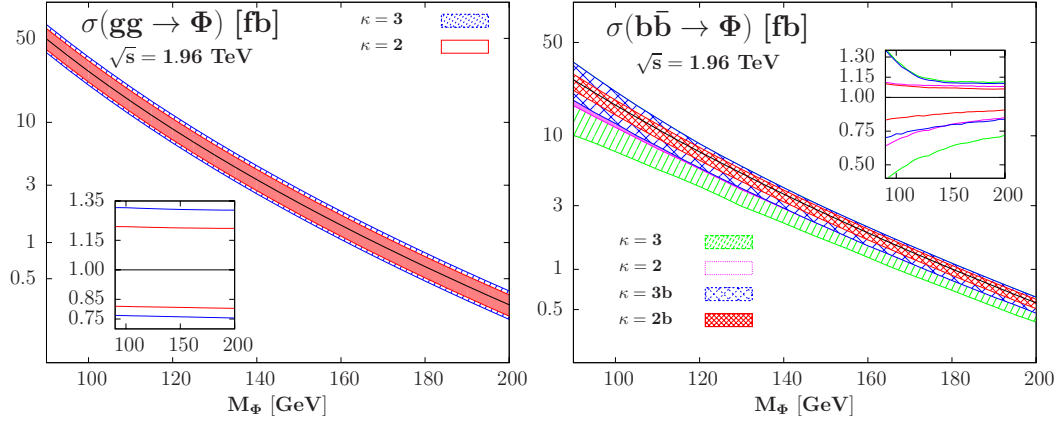


Figure 55: The scale uncertainty bands of the NLO $gg \rightarrow \Phi$ (left) and the NNLO $b\bar{b} \rightarrow \Phi$ (right) cross sections at the Tevatron as a function of M_Φ ; different values $\kappa = 2, 3$ are used and the results are shown when the additional constraint $1/\kappa \leq \mu_R/\mu_F \leq \kappa$ is imposed or not (marked as κb). In the inserts, the relative deviations (compared to the central cross section values) are shown.

We obtain in the gluon–gluon fusion process a relatively constant uncertainty of order +21%, –18% in the whole M_Φ mass range 90–200 GeV relevant at the Tevatron. In the case of the bottom quarks fusion, the right part of Fig. 55 shows clearly that there is an instability in the choice of the constant factor κ defining the interval of variation of the two scales μ_R, μ_F . If one chooses the factor $\kappa = 2$, the scale uncertainty is +15%, –9% at $M_\Phi \simeq 100$ GeV with the additional constrain on the ratio μ_R/μ_F and reduces to +9%, –6% at $M_\Phi \simeq 200$ GeV. However our final choice leads to a scale uncertainty of $\pm 27\%$ at $M_\Phi \simeq 100$ GeV which reduces to +15%, –10% at high $M_\Phi \simeq 200$ GeV.

11.3 The PDF and α_s uncertainties

We now turn our attention to the estimation of the uncertainties from the parton densities and α_s , following stictly the discussion lead in section 4.3 in the case of the SM Higgs gluon–gluon fusion production channel. The 90% CL PDF+ $\Delta^{\text{exp}}\alpha_s$ uncertainty, with $\alpha_s(M_Z^2) = 0.120 \pm 0.002$ at NLO for $gg \rightarrow \Phi$ and $\alpha_s(M_Z^2) = 0.1171 \pm 0.0014$ at NNLO for $b\bar{b} \rightarrow \Phi$, is evaluated within the MSTW parametrization when including the experimental error on α_s [128, 199, 234]. To that, we add in quadrature the effect of the theoretical error

on α_s , estimated by the MSTW collaboration to be $\Delta^{\text{th}}\alpha_s \approx 0.003$ at NLO and $\Delta^{\text{th}} \approx 0.002$ at NNLO, using the MSTW fixed α_s grid with central PDF sets. The 90%CL PDF, PDF+ $\Delta^{\text{exp}}\alpha_s$ and the PDF+ $\Delta^{\text{exp+th}}\alpha_s$ uncertainties at the Tevatron are shown in Fig. 56 as a function of M_Φ . In the case of the $gg \rightarrow \Phi$ process the PDF uncertainty is up to $\pm 10\%$ at high mass $M_\Phi = 200$ GeV and the total PDF+ $\Delta^{\text{exp+th}}\alpha_s$ uncertainty is $\pm 11\%$ at low Higgs mass $M_\Phi \simeq 100$ GeV and $\pm 15\%$ at high Higgs mass $M_\Phi \simeq 200$ GeV. This is then a rather controlled uncertainty, which is quite different in the case of the $b\bar{b} \rightarrow \Phi$ production channel. Indeed in the latter case we obtain a total PDF+ $\Delta^{\text{exp+th}}\alpha_s$ uncertainty of order $\pm 20\%$ at low Higgs mass values $M_\Phi \simeq 100$ GeV and up to $+28\%$, -24% at $M_\Phi = 200$ GeV.

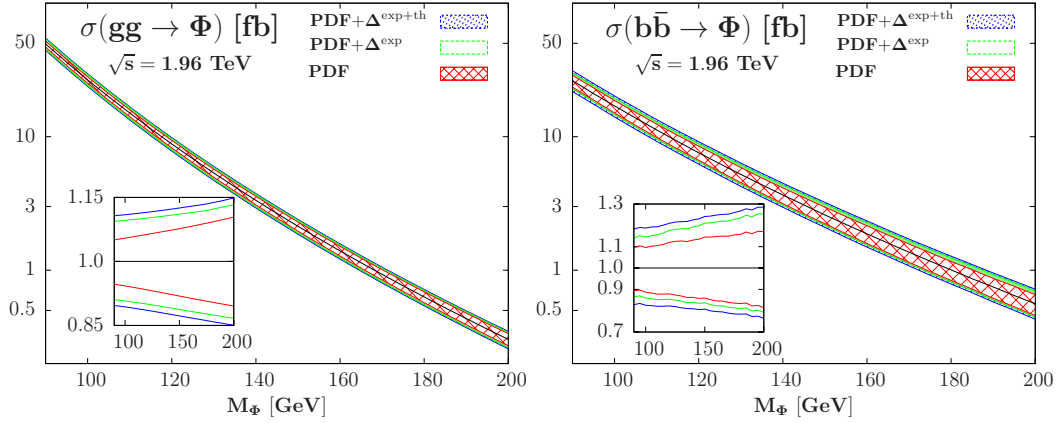


Figure 56: The PDF 90% CL PDF, PDF+ $\Delta^{\text{exp}}\alpha_s$ and PDF+ $\Delta^{\text{exp}}\alpha_s + \Delta^{\text{th}}\alpha_s$ uncertainties in the MSTW scheme in the $gg \rightarrow \Phi$ (left) and $b\bar{b} \rightarrow \Phi$ (right) cross sections at the Tevatron as a function of M_Φ . In the inserts, the relative deviations are shown.

This spectacular uncertainty in the case of the bottom quark fusion channel is in fact not as big if we recall the other way of estimating the PDF uncertainty, that is the comparison between the central predictions of the various NNLO PDFs sets on the market. We have chosen to display in Fig. 57 below the comparison between the MSTW PDF set [128], the JR09 PDF set [150] and the ABKM PDF set [206]. The difference between the ABKM and MSTW predictions is again huge: from 30% at low Higgs mass up to more than 40% at $M_\Phi = 200$ GeV. In this view the obtained PDF+ $\Delta^{\text{exp+th}}\alpha_s$ uncertainty within the MSTW set-up is acceptable. We have also evaluated the $gg \rightarrow \Phi$ sections with four other PDF sets and found that the maximal values are obtained with MSTW PDFs set while some other schemes give $\approx 20\%$ lower rates. The PDF discrepancy is then reduced in the case of the gluon-gluon fusion at the Tevatron in the MSSM.

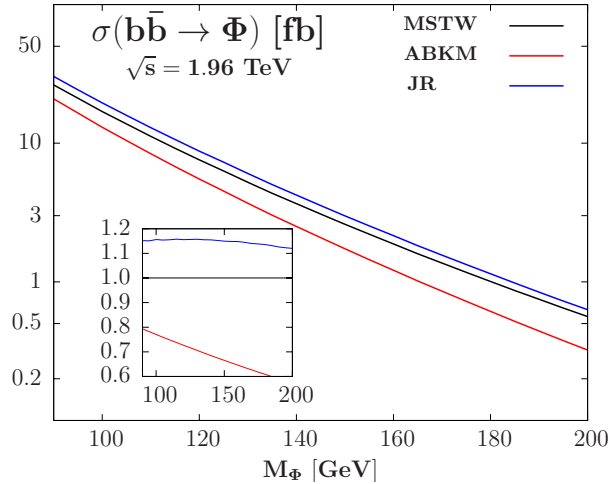


Figure 57: The MSTW, JR09 and ABKM predictions for $\sigma^{\text{NNLO}}(b\bar{b} \rightarrow \Phi)$ cross section at the Tevatron. In the inserts, the relative deviations compared to the central MSTW prediction are shown.

11.4 The b -quark mass uncertainty

The last piece of uncertainty that remains to be evaluated deals with the b quark issue. The impact of the b quark mass experimental error or the choice of the renormalization scheme was only marginal in the case of the SM Higgs boson both at the Tevatron and the LHC, mainly because the top loop is by far dominant in this latter case. There are three different sources of uncertainties related to the b quark, that are summarized below.

- The first one is of purely theoretical nature and is due to the choice of the renormalization scheme for the b -quark mass. In our analysis, we have adopted the $\overline{\text{MS}}$ renormalization scheme for two reasons: first because the natural scheme for any SUSY calculation would be the $\overline{\text{DR}}$ scheme which preserves SUSY, a scheme than can be traded in our case for the $\overline{\text{MS}}$ scheme without too much error as stated in the introduction of this section; then because the calculation of the $b\bar{b} \rightarrow \Phi$ process is available only in this scheme and we to have chosen to treat the same way both the $b\bar{b} \rightarrow \Phi$ and $gg \rightarrow \Phi$ channels. Nevertheless, one could choose another renormalization scheme such as the on-shell scheme as it was discussed in the case of the b -loop contribution in the gg fusion process for SM Higgs production. To estimate this scheme dependence, we evaluate the difference of the $gg \rightarrow \Phi$ cross section in the cases where the b -quark mass is defined in the on-shell and in the $\overline{\text{MS}}$ schemes. Using the program HIGLU, the obtained difference amounts to $\approx +5\%$. Bearing in mind the fact that the corrections could have been negative if we had adopted another scheme (as would have been the case if we have used the $\overline{\text{DR}}$ scheme for instance, although the difference from the $\overline{\text{MS}}$ result would have been at the level of a few percent only), an error $\Delta_{m_b}^{\text{scheme}} \approx \pm 5\%$ could be assigned to the $gg \rightarrow \Phi$ cross section. This is

the procedure that we will adopt here.

Note that there is one another way to estimate the renormalization scheme dependence of the b -quark mass: it would be to look at the differences that one obtains by using $\bar{m}_b(\frac{1}{2}\bar{m}_b)$ and $\bar{m}_b(2\bar{m}_b)$ as inputs in the $gg \rightarrow \Phi$ cross section⁷³. In this case, one obtains an uncertainty that is in fact much larger than the difference between the on-shell and $\overline{\text{MS}}$ schemes and which goes both ways, $\Delta_{m_b}^{\text{scheme}} \approx -10\%, +30\%$ for $M_\Phi = 90$ GeV for instance.

In the $b\bar{b} \rightarrow \Phi$ process, we cannot perform this exercise as the cross section, using the program `bbh@nnlo` can only be evaluated in the $\overline{\text{MS}}$ scheme with the Yukawa couplings evaluated at the scale μ_R . Nevertheless as stated a few lines above this scheme dependence can in this case be related to the scale uncertainty itself as in this process we use $\bar{m}_b(\mu_R)$. This is the reason why we extended the domain of scale variation in this case to $\frac{1}{3}\mu_0 \leq \mu_R, \mu_F \leq 3\mu_0$. The larger scale uncertainty obtained this way could be seen as indirectly taking care of the scheme dependence.

- The second source of uncertainty is of parametric nature and is the same as the one affecting the $H \rightarrow b\bar{b}$ partial decay width of the Higgs boson discussed in section 6. It is estimated as previously, i.e. by evaluating the maximal values of the cross sections when one includes the error on the input b -quark mass at the scale \bar{m}_b , $\bar{m}_b(\bar{m}_b) = 4.19_{-0.06}^{+0.18}$ GeV⁷⁴, and in the case of the $b\bar{b} \rightarrow \Phi$ process where the Yukawa coupling is defined at the high scale, the strong coupling constant, $\alpha_s(M_Z^2) = 0.1171 \pm 0.0014$ at NNLO, used to run the mass $\bar{m}_b(\bar{m}_b)$ upwards to $\bar{m}_b(\mu_R)$. In the considered Higgs mass range, one obtains an uncertainty of $\Delta_{m_b}^{\text{input}} \approx -4\%, +13\%$ and $\approx -3\%, +10\%$ in the case of, respectively, the $gg \rightarrow \Phi$ and $b\bar{b} \rightarrow \Phi$ processes (using the central MSTW PDF set). The difference is mainly due to the fact that the bottom quark masses in the two processes are not defined at the same scale and, also, in the case of the $gg \rightarrow \Phi$ process, additional corrections which involve the b -quark mass, $\propto \ln(\bar{m}_b^2/M_\Phi^2)$, occur at leading order.

⁷³We should note that the scheme dependence actually appears also as a result of the truncation of the perturbative series which, in principle, should already be accounted for by the scale variation. However, the scales which enter in the b -quark mass, that is defined at m_b itself, and in the rest of the $gg \rightarrow \Phi$ matrix element, which is the Higgs mass or the scale μ_R , are different. We have checked explicitly that the scale uncertainties due to the variation of μ_R (and μ_F) in both schemes are comparable. Adding this scheme dependence to the scale variation, as we will do here, is similar in practice to increase the domain of scale variation from the central scale while sticking to a given mass renormalization scheme. We thank Michael Spira for a discussion on this point.

⁷⁴We use our old set-up that was developed before the final stage of the thesis and published in Ref. [232]. Note that the final uncertainty obtained being quite small, the new choice for m_b presented in section 6 only changes marginally the final results, not to mention that this uncertainty will cancel out when taking into account the branching fraction, see in the following section 13.

- Finally, a third source of uncertainty originates from the choice of the b -mass value in the b -quark densities. The MSTW collaboration has released last year a set of PDFs with different bottom quark masses [234]: it involves six different central PDFs with a range of on-shell m_b values between 4.00 GeV and 5.50 GeV in 0.25 GeV steps, in addition to the central best-fit with $m_b = 4.75$ GeV. In order to distinguish between the parametric uncertainty in m_b and the one due to the correlated PDF- Δm_b uncertainty, we have chosen to calculate the latter uncertainty by taking the minimal and maximal values of the production cross sections when using the central value $m_b = 4.75$ GeV and the two closest ones upwards and downwards, i.e. $m_b = 4.5$ GeV and $m_b = 5$ GeV in the MSTW PDF set⁷⁵. However, we kept in the partonic calculation the central value of $\overline{m}_b(\overline{m}_b) = 4.19$ GeV which, approximately corresponds to the pole mass $m_b = 4.75$ GeV. One obtains an approximate 7–9% uncertainty depending on the considered Higgs mass range. Note that this uncertainty will not only affect the cross section in the $bb \rightarrow \Phi$ process in which the b -densities play the major role, but also the one of the $gg \rightarrow \Phi$ channel; however, in this case, the change is below the percent level and can be safely neglected.

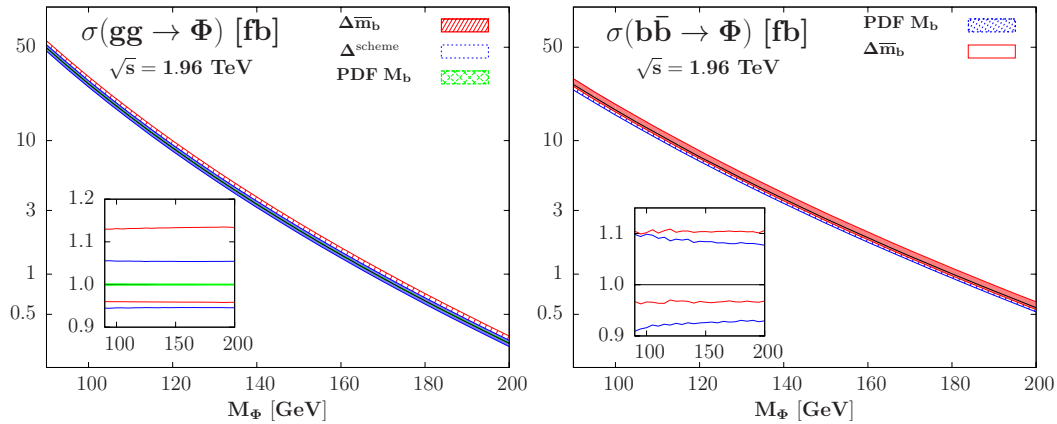


Figure 58: The scheme, parametric and PDF uncertainties due to the b -quark mass in the $gg \rightarrow \Phi$ (left) and $b\bar{b} \rightarrow \Phi$ (right) cross sections at the Tevatron as a function of M_Φ . In the inserts, the relative deviations are shown.

The effect of these three sources of uncertainties is displayed in Fig. 58 for $gg \rightarrow \Phi$ and $b\bar{b} \rightarrow \Phi$ as a function of M_Φ . As can be seen, quite large uncertainties occur, in particular in $gg \rightarrow \Phi$ where the scheme uncertainty that is absent in $b\bar{b} \rightarrow \Phi$ is of the same order than the specific b quark mass uncertainty.

⁷⁵Note that when including the 1σ errors on $\overline{m}_b(\overline{m}_b)$, while the upper value corresponds to the pole mass $m_b \approx 5$ GeV, the lower value does not correspond to $m_b = 4.5$ GeV; we will however adopt this smaller value to estimate the uncertainty as no other choice is possible within the MSTW set.

11.5 Summary and combination of the different sources of uncertainties

We now summarize and combine the different sources of uncertainties that have been discussed above and display them in the single Fig. 59 below where we display the $gg \rightarrow A$ and $b\bar{b} \rightarrow A$ with $\tan\beta$ set to unity. In the gg case and almost independently of M_A , the scale variation in a domain with $\kappa = 2$ leads to an uncertainty $\mathcal{O}(\pm 20\%)$, while the uncertainty from the scheme dependence in the renormalization of M_b is about $\pm 6\%$; they add up to $\approx 25\%$ that is only slightly lower than the scale uncertainty in the $b\bar{b}$ process, $\approx 30\%$ for low M_A , in which the domain of variation is extended to $\kappa = 3$. In the $gg \rightarrow A$ ($b\bar{b} \rightarrow A$) channel, the PDF+ $\Delta^{\text{exp+th}}\alpha_s$ (with ΔM_b in addition for $b\bar{b} \rightarrow A$) uncertainties are at the level of $\pm 10\%$ ($\pm 20\%$) for $M_A \approx 100$ GeV and larger ($\pm 30\%$ in $b\bar{b} \rightarrow A$) at $M_A \approx 200$ GeV where the more uncertain high Bjorken- x values for the gluon and bottom quark densities are probed. The parametric error on \bar{m}_b leads to a $\approx +13\%$, -4% uncertainty in the $gg \rightarrow A$ process and slightly less in the case of $b\bar{b} \rightarrow A$.

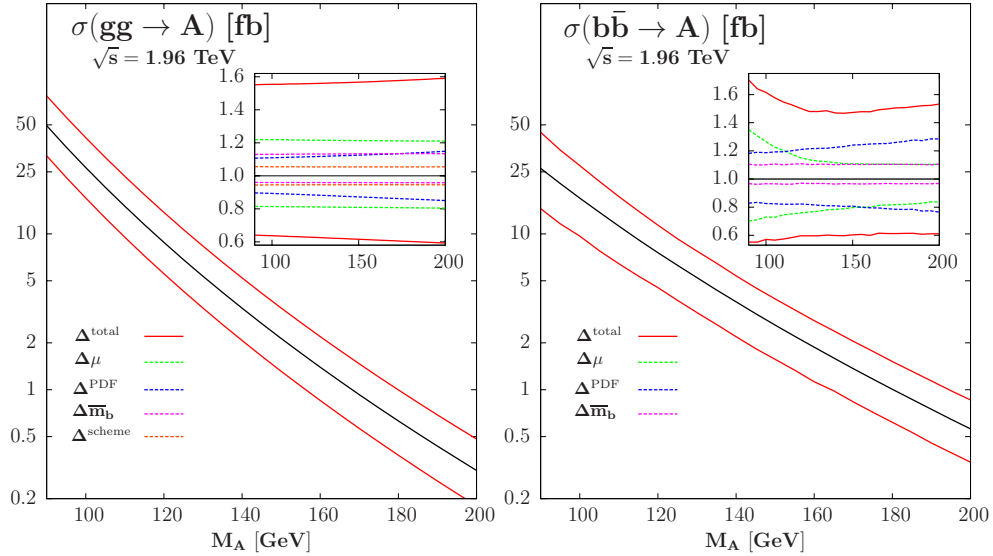


Figure 59: The normalization of the cross sections $\sigma_{gg \rightarrow A}^{\text{NLO}}$ (left) and $\sigma_{b\bar{b} \rightarrow A}^{\text{NNLO}}$ (right) at Tevatron energies as a function of M_A when using the MSTW PDFs and unit $A\bar{b}b$ couplings together with the total uncertainty. In the inserts, shown are the various sources of theoretical uncertainties when the rates are normalized to the central values.

How to combine these uncertainties together in the final total theoretical uncertainty? We will follow the same set-up developed in part II in the case of the SM Higgs production. To begin with the scheme and scale uncertainties being pure theoretical uncertainties they add up linearly. We then follow our recipe developed for the first time in Ref. [232] to deal with the combination of the scale/scheme and PDF+ $\Delta\alpha_s+\Delta m_b$ (the last one refers to the uncertainties related to the choice of the b quark mass within the PDFs): we would

like to view these uncertainties as a way of handling the theoretical ambiguities due to the parametrization of the PDF and we will evaluate them on the minimal and maximal values with respect to the scale variation. We then add linearly in the end the parametric uncertainties on the b quark mass. This last source of uncertainty will be discussed again in the following section when dealing with the combination with branching fractions.

The combined uncertainties on the cross sections, when using this procedure, are also shown in Fig. 59 for the two production channels. As shown they are very large: at low Higgs masses, $M_A \approx 100$ GeV, we obtain $\approx +55\%$, -35% for $\sigma(gg \rightarrow A)$ and $\approx +60\%$, -40% for $\sigma(b\bar{b} \rightarrow A)$ which become at masses $M_A \approx 200$ GeV, respectively, $\approx +60\%$, -40% and $\approx +50\%$, -40% .

We have ended the study of the main neutral MSSM Higgs bosons production channels at the Tevatron. We will now make the same exercise at the IHC collider, and leave the display of the table of results for the final section 13 where the combination with the branching fractions will also be presented.

12 MSSM Higgs production at the LHC

We now turn our attention to the study of the MSSM Higgs production at the CERN LHC collider. The LHC started its operations at 7 TeV in 2010 and has already provided interesting results regarding to MSSM searches, see Ref. [329, 330]. The quest for MSSM Higgs bosons has also started and some results have already been published [352, 353]. In the final stage of the writing of the thesis new results have been presented at HEP-EPS 2011 conference, but they will not be commented before section 13 and the final conclusion of this thesis.

We will reproduce the same outlines of section 11 and use the same set-up, that is neglecting the genuine SUSY corrections as justified in section 10.2, using SM-like couplings for the A boson and conducting our study in the case of the maximal mixing scenario where the upper bound on the mass of the lightest h boson is shifted from the tree level value M_Z to the value $M_h^{\max} \sim 110\text{--}135$ GeV [338–340], the H boson being almost degenerate with the A boson and having the same properties, or the no-mixing scenario where the role of the h boson and the H boson is exchanged. Ref. [327] gives widely used benchmark scenarios that fall into these two regimes. We will give the predictions for the bottom quarks fusion and gluon–gluon fusion production channels at the LHC together with a detailed study of the various theoretical uncertainties affecting the calculation: the unknown higher order corrections evaluated by the variation of the renormalization and factorization scales, the impact of the PDF and the associated uncertainty related to the value of the strong coupling constant α_s and finally the uncertainties due to the b quark mass, its experimental value together with its renormalization scheme choice. We will see in the next section the impact of these uncertainties on the $[M_A, \tan \beta]$ parameter space studied by the ATLAS and CMS experiments. All of the material was published in Refs. [232, 326].

12.1 Gluon–gluon fusion and bottom quarks fusion channels

As in the Tevatron case the two most important channels are the bottom quarks fusion and the gluon–gluon fusion at the LHC. As stated before, CP invariance forbids A couplings to gauge bosons at tree-level: the pseudoscalar A boson cannot be produced in the Higgsstrahlung and vector boson fusion processes. We concentrate on the high $\tan \beta$ regime that is relevant at the LHC which means that the b -quark will play the major role as its couplings to the CP -odd like Higgs bosons are enhanced.

We remind that in the $gg \rightarrow \Phi$ processes with only the b -quark loop included, the QCD corrections are known only to NLO for which the exact calculation with finite loop quark

masses is available [105]. We will again use the central scale $\mu_R = \mu_F = \mu_0 = \frac{1}{2}M_H$ to approach the SM case which is valid for the SM-like CP -even Higgs boson, thus having a consistent set-up for the three neutral Higgs bosons. In the case of the $pp \rightarrow b\bar{b}\Phi$ processes, the NLO QCD corrections have been calculated in Ref. [192, 333]. We will again use the five flavor scheme in which the bottom quarks are directly taken from the proton sea and the LO partonic process being $b\bar{b} \rightarrow \Phi$ [332]. The NNLO corrections are of moderate size when using the central scale $\mu_F = \mu_R = \mu_0 = \frac{1}{4}M_\Phi$ as recommended in Ref. [194] and the bottom quark mass in the $\overline{\text{MS}}$ renormalization scheme.

In order to evaluate the Higgs production cross sections at LHC energies in these two main processes, $gg \rightarrow \Phi$ and $b\bar{b} \rightarrow \Phi$, we will proceed as follows. We only evaluate the cross sections for the pseudoscalar A boson: in the $gg \rightarrow A$ process at NLO using the program HIGLU [152, 153] with a central scale $\mu_R = \mu_F = \mu_0 = \frac{1}{2}M_A$ (and where only the bottom quark loop contribution is included by setting $\lambda_{Att} = 0$), and in the $b\bar{b} \rightarrow A$ process up to NNLO using again the program `bbh@nnlo` [194] with a central scale $\mu_R = \mu_F = \mu_0 = \frac{1}{4}M_A$. In both cases, we work in the $\overline{\text{MS}}$ scheme for the renormalization of the bottom-quark mass. However, while $\overline{m}_b(\overline{m}_b)$ is used in the gg fusion process, $\overline{m}_b(\mu_R)$ is adopted in the $b\bar{b}$ fusion channel. In both processes, we assume the $Ab\bar{b}$ coupling to be SM-like, that is, we will not include the $\tan\beta$ term and the SUSY corrections to Δm_b . To obtain the actual cross section for both CP -even and CP -odd Higgs production, a factor of $2 \tan^2 \beta$ has to be included. As a consequence of chiral symmetry for $M_\Phi \gg \overline{m}_b$ and since the H (h) masses and couplings are very close to those of A , this turns out to be an excellent approximation as stated in section 10.2.

Within this set-up, the best values of the cross sections for $gg \rightarrow \Phi$ and $b\bar{b} \rightarrow \Phi$ are shown in Fig. 60 as a function of the Higgs mass M_Φ when the MSTW sets of (NLO for the former and NNLO for the latter process) PDFs are used to parametrize the gluon and bottom-quark densities. Center of mass energies in a range between $\sqrt{s} = 7$ TeV and 14 TeV relevant for the LHC are considered. It can be noticed that the cross sections for $gg \rightarrow \Phi$ and $b\bar{b} \rightarrow \Phi$ are comparable at a given energy and they significantly increase with increasing center of mass energies or decreasing Higgs mass. If, for example, the value $\tan\beta = 10$ is adopted, the numbers in Fig. 60 have to be multiplied by a factor $\simeq 200$ to obtain the true cross section for both A and $H(h)$ production. For low to moderate M_Φ values, the expected event rates are thus simply huge at the LHC, despite of the relatively low luminosities that are expected. This explains why the chances for observing a Higgs boson at the LHC are much higher in the MSSM than in the SM, as in the former case the production rates can be two to three orders of magnitude larger.

We are left to evaluate the theoretical uncertainties on the production cross sections

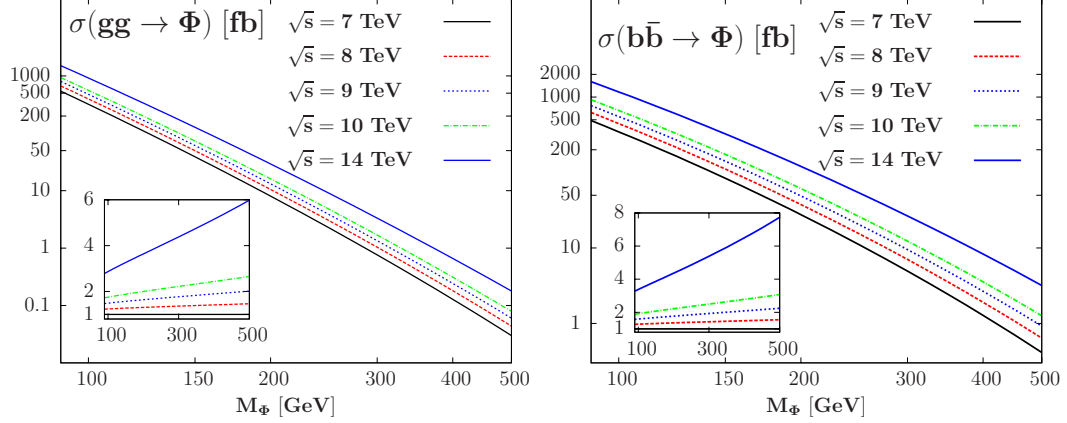


Figure 60: The production cross sections in the processes $gg \rightarrow \Phi$ (left) at a central scale $\mu_R = \mu_F = \mu_0 = \frac{1}{2}M_\Phi$ and $b\bar{b} \rightarrow \Phi$ (right) at a central scale $\mu_R = \mu_F = \mu_0 = \frac{1}{4}M_\Phi$ as a function of M_Φ for several center of mass energies relevant for the LHC. The MSTW sets of PDFs at the required perturbative order have been used. Only the cross section in the pseudoscalar A case but with a SM-like Yukawa coupling is included.

and, for this purpose, we will follow very closely the procedure developed for the SM Higgs boson and in particular in the end use the procedure A) for the total uncertainty. For the numerical analysis, we will only consider the case of the LHC at $\sqrt{s} = 7$ TeV: the uncertainties at center of mass energies slightly above this value, $\sqrt{s} = 8$ – 10 TeV, and even for the LHC energy $\sqrt{s} = 14$ TeV are expected to be comparable. We will start by the scale uncertainty, followed by the estimation of the PDF and α_s effects and end with the b quark issue, strictly following the procedure developed in the case of the Tevatron⁷⁶.

12.2 The scale uncertainty at the LHC

In the case of the $gg \rightarrow \Phi$ process, as for the SM Higgs boson, the scale uncertainty is evaluated by allowing for a variation of the renormalization and factorization scales within a factor of two around the central scale, $\frac{1}{2}\mu_0 \leq \mu_R, \mu_F \leq 2\mu_0$ with $\mu_0 = \frac{1}{2}M_\Phi$. For the $b\bar{b} \rightarrow \Phi$ case, we will extend the domain of scale variation to a factor of three around the central scale $\mu_0 = \frac{1}{4}M_\Phi$, $\frac{1}{3}\mu_0 \leq \mu_R, \mu_F \leq 3\mu_0$ but with the additional restriction $1/\kappa \leq \mu_R/\mu_F \leq \kappa$ imposed. We then follow strictly the procedure adopted in the case of the Tevatron in the previous subsection 11.2. Again, as to illustrate the much larger

⁷⁶Note that since in our analysis we are not considering the SUSY particle contributions and focus only on the standard QCD effects, additional uncertainties from the SUSY sector should, in principle, also be present. Nevertheless, at high $\tan\beta$, the genuine SUSY contributions should not be significant and can be ignored, while the corrections entering in Δ_b will almost cancel out when the $\tau^+\tau^-$ decays are considered. See section 10.2 for more details which justify this approach.

scale uncertainty that is possible in the $b\bar{b} \rightarrow \Phi$ case, we will also show results when this constraint is relaxed as also displayed in Ref. [210].

The results for $\sigma(gg \rightarrow \Phi)$ and $\sigma(b\bar{b} \rightarrow \Phi)$ at the LHC, for scale variations in the domains $\mu_0/\kappa \leq \mu_R, \mu_F \leq \kappa\mu_0$ with $\kappa = 2$ and 3 are shown in Fig. 61 as a function of M_Φ . One can see that the scale variation is moderate for $gg \rightarrow \Phi$ with $\kappa = 2$, despite of the fact that the process is known only at NLO, leading to an uncertainty of order $\pm 10\%$ in the entire Higgs mass range. Extending the variation domain to $\kappa = 3$ will increase the uncertainty by another $\approx 10\%$. As in the SM Higgs case, the maximal and minimal values of the cross sections are approximately obtained for $\mu_R \approx \mu_F$ and thus, varying independently the two scale does not affect the uncertainty. For $\kappa = 2$ when the restriction $\frac{1}{2} \leq \mu_R/\mu_F \leq 2$ is imposed, the uncertainty is also small in the case of $b\bar{b} \rightarrow \Phi$, $\approx \pm 10\%$ at low Higgs masses and less for higher masses; this was to be expected as the process is evaluated at NNLO. However, the extension to $\kappa = 3$, while keeping the restriction $\frac{1}{3} \leq \mu_R/\mu_F \leq 3$, will significantly increase the uncertainty: one would have $-18\%, +24\%$ at $M_\Phi = 100$ GeV and $-13\%, +6\%$ at $M_\Phi = 200$ GeV. If the restriction on μ_R/μ_F is ignored the uncertainty blows up, especially for very low Higgs masses: one would have a variation of $-45\%, +25\%$ at $M_\Phi = 100$ GeV, as also noticed in Ref. [210].

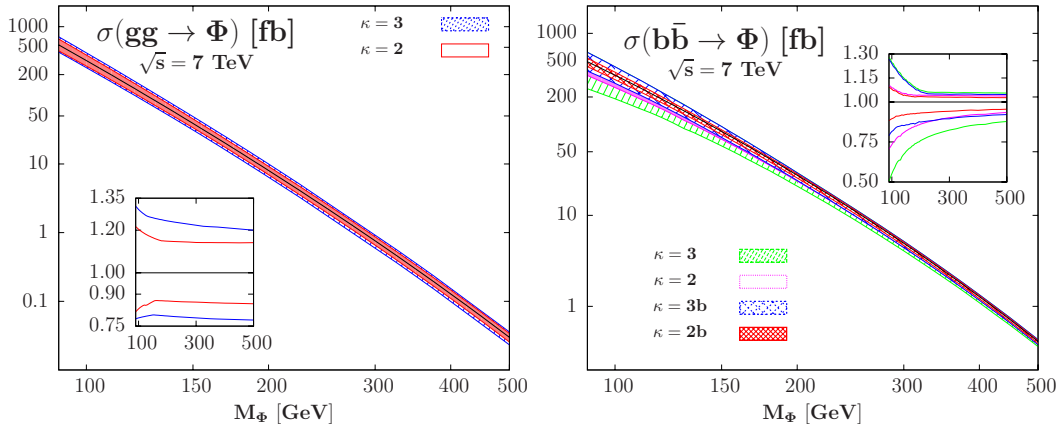


Figure 61: The scale uncertainty bands of the NLO $gg \rightarrow \Phi$ (left) and the NNLO $b\bar{b} \rightarrow \Phi$ (right) cross sections at the LHC at 7 TeV as a function of M_Φ ; different values $\kappa = 2, 3$ are used and the results are shown when the additional constraint $1/\kappa \leq \mu_R/\mu_F \leq \kappa$ is imposed or not (marked as κb). In the inserts, the relative deviations (compared to the central cross section values) are shown.

Hence, the cross section for $b\bar{b} \rightarrow \Phi$ is rather unstable against scale variation and this justifies, a posteriori, the choice of a larger domain of variation with $\kappa = 3$ in this case, a choice that does not appear to be a too extreme one when looking at Fig. 61.

12.3 The PDF and α_s uncertainties at the LHC

Let us now turn to the estimation of the uncertainties from the parton densities and α_s . The 90% CL PDF+ $\Delta^{\text{exp}}\alpha_s$ uncertainty, with $\alpha_s(M_Z^2) = 0.120 \pm 0.002$ at NLO for $gg \rightarrow \Phi$ and $\alpha_s(M_Z^2) = 0.1171 \pm 0.0014$ at NNLO for $b\bar{b} \rightarrow \Phi$, is evaluated within the MSTW parametrization when including the experimental error on α_s . To that, we add in quadrature the effect of the theoretical error on α_s , estimated by the MSTW collaboration to be $\Delta^{\text{th}}\alpha_s \approx 0.003$ at NLO and $\Delta^{\text{th}} \approx 0.002$ at NNLO, using the MSTW fixed α_s grid with central PDF sets. The 90%CL PDF, PDF+ $\Delta^{\text{exp}}\alpha_s$ and the PDF+ $\Delta^{\text{exp+th}}\alpha_s$ uncertainties at the LHC are shown in Fig. 62 as a function of M_Φ . In both the $gg \rightarrow \Phi$ and $b\bar{b} \rightarrow \Phi$ processes, the total uncertainty is below $\pm 10\%$ for $M_\Phi \lesssim 200$ GeV but increases at higher masses, in particular in the $b\bar{b} \rightarrow \Phi$ case.

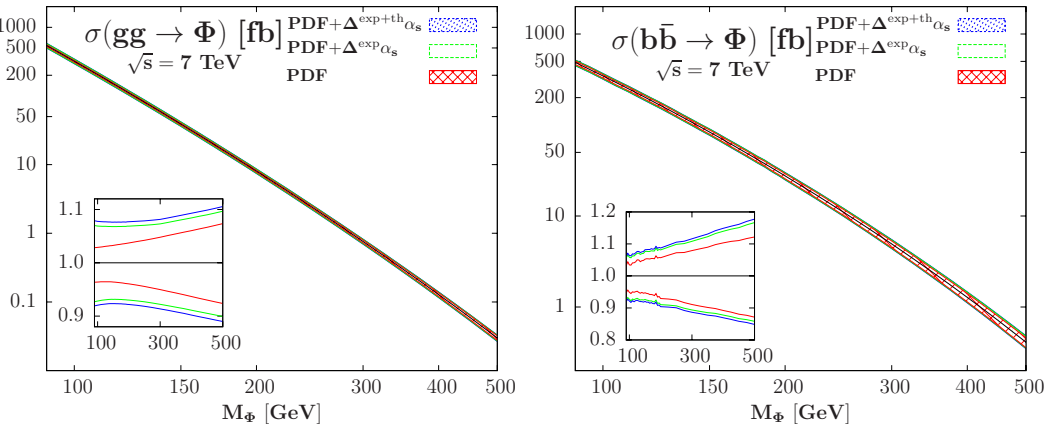


Figure 62: The PDF 90% CL PDF, PDF+ $\Delta^{\text{exp}}\alpha_s$ and PDF+ $\Delta^{\text{exp}}\alpha_s + \Delta^{\text{th}}\alpha_s$ uncertainties in the MSTW scheme in the $gg \rightarrow \Phi$ (left) and $b\bar{b} \rightarrow \Phi$ (right) cross sections at the LHC at 7 TeV as a function of M_Φ . In the inserts, the relative deviations are shown.

For completeness, we also display the two cross sections when one adopts two other PDF sets, ABKM and (G)JR, and compare the results with that of MSTW. As can be seen in Fig. 63, the deviations from the MSTW values are moderate in the case of $b\bar{b} \rightarrow \Phi$ for the JR scheme: a few percent at $M_\Phi = 100$ GeV, increasing to $\approx 10\%$ at $M_\Phi = 500$ GeV. The ABKM scheme leads to substantial deviations at high masses, $\approx 30\%$ at $M_\Phi = 500$ GeV. In the gg fusion process, the prediction with the GJR PDF set at $M_\Phi = 100$ GeV is $\approx 20\%$ lower than in the MSTW and ABKM cases which give comparable results. The GJR and ABKM parameterizations cross at ≈ 200 GeV and at higher masses, the gg cross sections with the ABKM parametrization are $\approx 20\%$ lower than for MSTW results while the predictions with the GJR set are $\approx 10\%$ higher than for MSTW.

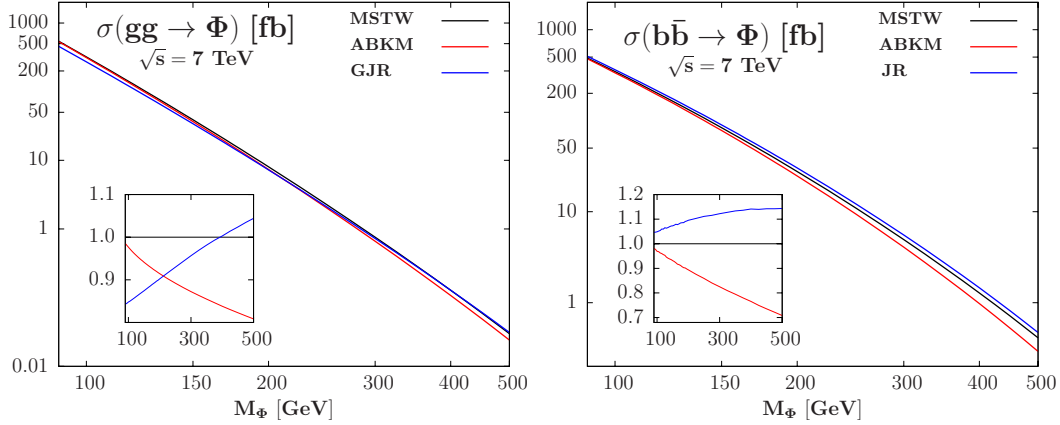


Figure 63: The cross sections in the $gg \rightarrow \Phi$ (left) and $b\bar{b} \rightarrow \Phi$ (right) at the LHC at 7 TeV as a function of M_Φ evaluated when using the ABKM and (G)JR PDF sets. In the inserts, the relative deviations from the value in the MSTW scheme are shown.

12.4 The b -quark mass issue

Finally, there is the effect of the uncertainty on the b -quark mass that was discussed in the case of the Tevatron in subsection 11.4. We reproduce the same outlines in this subsection and summarize the three different sources of uncertainties related to the b quark mass.

The first one is of purely theoretical nature and is due to the choice of the renormalization scheme for the b -quark mass. As in the Tevatron case we have adopted the $\overline{\text{MS}}$ renormalization scheme while other scheme could have been chosen. In order to estimate the effect of the other scheme we calculate the difference between on-shell and $\overline{\text{MS}}$ scheme predictions in the case of the gluon-gluon fusion process, and we include this scheme dependence in the scale uncertainty in the case of the bottom quarks fusion production channel. Using the program HIGLU, we obtain a $\approx +15\%$ difference in the $gg \rightarrow \Phi$ cross section⁷⁷. Bearing in mind the fact that the corrections could have been negative if we had adopted another scheme we assign an uncertainty $\Delta_{m_b}^{\text{scheme}} \approx \pm 15\%$ to the $gg \rightarrow \Phi$ cross section.

The second source of uncertainty is due to the experimental errors on the value of the b quark mass \bar{m}_b , $\bar{m}_b(\bar{m}_b) = 4.19_{-0.06}^{+0.18}$ GeV⁷⁸, and in the case of the $b\bar{b} \rightarrow \Phi$ process where the Yukawa coupling is defined at the high scale, the strong coupling constant, $\alpha_s(M_Z^2) = 0.1171 \pm 0.0014$ at NNLO, used to run the mass $\bar{m}_b(\bar{m}_b)$ upwards to $\bar{m}_b(\mu_R)$. In the considered Higgs mass range, one obtains an uncertainty of $\Delta_{m_b}^{\text{input}} \approx -4\%, +14\%$ and $\approx -3\%, +10\%$ in the case of, respectively, the $gg \rightarrow \Phi$ and $b\bar{b} \rightarrow \Phi$ processes (using

⁷⁷Using the second way of estimating this scheme uncertainty developed in subsection 11.4 we obtain a bigger uncertainty than the difference between the on-shell and $\overline{\text{MS}}$ schemes and which goes both ways, $\Delta_{m_b}^{\text{scheme}} \approx -20\%, +40\%$ for $M_\Phi = 90$ GeV for instance.

⁷⁸The same remark developed in the Tevatron study also applies in the LHC case, see subsection 11.4.

the central MSTW PDF set). The difference is mainly due to the fact that the bottom quark masses in the two processes are not defined at the same scale and, also, in the case of the $gg \rightarrow \Phi$ process, additional corrections which involve the b -quark mass, $\propto \ln(\bar{m}_b^2/M_\Phi^2)$, occur at leading order. It is interesting to note that this uncertainty is rather non sensible to center-of-mass energies as we obtain the uncertainty calculated at the Tevatron.

The last source of uncertainty originates from the choice of the b -mass value in the b -quark densities. Using the dedicated MSTW PDFs set with different bottom quark masses [234] as already done in the case of the Tevatron study, we have calculated the correlated PDF- Δm_b uncertainty by taking the minimal and maximal values of the production cross sections when using the central value $m_b = 4.75$ GeV and the two closest ones upwards and downwards, i.e. $m_b = 4.5$ GeV and $m_b = 5$ GeV in the MSTW PDF set while keeping in the partonic calculation the central value of $\bar{m}_b(\bar{m}_b) = 4.19$ GeV which approximately corresponds to the pole mass $m_b = 4.75$ GeV. We obtain at the LHC a ≈ 3 -5% uncertainty depending on the considered Higgs mass range in the $b\bar{b} \rightarrow \Phi$ channel, that is smaller than the uncertainty obtained at the Tevatron. As already mentioned in the Tevatron study the gluon-gluon fusion process is marginally affected, the uncertainty being below the percent level.

The effect of these three sources of uncertainties is displayed in Fig. 64 for $gg \rightarrow \Phi$ and $b\bar{b} \rightarrow \Phi$ as a function of M_Φ . As can be seen, large uncertainties occur, in particular in $gg \rightarrow \Phi$ where the $\approx 15\%$ scheme uncertainty that is absent in $b\bar{b} \rightarrow \Phi$ dominates.

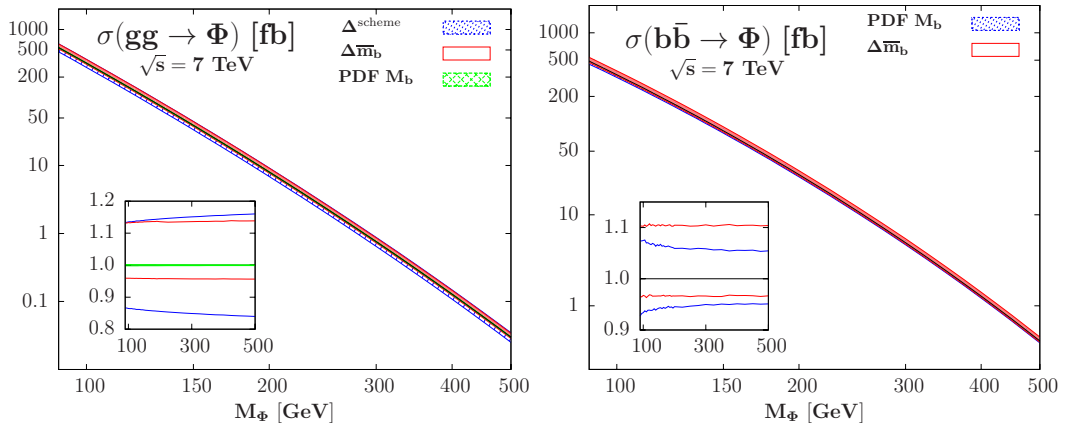


Figure 64: The scheme, parametric and PDF uncertainties due to the b -quark mass in the $gg \rightarrow \Phi$ (left) and $b\bar{b} \rightarrow \Phi$ (right) cross sections at the LHC at 7 TeV as a function of M_Φ . In the inserts, the relative deviations are shown.

12.5 Combination and total uncertainty

We end this section by the summary of the various sources of uncertainty discussed above then we give the final total uncertainty. This is displayed in Fig. 65 below for the two processes $gg \rightarrow \Phi$ and $b\bar{b} \rightarrow \Phi$ at the LHC; we recall again that $\tan\beta$ has been set to unity. The scale uncertainty has been taken in the $gg \rightarrow \Phi$ process with $\kappa = 2$ whereas $\kappa = 3$ has been used in the bottom quarks fusion process, with the additional restriction $1/3 \leq \mu_R/\mu_F \leq 3$. We have obtained almost independently of M_Φ an uncertainty of order $\pm 15\%$ for the gluon–gluon fusion process (a little higher for low Higgs masses $M_\Phi \simeq 90$ GeV) and of order $\pm 10\%$ in the bottom quarks fusion process nearly in the entire range; more precisely it is $-18\%, +24\%$ at $M_\Phi = 100$ GeV and $-13\%, +6\%$ at $M_\Phi = 200$ GeV. In the $gg \rightarrow A$ ($b\bar{b} \rightarrow A$) channel, the PDF + $\Delta^{\text{exp+th}}\alpha_s$ (with ΔM_b in addition for $b\bar{b} \rightarrow A$) uncertainties start from $\pm 10\%$ at low masses and reach the level of $\pm 15\%$ for $M_\Phi \approx 200$ GeV; in $b\bar{b} \rightarrow \Phi$ the situation is almost the same, with a bit higher uncertainty for high masses than in the gluon–gluon fusion process, where the more uncertain high Bjorken- x values for the gluon and bottom quark densities are probed. The parametric error on \bar{m}_b leads to a $+14\%, -3\%$ uncertainty in the $gg \rightarrow \Phi$ process and slightly less in the case of $b\bar{b} \rightarrow \Phi$, $+10\%, -4\%$. We also have an additional scheme uncertainty in the gluon–gluon fusion process that amounts to approximately $\pm 15\%$; this has been taken into account in the bottom quarks fusion channel when extending the scale interval from $\kappa = 2$ to $\kappa = 3$.

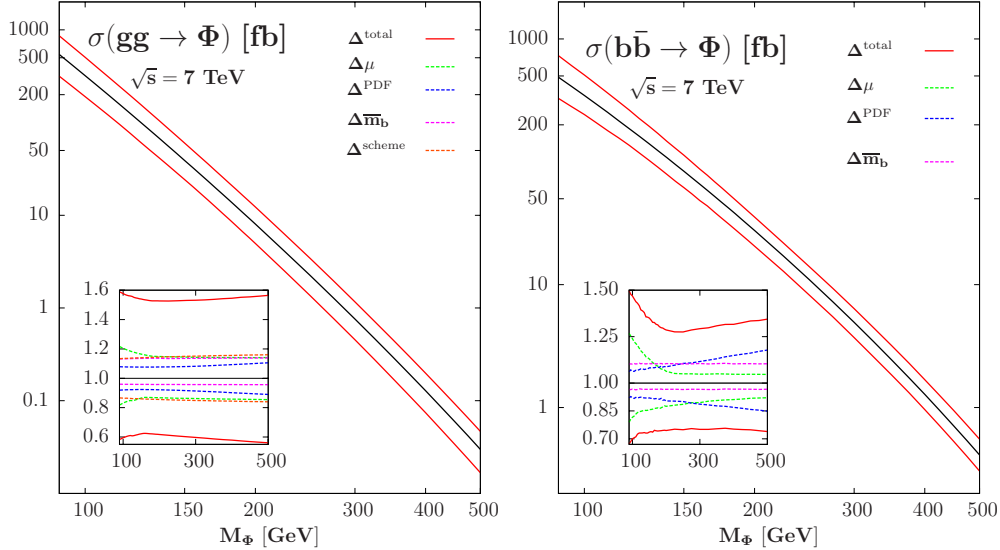


Figure 65: The normalization of the cross sections $\sigma_{gg \rightarrow \Phi}^{\text{NLO}}$ (left) and $\sigma_{b\bar{b} \rightarrow \Phi}^{\text{NNLO}}$ (right) at the LHC with $\sqrt{s} = 7$ TeV as a function of M_Φ when using the MSTW PDFs and unit $\Phi b\bar{b}$ couplings together with the total uncertainty. In the inserts, shown are the various sources of theoretical uncertainties when the rates are normalized to the central values.

We now combine the uncertainties following strictly what has been done in section 11.5

to handle this delicate issue, applying the procedure developed in Ref. [94] to obtain the results published in Ref. [232]. The overall uncertainty on the production cross section is obtained by applying the $\text{PDF} + \Delta^{\text{exp}}\alpha_s + \Delta^{\text{th}}\alpha_s$ uncertainty on the maximal and minimal cross sections from the scale variation, adding linearly the scheme uncertainty.

We detail again the procedure developed to handle the parametric b quark mass issue. The uncertainty from the scheme dependence in the $gg \rightarrow \Phi$ process should be simply, that is linearly, added to the scale uncertainty as both emerge as a result of the truncation of the perturbative series and are thus of pure theoretical nature. The uncertainties of the input b -quark mass which appears in the parton densities should be added (in quadrature, a reflect of its experimental nature) to the other $\text{PDF} + \alpha_s$ uncertainties. Since this uncertainty is much smaller than that of the $\text{PDF} + \Delta^{\text{exp+th}}\alpha_s$ it will have practically no impact on the total $\text{PDF} + \alpha_s$ error⁷⁹. Finally, the parametric uncertainty, which has a special status as it appears also in the Higgs branching ratios as seen later on, can be simply added linearly to the combined scale+scheme+PDF uncertainty; we will see in the next section that it will have no impact in practice.

Applying the procedure above for combining the uncertainties, the results for the processes $gg \rightarrow \Phi$ and $b\bar{b} \rightarrow \Phi$ at the LHC with $\sqrt{s} = 7$ TeV are displayed in Fig. 65 as a function of M_Φ ; the numerical values will be displayed in the next section when we will also quote the numbers from the cross section times branching fractions study. A total uncertainty of approximately +60%, -40% for $\sigma(gg \rightarrow \Phi)$ and +50%, -35% for $\sigma(b\bar{b} \rightarrow \Phi)$ is found in the low Higgs mass range and slightly less at higher masses. As mentioned previously, we expect that these numbers approximately hold at least for slightly higher energies, $\sqrt{s} = 8-10$ TeV, and probably also at the designed LHC with $\sqrt{s} = 14$ TeV.

This completes the analysis of the MSSM neutral Higgs bosons production at the LHC in the two main channels $gg \rightarrow \Phi$ and $b\bar{b} \rightarrow \Phi$. The next step that remains to be done before using these results to constrain the MSSM parameter space is to study the decay branching fractions and the combination of the latter with the production cross sections. This will be the subject of the next-to-next – and last – section of this thesis.

⁷⁹Note that one may also consider an uncertainty related to the charm-quark mass dependence of the PDFs. This can be estimated again as done in the SM case and we find at most $\simeq \pm 2.6\%$ at $M_\Phi = 500$ GeV in both channels. We then neglect this uncertainty added in quadrature to that of the other PDF-related.

12.6 The case of the charged Higgs production in association with top quark at the LHC

Before getting to the comparison with experimental results on the MSSM neutral Higgs bosons production, we wish to present the usefulness of the study of the charged Higgs production in association with one top quark at the LHC. We will see that a quite accurate measure of the fundamental parameter $\tan \beta$ can be done thanks to the left–right asymmetry in the channel $gb \rightarrow tH^-$ and in particular for some values of $\tan \beta$ we can distinguish between type II 2 Higgs Doublet Models (2HDM) which MSSM is an example, and type I 2HDM where only one Higgs field couples to all fermions whereas both couple to the weak and hypercharge bosons.

Once the Higgs bosons have been produced, their mass can be measured looking at the kinematical distributions of the decay products [236,237]. In the MSSM the parameter $\tan \beta$ can be determined looking at the total cross section of processes involving Higgs bosons. For instance in the MSSM the total cross sections $pp(\bar{p}) \rightarrow H, A$ are proportional to $\tan^2 \beta$ as seen in previous sections. A measurement of the relevant production cross sections at the LHC allows for a determination of $\tan \beta$ [131] with an uncertainty of the order of 30%.

Another interesting process is the production of the charged Higgs boson in association with a top quark in bottom–gluon fusion at hadron colliders [354–358]

$$bg \rightarrow tH^-, \quad \bar{b}g \rightarrow \bar{t}H^+, \quad (12.1)$$

in which the bottom quark is directly taken from the proton in a five flavor scheme. The cross section of this process is proportional to the square of the Yukawa coupling $g_{H^\pm tb}$. In type II 2HDMs, such as in the MSSM, $g_{H^\pm tb}$ reads as follows [44],

$$g_{H^\pm tb} = \frac{g}{\sqrt{2}M_W} V_{tb} \{H^+ \bar{t} [m_b \tan \beta P_R + m_t \cot \beta P_L] b + \text{h.c.}\}, \quad (12.2)$$

where $g = e/\sin(\theta_W)$ is the $SU(2)_L$ coupling and $P_{L/R} = (1 \mp \gamma_5)/2$ are the chiral projectors. The CKM matrix element V_{tb} can be set, to a good approximation, to unity [205]. At tree-level the total production cross sections of the processes in Eq. (12.1) are equal and proportional to $(m_t^2 \cot^2 \beta + m_b^2 \tan^2 \beta)$. They are significant both in the $\tan \beta \leq 1$ and in the $\tan \beta \gg 1$ regions⁸⁰. In type I 2HDMs, all fermions couple to only one Higgs field; thus the $g_{H^\pm tb}$ coupling is modified with the substitution $m_b \tan \beta \rightarrow m_b \cot \beta$ in Eq. (12.2). The sum of the total cross section of the two processes in Eq. (12.1) is proportional to $\cot^2 \beta$ and is enhanced for small $\tan \beta$ values only⁸¹.

⁸⁰The total cross section exhibits a minimum at $\tan \beta = \sqrt{m_t/m_b} \approx 7$.

⁸¹We recall that in the MSSM the lower bound of the mass of h requires that $\tan \beta \gtrsim 2\text{--}3$ [205,211]. In

Besides the experimental uncertainties, the cross section measurement is plagued with various theoretical uncertainties as seen in previous section 12. The most important uncertainties are related to the dependence of the observables on the renormalisation and factorisation scales, as well as the dependence on the choice of the parton distribution functions (PDFs), and the related errors on the strong coupling constant α_s . These theoretical uncertainties can be of the order of 20 – 30% [131] and are a major source of error in the determination of $\tan\beta$ directly from the Higgs production cross section. The study of the left–right top asymmetry in the $gb \rightarrow bH^-$ production, followed by the clean and detectable $H^\pm \rightarrow \tau^\pm\nu$ channel, will be proved to be nearly free of these theoretical uncertainties. The polarisation asymmetry A_{LR}^t is defined as the difference of cross sections for the production of left–handed and right–handed top quarks divided by their sum

$$A_{LR}^t \equiv \frac{\sigma_L - \sigma_R}{\sigma_L + \sigma_R}, \quad (12.3)$$

where $\sigma_{L/R}$ is the total hadronic cross section of the process of $t_{L/R}H^-$ associated production. The asymmetry is a ratio of observables of similar nature. Compared to the cross section, the asymmetry is then significantly less affected by the scale and PDF uncertainties. We are then mainly left only with the experimental uncertainties in the determination of the cross sections and with the measurement of the polarisation of the top quarks⁸². In the MSSM, the asymmetry will nevertheless remain sensitive to the electroweak and strong radiative corrections from supersymmetric particles which also strongly affect the cross sections at high $\tan\beta$ values [356, 362, 363]. All the work that will be presented in this section is taken from Ref. [364] and follow the works cited herein that originate from a first study of the asymmetry in the case of associated top–charged slepton production in the MSSM [365]. A detailed analysis of the top polarisation in $bg \rightarrow tH^-$ production has also been given in Ref. [358] which provides material that partly overlaps with the one presented here.

We will first discuss the asymmetry in the tree–level approximation and show its dependence on $\tan\beta$. We then move on to the demonstration that it is nearly independent of the scale and PDF distribution choice, but still remaining dependent on the important MSSM radiative corrections that indeed may help to distinguish between SUSY and non–SUSY scenarios.

a general 2HDM $\tan\beta$ is less constrained: the region $0.2 \lesssim \tan\beta \lesssim 50$ is not ruled out and preserves the perturbativity of the Higgs Yukawa coupling in Eq. 12.2.

⁸²This section will not address the issue of the experimental determination of the top quark polarization; we refer to Refs. [359–361] for this matter.

The A_{LR}^t asymmetry at tree-level

We will fix the notation, and begin with the process

$$b(p_b, \lambda_b) g(p_g, \lambda_g) \rightarrow t(p_t, \lambda_t) H^-(p_H). \quad (12.4)$$

The momentum (helicity) of the particle i is marked as p_i (λ_i). In the tree-level approximation the process is mediated by two Feynman diagrams, one with s -channel bottom quark exchange and another with u -channel top quark exchange. In the case of type II 2HDM couplings the helicity amplitude $F_{\lambda_b \lambda_g \lambda_t}$ reads as follows [357]

$$\begin{aligned} F_{\lambda_b \lambda_g \lambda_t} = & \frac{gg_s \lambda^l \sqrt{x_+}}{2M_W} \left\{ \frac{\delta_{\lambda_b \lambda_g}}{\sqrt{\hat{s}}} \left[\lambda(1-r_t) s_{\theta/2} \delta_{\lambda_b \lambda_t} + \frac{1+r_t}{2} c_{\theta/2} \delta_{\lambda_b - \lambda_t} \right] \right. \\ & + \frac{m_t \delta_{\lambda_b \lambda_g}}{\hat{u} - m_t^2} \left[(1+r_t) s_{\theta/2} \lambda \delta_{\lambda_b \lambda_t} + \frac{1-r_t}{2} c_{\theta/2} \delta_{\lambda_b - \lambda_t} \right] \\ & + \frac{(1-r_t) s_{\theta/2} \lambda \delta_{\lambda_b \lambda_t}}{\hat{u} - m_t^2} [-p(1+c_\theta) \delta_{\lambda_b - \lambda_g} + d_t \delta_{\lambda_b \lambda_g}] \\ & \left. + \frac{(1+r_t) c_{\theta/2} \delta_{\lambda_b - \lambda_t}}{2(\hat{u} - m_t^2)} [p(1-c_\theta) \delta_{\lambda_b - \lambda_g} + d_t \delta_{\lambda_b \lambda_g}] \right\} [m_t \cot \beta \delta_{\lambda_t L} + m_b \tan \beta \delta_{\lambda_t R}] \end{aligned} \quad (12.5)$$

We will define the partonic Mandelstam variables as $\hat{s} = (p_b + p_g)^2$ and $\hat{u} = (p_b - p_H)^2$. The angle θ is the azimuthal angle in the center-of-mass frame, g_s is the strong coupling constant. The abbreviations d_t , r_t , x_\pm and λ read as follows

$$d_t = \sqrt{\hat{s}} - E_t + p \cos \theta, \quad r_t = \sqrt{\frac{x_-}{x_+}}, \quad x_\pm = \left(\sqrt{\hat{s}} \pm m_t \right)^2 - M_{H^\pm}^2, \quad (12.6)$$

$$\lambda = \sqrt{(1 - (x_t + x_h)^2)(1 - (x_t - x_h)^2)},$$

while $p \equiv |\mathbf{p}_t|$, $c_\alpha \equiv \cos \alpha$, and $s_\alpha \equiv \sin \alpha$.

The partonic cross sections for L/R polarized top quarks in the final state is then

$$\hat{\sigma}_{L/R} = \frac{p}{384\pi \hat{s}^{3/2}} \int_{-1}^{+1} d\cos \theta \sum_{\lambda_b, \lambda_g} |F_{\lambda_b \lambda_g L/R}|^2. \quad (12.7)$$

The integration over the angle θ finally leads to

$$\begin{aligned}
\hat{\sigma}_L &= \frac{G_F \alpha_s}{24\sqrt{2}\hat{s}\lambda} \left\{ \lambda \left[m_t^2 \cotan^2 \beta \left(\frac{7}{2} \lambda x_{ht}^2 + 2x_{ht}^2 + 2(1-x_{ht}^2)^2 + \frac{3}{2}(\lambda-1)\lambda \right) \right. \right. \\
&\quad \left. \left. - m_b^2 \tan^2 \beta \left(-\frac{7}{2} \lambda x_{ht}^2 + 2x_{ht}^2 + 2(1-x_{ht}^2)^2 + \frac{3}{2}\lambda(\lambda+1) \right) \right] + \right. \\
&\quad \left. \Lambda \left[m_t^2 \cotan^2 \beta \left((x_{ht}^2 + 2\lambda)(1-x_{ht}^2)^2 + (\lambda+1)(x_{ht}^2(\lambda+1)-1) \right) \right. \right. \\
&\quad \left. \left. + m_b^2 \tan^2 \beta \left((2\lambda-x_{ht}^2)(1-x_{ht}^2)^2 + ((\lambda-1)x_{ht}^2+1)(1-\lambda) \right) \right] \right\}, \\
\hat{\sigma}_R &= \frac{G_F \alpha_s}{24\sqrt{2}\hat{s}\lambda} \left\{ \lambda \left[m_b^2 \tan^2 \beta \left(\frac{7}{2} \lambda x_{ht}^2 + 2x_{ht}^2 + 2(1-x_{ht}^2)^2 + \frac{3}{2}(\lambda-1)\lambda \right) \right. \right. \\
&\quad \left. \left. - m_t^2 \cotan^2 \beta \left(-\frac{7}{2} \lambda x_{ht}^2 + 2x_{ht}^2 + 2(1-x_{ht}^2)^2 + \frac{3}{2}\lambda(\lambda+1) \right) \right] + \right. \\
&\quad \left. \Lambda \left[m_b^2 \tan^2 \beta \left((x_{ht}^2 + 2\lambda)(1-x_{ht}^2)^2 + (\lambda+1)(x_{ht}^2(\lambda+1)-1) \right) \right. \right. \\
&\quad \left. \left. + m_t^2 \cotan^2 \beta \left((2\lambda-x_{ht}^2)(1-x_{ht}^2)^2 + ((\lambda-1)x_{ht}^2+1)(1-\lambda) \right) \right] \right\}. \quad (12.8)
\end{aligned}$$

where $x_i = m_i/\sqrt{\hat{s}}$ and $x_{ht}^2 = x_h^2 - x_t^2$ and Λ is defined as

$$\Lambda = \ln \left(\frac{1-x_{ht}^2+\lambda}{1-x_{ht}^2-\lambda} \right). \quad (12.9)$$

The total partonic cross section is then simply the sum of the cross sections $\hat{\sigma}_L$ and $\hat{\sigma}_R$

$$\hat{\sigma}_{\text{tot}} = \frac{G_F \alpha_s}{24\sqrt{2}\hat{s}} (m_t^2 \cot^2 \beta + m_b^2 \tan^2 \beta) \left\{ 2 [1-2x_{ht}^2(1-x_{ht}^2)] \Lambda - (3-7x_{ht}^2)\lambda \right\}. \quad (12.10)$$

The final hadronic cross sections $\sigma_{L,R}$ are the convolution of these partonic cross sections with the bottom-quark and gluon parton distribution functions. The results for the type I 2HDM are obtained once we perform the switch $m_b \tan \beta \rightarrow m_b \cot \beta$.

In Fig. 66 we display the left- and right-handed cross sections σ_L and σ_R as well as the asymmetry A_{LR}^t at the LHC with $\sqrt{s} = 7$ TeV as a function of $\tan \beta$. We choose two values of M_{H^\pm} , $M_{H^\pm} = 230$ and 412 GeV corresponding to the two MSSM scenarios proposed in Refs. [362] (LS2) and [366] (SPS1a) respectively. We have adopted the CTEQ6L1 leading order PDFs [145] with $\alpha_s(M_Z^2) = 0.130$. The factorisation scale μ_F has been set to the value $\mu_0 = (M_{H^\pm} + m_t)/6$ which according to Ref. [356] is known to minimize the higher order QCD corrections. For the H^-tb coupling, we use the on-shell top mass value $m_t = 173.1$ GeV and the $\overline{\text{MS}}$ mass of the bottom quark evaluated at a scale $\mu = \mu_F$. In the analysis

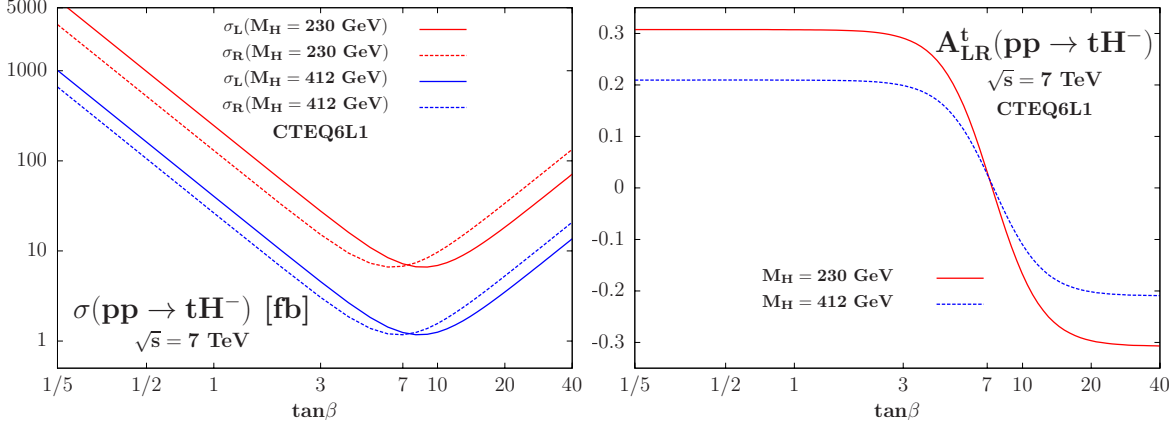


Figure 66: The LO cross sections σ_L and σ_R (left) and the left–right top asymmetry A_{LR} at leading order (right) at the LHC with $\sqrt{s} = 7$ TeV in two benchmark scenarios with $M_{H^\pm} = 230$ and 412 GeV in type II 2HDMs.

presented in this section, $m_b(\mu)$ is approximately equal to 3 GeV depending on the values of μ_F considered [364].

As we can see in Fig. 66, σ_L and σ_R have the same order of magnitude: they are large at small $\tan\beta$ values, when the component $m_t \cot\beta$ of the H^-tb coupling is significant, as well as at large $\tan\beta$ value when the $m_b \tan\beta$ component of the coupling is enhanced. The cross sections are equal and minimal at the value $\tan\beta = \sqrt{m_t/m_b} \simeq 7$ for which the H^-tb coupling is the smallest. This implies that in type II 2HDM (such as the MSSM) A_{LR}^t is maximal at low $\tan\beta$ values when the associated top quark is mostly left–handed and minimal at large $\tan\beta$ values when the top quarks are right handed. For a given value of the charged Higgs mass, the absolute value of A_{LR}^t is the same in the $\tan\beta \gg 1$ and in the $\tan\beta \leq 1$ region. In the scenarios under consideration $|A_{LR}^t| = 0.31$ (0.21) for $M_{H^\pm} = 230$ (412) GeV. The two $\tan\beta$ regions differ for the sign of the asymmetry. Therefore the sign of A_{LR}^t helps to distinguish between the low and large $\tan\beta$ scenarios. In the intermediate $\tan\beta$ region, $\tan\beta \simeq 7$ for which $\sigma_L \simeq \sigma_R$, the asymmetry goes through zero.

The behaviour in a type I 2HDM is completely different: the left– and right– components of the Yukawa coupling $g_{H^\pm tb}$ are both proportional to $\cot\beta$, and there is no $\tan\beta$ dependence in A_{LR}^t , which implies that the asymmetry is constant and simply given by the A_{LR}^t value in the corresponding type II model evaluated at $\tan\beta = 1$. For type I 2HDM characterized by $M_{H^\pm} = 230$ (412) GeV the value of A_{LR}^t can be read off Fig. 66, $A_{LR}^t = 0.31$ (0.21). Combining this value with the value of $\sigma_{\text{tot}} \propto \cot^2\beta$, the predictions of 2HDMs of type I and II can eventually be discriminated.

It is worth mentioning that while σ_L, σ_R and thus σ_{tot} strongly depend on the hadronic

center-of-mass energy, the asymmetry dependence of A_{LR}^t is mild. The asymmetry is comparable for $\sqrt{s} = 7$ and 14 TeV. For instance at $\sqrt{s} = 14$ TeV in the type I model one obtains $A_{LR}^t = 0.27$ (0.18) for $M_{H^\pm} = 230$ (412) GeV.

Scale and PDF dependence; impact of the SUSY NLO corrections

Up until now we have calculated the asymmetry only at leading order, and made central predictions. The yet uncalculated higher order QCD contributions on this observable can be estimated from its dependence on the factorisation scale μ_F at which the process is evaluated. Starting from our reference scale μ_0 we vary μ_F within the range $\mu_0/\kappa \leq \mu_F \leq \kappa\mu_0$ with the constant factor chosen to be $\kappa = 2, 3$ or 4. The left panel of Fig. 67 shows the variation of the polarisation asymmetry for the choices $\kappa = 2, 3$ and 4. The insert shows the scale variation relative to the asymmetry value when the central scale is adopted.

The main output of this calculation is that the scale dependence is very low. Indeed, in the low and in the high $\tan\beta$ region, it is at most at the level of 2%, even for the high $\kappa = 4$ choice for the scale interval. At moderate values of $\tan\beta$, $\tan\beta \simeq 7$, the relative variation is much larger since the asymmetry vanishes⁸³. However the absolute impact of the scale variation is comparable to the one obtained for low and high $\tan\beta$ values, and thus small in absolute terms. It is worth mentioning that the NLO QCD total cross section σ_{tot} exhibits a bigger residual scale uncertainty estimated to be of the order of 10–20% at the LHC with $\sqrt{s} = 7$ TeV, see Ref. [210].

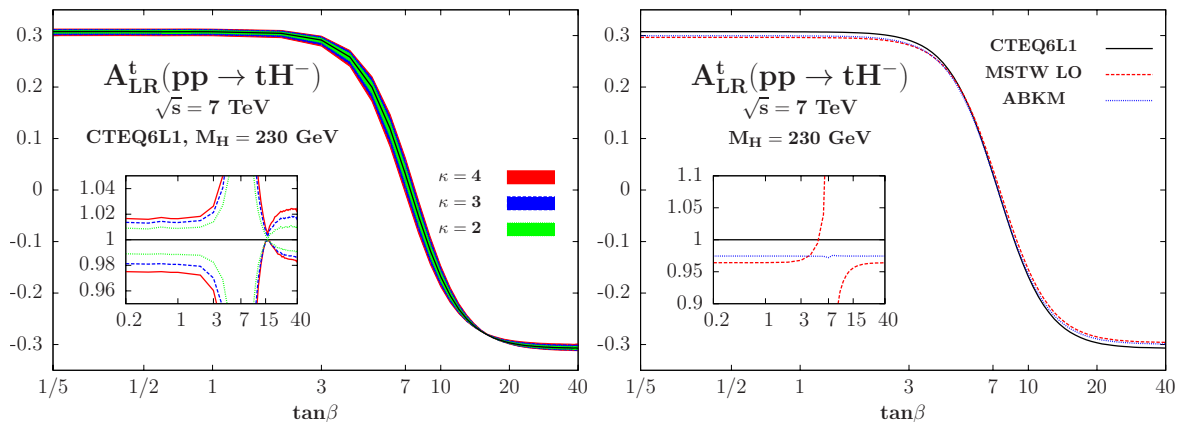


Figure 67: The scale variation (left) and the PDF dependence (right) of the asymmetry A_{LR}^t at leading order at the LHC with $\sqrt{s} = 7$ TeV as a function of $\tan\beta$. We consider the type II 2HDM characterized by $M_{H^\pm} = 230$ GeV. In the inserts, shown are the variations with respect to the central CTEQ value.

⁸³This is nothing more than a numerical effect: as the asymmetry vanishes, the precision of the numerical calculation is less than the true scale uncertainty.

The second potential source of uncertainty comes from the presently not satisfactory determination of the gluon and bottom quark PDFs. We have chosen to estimate the impact of the different choice of PDFs collaborations together with some differences in the choice of the value of $\alpha_s(M_Z^2)$. As already discussed in the case of SM Higgs production this is a way to estimate the PDF uncertainties. In the right panel of Fig. 67 we show the dependence of the asymmetry on $\tan\beta$ when the CTEQ, the MSTW [128], and the ABKM [147] PDF sets are used. We consider the type II 2HDM characterized by $M_{H^\pm} = 230$ GeV. As usual the asymmetry has been computed at the LHC with $\sqrt{s} = 7$ TeV. In the insert we show the relative deviation from the CTEQ central prediction. The difference between the various predictions is found to be rather small as displayed in the right panel of Fig. 67, less than few percents at low and high $\tan\beta$ values. Again the peaks in the insert for $\tan\beta \simeq 7$ correspond to the vanishing of A_{LR}^t and are nothing more than numerical effects. On the contrary, the impact of the PDF variation on the total cross section σ_{tot} is expected to be much larger. For instance, Ref. [210] has found that at NLO the PDF uncertainty is expected to be of the order of 10%.

The last piece that remains to be discussed is the impact of radiative corrections on the polarization asymmetry, in particular in the case of supersymmetric scenarios. In the MSSM, the process $gb \rightarrow tH^-$ is affected by radiative corrections involving the supersymmetric particle spectrum. The NLO QCD and electroweak corrections have been discussed in Ref. [356] and in Ref. [362] respectively. Some of these corrections are known to be large for high values of $\tan\beta$ and some other parameters such as the higgsino mass parameter μ . It turns out that the bulk of these radiative corrections can be accounted for by modifying the Yukawa coupling of Eq. 12.2 as described in Ref. [363], in much the same way as we have done in the case of MSSM neutral Higgs production in previous sections using the Δ_b approximation. The approximation is rather good for the SUSY-QCD corrections (in particular when the SUSY spectrum is rather heavy), and slightly worse in the case of the electroweak ones.

In Fig. 68, we display the impact of these NLO SUSY radiative corrections within the MSSM on both the total cross section and the left-right asymmetry as a function of $\tan\beta$, obtained in Ref. [364]. The other SUSY parameters are fixed according to the scenario presented in Ref. [362], characterized by a heavy superparticle spectrum and $M_{H^\pm} = 270$ GeV. The SUSY QCD corrections are included in the Δ_b approximation, while the electroweak and the (very small) QED corrections are computed exactly. In the $\tan\beta$ range considered the approximation for the SUSY QCD contributions is expected to be valid.

Fig. 68 shows that the NLO corrections can indeed be large in both the cross section and the asymmetry. In the case of the latter observable the effect is of the order of 10% in

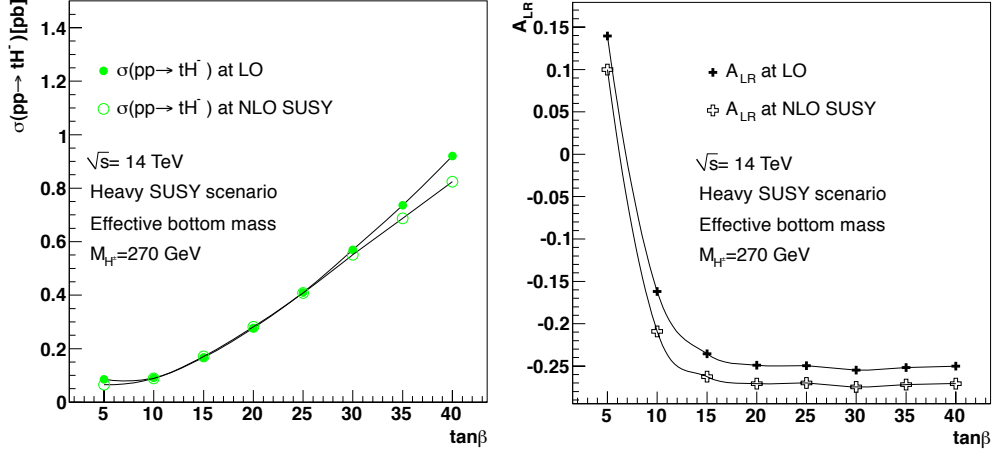


Figure 68: The total production cross section (left) and the asymmetry A_{LR}^t (right) at leading order and including the NLO SUSY corrections at the LHC with $\sqrt{s} = 14$ TeV. We consider the MSSM scenario of Ref. [362] characterized by a heavy sparticle spectrum and $M_{H^\pm} = 270$ GeV. $\tan\beta$ is varied from 5 to 40. Figure taken from Ref. [364].

the $\tan\beta \geq 15$ region, where the asymmetry dependence on $\tan\beta$ is almost flat. Therefore the asymmetry is sensitive to the quantum contributions of the superparticle spectrum: a precise measurement of the asymmetry could then allow to probe these additional supersymmetric corrections and, hence, could help to discriminate between supersymmetric and non-supersymmetric 2HDM of type II.

We have then seen that the associated top quark and charged Higgs production $bg \rightarrow tH^-$ at the LHC is a very interesting channel to measure the parameter $\tan\beta$ with some accuracy through the left-right top asymmetry, obtained by identifying the polarisation of the top quarks. This asymmetry has been proved to be essentially free from scale and PDF uncertainties, and still sensitive to radiative effects from new physics scenarios such as supersymmetry. The combined measurement of the production cross section and the polarisation asymmetry could discriminate between various new physics scenarios: two-Higgs doublet models of type I versus type II and the MSSM versus non-supersymmetric models, at least for intermediate values of $\tan\beta$. For $\tan\beta \gg 1$ or $\tan\beta \leq 1$ the method allows for the determination of the region of $\tan\beta$ but not for the exact value of $\tan\beta$, since in this two regions A_{LR}^t has a plateau. The only region where the distinction between type I and II 2HDM becomes challenging is for $\tan\beta \leq 1$ where the asymmetry is the same in both models. This polarisation asymmetry is thus worth investigating theoretically and experimentally in more detail.

This concludes the production of the MSSM Higgs bosons at the LHC. We will now end this part IV by giving the consequences of these theoretical results on the MSSM parameter

space and also on the SM Higgs boson search at the LHC.

13 Higgs $\rightarrow \tau\tau$ channel and limits on the MSSM parameter space

After having conducted a detailed study of the two main production channels for the MSSM neutral Higgs bosons at the Tevatron and the LHC, taking into account all QCD related uncertainties, we are nearly ready to study the impact of our predictions on the MSSM parameter space. The last step that remains to be done is the study of the main decay branching fraction that is of interest in the context of the thesis, that is the decay $\Phi \rightarrow \tau^+\tau^-$.

Indeed this decay channel together with its parent $\Phi \rightarrow b\bar{b}$ is the most sensitive channel for MSSM neutral Higgs bosons searches at hadron colliders [336, 352, 353]. We will reproduce the set-up that has been used in the case of the SM Higgs boson branching fraction in section 6 and take into account the uncertainties related to the b quark mass and the value of the strong coupling constant α_s . In this case the role of the c quark is negligible and will not be taken into account. We will see that even if the MSSM adds lots of new particles in the spectrum the major decay channels are up to a very good approximation the leptonic $\Phi \rightarrow \tau^+\tau^-$ channel and the hadronic $\Phi \rightarrow b\bar{b}$ channel.

We will then combine the decay branching fraction with the production channels at the Tevatron then at the LHC, giving the detailed tables of the central predictions for the two channels together with the different sources of uncertainties, the final uncertainty and the total uncertainty taking into account the $\Phi \rightarrow \tau^+\tau^-$ branching fraction, with all the relevant numbers for the two colliders. We will then give the impact of the theoretical uncertainties on the MSSM $[M_A, \tan\beta]$ plane and in particular revisit the limits obtained by the CDF and D0 collaborations [336]. We will also study this impact at the LHC and give some prospects for the higher luminosity in the 7 TeV run. We want to note that during the final stage of the writing of the thesis new results have been presented in HEP-EPS 2011 conference in July; they will not be commented in this section and postponed for the conclusion of this work. We will end the section by giving a very interesting consequence of the MSSM CMS search on the SM Higgs search in the channel $gg \rightarrow \Phi \rightarrow \tau^+\tau^-$ that has been presented in Ref. [326]. Again we will comment this important output in the light of the new HEP-EPS 2011 results in the conclusion of the thesis.

13.1 The main MSSM Higgs branching ratios

In the most general case, the decay pattern of the MSSM Higgs particles can be rather complicated, in particular for the heavy states. Indeed, besides the standard decays into

pairs of fermions and gauge bosons, the latter can have mixed decays into gauge and Higgs bosons (and the H bosons can decay into hh states) and, if some superparticles are light, SUSY decays would also occur. However, for the large values of $\tan\beta$ that we are interested in here, $\tan\beta \gtrsim 10$, the couplings of the non-SM like Higgs particles to bottom quarks and τ leptons are so strongly enhanced and those to top quarks and gauge bosons suppressed, that the pattern becomes very simple. To a very good approximation, the $\Phi = A$ or $H(h)$ bosons will decay almost exclusively into $b\bar{b}$ and $\tau^+\tau^-$ pairs with branching ratios of, respectively, $\approx 90\%$ and $\approx 10\%$, with the $t\bar{t}$ decay channel and the decay involving gauge or Higgs bosons suppressed to a level where the branching ratios are less than 1%. The CP -even h or H boson, depending on whether we are in the decoupling or anti-decoupling regime, will have the same decays as the SM Higgs boson in the mass range below $M_h^{\max} \lesssim 135$ GeV. The results presented in section 6 can therefore be used for the study of the decay pattern of the neutral SM-like Higgs boson⁸⁴

For the evaluation of the theoretical uncertainties in the $b\bar{b}$ and $\tau^+\tau^-$ decay branching ratios of the Φ states, the analysis of section 6 for the SM Higgs boson can be straightforwardly extended to the MSSM case. In this case we will ignore the experimental error on the input charm quark mass: indeed the decay $\Phi \rightarrow c\bar{c}$ being strongly suppressed the impact of the c quark mass on the $\Phi \rightarrow \tau^+\tau^-$ and $\Phi \rightarrow b\bar{b}$ branching fractions is totally negligible as its impact was mainly on the $\Phi \rightarrow c\bar{c}$ decay width which would translate on the branching fractions. As the QCD corrections to the dominant $\Phi \rightarrow b\bar{b}$ decays are large, they are resummed by switching from the b -quark pole mass M_b which appears at tree-level to the running quark mass in the $\overline{\text{MS}}$ scheme evaluated at the scale of the Higgs mass, $\overline{m}_b(M_\Phi)$. We will then consider only the uncertainties coming from the two other sources: the inputs $\overline{m}_b(\overline{m}_b) = 4.19_{-0.06}^{+0.18}$ GeV [205] where the central value corresponds to a pole mass of $M_b = 4.71$ GeV and the experimental errors on the QCD coupling constant $\alpha_s(M_Z^2) = 0.1171 \pm 0.0014$ at NNLO (the value adopted in the cross sections) [128, 199, 234] which is used to run the b -quark mass from \overline{m}_b up to M_Φ . Again, the impact of a scale variation in the range $\frac{1}{2}M_\Phi \leq \mu \leq 2M_\Phi$ is negligibly small. The uncertainties on the two branching ratios are displayed in Table 12 for some values of the Higgs boson mass, together with the total uncertainties when the individual uncertainties resulting from the “ 1σ ” errors on the inputs $\overline{m}_b(\overline{m}_b)$ and $\alpha_s(M_Z^2)$ are added in quadrature.

The $b\bar{b}$ branching ratios of the Φ states, $\text{BR}(\Phi \rightarrow b\bar{b}) \approx 3\overline{m}_b^2(M_\Phi)/[3\overline{m}_b^2(M_\Phi) + m_\tau^2]$, slightly decrease with increasing M_Φ as a result of the higher scale which reduces the b -quark mass $\overline{m}_b(M_\Phi)$, but the total uncertainty is practically constant on the entire mass

⁸⁴It is interesting to note that for $M_h^{\max} \sim 135$ GeV, we are in the regime where the decays into $b\bar{b}$ and WW are comparable and, thus, the uncertainties in the Higgs branching ratios are the largest.

M_Φ	$b\bar{b}$	Δm_b	$\Delta\alpha_s$	tot	$\tau\tau$	Δm_b	$\Delta\alpha_s$	tot
90	90.40	+0.9% -0.3%	+0.2% -0.2%	+0.9% -0.4%	9.60	+3.2% -8.6%	+1.9% -1.8%	+3.8% -8.8%
100	90.21	+0.9% -0.4%	+0.2% -0.2%	+1.0% -0.4%	9.79	+3.3% -8.6%	+1.9% -1.8%	+3.8% -8.8%
110	90.04	+0.9% -0.4%	+0.2% -0.2%	+1.0% -0.4%	9.96	+3.2% -8.6%	+2.0% -1.9%	+3.8% -8.8%
120	89.88	+1.0% -0.4%	+0.2% -0.2%	+1.0% -0.4%	10.12	+3.3% -8.6%	+2.0% -1.9%	+3.8% -8.8%
130	89.74	+1.0% -0.4%	+0.2% -0.2%	+1.0% -0.4%	10.26	+3.2% -8.5%	+2.0% -1.9%	+3.8% -8.7%
140	89.61	+1.0% -0.4%	+0.2% -0.2%	+1.0% -0.4%	10.39	+3.3% -8.5%	+2.0% -1.9%	+3.8% -8.7%
150	89.48	+1.0% -0.4%	+0.2% -0.2%	+1.0% -0.4%	10.52	+3.1% -8.6%	+2.0% -2.0%	+3.7% -8.8%
160	89.37	+1.0% -0.4%	+0.2% -0.2%	+1.0% -0.5%	10.63	+3.2% -8.5%	+2.1% -2.0%	+3.8% -8.7%
170	89.26	+1.0% -0.4%	+0.2% -0.2%	+1.1% -0.5%	10.74	+3.2% -8.5%	+2.0% -2.0%	+3.8% -8.8%
180	89.16	+1.0% -0.4%	+0.2% -0.3%	+1.1% -0.5%	10.84	+3.2% -8.5%	+2.1% -1.9%	+3.9% -8.7%
190	89.05	+1.0% -0.4%	+0.2% -0.2%	+1.1% -0.5%	10.95	+3.2% -8.5%	+2.0% -2.0%	+3.8% -8.7%
200	88.96	+1.0% -0.4%	+0.2% -0.3%	+1.1% -0.5%	11.04	+3.3% -8.4%	+2.2% -2.0%	+3.9% -8.7%
250	88.53	+1.1% -0.4%	+0.3% -0.3%	+1.1% -0.5%	11.47	+3.1% -8.5%	+2.1% -2.1%	+3.8% -8.7%
300	88.19	+1.1% -0.4%	+0.3% -0.3%	+1.2% -0.5%	11.81	+3.1% -8.5%	+2.1% -2.1%	+3.8% -8.7%
350	87.90	+1.2% -0.4%	+0.3% -0.3%	+1.2% -0.5%	12.10	+3.1% -8.4%	+2.1% -2.1%	+3.8% -8.7%
400	87.66	+1.2% -0.4%	+0.3% -0.3%	+1.2% -0.5%	12.34	+3.2% -8.3%	+2.2% -2.1%	+3.8% -8.6%
450	87.44	+1.2% -0.4%	+0.3% -0.3%	+1.2% -0.5%	12.56	+3.1% -8.4%	+2.2% -2.1%	+3.8% -8.6%
500	87.25	+1.2% -0.5%	+0.3% -0.3%	+1.3% -0.6%	12.75	+3.1% -8.3%	+2.3% -2.1%	+3.9% -8.6%

Table 12: The MSSM CP -odd like Higgs bosons decay branching ratios into $b\bar{b}$ and $\tau^+\tau^-$ final states (in %) for given Higgs mass values (in GeV) with the corresponding individual uncertainties as well as the global uncertainties assuming 1σ uncertainties on the inputs $\bar{m}_b(\bar{m}_b)$ and $\alpha_s(M_Z^2)$.

range $90 \leq M_\Phi \leq 200$ GeV and amounts to approximately $+1\%$, -0.5% as a consequence of the almost complete cancellation of the uncertainties in the numerator and denominator. In contrast, there is no such a cancellation in the branching fraction for Higgs decays into $\tau^+\tau^-$ pairs, $\text{BR}(\Phi \rightarrow \tau^+\tau^-) \approx m_\tau^2/[3\bar{m}_b^2(M_\Phi) + m_\tau^2]$, and the total uncertainty, that is dominated by the error on the b -quark mass, reaches the level of $+4\%$, -9% for all Higgs masses. If the error on the input b -quark mass is ignored, the total uncertainty in the $\tau^+\tau^-$ branching ratio will reduce to $\approx 3\%$.

Before closing this subsection it should be noted that in the MSSM at high $\tan\beta$, the total decay widths of the Φ particles should be taken into account. Indeed, they rise as $\Gamma(\Phi) \propto M_\Phi \tan^2\beta$ and thus, reach the level of $\mathcal{O}(10 \text{ GeV})$ for $M_\Phi \approx 200$ GeV and

$\tan\beta \approx 50$. The total Higgs width can thus possibly be larger than the experimental resolution on the $\tau^+\tau^-$ and $b\bar{b}$ invariant masses when decays into these final states are analyzed. If the total width has to be taken into account in the experimental analyses, the uncertainties that affect it should also be considered. These uncertainties are in fact simply those affecting the $\Phi \rightarrow b\bar{b}$ partial widths (being the dominant channel) and thus, to a good approximation, the $\Phi \rightarrow \tau^+\tau^-$ branching ratio. The numbers given in Table 12 for the uncertainties of $\text{BR}(\Phi \rightarrow \tau^+\tau^-)$ thus correspond (when multiplied by a factor ≈ 1.1) to the uncertainties on the total width $\Gamma(\Phi)$ with a good accuracy.

13.2 Combination of production cross section and Higgs $\rightarrow \tau\tau$ decay

This subsection will combine all the results obtained in the previous section in order to obtain the final predictions at the Tevatron and the LHC for the process $gg+b\bar{b} \rightarrow \Phi \rightarrow \tau^+\tau^-$ which is used by experimental collaborations to set up limit on the $[M_A, \tan\beta]$ MSSM parameter space. We will start by the Tevatron study and then give the LHC results.

13.2.1 The combination at the Tevatron

To obtain the total uncertainty on the cross section times branching ratio $\Delta(\sigma \times \text{BR})$, we use the simple scheme which consists in the addition of the total uncertainties on the production cross sections and the uncertainties on the branching fraction in Higgs decays into $\tau^+\tau^-$ pairs. In this addition, at least in the $b\bar{b} \rightarrow \Phi$ process where one defines the $\Phi b\bar{b}$ coupling at the scale μ_R , the uncertainty on the input b -mass, which is common to σ and to BR , almost cancels out; only $\approx 10\%$ of the error is left out as this uncertainty is anti-correlated between the production cross section and the decay branching fraction⁸⁵. In the case of $gg \rightarrow \Phi$ where the Yukawa coupling is defined at the scale m_b in contrast to the Higgs decay widths, the errors on α_s used for the running from m_b to M_Φ will induce a remaining uncertainty. This α_s uncertainty is correlated in $\sigma(gg \rightarrow \Phi)$ and $\text{BR}(\Phi \rightarrow \tau^+\tau^-)$: smaller α_s values lower $\sigma(gg \rightarrow \Phi) \propto \alpha_s^2$ at LO, and also $\text{BR}(\Phi \rightarrow \tau^+\tau^-)$ as the resulting $\bar{m}_b(M_\Phi)$ is higher, thus enhancing/reducing the $\Phi \rightarrow b\bar{b}/\tau^+\tau^-$ rates. This uncertainty should thus be added linearly to the overall scale+scheme+PDF uncertainty of the cross section.

We display the numerical results for the two processes $gg \rightarrow \Phi$ and $b\bar{b} \rightarrow \Phi$ in the Tables. 13 and 14 which include the individual uncertainties as well as the total uncertainty,

⁸⁵We remind that this is also the case of the Δ_b SUSY correction which enters both $\sigma(gg, b\bar{b} \rightarrow \Phi)$ and $\text{BR}(\Phi \rightarrow \tau^+\tau^-)$ and which thus cancels in the product as shown in section 10.2.

including or not the impact of the branching fraction. This impact is modest but sizable in the upper direction for both processes, and negligible in the lower direction in the case of the bottom quarks fusion.

We are now left with the final combination which is of utmost interest: the combination of the two production times decay processes. Indeed, to consider the final state topology that has been searched for by the D0 and CDF collaborations [336], that is $p\bar{p} \rightarrow \text{Higgs} \rightarrow \tau^+\tau^-$, we first have to add the cross sections for the two channels $gg \rightarrow A$ and $b\bar{b} \rightarrow A$, and then to multiply the resulting production cross section by the Higgs branching ratio $\text{BR}(A \rightarrow \tau^+\tau^-) \approx 10\%$ ⁸⁶. The resulting $\sigma(p\bar{p} \rightarrow A) \times \text{BR}(A \rightarrow \tau^+\tau^-)$ at the Tevatron is shown in Fig. 69 as a function of M_A . We stress again that to obtain the true rate for $\Phi = A + H(h)$, one has to multiply the values given in the figure by a factor $2 \tan^2 \beta$.

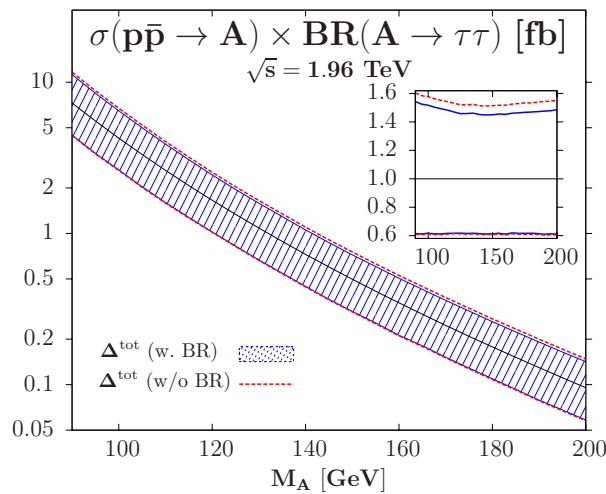


Figure 69: $\sigma(p\bar{p} \rightarrow A) \times \text{BR}(A \rightarrow \tau^+\tau^-)$ as a function of M_A at the Tevatron, together with the associated overall theoretical uncertainty; the uncertainty when excluding that on the branching ratio is also displayed. In the inserts, shown are the relative deviations from the central values.

In Fig. 69 we also display the associated overall theoretical uncertainties. The uncertainty from the cross section alone is dominated by that of $gg \rightarrow A$ at low Higgs masses and $b\bar{b} \rightarrow A$ at high masses as the corresponding cross sections are largest. In the product $\sigma(p\bar{p} \rightarrow A) \times \text{BR}(A \rightarrow \tau^+\tau^-)$, the parametric uncertainty that is common to the production and decay rates almost cancels out as shown by the solid curves in Fig. 69 and only a few percent are left. This leads to a smaller uncertainty in $\sigma(p\bar{p} \rightarrow A) \times \text{BR}(A \rightarrow \tau^+\tau^-)$ than in $\sigma(p\bar{p} \rightarrow A)$ alone. The final theoretical uncertainty for $p\bar{p} \rightarrow A \rightarrow \tau^+\tau^-$ at the Tevatron is of order $+50\%$, -40% .

⁸⁶We simply add all uncertainties linearly, in contrast to Ref. [210] in which the PDF uncertainties in gg and $b\bar{b} \rightarrow A$ are added in quadrature, with the total PDF+ α_s uncertainty added linearly to the scale uncertainty.

13.2.2 The combination at the IHC

We do the same exercise in the case of the IHC, reproducing the lines of argument presented in the Tevatron study above: the total uncertainty on the cross section times branching ratio, $\Delta(\sigma \times \text{BR})$ is obtained by adding the total uncertainties on the production cross sections and the uncertainties on the branching fraction in Higgs decays into $\tau^+\tau^-$ pairs. Again the uncertainty due to the parametric b quark mass will almost cancel out in the cross section times branching fraction because this uncertainty is anti-correlated between the production and the decay. Nevertheless, especially in the case of the bottom quarks fusion channel, there will remain a residual uncertainty related to the α_s running of the b quark mass: it will be added linearly to the scale+PDF+scheme uncertainty. The impact of the production cross section times branching fraction uncertainty is shown by the dotted lines of Fig. 70 where the uncertainty $\Delta(\sigma \times \text{BR})$ for tau decays is displayed for the two production processes.

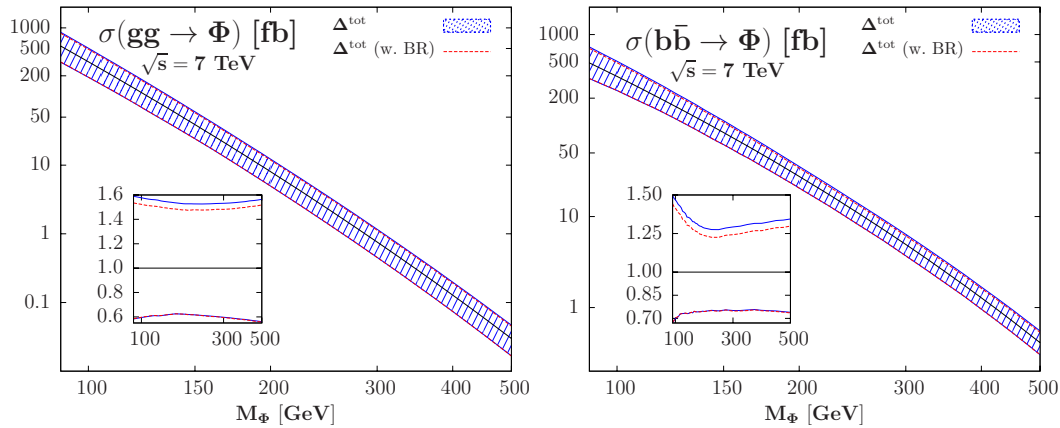


Figure 70: The total uncertainties due to the scale, PDF and b -quark mass in the $gg \rightarrow \Phi$ (left) and $b\bar{b} \rightarrow \Phi$ (right) cross sections at the IHC with 7 TeV as a function of M_Φ . The dotted lines show the uncertainties when those on the branching ratios for Higgs decays into $\tau^+\tau^-$ final states are added. In the inserts, the relative deviations are shown.

We display the numerical results for the two processes $gg \rightarrow \Phi$ and $b\bar{b} \rightarrow \Phi$ in the Tables. 15 and 16 which include the individual uncertainties as well as the total uncertainty, including or not the impact of the branching fraction. Again the impact of the branching fraction uncertainty is modest, sizable in the upper direction and nearly negligible in the lower direction. It should not be a surprise that the total uncertainty may sometimes be higher (of some 0.2%) in the cross section section times branching fraction than in the production cross section alone: indeed the additional α_s uncertainty on the branching fraction remains and is added to the total uncertainty on the cross section, thus sometimes overcompensating the cancellation of the parametric b quark mass uncertainty.

M_Φ	$\sigma_{gg \rightarrow \Phi}^{\text{NLO}}$	scale	scheme	PDFs	param	total	$\sigma \times \text{BR}$	
90	49.46	+22.0% -18.5%	+5.6% -5.6%	+10.7% -10.3%	+13.0% -4.0%	+55.2% -35.9%	4.75	+49.7% -35.7%
95	36.07	+22.0% -18.6%	+5.6% -5.6%	+10.8% -10.5%	+13.0% -4.0%	+55.3% -36.1%	3.50	+49.9% -35.9%
100	26.62	+21.9% -18.6%	+5.5% -5.5%	+10.9% -10.7%	+13.1% -4.0%	+55.4% -36.3%	2.61	+50.0% -36.0%
105	19.90	+21.9% -18.7%	+5.5% -5.5%	+11.1% -10.8%	+13.0% -4.0%	+55.5% -36.5%	1.97	+50.1% -36.3%
110	15.03	+21.8% -18.7%	+5.5% -5.5%	+11.2% -11.0%	+13.1% -4.1%	+55.7% -36.7%	1.50	+50.3% -36.6%
115	11.46	+21.7% -18.8%	+5.5% -5.5%	+11.4% -11.2%	+13.1% -4.0%	+55.7% -36.9%	1.15	+50.4% -36.7%
120	8.82	+21.6% -18.8%	+5.5% -5.5%	+11.5% -11.4%	+13.2% -4.1%	+55.8% -37.1%	0.89	+50.5% -37.0%
125	6.84	+21.6% -18.8%	+5.4% -5.4%	+11.7% -11.7%	+13.2% -4.1%	+56.0% -37.3%	0.70	+50.6% -37.1%
130	5.35	+21.5% -18.9%	+5.4% -5.4%	+11.8% -11.9%	+13.2% -4.1%	+56.0% -37.6%	0.55	+50.9% -37.4%
135	4.21	+21.5% -18.9%	+5.4% -5.4%	+12.0% -12.1%	+13.3% -4.1%	+56.3% -37.8%	0.43	+51.0% -37.8%
140	3.34	+21.4% -19.0%	+5.4% -5.4%	+12.2% -12.3%	+13.3% -4.1%	+56.4% -38.0%	0.35	+51.2% -37.9%
145	2.66	+21.4% -19.0%	+5.4% -5.4%	+12.3% -12.5%	+13.3% -4.1%	+56.6% -38.2%	0.28	+51.3% -38.4%
150	2.13	+21.3% -19.1%	+5.4% -5.4%	+12.5% -12.8%	+13.3% -4.1%	+56.8% -38.4%	0.22	+51.5% -38.6%
155	1.72	+21.3% -19.1%	+5.4% -5.4%	+12.7% -13.0%	+13.3% -4.1%	+56.9% -38.7%	0.18	+51.8% -38.5%
160	1.40	+21.2% -19.2%	+5.4% -5.4%	+12.9% -13.2%	+13.4% -4.1%	+57.1% -38.9%	0.15	+52.0% -38.9%
165	1.14	+21.2% -19.2%	+5.4% -5.4%	+13.1% -13.4%	+13.4% -4.1%	+57.4% -39.1%	0.12	+52.3% -39.1%
170	0.93	+21.2% -19.3%	+5.4% -5.4%	+13.3% -13.6%	+13.4% -4.1%	+57.6% -39.3%	0.10	+52.4% -39.4%
175	0.76	+21.2% -19.3%	+5.4% -5.4%	+13.5% -13.9%	+13.4% -4.2%	+57.8% -39.6%	0.08	+52.7% -39.5%
180	0.63	+21.1% -19.4%	+5.4% -5.4%	+13.7% -14.1%	+13.4% -4.1%	+58.1% -39.8%	0.07	+53.1% -39.7%
185	0.52	+21.1% -19.4%	+5.4% -5.4%	+14.0% -14.3%	+13.4% -4.2%	+58.3% -40.0%	0.06	+53.1% -40.2%
190	0.43	+21.1% -19.5%	+5.4% -5.4%	+14.3% -14.5%	+13.5% -4.2%	+58.5% -40.3%	0.05	+53.3% -40.4%
195	0.36	+21.1% -19.5%	+5.4% -5.4%	+14.6% -14.7%	+13.4% -4.2%	+58.8% -40.5%	0.04	+53.7% -40.6%
200	0.30	+21.1% -19.6%	+5.4% -5.4%	+14.9% -15.0%	+13.4% -4.2%	+59.0% -40.7%	0.03	+54.2% -40.7%

Table 13: The production cross sections in the $gg \rightarrow \Phi$ process at the Tevatron (in fb) for given A masses (in GeV) at a scale $\mu_F = \mu_R = \frac{1}{2}M_\Phi$ with MSTW PDFs. Shown also are the corresponding uncertainties from the various sources discussed as well as the total uncertainty. In the last column is displayed the product $\sigma(gg \rightarrow \Phi) \times \text{BR}(\Phi \rightarrow \tau^+ \tau^-)$ together with its total uncertainty.

M_Φ	$\sigma_{bb \rightarrow \Phi}^{\text{NNLO}}$	scale	PDFs	param	total	$\sigma \times \text{BR}$	
90	26.31	+35.1% -29.9%	+18.2% -17.2%	+10.5% -3.3%	+70.4% -44.9%	2.53	+63.4% -44.0%
95	21.04	+30.6% -29.0%	+19.0% -16.6%	+9.9% -3.7%	+64.1% -44.9%	2.04	+57.1% -43.9%
100	16.96	+26.6% -27.0%	+18.7% -17.5%	+10.2% -3.4%	+61.5% -42.9%	1.66	+54.5% -42.0%
105	13.78	+22.6% -27.2%	+19.2% -17.6%	+10.7% -3.4%	+57.8% -43.4%	1.36	+50.8% -42.4%
110	11.22	+20.3% -25.5%	+19.4% -17.9%	+10.1% -3.6%	+54.7% -42.6%	1.12	+47.9% -41.7%
115	9.18	+17.6% -24.8%	+20.1% -17.9%	+10.6% -3.6%	+52.7% -41.6%	0.92	+45.7% -40.6%
120	7.57	+15.1% -24.1%	+21.0% -17.8%	+10.9% -3.0%	+50.2% -40.3%	0.77	+43.1% -40.0%
125	6.29	+13.6% -23.5%	+21.5% -18.1%	+10.2% -3.2%	+47.9% -40.4%	0.64	+40.7% -39.5%
130	5.24	+12.8% -22.9%	+21.7% -18.6%	+10.5% -3.2%	+48.0% -40.4%	0.54	+41.0% -39.5%
135	4.36	+12.4% -21.9%	+21.8% -19.0%	+10.5% -3.3%	+48.5% -39.9%	0.45	+41.6% -38.9%
140	3.66	+11.6% -21.5%	+22.5% -19.1%	+10.2% -3.6%	+46.9% -40.2%	0.38	+39.8% -39.3%
145	3.08	+11.0% -21.2%	+23.0% -19.5%	+10.4% -3.3%	+46.7% -40.3%	0.32	+39.5% -39.4%
150	2.60	+10.8% -20.3%	+24.1% -19.3%	+10.4% -3.4%	+47.3% -39.7%	0.27	+39.9% -38.9%
155	2.20	+10.8% -20.0%	+24.3% -20.1%	+10.3% -3.5%	+47.8% -39.3%	0.23	+40.8% -38.2%
160	1.88	+10.5% -20.0%	+24.9% -20.4%	+10.4% -3.4%	+47.8% -40.0%	0.20	+40.5% -39.1%
165	1.60	+10.6% -18.7%	+25.1% -20.6%	+10.4% -3.3%	+49.2% -38.5%	0.17	+41.8% -37.4%
170	1.37	+10.6% -18.4%	+25.3% -21.1%	+10.5% -3.1%	+49.8% -38.7%	0.15	+42.4% -37.8%
175	1.17	+10.5% -18.2%	+26.0% -21.5%	+10.4% -3.4%	+50.5% -38.8%	0.13	+43.0% -37.6%
180	1.01	+10.3% -18.1%	+26.7% -21.6%	+10.4% -3.4%	+50.7% -38.6%	0.11	+43.2% -37.4%
185	0.87	+10.4% -17.6%	+27.8% -21.5%	+10.3% -3.2%	+51.4% -38.6%	0.09	+43.8% -37.6%
190	0.75	+10.3% -17.3%	+27.2% -22.7%	+10.4% -3.3%	+52.1% -39.2%	0.08	+44.4% -38.2%
195	0.65	+10.5% -16.2%	+28.5% -22.6%	+10.1% -3.4%	+52.3% -38.9%	0.07	+44.7% -37.7%
200	0.56	+10.4% -16.3%	+28.5% -23.6%	+10.6% -3.2%	+53.2% -38.9%	0.06	+45.8% -37.9%

Table 14: Same as in Table 13 for the $b\bar{b} \rightarrow \Phi$ channel.

M_Φ	$\sigma_{gg\rightarrow\Phi}^{\text{NLO}}$	Scale [%]	PDF+ $\Delta_{\alpha_s}^{\text{exp+th}}$ [%]	$\Delta\bar{m}_b$ [%]	Total [%]	$\sigma \times \text{BR}$	Total [%]
90	542.28	+21.7 -18.3	+7.9 -8.1	+26.7 -17.6	+58.9 -41.7	52.05	+53.5 -41.5
95	414.48	+21.1 -17.6	+7.8 -8.0	+26.8 -17.7	+58.3 -41.1	40.19	+52.8 -40.9
100	320.31	+20.4 -16.9	+7.8 -7.9	+27.0 -17.8	+57.7 -40.5	31.36	+52.3 -40.3
105	250.43	+19.9 -16.3	+7.8 -7.9	+27.0 -17.9	+57.1 -40.0	24.74	+51.7 -39.8
110	197.61	+19.4 -15.9	+7.7 -7.8	+27.1 -17.9	+56.6 -39.6	19.69	+51.3 -39.4
115	157.34	+18.9 -15.4	+7.7 -7.8	+27.2 -18.0	+56.2 -39.2	15.80	+51.0 -39.0
120	126.32	+18.5 -15.1	+7.7 -7.8	+27.3 -18.0	+56.1 -39.0	12.78	+50.7 -38.9
125	102.14	+18.1 -15.3	+7.7 -7.7	+27.4 -18.1	+55.8 -39.2	10.41	+50.4 -39.1
130	83.24	+17.7 -15.1	+7.7 -7.7	+27.4 -18.1	+55.1 -39.0	8.54	+50.0 -38.9
135	68.25	+17.4 -14.7	+7.7 -7.7	+27.5 -18.2	+54.8 -38.7	7.05	+49.6 -38.7
140	56.31	+17.1 -14.2	+7.7 -7.7	+27.6 -18.2	+54.5 -38.4	5.85	+49.3 -38.3
145	46.73	+16.7 -13.8	+7.6 -7.7	+27.6 -18.3	+54.1 -38.1	4.89	+48.9 -38.2
150	38.98	+16.4 -13.5	+7.6 -7.7	+27.7 -18.4	+54.0 -37.8	4.10	+48.7 -37.9
155	32.68	+16.1 -13.1	+7.6 -7.7	+27.8 -18.4	+53.7 -37.6	3.45	+48.6 -37.5
160	27.52	+15.9 -13.0	+7.6 -7.7	+27.9 -18.5	+53.5 -37.5	2.93	+48.3 -37.5
165	23.29	+15.7 -13.0	+7.6 -7.7	+27.9 -18.5	+53.3 -37.6	2.49	+48.2 -37.5
170	19.79	+15.4 -13.0	+7.6 -7.7	+28.0 -18.6	+53.0 -37.7	2.13	+47.9 -37.7
175	16.88	+15.2 -13.1	+7.6 -7.7	+28.0 -18.6	+52.8 -37.8	1.82	+47.7 -37.7
180	14.45	+15.0 -13.1	+7.7 -7.7	+28.1 -18.6	+52.7 -37.8	1.57	+47.7 -37.8
185	12.42	+15.0 -13.1	+7.7 -7.7	+28.1 -18.7	+52.7 -38.0	1.35	+47.5 -38.2
190	10.71	+14.9 -13.2	+7.6 -7.8	+28.2 -18.8	+52.8 -38.1	1.17	+47.6 -38.2
195	9.27	+14.9 -13.2	+7.7 -7.8	+28.2 -18.8	+52.7 -38.2	1.02	+47.6 -38.3
200	8.04	+14.8 -13.2	+7.7 -7.8	+28.0 -18.7	+52.7 -38.3	0.89	+47.8 -38.3
225	4.12	+14.7 -13.4	+7.8 -8.0	+28.3 -19.0	+52.6 -38.8	0.46	+47.6 -39.0
250	2.24	+14.5 -13.6	+7.9 -8.2	+28.4 -19.2	+52.8 -39.3	0.26	+47.8 -39.6
275	1.28	+14.4 -13.7	+8.0 -8.4	+28.7 -19.4	+53.0 -39.8	0.15	+48.3 -39.9
300	0.76	+14.2 -13.8	+8.2 -8.6	+28.9 -19.5	+53.2 -40.3	0.09	+48.2 -40.6
325	0.47	+14.2 -13.9	+8.4 -8.9	+29.0 -19.6	+53.4 -40.7	0.06	+48.5 -41.0
350	0.30	+14.2 -14.0	+8.7 -9.2	+29.1 -19.8	+53.8 -41.3	0.04	+48.9 -41.7
375	0.19	+14.1 -14.1	+9.0 -9.5	+29.4 -19.9	+54.2 -41.8	0.02	+49.5 -41.9
400	0.13	+14.1 -14.2	+9.3 -9.8	+29.4 -20.0	+54.5 -42.1	0.02	+49.8 -42.4
425	0.09	+14.1 -14.3	+9.6 -10.1	+29.7 -20.2	+55.1 -42.6	0.01	+50.5 -42.9
450	0.06	+14.1 -14.4	+9.9 -10.4	+29.8 -20.3	+55.4 -43.1	0.01	+50.8 -43.5
500	0.03	+14.2 -14.5	+10.6 -11.0	+30.0 -20.5	+56.5 -44.0	0.00	+51.9 -44.3

Table 15: The MSSM Higgs production cross sections in the $gg \rightarrow \Phi$ channel (for $\tan\beta = 1$) at the IHC with $\sqrt{s} = 7$ TeV as well as the individual uncertainties (first from scale, then from PDF+ $\Delta_{\alpha_s}^{\text{exp+th}}$ at 90%CL and from the input mass \bar{m}_b at 1σ) and the total uncertainties for selected values of the Higgs mass. The last column displays the cross section times $\Phi \rightarrow \tau^+\tau^-$ branching fraction together with the total uncertainty when including the combination with the total uncertainty on $\Phi \rightarrow \tau^+\tau^-$ branching ratio.

M_Φ	$\sigma_{gg\rightarrow\Phi}^{\text{NLO}}$	Scale [%]	PDF + $\Delta_{\alpha_s}^{\text{exp+th}}$ [%]	$\Delta\bar{m}_b$ [%]	Total [%]	$\sigma \times \text{BR}$	Total [%]
90	487.83	+26.8 -21.1	+6.2 -8.0	+17.8 -10.7	+49.8 -32.8	46.83	+44.3 -32.5
95	409.59	+25.4 -19.5	+7.1 -7.3	+17.7 -10.3	+47.8 -31.5	39.72	+42.4 -31.3
100	346.50	+23.9 -18.4	+6.4 -7.8	+17.8 -9.9	+46.9 -29.9	33.92	+41.4 -29.8
105	294.57	+22.2 -17.8	+6.3 -8.3	+18.1 -9.6	+45.4 -29.5	29.10	+40.0 -29.3
110	252.03	+21.3 -16.7	+6.9 -7.7	+17.2 -10.1	+43.8 -28.9	25.11	+38.5 -28.8
115	215.89	+20.3 -15.9	+6.8 -8.0	+17.5 -9.5	+43.0 -27.5	21.68	+37.7 -27.3
120	186.56	+18.8 -15.4	+7.2 -7.7	+17.6 -9.3	+41.7 -26.9	18.88	+36.4 -27.0
125	161.84	+17.4 -15.2	+7.7 -7.6	+17.1 -9.4	+39.4 -26.9	16.49	+34.1 -26.8
130	140.97	+16.4 -14.9	+7.6 -7.8	+17.5 -9.5	+38.8 -26.8	14.46	+33.7 -26.7
135	122.98	+15.5 -14.6	+7.3 -8.0	+17.2 -9.2	+38.0 -26.6	12.70	+32.8 -26.6
140	108.08	+14.1 -14.7	+7.5 -8.0	+16.6 -9.5	+35.6 -26.9	11.23	+30.5 -26.8
145	94.85	+13.7 -14.7	+7.7 -8.2	+17.1 -9.2	+35.5 -26.9	9.92	+30.2 -27.0
150	83.83	+13.0 -14.3	+8.2 -8.0	+17.0 -9.1	+35.0 -26.4	8.82	+29.7 -26.5
155	74.13	+12.0 -14.2	+8.2 -8.2	+17.1 -9.0	+34.0 -26.2	7.84	+28.9 -26.1
160	65.84	+11.0 -14.1	+8.3 -8.2	+16.9 -9.1	+32.7 -26.4	7.00	+27.6 -26.5
165	58.60	+10.4 -13.6	+8.2 -8.5	+16.9 -8.8	+32.6 -25.4	6.26	+27.5 -25.5
170	52.28	+9.6 -13.6	+8.5 -8.3	+16.6 -9.2	+31.7 -25.7	5.61	+26.5 -25.7
175	46.75	+9.1 -13.4	+8.4 -8.6	+16.7 -8.9	+31.3 -25.8	5.04	+26.2 -25.8
180	41.97	+8.3 -13.8	+8.5 -8.7	+16.9 -8.7	+30.4 -25.7	4.55	+25.4 -25.7
185	37.69	+7.5 -13.3	+9.2 -8.2	+16.8 -8.8	+29.8 -25.6	4.11	+24.6 -25.8
190	33.87	+7.5 -12.8	+8.6 -9.2	+16.5 -8.9	+29.6 -25.5	3.71	+24.4 -25.6
195	30.55	+7.0 -12.3	+8.9 -9.1	+16.4 -9.1	+29.0 -25.4	3.36	+23.9 -25.5
200	27.61	+6.3 -12.5	+8.7 -9.6	+16.4 -8.8	+28.6 -25.5	3.05	+23.7 -25.6
225	17.10	+5.1 -11.9	+9.6 -9.7	+16.4 -8.9	+27.6 -24.8	1.93	+22.6 -25.0
250	10.97	+5.0 -11.5	+10.6 -10.0	+16.1 -8.8	+27.5 -25.1	1.26	+22.5 -25.4
275	7.27	+5.0 -10.6	+10.9 -10.8	+16.3 -8.6	+28.6 -24.5	0.85	+23.9 -24.6
300	4.94	+4.8 -10.5	+11.6 -11.4	+16.4 -8.4	+29.3 -24.9	0.58	+24.3 -25.3
325	3.43	+4.8 -9.8	+12.4 -11.8	+15.9 -8.6	+29.7 -24.9	0.41	+24.9 -25.2
350	2.43	+5.0 -9.4	+13.1 -12.3	+16.2 -8.4	+30.8 -24.6	0.29	+25.9 -25.0
375	1.75	+4.9 -9.1	+14.1 -12.5	+16.0 -8.2	+31.6 -24.3	0.21	+26.9 -24.5
400	1.28	+4.7 -8.9	+14.9 -13.1	+15.9 -8.2	+31.6 -24.8	0.16	+26.9 -25.1
425	0.95	+4.7 -8.6	+15.5 -13.6	+16.0 -8.3	+32.5 -25.0	0.09	+27.8 -25.3
450	0.71	+4.7 -8.2	+16.1 -14.2	+16.1 -8.2	+33.4 -25.2	0.07	+28.8 -25.6
500	0.41	+4.7 -7.9	+17.8 -15.1	+15.8 -8.2	+34.4 -26.1	0.05	+29.8 -26.5

Table 16: The same as in Table.15 but for the $b\bar{b} \rightarrow \Phi$ channel.

We finally combine the two production channel together to obtain the final $pp \rightarrow \Phi \rightarrow \tau^+\tau^-$ central prediction and total uncertainty. This is the prediction to be compared with ATLAS and CMS experimental results as the search topology in the Higgs $\rightarrow \tau^+\tau^-$ channel use the two production processes. The resulting $\sigma(pp \rightarrow A) \times \text{BR}(A \rightarrow \tau^+\tau^-)$ at the IHC with $\sqrt{s} = 7$ TeV is shown in Fig. 71 as a function of M_A . As stated in the Tevatron study the true rates for the combined production of $\Phi = A + H(h)$ are obtained when our results are multiplied by a factor of $2 \tan^2 \beta$.

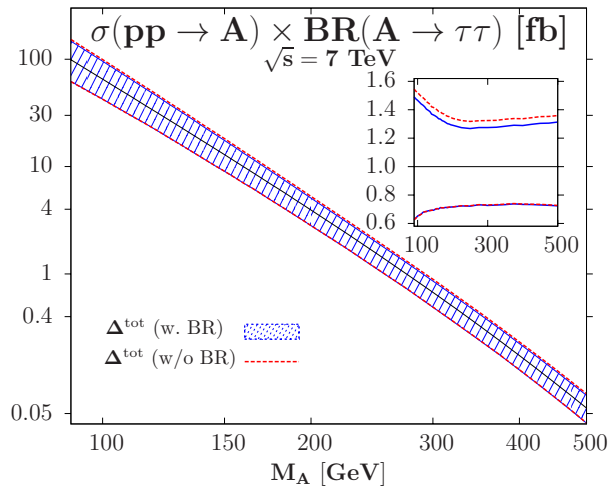


Figure 71: $\sigma(pp \rightarrow A) \times \text{BR}(A \rightarrow \tau^+\tau^-)$ as a function of M_A at the IHC with $\sqrt{s} = 7$ TeV, together with the associated overall theoretical uncertainty; the uncertainty when excluding that on the branching ratio is also displayed. In the inserts, shown are the relative deviations from the central values.

The impact of the theoretical uncertainties in both channels $b\bar{b}, gg \rightarrow \Phi \rightarrow \tau^+\tau^-$ for the MSSM CP -odd and one of the CP -even Higgs particles are then large. We will see in the next subsection that this has important consequences on the MSSM $[\tan \beta, M_A]$ parameter space that can be probed at the IHC.

13.3 Impact of the theoretical uncertainties on the limits on the MSSM parameter space

We are arrived nearly at the end of our journey. Thanks to the subsection 13.2 we will apply our study on the limits on the MSSM $[M_A, \tan \beta]$ parameter space, first using the Tevatron experimental results and then the early IHC experimental results.

13.3.1 The Tevatron results

The results that we have obtained in section 13.2 have to be compared with the experimental limits that have been obtained by the CDF/D0 collaborations in the $p\bar{p} \rightarrow \Phi \rightarrow \tau^+\tau^-$ search topology [336]. The major experimental output that is of use for such a theoretical comparison is the production cross section times branching fraction 95%CL limit for various A boson masses M_A . As the experiment has seen nothing, this translates into limits on the MSSM $[M_A, \tan\beta]$ parameter space that is probed. We thus generate for each $(M_A, \tan\beta)$ value a cross section by multiplying our results by $2 \tan^2\beta$ as already mentioned and then compare with the experimental results presented in Table X of ref [336]; if our theoretical expectation is above that means that the associated value $[M_A, \tan\beta]$ has been excluded at 95%CL.

To visualize the impact of these theoretical uncertainties on this MSSM $[M_A, \tan\beta]$ parameter space, we show in Fig. 72 the contour of the cross section times branching ratio in this plane, together with the contours when the uncertainties are included. We apply the model independent 95%CL expected and observed limits from the CDF/D0 analysis (Table X of Ref. [336]). We have displayed the expected limit with our central prediction (black dotted line) together with the expected limits using the maximal and minimal predictions (in blue dotted lines) in order to show the impact of the theoretical uncertainties on the $[M_A, \tan\beta]$ plane. However, rather than applying the observed limits on the central $\sigma \times \text{BR}$ rate, we apply them on the minimal one when the theory uncertainty is included. Indeed, since the latter has a flat prior, the minimal $\sigma \times \text{BR}$ value is as respectable and likely as the central value and the viable exclusion limit should take into account these uncertainties: the final exclusion limit should be viewed as the one obtained with the minimal cross section rather than the central cross section with respect to theoretical uncertainties.

Fig. 72 displays the obtained observed limit in this spirit in red solid line. Only values $\tan\beta \gtrsim 50$ are excluded in the mass ranges, $M_A \approx 95\text{--}125$ GeV and $M_A \gtrsim 165$ GeV. In the intermediate range $M_A \approx 125\text{--}165$ GeV, the exclusion limit is $\tan\beta \gtrsim 40\text{--}45$, to be contrasted with the values $\tan\beta \gtrsim 30$ excluded in the CDF/D0 analysis. Hence, the inclusion of the theory uncertainties has a drastic impact on the allowed $[M_A, \tan\beta]$ parameter space.

We conclude by mentioning that there is a subleading channel which has also been considered at the Tevatron, $bg \rightarrow \Phi b \rightarrow 3b$ [367]. The evaluation of the theory uncertainties in $bg \rightarrow \Phi b$ [193, 195] follows that of the parent process $b\bar{b} \rightarrow \Phi$, being part of the NLO contributions of the latter process. Similar results, that is an uncertainty of approximately $\pm 40\%$, are expected. However, in this case, it is the $\Phi \rightarrow b\bar{b}$ decay which is considered

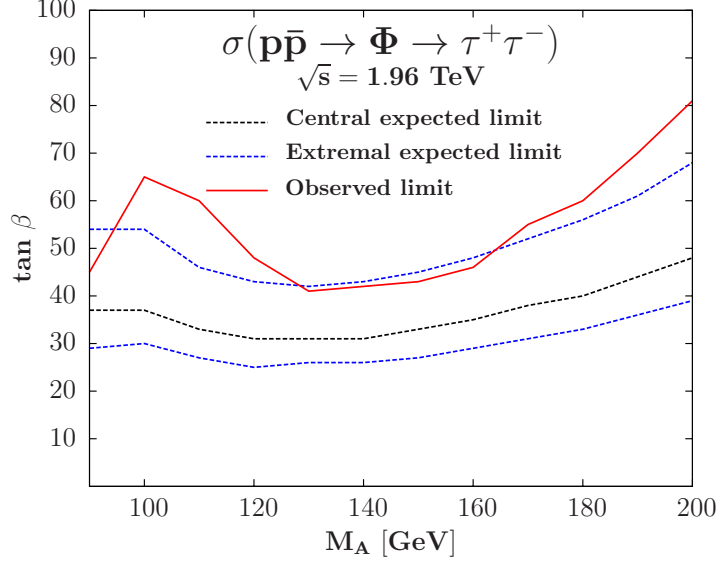


Figure 72: Contours for the expected $\sigma(p\bar{p} \rightarrow \Phi \rightarrow \tau^+\tau^-)$ rate at the Tevatron in the $[M_A, \tan\beta]$ plane with the associated theory uncertainties, confronted to the 95%CL exclusion limit.

experimentally and, since $\text{BR}(\Phi \rightarrow b\bar{b})$ has a small error, the uncertainties in σ and $\sigma \times \text{BR}$ are almost the same. These uncertainties will thus also have an impact on the excluded $[M_A, \tan\beta]$ parameter space⁸⁷.

13.3.2 The IHC results

We now discuss the ATLAS and CMS limits [352, 353] in the light of the theoretical uncertainties that affect the Higgs production cross section and the decay branching ratios. We use the same method presented in the Tevatron case a few lines above, with a comparison to the data provided by the CMS collaboration in Ref. [353]⁸⁸: we simply rescale the $\sigma(gg + b\bar{b} \rightarrow A \rightarrow \tau\tau)$ numbers by a factor $2 \times \tan^2\beta$ and then turn them into exclusion limits on the MSSM $[M_A, \tan\beta]$ parameter space that has been probed at the IHC thanks to the CMS numbers.

Our results are shown in Fig. 73 where the contour of the cross section times branching

⁸⁷Note that the 2σ excess observed by CDF in this channel cannot be a Higgs signal as it would correspond to a much larger excess in $p\bar{p} \rightarrow \tau^+\tau^-$ which has not been observed. In addition, for the huge $\tan\beta$ values probed in this $3b$ channel, $\tan\beta \gtrsim 100$, we are outside the theoretical favored range $\tan\beta \lesssim 50$ and the $\Phi b\bar{b}$ Yukawa coupling become non-perturbative. For such values, the total Higgs widths are to be included.

⁸⁸Unfortunately, the ATLAS collaboration had not given this important information in its note ATLAS-CONF-2011-024 which is the preliminary version of Ref. [352] that was available at the time of this analysis. But as the ATLAS exclusion limits are similar to those obtained by the CMS collaboration, the final result once the theory uncertainties have been included is the same as visualised in Ref. [352].

ratio in this plane is displayed, together with the contours when the uncertainties are included. As in Fig. 72 we display the central expected limit (black dotted line) obtained using our central predictions as well as the maximal and minimal expected limits (blue dotted lines) when using correspondingly the minimal and maximal theoretical rates. We also display in gray band the observed limit at the Tevatron according to Fig. 72.

However, rather than applying the observed limits on the central $\sigma \times \text{BR}$ rate (as the CMS and also ATLAS collaborations do), we apply them on the minimal one when the theory uncertainty is included. In this case, only values $\tan \beta \gtrsim 28$ are excluded for a Higgs mass $M_\Phi \approx 130$ GeV, compared to $\tan \beta \gtrsim 23$ if the central prediction is considered as in the CMS analysis. The inclusion of the theory uncertainties should lead to a slight reduction of the excluded $[M_A, \tan \beta]$ parameter space, which can also be viewed in Fig. 3 of Ref. [353], though our uncertainties are larger especially at low A Higgs boson masses.

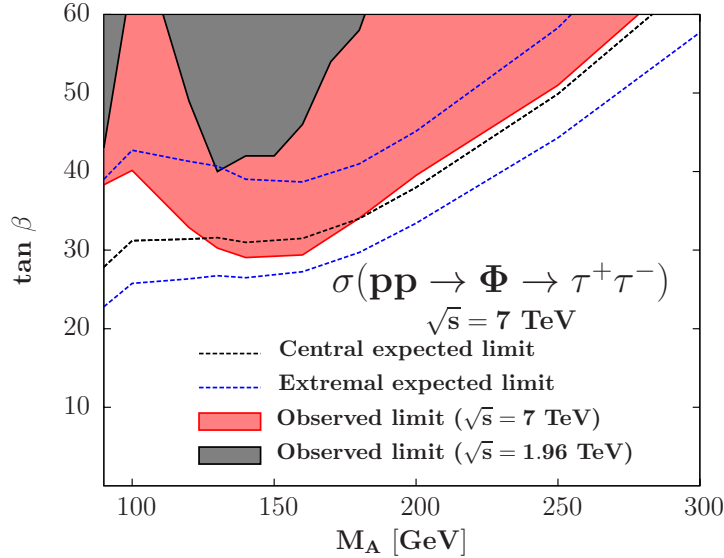


Figure 73: Contours for the expected $\sigma(pp \rightarrow \Phi \rightarrow \tau^+\tau^-)$ exclusion limits at the LHC in the $[M_A, \tan \beta]$ plane with the associated theory uncertainties, confronted to the 95%CL exclusion limits given by the CMS [353] and also CDF/D0 [336] collaborations when our procedure is applied.

13.3.3 The expectations at the LHC

The exclusion limits on the $[\tan \beta, M_A]$ MSSM parameter space obtained by the ATLAS and CMS collaborations with only 36 pb^{-1} data are very strong: indeed when taking into account our theoretical uncertainties we have just demonstrated that values $\tan \beta \gtrsim 29$ are excluded in the low mass range for the pseudoscalar Higgs boson, $M_A = 90\text{--}200$ GeV. We can draw some expectations in the view of higher luminosity and some consequences. We

note that the newest results from HEP–EPS 2011 conference confirm and even surpass our expectations, see below.

First of all, if the luminosity is increased to the fb^{-1} level as was expected to be the case at the end of this year and is actually already the case⁸⁹ at the level of 2 fb^{-1} [368], the values of $\tan\beta$ which can be probed will be significantly lower. We have drawn quantitative expectations assuming no improvement in the analysis, which may be proved to be pessimistic⁹⁰ and that the CMS sensitivity will simply scale as the square root of the integrated luminosity, the region of the $[\tan\beta, M_A]$ parameter space which can be excluded in the case where no signal is observed is displayed in Fig. 74 for several values of the accumulated luminosity. With 3 fb^{-1} data per experiment (or with 1.5 fb^{-1} when the ATLAS and CMS results are combined), we have found that values $\tan\beta \gtrsim 12$ could be excluded in the entire mass range $M_A \lesssim 200 \text{ GeV}$; the exclusion reduces to $\tan\beta \gtrsim 20$ for the mass range $M_A \lesssim 300 \text{ GeV}$. The comparison with Ref. [370] (page 24) from HEP–EPS 2011 conference with 1.1 fb^{-1} data shows that we are not far from the actual observations, thus nicely confirming our expectations.

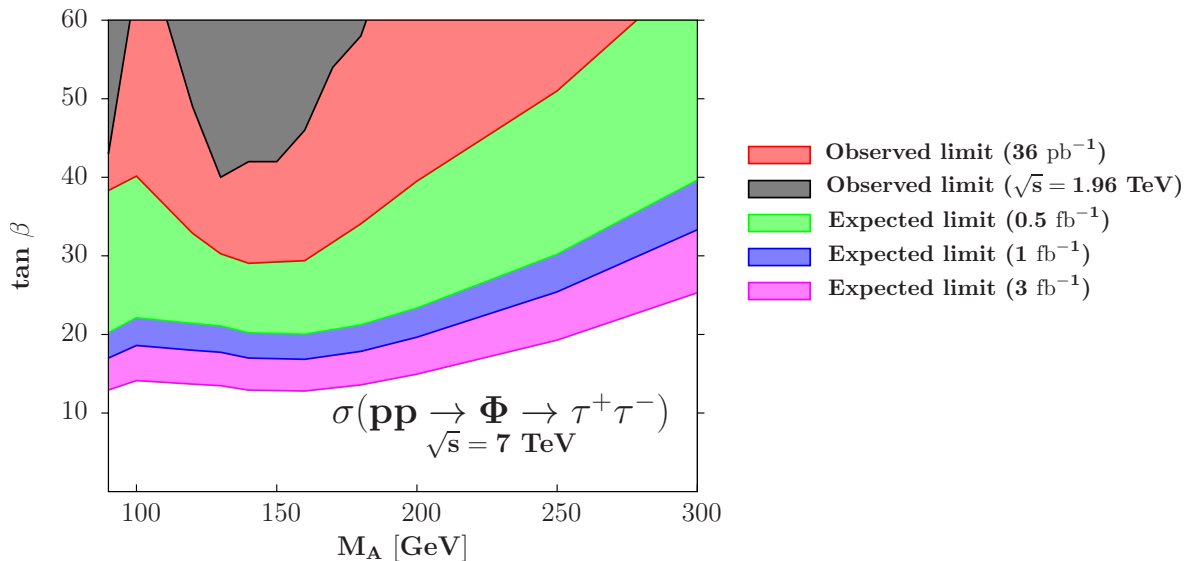


Figure 74: Contours for the “expected” $\sigma(pp \rightarrow \Phi \rightarrow \tau^+\tau^-)$ 95%CL exclusion limits at the LHC with $\sqrt{s} = 7 \text{ TeV}$ in the $[M_A, \tan\beta]$ plane for various integrated luminosities. The present limits from 36 pb^{-1} CMS and the Tevatron are also displayed.

We list below three ways to improve these limits by considering additional production channels.

a) *The process $gb \rightarrow \Phi b \rightarrow b\bar{b}\bar{b}$ where the all final bottom quarks are detected:* the production

⁸⁹The LHC technical team should be acclaimed for such an impressive effort.

⁹⁰For example the SM $H \rightarrow \tau^+\tau^-$ search has been greatly improved from winter 2011 to July 2011, see Ref. [369], page 15.

cross section $\sigma(bg \rightarrow b\Phi + g\bar{b} \rightarrow \Phi\bar{b})$ is one order of magnitude lower than that of the inclusive $gg + b\bar{b} \rightarrow \Phi$ process (the $bg \rightarrow b\Phi$ process is part of the NLO corrections to $b\bar{b} \rightarrow \Phi$ [195, 332], see also Ref. [131] page 5) but this is compensated by the larger fraction $\text{BR}(\Phi \rightarrow b\bar{b}) \approx 90\%$ compared to $\text{BR}(\Phi \rightarrow \tau^+\tau^-) \approx 10\%$; the QCD background are much larger though⁹¹;

- b) *the process $pp \rightarrow \Phi \rightarrow \mu^+\mu^-$* : its rate is simply given by $\sigma(pp \rightarrow \Phi \rightarrow \tau\tau)$ rescaled by $\text{BR}(\Phi \rightarrow \mu\mu)/\text{BR}(\Phi \rightarrow \tau\tau) = m_\mu^2/m_\tau^2 \approx 4 \times 10^{-3}$; the smallness of the rate is partly compensated by the much cleaner $\mu\mu$ final state and the better resolution on the $\mu\mu$ invariant mass. The efficiency of the $pp \rightarrow \Phi \rightarrow \tau\tau$ signal is estimated by the CMS collaboration (see Table 1 of Ref. [353]) to be 4.5% when all τ decay channels are considered. This is only a factor 10 larger than the ratio $\text{BR}(\Phi \rightarrow \mu\mu)/\text{BR}(\Phi \rightarrow \tau\tau)$ (which is approximately equal to the efficiency in the $\tau \rightarrow e\mu$ channel). Thus the $\Phi \rightarrow \mu\mu$ decay channel might be useful. In particular, the small resolution that can be achieved could allow to separate the three peaks of the almost degenerate h, H and A states in the intense coupling regime; see Ref. [325, 371];
- c) *the process $pp \rightarrow tbH^- \rightarrow tb\tau\nu$* : this leads to a cross section that is also proportional to $\tan^2\beta$ (and which might also be useful for very low $\tan\beta$ values) but that is two orders of magnitude smaller than $\sigma(pp \rightarrow \Phi)$ for $M_A \approx 100\text{--}300$ GeV;
- d) *charged Higgs production from top quark decays, $pp \rightarrow t\bar{t}$ with $t \rightarrow H^+b \rightarrow \tau^+\nu b$* : this has also been recently analyzed by the CMS collaboration [372]. With 36 pb^{-1} data, values of the branching ratio $\text{BR}(t \rightarrow H^+b) \gtrsim 25\%$ are excluded which means that only $\tan\beta$ values larger than 60 are probed for the time being⁹².

However the rates are small and would allow only for modest improvements over the limit obtained with the $\Phi \rightarrow \tau^+\tau^-$ search. Indeed according to the projections by the

⁹¹We estimate the theoretical uncertainties on the rate $\sigma(bg \rightarrow Ab \rightarrow b\bar{b})$ to be similar to that of the combined $gg + b\bar{b} \rightarrow \Phi$ process, that is $\pm 30\text{--}40\%$. However, the parametric and Δ_b supersymmetric corrections do not cancel this time in the cross section times branching ratio and have to be taken into account.

⁹²We note that in this case the theoretical uncertainties have not been estimated in Ref. [210] (contrary to the channel $pp \rightarrow tbH^- \rightarrow tb\tau\nu$ where an uncertainty of $\pm 30\%$ has been found). We have evaluated them with HATHOR [373] and, in the production channel $\sigma(pp \rightarrow t\bar{t})$ and for $m_t = 173.3 \pm 1.1 \text{ GeV}$, we find $\sigma(pp \rightarrow t\bar{t}) = 163^{+2.5\%}_{-5.6\%}$ (factor 2 from central m_t scale) $^{+10.4\%}_{-10.1\%}$ (PDF + $\Delta^{\text{exp+th}}\alpha_s @ 90\% \text{ CL}$) $\pm 3.3\%$ (Δm_t) pb, which leads using the procedure of Ref. [94, 95] presented in part II to a total uncertainty of $\Delta\sigma/\sigma = ^{+16\%}_{-19\%}$, that is three times larger than the one assumed in the CMS analysis. To that, one should add the uncertainty on the branching ratio $\text{BR}(t \rightarrow H^+b)$ for which the parametric one (from the input \bar{m}_b and α_s values) is about $+10\%, -4\%$ [232].

ATLAS and CMS collaborations in their technical reports [236, 237], in the context of the full LHC with $\sqrt{s} = 14$ TeV and 30 fb^{-1} data, the observation of these processes is only possible for not too large values of M_A and values of $\tan\beta \gtrsim 20$ that have mostly been excluded by the newest 1.1 fb^{-1} searches [370] (page 24). However, as is the case for the $pp \rightarrow \tau\tau$ channel, some (hopefully significant) improvement over these projections might be achieved.

13.4 Consequences on the SM $H \rightarrow \tau\tau$ search at the LHC

We now conclude our study of the consequences of our theoretical estimations by giving the very interesting consequence of the MSSM analysis on the SM Higgs boson search that has been presented in Ref. [326].

Indeed the ATLAS and CMS $pp \rightarrow \tau\tau$ inclusive analyses open the possibility of using this channel in the case of the Standard Model Higgs boson H . Indeed, in this case, the main production process is by far the $gg \rightarrow H$ channel which dominantly proceeds via a top quark loop with a small contribution of the bottom quark loop as studied in section 5 where the cross section for this process has been discussed in detail (see also Refs. [210, 232]). In the mass range $M_H = 115\text{--}140$ GeV, the SM rate is at the level of 10 to 20 pb. The branching ratio for the decay $H \rightarrow \tau^+\tau^-$ ranges from 8% at $M_H = 115$ GeV to 4% at $M_H = 140$ GeV, see section 6. The cross section times branching ratio $\sigma(gg \rightarrow H \rightarrow \tau^+\tau^-)$ is thus rather substantial at low Higgs masses⁹³.

We have then applied in Ref. [326] our numerical results of the SM Higgs cross section $\sigma(gg \rightarrow H)$ times $H \rightarrow \tau^+\tau^-$ branching fraction [232] to the median expected' and observed 95%CL limits obtained in the CMS analysis at $\sqrt{s} = 7$ TeV with 36 pb^{-1} data. This will be interpreted as “expected” and “observed” 95%CL limits on the SM process. This is displayed in blue (large dotted line for the “expected” limit, small dotted line for the “observed” limit) in Fig. 75 where the 95%CL observed and expected cross sections are normalized to our SM prediction. With the small amount of data that is available in a 36 pb^{-1} analysis it is shown that we are approximately 60 times above the expected SM rate in the mass range $M_H = 110\text{--}140$ GeV. It is nevertheless not that bad if we compare with the expected and observed rates in the $H \rightarrow \gamma\gamma$ analysis of ATLAS experiment [374] which is the most important and promising channel for the low SM Higgs mass searches. Indeed, the $gg \rightarrow H \rightarrow \tau\tau$ inclusive channel, which has not been considered neither by

⁹³The cross section in the SM is comparable to that of $A + H(h)$ production in the MSSM with values $\tan\beta \approx 4$ (and not $\tan\beta = 1$), a consequence of the dominance of the top-quark loop (in the SM) compared to bottom-quark loop (as is in general the case in the MSSM) in the gg fusion process.

the ATLAS nor the CMS collaborations before HEP-EPS 2011 results, is in fact rather powerful and competes rather well with the long celebrated $H \rightarrow \gamma\gamma$ detection channel, as it has a sensitivity that is only a factor of two smaller than the latter channel.

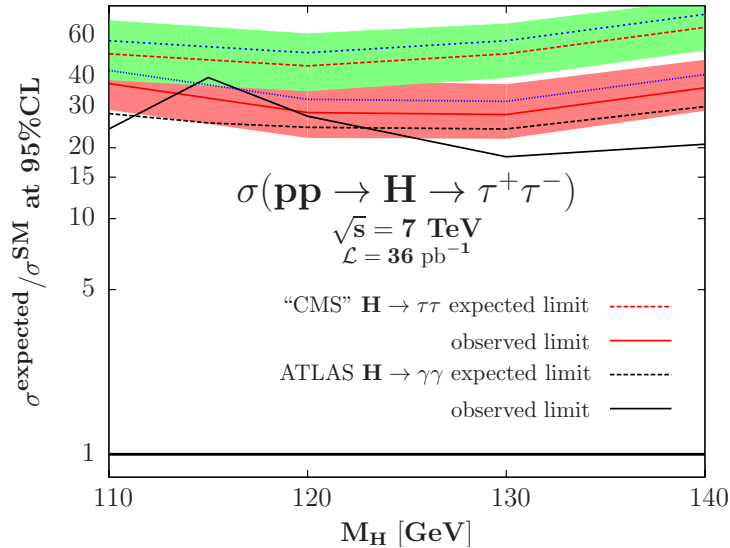


Figure 75: The median expected and observed cross sections at 95% CL for the production of the SM Higgs boson in the channels $gg \rightarrow H \rightarrow \tau\tau$ (blue lines) and $pp \rightarrow H \rightarrow \tau^+\tau^- + X$ (red lines captioned) from an extrapolation of the CMS analysis with 36 pb^{-1} data [353] normalised to the SM cross section. The green and red bands display the impact of our theoretical uncertainties on the “expected” and “observed” limits, respectively, using all the production channels. It is compared to the case of $H \rightarrow \gamma\gamma$ as recently analyzed by the ATLAS collaboration [374] with 37.6 pb^{-1} data.

Thus, the $gg \rightarrow H \rightarrow \tau^+\tau^-$ channel could be also used to search for the SM Higgs in the very difficult mass range $M_H \approx 115\text{--}130 \text{ GeV}$ where only the $H \rightarrow \gamma\gamma$ channel was considered to be effective. The two channels could be combined to reach a better sensitivity. In addition, while little improvement should be expected in $H \rightarrow \gamma\gamma$ (for which the analyses have been tuned and optimised for more than twenty years now), a better sensitivity could be achieved in the $H \rightarrow \tau^+\tau^-$ channel. Indeed, on the one hand, a possible improvement might come from the experimental side: novel and better mass reconstruction techniques of the $\tau\tau$ resonance can be used⁹⁴, splitting of the analysis into jet multiplicities as done for instance for the channel $H \rightarrow WW \rightarrow \ell\nu\nu$, inclusion of additional topologies such as same sign $\ell = e, \mu$ final states, etc⁹⁵. On the other hand, one can render the $H \rightarrow \tau\tau$ channel more effective by simply including the contribution of the other Higgs production mechanisms such as: vector boson fusion, which up until now is the only production channel that has

⁹⁴In Ref. [375], a new mass technique for reconstructing resonances decaying into τ lepton pairs has been proposed and it is claimed that it allows for a major improvement in the search for the Higgs $\rightarrow \tau\tau$ signal.

⁹⁵See for example the incredible improvement displayed in Ref. [369], page 15, where some experimental uncertainties have been reduced from 23% in winter 2011 down to the level of 6% in July 2011.

been analyzed by experimental collaborations in the $H \rightarrow \tau^+\tau^-$ search topology [236, 237] and first proposed in Ref. [376]⁹⁶; associated production with a W and Z bosons, which will increase the cross section for the inclusive $pp \rightarrow \tau\tau + X$ production mechanism by 15 to 20%. We have displayed in Fig. 75 the effect of including all these production channels (naively, that is without making use of the specific cut for vector boson fusion which significantly increases the sensitivity) in the inclusive $pp \rightarrow H \rightarrow \tau^+\tau^- + X$ signal, in dashed red line for the “expected” limit and in solid red line for the “observed” limit. We have also displayed correspondingly in green and red bands the effect of the theoretical uncertainties. Hence, the $pp \rightarrow \text{Higgs} \rightarrow \tau^+\tau^-$ inclusive channel turns out to be a very interesting and potentially very competitive Higgs detection channel also in the Standard Model.

13.5 Summary and outlook

We have presented two kinds of results in this section: the numerical theoretical predictions for the MSSM neutral Higgs bosons branching fractions and their combination with the production cross sections on the one hand, the consequence of the latter on the MSSM parameter space as well as a consequence on the SM Higgs search on the other hand.

We recall that we have updated the cross sections for the production of the MSSM CP -odd like Higgs bosons Φ at the Tevatron in the processes $gg \rightarrow \Phi$ and $b\bar{b} \rightarrow \Phi$ and found smaller rates in the high Higgs mass range compared to those assumed by the CDF and D0 experiments. We have then evaluated the associated theoretical uncertainties together with the impact of the $\Phi \rightarrow \tau^+\tau^-$ decay branching fractions and find that they are very large. These uncertainties, together with the correct normalization, affect significantly the exclusion limits set on the MSSM parameter space from the negative Higgs searches in the channel $pp \rightarrow \Phi \rightarrow \tau^+\tau^-$ at the Tevatron.

We have done the same exercise at the LHC with $\sqrt{s} = 7$ TeV. We have investigated the production of the CP -odd like particles, $\Phi = A$ as well as one of the CP -even H or h particles (depending on whether we are in the decoupling or anti-decoupling regimes) that are degenerate in mass with A and have the same couplings, in particular, enhanced couplings to bottom quarks for the high values of $\tan\beta$ than can be probed at the LHC. The two main production processes $gg \rightarrow \Phi$ and $b\bar{b} \rightarrow \Phi$, which could have cross sections that are order of magnitude larger than in the SM Higgs case, have been considered. Numerical results at energies $\sqrt{s} = 7\text{--}14$ TeV have been given and the associated theoretical

⁹⁶Because of the two additional forward jets, the sensitivity of this channel (the only one involving τ leptons that has been considered in the SM so far) is much larger than its contribution ($\approx 10\%$) to the total $pp \rightarrow H \rightarrow \tau\tau + X$ inclusive rate indicates.

uncertainties have been evaluated. The latter are due not only to the scale and PDF+ α_s uncertainties which appear in the SM case, but there are also uncertainties associated to the b -quark which plays a major role in the MSSM. The error on the input b -quark mass, the scheme dependence in the renormalization of the mass of the b -quark in its contribution to the $gg \rightarrow \Phi$ amplitude and the effect of m_b on the bottom quark densities in the process $b\bar{b} \rightarrow \Phi$ will induce additional uncertainties. To these results we have to add the parametric uncertainties in the branching ratio of the Higgs decay in tau lepton pairs, which is the cleanest detection channel at hadron colliders, that is found to be at the level of 10%.

The overall theoretical uncertainty in these two processes turn out to be extremely large at LHC energies, of the order of 50%. This large uncertainty have some impact on the MSSM parameter space that can be probed and this has been also discussed when comparing with the 36 pb $^{-1}$ data from CMS collaboration. Still the results lead to very strong constraints on the $[\tan\beta, M_A]$ MSSM parameter space. We also recall that these constraints are essentially model independent (for the values of M_A and $\tan\beta$ that are being probed so far) and slightly less effective when the theoretical uncertainties in the predictions for the Higgs cross sections and branching ratios are properly included, $\tan\beta \gtrsim 29$ excluded. We have also estimated that these limits can be significantly improved in the absence of a Higgs signal with a few inverse femtobarn data: $tb \gtrsim 20$ can be excluded with 1 fb $^{-1}$ data, a result that has been confirmed by the newest CMS analysis presented in the HEP-EPS 2011 conference [370] (page 24), $\tan\beta \lesssim 10$ can be excluded for not too heavy neutral Higgs bosons and a luminosity of order 3 fb $^{-1}$. At this stage, many channels such as $pp \rightarrow \Phi \rightarrow \mu^+\mu^-$, $pp \rightarrow btH^- \rightarrow bt\tau\nu$, $gb \rightarrow \Phi b \rightarrow 3b$ and $t \rightarrow H^+b$ will not be viable anymore even at the design energy and luminosity of the LHC.

The final most important consequence that we have drawn in that the inclusive $pp \rightarrow$ Higgs $\rightarrow \tau\tau$ process is also a very promising channel in the search for the Standard Model Higgs boson if the production rate $gg \rightarrow H$ is included. Indeed, this channel has a sensitivity that is only a factor of two smaller than the expected sensitivity of the main $pp \rightarrow H \rightarrow \gamma\gamma$ channel when compared to the ATLAS analysis with a luminosity of 36 pb $^{-1}$ in the $H \rightarrow \gamma\gamma$ search channel. While little improvement is expected in the later channel, there are ways to significantly enhance the sensitivity of the $pp \rightarrow H \rightarrow \tau\tau$ signal and render it a very powerful discovery channel for the SM Higgs boson in the difficult $M_H = 115$ –130 GeV mass range. Indeed, this $gg \rightarrow H \rightarrow \tau^+\tau^-$ channel is now considered by the experimental collaborations in their latest results presented at the HEP-EPS 2011 conference [377] (see also Ref. [378] page 13).

Part V

Perspectives

Summary

14 Exclusive study of the gluon–gluon fusion channel	242
14.1 Exclusive SM Higgs production	243
14.2 SM Backgrounds	246
Conclusion	248
A Appendix: Synopsis	252
A.1 Introduction	252
A.1.1 Le Modèle Standard	252
A.1.2 Le mécanisme de Brout–Englert–Higgs	254
A.2 Production et désintégration du boson de Higgs du Modèle Standard . .	256
A.2.1 Le cas du Tevatron	256
A.2.2 Le cas du LHC	261
A.2.3 Conséquences sur les résultats expérimentaux	262
A.3 Le Modèle Standard Supersymétrique Minimal (MSSM)	264
A.3.1 Bref aspect de la supersymétrie et du MSSM	264
A.3.2 Secteur de Higgs du MSSM	267
A.4 Production et désintégration des bosons de Higgs supersymétriques . . .	268
A.4.1 Les Higgs neutres du MSSM au Tevatron	269
A.4.2 Les Higgs neutres du MSSM au LHC	270
A.4.3 L’impact des incertitudes théoriques sur l’espace des paramètres du MSSM	272
A.4.4 Le canal $H \rightarrow \tau\tau$ dans le Modèle Standard revisité	273
A.5 Perspectives	274

14 Exclusive study of the gluon–gluon fusion channel

This last section is devoted to the perspectives of the work that has been done for the last three years. We have completed a detailed analysis of the inclusive production cross section times decay branching fractions at the Tevatron and LHC colliders both in the Standard Model and its minimal supersymmetric extension. The next step that is of utmost interest for experimentalists is the exclusive study of all the production and decay channels. Indeed, any experimental search is conducted in a specific channel with specific search topologies and cuts in order to maximize the signal over the background. We, as a theorist, are to give to experimental collaborations the most precise and detailed analysis of such search topologies. In addition the same work has to be done on the background analysis.

There are other perspectives to think of, for example:

- the study of the impact of the Higgs decay width on the predictions, as for heavy Higgs $M_H \gtrsim 500$ GeV this really has to be taken into account. Related to that effect is the study of the interference between the signal and the background, e.g. in the channel $pp \rightarrow H \rightarrow WW$ that means to make a detailed analysis of the $pp \rightarrow WW$ cross section in which the process $pp \rightarrow H \rightarrow WW$ is considered as part of the amplitude and not an isolated process;
- the impact of the cuts on the theoretical uncertainties in an exclusive study. Indeed it is well known that cuts and jet bin separation often enhance the scale uncertainties, see Ref. [112] in the case of the Tevatron; it may be interesting to make a study of the cuts that both improve the significance of the signal over the background and minimize the scale uncertainty.

We will present in this section some preliminary results on the Standard Model exclusive study of the channel $pp \rightarrow H \rightarrow W^+W^-$ at the LHC with $\sqrt{s} = 7$ TeV, in which well educated cuts on the phase space are implemented in order to maximize the signal significance over the backgrounds, which is the spirit of an exclusive study in comparison with an inclusive calculation where all the phase space is taken into account, see Refs. [112, 170] for studies of this channel at the Tevatron and the LHC. We will also give some results on the background study with the same set of cuts. This work is an on-going collaboration [379] in the context of the LHC Higgs Cross Section Working Group.

14.1 Exclusive SM Higgs production

We study the exclusive channel at the IHC $gg \rightarrow H \rightarrow W^+W^- \rightarrow \ell\nu\ell\nu$ in which two leptons have to be found together with missing transverse energy. This channel is a silver channel for Higgs discovery with a mass $M_H \geq 135$ GeV as stated in subsection 6.1. We will make use of the CMS cuts of Ref. [224] and summarized in Table 17 below:

M_H [GeV]	$p_T^{\ell,\max}$ [GeV]	$p_T^{\ell,\min}$ [GeV]	$m_{\ell\ell}$ [GeV]	$\Delta\Phi_{\ell\ell}$ [deg]
≥ 130	> 25	> 20	< 45	< 60
≥ 160	> 30	> 25	< 50	< 60
≥ 200	> 40	> 25	< 90	< 100
≥ 210	> 44	> 25	< 110	< 110
≥ 400	> 90	> 25	< 300	< 175

Table 17: CMS cuts on the charged leptons for the $gg \rightarrow H \rightarrow WW \rightarrow \ell\nu\nu$ final state.

Other cuts can further reduce the background: we can define a Z veto in the l^+l^- final states by which events with an invariant dilepton mass within 15 GeV around the Z mass are discarded, which reduces the Drell–Yan background. In addition we also impose the following cuts:

- $E_T^{\text{miss}} > 20$ GeV;
- $E_T^j > 25$ GeV for the jets, with $|\eta^j| < 5$ and a distance $R = 0.5$ between jets.

To calculate the signal cross section with the cuts defined in Table 17 we use the program HNNLO⁹⁷ [380]. We will use for the central prediction the MSTW2008 NNLO PDFs set if nothing else is indicated and the central scales are set to $\mu_R = \mu_F = \mu_0 = \frac{1}{2}M_H$ as in the inclusive study. This is known to absorb part of the higher order corrections already at the LO thus improving the perturbative expansion [112, 170]. The results presented in this perspective section are preliminary in the sense that the calculation is heavily time consuming: for the total Higgs cross section $\sigma_{\text{tot}}^{\text{NNLO}}$ and the Higgs+zero-jet (H+0j) $\sigma_{0j}^{\text{NNLO}}$ the program runs for more than 45 hours. The results that we display need to be checked against numerical instabilities and are not to be taken as serious but rather an indication at this stage.

For the H+1j and H+2j cross sections, the NLO and LO MSTW sets are adopted. We display in Table 18 the results for the most sensitive Higgs mass $M_H = 160$ GeV

⁹⁷The program can be found in Ref. [171].

together with the associated numerical errors (note that for NNLO there are still at the 3% level which is too much!). We have also calculated the Higgs+jet cross sections at NLO consistently (i.e. all PDFs and α_s at NLO) using the program MCFM [274] (for the H+2j cross section, there is an improvement here as the result is at NLO while with HNNLO is only at LO); the results are shown in the last column of Table 18.

M_H	σ_{jets} [fb]	LO	NLO	NNLO	MCFM@NLO
160	H+0jets	9.890 ± 0.004	11.598 ± 0.043	10.952 ± 0.186	11.173 ± 0.010
	H+1jet	8.981 ± 0.007	7.048 ± 0.090	–	6.834 ± 0.032
	H+2jets	5.778 ± 0.007	–	–	2.525 ± 0.086

Table 18: The $gg \rightarrow H+\text{jet}$ cross sections at the 7 TeV IHC calculated with HNNLO at the various perturbative orders with MSTW PDFs and central scale $\mu_F = \mu_R = \frac{1}{2}M_H$. In the last column, shown are the results when one uses the program MCFM at NLO.

Bearing in mind that these results as already mentioned are really preliminary, we can raise some remarks:

- a) the K-factors are $K^{\text{NLO}} = 1.173 \pm 0.005$ and $K^{\text{NNLO}} = 1.107 \pm 0.019$ which seems at first sight to be weird: $K^{\text{NLO}} > K^{\text{NNLO}}$ and both are really close to unity in contrast to what is known for the total exclusive cross section, even with $\mu_0 = \frac{1}{2}M_H$ which improves the perturbative calculation;
- b) the results between HNNLO and MCFM are consistent once the numerical errors are included. We note that for this comparison MCFM is fully at NLO which means that the H+0j calculation misses one order compared to HNNLO, the H+1j is at the same perturbative order and the H+2j is one perturbative order more than HNNLO calculation;
- c) the total Higgs cross section including the cuts is also given by HNNLO and is

$$\sigma_{\text{cuts}}^{\text{NNLO}}(\text{MSTWNNLO}) = 20.778 \pm 0.174 \text{ fb} \quad (14.1)$$

which is lower than what is obtained when summing the jet cross sections in Table 18, $\sigma_{0j}^{\text{NNLO}} + \sigma_{1j}^{\text{NLO}} + \sigma_{2j}^{\text{LO}} = 23.778 \pm 0.21 \text{ fb}$ (with a quadratic sum of the errors). The difference is due of course to the fact that in the total cross section $\sigma_{\text{cuts}}^{\text{NNLO}}$, the PDF for the 1j and 2j cross sections are both taken at NNLO consistently throughout the calculation. We need to think how to interpret this difference in term of PDF uncertainties on the cross section.

The next step is to apply the procedure that we have developed in part II to deal with the various sources of theoretical uncertainties that affect our predictions. In the case of

this exclusive study we deal with the scale uncertainty, the PDF+ α_s uncertainty and the specific jet cut uncertainty. All of these are calculated as stated below:

- i)* for the scale variation, rather than performing a scan in the usual domain $\frac{1}{2}\mu_0 \leq \mu_R, \mu_F \leq 2\mu_0$ with $\mu_0 = \frac{1}{2}M_H$ which is time consuming, we simply take the cross section values for $\mu_F = \mu_R = \frac{1}{2}\mu_0$ and $\mu_R = \mu_F = 2\mu_0$ which, in the case of the total inclusive cross section, provide the maximal and minimal values. This is nothing more than a mere assumption and it might indeed underestimate the scale uncertainty as in the case of the exclusive production two characteristic scales at least are present: the mass of the Higgs boson on the one hand and the p_T of the distribution on the other hand. Nevertheless our assumption will give an indication of the scale uncertainty that is sufficient for this preliminary study;
- ii)* The PDF4LHC recommendation [151] is adopted for the evaluation of the PDF+ α_s uncertainty: we use the 5×40 MSTW grids to obtain the 68%CL combined PDF+ α_s uncertainty of the various jet cross sections and multiply the result by a factor of two, see also Ref. [210];
- iii)* the uncertainty on the jet cut is calculated assuming simply that there is a 10% uncertainty on the jet energy. We thus calculate the cross section when the jet cut is either $E_T^{\text{jet}} = 22.5$ GeV or 27.5 GeV. We keep the same values for the rapidity η^{jet} and the distance R. We do not consider for the moment the problem that the errors for the various jet cross sections are correlated and that there should be no error in the sum;
- iv)* the total uncertainty is eventually calculated by a linear sum of the three individual uncertainties: for scale and PDF+ α_s , this follows the LHC Higgs working group recipe [210], while for the uncertainty on the jet energy which is of experimental nature, the situation might be slightly more complicated and we may have to think about correlations more carefully.

The results for the individual and total uncertainties are given (in %) in Table 19 below.

It has been checked that for the H+1j, H+2j and also H+0j cross sections, all evaluated at NLO, the same results are obtained with MCFM as shown in Table 20 below:

Some calculations remain to be done, and everything need to be checked against numerical instabilities in particular the PDFs uncertainties that are the most time consuming calculations.

M_H	σ_{jets}	$\Delta\mu$ [%]	PDF+ $\Delta\alpha_s$ [%]	ΔE_T^j [%]	total [%]
160	H+0jets	−0.1 +0.2	−55.7 +50.0	−7.6 +6.7	−63.4 +56.9
	H+1jet	−7.3 −9.9	−16.2 +12.7	−4.1 +4.2	to be calculated
	H+2jets	−43.3 +89.5	−16.4 +18.1	−13.9 +16.5	−73.6 +124.1

Table 19: The scale, PDF+ α_s and jet energy uncertainty on the various $gg \rightarrow H \rightarrow \ell\nu\ell\nu$ jet cross sections at the LHC with $\sqrt{s} = 7$ TeV for $M_H = 160$ GeV as well as the total uncertainty as obtained with HNNLO.

M_H	σ_{jets}	$\Delta\mu$ [%]	PDF+ $\Delta\alpha_s$ [%]	ΔE_T^j [%]	total [%]
160	H+0jets	−9.7 +8.5	−7.5 +8.1	−5.0 +4.0	−22.2 +20.6
	H+1jet	−7.7 −7.9	−11.8 +11.6	−5.3 +3.9	to be calculated
	H+2jets	−56.5 +30.1	to be calculated	−4.0 +3.0	to be calculated

Table 20: The scale, PDF+ α_s and jet energy uncertainty on the various $gg \rightarrow H \rightarrow \ell\nu\ell\nu$ jet cross sections at the LHC with $\sqrt{s} = 7$ TeV for $M_H = 160$ GeV as well as the total uncertainty as obtained with MCFM.

14.2 SM Backgrounds

In addition to the study of the signal cross section it is of utmost importance to study as well the background processes together with the selection cuts. We will consider four background processes leading to $\ell\nu\ell\nu+X$ final states with the cuts of Table 17:

1. $pp \rightarrow WW \rightarrow \ell\nu\ell\nu$: we evaluate this process at NLO using MCFM and we do not consider the interference between the signal and the background. As stated at the beginning of this perspective section, this is a separate study that remains to be done. The central scale is taken to be $\mu_0 = M_W$;
2. $pp \rightarrow ZZ \rightarrow \ell\nu\ell\nu$: this channel is also evaluated with MCFM at a central scale $\mu_0 = M_Z$. We recall that we use the Z jet veto that removes the contribution of a resonant Z boson;
3. $pp \rightarrow t\bar{t}$: this production channel will mainly affect the H+2jet cross section. The process is evaluated at NLO using MCFM and renormalised to NNLO by using the approximate inclusive NNLO to NLO rates obtained with the program HATHOR [373]. The scales are set to $\mu_F = \mu_R = m_t$;
4. single top production: we take into account the two processes $pp \rightarrow Wt$ and $pp \rightarrow Wt+1j$ that we evaluate again using MCFM with central scales $\mu_0 = \frac{M_W+m_t}{2}$.

There are many other background processes, involving the Z or the γ bosons, not to mention the huge QCD background that is inevitable at hadron colliders. However they will not have as much impact on the Higgs search in the diboson channel that we study in this section as we require the observation of two leptons.

The cross sections, using the cuts of Table 17, together with the cut on the transverse missing energy E_T^{miss} and the E_T, η and R of the jet, are displayed in Table 21 using MSTW2008 NLO PDFs⁹⁸. Together with the central cross sections, we also display the uncertainties on the cross sections due to scale variation (within a factor of two from the central scale) and due to the PDF+ α_s , applying again the PDF4LHC recipe [151] by taking 68%CL PDF+ α_s uncertainty multiplied by a factor of two. Whenever relevant, we also estimate the uncertainty on the jet energy. The total uncertainty is obtained by added linearly the three uncertainties as in the case of the signal cross section.

M_H	process	σ_{bkg} [fb]	$\Delta\mu$ [%]	PDF+ $\Delta\alpha_s$ [%]	ΔE_T^j [%]	total [%]
160	WW	8.85	-1.1 +2.1	-4.0 +5.6	-3.4 +3.3	-8.5 +11.0
	ZZ	0.26	-1.5 +2.3	-7.2 +4.5	-4.9 +4.2	-13.6 +11.0
	$t\bar{t}$	41.79	-23.2 +10.2	-6.6 +6.9	-4.5 +3.3	-34.3 +20.4
	tW	4.71	-9.9 +8.6	-24.7 +12.8	-9.7 +8.4	-44.3 +29.8

Table 21: The central values and the associated individual and total uncertainties for the various background cross sections at the IHC with 7 TeV using the cuts of Table 17. MCFM has been used with the default scales discussed in the text and the MSTW2008 NLO PDF sets adopted.

⁹⁸The numerical errors are very small and have been omitted.

Conclusion

The red line we have been guided by throughout this thesis has been the wish to unravel the mechanism that is behind the electroweak symmetry breaking, focusing of its realization through the Higgs mechanism of spontaneous symmetry breaking either in the Standard Model (SM) or in its minimal supersymmetric extension called the MSSM. The Standard Model itself has been the subject of a short review in part I while the MSSM and supersymmetry in general has been the subject of part III. We noted that if one Higgs boson is present in the SM, we have five Higgs bosons in the MSSM coming from the use of two Higgs doublet: two CP -odd neutral Higgs boson h and H , one CP -odd neutral Higgs boson A and two charged Higgs bosons H^\pm .

The two current best places we have to study this fascinating subject are the high energy hadron colliders, the Fermilab Tevatron collider on the one hand and the CERN Large Hadron Collider (LHC) on the other hand which has started its activities with a 7 TeV center-of-mass energy. We thus have focused on giving predictions for the Higgs bosons production and decay branching fractions at both colliders together with a detailed analysis of the theoretical uncertainties affecting those predictions.

The study of the SM Higgs boson production was the subject of part II. We started by a review of the current theoretical and experimental bounds on the Higgs boson mass in section 3 and then we moved on to the study of the SM Higgs boson production at the Tevatron in section 4. We focused on the two main production channels that are the gluon-gluon fusion with triangular top and bottom quarks loops and the Higgs-strahlung production with either a W^\pm or a Z boson in association with the Higgs boson. The first production channel is the major search channel for high Higgs mass searches $M_H \gtrsim 135$ GeV where the Tevatron is the most sensitive to a Higgs signal while the latter is used in low Higgs mass searches $M_H \lesssim 135$ GeV.

We have studied three kinds of uncertainties.

- The first is the scale uncertainty that estimates the effect of unknown higher-order terms in the perturbative expansion by varying the renormalization and factorization scales μ_R, μ_F within a definite interval $1/\kappa\mu_0 \leq \mu_R, \mu_F \leq \kappa\mu_0$ with μ_0 as the central scale and we exposed a way to define its (subjective) choice in subsection 4.2: choose the constant factor κ as the one that enables the lower order scale uncertainties bands to catch the central prediction of the highest order of the calculation. We then found that if $\kappa = 2$ is enough for the Higgs-strahlung process at next-to-next-to-leading order (NNLO) with a central scale $\mu_0 = M_{HV}$, M_{HV} being the invariant mass of the W and H boson system,

$\kappa = 3$ would be recommended for the gluon–gluon process at NNLO even with the central scale choice $\mu_0 = \frac{1}{2}M_H$ which is known to minimize the impact of higher order terms.

- The second source of uncertainties is related to the PDF puzzle. Indeed it is well known that there are many PDF collaborations on the market and they do not give the same predictions with sometimes dramatic variations up to 30%. A way to reconcile these different predictions is to take into account both the experimental and theoretical uncertainties on the value of α_s and we gave in subsection 4.3 numerical results within this scheme.
- We then introduced in subsection 4.4 the specific uncertainties of the gluon–gluon fusion channel related to the use of an effective theory approach to simplify the hard calculation: the infinite top mass approximation at NNLO which is excellent for the top loop but implies that we have to estimate the absence of the bottom loop; the use of an effective approach for the calculation of the mixed QCD–electroweak corrections at NNLO. We gave sizeable numerical results

We closed off the section 4 by the subsection 4.5 which was devoted to the combination of all the uncertainties into a single total uncertainty. We defined our method as to calculate the PDF+ $\Delta\alpha_s$ uncertainty on the maximal and minimal cross sections regarding to the scale uncertainty and then add linearly the small effective field theory uncertainty. This has to be contrasted with the quadratic addition used by the experimental collaborations, and has to be compared with the recommended linear addition of the LHC Higgs Cross Section Working Group recommendation [210]. We found an uncertainty that amounts to nearly $\pm 20\%$ in the gluon–gluon fusion channel in the Higgs mass range $115 \leq M_H \leq 200$ GeV that is of Tevatron interest and approximately $\pm 8\%$ in the case of the Higgs–strahlung channel.

We then moved on to section 5 when the same outlines were repeated for the study of the gluon–gluon fusion main production channel. We gave numerical results both for the LHC at 7 TeV that we call LHC for littler Hadron Collider, and for the LHC at 14 TeV. We found much more controlled uncertainties as they amount up to approximately $\pm 25\%$, either a bit more or a bit less depending on the Higgs mass range. This was followed by section 6 where we started by a short review of the most interesting decay channels for experimental searches in subsection 6.1 before turning on to the study of the SM Higgs decay branching fractions in subsection 6.2 where we found that their uncertainties should be taken into account in experimental searches even if they are quite small. We finished this section by the most important consequence of the combination of our results on the cross section and decay branching fractions that deals with the current Tevatron exclusion limit at 95%CL

for Higgs masses M_H between 156 GeV and 177 GeV [381]. We have estimated that if our uncertainties are properly taken into account the exclusion band obtained in Ref. [93] should be revisited and in particular in view of the PDF puzzle that is still pending in the community. We estimated that doubling the current luminosity would be required to obtain the current claimed sensitivity.

Section 10 opened our study of the MSSM neutral Higgs bosons production and decay at the hadron colliders. We showed that the predictions we presented in the following section 11 and 12 are somewhat model independent, we then move on to the study of the Higgs bosons production at the Tevatron in section 11 focusing on the two main production channels in the context of the MSSM at relatively high $\tan\beta$ values, $\tan\beta$ being the ratio of the two Higgs doublets: the gluon–gluon fusion channel through a triangular bottom quark loop, the top loop being suppressed, and the bottom quarks fusion channel. Our study of the uncertainties showed that they are quite large in the MSSM, including a new source of uncertainty compared to the SM study and coming from the b quark. We reproduced the same study in the case of the LHC in section 12 and then closed off this part IV by section 13 where we combined our results with the major Higgs to ditau decay branching fraction. We compared our predictions to the experimental results obtained both at the Tevatron and the LHC colliders and found that our uncertainties have a significant impact on the MSSM $[M_A, \tan\beta]$ parameter space that is probed by CDF/D0 and ATLAS/CMS experiments. We also gave some predictions for the expected exclusion by CMS with increased LHC luminosity that have been nicely confirmed by the latest HEP–EPS 2011 conference results [370] (page 24). We finished this section by giving one of the most important output of the thesis: the possibility to use the $gg \rightarrow H \rightarrow \tau^+\tau^-$ search channel for SM Higgs boson by comparing the limits obtained in the CMS MSSM search with the SM predictions. We found that this channel is not as bad compared to the long–celebrated $H \rightarrow \gamma\gamma$ for low Higgs mass searches $110 \leq M_H \leq 140$ GeV and proposed that it should be used by the experimental collaborations. This is now the case according to the latest HEP–EPS 2011 conference results [377].

We finally arrived at the end by the perspective section 14 where we gave some ideas for future work and in particular the exclusive study of the Higgs bosons production that is of utmost importance for experimental search as specific topology with dedicated cuts on the kinematic variables are actually used in a Higgs search. We gave some preliminary results from an ongoing study that remains to be finished.

What is the roadmap for the very close future? The latest HEP–EPS 2011 conference results [370, 378] have dramatically changed the hideouts for the SM Higgs boson: indeed thanks to the 1 fb^{-1} analysis of the ATLAS and CMS experiments the SM Higgs boson

mass is excluded at 95%CL in the mass ranges $149 \leq M_H \leq 206$ GeV and $270 \leq M_H \leq 450$ GeV which is a dramatic improvement over both the old LEP results $M_H \leq 114.4$ GeV and the (disputed) Tevatron results $157 \leq M_H \leq 177$ GeV. The latest HEP–EPS 2011 conference results are also very intriguing as both ATLAS and CMS experiments show some hints of a Higgs signal near $M_H = 140$ GeV, at the level of 2.9σ . This of course has to be carefully checked against statistical fluctuations but the fact that this is observed by the two experiments, not only in the $H \rightarrow WW$ channel but apparently also in the $H \rightarrow ZZ \rightarrow 4\ell$ channel, produces excitations within the community as we may be on the edge of finding the most elusive and searched particles of the past thirty years, which actually is the only thing that matters!

In any case, much work remains to be done: if these signals are indeed the first hints of a Higgs boson discovery we have to work hard to unravel its true nature: is it a SM Higgs boson, a MSSM Higgs boson and in this case which one of the three neutrals? Is it something more exotic as composite Higgs, or even not a Higgs at all but rather a scalar signal of something more exotic? And even if it is really the SM Higgs boson, lots remain to be done for the precise measurements of its mass, couplings and CP nature. On a theoretical side, theoretical uncertainties on these precision observables will be a critical issue, while this does not matter so much for a discovery as a peak in kinematic distribution would be clearly established if we have 5σ significance in the amount of data. On a more general view lots of mysteries remain to be solved, just to mention a few: the exact nature of dark matter, the matter–antimatter asymmetry, the origin of the three families, the unification of the electroweak and strong interactions and even with gravity, etc. We are on the very edges of exciting times!

A Appendix : Synopsis

A.1 Introduction

A.1.1 Le Modèle Standard

Cette thèse s'intéresse à l'étude théorique de la production et de la désintégration du boson de Higgs, la particule témoin du mécanisme de brisure électrofaible et qui reste à découvrir, dans les grands collisionneurs hadroniques actuels que sont le Tevatron au Fermilab et le grand collisionneur de hadrons (LHC) au CERN. Nous commençons l'étude par le Modèle Standard (SM), que nous décrivons dans les quelques lignes qui suivent, avant de nous intéresser à son extension supersymétrique minimale (MSSM).

Le Modèle Standard est un modèle des particules élémentaires et de leurs interactions dans le cadre de la théorie quantique des champs, et basé sur l'algèbre de Lie $SU(3)_c \times (SU(2)_L \times U(1)_Y)$ décrivant les symétries de jauge s'appliquant sur les champs fondamentaux du modèle.

Les champs de matière, fermioniques, se répartissent en deux catégories :

- Les quarks sensibles à toutes les interactions et en particulier à l'interaction forte décrite par l'algèbre de Lie $SU(3)_c$ et dont le nombre quantique est la couleur et la théorie quantique associée est la ChromoDynamique Quantique (QCD) ;
- Les leptons qui ne sont sensibles qu'à l'interaction électrofaible décrite par l'algèbre de Lie $SU(2)_L \times U(1)_Y$ dont les nombres quantiques sont respectivement l'isospin faible I et l'hypercharge Y .

Les générateurs des interactions sont des bosons de jauge, chacun associé aux algèbres de Lie correspondantes :

- huit gluons g pour l'interaction forte ;
- un boson B_μ pour l'algèbre $U(1)_Y$;
- trois bosons W_μ^a pour l'algèbre $SU(2)_L$.

L'interaction électrofaible viole la parité de façon maximale : les fermions sont divisés en doublets d'isospin faible et de chiralité gauche, et en singulets d'isospin faible et de chiralité

droite. Seul les neutrinos n'ont qu'une seule chiralité, gauche, dans le Modèle Standard et sont considérés de masse nulle⁹⁹.

Le tableau ci-dessous résume le contenu en champ fermionique du Modèle Standard.

Type	Nom	Masse [GeV]	Spin	Charge	$(I^W, I_3^W)_L$	rep. $SU(3)_c$
LEPTONS	ν_e	$< 2 \times 10^{-6}$	1/2	0	(1/2, 1/2)	1
	e	5.11×10^{-4}	1/2	-1	(1/2, -1/2)	1
	ν_μ	$< 1.9 \times 10^{-4}$	1/2	0	(1/2, 1/2)	1
	μ	1.06×10^{-1}	1/2	-1	(1/2, -1/2)	1
	ν_τ	$< 1.82 \times 10^{-2}$	1/2	0	(1/2, 1/2)	1
	τ	1.777	1/2	-1	(1/2, -1/2)	1
QUARKS	u	$(1.5 \leq m \leq 3.0) \times 10^{-3} (\overline{\text{MS}})$	1/2	2/3	(1/2, 1/2)	3
	d	$(3.0 \leq m \leq 7.0) \times 10^{-3} (\overline{\text{MS}})$	1/2	-1/3	(1/2, -1/2)	3
	c	1.28 ($\overline{\text{MS}}$)	1/2	2/3	(1/2, 1/2)	3
	s	$9.5 \times 10^{-2} (\overline{\text{MS}})$	1/2	-1/3	(1/2, -1/2)	3
	t	173.1	1/2	2/3	(1/2, 1/2)	3
	b	4.16 ($\overline{\text{MS}}$)	1/2	-1/3	(1/2, -1/2)	3

Table 22 – Description des champs fermioniques du Modèle Standard organisé en trois générations. Tous les champs ont une chiralité gauche et une chiralité droite, cette dernière étant singulet de $SU(2)_L$, sauf les neutrinos qui ne sont que des champs gauches.

Afin de respecter l'invariance de jauge et les symétries du Modèle Standard, il est nécessaire que les masses des fermions et des bosons de jauge soient nulles. Ceci est incompatible avec l'expérience : il est donc nécessaire d'avoir un mécanisme générant la masse aux particules tout en préservant l'invariance de jauge, ce qui est précisément le mécanisme de Brout–Englert–Higgs qui permet de briser spontanément la symétrie électrofaible : la symétrie est présente dans le lagrangien de la théorie mais brisée par la configuration du vide de la théorie. De ce mécanisme qui sera décrit ci-dessous émerge une particule supplémentaire au sein du Modèle Standard : le boson de Higgs, seule particule restante d'un isodoublet gauche scalaire appelé champs de Higgs.

⁹⁹Comme précisé dans le texte principal, nous savons aujourd'hui expérimentalement depuis 1998 que les neutrinos ont une masse très faible mais cependant non nulle car oscillants entre eux. Ce point est laissé de côté au sein du Modèle Standard.

A.1.2 Le mécanisme de Brout–Englert–Higgs

Le lagrangien du Modèle Standard complet est disponible dans le texte principal de la thèse, Eq. 1.7. Nous ne reprenons dans ce synopsis que la partie intéressante pour décrire le mécanisme de Brout–Englert–Higgs, donnée dans l'équation ci-dessous et qui ne concerne que la partie scalaire du lagrangien du Modèle Standard :

$$\mathcal{L}_{\text{scalaire}} = (D_\mu \Phi)^\dagger (D_\mu \Phi) - V(\Phi), \quad V(\Phi) = \mu^2 \Phi^\dagger \Phi + \lambda (\Phi^\dagger \Phi)^2 \quad (\text{A.1})$$

avec D_μ la dérivée covariante, construite de telle sorte que $(D_\mu \Phi)^\dagger (D_\mu \Phi)$ soit invariant de jauge :

$$D_\mu \psi = \left(\partial_\mu - ig_s U_a G_\mu^a - ig T_a W_\mu^a - ig_Y \frac{Y_q}{2} B_\mu \right) \psi \quad (\text{A.2})$$

Dans les équations A.1 et A.2 le champ Φ décrit l'isodoublet faible scalaire de Higgs suivant, avec hypercharge $Y = +1$:

$$\Phi = \begin{pmatrix} \phi^+ \\ \phi^0 \end{pmatrix}$$

Le mécanisme de Brout–Englert–Higgs repose sur la forme donnée au potentiel scalaire $V(\Phi) = \mu^2 \Phi^\dagger \Phi + \lambda (\Phi^\dagger \Phi)^2$. Son rôle est d'une part de donner la masse aux bosons de jauge faibles et aux fermions, d'autre part de permettre au Modèle Standard de respecter l'unitarité, c'est-à-dire la conservation des probabilités nécessaire dans toute théorie quantique cohérente, dans les processus de diffusion mettant en jeu justement les bosons de jauge faibles. Ces deux raisons sont développées en détail dans le texte principal, dans les sous-chapitres 2.1.1 et 2.1.2.

La valeur moyenne dans le vide (vev) du doublet de Higgs est donnée par le minimum du potentiel scalaire $V(\Phi)$. Afin d'avoir un minimum il faut que le potentiel soit borné inférieurement, donc $\lambda > 0$. Selon la valeur du terme μ^2 , deux situations se présentent, décrites dans la figure 76.

Pour un terme de masse positif $\mu^2 > 0$ le minimum est pour $\langle \Phi \rangle = 0$ ce qui paraît attendu. L'hypothèse du mécanisme de Brout–Englert–Higgs est de prendre $\mu^2 < 0$: dans ce cas il y a deux minima possibles, en réalité pour le doublet du Modèle Standard une infinité invariante sous $U(1)$. La vev (et donc le vide) est alors une configuration parmi toutes celles possibles et équivalentes : la symétrie de départ est alors brisée par le vide de la théorie, ce qu'on appelle une brisure spontanée de symétrie, cette dernière étant encore présente dans les équations de la théorie mais “cachée” par le vide qui lui brise la symétrie de jauge. Dans le cas du Modèle Standard on dit que la symétrie électrofaible $SU(2)_L \times U(1)_Y$

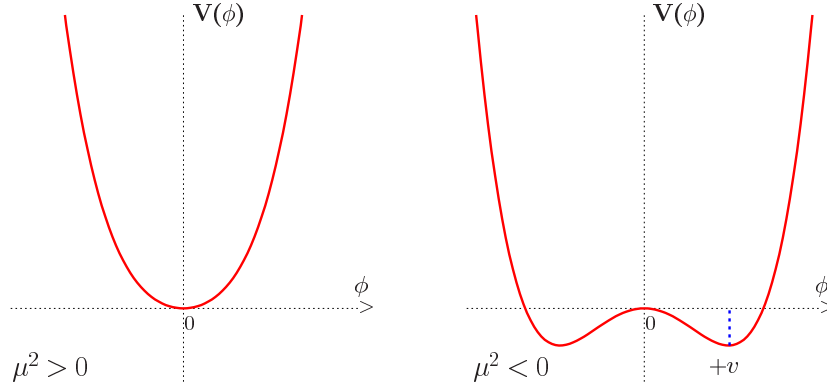


Figure 76 – Potentiel de Higgs dans le cas simplifié d'un seul champ scalaire réel selon le signe du terme de mass μ^2 . Cette figure est tirée de la référence [45].

se brise en la symétrie $U(1)_Q$ restante qui est l'électromagnétisme, non brisée. La relation entre charge électrique et isospin/hypercharge est donnée par $Q = I_3 + \frac{1}{2}Y$.

On fait un développement linéaire de l'isodoublet autour du minimum, qui fait apparaître le boson de Higgs comme seule composante réelle du doublet scalaire non absorbée par les bosons de jauge faibles. Dans la jauge dite unitaire, ceci donne :

$$\Phi = \begin{pmatrix} 0 \\ \frac{v + H}{\sqrt{2}} \end{pmatrix} \quad (\text{A.3})$$

où la vev v est donnée par

$$v^2 = -\frac{\mu^2}{\lambda} \quad (\text{A.4})$$

En introduisant les mélanges suivants entre les divers champs de jauge électrofaibles :

$$W^\pm = \frac{1}{\sqrt{2}}(W_\mu^1 \mp iW_\mu^2), \quad Z_\mu = \frac{gW_\mu^3 - g_Y B_\mu}{\sqrt{g^2 + g_Y^2}}, \quad A_\mu = \frac{gW_\mu^3 + g_Y B_\mu}{\sqrt{g^2 + g_Y^2}} \quad (\text{A.5})$$

ces derniers sont les champs physiques et ont acquis une masse grâce à la vev v du champ de Higgs dans le développement du lagrangien scalaire A.1 :

$$M_W = \frac{gv}{2}, \quad M_Z = \frac{v\sqrt{g^2 + g_Y^2}}{2}, \quad M_A = 0 \quad (\text{A.6})$$

Le champ électromagnétique (champ du photon) est bien de masse nulle, comme attendu pour une symétrie non brisée. Les termes de masses pour les fermions sont donnés grâce à l'interaction de Yukawa suivante :

$$\begin{aligned} \mathcal{L}_{\text{Yukawa}} = & - \left(\frac{\lambda_e v}{\sqrt{2}} \right) \bar{e}e - \left(\frac{\lambda_u v}{\sqrt{2}} \right) \bar{u}u - \left(\frac{\lambda_d v}{\sqrt{2}} \right) \bar{d}d \\ & - \left(\frac{\lambda_e}{\sqrt{2}} \right) \bar{e}He - \left(\frac{\lambda_u}{\sqrt{2}} \right) \bar{u}Hu - \left(\frac{\lambda_d}{\sqrt{2}} \right) \bar{d}Hd \end{aligned} \quad (\text{A.7})$$

ce qui donne les masses suivantes :

$$m_e = \frac{\lambda_e v}{\sqrt{2}} \quad , \quad m_u = \frac{\lambda_u v}{\sqrt{2}} \quad , \quad m_d = \frac{\lambda_d v}{\sqrt{2}} \quad (\text{A.8})$$

Les couplages entre le boson de Higgs et les autres particules du Modèle Standard sont donnés dans le texte principal, notamment dans l'équation 2.20. Rappelons notamment l'existence d'un couplage très important pour les collisionneurs hadroniques, qui apparaît à l'ordre des boucles et qui n'est pas présent directement dans le lagrangien du Modèle Standard : le couplage Higgs–gluon–gluon via une boucle triangulaire de quarks notamment les plus lourds, le top et le bottom.

Avant de conclure cette introduction nous indiquons au lecteur qu'il peut trouver dans le corps principal du texte, chapitre 3, une étude des bornes théoriques et expérimentales sur la masse du boson de Higgs du Modèle Standard. Mentionnons simplement que cette masse n'est pas prédite par la théorie ni même protégée des corrections radiatives¹⁰⁰ et que les bornes théoriques donnent $50 \lesssim M_H \lesssim 750$ GeV si le Modèle Standard est une théorie valide jusqu'à l'échelle du TeV, cet intervalle se restreignant à $130 \lesssim M_H \lesssim 180$ GeV si le Modèle Standard est valide jusqu'à l'échelle de Planck $\Lambda_P \simeq 10^{18}$ GeV¹⁰¹. Les bornes expérimentales qui étaient disponibles lors de l'établissement de ce travail de thèse sont $M_H > 114.4$ GeV (borne du LEP) ainsi que l'exclusion de la bande $158 \leq M_H \leq 177$ GeV au Tevatron, à 95% de niveau de confiance (CL).

A.2 Production et désintégration du boson de Higgs du Modèle Standard

A.2.1 Le cas du Tevatron

Le cœur de la thèse est l'étude de la production inclusive du boson de Higgs dans ses canaux principaux au Tevatron et au LHC et notamment l'étude exhaustive des incertitudes théoriques affectant le calcul. Nous allons voir qu'elles ont un impact significatif sur les prédictions théoriques et qu'elles vont jouer un rôle important lors de la comparaison de ces résultats avec les données expérimentales.

¹⁰⁰Ce que l'on appelle le problème de la hiérarchie des masses du Modèle Standard et qui est une (parmi beaucoup d'autres) des raisons motivant l'étude de théories allant au-delà du Modèle Standard.

¹⁰¹Comme indiqué dans le texte principal, le sentiment prévalant dans la communauté est que le Modèle Standard n'est pas valide jusqu'à de telles échelles ; on peut penser au problème de la matière noire en cosmologie qui requiert l'existence d'une nouvelle particule non décrite par le Modèle Standard, si d'aventure la relativité générale est bien valide aux échelles cosmologiques. Il s'agit aussi d'avoir du travail pour le futur en tant que jeune physicien, espérons donc que la Nature ne nous a pas joué un vilain tour !

Deux canaux de découverte ont un rôle majeur au Tevatron :

- pour des masses de Higgs petites, $M_H \lesssim 135$ GeV, le canal de recherche dominant est la production du boson de Higgs par Higgs–strahlung, $p\bar{p} \rightarrow VH$ qui est une production associée avec un boson de jauge faible $V = W^\pm, Z$, suivie de la désintégration du boson de Higgs H en paire de quarks bottom $H \rightarrow b\bar{b}$; même si le canal de production dominant est la fusion de gluons, ce dernier est noyé par un bruit de fond hadronique beaucoup trop important pour une recherche expérimentale efficace. Le canal de production $p\bar{p} \rightarrow VH$ est connue jusqu'à l'ordre α_s^2 c'est-à-dire au next-to-next-to-leading order (NNLO) en QCD où α_s est la constante de couplage fort, et aussi au NNLO en ce qui concerne les corrections électrofaibles;
- pour des masses de Higgs “grandes”, $M_H \gtrsim 135$ GeV, le canal de recherche dominant est la production par fusion de gluons $gg \rightarrow H$ suivie de la désintégration du boson de Higgs en paires de bosons $W, H \rightarrow WW^*$. Ces derniers vont ensuite se désintégrer et le produit de désintégration le plus intéressant est une paire de leptons accompagnée d'énergie manquante emportée par les neutrinos, un état final particulièrement propre, ce qui d'ailleurs est le canal le plus sensible au boson de Higgs au Tevatron. Le canal $gg \rightarrow H$ est connu jusqu'au NLO en QCD de manière exacte pour les contributions des boucles du quark top et du quark bottom, et jusqu'au NNLO en QCD dans une approche effective pour la boucle du quark top où ce dernier est pris de masse très grande par rapport à la masse du boson de Higgs. Les corrections électrofaibles sont connues jusqu'au NLO de façon exacte et jusqu'au NNLO de façon effective, dans un mélange entre corrections QCD et électrofaibles. Il existe aussi des corrections dite molles qui sont prises en compte dans une technique de resommation (NNLL) mais dont on ne tient pas directement compte dans cette thèse pour des raisons évoquées dans le texte principal, sous-chapitre 4.1.

Nous ne discuterons pas ici des deux autres canaux sous-dominants que sont la fusion de bosons faibles ainsi que la production en association avec une paire de quarks lourds (principalement de quarks top), quelques détails supplémentaires sont disponibles dans le corps principal de la thèse, sous-chapitre 4.1.

Les incertitudes théoriques se répartissent en trois grands groupes :

1. La première incertitude est reliée au calcul perturbatif que l'on effectue. En effet, d'une part l'on effectue un calcul jusqu'à un ordre donné dans une expansion en la constante de couplage fort α_s , d'autre part la section efficace hadronique est une convolution de

ce calcul perturbatif partonique avec les distributions de partons (PDFs) dans le proton/l'antiproton, ce qui est un processus non perturbatif. Le calcul partonique fait intervenir l'échelle de renormalisation μ_R , la convolution avec les PDFs fait intervenir l'échelle de factorisation μ_F . Ces deux échelles ne sont pas physiques et ne sont que le reflet de notre approximation dans le calcul : l'étude de la dépendance du résultat en fonction de ces deux échelles est ce que l'on nomme l'incertitude d'échelle et permet de donner une estimation de l'impact des corrections quantiques d'ordres supérieurs.

L'usage est de faire varier ces deux échelles dans l'intervalle de variation $\mu_0/\kappa \leq \mu_R, \mu_F \leq \kappa\mu_0$ où μ_0 est l'échelle de la prédiction centrale (ou meilleure prédiction) et κ un coefficient constant à choisir. Dans le cas de la fusion de gluons nous avons choisi $\mu_0 = \frac{1}{2}M_H$ ce qui permet une meilleure convergence des ordres supérieurs et permet de reproduire l'effet des corrections NNLL ; nous avons choisi $\mu_0 = M_{HV}$ pour la production en association avec les bosons de jauge faibles, où M_{HV} est la masse invariante de la paire $H + V$. Il est important de bien comprendre que le choix de l'intervalle est totalement subjectif, puisque en théorie cette dépendance devrait être nulle si on pouvait prendre en compte tous les ordres.

Nous avons défini un critère permettant de choisir κ de façon "raisonnable" : le coefficient que nous prendrons sera celui permettant d'atteindre la prédiction centrale à l'ordre le plus élevé dans le calcul avec les bandes d'incertitudes pour la prédiction à l'ordre le plus bas (LO) ou l'ordre d'après (NLO). Le calcul au LO pour le Higgs–strahlung étant un processus purement électrofaible, l'ordre le plus bas qui est choisi est le NLO, et prendre $\kappa = 2$ suffira. Par contre, comme le montre la partie gauche de la figure 77, le processus $gg \rightarrow H$ demande $\kappa = 4$ si on utilise ce critère en prenant comme ordre le plus bas l'ordre LO ; ceci dit nous voyons que la prédiction NNLO touche la bande $\kappa = 3$ à haute masse, et se trouve complètement dans cette bande si on compare la prédiction NNLO aux bandes NLO. Nous utiliserons donc $\kappa = 3$ pour la fusion de gluons et nous obtenons ainsi une incertitude d'ordre $+15\%$, -20% sur l'intervalle de masse du boson de Higgs pertinent au Tevatron dans le cas du canal $gg \rightarrow H$.

2. Le second type d'incertitude est celui qui concentre le plus de questions brûlantes dans la communauté à l'heure actuelle : l'incertitude due aux fonctions de distribution des partons (PDFs) dans le proton/l'antiproton. En effet ces variables physiques sont non-perturbatives et ne sont donc pas prédites par la QCD à partir des premiers principes, mais résultent d'un ajustement à un ensemble de données expérimentales. Il existe plusieurs collaborations qui fournissent des prédictions variées pour ces PDFs, qui ne sont pas toutes nécessairement en accord, et cela dans des proportions parfois frappantes comme le montre la figure 78 ci-dessus. L'incertitude due aux erreurs aussi bien théo-

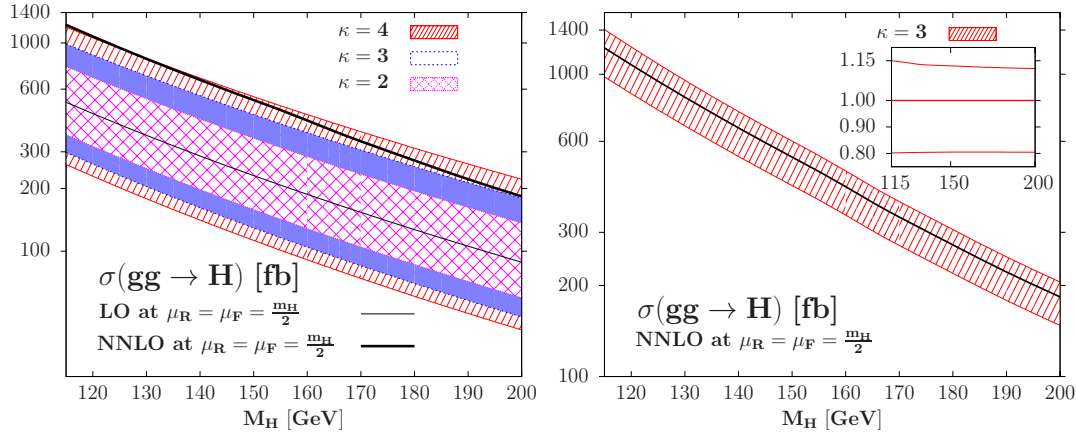


Figure 77 – Gauche : incertitude d'échelle au LO pour le canal $gg \rightarrow H$ au Tevatron dans le domaine $\mu_0/\kappa \leq \mu_R = \mu_F \leq \kappa\mu_0$ avec $\mu_0 = \frac{1}{2}M_H$, pour des choix du coefficient $\kappa = 2, 3$ et 4 comparée à la prédiction centrale au NNLO. Droite : l'incertitude d'échelle au NNLO du canal $gg \rightarrow H$ avec $\kappa = 3$ en fonction de M_H au Tevatron. Dans les deux figures les encarts donnent les incertitudes relatives à la prédiction centrale.

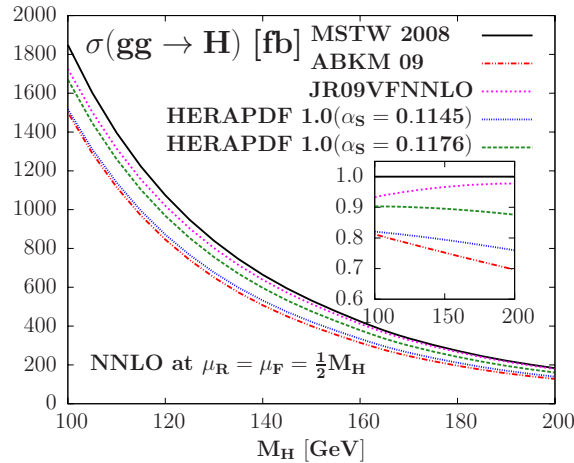


Figure 78 – Section efficace du canal $gg \rightarrow H$ au Tevatron en fonction de M_H en utilisant les quatre collaborations de PDFs au NNLO qui existent : MSTW, JR, HERA et ABKM. L'encart donne la déviation relative à la prédiction centrale obtenue avec MSTW.

riques qu'expérimentales sur la valeur de $\alpha_s(M_Z^2)$ est liée à cette incertitude sur les PDFs, tout autant qu'à l'ajustement des PDFs : en effet toutes les collaborations ne donnent pas une même valeur pour la constante de couplage forte. Comprendre pourquoi il existe tant de différences entre ces prédictions est encore à l'heure actuelle une question ouverte parmi les spécialistes, que nous ne sommes certainement pas à même de trancher. Nous invitons le lecteur intéressé à se référer au texte principal de la thèse où ces questions sont abordées en détail ainsi qu'aux références associées, voir le sous-chapitre 4.3. Nous allons nous contenter ici de résumer le résultat final que nous obtenons

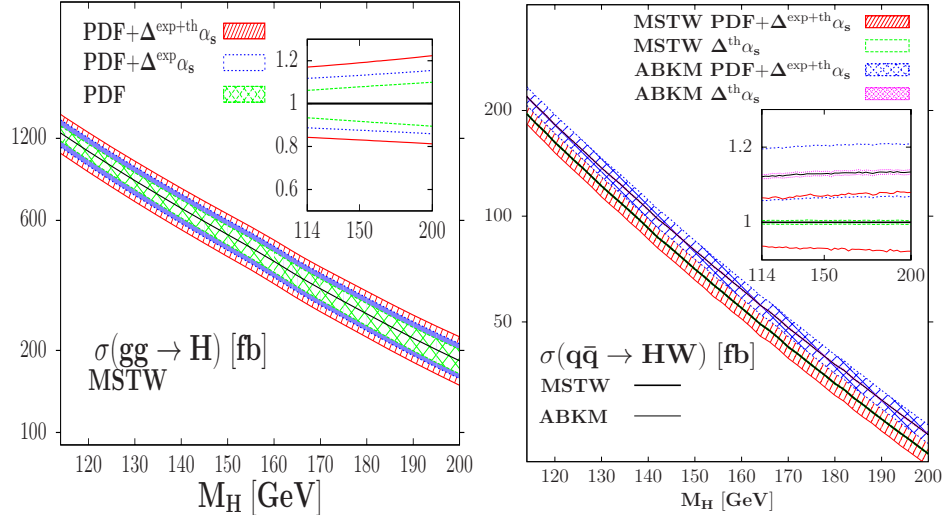


Figure 79 – Gauche : bandes d’incertitude PDF, PDF+ $\Delta^{\text{exp}}\alpha_s$ et PDF+ $\Delta^{\text{exp+th}}\alpha_s$ au Tevatron en fonction de M_H dans le canal $gg \rightarrow H$. Droite : la même chose mais pour le canal $p\bar{p} \rightarrow HW$ au Tevatron. Les incertitudes relatives à la prédiction centrale sont données dans les encarts.

dans le cadre de cette problématique. Nous utilisons la collaboration la plus utilisée dans la communauté pour les prédictions centrales, c’est-à-dire la collaboration MSTW, puis nous calculons dans son schéma l’incertitude PDF+ $\Delta^{\text{exp+th}}\alpha_s$ en utilisant leurs données publiques PDF et incertitudes expérimentales sur α_s corrélées d’une part, et en utilisant $\Delta^{\text{th}}\alpha_s = 0.004$ dans le cas du canal $gg \rightarrow H$, afin de réconcilier les prédictions d’ABKM et de MSTW (au moins en tenant compte de leurs bandes d’incertitudes PDFs respectives), et $\Delta^{\text{th}}\alpha_s = 0.002$ pour le canal Higgs–strahlung, d’autre part. Le résultat final est décrit dans la figure 79 ci-dessous. Nous trouvons une incertitude combinée de l’ordre de $\pm 15\%$ à $\pm 20\%$ dans le cas de la fusion de gluons et de l’ordre de $\pm 7\%$ dans le cas du Higgs–strahlung au Tevatron.

- La dernière classe d’incertitude ne concerne que le canal de production $gg \rightarrow H$. En effet le calcul jusqu’à l’ordre le plus élevé, le NNLO, requiert l’utilisation d’une théorie effective dans laquelle on fait tendre la masse du quark top vers l’infini. Il a été prouvé par différents groupes que cette approximation est excellente pour la boucle du quark top, pour $M_H \lesssim 300$ GeV, mais il est certain qu’elle ne l’est pas pour la boucle du quark bottom. Nous avons donc quantifié son absence au NNLO, et aussi étudié l’impact du schéma de renormalisation de la masse du quark b dans le calcul. En parallèle, et reliée à cette problématique de théorie effective, nous avons estimé l’incertitude des corrections électrofaibles au NNLO, qui sont aussi calculées de manière effective en supposant $M_H \ll M_W$. Les incertitudes obtenues sont de l’ordre de quelques pourcents, 5% au maximum.

Il s’agit enfin de combiner ces incertitudes pour obtenir l’incertitude finale. C’est une

problématique qui n'est pas complètement résolue, car une combinaison quadratique suppose que toutes les incertitudes sont totalement décorrélées, alors que l'alternative linéaire est clairement trop conservatrice. Nous avons choisi de combiner de la façon suivante : calculer l'incertitude $\text{PDF} + \Delta\alpha_s$ sur les extrema obtenus avec l'incertitude d'échelle, puis rajouter linéairement les incertitudes purement théoriques dues à l'usage d'une théorie effective dans le cas de $gg \rightarrow H$. Ceci est un bon compromis entre addition linéaire et addition quadratique. Nous obtenons ainsi une incertitude de l'ordre de $\pm 38\%$ dans le cas de la fusion de gluons et de l'ordre de $\pm 8\%$ dans le cas du Higgs–strahlung comme représenté dans la figure 80 ci-dessous. C'est quasiment deux fois plus que l'incertitude utilisée par CDF et D0 dans leur interprétation des résultats expérimentaux qu'ils obtiennent. Le lecteur trouvera les résultats numériques détaillés dans les tables 2 et 3.

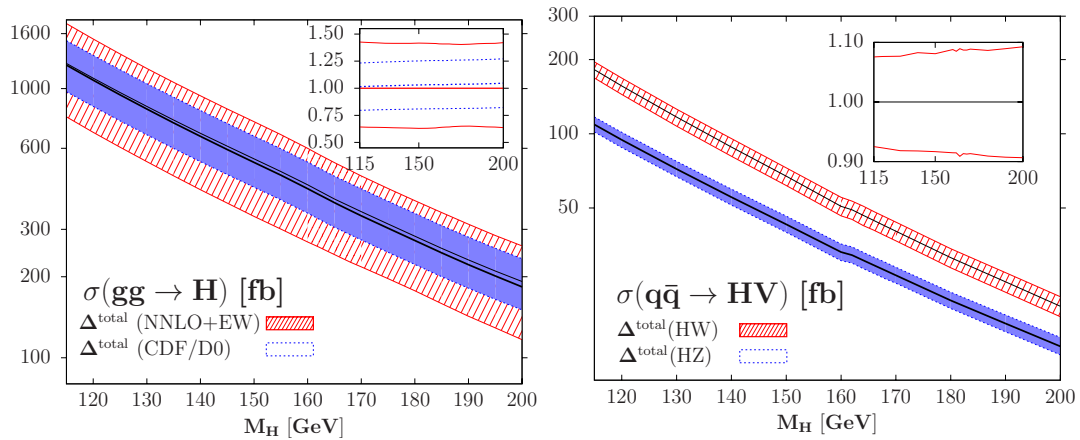


Figure 80 – Gauche : section efficace de production inclusive du canal $gg \rightarrow H$ (en fb) au Tevatron en fonction de M_H (en GeV) ainsi que la bande d'incertitude totale obtenue avec notre combinaison des incertitudes individuelles. Droite : la même chose au Tevatron pour le canal $p\bar{p} \rightarrow VH$, $V = W, Z$. Les incertitudes relatives à la prédiction centrale sont données dans les encarts.

A.2.2 Le cas du LHC

Après avoir mené une étude détaillée des incertitudes théoriques pesant sur les prédictions au Tevatron, nous avons réalisé le même travail dans le cas du LHC. L'énergie au centre de masse actuelle étant de 7 TeV nous avons concentré notre étude sur cette phase actuelle des recherches et nous avons distingué le LHC dans son fonctionnement nominal à 14 TeV de ce fonctionnement à 7 TeV en le nommant LHC. Le chapitre 5 aborde en détail cette étude pour le lecteur intéressé.

Nous avons effectué la même démarche que pour le cas du Tevatron, en se concentrant sur le canal dominant de production du boson de Higgs du Modèle Standard qu'est la fusion

de gluons. Nous n'allons donner ici que le résultat final, pour le cas du IHC à 7 TeV ainsi que le cas du LHC à 14 TeV. Nous avons aussi donné dans le chapitre 5 des résultats pour des énergies au centre de masse intermédiaires. Les incertitudes ne changent que marginalement entre 7 et 14 TeV, mais sont par contre significativement réduites en comparaison des résultats obtenus au Tevatron, pour deux raisons essentiellement : une meilleure convergence des ordres supérieurs, conduisant à une réduction de l'incertitude d'échelle (et expliquant le choix du coefficient constant $\kappa = 2$ pour l'intervalle de variation choisi), d'une part ; une meilleure connaissance de la fonction de distribution de gluons à cette fraction du moment du proton dans cette gamme d'énergie, réduisant l'incertitude due aux PDFs, d'autre part. Nous avons étudié trois façons distinctes de définir l'incertitude totale, détaillées dans le texte principal au sous-chapitre 5.5 et notées A, B et C ; l'incertitude que nous choisirons sera l'incertitude A qui suit la procédure présentée dans le cas du Tevatron. Nous obtenons au final une incertitude totale de l'ordre de $\pm 25\%$ pour le IHC, légèrement plus à basses masses $M_H \simeq 120$ GeV et légèrement moins à haute masse $M_H \simeq 500$ GeV. La figure 81 ci-dessous résume les résultats, le lecteur intéressé pouvant trouver les résultats numériques détaillés dans les tables 5 et 7.

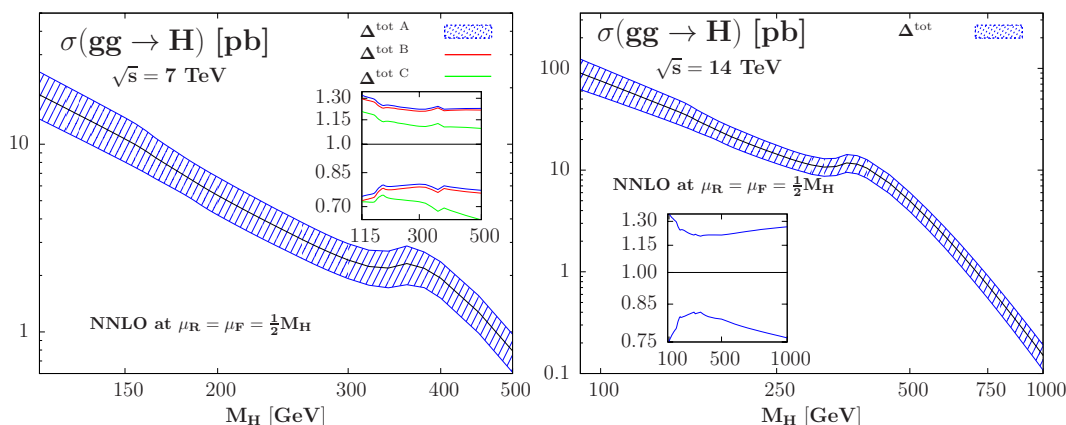


Figure 81 – Gauche : section efficace de production inclusive du canal $gg \rightarrow H$ (en pb) au IHC à 7 TeV en fonction de M_H (en GeV) ainsi que la bande d'incertitude totale obtenue avec notre combinaison des incertitudes individuelles. Droite : la même chose au LHC à 14 TeV ainsi que la bande d'incertitude totale selon notre procédure. Les incertitudes relatives à la prédiction centrale sont données dans les encarts ainsi que les trois manières de combiner les incertitudes à 7 TeV présentées dans le corps principal de la thèse au sous-chapitre 5.5.

A.2.3 Conséquences sur les résultats expérimentaux

Après avoir étudié les sections efficaces de production, nous avons tourné notre attention vers les rapports d'embranchement des désintégrations du boson de Higgs du Modèle Standard dans le chapitre 6. Nous avons, ici aussi, étudié l'impact de certaines incertitudes

pesant sur les prédictions théoriques, et notamment l'impact des erreurs expérimentales sur la masse des quarks bottom et charmé, ainsi que l'impact des erreurs expérimentales sur la détermination de la constante de couplage $\alpha_s(M_Z^2)$. Nous avons ainsi trouvé que cet impact peut être significatif dans les deux canaux $H \rightarrow b\bar{b}$ et $H \rightarrow WW$ autour de $M_H \approx 135$ GeV, où ces deux canaux de désintégration ont des rapports d'embranchement similaires. *A contrario*, à haute masse, où les canaux de désintégration en deux bosons faibles W, Z dominant, ces incertitudes sont quasiment nulles. Les résultats numériques sont donnés dans les tables 8 et 9 du corps principal de la thèse.

Il s'agit ensuite de combiner les sections efficaces de production et les rapports d'embranchement des canaux de désintégration du boson de Higgs. Nous avons choisi de travailler dans l'approximation dite de largeur étroite de désintégration, où cette combinaison se fait en multipliant simplement la section efficace par le rapport d'embranchement. C'est une approximation excellente pour les basses masses du boson de Higgs, mais il faut garder en tête que lorsque ladite masse approche les 500 GeV, cela devient une mauvaise approximation ; une étude plus fine serait nécessaire. Nous avons trouvé que l'impact sur le résultat final des erreurs sur les rapports d'embranchement sont négligeables à haute masse, et augmentent légèrement l'incertitude à basse masse.

L'étape finale du chapitre 6 a été la comparaison de nos calculs avec les résultats expérimentaux, en particulier les limites d'exclusion obtenues par les collaborations CDF et D0 au Tevatron. Une discussion beaucoup plus complète est disponible dans le corps principal du texte dans le sous-chapitre 6.5 ; nous n'indiquons ici que le résultat final de cette discussion. Une comparaison naïve indique que la bande d'exclusion $158 \leq M_H \leq 173$ GeV obtenue avec 7.1 fb^{-1} de luminosité est à questionner, mais afin d'avoir un résultat plus quantitatif nous avons cherché à obtenir la luminosité nécessaire pour avoir la sensibilité actuelle que prétendent les deux expériences en tenant compte de nos incertitudes qui sont le double de celles utilisées par les deux collaborations. Pour ce faire nous avons recalculé cette sensibilité en baissant de 20% à 30% la valeur centrale du calcul théorique comparé aux données en présupposant que les 20% restants sont déjà pris en compte par les expériences. Ceci est résumé dans la figure 82 ci-dessous, où nous avons effectué cet exercice pour une des masses du boson de Higgs à lesquelles le Tevatron est le plus sensible, avec la procédure détaillée dans le sous-chapitre 6.5. Nous voyons clairement que la luminosité nécessaire afin d'exclure effectivement le boson de Higgs à cette masse est de l'ordre de 10 à 11 fb^{-1} particulièrement si on tient compte des incertitudes qui pèsent aussi sur le calcul du bruit de fond du Modèle Standard. C'est pourquoi nous questionnons cette exclusion à la lumière de nos résultats théoriques, d'autant plus que cette exclusion est fortement dépendante de la PDF choisie. Nous rappelons aussi que cette exclusion est débattue dans la communauté

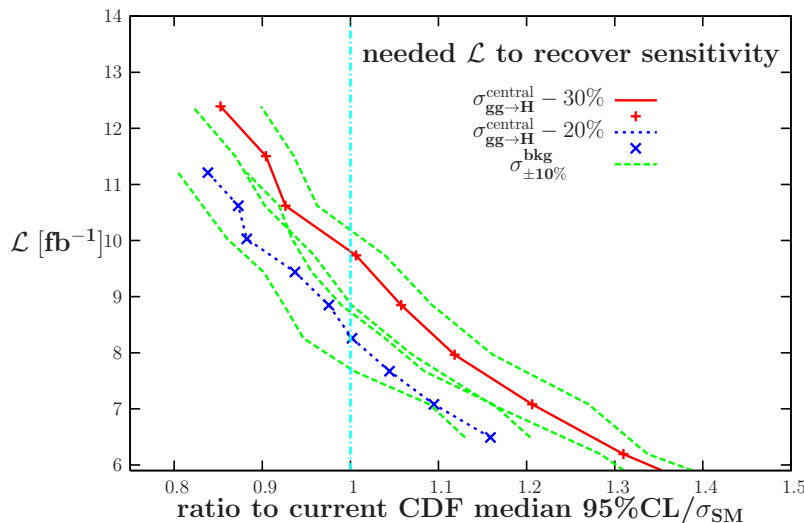


Figure 82 – Luminosité nécessaire à l’expérience CDF afin qu’elle obtienne la sensibilité qu’elle prétend avoir actuellement au boson de Higgs d’une masse de 160 GeV, lorsque le calcul théorique de la section efficace du canal $gg \rightarrow H \rightarrow \ell\ell\nu\nu$ est diminuée de 20% et de 30% ; l’impact d’un changement de 10% dans le bruit de fond dominant $p\bar{p} \rightarrow WW$ est aussi indiqué. Cette figure est extraite de la référence [95].

tout particulièrement à cause de l’impact des PDFs, dont la question n’est toujours pas résolue à l’heure actuelle parmi les spécialistes et dont on espère que les données futures du LHC permettront de mieux comprendre le problème d’une telle disparité de prédictions entre les différentes collaborations de PDFs.

A.3 Le Modèle Standard Supersymétrique Minimal (MSSM)

A.3.1 Bref aspect de la supersymétrie et du MSSM

Après avoir étudié la production du boson de Higgs du Modèle Standard au Tevatron et au LHC nous nous tournons vers l’étude de la brisure de symétrie électrofaible dans le cadre de l’extension supersymétrique minimale du Modèle Standard. Comme indiqué en détail dans le corps de la thèse, chapitre 7, il existe plusieurs raisons qui poussent les théoriciens à envisager des modèles allant au-delà du Modèle Standard, et en particulier à s’intéresser à la supersymétrie (SUSY). Nous allons brièvement présenter ces raisons ainsi que les aspects principaux de la supersymétrie, puis introduire le contenu en champs de l’extension supersymétrique minimale du Modèle Standard (MSSM) ainsi que ses caractéristiques.

Le chapitre 7 donne trois raisons (parmi beaucoup d’autres !) qui poussent les physiciens des hautes énergies à envisager des théories étendant le Modèle Standard et en particulier les théories supersymétriques :

- le problème de la hiérarchie : rien ne protège la masse du boson de Higgs dans le Modèle Standard, ce qui signifie que sa masse est naturellement de l'ordre de grandeur de l'échelle d'énergie la plus élevée de la théorie, sauf si l'on ajuste très finement les contre-terme dans les corrections radiatives. Techniquement cela signifie que les divergences ultraviolettes sont quadratiques. Or la supersymétrie, qui est une symétrie entre bosons et fermions, implique que les boucles bosoniques et les boucles fermioniques se compensent, stabilisant ainsi la masse du boson de Higgs ;
- dans le Modèle Standard, si on fait évoluer à l'aide des équations du groupe de renormalisation les constantes de couplage des trois algèbres de Lie $SU(2)_L$, $U(1)_Y$ et $SU(3)_c$, on constate qu'elles ne convergent pas tout à fait à haute énergie ; cependant si l'on rajoute de nouvelles particules dans le spectre, comme c'est le cas avec une extension supersymétrique, leurs contributions au groupe de renormalisation peuvent permettre une telle unification ; c'est bien le cas dans l'extension supersymétrique minimale du Modèle Standard, à une échelle de l'ordre de 10^{16} GeV, comme le montre la figure 49 du sous-chapitre 7.2 ;
- il existe en cosmologie le problème dit de la matière noire : en effet les observations cosmologiques¹⁰² pointent vers l'existence d'une composante de la matière de l'ordre de 23% du contenu énergétique de l'Univers, que l'on ne connaît pas. La particule supersymétrique la plus légère pourrait parfaitement jouer le rôle de cette matière noire.

Nous n'allons pas rentrer dans les détails techniques de la supersymétrie dans ce synopsis, le lecteur intéressé pourra lire avec profit le chapitre 8. Nous allons mentionner brièvement ses caractéristiques principales et notamment comment l'appliquer au Modèle Standard.

Dans une théorie supersymétrique les champs sont groupés en (super)multiplets associant bosons et fermions. Un lagrangien est supersymétrique lorsque l'échange entre bosons et fermions d'un même (super)multiplet laisse le lagrangien invariant à une dérivée totale près. Afin que la supersymétrie soit une symétrie présente dans le lagrangien sans tenir compte des équations du mouvement, il est alors nécessaire au sein des supermultiplets d'introduire des champs auxiliaires, permettant de respecter l'égalité entre les nombres de degrés de liberté fermioniques et bosoniques : ces champs auxiliaires ne sont pas dynamiques et peuvent être éliminés à l'aide des équations de Lagrange. Voici un exemple de lagrangien

¹⁰²Si l'on présuppose que la relativité générale est valide aux échelles cosmologiques ; cette hypothèse n'a pas été testée expérimentalement, et certains modèles alternatifs tentent d'expliquer les observations cosmologiques sans matière noire en modifiant la relativité générale. Néanmoins nous ne nous lançons pas ici dans une telle discussion.

supersymétrique, le modèle de Wess–Zumino libre :

$$\mathcal{L} = \bar{\psi}\bar{\sigma}^\mu\partial_\mu\psi - \partial^\mu\phi^*\partial_\mu\phi + F^*F \quad (\text{A.9})$$

Il y a un seul supermultiplet composé du champ F qui est un champ scalaire complexe jouant le rôle de champ auxiliaire, du champ scalaire complexe ϕ et du spineur à quatre composantes ψ . Il y a bien quatre degrés de liberté bosoniques et quatre degrés de liberté fermioniques. Si l'on applique les transformations supersymétriques suivantes, paramétrisées par la variable anti-commutante infinitésimale ϵ :

$$\begin{aligned} \delta_\epsilon\phi &= \sqrt{2}\epsilon\psi \\ \delta_\epsilon\psi &= \iota\sqrt{2}\sigma^\mu\bar{\epsilon}\partial_\mu\phi + \sqrt{2}\epsilon F \\ \delta_\epsilon F &= \iota\sqrt{2}\bar{\epsilon}\bar{\sigma}^\mu\partial_\mu\psi \end{aligned} \quad (\text{A.10})$$

le lagrangien A.9 est bien invariant à une dérivée totale près : c'est un lagrangien supersymétrique.

Afin de traiter les interactions dans un cadre supersymétrique nous avons introduit dans le sous-chapitre 8.2 le concept de superespace, qui étend l'espace-temps classique en rajoutant des variables anticommutantes qui vont permettre de réécrire les supermultiplets comme des superchamps vivant dans ce superespace. Nous invitons le lecteur intéressé à parcourir ce sous-chapitre qui décrit en détail la technique mathématique sous-jacente. L'étape suivante est d'appliquer ces concepts au Modèle Standard et notamment d'étendre ce dernier de manière minimale en champ : c'est le Modèle Standard Supersymétrique Minimal ou MSSM.

Si la supersymétrie était une symétrie exacte de la Nature, l'électron par exemple aurait un partenaire bosonique avec exactement la même charge et la même masse, mais de spin zéro ; l'expérience prouve que ce n'est pas le cas, ce qui signifie que la supersymétrie doit être une symétrie brisée. Cette problématique est majeure dans le champ d'étude de la supersymétrie et reste encore à l'heure actuelle un problème ouvert, notamment si l'on souhaite le faire de manière dynamique en réutilisant les concepts développés dans le cadre de la brisure électrofaible du Modèle Standard. Dans le cadre du MSSM, la brisure de la supersymétrie a été choisie de manière explicite, mais tout en préservant les qualités fondamentales de la supersymétrie comme par exemple de résoudre le problème de la hiérarchie du Modèle Standard : c'est ce que l'on appelle la brisure "douce". On introduit alors non seulement de nouvelles particules, partenaires des particules standards, mais aussi des termes explicites de brisure SUSY douce. Le tableau 23 ci-dessous résume les nouveaux champs du MSSM :

La brisure électrofaible nécessite maintenant deux doublets de Higgs et non plus un seul, qui vont fournir cinq bosons de Higgs physiques : deux bosons neutres h et H , un boson

Type	Nom	Spin	rep. $SU(3)_c$	rep. $SU(2)_L$	charge $U(1)_Y$
SLEPTONS	$\tilde{\nu}_e, \tilde{e}_L, \tilde{\nu}_\mu, \tilde{\mu}_L, \tilde{\nu}_\tau, \tilde{\tau}_L$	0	1	2	-1
	$\tilde{e}_R, \tilde{\mu}_R, \tilde{\tau}_R$	0	1	1	2
SQUARKS	$\tilde{u}_L, \tilde{d}_L, \tilde{s}_L, \tilde{c}_L, \tilde{t}_L, \tilde{b}_L$	0	3	2	1/3
	$\tilde{u}_R, \tilde{c}_R, \tilde{t}_R$	0	3	1	-4/3
	$\tilde{d}_R, \tilde{s}_R, \tilde{b}_R$	0	3	1	2/3
JAUGINOS	\tilde{B}	1/2	1	1	1
	$\tilde{W}_1, \tilde{W}_2, \tilde{W}_3$	1/2	1	3	0
	\tilde{g}	1/2	8	1	0
HIGGSINOS	$\tilde{h}_u^+, \tilde{h}_u^0$	1/2	1	2	1
	$\tilde{h}_d^0, \tilde{h}_d^-$	1/2	1	2	-1
HIGGS	h_u^+, h_u^0	0	1	2	1
	h_d^0, h_d^-	0	1	2	-1

Table 23 – Les superparticules et champs de Higgs du MSSM avant brisure électrofaible.

neutre pseudoscalaire A et deux bosons chargés H^\pm . Elle induit aussi un mélange entre les partenaires supersymétriques des bosons de jauge et des bosons de Higgs, donnant naissance à quatre fermions neutres appelés neutralinos $\tilde{\chi}_i^0$ et quatre fermions chargés appelés charginos $\tilde{\chi}_{1,2}^\pm$. Nous expliquons plus en détails ci-dessous le secteur de Higgs du MSSM qui nous intéresse tout particulièrement dans cette thèse.

A.3.2 Secteur de Higgs du MSSM

Pour des raisons techniques il est nécessaire d'avoir deux doublets de Higgs au sein du MSSM. Ces raisons sont données en détails dans le sous-chapitre 9.2, pour n'en citer qu'une seule nous rappelons que l'un des doublets donne la masse aux fermions de type up, le second doublet donne la masse aux fermions de type down, ceci afin d'à la fois respecter l'expérience qui nous indique qu'il est nécessaire de donner une masse aux fermions, et respecter la structure mathématique de la supersymétrie et notamment la nécessité d'annuler les anomalies de jauge. Nous avons donc les deux doublets suivants :

$$h_u = \begin{pmatrix} h_u^+ \\ h_u^0 \end{pmatrix}, \quad h_d = \begin{pmatrix} h_d^0 \\ h_d^- \end{pmatrix} \quad (\text{A.11})$$

qui ont tous les deux une vev non-nulle :

$$\langle h_u \rangle = \frac{1}{\sqrt{2}} \begin{pmatrix} 0 \\ v_u \end{pmatrix}, \quad \langle h_d \rangle = \frac{1}{\sqrt{2}} \begin{pmatrix} v_d \\ 0 \end{pmatrix} \quad (\text{A.12})$$

Les détails du potentiel scalaire du MSSM sont donnés dans le sous-chapitre 9.2 ; nous résumons les résultats en rappelant que de la brisure électrofaible, intimement liée à la brisure de supersymétrie, émergent cinq bosons de Higgs physiques qui sont :

- deux bosons de Higgs neutres scalaires h et H ;
- un boson de Higgs pseudoscalaire A ;
- deux bosons de Higgs chargés H^\pm .

dont les masses et couplages à l'ordre le plus bas (des arbres) sont paramétrés par la masse M_A du boson de Higgs pseudoscalaire et le rapport des vev $\tan \beta \equiv \frac{v_u}{v_d}$.

Nous nous concentrons dans la suite sur l'étude de la production et de la désintégration des bosons de Higgs neutres ; leurs couplages aux bosons de jauge standards et aux fermions du Modèle Standard sont une donnée essentielle dans l'optique de leur production au sein des collisionneurs hadroniques. Nous avons donné dans le sous-chapitre 9.2 les couplages des bosons de Higgs aux fermions en particulier. Les couplages aux fermions de type up sont supprimés d'un facteur $\tan \beta$ alors qu'au contraire les couplages aux fermions de type down sont renforcés de ce même facteur : cela signifie que la production des bosons de Higgs neutres à grand $\tan \beta$ va faire principalement intervenir le quark bottom et non plus le quark top. Ceci va être d'une importance cruciale dans la suite.

A.4 Production et désintégration des bosons de Higgs supersymétriques

La dernière partie de la thèse s'intéresse à l'étude de la production et de la désintégration des bosons de Higgs neutres du MSSM au Tevatron et au LHC. Du fait de la modification des couplages d'un facteur $\tan \beta$ comparés à ceux du Modèle Standard, les chances d'observer de tels bosons au sein des collisionneurs hadroniques sont renforcées comparativement au boson de Higgs standard. Nous reproduisons le même schéma d'étude développé dans le cas du Modèle Standard : l'étude exhaustive des incertitudes théoriques pesant sur la prédiction, dont les sources sont identiques à celles jouant un rôle dans le cas du Modèle Standard et

en y rajoutant l'impact des incertitudes sur le quark bottom qui joue cette fois-ci un rôle prépondérant.

Nous avons démontré dans le chapitre 10 que si les corrections QCD jouent évidemment un grand rôle dans les prédictions des sections efficace de production et les rapports d'embranchement des canaux de désintégration, les corrections supersymétriques dans une certaine classe de modèles assez large ont un impact relativement faible, quand on s'intéresse à la chaîne complète production–désintégration des bosons de Higgs neutres. Cette classe de modèles possède la particularité de présenter un spectre organisé ainsi : un des deux bosons scalaires se comporte comme le boson de Higgs du Modèle Standard tandis que le second se comporte comme le boson pseudoscalaire. L'étude en est ainsi simplifiée et nous présenterons nos résultats pour le boson de Higgs générique Φ représentant alternativement les deux particules semblables A et h/H . Nous négligerons les corrections SUSY¹⁰³ et nous nous placerons dans l'hypothèse d'étude des collisionneurs hadroniques à savoir $\tan\beta$ relativement élevé ce qui permet de négliger toute contribution due au quark top. Nous présenterons nos résultats avec $\tan\beta = 1$: il est entendu que le lecteur doit multiplier ces résultats par un facteur $2 \tan^2\beta$ afin d'obtenir la prédiction réelle pour la production de $A + h/H$.

A.4.1 Les Higgs neutres du MSSM au Tevatron

Dans le schéma d'étude résumé ci-dessus les deux canaux principaux de production du boson Φ au Tevatron (et au LHC) sont la fusion de gluons ainsi que la fusion de quarks bottom. Ce dernier canal devient même le canal dominant pour des masses $M_\Phi \gtrsim 135$ GeV. L'étude détaillée est disponible dans le chapitre 11.

Le calcul perturbatif de la section efficace inclusive de production du canal $b\bar{b} \rightarrow \Phi$ est connue jusqu'à l'ordre NNLO dans une modélisation dite "à 5 saveurs" pour les PDFs, en supposant que l'ordre le plus bas est effectivement une fusion des deux quarks bottom que l'on arrive à extraire de la mer des protons/antiprotons, au contraire d'une modélisation dite "à 4 saveurs" où les quarks bottom n'apparaissent qu'au NLO après séparation des gluons de la mer en paires bottom/antibottom. En ce qui concerne la fusion de gluons, dans la mesure où seule la boucle triangulaire de quarks bottom est prise en compte, le calcul s'effectue jusqu'à l'ordre NLO seulement contrairement au cas du Modèle Standard. Nous prenons en compte toutes les incertitudes théoriques déjà discutées dans le cas du Modèle Standard,

¹⁰³Il est bon de rappeler que si ces corrections sont prises en compte, non seulement elles sont faibles mais en plus elles génèrent aussi une incertitude théorique liée aux paramètres supersymétriques sous-jacents ; ces corrections sont ainsi noyées dans les incertitudes QCD standards et les incertitudes SUSY à estimer, ces dernières étant loin d'être négligeables.

hormis bien évidemment l'incertitude générée par l'usage d'une théorie effective puisque ici le calcul est exact à un ordre perturbatif donné. Par contre, une nouvelle incertitude joue un rôle majeur : celle reliée aux erreurs expérimentales de la masse du quark bottom ainsi que les incertitudes liées au choix du schéma de renormalisation de ladite masse.

En ce qui concerne les incertitudes d'échelle, nous utilisons un facteur d'intervalle $\kappa = 2$ dans le cas de la fusion de gluons, les contributions dues aux quarks bottom entraînant une plus grande stabilité de la prédiction comparativement au cas du Modèle Standard à boucle top dominante et où $\kappa = 3$ au Tevatron était nécessaire. Nous utilisons l'échelle centrale $\mu_R = \mu_F = \frac{1}{2}M_H$ afin de rester cohérent avec l'étude du Modèle Standard qui est valide pour le boson de Higgs neutre du MSSM se comportant comme le boson de Higgs du Modèle Standard. Par contre, comme indiqué dans le sous-chapitre 11.2 et illustré dans la figure 55, le choix $\kappa = 3$ assorti de la restriction $1/3 \leq \mu_R/\mu_F \leq 3$ est nécessaire dans le cas de la fusion de quarks bottom où l'incertitude d'échelle est instable ; ceci permet aussi de prendre en compte l'incertitude reliée au schéma de renormalisation du quark bottom puisque dans le schéma $\overline{\text{MS}}$ qui est choisi pour la prédiction centrale la masse du quark bottom dans le processus $b\bar{b} \rightarrow \Phi$ est prise à l'échelle de renormalisation. L'échelle centrale de ce processus est $\mu_R = \mu_F = \frac{1}{4}M_H$.

Le résultat final est décrit dans la figure 83 ci-dessous, les résultats numériques étant disponibles dans le corps principal de la thèse dans les tables 13 et 14. L'impact de ces incertitudes est significatif, puisque de l'ordre de $\pm 50\%$ dans les deux canaux, un peu plus pour la fusion de gluons et un peu moins pour la fusion de quarks bottom.

A.4.2 Les Higgs neutres du MSSM au LHC

L'étude présentée ci-dessus a été répétée dans le cas du LHC dans le même cadre théorique qui a été présenté en introduction de l'étude du MSSM. L'étude détaillée est disponible dans le chapitre 12. Plutôt qu'effectuer une répétition fastidieuse et inutilement longue dans le cadre d'un synopsis, nous allons donner les figures finales ainsi que l'incertitude totale dans les deux canaux $gg \rightarrow \Phi$ et $b\bar{b} \rightarrow \Phi$. La figure 84 résume l'étude, les données numériques étant disponibles dans le corps de la thèse, tables 15 et 16. La comparaison avec le Tevatron montre que les incertitudes sont fortement réduites dans le cas du canal (dominant) $b\bar{b} \rightarrow \Phi$, ce qui n'est pas une surprise car ne serait-ce que les incertitudes dues aux PDFs sont réduites du fait que l'on sonde des domaines de fraction d'impulsion mieux maîtrisés. Par contre assez paradoxalement l'incertitude totale dans le canal $gg \rightarrow \Phi$ ne diminue que marginalement, car en fait dominée par l'incertitude due au quark bottom qui ne dépend que peu de l'énergie au centre de masse. En résumé, l'incertitude totale est significative et peut avoir un certain

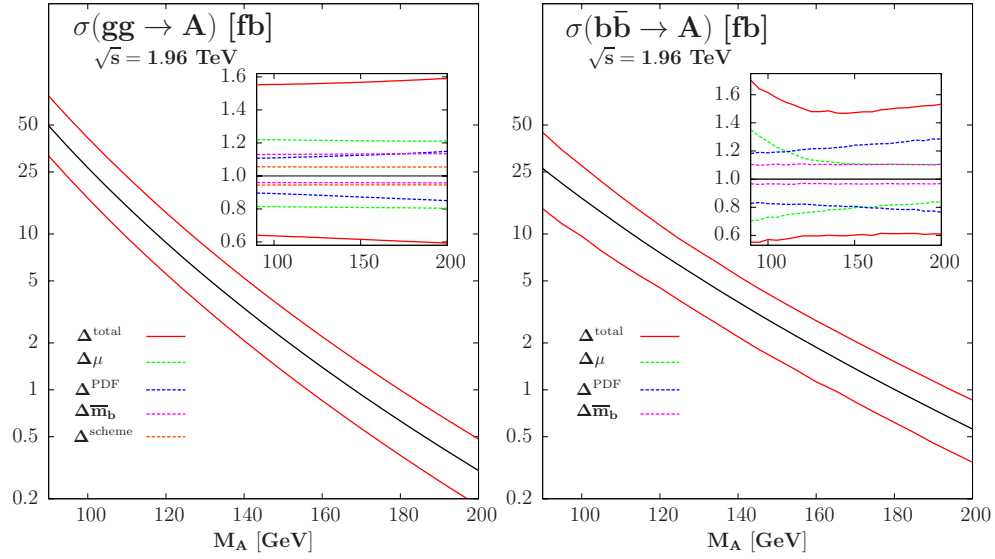


Figure 83 – Les prédictions centrales des sections efficaces inclusives de production $\sigma_{gg \rightarrow A}^{\text{NLO}}$ (gauche) et $\sigma_{b\bar{b} \rightarrow A}^{\text{NNLO}}$ (droite) au Tevatron en fonction de M_A avec les PDFs de MSTW et des couplages $A b\bar{b}$ unitaires, accompagnées des bandes d'incertitude théorique totale. Les différentes sources d'incertitude théorique ainsi que l'incertitude totale, relativement à la prédiction centrale, sont données dans les encarts pour chacun des canaux.

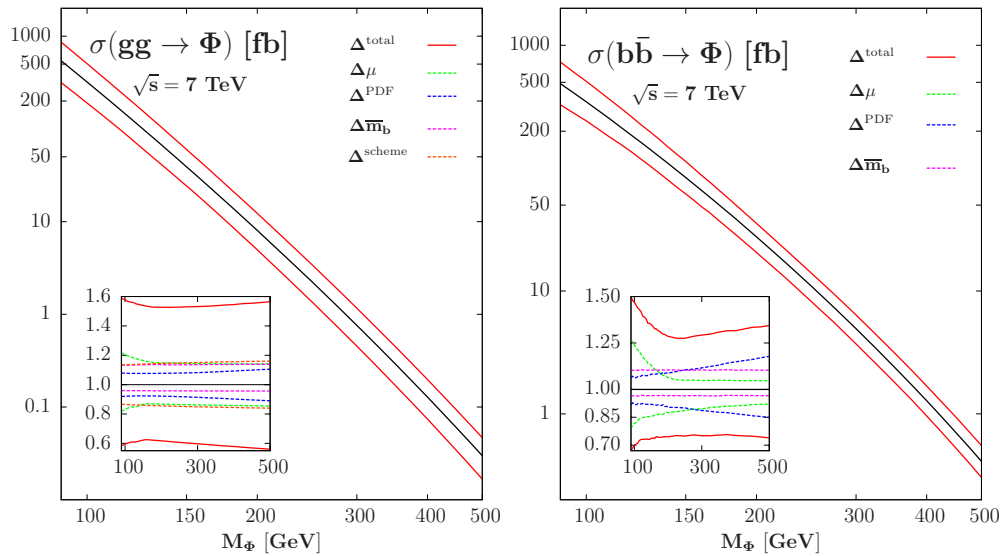


Figure 84 – Les prédictions centrales des sections efficaces inclusives de production $\sigma_{gg \rightarrow \Phi}^{\text{NLO}}$ (gauche) et $\sigma_{b\bar{b} \rightarrow \Phi}^{\text{NNLO}}$ (droite) au LHC avec $\sqrt{s} = 7$ TeV en fonction de M_Φ avec les PDFs de MSTW et des couplages $\Phi b\bar{b}$ unitaires, accompagnées des bandes d'incertitude théorique totale. Les différentes sources d'incertitude théorique ainsi que l'incertitude totale, relativement à la prédiction centrale, sont données dans les encarts pour chacun des canaux.

impact sur la comparaison avec les données expérimentales comme le montre le paragraphe qui suit.

A.4.3 L'impact des incertitudes théoriques sur l'espace des paramètres du MSSM

Il nous reste maintenant une dernière étape avant la comparaison finale avec les données expérimentales aussi bien du Tevatron que du LHC : la combinaison des sections efficaces de production avec les rapports d'embranchement des canaux de désintégration. Dans le cas du MSSM, et en particulier dans les classes de modèles que nous étudions où il y a une dégénérescence entre le boson de Higgs pseudoscalaire A et l'un des bosons de Higgs h/H , seuls deux canaux sont significatifs : le canal $\Phi \rightarrow b\bar{b}$ avec un rapport d'embranchement de l'ordre de 90% et le canal $\Phi \rightarrow \tau^+\tau^-$ avec un rapport d'embranchement de l'ordre de 10%. La table 12 du sous-chapitre 13.1 fournit les données numériques de notre étude et en particulier les incertitudes théoriques qui pèsent sur ces rapports d'embranchement, dues aux incertitudes sur la masse du quark bottom et sur la valeur de $\alpha_s(M_Z^2)$. Le canal de désintégration qui nous intéressera tout particulièrement dans l'optique d'une comparaison à l'expérience est le canal $\Phi \rightarrow \tau^+\tau^-$.

Il est très important de remarquer que l'incertitude sur la masse du quark bottom est anticorrélée entre section efficace de production et rapport d'embranchement : en définitive cette incertitude va quasiment s'annuler dans le processus final de production du boson Φ suivi de sa désintégration en paire de leptons taus. Ceci est illustré par les figures 69 et 70 dans le corps principal du texte.

Nous pouvons maintenant comparer nos prédictions combinant les deux canaux de production ainsi qu'avec le rapport d'embranchement $\Phi \rightarrow \tau^+\tau^-$ aux résultats expérimentaux du Tevatron et du LHC. Nous multiplions par un facteur $2 \tan^2 \beta$ les résultats que nous avons présentés afin d'avoir une prédiction donnée ainsi que son incertitude pour chaque couple de valeur $(M_A, \tan \beta)$. Comparées aux données expérimentales, ces prédictions théoriques fournissent une limite sur l'espace des paramètres $[M_A, \tan \beta]$ du MSSM. Les détails sont donnés dans le sous-chapitre 13.3 ; mentionons que nous soutenons qu'une exclusion à 95% de niveau de confiance doit se faire entre les données expérimentales et la prédiction théorique minimale et non la prédiction centrale, c'est-à-dire qu'il faut tenir compte des incertitudes théoriques séparées des erreurs expérimentales sur les données.

Nous voyons donc dans la figure 85 que l'impact des incertitudes théoriques est important dans le cas du Tevatron, bien moindre dans le cas du LHC mais cependant significatif. Avec nos incertitudes, le LHC exclut donc des valeurs $\tan \beta \geq 29$. Nous avons aussi donné quelques prédictions sur ce que l'on pourrait attendre comme exclusion avec une plus grande luminosité au LHC, nous invitons le lecteur intéressé à regarder la figure 74.

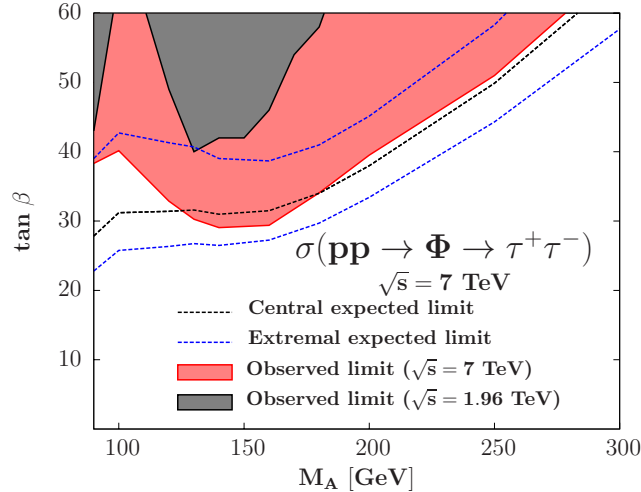


Figure 85 – Limites d’exclusion attendues et obtenues dans le canal $\sigma(pp \rightarrow \Phi \rightarrow \tau^+ \tau^-)$ au Tevatron et au LHC sur l’espace des paramètres du MSSM $[M_A, \tan \beta]$ en tenant compte de nos incertitudes théoriques, comparées aux résultats de CMS et de CDF/D0 lorsque notre procédure est appliquée.

A.4.4 Le canal $H \rightarrow \tau\tau$ dans le Modèle Standard révisité

Avant de terminer ce synopsis par une liste de perspectives à donner à cette thèse, nous présentons une des conséquences les plus intéressantes de ce travail pour la recherche du boson de Higgs du Modèle Standard. En effet, comme le présente en détail le sous-chapitre 13.4, nous avons eu l’idée de comparer les résultats expérimentaux obtenus par CMS dans la recherche des bosons de Higgs neutres du MSSM et notamment leurs limites à 95% de niveau de confiance sur la section efficace $pp \rightarrow \Phi \rightarrow \tau^+ \tau^-$ via fusion de gluons et fusion de quarks bottom, à nos prédictions au sein du Modèle Standard : en effet les états finaux à étudier expérimentalement sont les mêmes dans les deux cas, le seul changement significatif étant la comparaison des taux de production entre Modèle Standard et MSSM lorsque l’on cherche à comparer les données expérimentales aux prédictions théoriques.

La figure 86 ci-dessous montre le résultat de cette étude, à comparer avec la sensibilité qu’obtient ATLAS dans le canal $H \rightarrow \gamma\gamma$ qui est considéré comme le meilleur canal de recherche pour des bosons de Higgs du Modèle Standard dans la gamme 115–140 GeV. Le canal $gg \rightarrow H \rightarrow \tau^+ \tau^-$, qui n’est que peu ou pas considéré par les collaborations expérimentales, se révèle plutôt intéressant et compétitif, d’autant plus lorsque il est combiné avec le canal de la fusion de bosons faibles suivie de la désintégration $H \rightarrow \tau^+ \tau^-$, le seul réellement considéré par les collaborations expérimentales dans le canal de recherche en di-taus. Nous invitons donc les expériences à utiliser ce nouveau moyen de détection du boson de Higgs du Modèle Standard, et cela est d’ailleurs ce qui se fait dans les derniers

résultats présentés à Grenoble en juillet 2011 à la conférence HEP–EPS.

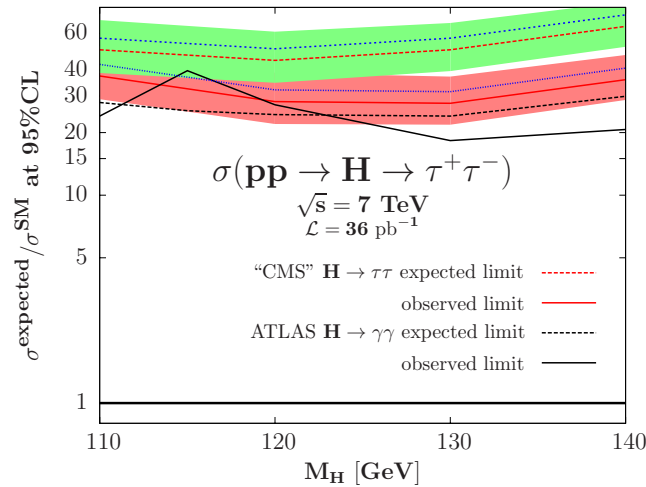


Figure 86 – Les sensibilités attendues et observées à 95% de niveau de confiance pour la production du boson de Higgs du Modèle Standard dans le canal $gg \rightarrow H \rightarrow \tau\tau$ (lignes bleues) et $pp \rightarrow H \rightarrow \tau^+\tau^- + X$ (lignes rouges et légende de la figure) à partir d’une extrapolation de l’analyse CMS du MSSM avec une luminosité de 36 pb^{-1} . Les bandes vertes et rouges décrivent l’impact de nos incertitudes théoriques sur les limites “attendues” et “observées”. Ces résultats sont comparés à l’analyse du canal $H \rightarrow \gamma\gamma$ faite par la collaboration ATLAS avec une luminosité de 37 pb^{-1} .

A.5 Perspectives

Nous avons vu qu’aussi bien dans le Modèle Standard que dans le MSSM, l’impact des incertitudes théoriques est certain. Les expériences ATLAS et CMS en cours au LHC n’ont toujours pas observé le boson de Higgs, même si quelques signaux intéressants ont fait leur apparition durant la fin de la rédaction de cette thèse, présentés à la conférence HEP–EPS à Grenoble en juillet 2011. Peut-être que le champagne pourra être débouché avant la fin de l’année! En attendant, nous pouvons donner quelques perspectives pour un travail futur :

- La suite importante à donner à ce travail est une étude exclusive où l’on calcule en particulier les incertitudes théoriques canal par canal en tenant compte des coupures cinématiques imposées pour maximiser le rapport signal sur bruit. Quelques résultats préliminaires sont donnés dans le texte principal de la thèse, section 14. Il faut aussi faire de même pour l’étude des bruits de fond standards eux-mêmes.
- Étudier l’impact de la largeur finie du boson de Higgs : tout le travail présenté dans cette thèse se place dans l’approximation d’une largeur étroite, ce qui a permis de faire le produit entre section efficace et rapport de branchement pour étudier le signal

complet, or pour des masses élevées du(des) boson(s) de Higgs la largeur totale de désintégration n'est plus négligeable.

- Il existe une étude complémentaire reliée au problème précédent : quel peut-être l'impact des interférences entre signal et bruit de fond ? En effet la production du boson de Higgs suivi de sa désintégration peut être vue comme n'étant qu'un processus intermédiaire parmi tant d'autres pour produire les produits de désintégration du boson de Higgs à partir des partons initiaux. Il s'agit donc d'étudier l'effet de l'interférence entre l'amplitude du signal et l'amplitude du bruit de fond sur l'observation du premier.
- Il pourrait être intéressant de faire une étude précise des coupures cinématiques vis-à-vis des incertitudes d'échelles, ces dernières étant sensibles aux coupures. Ainsi, quelles sont les coupures optimales pour à la fois maximiser le rapport signal sur bruit et minimiser les incertitudes d'échelle ?
- Dans l'hypothèse d'une découverte du boson de Higgs, il reste énormément de travail aux physiciens des hautes énergies : quelles sont ses propriétés exactes, est-il exactement celui du Modèle Standard, quelles informations nous apporte-t-il sur la brisure électrofaible ? Nous avons encore beaucoup de choses fascinantes à découvrir !

References

- [1] P. A. M. Dirac, *The Quantum theory of the Emission and Absorption of Radiation*, Proc. Roy. Soc. Lond. **A114** (1927) 243, [<http://rspa.royalsocietypublishing.org/content/114/767/243.full.pdf+html>].
- [2] E. Fermi, *Quantum theory of radiation*, Rev. Mod. Phys. **4** (1932) 87.
- [3] H. A. Bethe, *The Electromagnetic Shift of Energy Levels*, Phys. Rev. **72** (1947) 339–341.
- [4] S. Tomonaga, *On a Relativistically Invariant Formulation of the Quantum Theory of Wave Fields*, Prog. Theor. Phys. **1** (1946) 27–42.
- [5] F. J. Dyson, *The Radiation Theories of Tomonaga, Schwinger, and Feynman*, Phys. Rev. **75** (1949) 486–502.
- [6] R. P. Feynman, *Mathematical formulation of the quantum theory of electromagnetic interaction*, Phys. Rev. **80** (1950) 440–457.
- [7] T. D. Lee and C.-N. Yang, *Question of Parity Conservation in Weak Interactions*, Phys. Rev. **104** (1956) 254–258.
- [8] C. S. Wu, E. Ambler, R. W. Hayward, D. D. Hoppes and R. P. Hudson, *Experimental Test of Parity Conservation in Beta Decay*, Phys. Rev. **105** (1957) 1413–1414.
- [9] M. Gell-Mann, *A Schematic Model of Baryons and Mesons*, Phys. Lett. **8** (1964) 214–215.
- [10] G. Zweig, *An $SU(3)$ model for strong interaction symmetry and its breaking*, CERN Report (1964). CERN-TH-401.
- [11] M. Breidenbach *et al.*, *Observed Behavior of Highly Inelastic Electron–Proton Scattering*, Phys. Rev. Lett. **23** (1969) 935–939.
- [12] **E598** Collaboration, J. J. Aubert *et al.*, *Experimental Observation of a Heavy Particle J* , Phys. Rev. Lett. **33** (1974) 1404–1406.
- [13] **SLAC-SP-017** Collaboration, J. E. Augustin *et al.*, *Discovery of a Narrow Resonance in e^+e^- Annihilation*, Phys. Rev. Lett. **33** (1974) 1406–1408.
- [14] S. L. Glashow, J. Iliopoulos and L. Maiani, *Weak Interactions with Lepton-Hadron Symmetry*, Phys. Rev. **D2** (1970) 1285–1292.

- [15] **CDF** Collaboration, F. Abe *et al.*, *Observation of Top Quark Production in $p\bar{p}$ Collisions with the Collider Detector at Fermilab*, Phys. Rev. Lett. **74** (1995) 2626–2631, [[hep-ex/9503002](#)].
- [16] **D0** Collaboration, S. Abachi *et al.*, *Observation of the top quark*, Phys. Rev. Lett. **74** (1995) 2632–2637, [[hep-ex/9503003](#)].
- [17] N. Cabibbo, *Unitary Symmetry and Leptonic Decays*, Phys. Rev. Lett. **10** (1963) 531–533.
- [18] J. H. Christenson, J. W. Cronin, V. L. Fitch and R. Turlay, *Evidence for the 2π Decay of the K_2^0 Meson*, Phys. Rev. Lett. **13** (1964) 138–140.
- [19] M. Kobayashi and T. Maskawa, *CP–Violation in the Renormalizable Theory of Weak Interaction*, Prog. Theor. Phys. **49** (1973) 652–657.
- [20] C.-N. Yang and R. L. Mills, *Conservation of isotopic spin and isotopic gauge invariance*, Phys. Rev. **96** (1954) 191–195.
- [21] P. W. Higgs, *Broken symmetries, massless particles and gauge fields*, Phys. Lett. **12** (1964) 132–133.
- [22] F. Englert and R. Brout, *Broken symmetry and the mass of gauge vector mesons*, Phys. Rev. Lett. **13** (1964) 321–322.
- [23] G. S. Guralnik, C. R. Hagen and T. W. B. Kibble, *Global conservation laws and massless particles*, Phys. Rev. Lett. **13** (1964) 585–587.
- [24] P. W. Higgs, *Spontaneous Symmetry Breakdown without Massless Bosons*, Phys. Rev. **145** (1966) 1156–1163.
- [25] O. W. Greenberg, *Spin and Unitary Spin Independence in a Paraquark Model of Baryons and Mesons*, Phys. Rev. Lett. **13** (1964) 598–602.
- [26] D. J. Gross and F. Wilczek, *Ultraviolet Behavior of Non-Abelian Gauge Theories*, Phys. Rev. Lett. **30** (1973) 1343–1346.
- [27] H. D. Politzer, *Reliable Perturbative Results for Strong Interactions?*, Phys. Rev. Lett. **30** (1973) 1346–1349.
- [28] **PLUTO** Collaboration, C. Berger *et al.*, *Evidence for Gluon Bremsstrahlung in e^+e^- Annihilations at High-Energies*, Phys. Lett. **B86** (1979) 418.

- [29] S. L. Glashow, *Partial Symmetries of Weak Interactions*, Nucl. Phys. **22** (1961) 579–588.
- [30] A. Salam and J. C. Ward, *Electromagnetic and weak interactions*, Phys. Lett. **13** (1964) 168–171.
- [31] S. Weinberg, *A Model of Leptons*, Phys. Rev. Lett. **19** (1967) 1264–1266.
- [32] G. 't Hooft, *Renormalization of Massless Yang-Mills Fields*, Nucl. Phys. **B33** (1971) 173–199.
- [33] G. 't Hooft, *Renormalizable Lagrangians for massive Yang-Mills fields*, Nucl. Phys. **B35** (1971) 167–188.
- [34] G. 't Hooft and M. J. G. Veltman, *Regularization and Renormalization of Gauge Fields*, Nucl. Phys. **B44** (1972) 189–213.
- [35] **Gargamelle Neutrino** Collaboration, F. J. Hasert *et al.*, *Observation of neutrino-like interactions without muon or electron in the Gargamelle neutrino experiment*, Phys. Lett. **B46** (1973) 138–140.
- [36] **UA1** Collaboration, G. Arnison *et al.*, *Experimental observation of lepton pairs of invariant mass around 95 GeV/c² at the CERN SPS collider*, Phys. Lett. **B126** (1983) 398–410.
- [37] **UA1** Collaboration, G. Arnison *et al.*, *Experimental observation of isolated large transverse energy electrons with associated missing energy at $\sqrt{s} = 540$ GeV*, Phys. Lett. **B122** (1983) 103–116.
- [38] C. Quigg, *Gauge Theories Of The Strong, Weak and Electromagnetic Interactions*. Advanced Book Classics. Westview Press, 1983.
- [39] P. Binetruy, *Théorie de jauge des interactions électrofaibles*, Lecture notes in the theoretical physics master course at the ENS, Paris, 2008.
- [40] M. Davier, *Physique des particules*, Lecture notes in the theoretical physics master course at the ENS, Paris, 2008.
- [41] C. H. Llewellyn Smith, *High-Energy Behavior and Gauge Symmetry*, Phys. Lett. **B46** (1973) 233–236.
- [42] J. M. Cornwall, D. N. Levin and G. Tiktopoulos, *Uniqueness of spontaneously broken gauge theories*, Phys. Rev. Lett. **30** (1973) 1268–1270.

- [43] J. F. Gunion, H. E. Haber and J. Wudka, *Sum rules for Higgs bosons*, Phys. Rev. **D43** (1991) 904–912.
- [44] J. F. Gunion, H. E. Haber, G. Kane and S. Dawson, *The Higgs Hunter's Guide*. Advanced Book Classics. Westview Press, 1990.
- [45] A. Djouadi, *The Anatomy of electro-weak symmetry breaking. I: The Higgs boson in the standard model*, Phys. Rept. **457** (2008) 1–216, [[hep-ph/0503172](#)].
- [46] **LEP Working Group for Higgs boson searches** Collaboration, R. Barate *et al.*, *Search for the standard model Higgs boson at LEP*, Phys. Lett. **B565** (2003) 61–75, [[hep-ex/0306033](#)].
- [47] D. B. Kaplan, H. Georgi and S. Dimopoulos, *Composite Higgs Scalars*, Phys.Lett. **B136** (1984) 187.
- [48] K. Agashe, R. Contino and A. Pomarol, *The Minimal composite Higgs model*, Nucl.Phys. **B719** (2005) 165–187, [[hep-ph/0412089](#)].
- [49] M. Luscher and P. Weisz, *Is There a Strong Interaction Sector in the Standard Lattice Higgs Model?*, Phys. Lett. **B212** (1988) 472.
- [50] M. Luscher and P. Weisz, *Scaling Laws and Triviality Bounds in the Lattice ϕ^4 Theory. 3. N Component Model*, Nucl. Phys. **B318** (1989) 705.
- [51] W. J. Marciano and S. S. D. Willenbrock, *Radiative Corrections To Heavy Higgs Scalar Production And Radiative Corrections To Heavy Higgs Scalar Production And Decay*, Phys. Rev. **D37** (1988) 2509.
- [52] S. Dawson and S. Willenbrock, *Unitarity Constraints On Heavy Higgs Bosons*, Phys. Rev. Lett. **62** (1989) 1232.
- [53] W. J. Marciano, G. Valencia and S. Willenbrock, *Renormalization Group Improved Unitarity Bounds On The Higgs Boson And Top Quark Masses*, Phys. Rev. **D40** (1989) 1725.
- [54] M. S. Chanowitz and M. K. Gaillard, *Multiple Production of W and Z as a Signal of New Strong Interactions*, Phys. Lett. **B142** (1984) 85.
- [55] S. Dawson and S. Willenbrock, *Radiative Corrections To Longitudinal Vector Boson Scattering*, Phys. Rev. **D40** (1989) 2880.
- [56] L. Durand, P. N. Maher and K. Riesselmann, *Two loop unitarity constraints on the Higgs boson coupling*, Phys. Rev. **D48** (1993) 1084–1096, [[hep-ph/9303234](#)].

- [57] K. Riesselmann, *Large uncertainties in the cross-section of elastic $W_L^+W_L^-$ scattering*, Phys. Rev. **D53** (1996) 6226–6240, [[hep-ph/9507413](#)].
- [58] U. Nierste and K. Riesselmann, *Higgs Sector Renormalization Group in the \overline{MS} and OMS Scheme*, Phys. Rev. **D53** (1996) 6638–6652, [[hep-ph/9511407](#)].
- [59] K. G. Wilson and J. B. Kogut, *The Renormalization group and the epsilon expansion*, Phys. Rept. **12** (1974) 75–200.
- [60] N. Cabibbo, L. Maiani, G. Parisi and R. Petronzio, *Bounds on the Fermions and Higgs Boson Masses in Grand Unified Theories*, Nucl. Phys. **B158** (1979) 295–305.
- [61] R. F. Dashen and H. Neuberger, *How to Get an Upper Bound on the Higgs Mass*, Phys. Rev. Lett. **50** (1983) 1897.
- [62] D. J. E. Callaway, *Nontriviality Of Gauge Theories With Elementary Scalars And Upper Bounds On Higgs Masses*, Nucl. Phys. **B233** (1984) 189.
- [63] P. Hasenfratz and J. Nager, *The Cutoff Dependence of the Higgs Meson Mass and the Onset of New Physics in the Standard Model*, Z. Phys. **C37** (1988) 477.
- [64] J. Kuti, L. Lin and Y. Shen, *Upper Bound on the Higgs Mass in the Standard Model*, Phys. Rev. Lett. **61** (1988) 678.
- [65] R. S. Chivukula and E. H. Simmons, *Custodial symmetry and the triviality bound on the Higgs mass*, Phys. Lett. **B388** (1996) 788–792, [[hep-ph/9608320](#)].
- [66] T. P. Cheng, E. Eichten and L.-F. Li, *Higgs Phenomena in Asymptotically Free Gauge Theories*, Phys. Rev. **D9** (1974) 2259.
- [67] B. Pendleton and G. G. Ross, *Mass and Mixing Angle Predictions from Infrared Fixed Points*, Phys. Lett. **B98** (1981) 291.
- [68] C. T. Hill, *Quark and Lepton Masses from Renormalization Group Fixed Points*, Phys. Rev. **D24** (1981) 691.
- [69] J. Bagger, S. Dimopoulos and E. Masso, *Heavy Families: Masses And Mixings*, Nucl. Phys. **B253** (1985) 397.
- [70] M. A. B. Beg, C. Panagiotakopoulos and A. Sirlin, *Mass of the Higgs Boson in the Canonical Realization of the Weinberg-Salam Theory*, Phys. Rev. Lett. **52** (1984) 883.

- [71] M. J. Duncan, R. Philippe and M. Sher, *Theoretical Ceiling On Quark Masses In The Standard Model*, Phys. Lett. **B153** (1985) 165.
- [72] K. S. Babu and E. Ma, *Probing The Desert With Boson And Fermion Masses*, Phys. Rev. Lett. **55** (1985) 3005.
- [73] A. Hasenfratz, *Quantum Fields on the Computer*. World Scientific, 1992.
- [74] M. Gockeler, H. A. Kastrup, T. Neuhaus and F. Zimmermann, *Scaling analysis of the $O(4)$ symmetric Φ^4 theory in the broken phase*, Nucl. Phys. **B404** (1993) 517–555, [[hep-lat/9206025](#)].
- [75] M. Lindner, M. Sher and H. W. Zaglauer, *Probing Vacuum Stability Bounds at the Fermilab Collider*, Phys. Lett. **B228** (1989) 139.
- [76] M. Sher, *Precise vacuum stability bound in the standard model*, Phys. Lett. **B317** (1993) 159–163, [[hep-ph/9307342](#)].
- [77] G. Altarelli and G. Isidori, *Lower limit on the Higgs mass in the standard model: An Update*, Phys. Lett. **B337** (1994) 141–144.
- [78] J. A. Casas, J. R. Espinosa and M. Quiros, *Improved Higgs mass stability bound in the standard model and implications for supersymmetry*, Phys. Lett. **B342** (1995) 171–179, [[hep-ph/9409458](#)].
- [79] M. Sher, *Electroweak Higgs Potentials and Vacuum Stability*, Phys. Rept. **179** (1989) 273–418.
- [80] M. Lindner, *Implications of Triviality for the Standard Model*, Zeit. Phys. **C31** (1986) 295.
- [81] B. Grzadkowski and M. Lindner, *Stability Of Triviality Mass Bounds In The Standard Model*, Phys. Lett. **B178** (1986) 81.
- [82] T. Hambye and K. Riesselmann, *Matching conditions and Higgs mass upper bounds revisited*, Phys. Rev. **D55** (1997) 7255–7262, [[hep-ph/9610272](#)].
- [83] J. R. Ellis, M. K. Gaillard and D. V. Nanopoulos, *A Phenomenological Profile of the Higgs Boson*, Nucl. Phys. **B106** (1976) 292.
- [84] B. W. Lee, C. Quigg and H. B. Thacker, *Weak Interactions at Very High-Energies: The Role of the Higgs Boson Mass*, Phys. Rev. **D16** (1977) 1519.

- [85] D. R. T. Jones and S. T. Petcov, *Heavy Higgs Bosons at LEP*, Phys. Lett. **B84** (1979) 440.
- [86] B. L. Ioffe and V. A. Khoze, *What Can Be Expected from Experiments on Colliding e^+e^- Beams with e Approximately Equal to 100-GeV?*, Sov. J. Part. Nucl. **9** (1978) 50.
- [87] E. Ma and J. Okada, *Possible Means Of Detecting The Higgs Boson In e^+e^- Annihilation*, Phys. Rev. **D20** (1979) 1052.
- [88] J. Finjord, *A Light Higgs Boson: The Decay OF $Z^0 \rightarrow H^0\text{lepton}^+\text{lepton}^-$* , Phys. Scripta **21** (1980) 143.
- [89] F. A. Berends and R. Kleiss, *Initial State Radiation at LEP Energies and the Corrections to Higgs Boson Production*, Nucl. Phys. **B260** (1985) 32.
- [90] **CDF and D0** Collaboration, Tevatron New Phenomena & Higgs Working Group, *Combined CDF and D0 Upper Limits on Standard Model Higgs Boson Production with 2.1 - 5.4 fb^{-1} of Data*, [arXiv:0911.3930](#).
- [91] **CDF and D0** Collaboration, T. Aaltonen *et al.*, *Combination of Tevatron searches for the standard model Higgs boson in the W^+W^- decay mode*, Phys. Rev. Lett. **104** (2010) 061802, [[arXiv:1001.4162](#)].
- [92] **CDF and D0** Collaboration, Tevatron New Phenomena & Higgs Working Group, *Combined CDF and D0 Upper Limits on Standard Model Higgs Boson Production with up to 6.7 fb^{-1} of Data*, [arXiv:1007.4587](#).
- [93] **CDF and D0** Collaboration, T. Aaltonen *et al.*, *Combined CDF and D0 Upper Limits on Standard Model Higgs Boson Production with up to 8.2 fb^{-1} of Data*, [arXiv:1103.3233](#).
- [94] J. Baglio and A. Djouadi, *Predictions for Higgs production at the Tevatron and the associated uncertainties*, JHEP **10** (2010) 064, [[arXiv:1003.4266](#)].
- [95] J. Baglio, A. Djouadi, S. Ferrag and R. M. Godbole, *The Tevatron Higgs exclusion limits and theoretical uncertainties: a critical appraisal*, Phys. Lett. **B699** (2011) 368–371, [[arXiv:1101.1832](#)].
- [96] M. Cacciari, S. Frixione, M. L. Mangano, P. Nason and G. Ridolfi, *QCD analysis of first b cross-section data at 1.96-TeV*, JHEP **07** (2004) 033, [[hep-ph/0312132](#)].

- [97] A. Djouadi, J. Kalinowski and M. Spira, *HDECAY: A program for Higgs boson decays in the standard model and its supersymmetric extension*, Comput. Phys. Commun. **108** (1998) 56–74, [[hep-ph/9704448](#)].
- [98] J. M. Butterworth *et al.*, *The Tools and Monte Carlo working group Summary Report*, [arXiv:1003.1643](#).
- [99] H. M. Georgi, S. L. Glashow, M. E. Machacek and D. V. Nanopoulos, *Higgs Bosons from Two Gluon Annihilation in Proton Proton Collisions*, Phys. Rev. Lett. **40** (1978) 692.
- [100] M. Dittmar and H. K. Dreiner, *How to find a Higgs boson with a mass between 155-GeV - 180-GeV at the LHC*, Phys. Rev. **D55** (1997) 167–172, [[hep-ph/9608317](#)].
- [101] A. Djouadi, M. Spira and P. M. Zerwas, *Production of Higgs bosons in proton colliders: QCD corrections*, Phys. Lett. **B264** (1991) 440–446.
- [102] S. Dawson, *Radiative corrections to Higgs boson production*, Nucl. Phys. **B359** (1991) 283–300.
- [103] D. Graudenz, M. Spira and P. M. Zerwas, *QCD corrections to Higgs boson production at proton proton colliders*, Phys. Rev. Lett. **70** (1993) 1372–1375.
- [104] M. Spira, A. Djouadi, D. Graudenz and P. M. Zerwas, *SUSY Higgs production at proton colliders*, Phys. Lett. **B318** (1993) 347–353.
- [105] M. Spira, A. Djouadi, D. Graudenz and P. M. Zerwas, *Higgs boson production at the LHC*, Nucl. Phys. **B453** (1995) 17–82, [[hep-ph/9504378](#)].
- [106] M. Spira, *QCD effects in Higgs physics*, Fortsch. Phys. **46** (1998) 203–284, [[hep-ph/9705337](#)].
- [107] R. V. Harlander and W. B. Kilgore, *Next-to-next-to-leading order Higgs production at hadron colliders*, Phys. Rev. Lett. **88** (2002) 201801, [[hep-ph/0201206](#)].
- [108] C. Anastasiou and K. Melnikov, *Higgs boson production at hadron colliders in NNLO QCD*, Nucl. Phys. **B646** (2002) 220–256, [[hep-ph/0207004](#)].
- [109] V. Ravindran, J. Smith and W. L. van Neerven, *NNLO corrections to the total cross section for Higgs boson production in hadron hadron collisions*, Nucl. Phys. **B665** (2003) 325–366, [[hep-ph/0302135](#)].

- [110] S. Catani, D. de Florian, M. Grazzini and P. Nason, *Soft-gluon resummation for Higgs boson production at hadron colliders*, JHEP **07** (2003) 028, [[hep-ph/0306211](#)].
- [111] D. de Florian and M. Grazzini, *Higgs production through gluon fusion: updated cross sections at the Tevatron and the LHC*, Phys. Lett. **B674** (2009) 291–294, [[arXiv:0901.2427](#)].
- [112] C. Anastasiou, G. Dissertori, M. Grazzini, F. Stockli and B. R. Webber, *Perturbative QCD effects and the search for a $H \rightarrow WW \rightarrow \ell\nu\ell\nu$ signal at the Tevatron*, JHEP **08** (2009) 099, [[arXiv:0905.3529](#)].
- [113] A. Djouadi and P. Gambino, *Leading electroweak correction to Higgs boson production at proton colliders*, Phys. Rev. Lett. **73** (1994) 2528–2531, [[hep-ph/9406432](#)].
- [114] U. Aglietti, R. Bonciani, G. Degrossi and A. Vicini, *Two-loop light fermion contribution to Higgs production and decays*, Phys. Lett. **B595** (2004) 432–441, [[hep-ph/0404071](#)].
- [115] G. Degrossi and F. Maltoni, *Two-loop electroweak corrections to Higgs production at hadron colliders*, Phys. Lett. **B600** (2004) 255–260, [[hep-ph/0407249](#)].
- [116] S. Actis, G. Passarino, C. Sturm and S. Uccirati, *NLO Electroweak Corrections to Higgs Boson Production at Hadron Colliders*, Phys. Lett. **B670** (2008) 12–17, [[arXiv:0809.1301](#)].
- [117] S. Actis, G. Passarino, C. Sturm and S. Uccirati, *NNLO Computational Techniques: the Cases $H \rightarrow \gamma\gamma$ and $H \rightarrow gg$* , Nucl. Phys. **B811** (2009) 182–273, [[arXiv:0809.3667](#)].
- [118] C. Anastasiou, R. Boughezal and F. Petriello, *Mixed QCD-electroweak corrections to Higgs boson production in gluon fusion*, JHEP **04** (2009) 003, [[arXiv:0811.3458](#)].
- [119] S. L. Glashow, D. V. Nanopoulos and A. Yildiz, *Associated Production of Higgs Bosons and Z Particles*, Phys. Rev. **D18** (1978) 1724–1727.
- [120] A. Stange, W. J. Marciano and S. Willenbrock, *Associated production of Higgs and weak bosons, with $H \rightarrow b\bar{b}$, at hadron colliders*, Phys. Rev. **D50** (1994) 4491–4498, [[hep-ph/9404247](#)].
- [121] G. Altarelli, R. K. Ellis and G. Martinelli, *Large Perturbative Corrections to the Drell-Yan Process in QCD*, Nucl. Phys. **B157** (1979) 461.

- [122] J. Kubar-Andre and F. E. Paige, *Gluon Corrections to the Drell-Yan Model*, Phys. Rev. **D19** (1979) 221.
- [123] T. Han and S. Willenbrock, *QCD correction to the $pp \rightarrow WH$ and ZH total cross-sections*, Phys. Lett. **B273** (1991) 167–172.
- [124] J. Ohnemus and W. J. Stirling, *Order α_S corrections to the differential cross-section for the WH intermediate mass Higgs signal*, Phys. Rev. **D47** (1993) 2722–2729.
- [125] A. Djouadi and M. Spira, *SUSY-QCD corrections to Higgs boson production at hadron colliders*, Phys. Rev. **D62** (2000) 014004, [[hep-ph/9912476](#)].
- [126] O. Brein, A. Djouadi and R. Harlander, *NNLO QCD corrections to the Higgs-strahlung processes at hadron colliders*, Phys. Lett. **B579** (2004) 149–156, [[hep-ph/0307206](#)].
- [127] M. L. Ciccolini, S. Dittmaier and M. Kramer, *Electroweak radiative corrections to associated WH and ZH production at hadron colliders*, Phys. Rev. **D68** (2003) 073003, [[hep-ph/0306234](#)].
- [128] A. D. Martin, W. J. Stirling, R. S. Thorne and G. Watt, *Parton distributions for the LHC*, Eur. Phys. J. **C63** (2009) 189–285, [[arXiv:0901.0002](#)].
- [129] *MSTW parton distribution functions*, homepage. projects.hepforge.org/mstwpdf/.
- [130] O. Brein *et al.*, *Precision calculations for associated WH and ZH production at hadron colliders*, [hep-ph/0402003](#).
- [131] **Higgs Working Group** Collaboration, K. A. Assamagan *et al.*, *The Higgs working group: Summary report 2003*, [hep-ph/0406152](#).
- [132] A. D. Martin, R. G. Roberts, W. J. Stirling and R. S. Thorne, *NNLO global parton analysis*, Phys. Lett. **B531** (2002) 216–224, [[hep-ph/0201127](#)].
- [133] R. N. Cahn and S. Dawson, *Production of Very Massive Higgs Bosons*, Phys. Lett. **B136** (1984) 196.
- [134] M. Harn and H. Neuberger, *Self-consistent boundary conditions*, Phys. Lett. **B164** (1985) 337–341.
- [135] G. Altarelli, B. Mele and F. Pitolli, *Heavy Higgs Production at Future Colliders*, Nucl. Phys. **B287** (1987) 205–224.

- [136] T. Han, G. Valencia and S. Willenbrock, *Structure function approach to vector boson scattering in $p p$ collisions*, Phys. Rev. Lett. **69** (1992) 3274–3277, [[hep-ph/9206246](#)].
- [137] T. Figy, C. Oleari and D. Zeppenfeld, *Next-to-leading order jet distributions for Higgs boson production via weak-boson fusion*, Phys. Rev. **D68** (2003) 073005, [[hep-ph/0306109](#)].
- [138] R. Raitio and W. W. Wada, *Higgs boson production at large transverse momentum in QCD*, Phys. Rev. **D19** (1979) 941.
- [139] Z. Kunszt, *Associated Production of Heavy Higgs Boson with Top Quarks*, Nucl. Phys. **B247** (1984) 339.
- [140] J. N. Ng and P. Zakarauskas, *A QCD parton calculation of conjoined production of Higgs bosons and heavy flavors in $p\bar{p}$ collision*, Phys. Rev. **D29** (1984) 876.
- [141] W. Beenakker *et al.*, *Higgs radiation off top quarks at the Tevatron and the LHC*, Phys. Rev. Lett. **87** (2001) 201805, [[hep-ph/0107081](#)].
- [142] W. Beenakker *et al.*, *NLO QCD corrections to $t\bar{t}H$ production in hadron collisions. ((U))*, Nucl. Phys. **B653** (2003) 151–203, [[hep-ph/0211352](#)].
- [143] L. Reina and S. Dawson, *Next-to-leading order results for $t\bar{t}h$ production at the Tevatron*, Phys. Rev. Lett. **87** (2001) 201804, [[hep-ph/0107101](#)].
- [144] S. Dawson, L. H. Orr, L. Reina and D. Wackerroth, *Associated top quark Higgs boson production at the LHC*, Phys. Rev. **D67** (2003) 071503, [[hep-ph/0211438](#)].
- [145] P. M. Nadolsky *et al.*, *Implications of CTEQ global analysis for collider observables*, Phys. Rev. **D78** (2008) 013004, [[arXiv:0802.0007](#)].
- [146] *CTEQ: the Coordinated Theoretical-Experimental project on QCD*, homepage. www.phys.psu.edu/~cteq/.
- [147] S. Alekhin, J. Blumlein, S. Klein and S. Moch, *The 3-, 4-, and 5-flavor NNLO Parton from Deep-Inelastic-Scattering Data and at Hadron Colliders*, Phys. Rev. **D81** (2010) 014032, [[arXiv:0908.2766](#)].
- [148] *The Nucleon Parton Distribution Functions*, homepage. [mail.ihep.ru/~alekhin/pdfs.html](mailto:alekhin@ihep.ru).
- [149] *H1 and ZEUS public combined results*, official page. www.desy.de/h1zeus/combined_results.

- [150] P. Jimenez-Delgado and E. Reya, *Variable Flavor Number Parton Distributions and Weak Gauge and Higgs Boson Production at Hadron Colliders at NNLO of QCD*, Phys. Rev. **D80** (2009) 114011, [[arXiv:0909.1711](#)].
- [151] *PDF4LHC recommendation*, homepage.
www.hep.ucl.ac.uk/pdf4lh/PDF4LHCrecom.pdf.
- [152] M. Spira, *HIGLU: A Program for the Calculation of the Total Higgs Production Cross Section at Hadron Colliders via Gluon Fusion including QCD Corrections*, [hep-ph/9510347](#).
- [153] *Programs for SM and MSSM Higgs boson production at hadron colliders*, webpage.
people.web.psi.ch/spira/proglist.html.
- [154] M. Kramer, E. Laenen and M. Spira, *Soft gluon radiation in Higgs boson production at the LHC*, Nucl. Phys. **B511** (1998) 523–549, [[hep-ph/9611272](#)].
- [155] Tevatron New Phenomena & Higgs Working Group, *Responses to concerns about the theoretical modeling of the $gg \rightarrow H$ signal*, homepage. tevnpwhwg.fnal.gov/results/SMHPubWinter2010/ggtheoryreplies_may2010.html.
- [156] J. Baglio, *Higgs production at the Tevatron: Predictions and uncertainties*, PoS **ICHEP2010** (2010) 048.
- [157] **CDF and D0** Collaboration, B. Kilminster, *Higgs searches at the Tevatron*, PoS **ICHEP 2010** (July, 2010) 544.
- [158] J. Baglio, *Higgs in gluon-gluon fusion: follow-up*, in *Higgs Hunting 2010 workshop*, Orsay (France), July 29th–31st, 2010.
indico.lal.in2p3.fr/conferenceDisplay.py?confid=1109.
- [159] S. Moch and A. Vogt, *Higher-order soft corrections to lepton pair and Higgs boson production*, Phys. Lett. **B631** (2005) 48–57, [[hep-ph/0508265](#)].
- [160] V. Ravindran, *Higher-order threshold effects to inclusive processes in QCD*, Nucl. Phys. **B752** (2006) 173–196, [[hep-ph/0603041](#)].
- [161] A. Idilbi, X.-d. Ji, J.-P. Ma and F. Yuan, *Threshold resummation for Higgs production in effective field theory*, Phys. Rev. **D73** (2006) 077501, [[hep-ph/0509294](#)].
- [162] E. Laenen and L. Magnea, *Threshold resummation for electroweak annihilation from DIS data*, Phys. Lett. **B632** (2006) 270–276, [[hep-ph/0508284](#)].

- [163] V. Ahrens, T. Becher, M. Neubert and L. L. Yang, *Renormalization-Group Improved Prediction for Higgs Production at Hadron Colliders*, Eur. Phys. J. **C62** (2009) 333–353, [[arXiv:0809.4283](#)].
- [164] V. Ravindran, J. Smith and W. L. van Neerven, *Differential cross sections for Higgs production*, Mod. Phys. Lett. **A18** (2003) 1721–1734, [[hep-ph/0307005](#)].
- [165] C. Anastasiou, K. Melnikov and F. Petriello, *Fully differential Higgs boson production and the di-photon signal through next-to-next-to-leading order*, Nucl. Phys. **B724** (2005) 197–246, [[hep-ph/0501130](#)].
- [166] S. Catani and M. Grazzini, *An NNLO subtraction formalism in hadron collisions and its application to Higgs boson production at the LHC*, Phys. Rev. Lett. **98** (2007) 222002, [[hep-ph/0703012](#)].
- [167] C. Anastasiou, S. Bucherer and Z. Kunszt, *HPro: A NLO Monte-Carlo for Higgs production via gluon fusion with finite heavy quark masses*, JHEP **10** (2009) 068, [[arXiv:0907.2362](#)].
- [168] G. Corcella and L. Magnea, *Soft-gluon resummation effects on parton distributions*, Phys. Rev. **D72** (2005) 074017, [[hep-ph/0506278](#)].
- [169] C. Anastasiou, *Higgs production via gluon fusion*, in *Higgs Hunting 2010 workshop*, Orsay (France), July 29th–31st, 2010.
[indico.lal.in2p3.fr/conferenceDisplay.py?confid=1109](#).
- [170] M. Grazzini, *NNLO predictions for the Higgs boson signal in the $H \rightarrow WW \rightarrow \ell\nu\ell\nu$ and $H \rightarrow ZZ \rightarrow 4\ell$ decay channels*, JHEP **02** (2008) 043, [[arXiv:0801.3232](#)].
- [171] M. Grazzini, *Higgs cross section: compute reference SM Higgs production cross sections*, webpage. [theory.fi.infn.it/cgi-bin/hresum.pl](#).
- [172] S. D. Drell and T.-M. Yan, *Massive Lepton Pair Production in Hadron-Hadron Collisions at High-Energies*, Phys. Rev. Lett. **25** (1970) 316–320.
- [173] R. Hamberg, W. L. van Neerven and T. Matsuura, *A Complete calculation of the order α_S^2 correction to the Drell-Yan K factor*, Nucl. Phys. **B359** (1991) 343–405.
- [174] R. Hamberg, W. L. van Neerven and T. Matsuura, *Erratum to: "A Complete calculation of the order α_S^2 correction to the Drell-Yan K factor"*, Nucl. Phys. **B644** (2002) 403–404.

- [175] R. S. Thorne, A. D. Martin, W. J. Stirling and G. Watt, *The effects of combined HERA and recent Tevatron $W \rightarrow$ lepton neutrino charge asymmetry data on the MSTW PDFs*, PoS **DIS2010** (2010) 052, [[arXiv:1006.2753](#)].
- [176] M. Ciccolini, A. Denner and S. Dittmaier, *Electroweak and QCD corrections to Higgs production via vector-boson fusion at the LHC*, Phys. Rev. **D77** (2008) 013002, [[arXiv:0710.4749](#)].
- [177] P. Bolzoni, F. Maltoni, S.-O. Moch and M. Zaro, *Higgs production via vector-boson fusion at NNLO in QCD*, Phys. Rev. Lett. **105** (2010) 011801, [[arXiv:1003.4451](#)].
- [178] P. Bolzoni, M. Zaro, F. Maltoni and S.-O. Moch, *Higgs production at NNLO in QCD: the VBF channel*, Nucl. Phys. Proc. Suppl. **205-206** (2010) 314–319, [[arXiv:1006.2323](#)].
- [179] **CDF and D0** Collaboration, Tevatron Electroweak Working Group, *Combination of CDF and D0 Results on the Mass of the Top Quark*, [arXiv:0903.2503](#).
- [180] U. Aglietti *et al.*, *Tevatron for LHC report: Higgs*, [hep-ph/0612172](#).
- [181] **Tev4LHC Higgs Working Group** Collaboration, *Standard model Higgs cross sections at hadron colliders*, webpage.
[maltoni.web.cern.ch/maltoni/TeV4LHC/SM.html](#).
- [182] K. Melnikov and F. Petriello, *The W boson production cross section at the LHC through $O(\alpha_S^2)$* , Phys. Rev. Lett. **96** (2006) 231803, [[hep-ph/0603182](#)].
- [183] S. Catani, L. Cieri, G. Ferrera, D. de Florian and M. Grazzini, *Vector boson production at hadron colliders: a fully exclusive QCD calculation at NNLO*, Phys. Rev. Lett. **103** (2009) 082001, [[arXiv:0903.2120](#)].
- [184] J. Ohnemus, *An Order α_S calculation of hadronic W^-W^+ production*, Phys. Rev. **D44** (1991) 1403–1414.
- [185] S. Frixione, P. Nason and G. Ridolfi, *Strong corrections to $W Z$ production at hadron colliders*, Nucl. Phys. **B383** (1992) 3–44.
- [186] S. Frixione, *A Next-to-leading order calculation of the cross-section for the production of W^+W^- pairs in hadronic collisions*, Nucl. Phys. **B410** (1993) 280–324.
- [187] U. Baur, T. Han and J. Ohnemus, *QCD corrections to hadronic $W\gamma$ production with nonstandard $WW\gamma$ couplings*, Phys. Rev. **D48** (1993) 5140–5161, [[hep-ph/9305314](#)].

- [188] L. J. Dixon, Z. Kunszt and A. Signer, *Vector boson pair production in hadronic collisions at order α_S : Lepton correlations and anomalous couplings*, Phys. Rev. **D60** (1999) 114037, [[hep-ph/9907305](#)].
- [189] M. Cacciari, S. Frixione, M. L. Mangano, P. Nason and G. Ridolfi, *Updated predictions for the total production cross sections of top and of heavier quark pairs at the Tevatron and at the LHC*, JHEP **09** (2008) 127, [[arXiv:0804.2800](#)].
- [190] N. Kidonakis and R. Vogt, *The Theoretical top quark cross section at the Tevatron and the LHC*, Phys. Rev. **D78** (2008) 074005, [[arXiv:0805.3844](#)].
- [191] S. Moch and P. Uwer, *Theoretical status and prospects for top-quark pair production at hadron colliders*, Phys. Rev. **D78** (2008) 034003, [[arXiv:0804.1476](#)].
- [192] S. Dittmaier, M. Kramer and M. Spira, *Higgs radiation off bottom quarks at the Tevatron and the LHC*, Phys. Rev. **D70** (2004) 074010, [[hep-ph/0309204](#)].
- [193] J. M. Campbell, R. K. Ellis, F. Maltoni and S. Willenbrock, *Higgs boson production in association with a single bottom quark*, Phys. Rev. **D67** (2003) 095002, [[hep-ph/0204093](#)].
- [194] R. V. Harlander and W. B. Kilgore, *Higgs boson production in bottom quark fusion at next-to-next-to-leading order*, Phys. Rev. **D68** (2003) 013001, [[hep-ph/0304035](#)].
- [195] F. Maltoni, Z. Sullivan and S. Willenbrock, *Higgs-boson production via bottom-quark fusion*, Phys. Rev. **D67** (2003) 093005, [[hep-ph/0301033](#)].
- [196] V. Ravindran, J. Smith and W. L. van Neerven, *NNLO corrections to the Higgs production cross section*, Nucl. Phys. Proc. Suppl. **135** (2004) 35–40, [[hep-ph/0405263](#)].
- [197] R. V. Harlander and W. B. Kilgore, *Production of a pseudo-scalar Higgs boson at hadron colliders at next-to-next-to leading order*, JHEP **10** (2002) 017, [[hep-ph/0208096](#)].
- [198] A. Cafarella, C. Coriano, M. Guzzi and J. Smith, *On the scale variation of the total cross section for Higgs production at the LHC and at the Tevatron*, Eur. Phys. J. **C47** (2006) 703–721, [[hep-ph/0510179](#)].
- [199] A. D. Martin, W. J. Stirling, R. S. Thorne and G. Watt, *Uncertainties on α_S in global PDF analyses and implications for predicted hadronic cross sections*, Eur. Phys. J. **C64** (2009) 653–680, [[arXiv:0905.3531](#)].

- [200] A. Djouadi and S. Ferrag, *PDF uncertainties in Higgs production at hadron colliders*, Phys. Lett. **B586** (2004) 345–352, [[hep-ph/0310209](#)].
- [201] **NNPDF** Collaboration, R. D. Ball *et al.*, *Precision determination of electroweak parameters and the strange content of the proton from neutrino deep-inelastic scattering*, Nucl. Phys. **B823** (2009) 195–233, [[arXiv:0906.1958](#)].
- [202] M. Grazzini, *QCD effects in Higgs boson production at hadron colliders*, PoS **RADCOR2009** (2010) 047, [[arXiv:1001.3766](#)].
- [203] S. Alekhin, J. Blumlein, P. Jimenez-Delgado, S. Moch and E. Reya, *NNLO Benchmarks for Gauge and Higgs Boson Production at TeV Hadron Colliders*, Phys. Lett. **B697** (2011) 127–135, [[arXiv:1011.6259](#)].
- [204] M. Buza, Y. Matiounine, J. Smith and W. L. van Neerven, *Charm electroproduction viewed in the variable-flavour number scheme versus fixed-order perturbation theory*, Eur. Phys. J. **C1** (1998) 301–320, [[hep-ph/9612398](#)].
- [205] **Particle Data Group** Collaboration, K. Nakamura *et al.*, *Review of particle physics*, J. Phys. **G37** (2010) 075021.
- [206] S. Alekhin, *Parton distributions from deep-inelastic scattering data*, Phys. Rev. **D68** (2003) 014002, [[hep-ph/0211096](#)].
- [207] S. I. Alekhin, *Value of α_S from deep-inelastic scattering data*, JHEP **02** (2003) 015, [[hep-ph/0211294](#)].
- [208] S. Alekhin, J. Blumlein and S. Moch, *Higher order constraints on the Higgs production rate from fixed-target DIS data*, [arXiv:1101.5261](#).
- [209] R. S. Thorne, *PDFs, constraints and searches at LHC*, in *Higgs Hunting 2010 workshop*, Orsay (France), July 29th–31st, 2010. [indico.lal.in2p3.fr/conferenceDisplay.py?confid=1109](#).
- [210] **LHC Higgs Cross Section Working Group** Collaboration, S. Dittmaier *et al.*, *Handbook of LHC Higgs Cross Sections: 1. Inclusive Observables*, [arXiv:1101.0593](#).
- [211] A. Djouadi, *The Anatomy of electro-weak symmetry breaking. II. The Higgs bosons in the minimal supersymmetric model*, Phys. Rept. **459** (2008) 1–241, [[hep-ph/0503173](#)].
- [212] R. V. Harlander and K. J. Ozeren, *Finite top mass effects for hadronic Higgs production at next-to-next-to-leading order*, JHEP **11** (2009) 088, [[arXiv:0909.3420](#)].

- [213] A. Pak, M. Rogal and M. Steinhauser, *Finite top quark mass effects in NNLO Higgs boson production at LHC*, JHEP **02** (2010) 025, [[arXiv:0911.4662](#)].
- [214] R. V. Harlander, H. Mantler, S. Marzani and K. J. Ozeren, *Higgs production in gluon fusion at next-to-next-to-leading order QCD for finite top mass*, Eur. Phys. J. **C66** (2010) 359–372, [[arXiv:0912.2104](#)].
- [215] S. Marzani, R. D. Ball, V. Del Duca, S. Forte and A. Vicini, *Higgs production via gluon-gluon fusion with finite top mass beyond next-to-leading order*, Nucl. Phys. **B800** (2008) 127–145, [[arXiv:0801.2544](#)].
- [216] **CDF** Collaboration, T. Aaltonen *et al.*, *Inclusive Search for Standard Model Higgs Boson Production in the WW Decay Channel using the CDF II Detector*, Phys. Rev. Lett. **104** (2010) 061803, [[arXiv:1001.4468](#)].
- [217] G. Bernardi *et al.*, *Combined CDF and D0 Upper Limits on Standard Model Higgs Boson Production at High Mass (155-200-GeV/c²) with 3 fb⁻¹ of data*, [arXiv:0808.0534](#).
- [218] **D0** Collaboration, V. M. Abazov *et al.*, *Search for Higgs boson production in dilepton and missing energy final states with 5.4 fb⁻¹ of pp collisions at $\sqrt{s} = 1.96$ TeV*, Phys. Rev. Lett. **104** (2010) 061804, [[arXiv:1001.4481](#)].
- [219] M. Dittmar, F. Pauss and D. Zurcher, *Towards a precise parton luminosity determination at the CERN LHC*, Phys. Rev. **D56** (1997) 7284–7290, [[hep-ex/9705004](#)].
- [220] D. Zeppenfeld, R. Kinnunen, A. Nikitenko and E. Richter-Was, *Measuring Higgs boson couplings at the LHC*, Phys. Rev. **D62** (2000) 013009, [[hep-ph/0002036](#)].
- [221] M. Dührssen *et al.*, *Extracting Higgs boson couplings from LHC data*, Phys. Rev. **D70** (2004) 113009, [[hep-ph/0406323](#)].
- [222] C. Anastasiou, K. Melnikov and F. Petriello, *The gluon-fusion uncertainty in Higgs coupling extractions*, Phys. Rev. **D72** (2005) 097302, [[hep-ph/0509014](#)].
- [223] R. Heuer, *talk given in IWLC2010*, October, 2010.
- [224] **CMS** Collaboration, S. Chatrchyan *et al.*, *Measurement of WW Production and Search for the Higgs Boson in pp Collisions at $\sqrt{s} = 7$ TeV*, Phys. Lett. **B699** (2011) 25–47, [[arXiv:1102.5429](#)].

- [225] **ATLAS** Collaboration, G. Aad *et al.*, *Limits on the production of the Standard Model Higgs Boson in pp collisions at $\sqrt{s} = 7$ TeV with the ATLAS detector*, [arXiv:1106.2748](#).
- [226] **ATLAS** Collaboration, *ATLAS Sensitivity Prospects for 1 Higgs Boson Production at the LHC Running at 7, 8 or 9 TeV*, ATL-PHYS-PUB-2010-015, CERN, Geneva (Switzerland), November, 2010.
- [227] **CMS** Collaboration, *The CMS physics reach for searches at 7 TeV*, CMS-NOTE-2010-008. CERN-CMS-NOTE-2010-008, CERN, Geneva (Switzerland), May, 2010.
- [228] *ATLAS e-News*, February, 22nd, 2010.
atlas-service-enews.web.cern.ch/atlas-service-enews/2010/news_10/news_2010outlook.php.
- [229] E. L. Berger, Q.-H. Cao, C. B. Jackson, T. Liu and G. Shaughnessy, *Higgs Boson Search Sensitivity in the $H \rightarrow WW$ Dilepton Decay Mode at $\sqrt{s} = 7$ and 10 TeV*, Phys. Rev. **D82** (2010) 053003, [[arXiv:1003.3875](#)].
- [230] F. Demartin, S. Forte, E. Mariani, J. Rojo and A. Vicini, *The impact of PDF and α_S uncertainties on Higgs Production in gluon fusion at hadron colliders*, Phys. Rev. **D82** (2010) 014002, [[arXiv:1004.0962](#)].
- [231] V. Ahrens, T. Becher, M. Neubert and L. L. Yang, *Updated Predictions for Higgs Production at the Tevatron and the LHC*, Phys. Lett. **B698** (2011) 271–274, [[arXiv:1008.3162](#)].
- [232] J. Baglio and A. Djouadi, *Higgs production at the LHC*, JHEP **03** (2011) 055, [[arXiv:1012.0530](#)].
- [233] **NNPDF** Collaboration, D. R. Ball *et al.*, *Unbiased global determination of parton distributions and their uncertainties at NNLO and at LO*, [arXiv:1107.2652](#).
- [234] A. D. Martin, W. J. Stirling, R. S. Thorne and G. Watt, *Heavy-quark mass dependence in global PDF analyses and 3- and 4-flavour parton distributions*, Eur. Phys. J. **C70** (2010) 51–72, [[arXiv:1007.2624](#)].
- [235] A. Djouadi, M. Spira and P. M. Zerwas, *QCD Corrections to Hadronic Higgs Decays*, Z. Phys. **C70** (1996) 427–434, [[hep-ph/9511344](#)].
- [236] **CMS** Collaboration, G. L. Bayatian *et al.*, *CMS technical design report, volume II: Physics performance*, J. Phys. **G34** (2007) 995–1579.

- [237] **ATLAS** Collaboration, G. Aad *et al.*, *The ATLAS Experiment at the CERN Large Hadron Collider*, JINST **3** (2008) S08003.
- [238] **ATLAS** Collaboration, G. Aad *et al.*, *Expected Performance of the ATLAS Experiment - Detector, Trigger and Physics*, [arXiv:0901.0512](#).
- [239] B. A. Kniehl and A. Sirlin, *Comparative analysis of three methods to evaluate vacuum polarization functions*, Phys. Lett. **B318** (1993) 367–370.
- [240] B. A. Kniehl, *Two loop $\mathcal{O}(\alpha_s G_F M_t^2)$ corrections to the fermionic decay rates of the standard model Higgs boson*, Phys. Rev. **D50** (1994) 3314–3322, [[hep-ph/9405299](#)].
- [241] K. G. Chetyrkin, B. A. Kniehl and M. Steinhauser, *Three-loop $\mathcal{O}(\alpha_s^2 G_F M_t^2)$ corrections to hadronic Higgs decays*, Nucl. Phys. **B490** (1997) 19–39, [[hep-ph/9701277](#)].
- [242] K. G. Chetyrkin, B. A. Kniehl and M. Steinhauser, *Virtual top-quark effects on the $H \rightarrow b\bar{b}$ decay at next-to-leading order in QCD*, Phys. Rev. Lett. **78** (1997) 594–597, [[hep-ph/9610456](#)].
- [243] **Higgs Working Group** Collaboration, M. S. Carena *et al.*, *Report of the Tevatron Higgs working group*, [hep-ph/0010338](#).
- [244] P. C. Bhat, R. Gilmartin and H. B. Prosper, *A strategy for discovering a low-mass Higgs boson at the Tevatron*, Phys. Rev. **D62** (2000) 074022, [[hep-ph/0001152](#)].
- [245] E. Richter-Was, *Prospects for the observability of the $W H$ and $Z H$, $H \rightarrow b\bar{b}$ channel in 14-TeV pp and 2-TeV $p\bar{p}$ collisions (missing $E_T + b\bar{b}$ final state)*, Acta Phys. Polon. **B31** (2000) 1973–2019.
- [246] E. Richter-Was, *Revisiting the observability of the $W H$ and $Z H$, $H \rightarrow b\bar{b}$ channel in 14-TeV pp and 2-TeV $p\bar{p}$ collisions ($l\bar{b}\bar{b}$ and $l\bar{l}b\bar{b}$ final states)*, Acta Phys. Polon. **B31** (2000) 1931–1972.
- [247] E. Richter-Was and M. Sapinski, *Search for the SM and MSSM Higgs boson in the $t\bar{t}H$, $H \rightarrow b\bar{b}$ channel*, Acta Phys. Polon. **B30** (1999) 1001–1040.
- [248] V. Drollinger, T. Muller and D. Denegri, *Searching for Higgs bosons in association with top quark pairs in the $H^0 \rightarrow b\bar{b}$ decay mode*, [hep-ph/0111312](#).
- [249] D. Green, S. Kunori, K. Maeshima, R. Vidal and W. Wu, *A Study of $t\bar{t} + Higgs$ at CMS*, CMS-NOTE-2001-039, CERN, Geneva (Switzerland), July, 2001.

- [250] J. Cammin and M. Schumacher, *The ATLAS discovery potential for the channel ttH , $H \rightarrow bb$* , ATL-PHYS-2003-024, CERN, Geneva (Switzerland), June, 2003.
- [251] A. Grau, G. Panchieri and R. J. N. Phillips, *Contributions of off-shell top quarks to decay processes*, Phys. Lett. **B251** (1990) 293–298.
- [252] M. S. Chanowitz, M. A. Furman and I. Hinchliffe, *Weak Interactions of Ultraheavy Fermions*, Phys. Lett. **B78** (1978) 285.
- [253] M. S. Chanowitz, M. A. Furman and I. Hinchliffe, *Weak Interactions of Ultraheavy Fermions. 2*, Nucl. Phys. **B153** (1979) 402.
- [254] J. Fleischer and F. Jegerlehner, *Radiative Corrections to Higgs Decays in the Extended Weinberg-Salam Model*, Phys. Rev. **D23** (1981) 2001–2026.
- [255] S. Dawson and S. Willenbrock, *Heavy Fermion Corrections To Heavy Higgs Boson Production And Decay*, Phys. Lett. **B211** (1988) 200.
- [256] Z. Hioki, *Heavy Fermion Corrections To Higgs Couplings Revisited*, Phys. Lett. **B224** (1989) 417.
- [257] B. A. Kniehl, *Radiative corrections for $H \rightarrow ZZ$ in the standard model*, Nucl. Phys. **B352** (1991) 1–26.
- [258] B. A. Kniehl, *Radiative corrections for $H \rightarrow W^+W^-(\gamma)$ in the standard model*, Nucl. Phys. **B357** (1991) 439–466.
- [259] A. Bredenstein, A. Denner, S. Dittmaier and M. M. Weber, *Radiative corrections to the semileptonic and hadronic Higgs-boson decays $H \rightarrow WW/ZZ \rightarrow 4$ fermions*, JHEP **02** (2007) 080, [[hep-ph/0611234](#)].
- [260] E. W. N. Glover, J. Ohnemus and S. S. D. Willenbrock, *Higgs Boson Decay To One Real And One Virtual W Boson*, Phys. Rev. **D37** (1988) 3193.
- [261] S. Asai *et al.*, *Prospects for the search for a standard model Higgs boson in ATLAS using vector boson fusion*, Eur. Phys. J. **C32S2** (2004) 19–54, [[hep-ph/0402254](#)].
- [262] W. J. Stirling, R. Kleiss and S. D. Ellis, *W^+W^- Pair Production in High-Energy Hadronic Collisions: Signal Versus Background*, Phys. Lett. **B163** (1985) 261.
- [263] J. F. Gunion, Z. Kunszt and M. Soldate, *A Background to Higgs Detection*, Phys. Lett. **B163** (1985) 389.

- [264] J. F. Gunion and M. Soldate, *Overcoming a Critical Background to Higgs Detection*, Phys. Rev. **D34** (1986) 826.
- [265] L. Fayard and G. Unal, *Search for Higgs decay into photons with EAGLE. Add. 1 Addendum on the Higgs search with photons. Add. 2 (final?) update on Higgs decay to photons*, ATL-PHYS-92-001, CERN, Geneva (Switzerland), December, 1992.
- [266] C. Seez and T. S. Virdee, *The Higgs two photon decay in CMS: an update*, CMS-TN/94-289, CERN, Geneva (Switzerland), 1994.
- [267] D. Froidevaux, F. Gianotti and E. Richter-Was, *Comparison of the ATLAS and CMS discovery potential for the $H \rightarrow \gamma\gamma$ channel at the LHC*, ATL-PHYS-95-064, CERN, Geneva (Switzerland), February, 1995.
- [268] F. Gianotti and I. Vichou, *Study of γ /jet separation with the ATLAS detector*, ATL-PHYS-96-078, CERN, Geneva (Switzerland), February, 1996.
- [269] M. Wielers, *Isolation of Photons*, ATL-PHYS-2002-004, CERN, Geneva (Switzerland), November, 2001.
- [270] K. G. Chetyrkin, B. A. Kniehl and M. Steinhauser, *Hadronic Higgs decay to order α_s^4* , Phys. Rev. Lett. **79** (1997) 353–356, [[hep-ph/9705240](#)].
- [271] D. Cavalli *et al.*, *The Higgs working group: Summary report*, [hep-ph/0203056](#).
- [272] K. G. Chetyrkin *et al.*, *Charm and Bottom Quark Masses: an Update*, Phys. Rev. **D80** (2009) 074010, [[arXiv:0907.2110](#)].
- [273] A. Djouadi, N. Krauer and M. Kramer, in progress.
- [274] J. M. Campbell and R. K. Ellis, *MCFM for the Tevatron and the LHC*, Nucl. Phys. Proc. Suppl. **205-206** (2010) 10–15, [[arXiv:1007.3492](#)].
- [275] **CDF** Collaboration, *Search for $H \rightarrow WW^*$ Production at CDF Using 5.9 fb^{-1} of Data*, CDF note 10232, Fermilab, Batavia (U.S.A.), August, 2010.
- [276] T. Junk, *Confidence Level Computation for Combining Searches with Small Statistics*, Nucl. Instrum. Meth. **A434** (1999) 435–443, [[hep-ex/9902006](#)].
- [277] K. Peters, *talk at the LHC–HCG meeting*, December, 2010.
- [278] S. Alekhin, J. Blumlein and S. O. Moch, *Parton distributions and Tevatron jet data*, [arXiv:1105.5349](#).

- [279] A. Cooper-Sarkar, *PDFs for the LHC*, [arXiv:1107.5170](#).
- [280] R. S. Thorne and G. Watt, *PDF dependence of Higgs cross sections at the Tevatron and LHC: response to recent criticism*, [arXiv:1106.5789](#).
- [281] C. F. Berger, C. Marcantonini, I. W. Stewart, F. J. Tackmann and W. J. Waalewijn, *Higgs Production with a Central Jet Veto at NNLL+NNLO*, JHEP **04** (2011) 092, [[arXiv:1012.4480](#)].
- [282] S. Weinberg, *Gauge Hierarchies*, Phys. Lett. **B82** (1979) 387.
- [283] C. H. Llewellyn Smith and G. G. Ross, *The Real Gauge Hierarchy Problem*, Phys. Lett. **B105** (1981) 38.
- [284] M. Drees, R. M. Godbole and P. Roy, *Theory and Phenomenology of Sparticles*. World Scientific, 2004.
- [285] S. P. Martin, *A Supersymmetry Primer*, [hep-ph/9709356](#).
- [286] H. Georgi and S. L. Glashow, *Unity of All Elementary Particle Forces*, Phys. Rev. Lett. **32** (1974) 438–441.
- [287] A. J. Buras, J. R. Ellis, M. K. Gaillard and D. V. Nanopoulos, *Aspects of the Grand Unification of Strong, Weak and Electromagnetic Interactions*, Nucl. Phys. **B135** (1978) 66–92.
- [288] H. Georgi, H. R. Quinn and S. Weinberg, *Hierarchy of Interactions in Unified Gauge Theories*, Phys. Rev. Lett. **33** (1974) 451–454.
- [289] P. Langacker and M.-x. Luo, *Implications of precision electroweak experiments for M_t , ρ_0 , $\sin^2 \theta_W$ and grand unification*, Phys. Rev. **D44** (1991) 817–822.
- [290] R. H. Sanders and S. S. McGaugh, *Modified Newtonian Dynamics as an Alternative to Dark Matter*, Ann. Rev. Astron. Astrophys. **40** (2002) 263–317, [[astro-ph/0204521](#)].
- [291] J. D. Bekenstein, *Relativistic gravitation theory for the MOND paradigm*, Phys. Rev. **D70** (2004) 083509, [[astro-ph/0403694](#)].
- [292] **WMAP** Collaboration, D. N. Spergel *et al.*, *First Year Wilkinson Microwave Anisotropy Probe (WMAP) Observations: Determination of Cosmological Parameters*, Astrophys. J. Suppl. **148** (2003) 175–194, [[astro-ph/0302209](#)].

- [293] **WMAP** Collaboration, D. N. Spergel *et al.*, *Wilkinson Microwave Anisotropy Probe (WMAP) three year results: Implications for cosmology*, *Astrophys. J. Suppl.* **170** (2007) 377, [[astro-ph/0603449](#)].
- [294] **WMAP** Collaboration, E. Komatsu *et al.*, *Seven-Year Wilkinson Microwave Anisotropy Probe (WMAP) Observations: Cosmological Interpretation*, *Astrophys. J. Suppl.* **192** (2011) 18, [[arXiv:1001.4538](#)].
- [295] G. R. Farrar and P. Fayet, *Phenomenology of the Production, Decay, and Detection of New Hadronic States Associated with Supersymmetry*, *Phys. Lett.* **B76** (1978) 575–579.
- [296] J. L. Feng, *Supersymmetry and cosmology*, [hep-ph/0405215](#).
- [297] S. R. Coleman and J. Mandula, *All Possible Symmetries Of The S-Matrix*, *Phys. Rev.* **159** (1967) 1251–1256.
- [298] R. Haag, J. T. Lopuszanski and M. Sohnius, *All Possible Generators of Supersymmetries of the S Matrix*, *Nucl. Phys.* **B88** (1975) 257.
- [299] J. Wess and J. Bagger, *Supersymmetry and Supergravity*. Princeton Series in Physics. Princeton University Press, 1992.
- [300] J. Wess and B. Zumino, *Supergauge Transformations in Four-Dimensions*, *Nucl. Phys.* **B70** (1974) 39–50.
- [301] J. Iliopoulos and B. Zumino, *Broken Supergauge Symmetry and Renormalization*, *Nucl. Phys.* **B76** (1974) 310.
- [302] S. Dimopoulos and H. Georgi, *Softly Broken Supersymmetry and SU(5)*, *Nucl. Phys.* **B193** (1981) 150.
- [303] N. Sakai, *Naturalness in Supersymmetric Guts*, *Zeit. Phys.* **C11** (1981) 153.
- [304] L. O’Raifeartaigh, *Spontaneous Symmetry Breaking for Chiral Scalar Superfields*, *Nucl. Phys.* **B96** (1975) 331.
- [305] P. Fayet and J. Iliopoulos, *Spontaneously Broken Supergauge Symmetries and Goldstone Spinors*, *Phys. Lett.* **B51** (1974) 461–464.
- [306] **ATLAS** Collaboration, G. Aad *et al.*, *Search for supersymmetry using final states with one lepton, jets, and missing transverse momentum with the ATLAS detector in $\sqrt{s} = 7$ TeV pp* , *Phys. Rev. Lett.* **106** (2011) 131802, [[arXiv:1102.2357](#)].

- [307] **ATLAS** Collaboration, G. Aad *et al.*, *Search for supersymmetry in pp collisions at $\sqrt{s} = 7$ TeV in final states with missing transverse momentum and b-jets*, Phys. Lett. **B701** (2011) 398–416, [[arXiv:1103.4344](#)].
- [308] **CMS** Collaboration, S. Chatrchyan *et al.*, *Search for Supersymmetry in pp Collisions at $\sqrt{s} = 7$ TeV in Events with Two Photons and Missing Transverse Energy*, Phys. Rev. Lett. **106** (2011) 211802, [[arXiv:1103.0953](#)].
- [309] **CMS** Collaboration, S. Chatrchyan *et al.*, *Search for supersymmetry in events with a lepton, a photon, and large missing transverse energy in pp collisions at $\sqrt{s} = 7$ TeV*, JHEP **06** (2011) 093, [[arXiv:1105.3152](#)].
- [310] S. L. Adler and W. A. Bardeen, *Absence of higher order corrections in the anomalous axial vector divergence equation*, Phys. Rev. **182** (1969) 1517–1536.
- [311] L. Alvarez-Gaume and E. Witten, *Gravitational Anomalies*, Nucl. Phys. **B234** (1984) 269.
- [312] L. E. Ibanez and G. G. Ross, *$SU(2)$ - $L \times U(1)$ Symmetry Breaking as a Radiative Effect of Supersymmetry Breaking in Guts*, Phys. Lett. **B110** (1982) 215–220.
- [313] L. Alvarez-Gaume, J. Polchinski and M. B. Wise, *Minimal Low-Energy Supergravity*, Nucl. Phys. **B221** (1983) 495.
- [314] L. E. Ibanez, C. Lopez and C. Munoz, *The Low-Energy Supersymmetric Spectrum According to $N=1$ Supergravity Guts*, Nucl. Phys. **B256** (1985) 218–252.
- [315] M. Muehlleitner, *Theory SUSY Higgs and relation with SUSY*, in *Higgs Hunting 2011 workshop*, Orsay (France), July 28th–30st, 2011. [indico.lal.in2p3.fr/conferenceDisplay.py?confid=1507](#).
- [316] P. Fayet, *Supergauge Invariant Extension of the Higgs Mechanism and a Model for the electron and Its Neutrino*, Nucl. Phys. **B90** (1975) 104–124.
- [317] J. P. Derendinger and C. A. Savoy, *Quantum Effects and $SU(2) \times U(1)$ Breaking in Supergravity Gauge Theories*, Nucl. Phys. **B237** (1984) 307.
- [318] J. R. Ellis, J. F. Gunion, H. E. Haber, L. Roszkowski and F. Zwirner, *Higgs Bosons in a Nonminimal Supersymmetric Model*, Phys. Rev. **D39** (1989) 844.
- [319] U. Ellwanger, M. Rausch de Traubenberg and C. A. Savoy, *Phenomenology of supersymmetric models with a singlet*, Nucl. Phys. **B492** (1997) 21–50, [[hep-ph/9611251](#)].

- [320] U. Ellwanger, C. Hugonie and A. M. Teixeira, *The Next-to-Minimal Supersymmetric Standard Model*, Phys. Rept. **496** (2010) 1–77, [[arXiv:0910.1785](#)].
- [321] A. Djouadi, U. Ellwanger and A. M. Teixeira, *The constrained next-to-minimal supersymmetric standard model*, Phys. Rev. Lett. **101** (2008) 101802, [[arXiv:0803.0253](#)].
- [322] H. E. Haber, *Challenges for nonminimal Higgs searches at future colliders*, [hep-ph/9505240](#).
- [323] A. Djouadi, J. Kalinowski, P. Ohmann and P. M. Zerwas, *Heavy SUSY Higgs bosons at e^+e^- linear colliders*, Z. Phys. **C74** (1997) 93–111, [[hep-ph/9605339](#)].
- [324] J. F. Gunion, A. Stange and S. Willenbrock, *Weakly coupled Higgs bosons*, [hep-ph/9602238](#).
- [325] E. Boos, A. Djouadi and A. Nikitenko, *Detection of the neutral MSSM Higgs bosons in the intense-coupling regime at the LHC*, Phys. Lett. **B578** (2004) 384–393, [[hep-ph/0307079](#)].
- [326] J. Baglio and A. Djouadi, *Implications of the ATLAS and CMS searches in the channel $pp \rightarrow Higgs \rightarrow \tau^+\tau^-$ for the MSSM and SM Higgs bosons*, [arXiv:1103.6247](#).
- [327] M. S. Carena, S. Heinemeyer, C. E. M. Wagner and G. Weiglein, *Suggestions for benchmark scenarios for MSSM Higgs boson searches at hadron colliders*, Eur. Phys. J. **C26** (2003) 601–607, [[hep-ph/0202167](#)].
- [328] S. Heinemeyer, W. Hollik and G. Weiglein, *FeynHiggs: a program for the calculation of the masses of the neutral CP-even Higgs bosons in the MSSM*, Comput. Phys. Commun. **124** (2000) 76–89, [[hep-ph/9812320](#)].
- [329] **Atlas** Collaboration, J. B. G. da Costa *et al.*, *Search for squarks and gluinos using final states with jets and missing transverse momentum with the ATLAS detector in $\sqrt{s} = 7$ TeV proton-proton collisions*, Phys. Lett. **B701** (2011) 186–203, [[arXiv:1102.5290](#)].
- [330] **CMS** Collaboration, V. Khachatryan *et al.*, *Search for Supersymmetry in pp Collisions at 7 TeV in Events with Jets and Missing Transverse Energy*, Phys. Lett. **B698** (2011) 196–218, [[arXiv:1101.1628](#)].

- [331] S. Dawson, C. B. Jackson and P. Jaiswal, *SUSY QCD Corrections to Higgs-b Production : Is the Δ_b Approximation Accurate?*, Phys. Rev. **D83** (2011) 115007, [[arXiv:1104.1631](#)].
- [332] D. A. Dicus and S. Willenbrock, *Higgs Boson Production from Heavy Quark Fusion*, Phys. Rev. **D39** (1989) 751.
- [333] S. Dawson, C. B. Jackson, L. Reina and D. Wackerroth, *Exclusive Higgs boson production with bottom quarks at hadron colliders*, Phys. Rev. **D69** (2004) 074027, [[hep-ph/0311067](#)].
- [334] **CDF Collaboration**, T. Aaltonen *et al.*, *Search for Higgs bosons predicted in two-Higgs-doublet models via decays to tau lepton pairs in 1.96 TeV $p\bar{p}$ collisions*, Phys. Rev. Lett. **103** (2009) 201801, [[arXiv:0906.1014](#)].
- [335] **D0 Collaboration**, V. M. Abazov *et al.*, *Search for Higgs bosons decaying to tau pairs in $p\bar{p}$ collisions with the D0 detector*, Phys. Rev. Lett. **101** (2008) 071804, [[arXiv:0805.2491](#)].
- [336] **Tevatron New Phenomena & Higgs Working Group Collaboration**, D. Benjamin *et al.*, *Combined CDF and D0 upper limits on MSSM Higgs boson production in tau-tau final states with up to 2.2 fb^{-1}* , [arXiv:1003.3363](#).
- [337] J. Baglio and A. Djouadi, *Revisiting the constraints on the Supersymmetric Higgs sector at the Tevatron*, Phys. Lett. **B699** (2011) 372–376, [[arXiv:1012.2748](#)].
- [338] S. Heinemeyer, W. Hollik and G. Weiglein, *Electroweak precision observables in the minimal supersymmetric standard model*, Phys. Rept. **425** (2006) 265–368, [[hep-ph/0412214](#)].
- [339] S. Heinemeyer, *MSSM Higgs physics at higher orders*, Int. J. Mod. Phys. **A21** (2006) 2659–2772, [[hep-ph/0407244](#)].
- [340] B. C. Allanach, A. Djouadi, J. L. Kneur, W. Porod and P. Slavich, *Precise determination of the neutral Higgs boson masses in the MSSM*, JHEP **09** (2004) 044, [[hep-ph/0406166](#)].
- [341] D. M. Pierce, J. A. Bagger, K. T. Matchev and R.-j. Zhang, *Precision corrections in the minimal supersymmetric standard model*, Nucl. Phys. **B491** (1997) 3–67, [[hep-ph/9606211](#)].
- [342] S. Dawson, A. Djouadi and M. Spira, *QCD corrections to SUSY Higgs production: The Role of squark loops*, Phys. Rev. Lett. **77** (1996) 16–19, [[hep-ph/9603423](#)].

- [343] R. V. Harlander and M. Steinhauser, *Supersymmetric Higgs production in gluon fusion at next- to-leading order*, JHEP **09** (2004) 066, [[hep-ph/0409010](#)].
- [344] C. Anastasiou, S. Beerli, S. Bucherer, A. Daleo and Z. Kunszt, *Two-loop amplitudes and master integrals for the production of a Higgs boson via a massive quark and a scalar-quark loop*, JHEP **01** (2007) 082, [[hep-ph/0611236](#)].
- [345] U. Aglietti, R. Bonciani, G. Degrossi and A. Vicini, *Analytic results for virtual QCD corrections to Higgs production and decay*, JHEP **01** (2007) 021, [[hep-ph/0611266](#)].
- [346] R. Bonciani, G. Degrossi and A. Vicini, *Scalar Particle Contribution to Higgs Production via Gluon Fusion at NLO*, JHEP **11** (2007) 095, [[arXiv:0709.4227](#)].
- [347] M. Muehlleitner and M. Spira, *Higgs boson production via gluon fusion: Squark loops at NLO QCD*, Nucl. Phys. **B790** (2008) 1–27, [[hep-ph/0612254](#)].
- [348] G. Degrossi and P. Slavich, *On the NLO QCD corrections to Higgs production and decay in the MSSM*, Nucl. Phys. **B805** (2008) 267–286, [[arXiv:0806.1495](#)].
- [349] S. Dawson and C. B. Jackson, *SUSY QCD Corrections to Associated Higgs-bottom Quark Production*, Phys. Rev. **D77** (2008) 015019, [[arXiv:0709.4519](#)].
- [350] C. Anastasiou, S. Beerli and A. Daleo, *The two-loop QCD amplitude $gg \rightarrow h, H$ in the Minimal Supersymmetric Standard Model*, Phys. Rev. Lett. **100** (2008) 241806, [[arXiv:0803.3065](#)].
- [351] M. Muehlleitner, H. Rzehak and M. Spira, *SUSY-QCD corrections to MSSM Higgs boson production via gluon fusion*, PoS **RADCOR2009** (2010) 043, [[arXiv:1001.3214](#)].
- [352] **ATLAS** Collaboration, *Search for neutral MSSM Higgs bosons decaying to $\tau^+\tau^-$ pairs in proton-proton collisions at $\sqrt{s} = 7$ TeV with the ATLAS detector*, [arXiv:1107.5003](#).
- [353] **CMS** Collaboration, S. Chatrchyan *et al.*, *Search for Neutral MSSM Higgs Bosons Decaying to Tau Pairs in pp Collisions at $\sqrt{s} = 7$ TeV*, Phys. Rev. Lett. **106** (2011) 231801, [[arXiv:1104.1619](#)].
- [354] J. Gunion, H. Haber, F. Paige, W.-K. Tung and S. Willenbrock, *Neutral and Charged Higgs Detection: Heavy Quark Fusion, Top Quark Mass Dependence and Rare Decays*, Nucl.Phys. **B294** (1987) 621.

- [355] F. Borzumati, J.-L. Kneur and N. Polonsky, *Higgs-Strahlung and R-parity violating slepton-Strahlung at hadron colliders*, Phys.Rev. **D60** (1999) 115011, [[hep-ph/9905443](#)].
- [356] T. Plehn, *Charged Higgs boson production in bottom gluon fusion*, Phys.Rev. **D67** (2003) 014018, [[hep-ph/0206121](#)].
- [357] M. Beccaria, F. M. Renard and C. Verzegnassi, *Electroweak supersymmetric effects on high energy unpolarized and polarized single top production at CERN LHC*, Phys.Rev. **D71** (2005) 033005, [[hep-ph/0410089](#)].
- [358] K. Huitu, S. Kumar Rai, K. Rao, S. D. Rindani and P. Sharma, *Probing top charged-Higgs production using top polarization at the Large Hadron Collider*, JHEP **1104** (2011) 026, [[arXiv:1012.0527](#)].
- [359] M. Beneke, I. Efthymiopoulos, M. L. Mangano, J. Womersley, A. Ahmadov *et al.*, *Top quark physics*, [hep-ph/0003033](#).
- [360] W. Bernreuther, *Top quark physics at the LHC*, J.Phys.G **G35** (2008) 083001, [[arXiv:0805.1333](#)].
- [361] R. M. Godbole, K. Rao, S. D. Rindani and R. K. Singh, *On measurement of top polarization as a probe of $t\bar{t}$ production mechanisms at the LHC*, JHEP **1011** (2010) 144, [[arXiv:1010.1458](#)].
- [362] M. Beccaria, G. Macorini, L. Panizzi, F. Renard and C. Verzegnassi, *Associated production of charged Higgs and top at LHC: The Role of the complete electroweak supersymmetric contribution*, Phys.Rev. **D80** (2009) 053011, [[arXiv:0908.1332](#)].
- [363] M. S. Carena, D. Garcia, U. Nierste and C. E. M. Wagner, *Effective Lagrangian for the $\bar{t}bH^+$ interaction in the MSSM and charged Higgs phenomenology*, Nucl. Phys. **B577** (2000) 88–120, [[hep-ph/9912516](#)].
- [364] J. Baglio *et al.*, *The left-right asymmetry of top quarks in associated top- charged Higgs bosons at the LHC as a probe of the $\tan\beta$ parameter*, Phys. Lett. **B705** (2011) 212–216, [[arXiv:1109.2420](#)].
- [365] M. Arai, K. Huitu, S. K. Rai and K. Rao, *Single production of sleptons with polarized tops at the Large Hadron Collider*, JHEP **1008** (2010) 082, [[arXiv:1003.4708](#)].

- [366] B. Allanach, M. Battaglia, G. Blair, M. S. Carena, A. De Roeck *et al.*, *The Snowmass points and slopes: Benchmarks for SUSY searches*, Eur.Phys.J. **C25** (2002) 113–123, [[hep-ph/0202233](#)].
- [367] **CDF** Collaboration, *Search for Higgs Bosons Produced in Association with b -Quarks*, CDF note 10105, Fermilab, Batavia (U.S.A.), June, 2010.
- [368] *CERN bulletin*, issue No. 32-34/2011, Cern, Geneva Switzerland, 2009.
cdsweb.cern.ch/journal/CERNBulletin/2011/32/News%20Articles/1372204?ln=en.
- [369] **CMS** Collaboration, M. Bluj, *CMS Results on Low Mass Higgs Searches*, in *Higgs Hunting 2011 workshop*, Orsay (France), July 28th–30st, 2011.
indico.lal.in2p3.fr/conferenceDisplay.py?confid=1507.
- [370] **CMS** Collaboration, G. Tonelli, *Highlights and Searches in CMS*, in *HEP–EPS 2011*, Grenoble (France), July 20th–27st, 2011.
indico.in2p3.fr/conferenceTimeTable.py?confId=5116.
- [371] E. Boos, A. Djouadi, M. Muehlleitner and A. Vologdin, *The MSSM Higgs bosons in the intense coupling regime*, Phys. Rev. **D66** (2002) 055004, [[hep-ph/0205160](#)].
- [372] **CMS** Collaboration, *Search for the charged Higgs boson in the $e\tau$ and $\mu\tau$ dilepton channels of top quark pair decays*, CMS-PAS-HIG-11-002, CERN, Geneva (Switzerland), March, 2011.
- [373] M. Aliev *et al.*, *HATHOR – HAdronic Top and Heavy quarks crOss section calculatoR*, Comput. Phys. Commun. **182** (2011) 1034–1046, [[arXiv:1007.1327](#)].
- [374] **ATLAS** Collaboration, *Search for the Higgs boson in the diphoton final state with 38 pb^{-1} of data recorded by the ATLAS detector in proton-proton collisions at $\sqrt{s}=7\text{ TeV}$* , ATLAS-CONF-2011-025, CERN, Geneva, Mar, 2011.
- [375] A. Elagin, P. Murat, A. Pranko and A. Safonov, *A New Mass Reconstruction Technique for Resonances Decaying to di-tau*, [arXiv:1012.4686](#).
- [376] T. Plehn, D. L. Rainwater and D. Zeppenfeld, *A method for identifying $H \rightarrow \tau\tau \rightarrow e^\pm\mu^\mp$ missing p_T at the CERN LHC*, Phys. Rev. **D61** (2000) 093005, [[hep-ph/9911385](#)].
- [377] **CMS** Collaboration, S. Gennai, *Higgs search in Tau Tau final states at CMS*, in *HEP–EPS 2011*, Grenoble (France), July 20th–27st, 2011.
indico.in2p3.fr/conferenceTimeTable.py?confId=5116.

-
- [378] B. Murray, *LHC Higgs*, in *HEP–EPS 2011*, Grenoble (France), July 20th–27st, 2011. indico.in2p3.fr/conferenceTimeTable.py?confId=5116.
- [379] J. Baglio, A. Djouadi, M. Grazzini and J. Quevillon , in progress.
- [380] S. Catani and M. Grazzini, *HNNLO: a Monte Carlo program to compute Higgs boson production at hadron colliders*, PoS **RADCOR2007** (2007) 046, [[arXiv:0802.1410](https://arxiv.org/abs/0802.1410)].
- [381] **CDF and D0** Collaboration, Tevatron New Phenomena & Higgs Working Group, *Combined CDF and D0 Upper Limits on Standard Model Higgs Boson Production with up to 8.6 fb⁻¹ of Data*, [arXiv:1107.5518](https://arxiv.org/abs/1107.5518).